THE
PHYSICAL REVIEW

A journal of experimental and theoretical physics established by E. L. Nichols in 1893

SECOND SERIES, VOL. 74, NO. 9 NOVEMBER 1, 1948

The Natural Abundance of Isotopes of Stable Elements†

J. R. WHITE* AND A. E. CAMERON**
Clinton Engineer Works, Tennessee Eastman Corporation, Oak Ridge, Tennessee
(Received April 15, 1948)

The natural isotopic abundances of the following elements have been determined by mass spectrometric techniques:

Lithium	Copper	Tin
Magnesium	Selenium	Antimony
Silicon	Bromine	Tellurium
Potassium	Strontium	Tantalum
Calcium	Zirconium	Tungsten
Chromium	Silver	Rhenium
Iron	Cadmium	Thallium
Nickel	Indium	Lead

Different masses were focused by variation of the magnetic flux in Nier-type, 60° mass spectrometers. Ion currents were measured potentiometrically. Each measurement represents at least 15 determinations. Many measurements are averages of series with different spectrometers and ion sources. From available packing fraction data and these abundances the chemical atomic weights have been computed.

INTRODUCTION

THE determinations of the natural isotopic abundance of the 24 elements here described were made in connection with the program of separation of these isotopes in the electromagnetic process pilot plant operated by the Clinton Engineer Works, Tennessee Eastman Corporation. The measurements were made to check the values in the literature and to serve as pathfinding experiments for measurements of separated isotopes. In some cases these are repetitions of previous determinations, but were usually made by somewhat different techniques. In several cases the only previous data were those obtained by mass spectrographic determinations involving photometry of a photographic plate.

EXPERIMENTAL

The measurements were made with two 60° mass spectrometers built in the Clinton Engineer Works, Tennessee Eastman Corporation laboratory specifically for this work. These instruments were of the type developed by Professor A. O. C. Nier of the University of Minnesota and his coworkers. Each instrument was the equivalent of two, since one set of electronic controls was associated with two vacuum and magnet assemblies. The instruments embodied improvements resulting from three years of intensive use and development of equipment of this type.

The hard solder used in assembling the tubes and in attaching the envelopes contained no cadmium, zinc, or other volatile metals, so that

† This work was done under contract W-7401-Eng. 23.
* Present address: Socony-Vacuum Oil Company, Inc., Research and Development Department, Paulsboro, New Jersey.
** Present address: Distillation Products, Inc., 755 Ridge Road West, Rochester, New York.

background was not introduced by these elements. Three-stage, self-fractionating diffusion pumps with Octoil-S produced an ultimate vacuum of approximately 10^{-7} millimeters of mercury. Liquid nitrogen traps were used to prevent hydrocarbon background arising from traces of pump oil. The ion sources were variously fabricated from nichrome *V*, platinum-iridium alloy, copper, and tantalum. Of these materials the platinum-iridium alloy appeared to be least attacked by corrosive gases. Tantalum introduced a tantalum and tantalum-halide spectrum which was troublesome in some measurements. The sample vapor was ionized by electrons of between 30 and 75 volts energy, and the ions so formed were focused and accelerated through a potential drop of 1900 volts. Ions were also produced by thermionic evaporation from a tungsten filament. Mass positions were identified by reading the output voltage of a rotating coil fluxmeter driven by a synchronous motor. The coil was rotated in the magnet gap and the output obtained through the two-segment commutator was filtered and read with a slide-wire potentiometer.

The selection of the ion beams was made exclusively by variation of the magnetic flux to avoid disturbing the voltages applied to the ion source. The ion currents from the collector plate behind the receiver slit were measured by introducing voltage from a calibrated precision potentiometer between ground and the 4×10^{10} ohm grid resistor in the input of the FP-54 electrometer. The electrometer and galvanometer were used as a null indicator and no reliance upon linearity of response of other than the grid resistor was then necessary. The galvanometer zero was observed by applying deflecting voltage to a source element so as to prevent the ion beam from passing through the tube. Residual galvanometer deflections were converted to potentiometer readings by interpolation factors determined experimentally.

The element or compound used for measurements of this kind must be volatile below 1500°C. Small samples must be readily prepared, free from other elements which are isobaric with the substance to be determined, or which give rise to complex or multiply-charged ions isobaric with the ions to be measured. The compound should not be so hygroscopic that it requires handling totally in a desiccated atmosphere. It must give an abundant ion in a mass region in which there is no background interference in the tube. The material should preferably sublime since evaporation from the liquid phase is more likely to lead to distillation fractionation because of the difference in weight of the various isotopes. Fluorides are particularly useful for measurements of this type since the step-wise ionization which occurs permits readings to be made at a number of different mass positions. Most fluorides are not, however, sufficiently volatile.

Samples which were volatile at room temperature, such as tungsten hexafluoride, were admitted to the ionizing region of the tube through a controllable capillary leak and a glass or metal sample line. Materials like selenium metal were handled with an external heating furnace and a large bore heated sample line passing into the tube. For other materials it was necessary to provide a small furnace which could be mounted above the ion source so that the substance could be distilled into the ionization region. These furnaces were supported from the ground glass cap on the source envelope and were isolated from the ionization region by a platinum screen to prevent electrostatic disturbance of the electron beam. Furnaces constructed of Vycor and tantalum and heated with platinum or tungsten elements were necessary for many of the compounds. A thermocouple was mounted in the furnace to permit a rough check upon the temperature of distillation.

Lengthy evacuation was necessary to remove background spectra from the tube and to free the sample from volatile impurities. The tube was baked at about 200°C by furnaces wound on the envelopes. It was frequently necessary to spend three to five days in pumping to reduce the background to a usable level.

Background ion contributions not associated with instrumental resolution could be reduced to a level such that these contributions to the abundances of the principal ions being measured were orders of magnitude less than the abundance deviations reported. However, particularly when employing corrosive halide gases, background ions frequently rendered critical examination for unreported isotopes infeasible. Accord-

Physics Lib
Physics Library
QC
1
P5812
Physics Lib
Direct
copy 1.

ingly, only for lithium, zirconium, tantalum and rhenium are these examinations reported.

Each measurement series reported below represents between 15- and 300-ratio determinations. Many measurements are an average of several series of determinations with different spectrometers and ion sources. In the case of elements having more than two isotopes, measurements were made between a principal isotope and each of the other isotopes. Where the packing fraction data are accurately known and these abundance measurements are thought to make significant contributions, the computed chemical weights are given.

DISCUSSION

The discrepancy between observers is not any greater than that between instruments in cases where the measurements were made by identical techniques. The residual discrepancy may probably be ascribed to mass discrimination occurring in the ion lenses in the source. Reversal of the magnetic field in the ionization region, operation with widely varied voltages applied to the source elements, and variations in collector geometry and secondary electron suppression make it probable that this discrimination is a function of the actual structural geometry of the source, rather than being caused by conditions which can be varied or differences in instrument geometry. The measurements of copper are a good example.

It has been assumed that the most probable ion abundance results from averaging of the measurements from a variety of ion sources and instruments and assigning equal weight to each instrument and ion-source structural variation. Only where several series of different determinations have been averaged may the average deviations tabulated be regarded as indexing the uncertainty in the abundances reported. In all other data an uncertainty of one percent of the specific ion abundance tabulated appears likely for abundances above two percent. For abundances between two percent and 0.05 percent, the uncertainty may be regarded as increasing from one percent to fifteen percent.

Measurements on any one spectrometer and ion source agreed much more closely than is indicated for the agreement between measurements on different instruments and ion sources. It is accordingly possible to use differential techniques in estimating enhanced tracer samples whose enhancement may be less than the expected instrument-to-instrument variation.

Lithium

Previous measurements of the abundance of the lithium isotopes have, for the most part, utilized the thermionic properties of the lithium salts for the production of ions. Some uncertainty was introduced by the correction for the free evaporation of ions with a large percentile mass difference.[1–8] For the measurements reported here, lithium aluminum chloride ($LiAlCl_4$) was distilled from a Pyrex glass retort into the ionizing region where it was bombarded by 75-volt electrons. The retort was separated from the platinum-iridium ionizing case by a platinum gauze screen. The distillation of the heavy molecule, $LiAlCl_4$, reduced the effects caused by the mass difference between the lithium isotopes. Measurements were made on the Li^+ ion. Three different series of determinations are represented. (See Table I.)

TABLE I. Relative abundance of Li isotopes.

Mass	5	6	7	8
Mole percent	$<10^{-5}$	7.30	92.70	$<10^{-5}$
Average deviation		±0.04	±0.04	
	Ratio Li^7/Li^6			
This measurement			12.7±0.07	
Morand[a]			14.9	
Bainbridge[b]			11.28	
Aston[c]			11.0	
Harnwell and Bleakney[d]			8.4	
Brewer[e,g]			11.60 to 12.52	
Hoff Lu[f]			12.29	
McKellar[h]			8.57	

[a] See reference 1.
[b] See reference 2.
[c] See reference 3.
[d] See reference 4.
[e] See references 5–7.
[f] See reference 8.
[g] A. K. Brewer, Ind. Eng. Chem. **30**, 893 (1938); A. K. Brewer and O. Baudisch, J. Am. Chem. Soc. **59**, 1578 (1937); A. K. Brewer, Phys. Rev. **49**, 867 (1937).
[h] A. McKellar and F. A. Jenkins, Dominion Astrophys. Obs. Victoria, Pub. **7**, 155 (1939).

[1] M. Morand, Comptes rendus **182**, 460 (1926); Ann. de physique **7**, 164 (1927).
[2] K. T. Bainbridge, J. Franklin Inst. **212**, 317 (1931).
[3] F. W. Aston, Proc. Roy. Soc. **A134**, 574 (1931).
[4] G. P. Harnwell and W. Bleakney, Phys. Rev. **45**, 117 (1934).
[5] A. K. Brewer and P. D. Kueck, Phys. Rev. **46**, 894 (1934).
[6] A. K. Brewer, Phys. Rev. **47**, 571 (1935).
[7] A. K. Brewer, J. Chem. Phys. **4**, 350 (1936).
[8] Hoff Lu, Phys. Rev. **53**, 845 (1938).

TABLE II. Relative abundance of Mg isotopes.

Mass	24	25	26
This measurement mole percent	78.60	10.11	11.29
Average deviation	±0.13	±0.05	±0.08
Dempster;[a] electron ionization of Mg metal vapor	77.4	11.5	11.1

[a] A. J. Dempster, Phys. Rev. **18**, 421 (1921).

TABLE III. Relative abundance of Si isotopes.

Mass	28	29	30
This measurement mole percent	92.16	4.71	3.13
Average deviation	±0.06	±0.03	±0.04
McKellar;[a] photometry of SiN	89.6	6.2	4.2
Inghram;[b] electron ionization of SiF_4	92.28	4.67	3.05
Williams and Yuster;[c] electron ionization of SiF_4	92.27	4.68	3.05
Ney and McQueen;[d] electron ionization of SiF_4	92.24	4.69	3.07

[a] A. McKellar, Phys. Rev. **45**, 761 (1934).
[b] M. G. Inghram, Bull. Am. Phys. Soc. **21–3**, Sp-1 (1946).
[c] D. Williams and P. Yuster, Phys. Rev. **69**, 556 (1946).
[d] E. P. Ney and J. H. McQueen, Phys. Rev. **69**, 41 (1946).

This abundance ratio with the masses of $Li^6=6.01670$ and $Li^7=7.01799$ calculated by Allison[9] or the masses $Li^6=6.01682$ and $Li^7=7.0178_4$ calculated by Smith[10] yields a chemical atomic weight for lithium of 6.943. The international value is 6.940. A physical to chemical scale conversion factor of 1.000275 has been employed in this and subsequent calculations.

Magnesium

Magnesium metal was distilled from a Vycor retort into a platinum-iridium ionizing case. The retort was heated by a platinum resistance furnace. Ionization was produced by slow electrons and measurements were made on the Mg^+ ion. Three different series of determinations were conducted.

Measurements were made also by distilling magnesium acetyl acetonate. These were found to be unreliable because of interference at masses 24, 25, and 26 and the absence of a complex ion containing magnesium useful for analysis. The interfering ions were presumed to be C_2^+, C_2H^+, and $C_2H_2^+$. No compound was found which could be used for the determination of separated samples. The metal could not be prepared readily in micro-quantity. (See Table II.)

These abundance data taken with the isotopic masses $Mg^{24}=23.99189$, $Mg^{25}=24.99277$ and $Mg^{26}=25.99062$ computed by Pollard[11] yield a chemical atomic weight of 24.31. The present international value is 24.32.

Silicon

Silicon tetrafluoride vapor, produced by the action of fluorine on hot Pyrex glass, was subjected to slow electron bombardment. Measurements were made with ionizing cases of tantalum and of copper. All measurements were made on the SiF_3^+ ion. A total of 61 different determinations, representing about 800 ratio measurements for each isotope pair, using five different instruments, has been performed. In computing the average, each instrument has been given equal weight. (See Table III.)

Using either Aston's[12] packing fraction value of -4.90 for Si^{28} or Pollard's[11] computed values, $Si^{28}=27.98639$, $Si^{29}=28.98685$, and $Si^{30}=29.98294$,

TABLE IV. Abundance rations of K isotopes.

	Ratio K^{39}/K^{41}	Ratio K^{40}/K^{39}
This measurement	13.66±0.1	
Brewer and Kueck;[a] thermionic	13.88±0.4	
Nier;[b] electron ionization of K metal vapor	13.96±0.1	1/8600
Bondy, Johansen and Popper;[c] thermionic	16.2	
Manley;[d] magnetic moment separation of molecular beam	13.4±0.5	
Bondy and Vanicek;[e] thermionic	14.0	
Brewer;[f] thermionic (plant ash)	12.63 to 14.32	
Brewer;[f] thermionic (sea water)	14.2	
Brewer;[f] thermionic (mineral)	14.11 to 14.6	
		1/8300
Brewer;[g] thermionic	—	
Paul and Pahl[h]	13.96±0.1	
Cook;[i] thermionic	14.12±0.28	

[a] See reference 5.
[b] A. O. Nier, Phys. Rev. **48**, 283 (1935).
[c] H. Bondy, G. Johansen and K. Popper, Zeits. f. Physik **95**, 46 (1935).
[d] J. H. Manley, Phys. Rev. **49**, 921 (1936).
[e] H. Bondy and V. Vanicek, Zeits. f. Physik **101**, 186 (1936).
[f] A. K. Brewer, J. Am. Chem. Soc. **58**, 365 (1936).
[g] A. H. Brewer, Phys. Rev. **48**, 640 (1935).
See also:
A. K. Brewer and O. Bandisch, J. Am. Chem. Soc., **59**, 1578 (1937).
A. K. Brewer, Ind. Eng. Chem. **30**, 893 (1938).
A. K. Brewer, J. Am. Chem. Soc. **61**, 1597 (1939); *ibid.* **59**, 869 (1937).
[h] W. Paul and M. Pahl, Naturwiss. **32**, 228 (1944).
[i] K. L. Cook, Phys. Rev. **64**, 278 (1943).

[9] S. K. Allison, Phys. Rev. **55**, 624 (1939).
[10] N. M. Smith, Jr., Phys. Rev. **56**, 548 (1939).
[11] E. Pollard, Phys. Rev. **57**, 1186 (1940).
[12] F. W. Aston, Nature **138**, 1094 (1936); Mass Spectra and Isotopes (1933).

TABLE V. Relative abundance of Ca isotopes.

Mass	40	42	43	44	46	48
	Mole percent					
This measurement; thermal evaporation	96.92	0.64	0.132	2.13	0.0032	0.179
Average deviation	±0.03	±0.01	±0.004	±0.04	—	±0.001
Nier;[a] electron ionization of metal vapor	96.97	0.64	0.145	2.06	0.0033	0.185
Aston[b] photometry	96.76	0.77	0.17	2.30	—	—

[a] A. O. Nier, Phys. Rev. **53**, 282 (1938).
[b] F. W. Aston, Nature **133**, 684 (1934); Proc. Roy. Soc. **A149**, 396 (1935).

TABLE VI. Relative abundance of Cr isotopes.

Mass	50	52	53	54
This measurement mole percent	4.31	83.76	9.55	2.38
Average deviation	±0.04	±0.14	±0.09	±0.02
Aston;[a] photometry	4.9	81.6	10.4	3.1
Nier;[b] thermal evaporation from metal	4.49	83.78	9.43	2.30

[a] F. W. Aston, Proc. Roy. Soc. **A130**, 306 (1931).
[b] A. O. Nier, Phys. Rev. **55**, 1143 (1939).

these abundances permit computation of a chemical atomic weight of 28.08_8. The present international value is 28.06.

Potassium

Potassium aluminum chloride, prepared by the Chemical Development Group of the Clinton Engineer Works, Tennessee Eastman Corporation, was distilled into an ionizing case constructed of platinum-iridium alloy. Measurements were made on the K^+ ion. The traces of calcium which were present in the sample made exact measurement of the concentration of the mass 40 isotope impossible. (See Table IV.)

From either Aston's[12] or Bainbridge's[13] packing fraction data the packing fraction of potassium is about −7.0. Hahn, Flügge, and Mattauch[14] report −6. From transmutation data Pollard[11] has calculated $K^{39}=38.97518$ and $K^{41}=40.9739$ corresponding to packing fractions of −6.37. Combining these latter with the abundance ratio of this measurement yields a chemical weight of 39.10 for potassium. The present international value is 39.096.

[13] K. T. Bainbridge, Phys. Rev. **43**, 424 (1933).
[14] O. Hahn, S. Flügge, and J. Mattauch, Ber. **73A**, 1 (1940).

Calcium

Calcium ions were produced by thermal evaporation from a tungsten filament coated with calcium oxide. Measurements were made upon the Ca^+ ion. These measurements compare very favorably with those which were made by Nier by electron ionization of calcium metal vapor. (See Table V.)

Selecting a packing fraction of −6.3 in accord with that reported by Hahn, Flügge, and Mattauch,[14] −6.2, and the mass, $K^{41}=40.9725$ to 40.9739, computed by Davidson,[15] permits computation of a chemical weight of 40.08 from the data in Table V. The international value is 40.08.

Chromium

Chromium trichloride ($CrCl_3$) was distilled from a tungsten, platinum, Vycor retort assembly into the tantalum metal electron ionization source. Cr^+ ion abundances were measured. (See Table VI.)

TABLE VII. Relative abundance of Fe isotopes.

Mass	54	56	57	58
This measurement mole mole percent	5.81	91.64	2.21	0.34
Average deviation	±0.01	±0.02	±0.01	±0.01
Aston;[a] photometry	6.5	90.7	2.8	—
Nier;[b] electron ionization of Fe metal vapor	6.0	91.6	2.1	0.28
Valley;[c] electron ionization of Fe metal vapor	5.83	91.7	2.16	0.31
deGier and Zeeman;[d] photometry	6.5	90.2	2.8	0.5

[a] F. W. Aston, Nature **133**, 684 (1934); Proc. Roy. Soc. **A149**, 396 (1935).
[b] A. O. Nier, Phys. Rev. **55**, 1143 (1939).
[c] G. E. Valley and H. H. Anderson, Phys. Rev. **59**, 113 (1941).
[d] J. deGier and P. Zeeman, Proc. Akad. Sci. Amsterdam **38**, 959 (1935).

TABLE VIII. Relative abundance of Ni isotopes.

Mass	58	60	61	62	64
This measurement mole percent	67.76	26.16	1.25	3.66	1.16
Average deviation	±0.22	±0.66	±0.03	±0.01	±0.20
Aston;[a] photometry	67.5	27.0	1.7	3.7	?
Straus;[b] oscillating spark Faraday collector	62.8	29.5	1.7	4.7	1.3
Valley;[c] electrom bombardment of Ni vapor	67.4	26.7	1.2	3.8	0.88
Lub[d]	68.0	27.2	0.1	3.8	0.9

[a] F. W. Aston, Proc. Roy. Soc. **A130**, 306 (1931).
[b] H. A. Straus, Phys. Rev. **59**, 430 (1941).
[c] G. E. Valley, Phys. Rev. **59**, 836 (1941).
[d] W. A. Lub, Proc. Acad. Sci. Amsterdam **42**, 253 (1939).

[15] W. L. Davidson, Jr., Phys. Rev. **57**, 244 (1940).

TABLE IX. Relative abundance of Cu^{63} isotope.

	Mole percent Cu^{63}
This measurement	68.94±0.19*
Ewald;[a] photometry	70.16±0.27
Dempster;[b] oscillating spark Faraday collector	69.04±0.29
Duckworth and Hoge;[c] photometry	69.48±0.16

* Maximum value for any series, 69.41. Minimum value for any series, 68.62.
[a] H. Ewald, Zeits. f. Physik **122**, 487 (1944).
[b] A. J. Dempster, Report for February, 1946, CP-3445.
[c] H. E. Duckworth and B. J. Hoge, Phys. Rev. **71**, 212 (1947).

TABLE X. Relative abundance of Se isotopes.

Mass	74	76	77	78	80	82
This measurement; SeF_6 mole percent	0.86	9.08	7.51	23.54	50.02	8.99
Se	0.88	8.95	7.65	23.51	49.62	9.39
Mean	0.87	9.02	7.58	23.52	49.82	9.19
Average deviation	±0.01	±0.07	±0.07	±0.02	±0.20	±0.20
Aston;[a] photometry	0.9	9.5	8.3	24.0	48.0	9.3

[a] See reference 24.

With either Aston's[16] packing fraction, −8.18 ±0.15 or that of Hahn, Flügge, and Mattauch,[14] 7.9±0.2 the chemical weight computed from these abundances becomes 52.00. The international chemical weight is presently 52.01.

Iron

Ferrous chloride ($FeCl_2$) was distilled from a Pyrex glass retort into the electron ionizing case of the platinum-iridium ion source. Fe^+ ion abundances were measured. Two series of determinations are represented. (See Table VII.)

Dempster[17] gives −7.0±0.4 as the packing fraction for iron; Flügge and Mattauch[18] list −7.15±0.30; while Okuda *et al.*[19] report Fe^{56} = −7.7. Selection of a mean −7.3 permits calculation of a chemical weight of 55.85_6 from these abundance observations. The international value is 55.85.

TABLE XI. Relative abundance of Br isotopes.

Mass	79	81
This measurement mole percent	50.51	49.49
Average deviation	±0.06	±0.06
Blewett[a]	50.6	49.4
Williams and Yuster[b]	50.52	49.48

[a] J. P. Blewett, Phys. Rev. **49**, 900 (1935).
[b] D. Williams and P. Yuster, Phys. Rev. **69**, 556 (1946).

[16] F. W. Aston, Nature **141**, 1096 (1938).
[17] A. J. Dempster, Phys. Rev. **53**, 64 (1938).
[18] S. Flügge and J. Mattauch, Ber. d.d. chem. Ges. **76**, 1 (1943).
[19] T. Okuda, K. Ogata, K. Aoki, and Y. Sugawara, Phys. Rev. **58**, 578 (1940).

TABLE XII. Relative abundance of Sr isotopes.

Mass	84	86	87	88
This measurement mole percent	0.55	9.75	6.96	82.74
Average deviation	±0.01	±0.04	±0.01	±0.06
Sampson and Bleakney[a]	0.5	9.6	7.5	82.4
Nier;[b] electron ionization of Sr metal vapor	0.56	9.86	7.02	82.56

[a] M. B. Sampson and W. Bleakney, Phys. Rev. **50**, 456 (1936).
[b] A. O. Nier, Phys. Rev. **54**, 275 (1938).

Nickel

Nickelous chloride ($NiCl_2$) was distilled from a tungsten, platinum, Vycor retort assembly into the ionizing region of the tantalum metal electron bombardment source. The abundances of Ni^+ and $NiCl^+$ ions were measured.

A number of determinations of different samples of chloride yielded similar ratio behavior in all mass positions save 64. Prolonged distillation resulted in some upward shift in the ratios with respect to 64. An average of four series of determinations after prolonged distillation yields the following. Mass 64 abundance is least certain. It is probable that the abundance lies between the 0.88 percent reported by Valley and 1.16 percent. (See Table VIII.)

Employing the packing fractions, Ni^{58} = 6.97

TABLE XIII. Relative abundance of Zr isotopes.

Mass	90	91	92	94	96
This measurement:					
Zr^+ mole percent	51.51	11.27	17.14	17.30	2.78
ZrF_3^+	51.40	11.19	17.09	17.50	2.82
Average	51.46	11.23	17.11	17.40	2.80
Aston;[a] photometry of photographic plate	48	11.5	22	17	1.5

[a] F. W. Aston, Nature **133**, 684 (1934); Proc. Roy. Soc. **A149**, 396 (1935).

TABLE XIV. Relative abundance of Ag isotopes.

Mass	107	109
This measurement mole percent	51.35	48.65
Average deviation	±0.07	±0.07
Aston;[a] photometry	52.5	47.5
Paul[b]	51.92	48.08

[a] F. W. Aston, Nature **133**, 684 (1934); Proc. Roy. Soc. **A149**, 396 (1935).
[b] W. Pauli, Naturwiss. **31**, 419 (1943).

TABLE XV. Relative abundance of Cd isotopes.

Mass	106	108	110	111	112	113	114	116
This measurement mole percent	1.22	0.98	12.35	12.78	24.00	12.30	28.75	7.63
Average deviation	±0.01	±0.01	±0.04	±0.04	±0.10	±0.04	±0.20	±0.04
Aston;[a] photometry	1.5	1.0	15.2	15.2	21.8	14.9	23.7	5.9
Nier;[b] electron ionization of Cd metal vapor	1.4	1.0	12.8	13.0	24.2	12.3	28.0	7.3

[a] F. W. Aston, Nature, **133**, 684 (1934); Proc. Roy. Soc. **A149**, 396 (1935).
[b] A. O. Nier, Phys. Rev. **50**, 1041 (1936).

±0.07, $Ni^{60} = -8.37 \pm 0.06$, $Ni^{61} = -7.5 \pm 0.3$, $Ni^{62} = -8.14 \pm 0.06$, and $Ni^{64} = -8.22 \pm 0.09$ of Okuda *et al.*,[20] which are in fair accord with Aston's[16] $Ni^{58} = -8.35$, the chemical weight is calculated as 58.71. The international weight is 58.69.

Copper

This element has been very extensively investigated by distillation of cuprous chloride (Cu_2Cl_2) from a Pyrex glass retort into the electron region of a variety of sources constructed of platinum-iridium and tantalum. In all, 21 series of determinations, representing about 300 ratio measurements, have been conducted under a variety of measurement conditions. Four different spectrometers have been used in this work. Cuprous chloride was obtained from four different suppliers. Cu^+ and $CuCl^+$ ion abundances were measured. (See Table IX.)

With a packing fraction of -6.9 ± 0.2 measured by Dempster,[17] the chemical atomic weight of copper becomes 63.56 in good accord with the older international chemical weight, 63.57, and slightly higher than the recent determination of Hönigschmidt and Johansen,[21] 63.542, now accepted in the 1947 international table. With Flügge and Mattauch's[22] packing fraction of -8.13 ± 0.10 or Duckworth's[23] packing fraction of -7.92 ± 0.25 the computed chemical weight becomes 63.55.

Selenium

Selenium was measured using both the metal and the hexafluoride. Selenium metal was distilled into a platinum-iridium metal electron ionization source. A tantalum metal ion source was used for the selenium hexafluoride measurements. The Se^+ ion formed from the metal and the SeF_5^+ ion formed from the hexafluoride were measured. (See Table X.)

Aston[24] reports a packing fraction of -7.3 for Se^{80} with a large uncertainty. Flügge and Mattauch[18] list -7.1. With either the chemical weight of selenium computed from these abundance data is 78.99; the international chemical weight is 78.96.

Bromine

Silver bromide has been distilled from a high temperature Vycor retort into a tantalum electron bombardment ion source. Br^+ and HBr^+ ion abundances have been measured. (See Table XI.)

Aston[16] indicates a packing fraction for bromine of -7.4 while Flügge and Mattauch[18] list -7.1. Either leads to a computed chemical atomic weight of 79.91 for bromine; the international weight is 79.916.

Strontium

Metallic strontium was distilled into the electron ionization region of a tantalum metal ion source. The abundances of Sr^+ ions were measured. (See Table XII.)

TABLE XVI. Relative abundance of In isotopes.

Mass	113	115
This measurement mole percent	4.23	95.77
Average deviation	±0.03	±0.03
Aston;[a] photometry	4.5	95.5
Sampson and Bleakney;[b] thermal ionization	4.5	95.5

[a] F. W. Aston, Nature, **133**, 684 (1934); Proc. Roy. Soc. **A149**, 396 (1935).
[b] M. B. Sampson and W. Bleakney, Phys. Rev. **50**, 456 (1936).

[20] T. Okuda, K. Ogata, H. Kuroda, S. Shima, and S. Shindo, Phys. Rev. **59**, 104 (1941).
[21] O. Hönigschmidt and Th. Johansen, Naturwiss. **31**, 548 (1943).
[22] S. Flügge and J. Mattauch, Physik. Zeits. **44**, 181 (1943).
[23] H. E. Duckworth, Phys. Rev. **62**, 19 (1942).
[24] F. W. Aston, Proc. Roy. Soc. **A132**, 487 (1931).

TABLE XVII. Relative abundance of Sn isotopes.

Mass	112	114	115	116	117	118	119	120	122	124
This measurement mole percent	0.90	0.61	0.35	14.07	7.54	23.98	8.62	33.03	4.78	6.11
Average deviation	±0.003	±0.01	±0.006	±0.08	±0.03	±0.03	±0.003	±0.12	±0.01	±0.006
Aston;[a] photometry	1.1	0.8	0.4	15.5	9.1	22.5	9.8	28.5	5.5	6.8

[a] F. W. Aston, Proc. Roy. Soc. **A115**, 506 (1927).

Flügge and Mattauch[18] adopt a packing fraction for strontium of −7.0. A value of −6.3 may be deduced from Dempster's[25] packing fraction curve. The former leads to a computed chemical weight of 87.62 while the latter leads to 87.63; the accepted international weight is 87.63.

Zirconium

Ions were formed by 50-volt electrom bombardment of vapors of zirconium tetrachloride ($ZrCl_4$) and zirconium tetrafluoride (ZrF_4). Zr^+ ions formed in the tetrachloride bombardment, and ZrF_3^+ ions formed in the tetrafluoride bombardment, were measured. Masses 88, 89, 93, 95, 97, 98, and 99 are each not greater than 1/5000 of the total zirconium ion abundance. (See Table XIII.)

From Dempster's[25] packing fraction curve a value of about −6.0 is obtained for the isotopes of zirconium. Flügge and Mattauch[18] list −6.75. These abundance data reduce to a chemical atomic weight of 91.24 with the former value and of 91.23 with the latter value; the accepted international chemical weight is 91.22.

Silver

Silver chloride was distilled from a Vycor and platinum retort into the platinum-iridium electron bombardment source. Ag^+ ion abundances were measured. Two series of determinations are represented. With Dempster's[17] packing fraction value of −4.93±0.5, the chemical atomic weight is calculated as 107.89, in excellent agreement with the international chemical value of 107.880. (See Table XIV.)

TABLE XVIII. Relative abundance of Sb isotopes.

Mass	121	123
This measurement mole percent	57.25	42.75
Average deviation	±0.03	±0.03
Aston;[a] photometry	56.0	44.0

[a] F. W. Aston, Proc. Roy. Soc. **A132**, 492 (1931).

[25] A. J. Dempster, Phys. Rev. **53**, 869 (1938).

Cadmium

Anhydrous cadmium chloride ($CdCl_2$) was distilled into the ionizing case of a tantalum metal ion source. Cd^+ ion abundances were measured. (See Table XV.)

The packing fractions for the cadmium isotopes have been deduced as about −5.0 from Dempster's[25] curve. Flügge and Mattauch[18] list −5.3. With either value the computed chemical weight of cadmium becomes 112.44 as contrasted with an international value of 112.41.

Indium

Indium trichloride ($InCl_3$) was vaporized and subjected to electron bombardment in a platinum-iridium metal ion source. In^+ ion abundances were measured. An average of three series of determinations yields the values shown in Table XVI.

Flügge and Mattauch[18] assign a packing fraction of −5.1 for the isotopes of indium. Dempster's[25] curve indicates an essentially similar value. With these abundances the chemical weight of indium is calculated as 114.83; the international chemical value is 114.76.

Tin

Anhydrous stannous chloride ($SnCl_2$) was volatilized and ionized by electron impact. Metal parts were constructed of platinum-iridium alloy. Sn^+ ion abundances were measured. Three series of determinations yield an average of the values shown in Table XVII.

Using Aston's[26] packing fraction, −5.8, for the mass 118 and 120 isotopes of tin, the computed

[26] F. W. Aston, Proc. Roy. Soc. **A163**, 391 (1937).

TABLE XIX. Relative abundance of Te isotopes.

Mass	120	122	123	124	125	126	128	130
Metal* mole percent	0.092	2.32	0.88	4.51	6.99	18.53	32.57	34.11
Hexafluoride	0.091	2.49	0.89	4.63	7.01	18.72	31.72	34.46
Average deviation TeF_6	±0.001	±0.02	±0.02	±0.05	±0.01	±0.04	±0.01	±0.09
Bainbridge;[a] photometry	—	2.9	1.6	4.5	6.0	19.0	32.8	33.1
Aston;[b] photometry	—	—	—	—	6.6	20.9	36.1	36.4
Williams and Yuster;[c] electron ionization of TeF_6	0.090	2.43	0.85	4.59	6.97	18.70	31.85	34.5

* Distillation of Te metal; Te^+ ion abundance.
[a] K. T. Bainbridge, Phys. Rev. 39, 1021 (1932).
[b] F. W. Aston, Proc. Roy. Soc. A132, 487 (1931).
[c] D. Williams and P. Yuster, Phys. Rev. 69, 556 (1946).

chemical weight becomes 118.75. With Graves's[27] packing fraction, −4.56, or Dempster's[25] value of −5.0±0.5 for the 116 and 118 isotopes and −4.5±0.5 for the 122 and 124 isotopes, the computed chemical weight is 118.76. The present international value is 118.70.

Antimony

Metallic antimony was volatilized and ionized by electron bombardment. Sb^+ ion abundances were measured. (See Table XVIII.)

Flügge and Mattauch[18] indicate a packing fraction of −4.8 for the isotopes of antimony. From Dempster's[25] data on tin a value nearer −4.5 may be inferred. Either figure leads to a chemical weight computed from these abundances of 121.77; the international value is 121.76.

Tellurium

Tellurium hexafluoride was admitted to the electron flux region of the ion source through a controllable capillary leak. TeF_5^+ and TeF_2^+ ion abundances were measured. Tellurium metal has also been distilled from a Vycor, platinum retort into a tantalum ion source. The ion sources were constructed of tantalum and of copper. Five series of 24 determinations are represented in the hexafluoride data. (See Table XIX.)

Aston[24] has indicated a rough packing fraction value for tellurium of 5±2. Flügge and Mattauch[18] list −4.5, while Dempster's[25] curve suggests −4.5 to −4.0 over the range of ten mass units. Adopting this latter permits computation of a chemical atomic weight of 127.64 for tellurium; the international chemical weight is 127.61.

[27] A. C. Graves, Phys. Rev. 55, 863 (1939).

Tantalum

Ta^+, TaF^+, TaF_2^+, TaF_3^+, TaF_4^+, and TaF_5^+ ions have been formed by admitting uranium hexafluoride to an ionizing case constructed of tantalum metal. Tantalum may be regarded as simple; no other isotopes greater than one part in ten thousand of the principal mass, 181, are present.

Tungsten

Tungsten hexafluoride (WF_6) was admitted through a controllable capillary leak into the electron ionization case of ion sources constructed of tantalum and copper. WF_5^+ ion abundances were measured. Four series of 27 determinations have been averaged. (See Table XX.)

Computation of chemical weight from reported or deduced packing fractions of 0.0[24], +0.6[18], and +1.8[25] leads to values of 183.84, 183.85, and 183.87, respectively. The international chemical weight is 183.92.

Rhenium

The hemi-heptoxide of rhenium (Re_2O_7) has been distilled into the electron flux region of an ion source constructed of platinum-iridium. Re^+ ion abundances have been measured. The rhen-

TABLE XX. Relative abundance of W isotopes.

Mass	180	182	183	184	186
This measurement mole percent	0.126	26.31	14.28	30.64	28.64
Average deviation	±0.006	±0.03	±0.01	±0.03	±0.01
Aston;[a] photometry	0.2	22.6	17.3	30.1	29.8
Inghram;[b] electrion ionization of WF_6	0.122	25.77	14.24	30.68	29.17
Williams and Yuster;[c] electron ionization of hexacarbonyl	0.135	26.41	14.40	30.64	28.41

[a] F. W. Aston, Proc. Roy. Soc. A132, 492 (1931).
[b] M. B. Inghram, Bull. Am. Phys. Soc. 21-3, Sp-1 (1946).
[c] D. Williams and P. Yuster, Phys. Rev. 69, 556 (1946).

TABLE XXI. Relative abundance of Rh isotopes.

Mass	180–184	185	186	187	188–190
This measurement mole percent	$<10^{-4}$	37.07	$<10^{-4}$	62.93	$<10^{-4}$
Average deviation		±0.06		±0.06	
Aston;[a] photometry		38.2		61.8	

[a] See reference 24.

TABLE XXII. Relative abundance of Tl isotopes.

Mass	203	205
This measurement mole percent	29.46	70.54
Average deviation	±0.05	±0.05
Schuler and Keyston[a]	30.31	69.69
Nier;[b] electron ionization of Tl vapor	29.1	70.9
Aston;[c] photometry	29.43	70.57

[a] H. Schuler and J. E. Keyston, Zeits. f. Physik **70**, 1–2, 1 (1931).
[b] A. O. Nier, Phys. Rev. **54**, 275 (1938).
[c] See Ref. 3.

ium was obtained from Dr. G. E. Boyd of the Clinton Laboratories, Monsanto Chemical Company.

Assuming a packing fraction of $+1.0$[24], the computed chemical atomic weight becomes 186.22. The international value is 186.31. (See Table XXI.)

Thallium

The metal was distilled from a Pyrex glass retort into a platinum-iridium ion source. Ionization was by slow electron bombardment. Measurements were made upon the Tl^+ ion. These measurements and those of Nier have been corrected for the free evaporation of the metal vapor from the liquid phase. The correction factor is $(205/203)^{\frac{1}{2}}=1.005$. (See Table XXII.)

With a packing fraction of $+2.0$ deduced from Dempster's[25] curve or a value of $+2.65$ reported by Flügge and Mattauch[18] the corresponding chemical atomic weights of thallium computed from these abundance measurements are 204.40 and 204.41 respectively; the international chemical atomic weight is 204.39.

TABLE XXIII. Relative abundance of Pb isotopes.

Mass	204	206	207	208
This measurement mole percent	1.37	25.15	21.11	52.38
Average deviation	±0.02	±0.04	±0.04	±0.10
Aston;[a] photometry	1.5	28.3	20.1	50.1
Nier;[b] electron ionization of PbI vapor Great Bear Lake Galena	1.5	23.5	22.7	52.3*
Rose and Stranathan[c]	0.8	26.3	21.3	51.5
Mattauch[d]	1.15	24.55	21.35	52.95

[a] F. W. Aston, Proc. Roy. Soc. **A140**, 535 (1933).
[b] A. O. Nier, Phys. Rev. **53**, 680; J. Am. Chem. Soc. **60**, 1571 (1938).
* Variation with source of lead, A. O. Nier, R. W. Thompson, and B. F. Murphey, Phys. Rev. **60**, 112 (1941).
[c] J. L. Rose and R. K. Stranathan, Phys. Rev. **49**, 916 (1936).
[d] J. Mattauch, Naturwiss. **25**, 763 (1937).

Lead

Lead chloride ($PbCl_2$) was distilled into the electron flux region of ion sources constructed of platinum-iridium. Pb^+ and $PbCl^+$ ion abundances were measured. Nier and Hanson's[28] data for the 35/37 chlorine isotope ratio have been used for correction. The samples were assumed to be common lead of unspecified source. (See Table XXIII.)

ACKNOWLEDGMENT

Measurements upon tungsten, tellurium and silicon fluorides were made also by Mr. R. F. Hibbs and associates in this laboratory. Mr. John E. Brown assisted in the measurements upon many of the elements. The writers are also indebted to the Chemical Development Group of this organization for preparation and purification of some of the compounds used in this work.

[28] A. O. Nier and E. E. Hanson, Phys. Rev. **50**, 722 (1936).

PHYSICAL REVIEW VOLUME 74, NUMBER 9 NOVEMBER 1, 1948

Deuteron-Induced Reactions

D. C. PEASLEE
Massachusetts Institute of Technology, Cambridge, Massachusetts
(Received June 3, 1948)

A simple semiclassical model is described for the computation of *d-p* and *d-n* cross sections. It is found that the stripping process is responsible for practically the entire observed *d-p* cross section at any bombarding energy E_d. The few available quantitative *d-p* measurements—for Na^{23}, Co^{59}, Cu^{63}, Br^{81}, and Bi^{209}—agree with curves calculated by assuming that only the stripping process is effective. As E_d increases above the barrier height of the target nucleus, the measured *d-p* cross sections diminish; this is interpreted as due to effective *d-n* competition, in which the excited nucleus re-emits a neutron after acquiring one in the *d-p* stripping process. It is expected that the *d-n* excitation curves are also predominantly due to the stripping process for incident energies $E_d \gtrsim 10$ Mev.

To compare observed magnitudes with the calculated values, it is necessary to specify as a nuclear parameter the average "sticking probability" ξ of an elementary particle. Comparison of the *d-p* and *d-n* stripping processes indicates that for a given target the ratio σ_{dp}/σ_{dn} will exceed unity at all energies E_d comparable with the Coulomb barrier and may approach the limit $\sigma_{dp}/\sigma_{dn} \to \xi_n/\xi_p \approx 1$ as $E_d \to \infty$.

I. INTRODUCTION

THIS study discusses nuclear reactions induced by deuterons at moderate incident energies, 2–15 Mev. The models used for calculation are of the simplest type, so that the structural details of individual nuclei are neglected, and the computed results should be regarded as of a semiquantitative nature. Nevertheless, fair agreement is obtained with some absolute excitation curves, and it appears possible to draw certain general conclusions that have not previously been emphasized about the mechanism of these reactions and to give a very simple formula that accounts, to first order, for the observed excitation curves. It is found for all but perhaps the lightest elements (i) that the observed *d-p* excitation curve is due almost entirely to the Oppenheimer-Phillips or stripping reaction throughout the entire range of deuteron bombarding energies, and not just at energies well below the barrier height of the nucleus, and (ii) that the major portion of the observed *d-n* cross section is due to an analogous stripping effect with the roles of neutron and proton interchanged. Only a secondary contribution is made by the direct reaction, in which the deuteron is absorbed as a whole and a single particle subsequently emitted; the predominance of the stripping process is greater for *d-p* than for *d-n* reactions, and for both types this predominance increases with the atomic number of the target.

Excitation curves for the *d-p* reaction are computed for those elements of which thorough quantitative measurements have been made: Na^{24}, Co^{59}, Cu^{63}, Br^{81}, and Bi^{209}. These cross sections are obtained experimentally by measuring the specific activity of the residual nucleus, which has experienced a net gain of one neutron in the reaction. If the deuteron is absorbed as a whole with high incident energy, however, the most probable result is the emission of two or more particles, and the simple *d-p* reaction becomes very unlikely. Available statistical theories of nuclear level densities[1] suggest that the two-particle competition to the direct reaction usually becomes important in the region around $E_d > 10$ Mev. But in this energy region the stripping process still allows an appreciable probability that the proton, in escaping, will carry away all of the incident energy or even more, leaving the neutron in a negative energy (bound) state in the final nucleus. The energy of the neutron will be measured from a zero corresponding to the potential energy of infinite separation from the nucleus; therefore, a neutron bound in the nucleus will be called a "negative energy" neutron. The preponderance of the *d-p* stripping process at these energies is estimated more quantitatively in the examples below. Of course, even the stripping reaction yields relatively fewer negative energy neutrons as the incident deuteron energy increases: the neutrons tend to be more often absorbed with positive energy, causing the immediate re-emission of a

[1] V. F. Weisskopf and D. H. Ewing, Phys. Rev. **57**, 472 (1939).

neutron (an uncertainty of a few kev in the energy limit for re-emission is unimportant for these considerations). Therefore, as the deuteron energy is increased well above the nuclear barrier, the *d-p* cross section will decline because of effective *d-pn* competition in the stripping reaction, which has not been observed.

At low incident energies, the charge asymmetry of the deuteron greatly favors the *d-p* process by stripping, because the proton does not, on the average, have to penetrate so far into the Coulomb barrier as in the direct reaction. This is what is ordinarily known as the Oppenheimer-Phillips reaction.

The *d-n* reactions at high incident energies are also due to stripping in accord with the argument above: only the stripping process, in which the statistical distribution of emergent energies is largely governed by the internal wave function of the deuteron, permits the appreciable absorption of protons in energy states low enough to avoid emission of another particle by the residual nucleus. At low energies, the proton must penetrate the same Coulomb barrier to reach the nuclear surface, regardless of whether the entire deuteron is absorbed or not. Therefore, the stripping process is not tremendously favored, as in the corresponding *d-p* case, but the low binding energy and wide average separation of the deuteron components make it possible even in this instance to ascribe roughly half the observed cross section to a stripping type reaction in which the neutron escapes without encountering the nucleus.

These considerations indicate that for a given target nucleus, the observed *d-p* cross section will generally exceed the *d-n* cross section. For when both reactions are predominantly due to stripping, the Coulomb repulsion of the nucleus will always favor proton stripping relative to neutron stripping; and as a first approximation we may assume other (nuclear) factors to be the same. At high incident energies, the Coulomb field is less effective, so the ratio σ_{dp}/σ_{dn} decreases toward unity as E_d decreases. Observations of this sort have been made on Bi^{209}.[2,3]

In this simplified treatment, the nucleus is introduced merely as a geometrical surface characterized by the phenomenological constant ξ, the "sticking probability" for an elementary particle. Curves computed on this basis are compared with quantitative cross section measurements, and it is found possible to achieve a moderate fit by assigning a reasonable constant value to ξ. Unfortunately, quantitative measurements are now available for only a few elements, but the values of the parameter ξ obtained here lie generally within the range encompassed by other measurements of this quantity. The values of ξ_n derived here for heavy elements seem to be definitely smaller than those for light and medium elements. It might be of interest to extend these investigations of the sticking probability to a more complete list of nuclei than has previously been studied.

II. METHOD OF TREATMENT

The outstanding peculiarity of the deuteron is its relatively low binding energy of about $I=2.18$ Mev and the concomitant wide average separation of its constituents, about

$$1/2\alpha=\hbar/2(MI)^{\frac{1}{2}}=2.2\times10^{-13}\text{ cm}.$$

This wide separation is the dominant feature in deuteron reactions and accounts for the preponderance of the stripping process. For it is statistically rather unlikely that the two particles of the deuteron will arrive simultaneously at the surface of the nucleus; the first particle to arrive may be immediately absorbed by the nucleus, abandoning the second particle which will usually escape without encountering the nucleus, especially if it is the proton under the action of the repulsive Coulomb field.

Previous treatments of the Oppenheimer-Phillips process[4-6] take as a point of departure the usual perturbation formula for the cross section. Unfortunately, the corresponding matrix element includes nuclear wave functions and a nuclear potential for which no explicit expressions are known. The unknown factors may be evaluated approximately in terms of the neutron sticking probability ξ_n, derived from considering the absorption cross section when the target

[2] H. E. Tatel and J. M. Cork, Phys. Rev. **71**, 159 (1947).
[3] J. M. Cork, Phys. Rev. **70**, 563 (1946).
[4] J. R. Oppenheimer and M. Phillips, Phys. Rev. **48**, 500 (1935).
[5] H. A. Bethe, Phys. Rev. **53**, 39 (1938).
[6] G. M. Volkoff, Phys. Rev. **57**, 866 (1940).

nucleus is bombarded with a beam of fast neutrons. Of course, the sticking probability is a quasiclassical notion depending for its validity on the statistical behavior of the nucleus.

In the present study, quasiclassical concepts like ξ_n are used directly in setting up the problem, instead of entering in the evaluation of formal expressions which cannot be computed analytically. The statistical methods for dealing with nuclear behavior have been discussed by several authors;[1,7,8] we shall follow the outline of reference 1. Because of the short range and great intensity of nuclear forces, it is possible to consider the nucleus as having a fairly well-defined boundary, i.e., as a classical sphere of radius $R=r_0A^{\frac{1}{3}}$ if A is the mass number of the nucleus. The most popular value at present is about $r_0=1.5\times10^{-13}$ cm, although sizable fluctuations from this mean may be apparent in particular nuclei. With this classical notion of the nucleus as a solid sphere, the absorption process for an incident particle naturally decomposes into two stages: (i) first, the penetration of whatever potentials are effective in the region outside the nuclear surface, and (ii) the probability that after reaching the surface the particle will be bound into the nucleus by energy exchange with the other nuclear components. These two stages are not independent, as the probability of absorption at the surface depends on the slope or phase of the incoming wave function, giving rise to resonance phenomena. However, if the reaction involves an average over many resonance levels—as it certainly will in the case of deuteron bombardment—we may, as a first approximation, consider the phase relations at the surface to be purely random. Then one can simply compute factor (i) from well-known wave equations and assign to factor (ii) a parameter ξ which represents the average sticking probability of the particle at the nuclear surface. The sticking probability and the definite radius R are the two classical attributes used to characterize the nucleus.

The same considerations may be applied if the incident beam consists of deuterons instead of elementary particles. Since we neglect the effect on ξ of the phase of the incident wave function, the absorption of a neutron or proton depends simply on its sticking probability and the probability that, as a member of the incident deuteron, it will reach the nuclear surface; if this latter probability is computed with the restriction that the second particle of the deuteron remain *outside* the nucleus, we can obtain the cross section for a one-particle absorption process like the Oppenheimer-Phillips reaction. Furthermore, because of the random phase relations assumed at the nuclear surface, the absorption process is independent of the condition of the abandoned particle, and *vice versa*. In qualitative terms, the nucleus is simply assumed to "snatch up" the first particle of the deuteron which it encounters, while the second particle is abandoned in whatever state it happens to find itself at the time and generally escapes without striking the nucleus. An advantage of this approach to deuteron-induced reactions is that it seems to be free of embarrassment in application to deuteron energies at or above the Coulomb barrier. If we can find satisfactory wave functions for the region external to the nucleus, the validity of the method proposed should not alter greatly with increased energy—at least until the point where the nucleus begins to break up under the impact, which requires on the order of hundreds of Mev. The argument is equally applicable to *d-p* or *d-n* reactions, so the stripping process is expected to be of importance in both.

Suppose a beam of elementary particles like protons, for example, is incident on the nucleus. At very high energies the effect of the Coulomb barrier is negligible, and the geometrical cross section of the nucleus in the beam will be πR^2. The absorption cross section is then $\xi_p\pi R^2$ where ξ_p is the sticking probability of the protons. We assume that at lower energies the cross section decreases in a manner proportional to the average density $\rho_p(R)$ of the protons at the nuclear surface, so that

$$\sigma_{\text{abs}}=\xi_p\pi R^2\rho_p(R). \tag{1}$$

If the wave function $\varphi_i(r,\theta)$ represents a plane wave of unit amplitude of protons in the Coulomb field, we average over all angles to get

[7] E. J. Konopinski and H. A. Bethe, Phys. Rev. **54**, 130 (1938).
[8] V. F. Weisskopf, Phys. Rev. **52**, 295 (1937).

the mean density at the nuclear surface:

$$\rho_p(R)=1/4\pi\int|\varphi_i(R,\theta)|^2d\omega,$$

where $d\omega$ is the element of solid angle. As the incident energy $E_d\rightarrow\infty$, $\varphi_i\rightarrow\exp[i\mathbf{k}\cdot\mathbf{r}]$ and $\sigma_{abs}\rightarrow\xi_p\pi R^2$ as mentioned before; and, of course, for a plane wave of neutrons, $\varphi_i=\exp[i\mathbf{k}\cdot\mathbf{r}]$ for all energies and $\rho_n(R)$ is always unity. Notice that no angular momentum restrictions are imposed: at these high energies the nucleus is assumed able to absorb particles of all angular momenta with equal ease.

This form for σ_{abs} at once invites extension to the case where deuterons are the incident particles. For instance, we may wish to compute the absorption cross section for neutrons, while the proton is allowed to escape unscathed: this is the *d-p* stripping cross section. Then we have

$$\sigma_{dp}=\xi_n\pi R^2\rho_n(R), \tag{2}$$

where $\rho_n(R)$ is the average density of neutrons at the surface of the nucleus, supplied by deuterons whose protons are outside the nucleus. Thus, if the wave function for an incident plane wave of deuterons, normalized to unit amplitude at infinity, is $\varphi_i(\mathbf{r}_n,\mathbf{r}_p)$, we have

$$\rho_n(R)=\int_{p>R}dV_p\int(d\omega_n/4\pi)|\varphi_i(\mathbf{R},\mathbf{r}_p)|^2. \tag{3}$$

As in the case of bombardment with elementary particles, we do not analyze φ_i into terms corresponding to angular momentum $l\hbar$, because the nucleus is assumed to assimilate all angular momenta. For this reason it is also not necessary to consider the intrinsic spin moments of the neutron and proton. The tensor forces in the deuteron have been omitted as a refinement incommensurate with the approximations used here.

Although the preceding discussion supposes that the neutron is captured and the proton freed, the reverse case is exactly analogous, in which the proton is absorbed and the neutron escapes. Then we should have

$$\sigma_{\text{reverse}}=\pi R^2\xi_p\rho_p(R),$$

where the density of proton at the nucleus is

$$\rho_p(R)=\int_{r_n>R}dV_n\int(d\omega_p/4\pi)|\varphi_i(\mathbf{r}_n,\mathbf{R})|^2. \tag{4}$$

The density $\rho_p(R)$ is expected to be always less than the corresponding $\rho_n(R)$, as the proton has to penetrate less deeply into the Coulomb field in the latter case.

To evaluate the factor $\rho_n(R)$, we must find an expression for the wave function $\varphi_i(\mathbf{r}_n,\mathbf{r}_p)$. It is usual to introduce the relative and center of gravity coordinates, $\mathbf{s}=\mathbf{r}_p-\mathbf{r}_n$, $\mathbf{S}=\frac{1}{2}(\mathbf{r}_p+\mathbf{r}_n)$; then the wave function $\varphi_i(\mathbf{s},\mathbf{S})$ satisfies the equation

$$[(\hbar^2/4M)\nabla_S^2+(\hbar^2/M)\nabla_s^2+E-I-V_0(s)-Ze^2/|\mathbf{S}+\tfrac{1}{2}\mathbf{s}|]\varphi_i(\mathbf{s},\mathbf{S})=0, \tag{5}$$

where M is the proton or neutron mass, E is the kinetic energy of the deuteron, $I=2.18$ Mev is its binding energy, and $Ze^2/|\mathbf{S}+\frac{1}{2}\mathbf{s}|=Ze^2/r_p$ is the Coulomb repulsive potential of the nucleus, acting solely on the proton. The potential $V_0(s)$ represents the specifically nuclear forces between the neutron and proton and is taken to be a simple scalar potential dependent on the separation distance alone. We look for approximate solutions of this equation, among which the simplest are the following. The first and most obvious choice is approximation (a): the deuteron center of gravity motion is assumed to be given by the wave function $\varphi_c(\mathbf{S})$ for a plane wave in a Coulomb field, while the internal coordinate is described by the wave function $\chi_0(\mathbf{s})$, the solution for the bound state unperturbed by the Coulomb field,

$$[\hbar^2/M\nabla_s^2-I-V_0(s)]\chi_0(\mathbf{s})=0. \tag{6}$$

This implies that the most important factor determining the reaction is the "natural spread" of the deuteron due to its low binding energy, for it completely neglects the effect of the charge asymmetry of the deuteron in the Coulomb field, according to which the proton is less likely to reach the nuclear surface than the neutron. This neglect entails a serious objection, since it means that the *d-p* and *d-n* stripping cross sections would be the same for a given nucleus at all energies. Actually, however, the *d-p* cross section markedly exceeds the *d-n* cross section, especially at low energies.

An attempt to improve the zero-order approximation (a) leads to the so-called adiabatic approximation (b). The wave function cor-

responding to approximation (a) does not satisfy Eq. (5) but leaves a remainder term proportional to $(Ze^2/S)-(Ze^2/|\mathbf{S}+\frac{1}{2}\mathbf{s}|)$, which represents the Coulomb energy difference between the positions of the proton and center of gravity. This remainder term is introduced as an additional potential energy into Eq. (6) for the internal motion of the deuteron, and the center of gravity wave function remains $\varphi_c(S)$ as before; this amounts to assuming that all the Coulomb energy gained by the proton in moving out from the center of gravity position goes into distorting the internal motion of the duteron. As this would be true only if the center of gravity remained fixed in position, the accuracy of the adiabatic approximation is somewhat problematical. The adiabatic internal function cannot be found in closed form, although the W.K.B. approximation is available for the case in which the neutron and proton are collinear with the nucleus. This solution cannot be handled analytically, however.

In both solutions (a) and (b) the appearance of $\varphi_c(S)$ implies that the internal motion of the deuteron is much more rapid than its passage through the Coulomb field, so that the average center of charge coincides with the center of gravity. This in turn implies a high binding energy and narrow intrinsic spread of the deuteron, which is almost the reverse of the truth. Approximation (b) is further inconsistent by distorting the internal motion so that the centers of charge and of gravity do not coincide, while continuing to treat the external motion as if they did.

A third approximation (c) suggests itself as the antithesis of the previous two: assume that the internal motion of the deuteron is much *slower* than its passage through the Coulomb field, or at least through that part of the field where the neutron has an appreciable probability of striking the nucleus. This is reasonable at high incident energies, and in the extreme limit it describes the deuteron behavior as that of a rigid framework which maintains a fixed magnitude and orientation as it traverses the Coulomb field. The distribution of this magnitude and orientation is specified by χ_0^2. Thus, the Coulomb wave function applies to the proton coordinate, and the incident wave function is $\varphi_i=\varphi_c(\mathbf{r}_p)\chi_0(\mathbf{s})$. The wave function φ_c, however, still refers to a particle of mass $2M$ as long as the deuteron is not dissociated by photoelectric action of the Coulomb field. Such a photoelectric process is of second order relative to the reaction considered here, so that it may be neglected. With this neglect, we have approximation (c) for the incident wave function: $\varphi_i=\varphi_c(\mathbf{r}_p)\chi_0(\mathbf{s})=\varphi_c(\mathbf{r}_p)\chi_0(\mathbf{r}_n-\mathbf{r}_p)$. This approximation has the cardinal advantage of being very tractable analytically.

We may now write an explicit form for $\rho_n(R)$. Substituting approximation (c) into Eq. (3), we have

$$\rho_n(R)=\int_{r_p>R}|\varphi_c(\mathbf{r}_p)|^2(dV_p/4\pi)\times\int d\omega_n|\chi_0(\mathbf{R}-\mathbf{r}_p)|^2. \quad (7)$$

The second integral, over the nuclear surface, can be performed at once by assuming the usual square-well model for the potential $V(s)$. We obtain

$$\int|\chi_0|^2d\omega_n=(\alpha/r_pR)(e^{2\alpha a}/(1+\alpha a))\times\{F[2\alpha(r_p-R)]-E[2\alpha(r_p+R)]\}, \quad (8a)$$

where the assumed radius of the square-well potential is $a=2.8\times10^{-13}$ cm, and

$$\begin{aligned}F(x)=E(x)&=\int_x^\infty\frac{dt}{t}e^{-t} \qquad \text{for } x\geq2\alpha a,\\ &=E(2\alpha a)+\tfrac{1}{2}e^{-2\alpha a}[\ln(2\alpha a/x)\\ &\quad+Ci(2\alpha a\pi/x)-Ci(\pi)] \quad \text{for } x\leq2\alpha a.\end{aligned} \quad (9)$$

Here

$$Ci(x)=-\int_x^\infty(\cos t/t)dt,$$

and the numerical factor $e^{2\alpha a}/(1+\alpha a)$ has the value 1.59. For nuclei with $2\alpha R>2$,

$$F[2\alpha(r_p-R)]\gg E[2\alpha(r_p+R)],$$

so we may take

$$\int|\chi_0|^2d\omega_n=(\alpha/r_pR)(e^{2\alpha a}/(1+\alpha a))\times F[2\alpha(r_p-R)]. \quad (8b)$$

Substituting in Eq. (7), with $dV_p/4\pi=r_p^2dr_p$, we

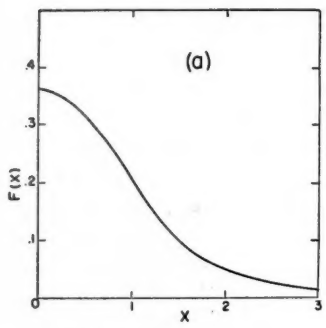

FIG. 1a. The average of the internal function over the nuclear surface,
$\int |\chi_0|^2(d\omega_n/4\pi) \approx F[2\alpha(r_p-R)]$.

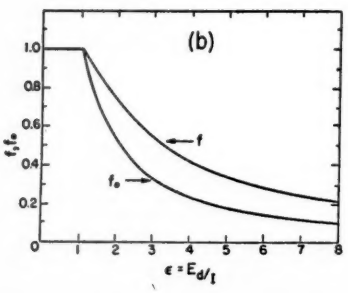

FIG. 1b. The reduction factors due to energy distribution of the stripped particle. The upper curve is $f(E_d)$ for d–p stripping; the lower curve f_0 is just $f'(E_d)$ for d-n stripping, computed for the case that $E_d' = E_d - Ze^2/R \leq 0$. In case $E_d' > 0$, a rough approximation if
$f'(E_d) = f(E_d) - Ze^2/E_dR[f(E_d) - f_0(E_d)]$.

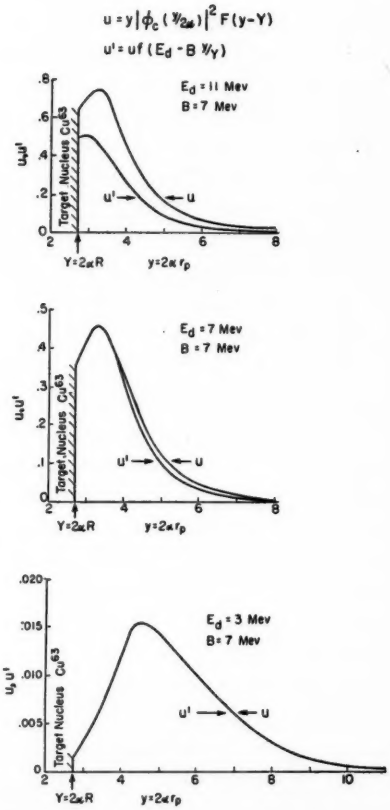

FIG. 1c. Comparison of integrand functions for $\rho_n(R)$ for Cu^{63}, at deuteron energies $E_d = 3$, 7, and 11 Mev; the nuclear barrier height is $B = 7$ Mev. Function u is without correction for d-pn competition as calculated from energy distribution of stripped protons; function u' is reduced by this correction.

obtain finally

$$\rho_n(R) = 0.8\int_Y^\infty (ydy/Y)\,|\varphi_c(y/2\alpha)|^2 F(y-Y), \quad (10)$$

where $y = 2\alpha r_p$, $Y = 2\alpha R$. For the purpose of computation, a curve of $F(x)$ is presented in Fig. 1a. For the factor $|\varphi_c|^2$ representing the deuteron plane wave in the Coulomb field, the expressions in Konopinski and Bethe[7] were used. No angular momentum restrictions were imposed, so that partial waves of all l values were included. In the notation of reference (7),

$$|\varphi_c(r)|^2 = l_c^2/l_0^2 = \sum_{l=0}^{\infty} (2l+1)P_l(r)/(kr)^2,$$

representing the intensity at a position r of a beam of unit intensity at infinity. The variation of ρ_n with E_d for a particular nucleus is to be obtained by integrating graphically Eq. (10). The expressions used tend to overestimate $|\varphi_c|^2$ at high energies, so that our computed $\rho_n(R)$ will also be somewhat too large for high E_d.

Equation (10) is not complete, for it is necessary to consider the effect of the energy distribution of the liberated protons. Although we have assumed no coherence between the neutron absorption process and the final proton state, conservation of energy requires that if the neutron is to be captured in a negative energy state (and essentially only such neutrons will contribute to the observed d-p activity, the rest causing re-emission in a d-pn reaction), the proton must escape with an energy E_p for which $E_d - I \leq E_p \leq E_d - I + E_0$. Here E_0 is the maximum binding energy of the neutron in the residual nucleus, taken in these calculations to be $E_0 = 3.5I = 7.6$ Mev. This range represents only a fraction

of the total proton spectrum, so that the effective $\rho_n(R)$ must be somewhat reduced from the expression calculated above.

By virtue of the assumption that the absorption process is very rapid and of random phase relative to the deuteron's internal motion, we can, in first approximation, take the proton energy to be specified simply by its membership in the deuteron. For a deuteron in the absence of a Coulomb field, moving with kinetic energy E_d and wave vector $\mathbf{K}$, the usual Fourier inversion shows that the proton has a momentum distribution

$$P(\mathbf{k})d\mathbf{k} \sim k^2 dk d\Omega/[\alpha^2+|\tfrac{1}{2}\mathbf{K}-\mathbf{k}|^2]^2, \quad (11)$$

where $K^2=4ME_d/\hbar^2$, $k^2=2ME_p/\hbar^2$, $\alpha^2=MI/\hbar^2$. Integrating over the solid angle $d\Omega$ and expressing the results in terms of energy,

$$P(E_p)dE_p \sim E_p^{\frac{1}{2}}dE_p/[I+2E_p-E_d]^2+4IE_d. \quad (12)$$

To carry this over to the deuteron in a classically accessible region of the Coulomb field, we assume that an equation of the form (12) applies, except that the zero point of the energy scale is shifted by an amount Ze^2/r_p for E_p and E_d, so that the effective distribution is

$$P(E_p')dE_p' \sim E_p'^{\frac{1}{2}}dE_p'/[I+2E_p'+E_d']^2+4IE_d', \quad (13)$$

with

$$E_p'-E_p=E_d'-E_d=Ze^2/r_p. \quad (14)$$

This is based on the classical idea that the energy Ze^2/r_p is stored by the incident deuteron in the Coulomb field and is regained by the proton as it escapes to an infinite distance, but is therefore not available when the deuteron breaks up at r_p. Then for a given proton position r_p at breakup, the fraction of escaping protons corresponding to neutrons captured in negative energy states is

$$f(E_d')=\frac{\int_{E_d'-I}^{E_d'-I+E_0} P(E_p')dE_p'}{\int_0^{E_d'-I+E_0} P(E_p')dE_p'}. \quad (15)$$

For a given incident energy, E_d' decreases and $f(E_d')$ increases as r_p moves in from infinity; and $f(E_d')$ reaches the value unity at $r_p=r_0$, where $E_d-Ze^2/r_0=I$. From this point on we take $f\equiv 1$, $r_p\leq r_0$. This means that the proton is assumed always to seize enough energy to escape without having to penetrate through a Coulomb barrier, and this condition requires that all neutrons be left bound in the nucleus if the reaction occurs at $r_p\leq r_0$.

This method of estimating the energy distribution of the released protons is admittedly crude but should impart at least the right direction to our results. The estimate is somewhat biased toward the high energy end of the proton spectrum, because no allowance is made for the possibility that the proton may penetrate out through the Coulomb barrier. This means that we overestimate the percentage of low energy neutrons and hence the observed cross section. The reduction factor $f(E_d)$ is plotted in Fig. 1b.

We have also assumed that all the stripping protons will escape without further encounter, whereas actually a small fraction of them will subsequently reach the nucleus and be absorbed. This effect is equivalent to absorption of the deuteron as a whole, and its inclusion would therefore reduce the computed cross section for stripping. At incident energies on the order of the target barrier height B, however, this is a second-order effect, although for $E_d \gg B$, it greatly reduces[9] the stripping cross section from about $\pi/2R^2$ to $\pi R/4\alpha$. Furthermore, at low E_d the reduction in d-p stripping appears to be roughly compensated by the d-p contribution from the direct reaction, so that to a first approximation the entire d-p cross section may be computed from Eq. (2) above.

Accordingly, we write

$$\sigma_{dp}=\pi R^2 \xi_n \rho_n(R), \quad (16)$$

$$\rho_n(R)=0.8\int_Y^\infty dy(y/Y)\,|\varphi_c(y/2\alpha)|^2 \times F(y-Y)f(E_d-B(y/Y)),$$

where $B=Ze^2/R$ is the Coulomb barrier of the target nucleus. The effect of the factor $f(E_d')=f(E_d-BY/y)$ is illustrated in Fig. 1c, where the integrand of ρ_n for Cu^{63} is plotted for several values of E_d. The reduction is negligible for low E_d, and of predominant importance for energies above the barrier height of 7 Mev, where it

[9] R. Serber, Phys. Rev. **72**, 1114 (1947).

accounts for the decline of σ_{dp} with increasing energy. Each curve displays a fairly sharp peak, which persists for E_d well above the barrier height, because the increase of $|\varphi_c(r_p)|^2$ with r_p in the neighborhood of R is still strong for these energies if all values of l are included in $|\varphi_c|^2$. The variation of these peak values with E_d is not a good approximation to the variation of ρ_n because of the variable width of the curves, as illustrated in Fig. 1c.

The present method of treatment has been discussed in terms of the *d-p* reaction, because it has been more extensively studied than the *d-n* reaction, which has generally been tacitly assumed to proceed entirely by direct absorption of the deuteron. Application of the same approach to the *d-n* case, however, indicates that an appreciable or even major fraction of the observed cross section is again due to a stripping process. In an analogous fashion to that above, the *d-n* stripping cross section is

$$\sigma_{dn}=\pi R^2\xi_p\rho_p(R), \tag{17}$$

where ξ_p is the proton-sticking probability. The proton density at the nuclear surface is

$$\begin{aligned}\rho_p(R)&=\int_{r_n>R}dV_n\int(d\omega_p/4\pi)\,|\,\varphi_i(\mathbf{r}_n,\mathbf{R})\,|^2\\&=\int(d\omega_p/4\pi)\,|\,\varphi_c(\mathbf{R})\,|^2\\&\quad\times\int_{r_n>R}dV_n|\,\chi_0(\mathbf{r}_n-\mathbf{R})\,|^2 \qquad (18)\\&\approx|\,\varphi_c(R)\,|^2[\tfrac{1}{2}+((1-e^{-4\alpha R})/8\alpha R)]\\&=|\,\varphi_c(R)\,|^2F_0(R),\end{aligned}$$

where $F_0(R)$ is simply the fraction of deuterons whose neutrons happen to lie outside the nucleus when the proton arrives at the surface.

Some of these neutrons will subsequently strike the nucleus and be absorbed, but at low E_d such absorption will most probably be followed by single neutron emission, so that the *d-n* stripping cross section will not be much reduced by this effect which is neglected in Eq. (18). At very high E_d, however, the *d-n* and *d-p* stripping cross sections are reduced in the same manner.[9] Therefore, although our absolute σ_{dp} and σ_{dn} may not be valid for $E_d\gg B$, the ratio σ_{dp}/σ_{dn} should remain correct to first order for all energies.

This also permits us a crude means of estimating the cross section for the absorption of the entire deuteron: without allowing for the detailed, compound nature of the process, these simple geometrical considerations would indicate that the cross section for formation of a compound nucleus with the addition of the entire deuteron is, for E_d comparable with B,

$$\sigma_d=\pi R^2\xi_p|\,\varphi_c(R)\,|^2[1-F_0(R)], \tag{19}$$

corresponding to the condition that the neutron is *inside* the nucleus when the proton arrives at the surface and is also absorbed. Since $F_0(R)>1-F_0(R)$ for finite R, it is expected that even for the *d-n* reaction the stripping process will roughly equal the direct absorption, although the ratio of compound nucleus formation by the two methods is only

$$\begin{aligned}F_0(R)/1-F_0(R)&\approx(1+1/4\alpha R)/(1-1/4\alpha R)\\&\approx1+1/2\alpha R=1.2\text{–}1.5,\end{aligned}$$

so that the disparity is of a much lower order than in the *d-p* reactions.

For high deuteron energies (above 10 Mev) the observed *d-n* activity is almost entirely due to stripping because the compound nucleus which has absorbed the whole deuteron is so highly excited that single particle emission is much less probable than the stripping process in which a proton is retained. In the *d-n* stripping reaction, we must also apply a reduction factor $f'(E_d)$ to account for the fact that the observed cross section is produced only by protons that are absorbed into the nucleus with energies less than E_0 above the ground state, for otherwise, a neutron is almost certain to be emitted, and a *d-2n* reaction will be observed instead. In this case, however, the escaping particle is not subject to the Coulomb field. Therefore, to specify the neutron energy distribution $P'(E_n)$, we replace E_p by E_n in Eq. (12) and E_d by $E_d'=E_d-Ze^2/r_p=E_d-Ze^2/R$ (or by zero if $E_d\leq Ze^2/R$, the nuclear Coulomb barrier). The reduction factor $f'(E_d)$ is then determined from $P'(E_n)$ in the same manner as $f(E_d)$ from $P(E_p)$. In Fig. 1b, the curve designated as $f_0(E_d)$ is the factor $f'(E_d)$ computed for $E_d'\leq0$, the case most frequently

encountered for heavy targets. If $E_d'>0$, one may take as a crude approximation

$$f'(E_d)\approx f_0(E_d)+(E_d'/E_d)[f(E_d)-f_0(E_d)]$$
$$=f(E_d)-Ze^2/E_dR[f(E_d)-f_0(E_d)].$$

The total *d-n* cross section to be observed from stripping is then

$$\sigma_{dn}=\pi R^2\xi_p|\varphi_c(R)|^2F_0(R)f'(E_d). \quad (20)$$

For incident deuteron energies well below the barrier height, the dominant factor in expressions 19 and 20 is $|\varphi_c(R)|^2$, and hence the decrease in the observed σ_{dn} with decreasing E_d is sharper than for the corresponding σ_{dp}. This also means that a quantitative fit with experimental cross sections at $E_d\lesssim B$ is more sensitive to the choice of R for *d-n* than for *d-p* reactions, so that Eq. (20) should be used to fit experimental curves only over a wide energy range. As in the *d-p* reaction, the *d-n* curve will show a maximum in the neighborhood of the barrier height. As E_d increases beyond this point, the contribution of the direct *d-n* reaction is generally negligible; while the decreasing factor $f'(E_d)$ and the increasing factor $|\varphi_c(R)|^2$ of Eq. (20) are more equally balanced than in the corresponding *d-p* formula. Therefore, the observed *d-n* curves should decline more slowly than the *d-p* for energies above their peaks. It is also clear that the ratio σ_{dp}/σ_{dn} should, in general, exceed unity; for example, compare the expressions (16) and (20) for σ_{dp} and σ_{dn} from stripping at $E_d\approx B$:

$$\sigma_{dp}/\sigma_{dn}=\xi_n/\xi_p\cdot\rho_n/\rho_p. \quad (21)$$

The terms ρ_n and ρ_P are computed in the same way, except that where $|\varphi_c(r)|^2f(E_d')$, $r\geq R$ occurs in the integrand for ρ_n, it is replaced by $|\varphi_c(R)|^2f'(E_d)$ in the integrand for ρ_p. Since

$$f'(E_d)<f(E_d)\leq f(E-Ze^2/r),$$

and $|\varphi_c(r)|^2>|\varphi_c(R)|^2$ for $r>R$, and ξ_p and ξ_n should generally be of the same order of magnitude, we have

$$\sigma_{dp}/\sigma_{dn}\gg\xi_n/\xi_p\approx 1 \quad (22)$$

for incident deuteron energies comparable with the nuclear barrier height. At low deuteron energies, the direct *d-n* reaction will also contribute to σ_{dn}; but this will no more than double the σ_{dn} computed from stripping alone, so that the inequality (22) still should hold. At very high energies, $|\varphi_c(r)|^2\approx|\varphi_c(R)|^2\approx 1$, and $f'(E_d)\approx f(E_d-Ze^2/r)\to 0$, so that $\rho_p\to\rho_n\to 0$, and $\sigma_{dp}/\sigma_{dn}\to\xi_n/\xi_p$. This suggests the only case in which the observed σ_{dn} might exceed σ_{dp}: if for some nucleus ξ_p happens to exceed ξ_n, then for high energies (E_d several times the barrier height), we may find $\sigma_{dp}/\sigma_{dn}\lesssim 1$. Observations at these energies have not yet been reported even qualitatively, although a study of the σ_{dp}/σ_{dn} ratio in Bi^{209} up to $E_d=18$ Mev. (12) shows that $\sigma_{dp}/\sigma_{dn}>1$ in this energy range.

Of course many-particle reactions induced by deuteron bombardment, such as the *d-2n*, *d-3n*, *d-(p,α)*, *d-(p,2n)*, may also be separated into two components, one due to the formation of the original compound nucleus by a stripping process, the other due to the formation of a different compound nucleus by the absorption of the deuteron as a whole. In these complex reactions, however, the chief determining factor appears to be the level density of the compound nucleus and its behavior in emitting several particles in cascade. Therefore, the method of formation of the compound nucleus is of secondary importance, and an analysis to distinguish between the two modes of formation is scarcely possible with the present limited knowledge of level densities.

III. APPLICATION

Quantitative cross section measurements for deuteron-induced reactions have been made up to the present time only on a limited number of elements, and there mostly for the *d-p* reaction. We compare the formulas obtained above with these measurements.

Figure 2 shows the case of $_{29}Cu^{63}$, using an

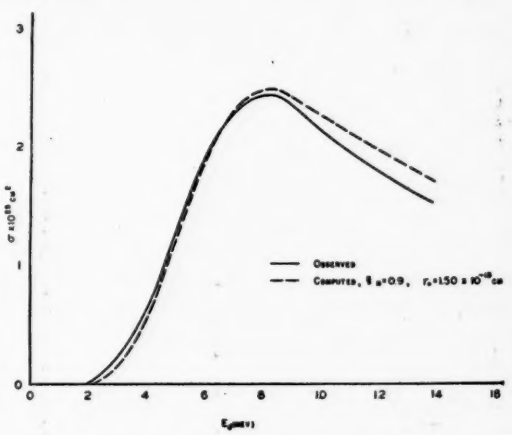

FIG. 2. *d-p* excitation curves for Cu^{63}.

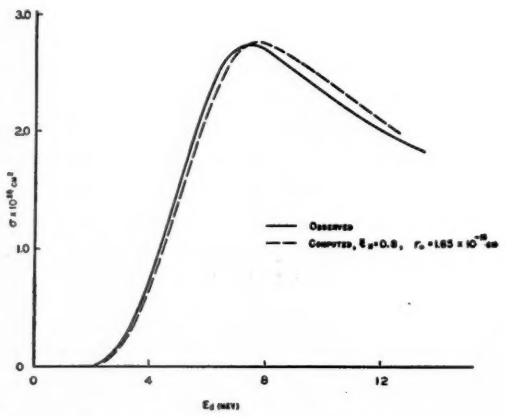

FIG. 3. *d-p* excitation curves for Co^{59}.

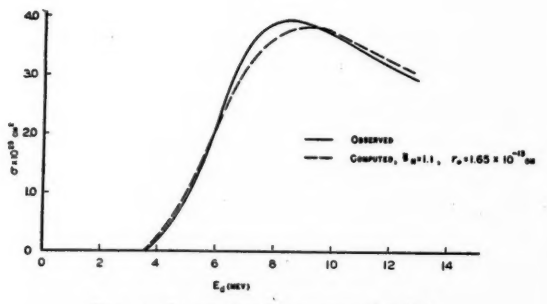

FIG. 4. *d-p* excitation curves for Br^{83}.

unpublished curve measured by Clarke and Irvine. The computed curve was obtained from Eq. (16), using $r_0=1.50\times10^{-13}$ cm, so that the nuclear radius was $R=6.0\times10^{-13}$ cm, and the effective barrier height (corrected by a factor $A+2/A$ for the center-of-gravity motion of the system of deuteron plus nucleus) is (Ze^2/R) eff $=7.0$ Mev. The general features of this curve are typical of all *d-p* excitation functions over wide enough energy ranges: at energies below the barrier, it rises toward a fairly well-defined peak, above which it declines again rather slowly. The rising portion of the curve is relatively flat compared with the excitation curve expected in case the entire deuteron were absorbed by the nucleus; this is due, of course, to the effect of the deuteron's wide natural spread. It is to be noted that the peak of the curve generally occurs at incident energies a Mev or two above the Coulomb barrier, and not at the barrier height itself. This arises from a combination of two factors. Since the expression for $|\varphi_c|^2$ includes the partial waves for all angular momenta, the value of $|\varphi_c|^2$ will continue to increase fairly rapidly with increasing deuteron energy, even above the barrier height. On the other hand, the reduction factor $f(E_d')$, determined by the energy distribution of the escaping protons, begins to become effective only for energies above the Coulomb barrier, and tends to reduce the cross section more and more as the deuteron energy increases. The opposing tendencies of $|\varphi_c|^2$ and $f(E_d')$ therefore result in a maximum that occurs somewhat above the barrier energy; beyond this point, the factor $f(E_d')$ is predominant, and the excitation curve declines. This decline may be thought of as due to competition with the unobservable *d-pn* reaction that follows when the stripping neutron is absorbed with positive energy. An effort has been made to explain this decline at high energies by assuming limitations on the angular momentum[10] so that only the first few partial waves contribute to $|\varphi_c|^2$, but this seems a rather artificial restriction in contrast to the present interpretation.

The computed curve in Fig. 2 is fitted to the observations by assuming a sticking probability of $\xi_n=0.9$. It is at once evident that the agreement is close enough to suggest that practically the entire observed *d-p* cross section is due to this stripping process, and that the contribution of the direct *d-p* reaction may be neglected in first approximation. Indeed, upon examination this direct contribution proves to be very small for all energies of the incident deuteron. This is essentially because at low energies the deuteron has difficulty penetrating as a whole through the Coulomb barrier, and, more important, the proton is inhibited from escaping from the compound nucleus because of the same Coulomb barrier. This unfavorable ratio for *p* emission relative to *n* emission persists up to incident deuteron energies above the barrier height, beyond which appreciable competition begins to occur from the *d-pn* reaction. Thus, the direct *d-p* reaction hardly appears at all, because of strong *d-n* competition at low energies, and (*d*-2 particle) processes at higher energies.

The smallness of the *d-p* reaction may be estimated in a quantitative fashion by using the results of Weisskopf and Ewing[1] on the evaporation model of the nucleus. Equation (19) gives

[10] E. T. Clarke and J. W. Irvine, Jr., Phys. Rev. 66, 231 (1944).

the cross section σ_d for the formation of a compound nucleus by absorption of the entire deuteron; the corresponding *d-p* cross section is then

$$\sigma_{dp}=\sigma_d(\Gamma_p/\Gamma)(\epsilon), \quad (21)$$

where Γ_p and Γ are the proton and total emission widths and ϵ is the maximum kinetic energy with which the proton may be emitted. If the energy of the incident deuteron is E_d and the neutron binding energy is $E_0=8$ Mev, we have

$$\epsilon=E_d+E_0-I=E_d+6 \text{ Mev}.$$

For $E_d=9$ Mev, $\epsilon=15$ Mev, and from Fig. 2 of reference 1 we find $\Gamma_p/\Gamma(15 \text{ Mev})=0.05$; and at this energy $|\varphi_c(R)|^2=0.5$. Also, for Cu^{63}, $1-F_0(R)=0.4$, and we take $\xi_p=\xi_n=0.9$ as already determined. Then the direct *d-p* cross section for Cu^{63} at 9 Mev is, according to Eqs. (19) and (21),

$$\sigma_{dp}=\pi R^2\xi_p|\varphi_c(R)|^2(\Gamma_p/\Gamma)[1-F_0(R)] =0.1\times10^{-25} \text{ cm}^2.$$

This is less than five percent of the observed cross section at this energy, and the percentage will decrease at lower energies as Γ_p/Γ becomes less favorable and $|\varphi_c(R)|^2$ diminishes. At a high energy like $E_d=15$ Mev, on the other hand, we must be concerned with competition from the *d-pn* reaction. The relative probability of single proton emission is, according to the statistical formula, approximately

$$f_p=(1+(\Delta\epsilon'/T_B'))\exp[-\Delta\epsilon'/T_B'], \quad (22)$$

with

$$\Delta\epsilon'=\epsilon-V-E_0=(E_d+6)-V-8=E_d-9$$

with $V=7$ Mev, the Coulomb barrier of the nucleus. $T_B'=T_B(\epsilon-V)=2[5(E_d-1)/A_{Cu}]^{\frac{1}{2}}$. For Cu^{63} at $E_d=15$ Mev, we have $\Delta\epsilon'=6$, $T_B'=2.1$, so $f_p=0.2$. The other factors in σ_{dp} remain the same, except for $|\varphi_c(R)|^2$, which has increased to 0.8, and Γ_p/Γ (21 Mev), which may be estimated as about 0.1. Then the direct *d-p* cross section is

$$\sigma_{dp}=\pi R^2\xi_p|\varphi_c(R)|^2[1-F_0(R)](\Gamma_p/\Gamma)f_p =0.07\times10^{-25} \text{ cm}^2,$$

again about five percent of the observed cross section. This percentage will now decrease with increasing energy, as the direct reaction cross section will be dominated by the $\exp[-\Delta\epsilon'/T_B']$ factor for single proton emission.

In Figs. 3 and 4 are shown similar comparisons of observed and computed curves for $_{27}Co^{59}$ [11] and $_{35}Br^{81}$.[10] In each case the computed curves show only the cross section expected from stripping; the values of ξ_n used to fit the curves were $\xi_n=0.8$ for cobalt and $\xi_n=1.1$ for bromine. These cases show no distinctive features, except that for both elements it was necessary to assume $r_0=1.65\times10^{-13}$ cm to fit the experimental curves. The computed curves are not particularly sensitive to variations in r_0 because of the smoothing effect of the integrations involved but, as in these cases, it should be possible to assign a value for r_0 to within ten percent from comparison with experiment.

The *d-p* reaction has been studied quantitatively[11] for one light element, $_{11}Na^{23}$. Although the statistical attitude underlying our formulation may not be valid in this case, it is of interest to see how closely the curve computed on this basis may resemble the observations. In Fig. 5 are shown the excitation curves: the computed curve involves only the *d-p* stripping process with an assumed $r_0=1.50\times10^{-13}$ cm, and a value of $\xi_n=1.8$. The agreement in shape of the curves is quite good, except at very low energies, but agreement in magnitude is achieved only by taking $\xi_n=1.8$, whereas from its definition we should expect $\xi_n\leq1$. Of course, some irregularity in the effective ξ values is expected for light nuclei, where the conditions for definition of the sticking probability as an independent nuclear

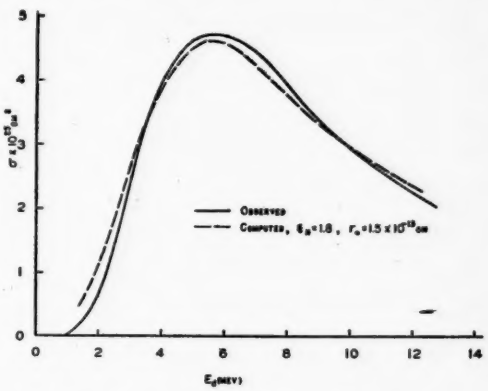

FIG. 5. *d-p* excitation curves for Na^{24}.

[11] E. T. Clarke and J. W. Irvine, Jr., unpublished.

parameter are least likely to be satisfied. A possible explanation might be that for such a light nucleus the *d-p* reaction by direct absorption would make a strong contribution. In the particular case of Na^{23}, however, it appears that the direct reaction is again negligible. It happens that the binding energy of a proton in the Mg^{24} nucleus is about 3.7 Mev greater than the binding energy of a neutron in the Na^{24} nucleus; in addition, the proton must overcome a 4-Mev Coulomb barrier in escaping. Thus, in an excited Mg^{25} nucleus there is effectively some 7.7 Mev more energy available for the emission of a neutron than of a proton, so that the direct *d-n* reaction is expected to overwhelm the *d-p* until incident deuteron energies are reached at which two-particle emission becomes prominent. For a very rough estimate of the σ_{dp}/σ_{dn} ratio we may use the statistical model as employed in reference 1; this shows that σ_{dp} (direct) $<0.05\times\sigma_{dp}$ (stripping) at $E_d=6$ Mev, the peak of the observed curve. Thus the stripping mechanism is expected to account for practically all the observed *d-p* cross section on Na^{23}. The sticking probability in this case might be reduced to approximately unity by taking $r_0\approx1.8\times10^{-13}$ cm; this would shift the peak of the computed curve to around 0.5 Mev lower energy.

The only heavy element for which a thorough quantitative study has been made on deuteron-induced reactions is Bi^{209}. Figure 6 shows the computed curves for both the *d-p* and *d-n* cross sections, as compared with a recent set of observations reported by E. Segrè.[12] For both

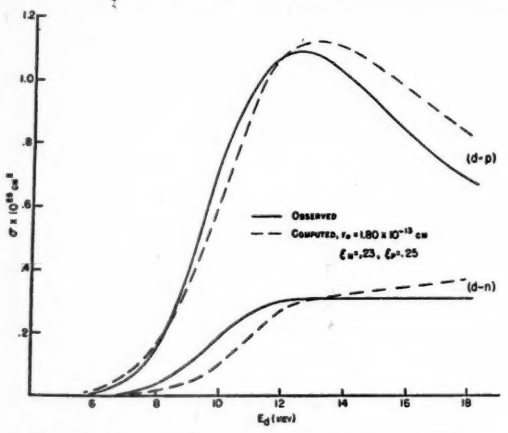

FIG. 6. *d-p* and *d-n* excitation curves for Bi^{209}.

[12] E. Segrè, unpublished.

TABLE I. Sticking probabilities.

Element	ξ_n	Element	ξ_n
Pt^{196}	0.2	Tl^{205}	0.5
Pt^{198}	0.4	Pb^{208}	0.3
Au^{197}	0.3	Bi^{209}	0.1
Hg^{196}	1.7	Th^{232}	0.2
Hg^{204}	0.3	U^{238}	0.2

computed curves a standard radius of $r_0=1.80\times10^{-13}$ cm was assumed, leading to a nuclear radius of $R=10.7\times10^{-13}$ cm. The values of the sticking probabilities were taken as $\xi_n=0.23$ and $\xi_p=0.25$ for the σ_{dp} and σ_{dn} curves, respectively. In computing the σ_{dn} curve with Eq. 20, the additional assumption was made that the threshold for a $Bi^{209}(p, n)Po^{209}$ reaction is some 2–3 Mev, in accordance with the presumed great instability of the Po^{209} nucleus. Only the component from the stripping process was considered in computing the σ_{dn} as well as the σ_{dp} curve; the direct *d-n* reaction is expected to encounter not only *d-2n* competition at energies around $E_d=10$ Mev, but strong *d-α* competition at all observable energies, as the compound Po^{211} is a very likely α-emitter.

The *d-p* and *d-n* reactions on Bi^{209} have previously been studied[3] at energies up to 14 Mev in an effort to determine the point at which the ratio σ_{dp}/σ_{dn} fell below unity, in accordance with the view that the Oppenheimer-Phillips supremacy of the *d-p* reaction would vanish as E_d approached the nuclear Coulomb barrier. This expectation is not fulfilled experimentally, and the present treatment indicates that since for Bi^{209} $\xi_p\approx\xi_n$ the observed ratio σ_{dp}/σ_{dn} will exceed or equal unity for all deuteron energies. This ratio approaches ξ_n/ξ_p as $E_d\rightarrow\infty$, so that the σ_{dp} and σ_{dn} curves will cross only at high E_d and only in the fortuitous (for this simple theory) circumstance that $\xi_n/\xi_p<1$.

This exhausts the list of elements for which quantitative excitation curves are available over a wide range of energies. Another set of measurements has been published[13,14] on quantitative cross sections for a series of heavy elements at the relatively low energies of $E_d=6$–9 Mev. The

[13] R. S. Krishnan and E. A. Nahum, Proc. Roy. Soc. **A180**, 321 (1942).

[14] R. S. Krishnan and E. A. Nahum, Proc. Roy. Soc. **A180**, 332 (1942).

shapes of the curves over this narrow region are not particularly informative, but in Fig. 7 are shown a couple of typical cases, the d-p excitation functions for Au^{197} and Th^{232}, representing examples from each end of the range of elements studied. For all calculations on these elements, a standard radius of $r_0=1.50\times10^{-13}$ cm was assumed, and the stripping reaction only was considered. The observed and computed curves for all intervening elements lie between these respective limiting cases, except for Bi^{209}, where these authors report an exceptionally steep curve, markedly steeper than that for any other element. Just for Bi^{209}, however, there exists an independent set of measurements over the same energy range,[2] which by contrast show a normal excitation curve with slope similar to that of the computed functions.

The quantitative values given in reference 14 may be used to calculate the corresponding sticking probabilities for the elements concerned; these are shown in Table I.

The corresponding ξ_p values were not computed from the few cross sections given for σ_{dn}, because at $E_d=9$ Mev the results are extremely sensitive to the choice of nuclear radius, and it is not certain that the contribution from the direct reaction is negligible. A reasonable value of ξ_p could be obtained only from fitting a quantitative curve over an energy range exceeding the barrier height of the nucleus, as in the case of Bi^{209}.

The ξ_n values were all fitted to the experimental cross sections reported at 9 Mev, using Eq. (16) for the cross sections due to the stripping process alone. The direct d-p reaction can be neglected as usual. These values for ξ_n are not so reliable as those obtained from fitting the over-all curve, as in the case of the lighter elements, because the computed cross sections at 9 Mev—below the barrier height in all cases—are rather sensitive to the value selected for the nuclear radius. There remains, however, the suggestion that the sticking probabilities for the heavy elements are consistently lower than those of the light and medium nuclei, where $\xi_n\approx1$. In this connection, it would be of interest to study the reactions of Table I quantitatively over a wide energy range in order to fix the values of ξ_n with more certainty, and to extend the measurements to elements in the range $83<A<196$.

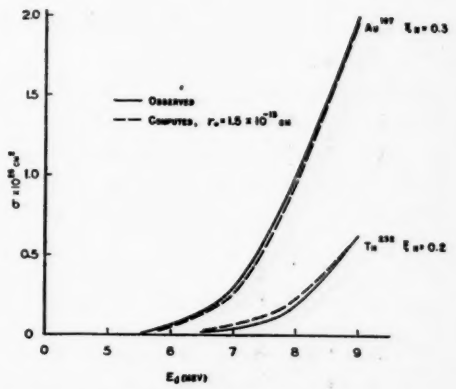

FIG. 7. d-p excitation curves for Au^{197} and Th^{232}.

The values of r_0 used to fit the over-all curves in Figs. 2–6 tend to be larger than the usually assumed value of 1.5×10^{-13} cm. This might be ameliorated by assuming that for d-p stripping to occur the proton must be outside the range of the n-p forces in the deuteron, as well as outside the nuclear surface. The actual radius of the nucleus would then be somewhat smaller than the effective radius appearing in the calculation.

ACKNOWLEDGMENTS

The author wishes to thank Dr. E. T. Clarke and Dr. J. W. Irvine, Jr., for the use of previously unpublished data on Co^{59} and Cu^{63}, and Professor E. Segrè for the opportunity to see the data on Bi^{209} prior to publication. He also wishes to express his appreciation to Professor Victor F. Weisskopf for suggestions and continued advice concerning this problem.*

* This work was supported in part by the Office of Naval Research.

PHYSICAL REVIEW VOLUME 74, NUMBER 9 NOVEMBER 1, 1948

The Binding Energy for a Self-Trapped Electron in NaCl*

JORDAN J. MARKHAM**
Randal Morgan Laboratory of Physics, University of Pennsylvania, Philadelphia, Pennsylvania

AND

FREDERICK SEITZ
Carnegie Institute of Technology, Pittsburgh, Pennsylvania

(Received July 2, 1948)

A calculation has been made of the binding energy of a self-trapped electron in NaCl. The potential well, caused by the ionic displacements, was assumed to be a sawed-off Coulomb field, the sides being given by $(1/\kappa_0-1/\kappa)1/r$, where the κ's are the dielectric constants. The depth of the well was calculated by the method of Mott and Littleton. In the present problem, however, we require a self-consistent solution; that is, the initial wave function which is employed in calculating the depth of the trapping potential hole must be identical to the one obtained from this potential hole on solving the Schroedinger equation. The electron is smeared over a sphere whose radius equals approximately three interatomic distances. The outer displacements are calculated by a semicontinuum theory, whereas the dipoles of the three ions nearest the trapping center are calculated from the condition of equilibrium. The optical dissociation energy is found to be 0.68 ev, whereas the thermal energy is 0.13 ev. The low value of the second quantity presumably explains why self-trapping has not been observed to date. This energy should be about twice as large in LiF. These results suggest that self-trapping should be sought at a very low temperature.

I. INTRODUCTION

THE possibility that an electron can trap itself in a polar crystal was predicted by Landau. The trapping potential well is produced as a result of the ionic displacements induced by the field of the electron. Formerly this type of trapping was believed to be a possible explanation of the F centers studied by Pohl.[1] Experimental studies of the way F centers are produced, when there is stoichiometric excess of metal in an ionic crystal, indicate that they actually are caused by an alternate mechanism suggested by de Boer. He proposed that the electrons are trapped in the vacant negative lattice sites. Further rough estimates of the energy required to form an F center from a vaporized alkali metal implies that Landau's mechanism does not compete favorably with de Boer's on energetic grounds.

The problem remains, however, to calculate the binding energy of a self-trapped electron sufficiently accurately to be sure that this process does not compete with the other. Further, one might hope that by a calculation of this type sufficient information would be gained to predict under what conditions, if any, self-trapping would be observed.

A rough set of calculations of the binding energy of a self-trapped electron in ionic crystals has been made by Gurney and Mott,[2] and they report the binding energy to be several electron volts. Details of the calculations are not given, but the problem of a self-consistent solution does not appear to have been considered. These values seem extremely high and make it very difficult to understand why self-trapping has not been observed during some of the experimentation of Pohl or his co-workers. Recently, Pekar[3] has calculated this binding energy on the assumption of a continuous medium. His solution is self-consistent and gives an optical activation energy of -0.32 ev for NaCl. To calculate this value from his equations, we have placed the effective mass of the self-trapped electron equal to the free electron mass.

* This work was started while the writers were connected with the Training Program of Clinton Laboratory, Oak Ridge, Tennessee. It was in part supported by Contract NObs-34144 with the University of Pennsylvania.

** Now at Brown University, Providence, Rhode Island.

[1] For a recent review of this field see F. Seitz, Rev. Mod. Phys. 18, 384 (1946), where a more detailed bibliography is given.

[2] R. W. Gurney and N. F. Mott, Proc. Phys. Soc. 49, 32 (1937).

[3] S. Pekar, J. Phys. U.S.S.R. 10, 341, 347 (1946).

In view of the importance of self-trapping, we deemed it worth while to carry through a detailed calculation of the binding energy. In these calculations the method developed by Mott and Littleton[4] to calculate lattice defects was used. It is based on the simple and reliable theory of ionic crystal of Born with appropriate modifications. The electron wave function determines the field which causes the displacement of the ions in the crystal; these displacements determine the potential hole the electron is found in, and, finally, the hole determines the wave function. We thus require a self-consistent solution. Further, as we shall see, the electron is smeared out over several neighboring ions. This implies that the more distant ions may be more important than in the calculations of Mott and Littleton and that the total charge which determines the polarization of an ion varies with the distance from the trapping center.

II. THE WAVE FUNCTION

Let us now consider in detail the Schroedinger's wave equation for a self-trapped electron in a crystal, namely,

$$\frac{\hbar^2}{2m}\nabla^2\psi+(E_T-eV_T)\psi=0, \tag{1}$$

where E_T is the total energy of the electron and V_T is the total potential at r. The other terms have their conventional meaning. V_T is a combination of two terms, namely, the undisturbed potential, which is present whether or not there is a distortion of the lattice due to self-trapping, and an additional potential from the distortion. We may thus write it in the form

$$V_T=V_I+V, \tag{2}$$

where V_I is the ionic potential, which is essentially the Hartree potential of the ion corrected for the fact that the ion is in a perfect crystal and V is the potential due to the lattice distortion. In line with Eq. (2) we write

$$E_T=E_I+E. \tag{3}$$

We now make the assumption that we may write the wave function, ψ, as a product of two wave functions

$$\psi=\varphi\chi. \tag{4}$$

χ is taken as the undistorted wave function—a Bloch function for an electron in the conduction band. We may picture φ as modulating χ. Admittedly (4) is just a first-order approximation. We assume that V_I, E_I, and χ are related by the equation

$$(\hbar^2/2m)\nabla^2\chi+(E_I-eV_I)\chi=0. \tag{5}$$

Substituting back into (1) we obtain

$$(\hbar^2/2m)\nabla^2\varphi+(\hbar^2/m)\nabla\varphi\cdot(\nabla\chi/\chi)+(E-eV)\varphi=0. \tag{6}$$

Let us now examine Eq. (5) so that we may find a way to handle the second term in Eq. (6). Tibbs[5] has calculated χ for NaCl. His calculations follow the standard method of calculating Bloch functions in solids.[6] Tibbs employed the calculations of Prokofjew[7] on Na and of Hartree[8] on Cl to determine the ionic fields, but added a term to take care of the Ewald potential. Its form is

$$Ar^2+Br^3\pm1.748e^2/a,$$

where r is the radial distance, A and B are constants, different for Na and Cl, "a" is the distance between nearest neighbors, and 1.748 is Madelung's constant. The positive sign goes with Na, and the negative with Cl. A and B are evaluated so that the Ewald term is zero at the point where the ionic spheres (Tibbs replaced the ionic polyhedrons by spheres) are in contact, and the potential is due only to the overlapping ions. By numerical integration Tibbs found the energy for which the condition

$$\chi(\mathrm{Cl})/\chi(\mathrm{Cl})=-\chi(\mathrm{Na})/\chi(\mathrm{Na})$$

is satisfied at the boundary of the ionic spheres. Tibbs' value of E_I is 3.2 ev.

We recalculated χ using more recent ionic fields, which include exchange terms. We used the field of Fock and Petrachen[9] for Na and the field

[4] N. F. Mott and M. J. Littleton, Trans. Faraday Soc. **34**, 485 (1938).

[5] S. R. Tibbs, Trans. Faraday Soc. **35**, 1471 (1939). Also N. F. Mott and R. W. Gurney, *Electronic Processes in Ionic Crystals* (Oxford University Press, New York, 1940), p. 69.

[6] F. Seitz, *The Modern Theory of Solids* (McGraw-Hill Book Company, Inc., New York, 1940).

[7] W. Prokofjew, Zeits. f. Physik **58**, 255 (1929).

[8] D. R. Hartree, Proc. Roy. Soc. **A141**, 282 (1933).

[9] V. Fock and Mary Petrachen, Physik. Zeits. Sowjet union **6**, 368 (1934).

of Hartree and Hartree[10] for Cl. The wave function obtained in this way is very similar to that found by Tibbs. However, E_I is 12.8 ev. Our value is considerably larger than Tibbs' for the following reason. He made a correction for the use of the self-consistent field calculations without exchange. The diamagnetic susceptibility for Cl^- calculated from the field he used is 25×10^{-6} cm^3, while the measured value for Cl^- is 41.3×10^{-6} cm^3. Therefore, he multiplied his ionic radii by $(41.3/25)^{\frac{1}{3}}$ and obtained approximately 4.0 atomic units. We did not make this correction and used for the atomic radius the value obtained directly from the lattice constant. In addition, of course, we used slightly different fields from those used by Tibbs.

In treating Eq. (6) we shall neglect the second term and use the simplified form of the equation, namely,

$$(\hbar^2/2m)\nabla^2\varphi+(E-eV)\varphi=0. \tag{7}$$

The principal justification for this procedure rests on the fact that φ varies slowly in comparison with χ so that $\nabla\chi/\chi$ may be replaced by its mean value over any single cell of the lattice to a good approximation. This mean value is readily seen to be zero because χ is an even function relative to the center of symmetry represented by each ion in the lattice.

To determine the effect on the energy of omitting the second term of Eq. (6), we calculate its value by the mean value theorem. To do this, we assume that ψ is given by (4), where φ and χ are given by Eqs. (5) and (7). If H is the total Hamiltonian obtained from Eq. (1), we have

$$E_T=\int\psi^*H\psi d\tau$$

$$=E+E_I-(\hbar/m)\int\chi^*\varphi^*\,\mathrm{grad}\chi\cdot\mathrm{grad}\varphi d\tau. \tag{3a}$$

We shall see that φ is a slowly varying function of position, and therefore, the last term can be written as

$$\sum_{\text{ll cells}}-\frac{\hbar}{m}\langle\varphi^*\,\mathrm{grad}\varphi\rangle_{Av}\cdot\int\chi^*\,\mathrm{grad}\chi d\tau.$$

We have substituted an average (over a cell) for $\varphi^*\,\mathrm{grad}\varphi$, taken it out of the integrand, and summed over all the cells. Since χ is an even function of position, the integral vanishes and one obtains Eq. (3).

This same argument can be used to show that the higher approximation in a perturbation scheme vanishes. The perturbation scheme can be built up of product functions of the type $\chi\varphi_i$ in which the φ_i are the excited states' wave functions going with the wave (7) (φ being the ground state of Eq. (5)). We may therefore consider the wave function (4) as the leading term of the actual function given by $\chi\sum_i\varphi_i$.

We note that E is the energy relative to the electron in the conduction band, and we are, therefore, interested in it, not E_T.

Equation (7) is the form that was used by Pekar, although, in principle at least, he made allowances for the band structure by substituting an effective mass for m.

III. THE DISPLACEMENT POTENTIAL

Since χ does not enter into the evaluation of Eq. (7), we may use Born's[11] model of an ionic crystal. Therefore, we assume that the crystal is made of ions, whose internal structure is of no interest here except for the fact that they may become polarized when placed in an electric field. There are two main types of forces in this crystal, the short-range Born-Mayer force and the long-range electric force which arises from the additional electron and the polarization associated with displacements of the ions from their equilibrium positions. The equilibrium electric forces have, of course, been taken into account in V_I.

To simplify the problem, we assume that it is possible to separate the polarization of the electrons in the ion core from the displacement polarization of the ions. This separation is necessary because of a difference in the time of relaxation. Thus, if by some mechanism the electron is held constant for a period which is long compared to the time of a single lattice oscillation, 10^{-12} sec., the surrounding ions would be displaced. Effectively then, the electron would be surrounded by dipoles. The displacements would not follow the rapid motion of the electron after it is released, because of the long period of relaxa-

[10] D. R. Hartree and W. Hartree, Proc. Roy. Soc. **A156**, 45 (1936).

[11] See N. F. Mott and R. W. Gurney, reference 5, Chapter I; F. Seitz, reference 6, Chapter II.

tion. Thus the displacement polarization would create a potential hole to which the electron would be bound. The core electrons will, however, follow the detailed motion of the trapped electron, since the velocities of the electrons are roughly comparable. This means that the susceptibility of the core will not enter directly into the creation of the potential hole. Strictly speaking, these two effects are not entirely separable because the local field (field at a given ion site within the crystal) is affected by the state of polarization of the neighboring ions. Nevertheless, we shall start with the assumption that the two are separable, so as to simplify the problem.

To make this argument quantitative, we consider two cases—first, for static charges the field is given by $\mathbf{D}/\kappa$, where $\mathbf{D}$ is Maxwell's displacement vector and κ is the static dielectric constant. This implies that there is an induced dipole of strength per unit volume,

$$(1/4\pi)(1-1/\kappa)\mathbf{D}. \tag{8}$$

If, on the other hand, we have a rapidly varying field, which cannot be followed by the ionic displacements, the field is $\mathbf{D}/\kappa_0$, where κ_0 is the high frequency dielectric constant. For this case the induced dipole is

$$(1/4\pi)(1-1/\kappa_0)\mathbf{D}. \tag{9}$$

To separate the effect of core polarization from the effects of displacements, we may use a method of Mott and Littleton.[4] If we impress a uniform field on our crystal, the positive ions will be displaced a distance $a\xi$ in one direction, while the negative ions are displaced $a\xi$ in the other. For small displacements the equation of equilibrium is:

$$pa\xi = eE_{(\text{local})}, \tag{10}$$

where p is an elastic constant. If we assume that the repulsive forces are represented by a short-ranged potential of the form (Born-Mayer)

$$w(r) = Ae^{-r/\rho}, \tag{11}$$

where $\rho = 0.326\times10^{-8}$ cm, and that these forces act only between nearest neighbors, we obtain

$$p = \frac{2(1.748)e^2}{3a^2}\left[\frac{1}{\rho} - 2/a\right]. \tag{12}$$

The induced dipole due to the displacement is simply

$$(e^2/p)E_{\text{local}}.$$

Thus e^2/p behaves just like a susceptibility, whence we may set $\alpha = e^2/p$. For static fields, we may define

$$f_e = (\alpha_1+\alpha_2)/(\alpha_1+\alpha_2+2\alpha), \tag{13}$$

$$f_d = 2\alpha/(\alpha_1+\alpha_2+2\alpha), \tag{14}$$

where α_1 and α_2 are the core polarizations for the odd and even ions (see below). f_d is the fraction of polarization arising from the displacements of the ions, and f_e is the fraction resulting from core polarization. In the equation, we have omitted corrections for the overlap terms,[11] since Mott and Littleton's calculations indicate that this correction is small.

One may arrive at an alternate expression for the f's by regarding the difference between the expressions (8) and (9) as the displacement dipoles per unit volume. According to this viewpoint, it follows that

$$f_e = (1-1/\kappa_0)/(1-1/\kappa), \tag{15}$$

and

$$f_d = (1/\kappa_0-1/\kappa)/(1-1/\kappa). \tag{16}$$

The definitions (13) and (14) are not equivalent to (15) and (16). For NaCl, the first set gives

$$\begin{aligned} f_e &= 0.38, \\ f_d &= 0.62. \end{aligned} \tag{17a}$$

In calculating Eq. (17a) the polarization used for Na was 0.195×10^{-24} and for Cl, 3.41×10^{-24} in cm^3. These are averages of values quoted by Fajan and Joos, Born and Heisenberg, and Pauling (see reference 11). The second definition gives

$$\begin{aligned} f_e &= 0.68, \\ f_d &= 0.32. \end{aligned} \tag{17b}$$

That these definitions are not equivalent in general can be seen with the use of the Lorentz term[12] for the local fields $\mathbf{E}+(4\pi/3)\mathbf{P}$. According to this relation, κ is related to the polarizability per unit cell α_c by the equation

$$(\kappa-1)/(\kappa+2) = (4\pi/3)n_0\alpha_c. \tag{18}$$

Here α_c is the total polarizability per unit cell and n_0 is the number of molecules per unit vol-

[12] See, for example, J. N. Van Vleck, *The Theory of Electric and Magnetic Susceptibility* (Oxford University Press, New York, 1932), p. 14ff.

ume. α_e may be replaced by the electron polarizability per unit cell when displacement does occur, in which case κ is to be replaced by κ_0. With the use of Eqs. (13), (14), and (18) we may conclude that

$$f_e=[(\kappa_0-1)/(\kappa_0+2)][(\kappa+2)/(\kappa-1)]. \quad (19)$$

The derivation of this equation uses the fact that the total polarizability per unit cell is proportional to $\alpha_1+\alpha_2+2\alpha$ and the electronic polarizability is proportional to $\alpha_1+\alpha_2$ with the same proportionality factor.

If the electron polarization were the same before and after displacement, we would expect the relation

$$[1-(1/\kappa_0)]=[1-(1/\kappa)]f_e$$
$$=[(\kappa_0-1)/(\kappa_0+2)][(\kappa+2)/\kappa]. \quad (20)$$

or

$$\kappa/\kappa_0=(\kappa+2)/(\kappa_0+2).$$

This evidently is not identically satisfied. However, the condition approximately valid is at least partly satisfied. It is interesting to note that the right-hand side of (20) is smaller than the left, which means that the electron polarization decreases somewhat when the displacement polarization occurs.

The actual calculations were carried through, using Eqs. (15) and (16). That is, with the assumption that the electron polarizability is unchanged by the displacement, it is difficult to tell what error this introduced without carrying through some lengthy calculations. To be exact, one should take account of the core polarization in a more careful manner than we have done. Undoubtedly, the calculations presented in this paper give values that are correct to within an order of magnitude.

Equations (15) and (16) give the usual expression for the displacement dipole per unit volume,[3,13] namely,

$$(1/4\pi)(1/\kappa_0-1/\kappa). \quad (21)$$

The use of this expression is equivalent to assuming a continuous medium and completely disregarding the detailed crystal structure. For distant lattice points, one may assume the foregoing relation to hold approximately, but for neighboring ions we will have to consider the crystal structure in detail.

[13] See N. F. Mott and R. W. Gurney, reference 2, p. 86.

Zeroth Approximation

Let us, for the moment, assume that (21) holds for all the ions. Thus the displacement dipole induced on an ion a distance r (to be measured in interionic units) from the self-trapping center is

$$ea\delta(r_i)=(a^3/4\pi)(1/\kappa_0-1/\kappa)\mathbf{D}(r_i), \quad (22)$$

where δ is the displacement of the r_ith ion in units of "a." Here the problem is to calculate Maxwell's displacement vector. As we shall see subsequently, the electron is smeared over a sphere whose diameter is approximately $10a$. At points outside this sphere, $\mathbf{D}$ clearly equals $e/a^2r_i^2$. Since we are only interested in the time average dipole, we may use the time average displacement vector obtained from the trapped electron's wave function for points inside the sphere. In general, we may write

$$ea\delta(r_i)=(a/4\pi r_i^2)(1/\kappa_0-1/\kappa)eQ(r_i), \quad (23)$$

where

$$Q(r)=4\pi\int_0^{ar}|\varphi(\xi)|^2\xi^2d\xi.$$

Here we used only the envelope of ψ—i.e., φ ignoring the modulating function χ in computing Q. At large distances, $Q(r)$ equals unity, and further, we note "a" appears only in the first power on the right-hand side because of the units selected. Equation (23) shows the nature of the problem to be solved. To calculate the dipoles we must know φ from Eq. (7), but to evaluate that equation we must know the δ's.

Using Eq. (23) one could calculate V at any point in the crystal. This procedure is too complicated for actual use. However, we approximate V as follows. At large distances, where the continuum approximation is applicable, the potential due to the displacement dipoles is the difference between the static and the high frequency potential,

$$(1/\kappa_0-1/\kappa)e/ar, \quad (24)$$

in which we have let $Q(r)$ equal unity. Near the center of trapping, the field undoubtedly is neither a simple function nor is it completely spherically symmetric. We believe, however, that

we can obtain a sufficiently good approximation by cutting off expression (24) at a distance r_0, and assuming that for smaller values of r_0 the potential is a constant. That the self-trapping potential behaves approximately in this manner can be seen from the fact that the potential at the very center is finite. We shall let the constant value at which (24) is cut off be this constant value. Our problem thus reduces itself to finding the potential once φ is known.

From Eq. (23) we obtain the desired value of the potential which we call $V_0(0)$, namely,

$$V_0(0)=(e/4\pi a)(1/\kappa_0-1/\kappa)\sum_{\text{all ions}} Q(r_i)/r_i^4. \quad (25)$$

The subscript denotes the order of the approximation. The summation converges slowly, since the number of ions per shell increases as the square of the distance. Until now we have made no assumption concerning the geometric arrangement of ions near the center of the self-trapped electron. For simplicity, we shall assume the center coincides with a positive ion site. In the zeroth approximation one would obtain exactly the same value of wave function φ and energy by locating the center at a negative ion site. This may seem paradoxical at first sight, but it should be recalled that the detailed internal structure, even the total charge of the ions, enters into the problem only through χ. However, the wave function χ is approximately equally distributed between the two ions, that is $\int|\chi|^2 d\tau$ over the negative ion approximately equals $\int|\chi|^2 d\tau$ over the positive ion. This shows that the electron does not distinguish strongly between the two ions.

Sums of the type found in (25) have been carried out by Ingham and Jones[14] for $Q(r)=1$. When the origin is at a positive ion, their result may be stated as follows:

$$\begin{aligned}\sum_{\text{neg. ions}} 1/r_i^4&=10.1977,\\ \sum_{\text{pos. ions}} 1/r_i^4&=6.3346.\end{aligned} \quad (26)$$

We can evaluate (25) accurately by assuming $Q(r)=1$ for the outer ions and write

$$\sum_{\text{all}} Q(r_i)/r_i^4=\sum_{\text{near}} Q(r_i)/r_i^4+\sum_{\text{far}} 1/r_i^4. \quad (27)$$

The division between "near" and "far" ions depends on φ. At first the 25 nearest shells were considered "near." However, it was found subsequently that $Q(r)$ converged sufficiently rapidly that it is necessary to consider only about half that number.

We started by using Pekar's wave function with the assumption that the free electron mass may be used for the effective mass. His equation leads to a value 20.3×10^{-4} e.s.u. for $V_0(0)$ while Eq. (25) gives 20.1×10^{-4} e.s.u. This implies that to the zeroth approximation both methods give the same results, as might have been expected. We must go to higher approximations to include the details of the crystal structure.

Higher Approximations

Mott and Littleton found when calculating $V(0)$ for a missing ion site that one may assume that an equation analogous to (22) holds for all but the nearest ions. It is not clear that this approximation is valid in the present case, because the electric charge is spread out over neighboring ions. Therefore, to be on the safe side, we assumed that (22) does not hold for the three sets of nearest ions, namely the (1, 0, 0), the (1, 1, 0) and the (1, 1, 1) sets. The cases in which these sets are successively included were referred to as the first, second and third approximations respectively. The displacements of these ions (which we shall call ξ to distinguish them from the δ's obtained by (22)) are calculated from the equations of equilibrium,

$$F_r+eE_i=0, \quad (28)$$

where F_r is the repulsive (Born-Mayer) force due to the neighboring six ions and E_i is the local field at the point of equilibrium. Here we ignore all effects of lattice vibrations. Strictly speaking, Eq. (28) gives the equilibrium position about which the ion is vibrating. The electric field is caused, to a good approximation, only by the lattice dipoles and the extra charge. The Madelung field is virtually zero near an ion site and is included in χ.

As stated, the trapped electron is not affected by the polarization of the ion core. The field E_i, to be used in Eq. (28), however, must include two effects; the field due to the displacements of the surrounding ions and the average core polar-

[14] A. E. Ingham and J. E. Jones, Proc. Roy. Soc. **A107**, 636 (1927).

ization of the surrounding ions. The latter must be included because of the relatively long relaxation time of the ions. The average core polarization is simply given by the average field E_i times the ionic polarization. Hence we have the additional set of equations,

$$m_i=\alpha_i E_i. \tag{29}$$

Here α_i is the susceptibility of the ith ion, m_i is the average core dipole, and E_i is the time average field. The subscript i on the ξ's and the α's refers to the inner ions in accordance with the following scheme:

1 for the (1, 0, 0) ion,
2 for the (1, 1, 0) ion,
3 for the (1, 1, 1) ion.

In the case of the third approximation, Eqs. (28) and (29) give six conditions between six unknowns. From the solution of these equations we obtain information needed to determine $V(0)$. We shall now derive explicit expressions for the E's and the F_r's in terms of the other variables.

The E's are composed of three parts:

(a) *The Outer Dipoles.*—This term includes those dipoles whose strength is given by the continuum theory. Thus for the third approximation this includes all ions outside of (1, 0, 0), (1, 1, 0) and (1, 1, 1). To calculate their contribution to the field, we note that the dipoles must be oriented radial relative to the center of the trapped electron. From the geometry of the lattice it follows that the net field at a lattice site arising from a shell of ions is also radial. By "shell of ions" we mean all the ions given by the permutation of (x, y, z) when the x, y, and z have both a positive and a negative sign. For NaCl, the ion is of one type if the sum of x, y, and z is odd and is of another type if the sum is even. For our case, an odd sum represents a negative (Cl) ion site. The outward field at about $R-$ having coordinates (X, Y, Z) due to a radial dipole of strength d at a point $r-$ having coordinates (x, y, z), can be calculated from the standard expression for the field due to a dipole. We find

$$\begin{aligned}E(R, r)=(d/rR|\mathbf{r}-\mathbf{R}|^5)\{&[(Xy-Yx)^2\\&+(Xz-Zx)^2+(Yz-Zy)^2]\\&-2[(r^2-Xx-Yy-Zz)\\&\times(Xx+Yy+Zz-R^2)]\}.\end{aligned} \tag{30}$$

The strength d of the dipole includes the effects due both to the displacement and to the core susceptibility. In view of our discussion in connection with the derivation of Eqs. (13) and (14) it would seem logical to define the average total (displacement plus ionic core) dipole induced at an odd (Cl^-) site as

$$(M_1a^3eQ(r)/a^2r^2)(1/4\pi)(1-1/\kappa), \tag{31a}$$

and that for an even (Na^+) site as

$$(M_2a^3eQ(r)/a^2r^2)(1/4\pi)(1-1/\kappa), \tag{31b}$$

where

$$\begin{aligned}M_1&=(\alpha+\alpha_1)/(\alpha+\tfrac{1}{2}(\alpha_1+\alpha_2)),\\M_2&=(\alpha+\alpha_2)/(\alpha+\tfrac{1}{2}(\alpha_1+\alpha_2)).\end{aligned} \tag{31c}$$

Here the α_1 and α_2 are the core susceptibilities of the odd and even ions.

Using Eqs. (12), (30), and (31), we obtain for the field from an odd (Cl^-) ion shell

$$-5.346\times10^4Q(r)I_{ij}/r_j^2, \tag{32a}$$

and from an even (Na^+) shell

$$-2.612\times10^4Q(r)I_{ij}/r^2j. \tag{32b}$$

The I's relate the field at site i to the dipoles in the jth shell. The evaluation of the I's requires lengthy calculations using (30). Mott and Littleton calculated the net effect (for $Q(r)=1$) due to the 23 nearest rings at some sites. We used only the 17 nearest rings, since a comparison with their value indicated that our other approximations give a much larger error. The individual values of the I's for the inner rings are given in Mott and Littleton.

(b) *The Inner Dipoles.*—We consider the effect of the ions in the "near" shells where (22) no longer holds. Here the displacements are given by ξ_i and the core susceptibility by m_i. Their contributions follow directly from Eq. (30) and are

$$-(e/a^2)\xi_jI_{ij}, \tag{33a}$$

and

$$-(m_j/a^3)I_{ij}. \tag{33b}$$

TABLE I. Comparison of the various approximations used.

Approximation	Potential $\times10^4$ e.s.u. at (000)	$\xi_1\times10^3$	$\xi_2\times10^3$	$\xi_3\times10^3$
0	35.8			
1	56.7	26.5		
2	67.2	23.6	18.3	
3	70.6	23.4	17.4	14.1

TABLE II. Summary of data for third approximation.

V (assumed) 10^4 e.s.u.	$\xi_1\times10^{+3}$	$\xi_2\times10^{+3}$	$\xi_3\times10^{+3}$	$m_1\times10^{+20}$ e.s.u.	$m_2\times10^{+20}$ e.s.u.	$m_3\times10^{+20}$ e.s.u.	$\beta\times10^{-8}$ cm^{-1}	V (cal.) 10^4 e.s.u.
70	23.5	17.4	14.1	17.8	0.72	10.6	0.3311	70.57
75	24.7	18.2	14.3	18.7	0.75	10.7	0.3405	72.89
80	25.8	18.8	14.4	19.4	0.77	10.8	0.3489	74.81

(c) *The Electron Charge.*—Superposed on the effects described in (a) and (b) are those of the field due to the electron. This is given to a satisfactory approximation by

$$eQ(r_i)/a^2(r_i\pm\xi_i)^2=(eQ(r_i)/a^2r_i^2)(1\mp2\xi_i/r_i), \quad (34)$$

where we adopt a sign convention in which outward displacements are positive for odd ions but negative for even ions. Combining (a), (b), and (c), we can calculate E_i for Eqs. (28) and (29).

We turn now to describe the method used to obtain F_r. This term can be obtained from (11) by calculating the potential of the inner ions and differentiating with respect to the ξ's, with due regard to the sign convention adopted. This gives us for F_r:

$$F_r(100)=(-A/\rho)\exp(-a/\rho)[\xi_1(2a/\rho-4)+\delta(2,0,0)a/\rho-2\sqrt{2}\xi_2], \quad (35a)$$

$$F_r(1,1,0)=(-A/\rho)\exp(-a/\rho)\times[\sqrt{2}\xi_1+(4-a/\rho)\xi_2+4/(6)^{\frac{1}{2}}\xi_3 2/(10)^{\frac{1}{2}}+(1-2a/\rho)\delta(1,2,0)], \quad (35b)$$

$$F_r(1,1,1)=(-A/\rho)\exp(-a/\rho)\times[-(6)^{\frac{1}{2}}\xi_2+(2a/\rho-4)\xi_3+\sqrt{2}(a/\rho-1)\delta(2,1,1)]. \quad (35c)$$

A is evaluated by requiring that the net force at the position of equilibrium be zero. This consideration gives

$$(1.748)e^2/a^2=(6A/\rho)\exp(-a/\rho). \quad (36)$$

To obtain (35) we have expanded terms of the type $\exp\{(1/\rho)(a+\xi_i)\}$. *A priori*, one would expect the leading term to be of the type $(a/\rho)\xi_i\times\exp(-a/\rho)$ and the next term of the type $(a/\rho)^2\xi_i^2\exp(-a/\rho)$. The geometry of the lattice clearly shows, upon detailed consideration, that terms of the order of $\exp(-a/\rho)$ will not appear. When one carries through the expansion, however, one sees that the next term after $(a/\rho)\xi_i\times\exp(-a/\rho)$ is of the type $(a/\rho)^2\xi_i\delta_j\exp(-a/\rho)$. Since actual calculations show that the δ's are considerably smaller than the ξ's, the second term is small enough to be neglected in this approximation. The physical reason for the cancellation of terms quadratic in $a/\rho\xi_i$ is not obvious. It is associated with the lattice structure and the approximation used. Had higher approximations been necessary, the terms of the type $(a/\rho)^2\xi_i\xi_j$ would have come in, and they might well have introduced a larger error.

We have all the necessary information to be able to substitute the appropriate terms into Eqs. (28) and (29). In the third approximation we thus have six unknowns and six equations. Using standard methods,[15] we solved these to evaluate the ξ's and the m's. Finally, to obtain the potential at (0, 0, 0) we subtract from (25) the contributions of the three inner shells and add

$$\sum_{i=1,2,3} n_i ea\xi_i/a^2r_i^2,$$

where n_i is the number of particles in the ith shell.

We have thus developed a method to calculate $V(0)$ to the desired approximation once φ is known.

IV. THE WAVE FUNCTION

We now require the wave function for a spherically symmetric well given by

$$\begin{aligned} V(r)&=V(0) \quad \text{for} \quad r<r_0,\\ V(r)&=c/r \quad \text{for} \quad r>r_0, \end{aligned} \quad (37)$$

where

$$c=(1/\kappa_0-1/\kappa)e.$$

Further, we define r_0 by the relation

$$c/r_0=V(0). \quad (37a)$$

It would be possible to solve the wave equation directly for the potential (37). However, since our solution will be only approximate and a series of

[15] R. A. Frazer, W. J. Duncan, and A. R. Collar, *Elementary Matrices* (Cambridge University Press, New York, 1938), p. 125.

TABLE III. Summary of data for first approximation.

V (assumed) $\times 10^{-4}$ e.s.u.	$\xi_1 \times 10^{+3}$	$m_1 \times 10^{+20}$ e.s.u.	$\beta \times 10^{-8}$ cm^{-1}	V (cal.) $\times 10^{4}$ e.s.u.
40	16.1	13.9	0.2572	42.0
61.4	23.9	20.2	0.3138	52.9
70	26.5	22.3	0.3311	56.7

wave functions will be required for various trial $V(0)$, we decided to use the standard variational method.[16] We approximated φ by the simple, normalized, wave function $(\beta^3/\pi)\exp(-\beta r)$. We desire the best β for the potential (37).

The energy calculated by this method is the optical activation energy,[17] that is, the energy to excite the trapped electron into the conduction band without causing any other effect. The energy released by the relaxation of the displacement dipoles is not included. By the Frank-Condon principle, this is the energy required to excite the self-trapped electron optically. The energy is given by

$$E_0=(\beta^2\hbar^2/2m)-eV(0) \times\{1-(1+\beta r_0)\exp(-2\beta r_0)\}. \quad (38a)$$

The first term gives the kinetic energy of the electron, while the second term gives the potential energy. β is determined in such a way that E_0 has an extreme value.

When a charge induces a displacement on the neighboring ions, there are two potential energy terms. One arises from the fact that the charge finds itself in a potential hole. This is given by the second term of Eq. (38a). A second potential arises from the work required to displace the neighboring charges. If the displacements are small, Hooke's law will hold approximately, and it follows that the second term is just half the first term. If the trapped electron escapes, due to thermal vibrations, the energy stored in the surrounding dipoles will be released. The thermal activation energy is thus E_0 plus half the potential energy in Eq. (38a) or is given by

$$E_t=(\beta^2\hbar^2/2m)-\tfrac{1}{2}eV(0) \times\{1-(1+\beta r_0)\exp(-2\beta r_0)\}. \quad (38b)$$

For consideration of thermal equilibrium, we use (38b), but for the considerations of the optical properties we use (38a).

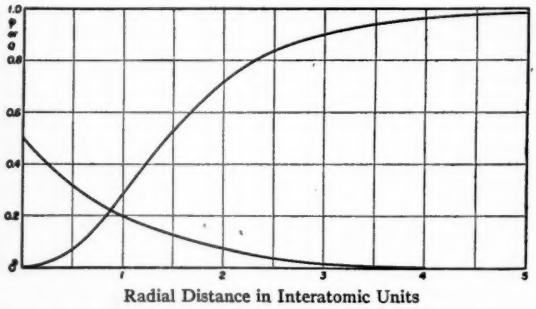

FIG. 1. Self-trapped electron's wave function "φ" (decreasing function) and charge distribution "Q" (increasing function) for NaCl.

V. SUMMARY OF THE CALCULATIONS

On starting to make this calculation the first question one must answer is: To what order of approximation should one carry the calculation of $V(0)$? To answer this question, we calculated $V(0)$ by four approximations (starting with the zeroth), using the wave function corresponding to a well depth of 70×10^{-4} e.s.u. This value of $V(0)$ was selected because a preliminary calculation, starting with Pekar's wave function, indicated that that depth gives approximately a self-consistent solution. The values of a, κ_0, and κ used were 2.81×10^{-8} cm, 2.24, and 5.62, respectively. Table I gives the results. The value of V seems to converge rapidly after the second approximation. The sudden jump between the zeroth and first approximation is due, in part, to the use of Eqs. (15) and (16) in place of Eqs. (13) and (14). To be on the safe side, we carried the problem to the third. However, a great deal of labor would have been saved with little loss in accuracy had we used only the second approximation. The variations in the value of the ξ's which are larger than those in $V(0)$'s are of no importance for the problem at hand. Table II summarizes our calculations. This table contains three (assumed) values of $V(0)$, the calculated values of β, the ξ's, the m's, and the (computed) $V(0)$. From these values we obtained the self-consistent solution by plotting the difference between the two types of V's and the assumed V.

[16] L. Pauling and E. B. Wilson, Jr., *Introduction to Quantum Mechanics* (McGraw-Hill Book Company, Inc., New York, 1935), p. 180.

[17] See N. F. Mott and R. W. Gurney, reference 5, p. 160.

The final values are:

$$V(0)=71.2\times10^{-4}\text{ e.s.u.},$$
$$\beta=0.331\times10^{8}\text{ cm}^{-1},$$
$$E_0=-0.68\text{ ev}$$
$$E_t=-0.13\text{ ev}.$$

In Fig. 1 the final wave function φ and $Q(r)$ are plotted against r in interatomic units. Table III summarizes a similar calculation, but here only the ξ_1 and m_1 of the (1, 0, 0) ion are assumed unknown. In other words, this is the first approximation. The self-consistent values here are

$$V(0)=44.7\times10^{-4}\text{ e.s.u.},$$
$$\beta=0.27\times10^{8}\text{ cm}^{-1},\quad\text{(First approximation)}$$
$$E_0=-0.56\text{ ev},$$
$$E_t=-0.14\text{ ev}.$$

It is difficult to estimate the relative errors introduced due to the various approximations made. One may check roughly the method used to find β from $V(0)$ by comparing our wave function with Pekar's, for the same depth of the potential hole. He also used the variational procedure. However, he had two parameters instead of one, his function being of the form

$$A(1+\beta r+\gamma r^2)\exp(-\beta r),$$

in which A is a normalizing factor. In his potential there is no abrupt cut-off like ours. For comparison we have plotted in Fig. 2 his $Q(r)$ against r for a free electron mass and the $Q(r)$ obtained by our method for $V(0)=20.3\times10^{-4}$ e.s.u., the value of $V(0)$ he obtained. Pekar notes that γ does not affect his results appreciably, and concludes that his method is quite accurate. Further, Pekar's E_0 is 0.32 ev, while the value obtained by our approximation is 0.35 ev. There are, however, undoubtedly other errors in our method such as the use of Eq. (15) and (16) in place of (13) and (14), and one would hardly expect agreement with experimental results to higher accuracy than 25 percent. Actually, our results may be somewhat less accurate.

VI. CONCLUSION

We may now examine some of the conclusions that may be inferred from the calculated values of E_t and E_0. First let us examine the life-time of a self-trapped electron. Its magnitude is given

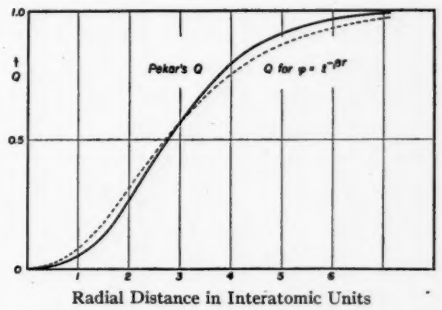

FIG. 2. Comparisons of $Q(r)$ obtained from Pekar's wave function, with that derived in this paper.

approximately by

$$10^{-12}\exp(E_t/kT)\text{ sec.}$$

This yields a value of 10^{-10} sec. for room temperature ($kT=1/40$ ev). The self-trapped electron will have a very short lifetime even at the boiling point of oxygen (90°K), namely, about 10^{-5} sec. This means that if an electron were trapped it could not be observed unless one worked at very low temperatures.

In an actual crystal, there are processes which compete with self-trapping, in particular the trapping of an electron in a vacant lattice site. We would like to know the differences between the energies involved in trapping an electron by the de Boer and Landau mechanisms. Let us consider the energy required to absorb a free sodium atom into the crystal, during which process the atom becomes an ion, and the extra electron gets trapped. This energy has been calculated for the de Boer process by Gurney and Mott[18] and is +0.23 ev. Let us now calculate this energy for a mechanism in which the positive ion is assumed to go into an interstitial position and the electron becomes self-trapped. We proceed as follows:

1. We ionize the free sodium atom; the necessary work is I, the ionization potential of sodium, namely 5.11 ev.

2. Next we place the electron into the conduction band; the energy E_c required to do this has been calculated by Mott[19] who obtains a value of −0.53 ev.

---

[18] R. W. Gurney and N. F. Mott, Trans. Faraday Soc. **34**, 506 (1938); also ref. 12, p. 144.

[19] N. F. Mott, Trans. Faraday Soc. **34**, 500 (1938); also reference 13, p. 95.

3. The free sodium ion is placed in an interstitial site $(\frac{1}{2}, \frac{1}{2}, \frac{1}{2})$. This process takes -1.71 ev.

4. Finally, we assume that the electron is trapped thermally, so that it gains 0.13 ev. Thus it takes $+2.74$ ev to form an F center by Landau's hypothesis, compared to 0.23 ev on the de Boer picture.

We may conclude that very few self-trapped electrons are formed during usual experimental procedures, and those trapped have a very short life. While some of the values used above and by Gurney and Mott may be questioned, there is little doubt that these calculations give values to an order of magnitude, and that the qualitative picture is correct.

One may wonder if self-trapping might be observed under reasonably static conditions in any crystal. In the zeroth approximation the quantity which determines the depth of the hole is primarily $(1/\kappa_0 - 1/\kappa)$. Further, in Pekar's treatment of this approximation the square of this is the only quantity which characterizes the crystal behavior provided it is assumed that the effective electron mass is about the same as the free value. Thus $(1/\kappa_0 - 1/\kappa)$ provides a rough measure of the relative ability of a crystal to trap an electron. We conclude that of the common ionic crystals LiF will have the largest energy for self-trapping, since $(1/\kappa_0 - 1/\kappa)$ is largest for it. The value for LiF is 0.41 compared to the value 0.27 for NaCl. If the energy parameters increase as the square of this quantity, we would expect E_0 to be about 1.6 ev and E_t about 0.3 ev. This second value means that the lifetime at the boiling point of oxygen is about 10^5 sec. Moreover the relatively large value of E_0 implies that Landau trapping could be observed in LiF with a relatively simple spectrograph if not visually. One would expect the nature of the absorption bands produced in LiF, when irradiated by x-ray, to be strongly temperature dependent in the neighborhood of 100°K. Of course, one would have to be careful to separate this effect from that caused by other trapping centers, which have their characteristic temperature dependence.

Little is known at present about the cross section for the process of self-trapping. Experimental studies of the capture of electrons by halogen ion vacancies in the formation of F centers, and of the capture of electrons by F centers in the formation of F' centers, show that the cross section for these processes is of the order of 10^{-15} cm^2. The experimental evidence concerning the formation of F centers also indicates that the initial trapping step which determines the magnitude of the trapping cross section rests on the transfer of energy from the electron to the lattice presumably by excitation of the polarization modes of vibration. This result strongly suggests that the cross section for self-trapping may also be of the order of 10^{-15} cm^2.

It should be pointed out that the electron need not be trapped about a sodium ion, although our calculations have been based on this premise. Undoubtedly there will be small variations in the trapping energy, depending upon the site which is chosen for the center of the trapping polarization. Since we have found that the trapped electron is distributed over a very large volume of the crystal, it seems reasonable to suppose that the trapping energy is relatively insensitive to the center chosen. This conclusion also suggests that the self-trapped electron may require only a small activation energy to move from one site to another. In other words, it is possible that at any but the very lowest temperatures the trapped electron may diffuse through the crystal with a velocity approaching sonic velocity. In this case, self-trapped electrons would find other trapping sites, such as halogen ion vacancies, in a time of the order of 10^{-8} sec. for normal densities of the latter.

The authors would like to thank Clinton Laboratories of Oak Ridge, Tennessee, for the opportunity of starting this research while taking part in their training program.

PHYSICAL REVIEW VOLUME 74, NUMBER 9 NOVEMBER 1, 1948

A Quantitative Determination of the Magnetic Moment of the Neutron in Units of the Proton Moment*

F. BLOCH, D. NICODEMUS, AND H. H. STAUB
Stanford University, Stanford, California

(Received July 23, 1948)

A precision determination of the ratio of the magnetic moments of neutron and proton is presented. The method consists in determining the Larmor precession frequencies of neutrons and protons simultaneously in the same extremely homogeneous magnetic field. In this manner the ratio of the two Larmor frequencies gives directly the ratio of the two magnetic moments. The precession frequency of the neutrons is obtained by the occurrence of non-adiabatic transitions of a polarized neutron beam, the precession frequency of the protons by nuclear induction. Measurements are made so that only small differences in frequency have to be measured in terms of a constant but otherwise unknown standard. The value of the ratio of the two moments is found to be $|\mu_N|/\mu_P=0.685001\pm0.00003$. By use of this value in connection with the recent determination of the ratio of the moments of proton and deuteron by Bloch, Levinthal, and Packard, the deviation of the deuteron moment from additivity is found to be 0.02230 ± 0.00009 nuclear magnetons.

INTRODUCTION

AMONG the moments of atomic nuclei, those of the elementary constituents, the proton and the neutron, are of central significance. Their values are not only basic in order to discuss the moments of more complex nuclear structures, but they are also of greatest interest in themselves in view of their bearing upon the constitution of fundamental particles.

As a most important first step towards the knowledge of these elementary moments, Stern and his collaborators have shown that the magnetic moment μ_P of the proton[1] is about 2.5 times larger than the nuclear magneton, $\mu_n=(m/M)\mu_B$, defined through the Bohr magneton μ_B and the mass ratio m/M of electron and proton. From a later measurement of the magnetic moment μ_D of the deuteron[2] and the assumption of the simple law of additivity, $\mu_D=\mu_N+\mu_P$, they have also been led to the conclusion that the neutron has a finite and negative moment μ_N of about 2 nuclear magnetons. Both results are equally significant since they indicate that neither the proton nor the neutron is adequately described through the relativistic wave equation of Dirac, which explains the magnetic moment of the electron but would lead here to the wrong values $\mu_P=\mu_n$, $\mu_N=0$. The ingenious new methods of Rabi and his collaborators have subsequently led to the far more accurate value

$$\mu_P=(2.7928\pm0.0008)\mu_N \qquad (1)^{**}$$

for the magnetic moment of the proton.[3]

The direct proof that the free neutron possesses a magnetic moment has originated from the effect of magnetic scattering.[4] The interaction of the neutron moment with the atomic moments in a ferromagnetic substance causes polarization of an originally unpolarized neutron beam and, as one of its consequences, an increase of the transmission upon magnetization of the substance. While this change in single transmission has been actually demonstrated,[5] it was not possible to infer from the measurement more than the expected order of magnitude of the neutron moment since the effect depends not only upon the neutron but also upon various complicating features of the scattering substance.

The quantitative determination of the neutron moment requires, besides the polarization of neutron beams, another independent principle which is closely related to the one first described

* Assisted by the Joint Program of the Office of Naval Research and the Atomic Energy Commission.

[1] R. Frisch and O. Stern, Zeits. f. Physik **85**, 4 (1933).

[2] I. Estermann and O. Stern, Zeits. f. Physik **85**, 17 (1933); Phys. Rev. **45**, 665 (1934).

** This value differs from the originally given value 2.7896 by the factor $(1+\alpha/2\pi)$, as a result of a recent radiative correction for the magnetic moment of the electron. (See Section V.)

[3] S. Millman and P. Kusch, Phys. Rev. **60**, 91 (1941).

[4] F. Bloch, Phys. Rev. **50**, 259 (1936).

[5] P. N. Powers, H. Beyer, and J. R. Dunning, Phys. Rev. **51**, 371 (1937).

by Rabi[6] as a means for the sign determination of nuclear moments and which was simultaneously conceived by Gorter and one of us (F.B.). It is based upon the resonance of a rotating or oscillating magnetic field with the Larmor frequency of the nuclear moment in a constant field at right angles. The initial use of this magnetic resonance method has been made by Rabi and his collaborators[7] in their famous experiments on molecular and atomic beams.

Alvarez and Bloch[8] have succeeded in applying the method to the neutron. In their experimental arrangement a beam of thermal neutrons passes through a polarizing and analyzing plate of magnetized iron. Between these two plates the neutrons are exposed to a magnetic field which has a constant component H_0 and at right angles to it an oscillating component with circular frequency ω and amplitude H_1. Under resonance conditions, there occurs in this field a reorientation of the neutron moments and thus a partial depolarization of the beam. Consequently, the total transmission through the analyzer is lowered so that resonance depolarization manifests itself by a drop in the transmitted intensity detected as one passes through resonance. From the measured value H_0 of the constant field at which resonance is observed and the frequency ω of the oscillating field, one obtains

$$\frac{\mu_N}{\hbar I_N}=\gamma_N=\frac{\omega}{H_0} \tag{2}$$

for the gyromagnetic ratio γ_N, defined as the magnetic moment of the neutron μ_N, divided by its angular momentum $\hbar I_N$. Assuming the spin of the neutron to be $I_N=\frac{1}{2}$, the absolute value of the neutron moment was determined to be

$$|\mu_N|=(1.93\pm0.02)\mu_n. \tag{3}$$

The fact that the sign of the neutron moment is actually negative has been shown in an earlier experiment of Powers.[9]

The limitation in accuracy of the result (3) was due to two major causes. In the first place the depolarization effects, although clearly established, were rather small. The largest observed drop of intensity amounted to about only 1.5 percent, so that the location of the exact resonance condition was only possible to within the width of the resonance line. A higher percentage accuracy could have been obtained with the same line width by carrying out the experiment at larger values of the constant field H_0 than those of about 600 gauss, which were actually used. This, however, would not have eliminated the second comparable error, originating in the determination of the resonance value of H_0. Although this field was determined by two independent procedures, one using flip coils directly, the other based upon a comparison with the field of a proton accelerating cyclotron, the consistency and accuracy of these two methods did not exceed $\frac{1}{2}$ percent.

A vast improvement of the experimental conditions has been made possible through our recent work. To a large extent, the two previously mentioned handicaps were eliminated, and thereby a far more accurate determination of the neutron moment has been achieved. The experiments have been extended over a considerable period, although preliminary results were obtained at an early stage and could easily have been trusted to within 0.1 percent. The indispensable part of a precision measurement which consists in the examination of detailed features required a more time-consuming effort which, however, seemed well justified in view of the importance of obtaining a reliable result of the highest accuracy compatible with the experimental conditions.

II. METHOD

With the principle of our method, to observe resonance depolarization of a collimated neutron beam between the polarizer and analyzer, being the same as in the experiment of Alvarez and Bloch,[8] we shall restrict ourselves to the description of those features which represent essential innovations.

An important improvement of the experimental conditions has been achieved by a very close approach to magnetic saturation in the polarizing and analyzing plates of iron. Our previous investigations[10] of the transmission

[6] I. I. Rabi, Phys. Rev. **51**, 652 (1937).
[7] Rabi, Zacharias, Millman, and Kusch, Phys. Rev. **55**, 526 (1939).
[8] L. W. Alvarez and F. Bloch, Phys. Rev. **57**, 111 (1940).
[9] P. N. Powers, Phys. Rev. **54**, 827 (1938).
[10] F. Bloch, M. Hamermesh, and H. Staub, Phys. Rev. **64**, 47 (1943); F. Bloch, R. I. Condit, and H. H. Staub, Phys. Rev. **70**, 972 (1946).

effect caused by magnetic scattering have shown that saturation to within less than 0.1 percent is necessary in order to approach the full effect in a single plate of hot-rolled steel of 3.8-cm thickness. By the use of strong magnetizing fields of the order of 10,000 gauss, we were able to observe an increase of the transmission by magnetization of as much as 22 percent, while the largest effects observed before did not exceed 6 percent. The dependence of the effect upon saturation was found to be in full agreement with the theory of Halpern and Holstein,[11] who investigated the influence of magnetic deviations from the field direction as a result of the microcrystalline structure. They have shown that such deviations, even if they are small, can cause an appreciable depolarization of the neutrons in the steel and thereby result in a reduction of the single transmission effect; besides, they have pointed out that this reduction must become even more pronounced if one deals with double transmission, as in our arrangement, where the combined result of the passage through polarizer and analyzer is observed.

This can best be seen by expressing the observed effect for double transmission in terms of likewise observable single transmission effects: Let $f_0(v)dv$ be the number of neutrons with velocity between v and $v+dv$ which are recorded in the detection chamber per unit time after having passed through the polarizer and analyzer plate, if both are unmagnetized. This number will be increased by a different characteristic factor $C(v)$ if either or both of the two plates are magnetized without any change of orientation of the neutrons occurring between them, and one has to consider the following cases:

(a) Polarizer and analyzer both magnetized; $C(v)=C_D(v)$.
(b) Polarizer magnetized; analyzer unmagnetized; $C(v)=C_P(v)$.
(c) Analyzer magnetized; polarizer unmagnetized; $C(v)=C_A(v)$.

Assuming the spin of the neutron to be $\frac{1}{2}$, we shall now consider the case that there exists a finite probability $P(v)$ for a neutron of velocity v to change its orientation between polarizer and analyzer. The total recorded intensity can then be expressed in the form

$$I=\int f_0[(1-2P)C_D+2PC_PC_A]dv, \tag{4}$$

where f_0, C_D, C_P, C_A, and P are all functions of the velocity. The proof of this formula requires merely that the recorded neutrons have not changed their velocity in their passage through the apparatus, and that the steel plates of the polarizer and analyzer are sufficiently thick so that an originally polarized beam of neutrons would emerge completely depolarized upon passage through the unmagnetized plates. Both conditions are certainly well satisfied under our experimental conditions. Let the recorded intensities corresponding to the three cases *a*, *b*, and *c* previously mentioned be

$$I_D=\int f_0C_Ddv, \tag{5a}$$

$$I_P=\int f_0C_Pdv, \tag{5b}$$

$$I_A=\int f_0C_Adv, \tag{5c}$$

and, furthermore, let

$$I_0=\int f_0dv \tag{6}$$

represent the intensity if polarizer and analyzer are both unmagnetized. Then we shall define the observable effect E_T resulting from transitions as

$$E_T=\frac{I-I_D}{I_D}=-2\frac{\int f_0(C_D-C_AC_P)Pdv}{\int f_0C_Ddv}. \tag{7}$$

The case where one has complete depolarization for all neutron velocities, i.e., where $P(v)=\frac{1}{2}$, is of special practical interest. To obtain here a simple form for E_T, one must consider that for normal thickness of polarizer and analyzer the factors C_A and C_P will differ only little from unity so that the product $(C_A-1)(C_P-1)$ can safely be neglected. With this simplification expression (7) becomes

$$E_T^*=-\frac{[E_D-(E_A+E_P)]}{1+E_D}, \tag{8}$$

[11] O. Halpern and T. Holstein, Phys. Rev. 59, 960 (1941).

where

$$E_D=\frac{I_D-I_0}{I_0}, \tag{9a}$$

$$E_P=\frac{I_P-I_0}{I_0}, \tag{9b}$$

$$E_A=\frac{I_A-I_0}{I_0} \tag{9c}$$

measure the relative increase of intensity upon magnetization, corresponding to the three previously mentioned cases. It is thus possible, in the case of complete depolarization, to compare directly the effect E_T^* with the independently observable transmission effects (9).

The importance of having polarizer and analyzer very close to magnetic saturation can be seen directly from (8). It follows from the theory of Halpern and Holstein,[11] and has been verified in our previous investigations, that the transmission effect for insufficient saturation is essentially proportional to the total thickness of the traversed magnetized iron. Thus, with d_A and d_P for the thicknesses of analyzer and polarizer, respectively, one has $E_A\sim d_A$, $E_P\sim d_P$, and $E_D\sim(d_A+d_P)$, so that the transition effect (8) vanishes in this approximation and will be greatly reduced as long as the experimental conditions are close to this limit. The fact that Alvarez and Bloch[8] with a transmission effect E_D of 6 percent observed values of E_T which did not exceed 1.5 percent can be quantitatively ascribed to this circumstance.

The maximum value for E_T^* is obtained at complete saturation, where one has for normal thicknesses $E_A\sim d_A^2$, $E_P\sim d_P^2$, and $E_D\sim(d_A+d_P)^2$, and, therefore, for $d_A=d_P$

$$E_T^*=-\frac{1}{2}\frac{E_D}{(1+E_D)}. \tag{10}$$

Actually, this formula for complete saturation is valid even for large thicknesses, where the previously made assumptions do not hold. One has then for $d_A=d_P=d$, $C_A=C_P=\cosh dK$ and $C_D=\cosh 2dK$, where $K=K(v)$ is a function of the neutron velocity. Also, $C_D-C_AC_P=(1/2)\times(\cosh 2dK-1)$, so that for $P(v)=\frac{1}{2}$, and with the definitions (5a) and (9a), one obtains (10) directly from the general expression (7).

It is essential, for a quantitative investigation of neutron resonances, not only to consider the limiting case of complete depolarization, but also to have an insight into the more general situation which one meets in tracing out a complete resonance curve and, hence, to have a theory of the expected line shape which must be tested experimentally. A completely general theory of the line shape, which involves the detailed actual geometry of the field in which the transitions occur, meets with considerable mathematical difficulties. It is sufficient, however, to base the discussion upon a simple geometry which could be used in principle, and which, in practice, closely describes the actual conditions of our experiment.

Disregarding the inevitable slight deviations from homogeneity, we shall consider the constant field H_0 as homogeneous over the distance l of the path where the neutrons are exposed to the oscillating field, and we shall furthermore assume that the oscillating field has a single component at right angles to H_0, with an amplitude H_1 which is constant within and zero outside of l. We consider thus the transitions of the neutrons in a field, given by

$$H_x=H_1\cos\omega t,\quad H_y=0,\quad H_z=H_0. \tag{11}$$

With the gyromagnetic ratio γ_N for neutrons, and using

$$\Delta=\omega-\gamma_N H_0 \tag{12}$$

for the deviation of the applied circular frequency from the resonance value $\gamma_N H_0$, one obtains[6] for the transition probability of neutrons with velocity v

$$P(v)=\frac{\sin^2\left(\frac{l}{2v}(\Gamma^2+\Delta^2)^{\frac{1}{2}}\right)}{1+(\Delta/\Gamma)^2}, \tag{13}$$

where the frequency

$$\Gamma=\frac{\gamma_N H_1}{2} \tag{14}$$

is assumed to be small compared to the resonance frequency $\gamma_N H_0$ (i.e., $H_1\ll H_0$), so that the oscillating field can be replaced by an effective rotating field of magnitude $H_1/2$.[12]

[12] F. Bloch and A. Siegert, Phys. Rev. **57**, 522 (1940).

Substituting (13) into the general expression (7) for the transition effect, one obtains

$$E_T = -\frac{F((\Gamma^2+\Delta^2)^{\frac{1}{2}})}{[1+(\Delta/\Gamma)^2][1+E_D]}, \quad (15)$$

where

$$F(\xi) = \frac{2\int f_0(C_D - C_A C_P)\sin^2(l\xi/2v)dv}{\int f_0 dv}. \quad (16)$$

This function can evidently not be evaluated without knowledge of f_0, C_D, C_A, and C_P in their dependence upon the neutron velocity v. It is possible, however, to determine the function experimentally by measuring the dependence of the transition effect at resonance upon Γ, or through (14) its dependence upon the amplitude H_1 of the oscillating field, since for $\Delta=0$ one has $E_T=-F(\Gamma)/(1+E_D)$. Equation (15) then allows one to obtain the transition effect E_T in its dependence upon Δ. Denoting by $F_0(\Gamma)$ the function F at resonance, one obtains

$$E_T(\Delta,\Gamma) = -\frac{F_0((\Gamma^2+\Delta^2)^{\frac{1}{2}})}{[1+(\Delta/\Gamma)^2][1+E_D]}, \quad (17)$$

which predicts the shape of the resonance line for fixed amplitude of the oscillating field and for varying deviation Δ of its frequency from resonance.

It is seen from (15) and (16) that the simple shape of a resonance line with $E_T \sim 1/[1+(\Delta/\Gamma)^2]$ can be expected only for large values of the oscillating field. Denoting by $\bar{v}$ an average velocity of the neutrons, the term $\sin^2(l\xi/2v)$ in (16) will become rapidly varying and can be replaced by its average value $\frac{1}{2}$ if

$$\Gamma = \frac{\gamma_N H_1}{2} \gg \frac{\pi\bar{v}}{l}. \quad (18)$$

The characteristic value of $\Gamma=\pi\bar{v}/l$ is that for which the neutrons of velocity $\bar{v}$ will with certainty, according to (13), undergo a transition at resonance. With the condition (18) being satisfied one has

$$F = \frac{\int f_0(C_D - C_A C_P)dv}{\int f_0 dv} \quad (19)$$

independently of Δ and Γ, and

$$E_T = \frac{E_T^*}{1+(\Delta/\Gamma)^2}, \quad (20)$$

where E_T^* is the effect observed for complete depolarization of the beam between polarizer and analyzer, which has been previously discussed.

It must be remarked, however, that the condition (18), which leads to the simple line shape (20), is not conducive to a good determination of the resonance frequency, since large values of H_1 or Γ lead at the same time to unnecessarily broad resonance lines. The extreme opposite case $\Gamma \ll \pi\bar{v}/l$, although it would lead to very sharp lines, is likewise unfavorable since it would also lead to an appreciable reduction of the resonance effect and consequently to difficulty in its observation. The optimum condition is obtained for values of H_1 in the neighborhood of

$$H_1 = \frac{2}{\gamma_N}\Gamma = \frac{2\pi\bar{v}}{\gamma_N l}, \quad (21)$$

where, according to (13),

$$P(\bar{v}) = \frac{\sin^2((\pi/2)(1+(\Delta/\Gamma)^2)^{\frac{1}{2}})}{1+(\Delta/\Gamma)^2}, \quad (22)$$

so that a neutron with the average velocity $\bar{v}$ will, with certainty, undergo a transition at resonance, where $\Delta=0$. For this case the analysis of the line shape cannot be carried out with the assumption of a constant F, but requires the use of the more refined formula (15).

The gyromagnetic ratio γ_N of the neutron is measured by determining the resonance value ω^* of the circular frequency ω for which $\Delta=0$, so that from (12)

$$\gamma_N = \frac{\omega^*}{H_0}, \quad (23)$$

and it is worth while to obtain an estimate for the accuracy to be expected in ascertaining the resonance value ω^*. Assuming that the resonance is established merely within the half-width of the line, which is of the order of 2Γ in frequency scale, a measure of the relative accuracy is $a=2\Gamma/\omega^*$ and one has

$$a = \frac{\bar{v}}{l\nu^*} \quad (24)$$

for the optimum value of Γ given by (21) and where $\nu_N^*=\omega^*/2\pi$ is the neutron resonance frequency. Using as characteristic figures for our experimental conditions $\bar{v}=2\times10^5$ cm/sec., $l=10$ cm, and $\nu_N^*=3\times10^7$ sec.$^{-1}$, one obtains from (24) $a=6.7\times10^{-4}$. The accuracy of a crude experiment without any analysis of the line shape would indeed be essentially limited by this number. It is clear, on the other hand, that such an analysis is necessary in a precision measurement; its completion has allowed us, at the same time, to improve appreciably upon the previously mentioned accuracy.

Before entering into a discussion of the finer features caused by the deviations of the actual geometry from the one which has led to (15), we shall give a qualitative derivation of the function $F(\xi)$, defined through (16). It is based upon a simple assumptions that the velocity distribution $f_0(v)$ of the neutrons has the quasi-Maxwellian form $f_0(v)=Av^n\exp(-\beta v^2)$, and that the factor $(C_D-C_AC_P)$ can be considered within the important velocity range to be independent of the velocity. It is particularly this last simplification which is certainly no more than qualitatively justified. With these assumptions one obtains from (16)

$$F(\xi)=-(1+E_D)E_T^*\phi_n(l\xi(\beta)^{\frac{1}{2}}), \qquad (25)$$

where

$$\phi_n(x)=\frac{\int_0^\infty u^n\exp(-u^2)\left(1-\cos\frac{x}{u}\right)du}{\int_0^\infty u^n\exp(-u^2)du}. \qquad (26)$$

The appearance in (25) of the factor E_T^*, representing the transition effect for complete depolarization, arises from the fact that ϕ_n approaches unity for large values of its argument, and that for $\Delta=0$ and large values of Γ, the expression (15) becomes $E_T=E_T^*$.

The function $\phi_n(x)$ has been computed for $n=2$ and $n=3$. The corresponding curves, showing the dependence of E_T on H_1, are plotted in Fig. 10, together with the experimental results. The curves were obtained from ϕ_2 and ϕ_3 by a suitable choice of the scale parameters β and E_T^*. They show essentially the same characteristic behavior, i.e., a quadratic dependence for very small values of the argument followed by a rather large interval, in which they are almost linear with x; an outspoken maximum is reached with $\phi_2=1.46$ for $x=3.3$ and $\phi_3=1.54$ for $x=3.8$, followed finally by a strongly damped oscillation around the asymptotic value $\phi=1$. The fact that the experimental results show the characteristic features of the calculated functions is most gratifying; the complete fit within the experimental error, obtained particularly for $n=3$, must, however, be considered as accidental. It shall be remarked that a Fourier transformation of (16) allows one, in principle, to determine the velocity dependence of $f_0(C_D-C_AC_P)$ in the integrand of (16) from the experimentally determined function $F(\xi)$. It seemed more convenient, however, to follow the opposite procedure, i.e., to show that a not unreasonable assumption about the velocity dependence leads to a sufficient agreement with the experiment.

While the preceding analysis offers the essential features which enter in a discussion of the magnitude of the effect and of the line shape, it is not sufficiently rigorous to be used as a perfect guide for the establishment of the resonance frequency. Deviations of the actual field in which the transitions occur from the form assumed in (11) require certain corrections which have to be considered.

A first correction arises if H_1, the amplitude of H_x, although constant in time is not constant in space so that, dependent upon its velocity, a neutron is exposed to a field with a time-dependent amplitude of its x component. It is, of course, possible in this case to obtain the transition probability $P(v)$ through a numerical integration by inserting the measured local variation of H_1, but it cannot be expected, in general, to be of any simple form. One can show, however, that the formulae (13) and (15) still remain valid in the special case of resonance ($\Delta=0$) if the quantity H_1l is replaced by $\int_0^l H_1dx$. A simple and, for practical purposes, sufficient correction for the case $\Delta\neq0$ can be obtained by replacing H_1 by its average value and correspondingly by writing

$$\Gamma=\frac{\gamma_N}{2l}\int_0^l H_1dx$$

in place of (14). Apart from these minor cor-

rections the expression (15) will not be essentially invalidated by the spatial variation of H_1. Particularly, the important feature that the line is symmetrical around the resonance value $\Delta=0$ can be seen to be unaffected by this variation.

A more serious correction arises if the assumption of a vanishing y component of the oscillating field made in (11) is not satisfied, and particularly if this component shows likewise a spatial variation. Writing generally,

$$H_x=H_1\cos(\omega t+\delta_1),\quad H_y=H_2\cos(\omega t+\delta_2),\quad H_z=H_0. \tag{27}$$

Hence, both H_1 and H_2 must be considered, for a neutron with given velocity, to be functions of time. The phases δ_1 and δ_2 might differ as a result of energy-dissipating elements. However, the high Q value of our coil arrangement ($Q\sim100$) justifies the assumption of equal phases. The effect of the field (27) upon a moving neutron can then be expressed by the modification of (11),

$$H_x'=H_1'\cos\omega t,\quad H_y'=0,\quad H_z'=H_0\mp\frac{d\theta}{dt}\Big/\gamma_N, \tag{28}$$

where $H_1'=(H_1^2+H_2^2)^{\frac{1}{2}}$, and $\theta=\arctan(H_2/H_1)$. The time derivative of θ in (28) is to be taken in a system moving with the neutron. It appears with the $-$ or $+$ sign, depending upon whether the sense of rotation of the Larmor precession which the neutron moment performs in the field H_0 is the same or opposite to that corresponding to a positive variation of θ.

The effect caused by the variation of θ is seen to be the same as that caused by an additional field in the z direction superimposed upon H_0. As long as θ can be considered as a linear function of the time, it causes the resonance curve to be shifted by the amount $d\theta/dt$ in frequency, thereby causing an error in the determination of the resonance value. A non-linear variation, on the other hand, has the same effect as an inhomogeneity of the field H_0, since both will manifest themselves in the frame of reference of the neutron as a time variation of the effective z component H_z'.

It is clear that such an inhomogeneity will, in general, destroy the symmetry of the resonance curve around any point. As far as the field H_0 is concerned it is important to reduce the actual inhomogeneity as much as possible by careful shimming, both for minimizing this undesirable asymmetry and also in view of improving the total accuracy of the measurement. In order to eliminate any possible error attributable to the variation of θ, it is essential to observe that it appears in (28) with the opposite sign upon reversal of the field H_0, and thereby upon reversal of the sense of rotation in which the neutron precession occurs. By observing the transition effect twice, i.e., leaving the magnitude of H_0 unchanged but reversing its polarity, any falsifying shift of the resonance curve, as well as its asymmetry due to this cause is thus avoided. It should be remarked that similar to the feature used by Millman[13] to determine the sign of nuclear moments, the sign of the neutron moment can be ascertained from the direction in which an observable shift of the resonance curve takes place upon reversing the polarity of H_0.

By applying the previous considerations to a sufficient set of experimental data it is possible to establish the resonance value ω^* of the applied frequency well within the width of the resonance line and, hence, to determine with high accuracy the gyromagnetic ratio γ_N of the neutron from (23) in terms of the field H_0. The conventional methods of determining this field are, however, inadequate to obtain a precision which appreciably exceeds the order of one percent. It was, in fact, this circumstance which limited to a large extent the accuracy of the original result obtained by Alvarez and Bloch.

The method of nuclear induction is ideally suited to overcome this limitation in the measurement of the neutron moment. As pointed out in the original paper,[14] it was indeed the search for a suitable method of field comparison which led to the thought of nuclear induction, and preparations to apply it to the determination of the neutron moment were announced at the same time.

The essential improvement over the earlier methods of determining the field lies in the direct comparison of the conditions for reso-

[13] S. Millman, Phys. Rev. **55**, 628 (1939).
[14] F. Bloch, Phys. Rev. **70**, 460 (1946).

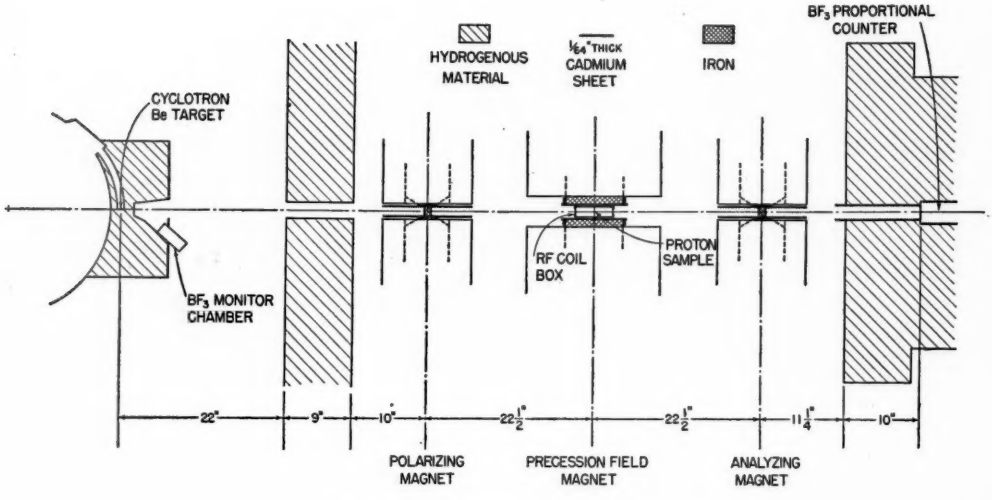

FIG. 1. Experimental arrangement.

nance observed simultaneously for neutrons and protons. By placing a sample containing protons into the same field H_0 in which the neutron transitions occur and by observing the proton resonance frequency $\nu_P=\omega_P/2\pi$ through nuclear induction, one obtains in analogy to (23) for the gyromagnetic ratio of the proton

$$\gamma_P=\frac{\omega_P}{H_0} \tag{29}$$

and, therefore, by division of (23) and (29)

$$\frac{\gamma_N}{\gamma_P}=\frac{\omega^*}{\omega_P}=\frac{\nu_N^*}{\nu_P}. \tag{30}$$

The determination of the gyromagnetic ratio of the neutron in terms of that of the proton is thus immediately obtained by a measurement of the ratio of two resonance frequencies ν_N^* and ν_P which can be carried out with high accuracy.

The actual value of H_0 does not enter at all in this determination. In fact, a stabilizing device was used in our experiment which held H_0 constantly at the value required for proton resonance so that the condition (29) was constantly and automatically fulfilled while establishing the neutron resonance (see below).

III. APPARATUS

Figure 1 shows the arrangement of the apparatus used in our present measurements. Thermalized neutrons emerge from a $2\frac{1}{2}''\times2\frac{1}{2}''$ hole in a block of paraffin surrounding the target of the cyclotron. They are collimated by a $2''\times2''$ opening in the 9″ thick hydrogenous wall in front of the target and enter and leave the polarizing magnet through cadmium channels $5\frac{3}{4}''$ long with openings $1\frac{1}{2}''\times2''$. These channels sit directly in front and in back of the polarizing iron plate. After passing through the polarizer, the neutrons enter the gap of the magnet for the constant precession field H_0. A copper box containing the coil for the radiofrequency field is located between the poles of this magnet. The neutrons enter and leave this box through copper windows of 5-mil thickness which, as experiments showed, have no noticeable effect on the state of the polarization. Front and back of the box are covered with cadmium diaphragms with $\frac{3}{4}''\times1\frac{1}{2}''$ openings, which prevent passage of the neutrons very close to the windings of the radiofrequency coil. While in the arrangement of Alvarez and Bloch the radiofrequency coil was a long solenoid with its axis perpendicular to the neutron beam, we used a shorter coil surrounding the beam. This choice results in a less homogeneous radiofrequency field, but it has the great advantage of avoiding neutron absorption in the coil windings. The axis of the precession field magnet is $21\frac{1}{2}''$ from the axes of both the polarizer and analyzer. The neutrons enter and leave the analyzer through an arrangement of cadmium channels similar to the one used for the polarizer. Finally, the neutrons enter the detector, located

at a distance of about 16″ from the analyzing magnet. The detector for the present measurement was identical with the one used in the previous work of Bloch, Condit, and Staub,[10] except that enriched boron trifluoride, containing 96 percent B_{10}, furnished by the Atomic Energy Commission, was used. This filling resulted in an increase in counting efficiency from about 20 to 70 percent for thermal neutrons (2200 m/sec.). The detector is, therefore, not shallow for most polarized neutrons. It was imbedded in a large block of paraffin surrounded by oil-filled cans. A shield of $\frac{1}{4}$″ of boron carbide and cadmium enveloped the detector with the exception of an opening of 2-in. diameter at the front face.

With the two blocks of iron, each 1.9 cm thick, in the gaps of polarizing and analyzing magnet, the cadmium ratio of the recorded neutron beam was about 4. This ratio was regularly measured by placing a piece of cadmium sheet, 1/64″ thick and just slightly larger than the cross section of the beam, over the opening of the exit diaphragm of the radio frequency coil box.

A neutron beam monitor, using an integrating boron trifluoride chamber and a circuit described earlier,[15] was employed to change the conditions of the experiment in intervals of equal numbers of primary slow neutrons. The monitor chamber was located as close as possible to the region where the neutron beam originated, and the chamber was operated at a collecting potential of 5000 v. Checks showed only a very slight dependence of the monitor performance on variations in the position of the target spot as caused by changes in the deflecting voltage or resonance condition of the cyclotron. Saturation of the ionization current was quite high. For a change in deuteron beam intensity from 5 to 15μ amp., the number of counts per monitor interval increased by only 7 percent. All final measurements were taken with a beam current of 7μ amp., and this current was carefully kept as constant as possible.

The pulses of the detector were fed into a conventional amplifier, discriminator, and scale of 16, from which the output pulses alternately operated one of two different registers during each monitor interval.

[15] E. Fryer and H. Staub, Rev. Sci. Inst. **13**, 187 (1942).

The magnets for polarizer and analyzer are identical. One of them had been previously used for the measurements of polarization effects.[10] The plane pole faces of these magnets have an area of 2″×3″ tapered down by a 60° angle from pole pieces of 6-in. diameter. The gap is $1\frac{1}{2}$″ wide. The polarizing and analyzing blocks consisted, as in the previous work, of hot-rolled steel $1\frac{1}{2}$″×2″ and $\frac{3}{4}$″ thick in the direction of the neutron beam. For all the present experiments the magnets were operated at a magnetizing current which produces a field of 11,900 gauss. The direction of magnetization was always the same for polarizing, analyzing, and precession field magnet so as to avoid any region of weak field in which the polarization of the neutrons could be changed through non-adiabatic transitions.

The currents of polarizer and analyzer magnets, both about 34 amps., were kept constant to about 2 percent by manual control. Since the contribution of these two magnets to the precession field ($\sim 10^4$ gauss) was only about 100 gauss, a two percent variation of the current would, on account of saturation, produce only a variation of $\frac{1}{2}$ gauss. Moreover, the control mechanism which was employed for the precession field would also take care of these variations provided that they were uniform over the region occupied by the proton sample and the radio-frequency field. It was indeed verified that such small variations did not affect the necessary homogeneity of the precession field H_0.

The precession field magnet has circular plane pole faces of $7\frac{13}{16}$-in. diameter and a $1\frac{3}{4}$-in gap width. Circular brass plates $\frac{1}{16}$″ thick, which carried the system of shims to correct the field, were clamped onto the pole pieces. Two carefully machined brass spacers were tightly fitted between the two pole faces. They very effectively prevented major changes of the gap configuration upon magnetization of the pole pieces. The magnet was energized by two coils, each having 17,000 turns. A current of about 1.4 amp. was necessary to produce a field of about 9800 gauss (corresponding roughly to a Larmor frequency of the neutrons of 29 Mc, and it was supplied by a 3000 v full-wave, three-phase rectifier. The useful region of the precession field in which transitions can occur, defined by the length of

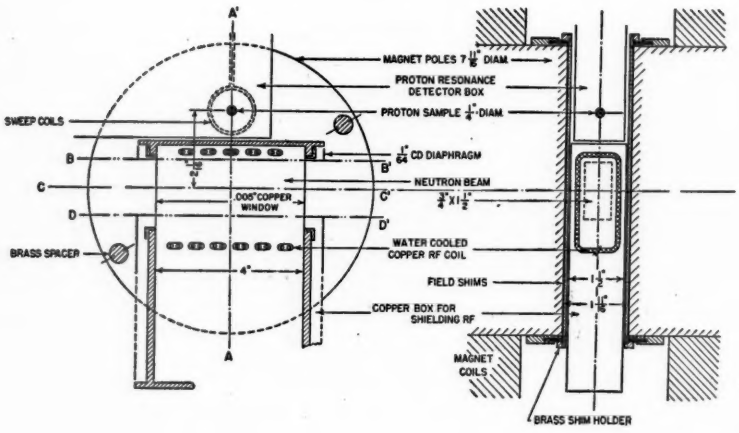

FIG. 2. Gap of precession field magnet, radiofrequency coil, and proton sample.

the copper box and the aperture of the cadmium diaphragms, was a volume 4″ long in the direction of the neutron beam, $\frac{3}{4}$″ wide across the gap, and $1\frac{1}{2}$″ high, and symmetric with respect to the center of the gap. The proton sample was approximately of spherical shape about $\frac{1}{4}$″ in diameter, with its center located $2\frac{1}{16}$″ above the axis of the magnet (Fig. 2). Two small coils which were mounted coaxially with the proton sample on the walls of the box containing the sample and the rectifier, provided the modulation for the proton resonance. For measurements of the magnetic field (see below), the modulation frequency was 60 c.p.s. with an amplitude of about 3 gauss. For the actual measurements of the neutron resonance, 500 c.p.s. modulation at an amplitude of 0.3 gauss was employed. The effect of this alternating field in the region of the neutron passage is, of course, completely negligible. The magnet current passed through 8 parallel-connected 304 TH tubes in series with the magnet windings. The grids of these tubes were controlled by the output voltage of a differential amplifier with a gain of about 10,000. This differential amplifier compared a constant voltage derived from dry cells with the voltage drop of the magnet current across a 30-ohm resistor. The stabilization of the current was such that for a line-voltage fluctuation of 10 percent the field varied about 3 gauss at 10,000 gauss. This manner of stabilization was employed whenever measurements of the inhomogeneities of the precession field were performed. For the actual measurements of the neutron resonances, an additional stabilizer, designed and built by M. Packard,[16] was used. It injects into the differential amplifier a voltage derived from the proton resonance signal in such a manner as to keep the magnetic field at resonance with the proton excitation frequency. With this additional stabilization, the field varied about 0.02 gauss for a 10 percent line-voltage change, and, in addition, was stabilized by a factor of 150 against any other causes of field variation, such as temperature and extraneous fields.

The accuracy of the present experiment is largely determined by the degree of homogeneity of the precession field over the region occupied by the proton sample and the region in which neutron transitions can occur. Consequently, a great deal of time and effort was spent in making this field as perfect as possible.

Inhomogeneities of the field were measured by observing the change of the proton resonance frequency upon the displacement of the proton sample from the center of the magnet to the point under investigation. For these measurements the magnet current was stabilized in the manner described above. The proton resonance obtained by 60-cycle field modulation was observed on the screen of a cathode-ray tube, and the frequency adjusted until the maximum of the resonance peak coincided with a reference line. The accuracy of this procedure is limited mainly by the unavoidable fluctuations of the field caused by the finite stabilization against line-voltage fluctuations. At points near the outer boundaries of the useful region of the field, the proton signal becomes somewhat wider, since the

[16] M. E. Packard, Rev. Sci. Inst. **19**, 435 (1948).

field is less homogeneous there than at the center. The accuracy of this measurement was about $\frac{1}{4}$ gauss for fields of about 10,000 gauss. All measurements were made with the fields of polarizing and analyzing magnets on so as to correct also for inhomogeneities caused by these fields. Within the above-stated accuracy, their contribution to the H_0 field was uniform over the useful region.

It was, of course, to be expected that a region of about $4'' \times 2''$ within the gap of the circular pole pieces of $7\frac{13}{16}$-in. diameter would not be nearly homogeneous enough for our measurements. Even if the pole pieces were perfectly symmetric and uniform, the fringing of the field would be considerable. Suitable shims were, therefore, mounted on the brass plates which held them directly against the pole faces. The first step in homogenizing the field consisted in using 90-degree sectors of annular rings cut from 5-mil shim steel, and of suitable radii so as to produce a slight increase of the field strength with increasing distance from the center. The second step was to place strips of 1-mil brass foil electroplated with nickel to thicknesses up to 0.3 mil wherever the field showed a dip. Every step was, of course, carefully checked by moving the proton sample along the four directions marked *ABCD* in Fig. 2 and by measuring the deviation of the resonance frequency from its value at the center of the magnet. A typical plot of the field variations along these four directions after completion of the shimming is shown in Fig. 3. The deviations given in kc represent a sixth of the actual frequency variation, since all proton frequencies were measured at one-sixth of the actual frequency (see below). Thus, a variation of 1 kc in Fig. 3 represents a variation of about 1 part in 7000 or about 1.4 gauss. Correction of the field was continued until no single point deviated by more than 0.5 kc, and the midpoint of the proton sample ($2\frac{1}{16}''$ vertically above the center) deviated not more than 0.2 kc from the average value. The largest deviations were always encountered at the end points ($\pm 2''$ from center) of the horizontal directions *BCD*, where their effect on the measurements is considerably reduced by the fact that at these points the effective radiofrequency field is quite small.

The rather severe requirements for the homogeneity of the precession field made it necessary to correct the field separately for every value of H_0 at which measurements were taken, since even changes of 5 percent in H_0 changed the configuration of the field entirely on account of saturation of the pole pieces and shims. A further complication, which was rather troublesome, was caused by variations of the field configuration with time. Although the magnet current and the cooling water were left on continuously, inhomogeneities developed over periods of several hours. It was found that the original situation could always be regained by alternately raising and lowering the current through a well defined cycle. The field configuration was, therefore, checked during the measurements at intervals of three hours and readjusted in the above manner if inhomogeneities could be detected. These field measurements also provided the information needed to correct the data for possible small differences in the value of the precession field H_0 for neutrons and protons.

The determination of the ratio of the resonance frequencies of protons and neutrons is greatly facilitated by the fact that the ratio of the neutron and proton magnetic moments is approximately $\frac{2}{3}$. The radiofrequency field of the protons was excited by the sixth harmonic of its master oscillator with frequency $\nu_P' = \nu_P/6$. Similarly, the fourth harmonic of another master oscillator with frequency $\nu_N' = \nu_N/4$ was used for the radiofrequency field of the neutrons. If one denotes the difference in the frequencies of the two master oscillators by $\Delta\nu_N'$, which has the

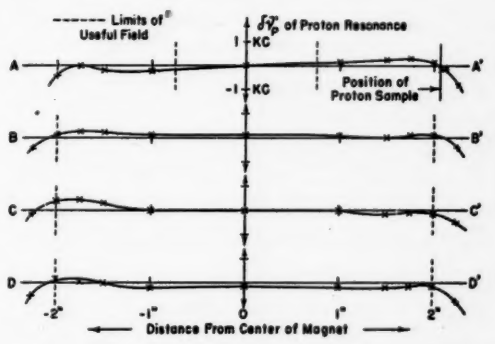

FIG. 3. Typical plot of the deviation of H_0 from value at center measured along the four directions *A*, *B*, *C*, *D* of Fig. 2. Deviations $\delta\nu_P'$ are measured in terms of one-sixth of the corresponding proton resonance frequency.

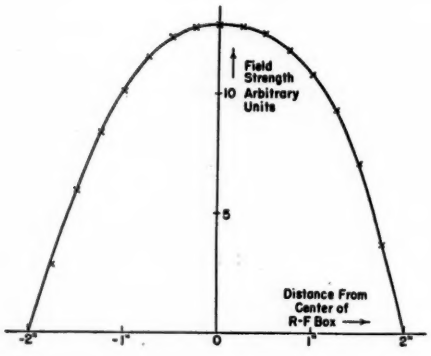

FIG. 4. X component (direction of propagation of neutrons) of the radiofrequency field.

value $\Delta\nu_N'^*$ at the neutron resonance, and by ν_P', the frequency of the proton master oscillator which was always set for the proton resonance, the desired ratio is given by

$$R=\frac{|\mu_N|}{\mu_P}=\frac{\nu_N^*}{\nu_P}=\frac{2}{3}\left(1+\frac{\Delta\nu_N'^*}{\nu_P'}\right). \qquad (31)$$

It follows from the approximately known values of the two moments that the relative error in R is only about one-fortieth of the relative error of $\Delta\nu_N'^*/\nu_N'$. The two frequencies $\Delta\nu_N'$ and ν_P' were measured with a General Radio combined heterodyne-frequency meter and crystal-controlled calibrator. This device produces the fundamental and the harmonics of a crystal-controlled frequency of 100 kc as well as of frequencies exactly one-fifth and one-tenth of this basic frequency. A second generator with continuously variable frequency can be set to any desired frequency by visual interpolation or with the aid of an interpolation meter. This secondary frequency can thus be adjusted to zero beat with the unknown external frequency. From the working principle of the apparatus, it is apparent that the fundamental crystal frequency does not enter in our measurements, since it is only the ratio of two frequencies which determines R. In terms of the errors $\delta\Delta\nu_N'^*$ of $\Delta\nu_N'^*$ and $\delta\nu_P'$ of ν_P', the relative error in the ratio R of the magnetic moments is given by

$$\frac{\delta R}{R}=\frac{\Delta\nu_N'^*/\nu_P'}{1+\Delta\nu_N'^*/\nu_P'}\left(\left(\frac{\delta\Delta\nu_N'^*}{\Delta\nu_N'^*}\right)^2+\left(\frac{\delta\nu_P'}{\nu_P'}\right)^2\right)^{\frac{1}{2}}. \qquad (32)$$

$\nu_P'\cong 7$ Mc was determined to within 1 kc, and $\Delta\nu_N'^*\cong 200$ kc was obtained by beating ν_N' and ν_P' and measuring this beat frequency with the above-described frequency meter to about 0.2 kc. The value of $\Delta\nu_N'$ was checked continuously and kept at zero beat with the frequency meter by manual adjustment of ν_N'. The proton frequency ν_P' was checked at frequent intervals during all measurements. Since $(\delta\nu_P'/\nu_P')^2\ll(\delta\Delta\nu_N'^*/\Delta\nu_N'^*)^2$ and $\Delta\nu_N'^*/\nu_P'\ll 1$, one can, to a very good approximation, replace (32) by

$$\frac{\delta R}{R}=\frac{\delta\Delta\nu_N'^*}{\nu_P'}. \qquad (33)$$

With the above figures this number amounts thus to 1/35,000.

The radiofrequency generator and receiver for the protons are of the usual design and are described elsewhere.[16] The generator for the neutron radiofrequency field consisted of an electron-coupled master oscillator with continuously variable frequency from 7 to 8 Mc, followed by a buffer and output stage, employing the second and fourth harmonics, respectively. The output stage is capable of delivering about 700 watts through a coaxial line and impedance-matching network to the coil. This coil (Fig. 2) was water cooled and consisted of 5 turns of $\frac{7}{16}''\times\frac{1}{8}''$ copper tubing wound with a rectangular cross section $2\frac{3}{8}''$ by $1\frac{1}{8}''$, and an over-all length of $3\frac{1}{2}''$. It was completely enclosed in a copper box 4" long, located, as shown in Fig. 2, between the magnet poles. A tap at a short distance from

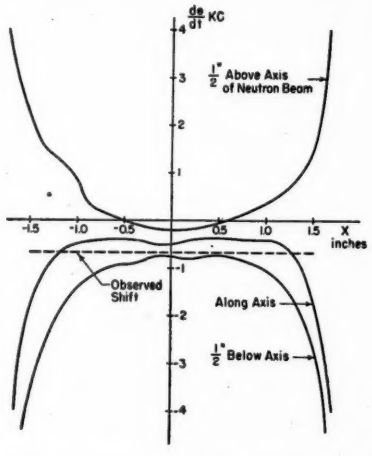

FIG. 5. Angular velocity $d\theta/dt$ of oscillating field H_1 as experienced by neutrons moving at a velocity of 2.2×10^5 cm sec.$^{-1}$ along the axis of the neutron beam and $\frac{1}{2}''$ above and below the axis, respectively.

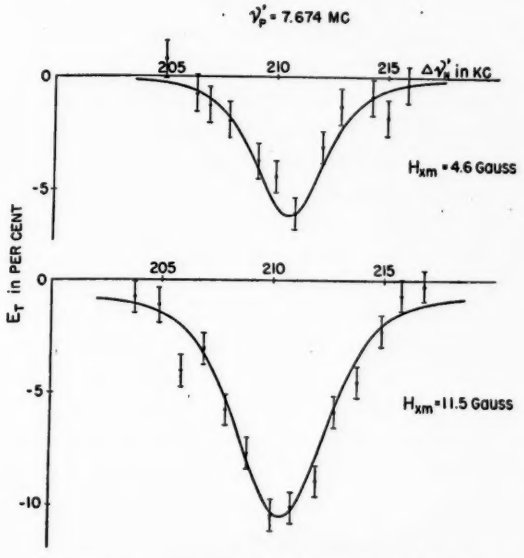

FIG. 6. Neutron resonances observed at $\nu_P' = 7.674$ Mc. Solid curves computed from curve of Fig. 10.

the grounded end of the coil served as a connection for a radiofrequency current meter.

The radiofrequency magnetic field was carefully calibrated and its configuration measured, by means of a small $\frac{1}{4}$-in. diameter search coil connected to a radiofrequency voltmeter. The coil was introduced through a small hole in the window of the casing. The distribution of the radiofrequency field component in the x direction (direction of propagation of neutrons) along the axis of the neutron beam is shown in Fig. 4. As expected, the field drops rather rapidly from its maximum value H_{xm} at the center to zero at the walls. No great variation of this distribution throughout the area occupied by the neutron beam was found. As pointed out in Section II, a serious asymmetry and shift of the resonance curve can be caused if the moving neutrons encounter an effectively rotating field perpendicular to H_0. This shift can be expressed as an effective change of H_0 by means of (28). The shift of the resonance frequency caused by this effect was measured in the most obvious manner (see Sections II and IV) by inversion of the precession field. However, in order to ascertain whether the determined shift is compatible with the actual distribution of H_x and H_y, the latter component was also measured as a function of x along the axis of the neutron beam and along two parallel lines $\frac{1}{2}''$ above and below the axis. From these data the quantity $d\theta/dt$, representing the effective shift of the resonance frequency for neutrons of an average velocity, was computed and is represented in Fig. 5 as measured along the three lines in the x direction. The frequencies refer again to one-quarter of the actual neutron resonance frequencies. The average velocity $\bar{v}$ was determined from the measurements of the dependence of the resonance effect on the amplitude of the radiofrequency field. Assigning a transition probability of unity for the average velocity neutrons at the maximum resonance effect, $\bar{v}$ is given by the relation (see Section II)

$$\bar{v} = \frac{\gamma_N}{2\pi} \int_0^l H_1 dx. \tag{34}$$

Figure 5 shows clearly that with our experimental arrangement the average frequency shift differs markedly from zero. This is easily understood, since the axis of the neutron beam is located above the axis of the radiofrequency coil, and since, furthermore, the shielding is not sym-

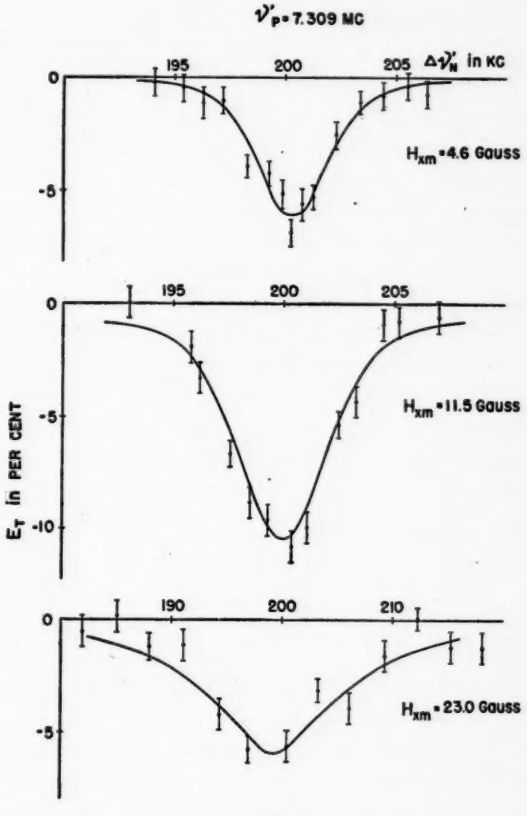

FIG. 7. Neutron resonances observed at $\nu_P' = 7.309$ Mc.

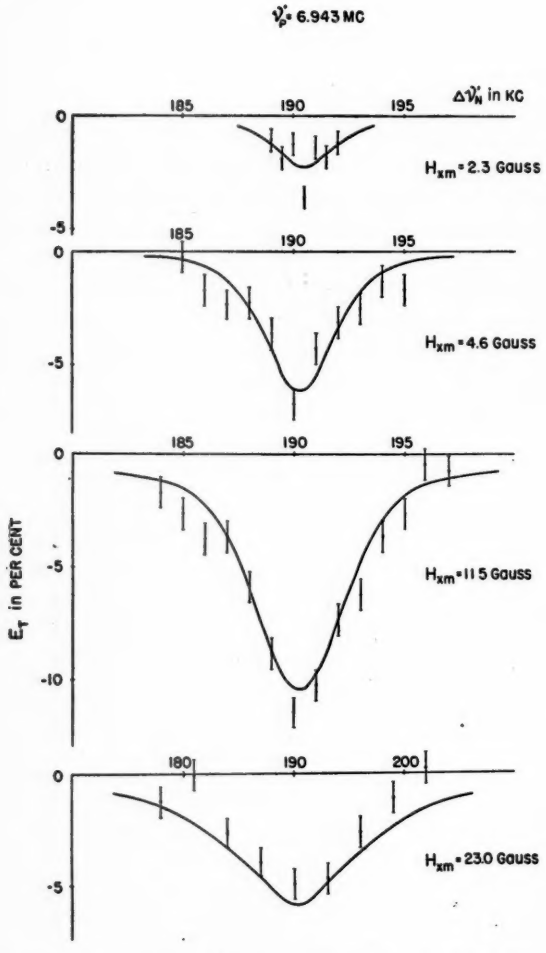

FIG. 8. Neutron resonances observed at $\nu_P' = 6.943$ Mc.

metric and consequently diverts the magnetic lines of force asymmetrically with respect to the axis. Also, as pointed out earlier, if one takes the geometrical features of the arrangement into account, the direction in which the shift occurs upon changing polarity of the precession field is directly connected with the sign of the neutron moment.

IV. MEASUREMENTS

All measurements were performed with analyzer and polarizer operating at the highest possible field of about 11,900 gauss, corresponding to a magnetization within less than 0.02 percent of saturation. Both oscillators were always turned on several hours before the start of the measurements. With this precaution only small and slow drifts of the frequencies were encountered. The inhomogeneities of the H_0 field were checked as previously mentioned at regular intervals. The performance of the proton-controlled regulator for the precession field was continuously checked with the aid of a cathode-ray oscilloscope, as described by Packard.[16] Great care was taken to have always a pattern of pure second harmonic, or zero-average control voltage. Any deviation was corrected manually by changing the current setting of the automatic current control. It is estimated that no deviation from exact proton resonance amounting to an error in $\Delta\nu_N'$ of more than 0.1 kc was permitted. All measurements of neutron resonances were performed by counting detector pulses for each monitor interval with the neutron radiofrequency field alternately on and off. Each interval lasted for about 80 sec. After 20 intervals, conditions were usually changed by varying either the magnitude of the radiofrequency field or the neutron frequency, depending on the type of measurements. During the measurements of the neutron resonances, frequencies were changed in such a manner as to measure alternately at frequencies located approximately symmetrical to the expected resonance frequency. For each group of measurement the background was determined several times by placing a cadmium sheet over the exit diaphragm of the radiofrequency coil box. In every case, sufficient data were taken to make the contribution from the background measurement to the statistical error negligible. Cadmium ratios were always measured with the radiofrequency field alternately turned on and off. As it was expected, the neutron intensity recorded with the cadmium shield intercepting the beam did not exhibit any resonance feature. Likewise, no transmission effects could be detected in this case.

The measurement of the neutron resonance dip was carried out at three different proton frequencies $\nu_P' = 7.674$ Mc, 7.309 Mc, and 6.943 Mc. These frequencies were chosen because with these values for ν_P', $\Delta\nu_N'$ at resonance has values very near to 210, 200, and 190 kc, respectively: consequently, frequencies close to resonance could be determined without a large interpolation between two values of the crystal oscillator of the frequency meter. At every one of these frequencies several resonance curves were measured

using different values of the radiofrequency field. Figure 6 shows the results at $\nu_P' = 7.674$ Mc for peak values of $H_{xm} = 11.5$ and 4.6 gauss at the center of the coil. Denoting by I_{on} and I_{off} the counting rates with and without the applied radiofrequency field, and by I_{Cd} the counting rate with cadmium intercepting the beam, the ordinate represents the quantity

$$E_T = \frac{I_{on} - I_{off}}{I_{off} - I_{Cd}}. \tag{35}$$

The errors indicated are mean errors. The measurements were taken at frequency intervals of 1 kc and corrected for any measurable difference (>0.1 kc) of H_0 at the center and at the proton sample. The solid curves shown in Fig. 6 were calculated according to the procedure outlined in Sections II and V. Since the absolute values of H_1 involve the knowledge of the area of a small radiofrequency search coil, their accuracy is probably about 20 percent. No correction for the frequency shift caused by the spatial variation of the radiofrequency field was made for this and the following figures. Figure 7 shows the results of the measurements at $\nu_P' = 7.309$ Mc taken with radiofrequency fields of $H_{xm} = 23.0$, 11.5, and 4.6 gauss. These measurements were actually the first ones performed, and the H_0 field was not nearly so homogeneous as in the later measurements. Consequently, corrections for deviations of as much as 0.8 kc had to be applied for differences of H_0 for neutrons and protons. This caused the uneven spacing of the measured points. We, therefore, believe that these data are considerably less reliable than the ones at 7.674 and 6.943 Mc. Again, the solid curves were calculated as before.

Figure 8 finally shows the results of the measurements at $\nu_P' = 6.943$ Mc. For this proton frequency the H_0 field was almost perfect; thus no correction at all had to be applied for field differences, and it was felt that with this field the most reliable data were obtained. Consequently, data were taken for $H_{xm} = 23.0$, 11.5, 4.6, and 2.3 gauss, as shown in Fig. 8. Furthermore, an experiment to determine the shift of the resonance maximum caused by the presence of the H_y component of the radiofrequency field was performed, as indicated in Section II, by reversing the polarity of the precession field. Upon reversal of the polarity, and after raising and lowering the magnet current according to the adopted procedure, it was found that no additional shimming was required. At the same time, the directions of polarizing and analyzing fields were inverted so as to have field reversal along the whole neutron path. The two measurements were taken with a radiofrequency field of 11.5 gauss, a value very near to that for which the maximum resonance effect occurs. The results are shown in Fig. 9. The points labeled "positive field" are those taken with the field in the same direction as for the preceding measurements. The points labeled "negative field" are those taken with the opposite field direction. The figure shows clearly a displacement between the two sets of data corresponding to about 1.3 kc. This difference represents, of course, twice the actual shift. The observed shift of 0.67 kc is indicated in Fig. 5 and is seen to be compatible with that expected from the measurements of the spatial variation H_x and H_y.

A check was performed to ascertain whether the sign of this shift was in agreement with the negative sign of the neutron magnetic moment. This was done by determining the relative orientations of the precession field and the magnetic field of the cyclotron magnet. The sense of rotation of the positive ions in the cyclotron is known from the arrangement of the deflector. It follows from the geometrical arrangement that, in the average, the lines of force of the neutron radiofrequency field, $\frac{1}{2}$ inch below the axis of the beam, curve downwards at the ends. The sense of rotation of the radiofrequency field thus seen

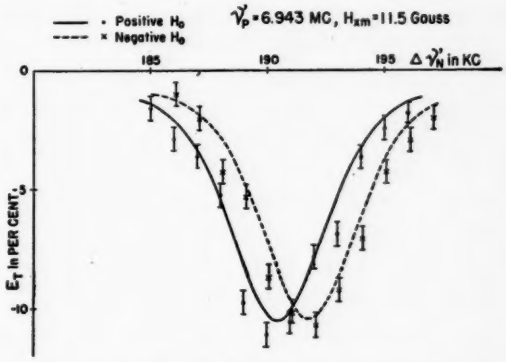

FIG. 9. Shift of resonance maximum caused by reversal of direction of precession field.

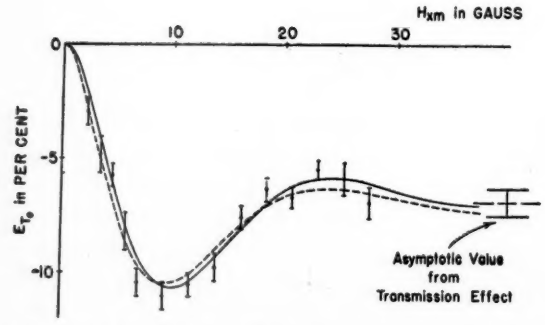

FIG. 10. Transmission effect at resonance *versus* amplitude of radiofrequency field. Values of H_1 are measured by H_{xm}, the x component of H_1 at center of coil. Solid curve: best fit obtained with $v^3\exp(-\beta v^2)$ distribution. Dotted curve: best fit obtained with $v^2\exp(-\beta v^2)$ distribution.

by the moving neutrons and the direction of the observed shift were indeed found to indicate the negative sign of the neutron moment.

As shown in Section II, the shape of the neutron resonance dips can be predicted (assuming homogeneity of H_0) if the dependence of E_T at resonance on the amplitude H_1 of the radiofrequency field is known (cf. (15) and (16)). Since the experimental results certainly do not exhibit a simple relation between H_1 and the observed width of the resonance dips, the values E_{T_0} of E_T at resonance were carefully measured over the full available region of H_1 measured in terms of H_{xm}. The resonance frequencies for these experiments were obtained by inspection from the preceding measurements. Data were taken at the three proton resonance frequencies. The combined results are shown in Fig. 10. The errors are the mean statistical errors increased by an amount corresponding to a possible error $\delta\nu_P'$ in the resonance frequency of 0.5 kc. Whereas the dependence of E_{T_0} on H_{xm} would obey a simple $\sin^2$ law if the neutrons were monoenergetic, the results show clearly the rapid damping and asymptotic approach to a finite value for a sufficiently large radiofrequency amplitude corresponding to a uniform transition probability $\frac{1}{2}$ for all neutrons of different velocity. This asymptotic value E_T^* is related by expression (8) to the three transmission effects E_D, E_A, E_P, which were measured directly several times. In addition, a check measurement of the quantity E_D-E_A was performed by leaving the analyzer magnetized and observing the intensity change upon magnetization of the polarizer. All these measurements were consistent and gave:†

$$E_A=E_P=(6.3\pm0.3)\text{ percent} \tag{36}$$

and

$$E_D=(21.1\pm0.5)\text{ percent.} \tag{37}$$

The asymptotic value E_T^* is, therefore,

$$E_T^*=(-6.9\pm0.6)\text{ percent,} \tag{38}$$

as indicated in Fig. 10. The observed and calculated value of the asymptotic effect are in good agreement. The fact that the proper and quantitative relation between the single-transmission effects and the double-transmission resonance effect could be established must be considered as an important factor in evaluating the reliability of the data. The solid curve in Fig. 10 represents the best fit with $f_0(v)=Av^3\exp(-\beta v^2)$ (cf. Section II), the dotted one with $f_0(v)=Av^2\exp(-\beta v^2)$.

A last series of measurements was undertaken to ascertain that within a region extending on both sides of the established resonance over a one percent range in frequency scale no other resonance dips of real, spurious, or instrumental nature could be found. Measurements were taken at a proton frequency $\nu_P'=7.309$ Mc, with a radiofrequency field of 11.5 gauss from $\Delta\nu_N'=133$ kc to $\Delta\nu_N'=267$ kc in steps of 6 kc, which is approximately the half-width of the previously observed resonance dip. The results of these measurements are shown in Fig. 11. Outside the resonance dip at 200 kc none of the observed points shows a deviation from zero towards negative values by more than about (1 ± 0.7) percent, or $\frac{1}{10}$ of the resonance maximum. It can, therefore, be safely stated that no other resonance dip with an intensity of more than $\frac{1}{3}$ of the observed main dip can be present within the explored region.

V. RESULTS

As pointed out in Section II, it is not possible to predict the exact dependence of E_{T_0}, the value of the transition effect at resonance, on the value of H_1 without the complete knowledge of the dependence of C_D, C_A, C_P, and f_0 upon the

† It should be noted that the values of the transmission effects are smaller than those previously quoted (see reference 10). These data were taken with the same arrangement but with the proportional counter filled with ordinary BF_3. The counter used in the present measurements favors fast neutrons and consequently the transmission effects are somewhat smaller.

velocity v. However, it was tried to match the observed points to a curve computed under reasonable assumptions. For this purpose C_D and $C_A C_P$ in expression (16) were replaced by their average values, such that:

$$E_{T0}=E_T^*\frac{2\int_0^\infty f_0(v)\sin^2\left(\frac{l}{2v}\Gamma\right)dv}{\int_0^\infty f_0(v)dv}. \quad (39)$$

For $f_0(v)$, the two most obvious functions $f_0(v)=Av^2\exp(-\beta v^2)$ and $f_0(v)=Av^3\exp(-\beta v^2)$, were chosen and the expressions for $E_{T0}(H_1)$ integrated numerically. The appropriate values of β and E_T^* were determined by the best-fitting curves, as shown in Fig. 10. It should be emphasized, of course, that actually there is hardly any justification for using a Maxwellian distribution in conjunction with the average values of C_A, C_P, and C_D. However, the very fact that excellent agreement with the experimental results can be obtained, as shown particularly by the relative position and magnitude of the two extrema, can be taken as proof that the adopted procedure cannot be very far from being correct. Between the two distribution functions there is not too large a difference; however, the $v^3\exp(-\beta v^2)$ distribution gives definitely a better fit. Since the detector used in our experiment was rather thick, this fact agrees with the expectation. From the value of β in the best-fitting curve one obtains a most probable velocity of the neutrons, $\bar{v}=2200$ m/sec. For a distribution of the form $Av^3\exp(-\beta v^2)$, characteristic for thermal neutrons and a thick detector, the most probable velocity at room temperature is 2690 m/sec. Our result, therefore, indicates that the effective temperature of the polarized neutrons is lower than room temperature as one would expect, since the polarization cross section increases with decreasing velocity. The first maximum of the E_{T0} curve occurs at a field $H_{xm}=10.0$ gauss at the center. If one assigns a transition probability of one at this field to the neutrons of the most probable velocity, $\bar{v}=2\mu_N H_1 l/h$, inserting for H_1 its measured average value over the length of the coil box, one obtains the former value of 2200 m/sec. for $\bar{v}$. The second parameter of E_T^* for the best fit is

$$E_T^*=-7.0 \text{ percent}, \quad (40)$$

in excellent agreement with the value (38) as observed by the transmission experiments. It was, therefore, felt that the observed resonance dips were fully understood and that the calculation of the shape of the resonance curves could be safely based upon the E_{T0} (H_{xm}) curve.

A difficulty in the calculation of the resonance curves arises from the fact that H_1 varies strongly over the region where transitions occur. As a first approximation, the value of H_1 entering in Γ was taken as the average value of H_x over the length l of the radiofrequency coil box. For one case, the calculation was carried out by approximating $H_x(x)$ by four step-functions, and integrating the quantum-mechanical equations for neutrons of the most probable velocity over these steps. The result showed no noticeable difference from the one obtained with the average value of H_x. Thus the theoretical curves shown in Figs. 6, 7, 8, and 9 were obtained from (17) with the deviation Δ expressed in terms of frequency deviation, and through (14) with the average value of H_1 (instead of H_x) obtained from the measurements of H_x and H_y along the three lines C, D, B, on the axis and $\frac{1}{2}''$ below and above, respectively. The average value of H_1 thus determined is 0.74 H_{xm}, where H_{xm} is the peak value of H_x at the center.

The over-all agreement between observed points and theoretical curves is quite good, as shown in Figs. 6, 7, and 8. Significant dis-

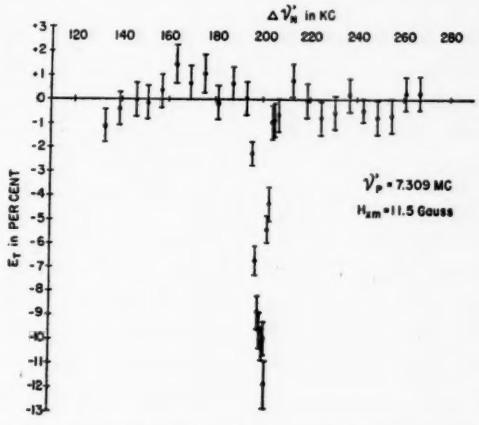

FIG. 11. Exploration of neighborhood of resonances at $\nu_P'=7.309$ Mc.

TABLE I.

ν_P' Mc	H_0	H_{xm} gauss	$\Delta\nu_N'^*$ kc	ν_N^*/ν_P
7.674	+	11.5	210.39±0.12	0.685003±0.000013
	+	4.6	210.62±0.20	0.685022±0.000019
7.309	+	23.0	199.30±0.40	0.684906±0.000037
	+	11.5	200.05±0.20	0.684975±0.000020
	+	4.6	200.33±0.14	0.685000±0.000015
6.943	+	23.0	190.19±0.40	0.684993±0.000039
	+	11.5	190.26±0.13	0.685000±0.000015
	+	4.6	190.25±0.19	0.684999±0.000020
	+	2.3	190.47±0.16	0.685020±0.000017
	+	11.5	190.46±0.12	0.685019±0.000014
	−	11.5	191.79±0.12	

crepancies can be found in the maximum value of E_T at resonance for the lowest field $H_{xm}=2.3$ gauss. This discrepancy is probably caused by the inaccuracy of the radiofrequency field measurements to which this value is particularly sensitive. At the values $H_{xm}=11.5$ gauss the theoretical curves seem to be somewhat too narrow, and at 23.0 gauss somewhat too wide. However, in view of the approximations made in the calculation it is felt that a better agreement could hardly be expected. It is worth while to notice that for the relatively weak radiofrequency fields, i.e., fields for which ET_0 still deviates considerably from its asymptotic value, the half-width of the resonance curves differs considerably from proportionality with H_1. In fact, the half-width of the curves taken with $H_{xm}=4.6$ gauss and $H_{xm}=11.5$ gauss differ by only a factor 1.3. This is understood readily by considering Fig. 10, which shows that in the most important region near resonance and for increasing values of Δ, $F(\xi)$ increases for the lower value of H_1 and decreases for the higher value. This results in an increase of the width for the 4.6-gauss curve and a decrease for the 11.5-gauss curve, in very good agreement with the observations.

For the determination of the exact resonance frequency, one could, in principle, find its value by adjusting the abscissa of the theoretical curves to the best fit with the observed points. However, it was felt that in view of the approximations made in the calculation of these curves a more general procedure which would not be based on special assumptions was indicated. Since no evidence for any asymmetry of the observed resonance curves could be found, the resonance frequencies were determined by assuming that the measured points represent a curve symmetric with respect to a resonance frequency. The axis of symmetry was then determined by pairing each of the observed points on the one side with a linearly interpolated point on the other side of the approximate resonance value. The average value of the resonance frequency was obtained by a properly weighted average of the resonance values obtained from each pair. This procedure was carried out by once choosing the interpolated values on the right and once on the left side of the axis of symmetry. In the same manner the mean error was determined. The final values represent the average of the two calculations, which in no case differed by more than their errors. For each measured point the following errors were considered:

(a) Statistical error in E_T;

(b) error in frequency measurement of $\Delta\nu_N'$, estimated to be ± 0.2 kc;

(c) error caused by differences in the value of H_0 for neutrons and protons. This difference was always carefully measured, as stated in Section III, and the results accordingly corrected. The remaining error is equal to the accuracy of the magnetic field measurements and taken to be ± 0.2 kc.

(d) error caused by drift of the neutron frequency, the proton frequency, and drift of the operating point of the magnetic field control from exact proton resonance. The difference of the two master oscillator frequencies, equal to $\frac{1}{4}$ and $\frac{1}{6}$ of the neutron and the proton frequency, respectively, was at no time allowed to drift by more than 0.1 kc. The absolute value of the proton frequency could drift or be mis-set by as much as 1 kc; this, however, would only cause a very small error in the ratio of the two frequencies (see Section III). The drift of the operating point of the proton-controlled field stabilizer, manually kept at exact resonance, is estimated to cause an error of ± 0.1 kc.

Since all these errors are statistically independent, an over-all error of 0.3 kc was assumed for the values of $\Delta\nu_N'$ for all the measurements, except those at 7.309 Mc, for which the error was increased to 0.4 kc. Table I shows the values of

$\Delta\nu_N'^*$ for the resonance maximum as obtained for the various experiments. In the first column the values of one-sixth of the proton frequency and the direction of the H_0 field are listed. The second column contains the value of the radiofrequency field H_{rm} at the center of the coil. In the third column the average value $\Delta\nu_N'^*$ of the axis of symmetry is given with its error. The last column finally shows the value of the ratio of ν_N^*/ν_P. These last values were obtained by correcting the values of $\Delta\nu_N'^*$ for the frequency shift caused by the asymmetry of the radiofrequency field. The magnitude of this shift, obtained from the last two measurements listed in the table and being equal to one-half the difference of their observed resonance frequencies, was found to be $+(0.67\pm0.09)$ kc for the positive field direction. Comparing this value with Fig. 5 shows that it represents a not unreasonable average value of $d\theta/dt$. It is worth while noticing that the actual spread of the values of ν_N^*/ν_P in Table I is in excellent agreement with the errors computed for each value.

The final value of ν_N^*/ν_P or of the ratio of the magnetic moments of neutron and proton was obtained by averaging the various values listed in Table I, excluding the last. In order to state the mean error of this final result, proper consideration should be given to systematic errors, such as the error in the frequency shift discussed above. The following other possible errors of this type were considered:

(a) A deviation of the fundamental standard frequency of the frequency meter cannot affect the result if the frequency subdivision to $\frac{1}{10}$ or $\frac{1}{5}$, respectively, is maintained, since only frequency ratios enter into the final value.

(b) An additional error could be introduced by a deviation of the average value of the field H_0 over the region in which transitions take place from its value at the center. Since in every case the field configuration was very similar, this error, as being systematic, was not included in the above evaluation, and due allowance has to be made for it in the final result. It is estimated that this error corresponds to a systematic deviation of ±0.2 kc in $\Delta\nu_N'^*$.

(c) A correction of $\Delta\nu_N'^*$ because of the fact that the radiofrequency field is actually an oscillating rather than a rotating, field is too small to be important.[12]

(d) A final possible source of error arises from the fact that the neutrons were observed in air, while the protons were contained in an approximately 0.1-molar solution of $MnSO_4$ in water. The electron of the hydrogen atom, as well as the surrounding other molecules, could cause a modification of the effective resonance field to which the proton is exposed, and this effect would necessitate a correction in the measured ratio of the moments. While the effect caused by the diamagnetism of the water is far too small to be considered, the paramagnetism of the manganese ions would for a spherical sample raise the magnetic induction by about 1/90,000 over its value in air. It is clear, however, that even this small correction would represent a gross over-estimate of the paramagnetic effect, since a proton is on the average isotropically surrounded by manganese ions so that they effect merely a broadening of the resonance line, while its shift cancels out. The only effect which remains is the shielding of the applied field by the electron surrounding the proton, which was treated by Lamb.[17] Neglecting the distortion of the electron eigenfunction as a result of chemical binding, this shielding would cause a relative reduction of the effective field by $\alpha^2/3=1/57{,}000$ ($\alpha=$fine structure constant) which is negligible within our accuracy and again represents an overestimate because of the partial sharing of the electron with the oxygen of the H_2O molecule. Summarizing, it therefore appears that even with our high accuracy, no correction for the resonance field of the proton has to be applied.

Thus the ratio of the two magnetic moments is found to be

$$\frac{|\mu_N|}{\mu_P}=0.685001\pm0.00003. \qquad (41)$$

A previous and considerably less accurate determination by Arnold and Roberts[18] gave for this ratio a value 0.68479 ± 0.0004, which within its error agrees with the above value.

The absolute value of the neutron magnetic moment can be obtained from the value of the

[17] W. E. Lamb, Phys. Rev. **60**, 817 (1941).
[18] W. R. Arnold and A. Roberts, Phys. Rev. **71**, 878 (1947).

proton moment measured by Millman and Kusch[3] in terms of the electronic moment. The value given by these authors is

$$\mu_P=(2.7896\pm0.0008)\mu_n'.$$

The value of μ_n' deviates from a true nuclear Bohr magneton by a radiative correction, as pointed out by Schwinger.[19] According to his investigation, this correction raises the above value of μ_P by a factor $(1+\alpha/2\pi)=1.001162$ if referred to a true nuclear magneton $\mu_n=e\hbar/2Mc$, yielding thus the previously given value (1). In units of the present best known value of the nuclear magneton, and by using

$$\frac{\mu_D}{\mu_P}=0.3070126\pm0.000002, \tag{42}$$

as determined by Bloch, Levinthal, and Packard,[20] the values of the moments of the neutron, proton, and deuteron are

$$\begin{aligned}\mu_N&=-1.91307\pm0.0006,\\ \mu_P&=2.7928\pm0.0008,\\ \mu_D&=0.85742\pm0.0003.\end{aligned} \tag{43}$$

The value $|\mu_N|=(1.935\pm0.02)\mu_n$, which was found by Alvarez and Bloch,[8] agrees with the present more accurate determination.

VI. DISCUSSION

The most outstanding information which has been gained from the investigation of nuclear moments is still contained in the result that the neutron has a finite magnetic moment and that the proton moment differs from the nuclear magneton. It clearly signifies that neither of the two particles is of the same nature as the electron, which has been successfully described by the famous relativistic wave equation of Dirac. The same theory, applied to the neutron and the proton, would give $\mu_N=0$, $\mu_P=\mu_n$, and it seems plausible that the different values, which have been observed for both moments, are of common origin. Using the values (41) and (43) for $|\mu_N|/\mu_P$ and μ_P/μ_n, respectively, one finds

$$\begin{aligned}\frac{\mu_P+\mu_N}{\mu_n}&=\left(1-\frac{|\mu_N|}{\mu_P}\right)\left(\frac{\mu_P}{\mu_n}\right)\\ &=(0.8797\pm0.0003).\end{aligned} \tag{44}$$

The fact that this number is close to unity suggests that the mechanism, which provides the magnetic moment of the neutron, adds, in the case of the proton, an approximately equal and opposite excess to the magnetic moment μ_n, which one would expect to find as a direct consequence of relativity. Frohlich, Heitler, and Kemmer[21] have shown that such a mechanism is rather naturally found if one accepts Yukawa's hypothesis of the meson field for the nuclear forces. Both the negative neutron moment and the positive excess moment of the proton are here explained by the magnetic moment of the negative and positive mesons, respectively, which exist with a finite probability within the range of nuclear forces from the heavy particle. The calculations are based upon a weak coupling between the heavy particle and the meson field, and the relatively small difference of the value (44) from unity appears here as an effect resulting from the small but finite ratio of the masses of meson and heavy particles. Pauli and Dancoff[22] have shown, however, that in a theory with strong coupling, the magnetic moments of proton and neutron would appear as equal and opposite so that a vanishing result would be obtained instead of the value (44); the fact that this actual value lies between zero and unity might thus call for a theory with intermediate coupling.

Another interesting feature of the value (44) is found in the fact that it is very closely equal to the magnetic moment of the deuteron, measured in units μ_n. Using here also the value (42), one has

$$\begin{aligned}\frac{\mu_P+\mu_N-\mu_D}{\mu_n}&=\left(1-\frac{|\mu_N|}{\mu_P}-\frac{\mu_D}{\mu_P}\right)\left(\frac{\mu_P}{\mu_n}\right)\\ &=0.02230\pm0.00009.\end{aligned} \tag{45}$$

A vanishing result instead of this small number would indicate that the magnetic moments of the proton and neutron are additive in the deuteron, and the first approximate data for the neutron moment were actually derived under this assumption. The value (45) represents the measure of a small but well established deviation

[19] J. Schwinger, Phys. Rev. **73**, 416 (1948).
[20] F. Bloch, E. C. Levinthal, and M. E. Packard, Phys. Rev. **72**, 1125 (1947).
[21] H. Frohlich, W. Heitler, and N. Kemmer, Proc. Roy. Soc. **166**, 154 (1938).
[22] W. Pauli and S. M. Dancoff, Phys. Rev. **62**, 85 (1942).

from additivity which can be ascribed to various causes.

A first and in fact very accurate prediction of the non-additivity has been given by Rarita and Schwinger[23] in connection with the quadrupole moment Q_D of the deuteron. Although the observed finite value of Q_D is compatible with the spin $I_D=1$ of the deuteron, it would vanish, if the orbital angular momentum of the proton and the neutron were zero, i.e., if the ground state of the deuteron were a pure S state. Such a vanishing result would not be accidental, but it would necessarily follow if the interaction potential between proton and neutron were spherically symmetrical. Through the assumption of a spin-dependent spherical asymmetry, it is found, however, that the ground state of the deuteron is not a pure S state but rather a mixture of an S and a D state. With the simplest assumptions about the form of the interaction, Rarita and Schwinger were able, from the observed value of Q_D, to estimate the relative strength of the spin-dependent part.

Through the orbital contribution to the magnetic moment of the D state, there enters a correction to the total magnetic moment of the deuteron. It is directly related to the probability of finding the deuteron in the D state. With the form of interaction, which leads to the observed value of Q_D, this probability was found to be 0.039; introducing the observed values for μ_P and μ_N one obtains then from the theory of Rarita and Schwinger $(\mu_P+\mu_N-\mu_D)/\mu_n=0.022$. This excellent agreement with the observed value (45) is, however, largely coincidental; it could easily be spoiled by altering the simple but implausible assumption that the radial dependence of the interaction energy has the form of a square well.

The agreement seems even more accidental if one considers that another major cause of non-additivity has been entirely omitted in the calculations of Schwinger and Rarita. It has been pointed out by several authors[24] that relativistic effects, resulting from the motion of the constituents in the deuteron, could likewise cause deviations from additivity in the same direction and of comparable magnitude as those introduced through the mere presence of the D state. The estimates vary widely, dependent on the different assumptions about the type of interaction between the proton and the neutron. While no definite answer can thus be given at the present state of the theory, it is not justifiable, either, to overlook these relativistic corrections.

Finally, deviations from additivity for the magnetic moments can appear for a third independent reason. If one assumes that the excess moment of the proton and the moment of the neutron are due to the meson field, one is led to the possibility that the modification of this field, which causes their interaction, affects also the resultant magnetic moment of proton and neutron in the deuteron. The existing theories indeed contain features which lead in general to a modification of the intrinsic moments through that of the meson field.[25] In the special case of the deuteron, however, this mechanism contributes no correction by virtue of the particular symmetry properties with respect to an interchange of proton and neutron.

It is evident that the present knowledge of nuclear forces is insufficient to give a satisfactory explanation of the observed value (45). With its considerable accuracy this experimental number may serve as an important and rather severe test for future theories.

VII. ACKNOWLEDGMENT

The authors wish to thank Mr. M. Packard who developed the proton-controlled field stabilizer for the present work, Mr. R. K. Wangsness for his numerical calculations of the curves represented in Fig. 10, and Messrs. J. Fleeman, C. Jeffries, and E. Rogers for their tireless help in taking data. We further wish to acknowledge with thanks the additional support of a Frederick Gardner Cottrell Special Grant-in-Aid from the Research Corporation.

[23] W. Rarita and J. Schwinger, Phys. Rev. **59**, 436 (1941).

[24] H. Margenau, Phys. Rev. **57**, 383 (1940); P. Caldirola, Phys. Rev. **69**, 608 (1946); R. G. Sachs, Phys. Rev. **72**, 91 (1947); H. Primakoff, Phys. Rev. **72**, 118 (1947); G. Breit and I. Bloch, Phys. Rev. **72**, 135 (1947); G. Breit, Phys. Rev. **71**, 400 (1947).

[25] W. E. Lamb and L. I. Schiff, Phys. Rev. **53**, 651 (1938); S. T. Ma and F. C. Yu, Phys. Rev. **62**, 118 (1942); W. Pauli and S. Kusaka, Phys. Rev. **63**, 400 (1943).

PHYSICAL REVIEW VOLUME 74, NUMBER 9 NOVEMBER 1, 1948

On Nuclear Dipole Vibrations

M. GOLDHABER
Department of Physics, University of Illinois, Urbana, Illinois

AND

E. TELLER
Institute of Nuclear Studies, University of Chicago, Chicago, Illinois

(Received July 22, 1948)

The high frequency resonances recently observed for (γ,n) reactions as well as photo-fission are interpreted in analogy with the "reststrahl frequencies" of polar crystals. The estimated frequencies are in good agreement with the experimental results. An interesting consequence of this interpretation is the conclusion that strong resonance scattering of γ-rays should take place at a frequency characteristic of the scattering nucleus.

IT has been observed recently[1] that some nuclear photo-disintegrations, (γ,n) reactions as well as photo-fission, exhibit a behavior which has the appearance of a high frequency resonance. Such a resonance was observed in carbon at 30 Mev,[1] in copper at 22 Mev,[1] in tantalum at 16 Mev,[2] and for photofission in thorium and in uranium at 16–18 Mev.[1] The suggestion was made that this phenomenon may be due to the interplay of increasing level density and increasing competition from other processes such as, for instance, the $(\gamma,2n)$ process. Recent experiments[3] show, however, that in the case of Cu^{63} as well as other nuclei the decrease in the (γ,n) cross section in the high energy region is not compensated to any considerable extent by an increase in the $(\gamma,2n)$ cross section. It is, furthermore, desirable to explain why such different processes as (γ,n) reactions and photo-fission should have maximum cross sections at so similar γ-energies.

We propose to interpret these frequencies as resonances, somewhat different from those caused by definite nuclear levels, and analogous to the "reststrahl frequencies" of polar crystals. We assume that the γ-rays excite a motion in the nucleus in which the bulk of the protons move in one direction while the neutrons move in the opposite direction. We shall call this motion the "dipole vibration." Such a vibration will have a high frequency as a result of the partial separation of the protons from the neutrons to which they are strongly bound. The maximum in the γ-absorption cross section will give rise to similar maxima for several nuclear processes in which γ-absorption is the first step. We shall see below that the magnitude of the integrated cross sections deduced from experiments is too great to be explained by the motion of a single proton or of a small fraction of the protons contained in the nucleus.

The breadth of the resonance—so far only crudely known—is probably due to the transfer of energy from the orderly vibration described above into other modes of nuclear motion. Thus, the breadth is due to a process analogous to damping by friction. One may use a nuclear model in which the ordered dipole vibration of protons and neutrons in opposite directions correspond to well defined quantum states. Coupling with other degrees of freedom will broaden these states. Our resonance will then correspond to the transition of the nucleus from the lowest state to the first excited state of the dipole vibration. A more complete nuclear model will include from the beginning the coupling between the dipole vibration and the other nuclear motions. In this case we shall obtain a great number of nuclear levels each of which contains to some extent the dipole vibration. If, however, the coupling is weak, only such levels will contain considerable contributions from the first excited state of the dipole vibration whose energy does

[1] G. C. Baldwin and G. S. Klaiber, Phys. Rev. **71**, 3 (1947) and Phys. Rev. **73**, 1156 (1948).
[2] J. McElhinney and A. O. Hanson, private communication.
[3] M. L. Perlman and G. Friedlander, Phys. Rev. **74**, 442 (1948). We are indebted to Dr. Friedlander for informing us of these results before publication.

not differ greatly from the energy of this first excited state. Absorption of γ-rays by an energy level is due to the contribution from the dipole vibration. Thus, a great number of nuclear levels actually contribute to the γ-absorption, but they all cluster around the first excited state of the idealized dipole-vibration. In the following we shall discuss this idealized vibration.

In order to gain some insight into the change of the resonance frequency with nuclear properties we shall consider the dipole vibration on the basis of three simple models.

I. We assume that the displacements of the average position of a proton from its original location in the nucleus requires a force which is proportional to the displacement. The proportionality constant shall be the same for every kind of nucleus and for every proton within the nucleus. These assumptions should be well approximated in nuclei consisting of α-particles. It is clear that in this model the frequency of the dipole vibration will be the same for all nuclei.

II. We assume that the protons and neutrons on the surface of the nuclei have fixed positions with respect to each other. Motion of protons and neutrons inside the nucleus causes density changes in the proton-fluid and neutron fluid. The restoring forces per unit mass will be proportional to the gradients of these densities. For a given displacement in the nucleus the maximum density change is inversely proportional to the nuclear radius R and the gradient will be proportional to $1/R^2$. Thus, the frequency, which must vary as the square root of the restoring force, is proportional to $1/R$ or to the inverse cube root of the nuclear mass.

III. We assume that the protons and the neutrons behave as two inter-penetrating incompressible fluids. During the dipole vibration the two fluids suffer a relative displacement so that near the nuclear surface the two fluids no longer overlap. The total restoring force will be proportional to the surface, that is, to R^2. For small displacements we may again assume proportionality between displacement and force. The frequency ω of the resulting harmonic motion is proportional to the square root of force over mass. Thus we have $\omega \sim (R^2/R^3)^{\frac{1}{2}} \sim R^{-\frac{1}{2}}$, and the frequency varies inversely as the sixth root of the nuclear mass.

The experimental variation of the frequency seems to be best described by hypothesis III. It is of interest to explore this model in a more quantitative way even though it is clear that the picture used is too idealized. Indeed we shall further simplify our calculation by assuming that the number of protons and neutrons is equal.

The relative displacement of the neutrons and protons shall be denoted by ξ. We consider the case $\xi \ll R$, where R is the nuclear radius. We shall, however, not assume at first that ξ is infinitesimal. Because of this displacement a volume $\pi R^2|\xi|$ of the proton-fluid no longer overlaps the neutron-fluid and a similar volume of the neutron-fluid extrudes on the other side of the nucleus. If ρ is the density of protons (and neutrons) within the nucleus there will be $\pi R^2|\xi|\rho$ protons separated from the neutron-fluid (and a similar number of neutrons separated from the proton fluid). The total increase in potential energy will then be $2\pi R^2|\xi|\rho\varphi$, where φ is the energy needed to extract one proton from its neutron environment (or one neutron from its proton environment). It is to be noted that φ is not the binding energy of protons (or neutrons). This latter quantity is the difference of the potential energy and of the "zero-point" kinetic energy, whereas φ is that part of the potential energy which is due to the neutron-proton interaction.

For infinitesimal ξ-values the potential should vary as ξ^2 rather than as $|\xi|$. We write $k\xi^2/2$ +const. for the potential at small ξ-values. At a certain point $\xi=\epsilon$ we shall require the two approximate potentials to join smoothly. Here ϵ is the length within which the interaction between a neutron and a nucleus changes from a zero-value outside the nucleus to a high value inside. Setting derivatives equal at $\xi=\epsilon$ we get

$$2\pi R^2\rho\varphi = k\epsilon,$$

or $k=2\pi R^2\rho\varphi/\epsilon$. The reduced mass to be used in the vibration is one-half of the mass of the protons (or neutrons), that is $(2\pi/3)R^3\rho m$, where m is the mass of a single nucleon. Vibrations with zero or one quantum of excitation have amplitudes small compared to ϵ so that the frequency of the vibration is that of a harmonic oscillator. Taking the square root of the force constant divided by the mass we get for the angular fre-

quency

$$\omega=\left(\frac{3\varphi}{\epsilon Rm}\right)^{\frac{1}{2}},$$

and for the resonance energy

$$\hbar\omega=\left(\frac{3\varphi\hbar^2}{\epsilon Rm}\right)^{\frac{1}{2}}.$$

Setting $\epsilon=2\times10^{-13}$ cm, $\varphi=40$ Mev and using $R=10^{-12}$ cm for uranium, we obtain $\hbar\omega=16$ Mev. For copper we get $\hbar\omega=20$ Mev and for carbon $\hbar\omega=26.5$ Mev. The agreement with the experiments is good. It must be remembered, however, that the assumed values of ϵ and φ are quite uncertain and thus the agreement obtained above is significant only in that the correct order of magnitude of the resonance energy is found.

For the vibration described above one finds that the total absorption is given by

$$\int\sigma d\omega=\frac{\pi^2Ae^2}{2mc}$$

where A is the mass-number of the nucleus. For copper this gives $\hbar\int\sigma d\omega=1$ Mev×barn. Comparison with experiment is difficult, since Baldwin and Klaiber do not give absolute values of the cross section in this case. The cross section of the $Cu^{63}(\gamma,n)$ reaction for 17.5 Mev photons was, however, determined by Bothe and Gentner,[4] who find $\sigma=5\times10^{-26}$ cm². Using their value and the relative curve given by Baldwin and Klaiber one obtains 1 Mev×barn. The value deduced from these two experiments may easily be in error by a factor of about 5. The theoretical formula would change somewhat, if model III should be abandoned or if the difference in proton and neutron numbers should be taken into account. Furthermore, the value $\int\sigma d\omega$ was derived under the assumption that the wave-length of the γ-ray is long compared to the nuclear radius. In the present case this condition is not very well satisfied. Finally, the effect of reactions competing with the (γ,n) process has been neglected. All these effects would result in a decrease in the theoretical $\int\sigma d\omega$-values. Thus it seems clear that the observed large values for this integral can be explained only if it is assumed that a considerable fraction of the nuclear charge participates in the absorption process.

In the case of photo-fission in uranium, the experimental value of $\int\sigma d\omega$ is about 15 times smaller than the theoretical figure. This may well be due to competition from the (γ,n) reaction. In thorium the experimental value of $\int\sigma d\omega$ for photo-fission is about 30 times smaller than the calculated value for the absorption cross section.

The dependence of the frequency of the dipole vibration on the nuclear radius has further interesting consequences. For light nuclei the (γ,n) reaction will occur with comparatively small probability, if a nucleus is exposed to a continuous x-ray spectrum with a fairly high upper limit. The nucleus absorbs only a narrow band of photon energies and, in light nuclei, these energies are so high that they are apt to produce other reactions than the (γ,n) process. For the lightest nuclei up to $Z\approx7$, it seems most likely that the excited nucleus will first emit an α-particle. This may be followed by further disintegration. For heavier nuclei the decrease in the resonance energy may cause the (γ,n) process to become more probable, while for the heaviest nuclei the decrease in the binding energy of the neutron may favor the $(\gamma,2n)$ process.

Photo-fission for bismuth and lighter elements is likely to have small cross sections for the following reason. The theoretical photo-fission threshold, according to Frankel and Metropolis,[5] is 16 Mev for bismuth and it is higher for lighter elements. According to our present picture bismuth does not absorb photons strongly above 17 Mev. Thus the cross section is low at high energies because the γ-ray is not absorbed, whereas the resonance energy is so close to the threshold that competition from the (γ,n) reaction becomes strong. For lighter nuclei the frequency of the dipole vibration will be actually lower than the threshold. It is not clear how small the absorption of γ-rays above the resonance will be and whether there are other reasons that make photo-fission an unlikely process for bismuth and lighter nuclei. Baldwin and Klaiber

[4] W. Bothe and W. Gentner, Zeits. f. Physik **106**, 236 (1937).

[5] S. Frankel and N. Metropolis, Phys. Rev. **72**, 914 (1947).

find that the photo-fission cross section of bismuth is at least 10^3 times smaller than the cross section of uranium.

It would be interesting to investigate the resonance scattering of photons by the dipole vibration. The value of $\int \sigma_{\text{scatt}} d\omega$ for this process should be a considerable fraction of the theoretical value derived above for the absorption cross section. The resonance scattering will be, therefore, comparable in intensity to the Compton scattering. The two kinds of scattering processes can be distinguished by their angular dependence. The Compton scattering will be observed in the forward direction. The resonance scattering has, in the first approximation, an intensity proportional to $\sin^2\vartheta$, where ϑ is the angle included by the direction of the scattered radiation and the polarization direction of the primary γ-ray. Deviations from the $\sin^2\vartheta$ law are to be expected due to the finite radius of the nucleus. The scattered radiation may turn out to be a good source of fairly monochromatic γ-rays. The investigation of the spectrum of these scattered rays may open a convenient way to study the breadth of the resonance, while a detailed study of the angular distribution may yield information about the current distribution in the dipole vibration.

PHYSICAL REVIEW VOLUME 74, NUMBER 9 NOVEMBER 1, 1948

Coincidence Experiments on Sc^{46}, Ga^{72}, Au^{198}, and Rb^{86}

E. T. JURNEY
Department of Physics, Indiana University, Bloomington, Indiana
(Received July 9, 1948)

Gamma-gamma- and beta-gamma-coincidences have been investigated in the disintegration of the active isotopes Sc^{46}, Ga^{72}, Au^{198}, and Rb^{86}. Gamma-gamma-correlation was found in Sc^{46} and in Ga^{72} but not in Au^{198} or Rb^{86}. The beta-ray spectra of Sc^{46} and Au^{198} are found to be simple on the basis of beta-gamma-coincidence measurements, while those of Ga^{72} and Rb^{86} are complex. Gamma-ray energies and beta-ray maximum energies were determined by absorption methods.

I. INTRODUCTION

COINCIDENCE experiments, as described by Mitchell,[1] frequently are a great aid in establishing decay schemes for radioactive isotopes. Experiments on the radiations from Sc^{46}, Ga^{72}, Au^{198}, and Rb^{86} have been done, and the results are to be reported herein. The coincidence amplifier, which has a resolving time of about two microseconds, and its associated counting apparatus have been described previously.[2]

II. SCANDIUM 46

Peacock and Wilkinson[3] have measured the energies of the beta- and gamma-rays from Sc^{46} with a 180°-type magnetic spectrometer and find gamma-ray energies of 0.89 Mev and 1.12 Mev and beta-ray groups with end-point energies of 0.36 Mev and 1.49 Mev, with the 1.49 Mev beta-ray group very weak.

A source was prepared on the Indiana University cyclotron according to the reaction $Sc^{45}(d,p)Sc^{46}$, and the resulting Sc^{46} was purified chemically. Two silver-cathode glass counters were arranged with thick aluminum radiators to obtain gamma-gamma-coincidences. For the particular geometrical arrangement which was used, the ratio of the gamma-gamma-coincidence rate to the rate of counting gamma-rays in one of the counters was measured to be $(0.72\pm0.08)\times10^{-3}$. From this it can be concluded that cascaded gamma-rays occur in the disintegration.

Figure 1 shows that the ratio of the beta-gamma-coincidence rate to the beta-ray counting rate is independent of the thickness of absorber

[1] A. C. G. Mitchell, Rev. Mod. Phys. **20**, 296 (1948).
[2] E. T. Jurney and A. C. G. Mitchell, Phys. Rev. **73**, 1153 (1948).
[3] C. L. Peacock and R. G. Wilkinson, Phys. Rev. **74**, 297 (1948).

placed between the source and the counter up to thicknesses around 0.06 g/cm², which is only a little less than the thickness required to absorb completely the 0.36 Mev group. One concludes that the low-energy group is followed by at least one gamma-ray. The intensity of the high energy group reported by Peacock and Wilkinson is so low that it cannot be detected by absorption methods; it is clearly impossible, then, to measure the ratio $N_{\beta\gamma}/N_{\beta}$ for this group.

The results described here are in good agreement with those obtained by Mandeville and Scherb[4] and also are compatible with the disintegration scheme proposed by Peacock and Wilkinson.

III. GALLIUM 72

The method of coincidence counting has been used with Ga^{72} by Mitchell, Jurney, and Ramsey[5] and by Mandeville and Scherb.[6] These two investigations yielded results which were in very close agreement, namely, that the beta-ray spectrum consists of two groups, with the low energy group having an end point somewhat under 1 Mev. A more careful investigation than the one reported by Mitchell, Jurney, and Ramsey has recently been made here. Again gamma-gamma-coincidences were observed, which indicate the presence of cascaded gamma-rays in the disintegration. Figure 2 shows the result of the beta-gamma-coincidence measurements; the beta-ray spectrum is seen to be complex, with an inner end point in the neighborhood of 0.38 g/cm² or 0.92 Mev, according to the Feather range-energy relation.

Mitchell, Zaffarano, and Kern[7] have proposed a disintegration scheme for Ga^{72} based on measurements made with a magnetic lens spectrometer, in which there are seven possible excited levels in the resulting Ge^{72} nucleus. In their scheme roughly three-quarters of the transitions from Ga^{72} involve beta-ray groups having end-point energies of 1.0, 0.74, and 0.56 Mev. The remaining transitions to Ge^{72} are through one of four relatively weak groups, the most energetic of which has an end point at 3.17 Mev. One would expect the ratio $N_{\beta\gamma}/N_{\beta}$ to increase slowly from an absorber thickness corresponding to this energy to a thickness corresponding to about 1 Mev, according to this scheme, and to increase much more rapidly from there up to zero thickness. The counting errors are too large to determine the slope of the curve in the 1–3 Mev region; Mandeville and Scherb's curve appears to indicate a dependence of $N_{\beta\gamma}/N_{\beta}$ on the absorber thickness there, however. Coincidence methods cannot be expected to confirm completely such a complex scheme as Mitchell, Kern, and Zaffarano's, but the results here are not in disagreement with their scheme.

IV. GOLD 198

Clark,[8] Norling,[9] and Mandeville and Scherb[10] have performed experiments on Au^{198} which

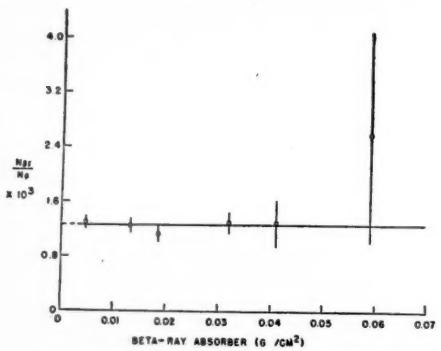

FIG. 1. Beta-gamma-coincidences in Sc^{46}.

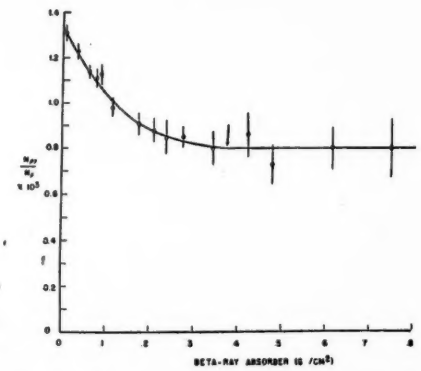

FIG. 2. Beta-gamma-coincidences in Ga^{72}.

[4] C. E. Mandeville and M. V. Scherb, Phys. Rev. **73**, 141 (1948).
[5] A. C. G. Mitchell, E. T. Jurney, and M. Ramsey, Phys. Rev. **71**, 324 (1947).
[6] C. E. Mandeville and M. V. Scherb, Phys. Rev. **72**, 520 (1947).
[7] A. C. G. Mitchell, D. J. Zaffarano, and B. D. Kern, Phys. Rev. **73**, 1424 (1948).
[8] A. F. Clark, Phys. Rev. **61**, 242 (1942).
[9] F. Norling, Arkiv. f. Mat. Ast. Och Fys. **B27** (3), 4 (1941).
[10] C. E. Mandeville and M. V. Scherb, Phys. Rev. **73**, 634 (1948).

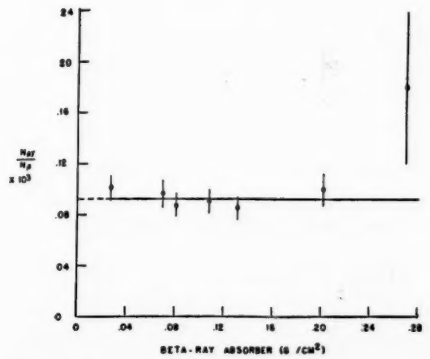

FIG. 3. Beta-gamma-coincidences in Au^{198}.

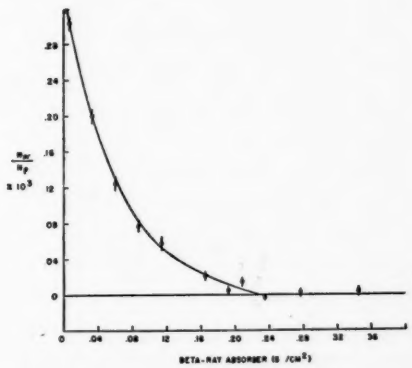

FIG. 4. Beta-gamma-coincidences in Rb^{86}.

give a value of $N_{\beta\gamma}/N_\beta$ which is independent of beta-ray absorber thickness. These authors disagree, however, in that Clark and Mandeville and Scherb find gamma-gamma-coincidences while Norling does not. The findings of Clark and of Mandeville and Scherb are supported by the spectrographic measurements of Levy and Greuling[11] in which gamma-rays of 0.157, 0.208, and 0.408 Mev were detected. Measurements by Siegbahn[12] and by Peacock and Wilkinson[3] fail to show more than one gamma-ray occurring in the disintegration.

A preliminary investigation here[13] yielded a value of $N_{\gamma\gamma}/N_\gamma=(-0.038\pm0.02)\times10^{-3}$ for Au^{198}. The counters which were used for that measurement had lead cathodes to improve the sensitivity for counting gamma-rays. Absorption of low-energy gamma-rays by the counter walls was rather high, although the 0.157 and 0.208 Mev lines reported by Levy and Greuling still would reach the counter gas with 25 percent and 42 percent of their initial respective intensities.

Recently another attempt has been made to find gamma-gamma-coincidences. Two silver cathode glass counters were arranged 6.3 cm apart with the source midway between them. Each counter was shielded from the source by a 0.4 cm thickness of aluminum. Using an unpurified source which was prepared according to $Au^{197}(n,\gamma)Au^{198}$ a value of $N_{\gamma\gamma}/N_\gamma=(0.043\pm0.012)\times10^{-3}$ was found. The experiment was then repeated, with the same geometry, but with a source which had been given chemical separation from possible mercury contamination, and a value of $N_{\gamma\gamma}/N_\gamma=(0.022\pm0.01)\times10^{-3}$ was found. This small value is not interpreted as being significant, especially since no particular pains were taken to prevent coincidences arising from scattering.

The gamma-gamma-correlation found by Clark was very low, and might be ascribed to a small amount of contamination of his source by some other active isotope, as he does not indicate that his source had been given any chemical purification after bombardment. The gamma-gamma-coincidence rate found by Mandeville and Scherb might also be due to an impurity, especially if their pile irradiation was a long one.

Figure 3 gives the ratio $N_{\beta\gamma}/N_\beta$ as a function of beta-ray absorber thickness, of which it is seen to be independent. This indicates a simple beta-ray spectrum and is in agreement with the results of Clark, Norling, and Mandeville and Scherb.

From the results here one would conclude that Au^{198} disintegrates by the emission of a single beta-ray, and that the resulting excited Hg^{198} nucleus reaches its ground state by the emission of a single gamma-ray.

V. RUBIDIUM 86

A source of Rb^{86} was produced by neutron irradiation in the Clinton pile and was separated from cesium in an ion exchange column. The absorption of the beta-rays in aluminum was determined, and the resulting data were analyzed by the method proposed by Bleuler and Zünti,[14] which showed beta-ray groups with end points

[11] P. W. Levy and E. Greuling, Phys. Rev. **73**, 83 (1948).
[12] K. Siegbahn, Proc. Roy. Soc. **189**, 527 (1947).
[13] E. T. Jurney and M. R. Keck, Phys. Rev. **73**, 1220 (1948).
[14] E. Bleuler and W. Zünti, Helv. Phys. Acta **19**, 375 (1946).

at 1.82 Mev (~67 percent) and 0.56 Mev (~33 percent). The maximum gamma-ray energy was found to be 1.12 Mev by coincidence absorption of Compton recoil electrons produced in an aluminum target.

Figure 4 shows the result of beta-gamma-coincidence measurements. It is evident that no coincidences are present for beta-ray absorption thicknesses greater than 0.23 g/cm^2 of aluminum, which corresponds to 0.62 Mev. Hence the transitions which involve the 1.76 Mev beta-ray group lead directly to the ground state of Sr^{86}. Those coincidences which appear between this absorber thickness and zero absorber thickness are to be ascribed to disintegrations which involve the low-energy beta-ray group. No evidence of gamma-gamma-coincidence could be found; it is to be concluded that the low energy group of beta-rays leads to a 1.12 Mev level of Sr^{86}, which in turn goes to the ground state with the emission of a single gamma-ray.

The spectrum of Rb^{86} has recently been measured in a magnetic lens by Zaffarano, Kern, and Mitchell,[15] who found one gamma-ray of energy 1.081 Mev and two beta-ray groups with end points at 1.822 and 0.716 Mev. The results described in the present paper confirm their results.

VI. ACKNOWLEDGMENTS

The author expresses his thanks to Dr. R. G. Wilkinson who generously provided the use of Sc^{46} and Au^{198} sources which he had prepared for spectrographic measurements, and to Professor A. C. G. Mitchell for the use of his purified Rb^{86} source. He also wishes to thank Professor Mitchell for interest and suggestions throughout the course of the experiments. This work was supported by the Office of Naval Research under Contract N6ori-48, T. O. 1.

[15] D. J. Zaffarano, B. D. Kern, and A. C. G. Mitchell, Phys. Rev. **74**, 682 (1948).

PHYSICAL REVIEW VOLUME 74, NUMBER 9 NOVEMBER 1, 1948

Additional Rotational Energy Levels of H_2O and D_2O Molecules*

N. GINSBURG
Physics Department, Syracuse University, Syracuse, New York
(Received July 6, 1948)

An extension of the pure rotational energy levels for H_2O and D_2O is made in order to obtain new possible microwave transitions. For H_2O the levels are given through $J=14$ and for D_2O through $J=15$. Additional assignments are made in the previously observed absorption spectra. The Wang secular determinant for the asymmetric rotator is expanded, and equations for the the energy levels of $J=12$, 13, 14, and 15 are given in terms of the asymmetry parameter.

INTRODUCTION

THE calculation by Van Vleck[1] on the absorption of microwaves by water vapor showed an absorption greater than the amount predicted by the theory as developed. An effort to account for the residual absorption on the basis of line widths was unsuccessful. It was thought that the additional intensity might be accounted for by an accidental coincidence with a line corresponding to a transition value between levels of J higher than 11. The absorption spectrum of water vapor had previously been observed and analyzed by several investigators, the most satisfactory and complete analysis being that of Randall, Dennison, Ginsburg, and Weber[2] (hereafter referred to as RDGW). They obtained the pure rotational spectrum in the region from 140 to 555 cm^{-1} and combined their results with those of Wright and Randall[3] in the longer wave-

* The calculations and energy levels for H_2O were presented at the Symposium on Molecular Structure and Spectroscopy, Ohio State University, Columbus, Ohio (June, 1947).

[1] J. H. Van Vleck, Phys. Rev. **71**, 425 (1947).

[2] Randall, Dennison, Ginsburg, and Weber, Phys. Rev. **52**, 160 (1937).

[3] N. Wright and H. M. Randall, Phys. Rev. **44**, 39 (1933).

TABLE I. The rotational energy levels of the H_2O molecule. The levels for the $J=11$ and the lower levels for the higher J values are taken from RDGW. W is the difference between levels obtained from the spectrum and those calculated from solution of the rigid asymmetric top equations.

J / τ	11		12		13		14	
	W	δW	W	δW	W	δW	W	δW
14							4971.3	648.2
13					4353.6	503.0	4971.3	648.2
12			3768.88	380.49	4353.6	503.0	4701.5	494.6
11	3218.55	279.19	3768.88	380.49	4090.9	373.6	4701.5	494.6
10	3218.55	279.19	3514.88	273.90	4090.9	373.6	4432.0	372.7
9	2974.88	193.68	3514.88	273.90	3832.0	272.7	4432.0	372.7
8	2974.88	193.68	3267.69	192.57	3832.0	272.7	4172.5	273.0
7	2741.42	130.06	3267.69	192.57	3584.1	192.9	4172.5	273.0
6	2741.42	130.06	3033.78	130.31	3584.1	192.9	3943.5	197.9
5	2523.08	83.77	3033.78	130.31	3351.5	130.5	3943.5	197.9
4	2523.08	83.77	2815.03	85.73	3351.5	130.5	3689.0	136.4
3	2322.82	52,51	2815.03	85.71	3128.5	91.9	3689.0	136.4
2	2322.77	52.47	2612.94	58.39	3128.5	91.8	3466.9	99.1
1	2145.17	33.80	2613.21	57.79	2933.2	62.3	3466.9	99.2
0	2144.06	33.26	2438.16	41.51	2930.4	62.4	3273.8	69.8
− 1	2000.71	25.74	2435.69	39.46	2765.6	44.0	3273.9	66.0
− 2	1984.20	26.65	2297.61	41.02	2756.7	42.1	3118.7	55.6
− 3	1898.56	27.39	2273.36	34.52	2636.1	45.3	3094.1	53.7
− 4	1840.14	22.39	2209.98	32.98	2594.2	34.3	3003.2	49.7
− 5	1811.21	25.36	2116.21	34.64	2543.1	39.7	2928.7	42.9
− 6	1694.71	14.26	2107.08	28.68	2431.0	28.6	2896.2	46.2
− 7	1691.13	14.64	1962.20	18.55	2419.2	32.4	2754.6	33.5
− 8	1525.65	7.68	1961.00	18.30	2243.5	27.9	2746.3	37.8
− 9	1525.36	7.80	1775.26	10.36	2242.7	28.1	2545.7	35.0
−10	1327.58	4.33	1775.26	10.30	2043.0	13.5	2545.4	34.9
−11	1327.58	4.33	1558.42	6.03	2043.0	13.5	2332.6	18.8
−12			1558.42	6.03	1807.4	8.2	2332.6	18.8
−13					1807.4	8.2	2074.3	10.9
−14							2074.3	10.9

length region to obtain all energy levels through $J=11$, together with some for higher J values. Some of the lines they observed were not assigned. In addition there was available the prism measurements made by Weber and Randall[4] which extended the absorption spectrum of water vapor to shorter wave-lengths. It was thought possible, by using these measurements, to extend the analysis.

A number of absorption lines in the spectrum of D_2O as observed by Fuson, Randall, and Dennison[5] (hereafter referred to as FRD) had not been assigned. It was thought worth while to extend the calculations made for H_2O to include the D_2O molecule as well and obtain assignments for as many of these lines as possible.

CALCULATION

It was necessary to extend the equations obtained by Nielsen[6] from the Wang secular determinant for the asymmetrical rotator. He had obtained the equations through $J=10$, and in the paper of RDGW that for $J=11$ was added. The equations for the higher J values, through $J=15$, are given in the Appendix.

Making use of the values previously assigned by RDGW for the moments of inertia of the water molecule, namely

$$h/8\pi^2cA=27.8055,\quad h/8\pi^2cB=14.499724,$$
$$h/8\pi^2cC=9.279276$$

giving the parameter of b the value -0.164 exactly, these equations were solved for the energy levels. The values through $J=14$ were obtained for H_2O and through $J=15$ for D_2O. Since the mass of the molecule is less for the former than for the latter, the spectrum extends to higher frequencies. In this region the wave-lengths, and consequently the frequencies, are known with much less accuracy since they were obtained by prism spectrometer measurements.

TABLE II. New assignments in the spectrum of H_2O. The last fourteen lines are from Weber and Randall's prism measurements.

cm^{-1}	Assignment $J_{\tau'}\leftarrow J_\tau$	cm^{-1}	Assignment $J_{\tau'}\leftarrow J_\tau$
550.33	$12_{12}-11_{10}$	280.46	$13_{-9}-12_{-7}$
	$12_{11}-11_{11}$	267.73	$13_{-10}-12_{-10}$
	13_7-12_5	266.94	$12_{-6}-11_{-4}$
	13_6-12_6	266.29	$12_{-8}-11_{-6}$
536.48	13_5-12_3	200.44	$13_{-3}-12_{-1}$
	13_4-12_4	188.28	$14_{-2}-13_0$
	14_2-13_0	152.55	$13_{-1}-12_1$
526.27	12_8-11_6	139.84	$12_{-2}-11_0$
	12_7-11_7		
519.81	$13_{-3}-12_{-5}$	617.7	$14_{14}-13_{12}$
518.09	14_0-13_{-2}		$14_{13}-13_{13}$
515.27	$12_{-4}-11_{-6}$	610.6	$14_{12}-13_{10}$
	13_3-12_1		$14_{11}-13_{11}$
	13_2-12_2	600.0	$14_{10}-13_8$
502.45	$14_{-10}-13_{-8}$		14_9-13_9
492.22	12_4-11_2	592.0	14_8-13_6
	12_3-11_3		14_7-13_7
	13_0-12_0	584.7	$13_{13}-12_{11}$
	$13_{-1}-12_{-3}$		$13_{12}-12_{12}$
472.68	$13_{-2}-12_{-2}$		14_6-13_4
468.88	12_2-11_0		14_5-13_5
468.04	12_1-11_1	580.7	$13_{-5}-12_{-7}$
458.05	$14_{-3}-13_{-3}$	576.0	$13_{11}-12_9$
453.96	12_0-11_{-2}		$13_{10}-12_{10}$
443.90	$12_{-2}-11_{-4}$	564.3	13_9-12_7
434.98	$12_{-1}-11_{-1}$		13_8-12_8
385.58	$14_{-5}-13_{-5}$	560.5	14_4-13_2
384.21	$13_{-4}-12_{-4}$		14_3-13_3
374.80	$12_{-3}-11_{-3}$	540.0	$12_{10}-11_8$
335.34	$14_{-7}-13_{-7}$		12_9-11_9
323.90	$13_{-6}-12_{-6}$	533.7	14_1-13_1
303.00	$13_{-7}-12_{-5}$	497.5	13_1-12_{-1}
	$14_{-9}-13_{-9}$	315.32	$14_{-8}-13_{-6}$
302.04	$14_{-6}-13_{-4}$	305.00	$12_{-5}-11_{-5}$
289.65	$14_{-11}-13_{-11}$		
282.45	$13_{-8}-12_{-8}$		

[4] L. R. Weber and H. M. Randall, Phys. Rev. **40**, 835 (1932).
[5] N. Fuson, H. M. Randall, and D. M. Dennison, Phys. Rev. **56**, 983 (1939).
[6] H. H. Nielsen, Phys. Rev. **38**, 1432 (1931).

TABLE III. The rotational levels of the D_2O molecule. The $J=11$ levels are taken from FRD as are some of the levels for the higher J values. The levels with subscript c are calculated from series. $W-W_k$ is the difference from the "key" energy levels and W the difference from the rigid asymmetric rotator calculations.

J / τ	11 W	11 $W-W_k$	12 W	12 $W-W_k$	13 W	13 $W-W_k$	14 W	14 $W-W_k$	15 W	15 δW
15									3280.37$_c$	271.95
14							2885.21	−12.56	3280.37$_c$	271.95
13					2512.54	−8.60	2885.21	−12.56	3069.20	213.73
12			2164.14	−6.86	2512.54	−8.60	2685.50	−12.47	3069.20	213.73
11	1837.89	−4.45	2164.14	−6.86	2324.30	−7.13	2685.50	−12.47	2871.84	162.44
10	1837.89	−4.45	1986.60	−4.66	2324.30	−7.13	2499.17	−5.23	2871.84	162.44
9	1672.71	−1.68	1986.60	−4.66	2147.87	−3.01	2499.17	−5.23	2680.94	122.50
8	1672.71	−1.68	1821.62	−0.38	2147.87	−3.01	2319.74	−3.08	2680.94	122.50
7	1519.60	1.14	1821.62	−0.38	1982.04	0.31	2319.74	−3.08	2502.97	88.54
6	1519.60	1.14	1668.15	2.16	1982.04	0.31	2154.61	2.03	2502.97	88.54
5	1378.56	2.45	1668.15	2.16	1828.36	2.18	2154.61	2.03	2340.65	58.96
4	1378.56	2.45	1526.34	2.77	1828.36	2.18	2001.15	3.86	2340.65	58.96
3	1250.97	2.72	1526.34	2.77	1687.26	4.62	2001.15	3.86	2189.98	37.29
2	1250.95	2.70	1400.00	4.70	1687.26	4.62	1861.08	7.09	2189.98	37.29
1	1139.78	3.56	1400.00	4.70	1561.23	5.43	1861.08	7.09	2045.71	25.53
0	1139.63	3.49	1287.55	3.54	1561.23	5.55	1737.00	7.87	2045.71	25.53
−1	1046.21	2.96	1287.50	3.57	1449.93	2.73	1737.19	7.36	1922.11	16.44
−2	1042.03	2.39	1196.28	3.61	1448.37	2.16	1625.05	2.46	1921.60	15.95
−3	979.36	3.15	1190.75	3.32	1367.36	3.10	1624.73	5.68	1819.58	12.14
−4	960.32	2.84	1136.25	2.32	1352.40	1.91	1549.64	5.25	1815.36	7.95
−5	931.60	1.21	1105.18	3.60	1307.28	1.90	1526.80	3.55	1750.13	8.15
−6	882.26	2.43	1087.58	3.64	1265.40	3.01	1490.80	1.72	1712.21	9.60
−7	876.94	1.89	1022.15	2.82	1253.78	4.06	1431.50	1.95	1688.50	9.76
−8	794.33	1.48	1019.15	2.25	1172.80	5.39	1427.90	5.46	1616.18	3.60
−9	793.96	1.46	925.15	1.91	1170.75	4.68	1331.60	5.23	1613.05	2.90
−10	692.57	1.39	924.95	1.86	1065.25	2.10	1331.35	5.61	1508.28	2.20
−11	692.57	1.39	813.35	1.65	1065.25	2.10	1215.2	3.01	1507.79	2.00
−12			813.35	1.65	943.75	1.99	1215.0	3.01	1374.7	2.5
−13					943.75	1.99	1083.8	2.47	1374.8	2.5
−14							1083.8	2.47	1233.4	0.82
−15									1233.4	0.82

Thus it was not thought worth while to go beyond $J=14$ values for H_2O.

The calculated energy levels were then corrected for centrifugal stretching by the method of RDGW and compared with the observed spectrum. It was possible to extend the energy level scheme through $J=14$. The results are given in Table I. The table includes the results for $J=11$ as given by RDGW. δW is the difference between the experimentally determined energy, W, and the calculated value as obtained from the solution of the equations. The progressions of the δW continue in much the same fashion as for smaller J values. Similarly, various series approximating the symmetric rotator[7] with rotation about either the axis of greatest or least moment of inertia can be extended. Both methods apply to these additional energy levels. Table II gives the observed rotational lines used in this extension with the new assignments.

For the case of the rotational levels of D_2O, a similar method was applied. As in the paper of FRD, it was possible to apply the proper mass correction to the δW's as obtained from H_2O. This gave a set of "key" levels which were then used to obtain the proper transition frequencies. It was possible to do this for all levels through $J=14$. For the 31 levels of $J=15$, only the extrapolated progression of the δW's was possible since no terms for H_2O were available. Table III gives the additional energy levels thus obtained for D_2O and the difference between the actual and "key" levels. For $J=15$, δW is given. Table IV gives the observed lines used and their new assignments.

DISCUSSION AND SUMMARY

The results for H_2O are a straightforward extension of previous work. There are one or two

[7] The two levels of greatest τ value degenerate into a single level with $k=J$, the next two have a $k=J-1$, and so on. For the rotation about the axis of greatest moment the two levels with the largest negative value of τ degenerate into a single level with $k=J$, the next two higher into a level with $k=J-1$, and so on.

TABLE IV. New assignments in the spectrum of D_2O.

cm^{-1}	Assignment $J_\tau' \leftarrow J_\tau$	cm^{-1}	Assignment $J_\tau' \leftarrow J_\tau$	cm^{-1}	Assignment $J_\tau' \leftarrow J_\tau$	cm^{-1}	Assignment $J_\tau' \leftarrow J_\tau$
383.70	$15_{13} - 14_{11}$	297.38	$15_{-1} - 14_{-2}$	328.90	$13_{-7} - 12_{-9}$	216.05	$13_{-4} - 12_{-4}$
	$15_{12} - 14_{12}$	296.52	$15_{-2} - 14_{-2}$		$15_{3} - 14_{1}$	211.35	$12_{-3} - 11_{-3}$
372.67	$14_{14} - 13_{12}$	293.25	$12_{-6} - 11_{-8}$		$15_{2} - 14_{2}$	188.28	$15_{-3} - 14_{-3}$
	$14_{13} - 13_{13}$	289.59	$12_{6} - 11_{4}$	326.25	$12_{12} - 11_{10}$	181.55	$15_{-9} - 14_{-7}$
	$15_{11} - 14_{9}$		$12_{5} - 11_{5}$		$12_{11} - 11_{11}$	177.72	$13_{-6} - 12_{-6}$
	$15_{10} - 14_{10}$	288.56	$14_{0} - 13_{-2}$		$13_{9} - 12_{7}$		$14_{-7} - 13_{-7}$
361.20	$14_{12} - 13_{10}$	287.26	$13_{3} - 12_{1}$		$13_{8} - 12_{8}$	176.93	$15_{-10} - 14_{-10}$
	$14_{11} - 13_{11}$		$13_{2} - 12_{2}$		$14_{6} - 13_{4}$	176.19	$15_{-11} - 14_{-9}$
	$15_{9} - 14_{7}$		$14_{-1} - 13_{-1}$		$14_{5} - 13_{5}$	173.58	$12_{-5} - 11_{-5}$
	$15_{8} - 14_{8}$	285.13	$13_{-5} - 12_{-7}$	313.89	$12_{10} - 11_{8}$	162.50	$14_{-8} - 13_{-6}$
351.30	$14_{10} - 13_{8}$	284.22	$14_{-4} - 13_{-6}$		$12_{9} - 11_{9}$	160.95	$14_{-9} - 13_{-9}$
	$14_{9} - 13_{9}$	273.48	$13_{1} - 12_{-1}$		$13_{7} - 12_{5}$	158.55	$14_{-10} - 13_{-8}$
348.36	$13_{13} - 12_{11}$		$13_{0} - 12_{0}$		$13_{6} - 12_{6}$	153.65	$13_{-8} - 12_{-8}$
	$13_{12} - 12_{12}$	272.65	$14_{-2} - 13_{-4}$		$14_{4} - 13_{2}$	148.60	$13_{-9} - 12_{-7}$
	$15_{7} - 14_{5}$	265.54	$15_{-4} - 14_{-4}$		$14_{3} - 13_{3}$		$13_{-7} - 12_{-5}$
	$15_{6} - 14_{6}$	262.18	$13_{-3} - 12_{-5}$	308.65	$15_{1} - 14_{-1}$	138.40	$14_{-6} - 13_{-4}$
339.50	$15_{5} - 14_{3}$	259.18	$13_{-1} - 12_{-3}$		$15_{0} - 14_{0}$	127.36	$12_{-6} - 11_{-4}$
	$15_{4} - 14_{4}$	257.37	$14_{-3} - 13_{-3}$	302.02	$12_{8} - 11_{6}$	125.40	$15_{-5} - 14_{-3}$
337.70	$13_{11} - 12_{9}$	252.09	$13_{-2} - 12_{-2}$		$12_{7} - 11_{7}$	121.95	$15_{-7} - 14_{-5}$
	$13_{10} - 12_{10}$	235.96	$12_{-2} - 11_{-4}$		$13_{5} - 12_{3}$	101.28	$14_{-5} - 13_{-2}$
	$14_{8} - 13_{6}$	221.41	$15_{-6} - 14_{-6}$		$13_{4} - 12_{4}$		
	$14_{7} - 13_{7}$	219.52	$14_{-5} - 13_{-5}$				

slight irregularities in the symmetric top approximation series necessitated by the probable inaccuracies of the prism data. It will be observed that the δW values increase until for the highest τ value for $J=14$ group of levels, it reaches 648.2 cm^{-1}. Most of this is a centrifugal stretching correction and its magnitude indicates that higher order terms than the first must be used in a perturbation calculation.

In the case of the D_2O rotation terms, the calculations revealed that some changes should be made in the FRD assignments for the levels beyond $J=11$. Those for which new values have been obtained are 12_{12}, 12_{11}, 13_3, 13_2, 13_1, 13_0, 13_{-8}, and 14_2. The changes in these levels were made in order to satisfy observed δW progressions and at the same time keep the series regular. An additional 42 lines observed by FRD were given assignments. The top levels for $J=15$ were calculated since the transitions from the comparable levels for $J=14$ were beyond the range of the observations of FRD. This is indicated in Table III.

It will be noticed that most of the levels are based on the assignment of one transition only. Calculations on intensities have shown that lines other than those given are weaker by a factor of five at best. Since the intensities of the lines used are nearly at the weakest observable strength, it is probable that the others would not have been observed.

On the basis of these extended assignments for the energy levels of H_2O, it will be observed that only one other transition could be expected to contribute absorption in the spectral region now available to microwave technique. This is the transition $13_{-5} \rightarrow 14_{-9}$. It would give rise to an absorption at 2.5 cm^{-1}. By virtue of Boltzmann factors only, the lower state for this transition, which is at 2543.1 cm^{-1}, has a population 0.33 percent of the population of the lower state for the well-known 1.35 cm^{-1} ($5_{-1} \rightarrow 6_{-5}$) absorption. It is difficult to see how this 2.5 cm^{-1} transition could influence the Van Vleck calculation sufficiently to account for the observed difference.

In the D_2O energy level extension, it can be seen that several more transitions would be allowed on the basis of selection rules. A group of transitions should appear at 4.56 cm^{-1}. These are $12_5 \rightarrow 11_9$, $12_6 \rightarrow 11_8$,[8] $13_7 \rightarrow 12_9$, $13_6 \rightarrow 12_{10}$, $14_8 \rightarrow 13_{10}$, $14_7 - 13_{11}$, $15_9 - 14_{11}$, $15_8 - 14_{12}$. Another pair of allowed transitions, $14_{10} - 15_6$ and $14_9 - 15_7$, should give rise to an absorption at 3.80 cm^{-1}.

[8] Previously calculated by G. W. King, R. M. Hainer, and P. C. Cross, Phys. Rev. 71, 433 (1947).

APPENDIX

The extension of the asymmetric rotator equations, which were solved for the H_2O and D_2O molecules, are here given.

Equations for $J=12$

$$W^6-W^5(286\pm 78b)+W^4(28{,}743\pm 22{,}230b-17{,}121b^2)-W^3(1{,}234{,}948\pm 2{,}219{,}724b-3{,}980{,}340b^2 \mp 884{,}988b^3)+W^2(21{,}967{,}231\pm 94{,}106{,}220b-301{,}092{,}246b^2\mp 185{,}257{,}332b^3+53{,}971{,}983b^4) -W(128{,}816{,}766\pm 1{,}619{,}337{,}798b-8{,}499{,}796{,}500b^2\mp 11{,}599{,}949{,}556b^3+7{,}751{,}468{,}790b^4 \pm 1{,}304{,}412{,}174b^5)+108{,}056{,}025\pm 8{,}428{,}369{,}950b-72{,}069{,}547{,}473b^2\mp 213{,}220{,}651{,}644b^3 +246{,}759{,}212{,}007b^4\pm 113{,}153{,}886{,}846b^5-15{,}740{,}160{,}975b^6=0.$$

$$W^6-364W^5+(48{,}048-14{,}196b^2)W^4-(2{,}846{,}272-4{,}256{,}928b^2)W^3+(75{,}851{,}776-424{,}427{,}328b^2 +32{,}271{,}408b^4)W^2-(791{,}691{,}264-16{,}313{,}696{,}256b^2+6{,}226{,}294{,}464b^4)W+2{,}123{,}366{,}400 +2{,}123{,}366{,}400-198{,}078{,}676{,}992b^2+267{,}622{,}115{,}328b^4-4{,}247{,}640{,}000b^6=0.$$

$$W^7-364W^6+(48{,}048-26{,}208b^2)W^5-(2{,}846{,}272-8{,}581{,}248b^2)W^4+(75{,}851{,}776-984{,}282{,}624b^2 +137{,}928{,}960b^4)W^3-(791{,}691{,}264-48{,}263{,}694{,}336b^2+137{,}928{,}960b^4)W^3-(791{,}691{,}264 -48{,}263{,}694{,}336b^2+34{,}624{,}392{,}192b^4)W^2+(2{,}123{,}366{,}400-981{,}410{,}217{,}984b^2 +2{,}586{,}048{,}049{,}152b^4-99{,}221{,}815{,}296b^6)W+6{,}376{,}469{,}299{,}200b^2-56{,}815{,}669{,}886{,}976b^4 +11{,}330{,}631{,}696{,}384b^6=0.$$

Equations for $J=13$

$$W^6-364W^5+(48{,}048-21{,}476b^2)W^4-(2{,}846{,}272-6{,}272{,}032b^2)W^3+(75{,}851{,}776-611{,}444{,}288b^2 +83{,}727{,}280b^4)W^2-(791{,}691{,}264-23{,}066{,}394{,}624b^2+14{,}889{,}551{,}040b^4)W+2{,}123{,}366{,}400 -275{,}898{,}286{,}080b^2+599{,}267{,}911{,}680b^4-29{,}688{,}120{,}000b^6=0.$$

$$W^7-364W^6+(48{,}048-37{,}856b^2)W^5-(2{,}846{,}272-12{,}168{,}832b^2)W^4+(75{,}851{,}776-1{,}374{,}883{,}328b^2 +312{,}981{,}760b^4)W^3-(791{,}691{,}264-66{,}634{,}573{,}824b^2+74{,}560{,}711{,}680b^4)W^2+(2{,}123{,}366{,}400 -1{,}344{,}077{,}660{,}160b^2+5{,}339{,}879{,}976{,}960b^4-440{,}565{,}350{,}400b^6)W+8{,}695{,}185{,}408{,}000b^2 -113{,}553{,}686{,}937{,}600b^4+43{,}584{,}616{,}857{,}600b^6=0.$$

$$W^7-(455\pm 91b)W^6+(77{,}077\pm 41{,}314b-25{,}571b^2)W^5-(6{,}092{,}515\pm 6{,}972{,}693b-10{,}048{,}623b^2 \mp 1{,}606{,}241b^3)W^4+(230{,}673{,}443\pm 547{,}446{,}172b-1{,}395{,}802{,}590b^2\mp 592{,}098{,}052b^3 +134{,}427{,}475b^4)W^3-(3{,}841{,}278{,}805\pm 20{,}443{,}837{,}141b-83{,}663{,}110{,}622b^2\mp 74{,}088{,}692{,}678b^3 +39{,}368{,}434{,}105b^4\pm 4{,}473{,}628{,}705b^5)W^2+(21{,}878{,}089{,}479\pm 329{,}112{,}534{,}114b-2{,}094{,}866{,}377{,}839b^2 \mp 3{,}674{,}515{,}896{,}324b^3+3{,}427{,}662{,}556{,}665b^4\pm 1{,}042{,}576{,}770{,}690b^5-100{,}140{,}527{,}025b^6)W -(18{,}261{,}468{,}225\pm 1{,}661{,}793{,}608{,}475b-16{,}727{,}518{,}198{,}755b^2\mp 59{,}825{,}780{,}628{,}705b^3 +87{,}396{,}258{,}340{,}755b^4\pm 55{,}150{,}844{,}763{,}105b^5-13{,}131{,}815{,}922{,}225b^6\mp 705{,}556{,}726{,}875b^7)=0.$$

Equations for $J=14$

$$W^7-(455\pm 105b)W^6+(77{,}077\pm 47{,}670b-36{,}939b^2)W^5-(6{,}092{,}515\pm 8{,}045{,}415b-14{,}419{,}895b^2 \mp 2{,}764{,}755b^3)W^4+(230{,}673{,}443\pm 631{,}668{,}660b-1{,}940{,}497{,}902b^2\mp 994{,}665{,}420b^3 +303{,}873{,}507b^4)W^3-(3{,}841{,}278{,}805\pm 23{,}589{,}042{,}855b-114{,}588{,}599{,}790b^2\mp 121{,}872{,}781{,}170b^3 +83{,}968{,}308{,}585b^4\pm 13{,}053{,}862{,}395b^5)W^2+(21{,}878{,}089{,}479\pm 379{,}745{,}231{,}670b-2{,}834{,}763{,}235{,}959b^2 \mp 5{,}937{,}152{,}549{,}580b^3+6{,}965{,}688{,}307{,}113b^4\pm 2{,}821{,}662{,}850{,}230b^5-437{,}000{,}843{,}097b^6)W -(18{,}261{,}468{,}225\pm 1{,}917{,}454{,}163{,}625b-22{,}431{,}187{,}875{,}915b^2\mp 95{,}235{,}419{,}445{,}075b^3 +170{,}680{,}813{,}811{,}235b^4\pm 140{,}314{,}118{,}838{,}075b^5-49{,}036{,}115{,}840{,}985b^6\mp 5{,}524{,}796{,}502{,}225b^7)=0$$

$$W^7-560W^6+(119{,}392-31{,}584b^2)W^5-(12{,}263{,}680-15{,}110{,}400b^2)W^4+(633{,}721{,}088 -2{,}605{,}220{,}352b^2+202{,}551{,}552b^4)W^3-(15{,}658{,}639{,}360-198{,}942{,}965{,}760b^2+71{,}275{,}438{,}080b^4)W^2 +(157{,}294{,}854{,}144-6{,}582{,}989{,}144{,}064b^2+7{,}586{,}985{,}443{,}328b^4-181{,}233{,}303{,}552b^6)W -(416{,}179{,}814{,}400-73{,}342{,}526{,}423{,}040b^2+241{,}683{,}710{,}607{,}360b^4-28{,}054{,}235{,}381{,}760b^6)=0.$$

$$W^8-560W^7+(119{,}392-53{,}424b^2)W^6-(12{,}263{,}680-27{,}253{,}440b^2)W^5+(633{,}721{,}088$$
$$-5{,}164{,}169{,}472b^2+671{,}805{,}792b^4)W^4-(15{,}658{,}639{,}360-456{,}545{,}940{,}480b^2$$
$$+280{,}317{,}784{,}320b^4)W^3+(157{,}294{,}854{,}144-19{,}393{,}045{,}807{,}104b^2+39{,}714{,}028{,}697{,}088b^4$$
$$-1{,}752{,}049{,}619{,}712b^6)W^2-(416{,}179{,}814{,}400-364{,}086{,}983{,}393{,}280b^2+2{,}239{,}771{,}868{,}651{,}520b^4$$
$$-463{,}515{,}825{,}669{,}120b^6)W-2{,}272{,}341{,}786{,}624{,}000b^2+41{,}917{,}266{,}749{,}030{,}400b^4$$
$$-27{,}807{,}458{,}557{,}132{,}800b^6+292{,}220{,}641{,}440{,}000b^8=0.$$

Equations for $J=15$

$$W^7-560W^6+(119{,}392-45{,}024b^2)W^5-(12{,}263{,}680-21{,}131{,}520b^2)W^4+(633{,}721{,}088$$
$$-3{,}582{,}761{,}472b^2+446{,}683{,}392b^4)W^3-(15{,}658{,}639{,}360-269{,}665{,}566{,}720b^2+148{,}917{,}557{,}600b^4)W^2$$
$$+(157{,}294{,}854{,}144-8{,}815{,}336{,}341{,}504b^2+15{,}143{,}568{,}703{,}488b^4-765{,}344{,}858{,}112b^6)W$$
$$-(416{,}179{,}814{,}400-97{,}254{,}038{,}568{,}960b^2+464{,}234{,}875{,}453{,}440b^4-102{,}410{,}704{,}650{,}240b^6)=0.$$

$$W^8-560W^7+(119{,}392-73{,}584b^2)W^6-(12{,}263{,}680-37{,}010{,}880b^2)W^5+(633{,}721{,}088-6{,}929{,}079{,}552b^2$$
$$+1{,}351{,}635{,}552b^4)W^4-(15{,}658{,}639{,}360-606{,}530{,}995{,}200b^2+543{,}110{,}088{,}960b^4)W^3$$
$$+(157{,}294{,}854{,}144-25{,}566{,}948{,}900{,}864b^2+74{,}548{,}539{,}606{,}528b^4-5{,}852{,}150{,}007{,}552b^6)W^2$$
$$-(416{,}179{,}814{,}400-477{,}458{,}328{,}453{,}120b^2+4{,}096{,}623{,}324{,}487{,}680b^4-1{,}417{,}629{,}505{,}582{,}080b^6)W$$
$$-2{,}971{,}523{,}874{,}816{,}000b^2+75{,}109{,}687{,}846{,}502{,}400b^4-79{,}245{,}961{,}379{,}020{,}800b^6$$
$$+2{,}531{,}209{,}111{,}200{,}000b^8=0.$$

$$W^8-(680\pm120b)W^7+(179{,}452\pm81{,}480b-52{,}164b^2)W^6-(23{,}434{,}840\pm21{,}452{,}760b-31{,}318{,}200b^2$$
$$\mp4{,}588{,}920b^3)W^5+(1{,}601{,}489{,}318\pm2{,}790{,}728{,}040b-7{,}040{,}225{,}052b^2\mp2{,}634{,}185{,}880b^3$$
$$+651{,}554{,}982b^4)W^4-(55{,}742{,}803{,}480\pm189{,}387{,}990{,}120b-745{,}037{,}531{,}280b^2\mp553{,}580{,}725{,}680b^3$$
$$+312{,}586{,}120{,}440b^4\pm35{,}246{,}395{,}080b^5)W^3+(886{,}165{,}820{,}604\pm6{,}499{,}748{,}427{,}480b$$
$$-38{,}237{,}034{,}993{,}084b^2\mp52{,}593{,}125{,}379{,}120b^3+50{,}971{,}318{,}438{,}788b^4\pm14{,}699{,}387{,}983{,}320b^5$$
$$-1{,}727{,}702{,}682{,}372b^6)W^2-(4{,}940{,}831{,}601{,}000\pm99{,}840{,}150{,}045{,}000b-873{,}799{,}877{,}112{,}120b^2$$
$$\mp2{,}225{,}322{,}266{,}189{,}400b^3+3{,}306{,}291{,}533{,}482{,}680b^4\pm1{,}880{,}691{,}146{,}285{,}400b^5$$
$$-517{,}541{,}613{,}851{,}880b^6\mp37{,}269{,}826{,}288{,}200b^7)W+4{,}108{,}830{,}350{,}625\pm493{,}059{,}642{,}075{,}000b$$
$$-6{,}630{,}772{,}426{,}582{,}500b^2\mp32{,}929{,}424{,}899{,}875{,}000b^3+70{,}864{,}421{,}323{,}062{,}150b^4$$
$$\pm73{,}249{,}613{,}224{,}893{,}000b^5-35{,}034{,}611{,}605{,}251{,}300b^6\mp6{,}726{,}596{,}373{,}189{,}000b^7$$
$$+306{,}917{,}176{,}190{,}625b^8=0.$$

The Focusing in Crossed Fields of Charged Particles at Relativistic Energies

WALTER E. MILLETT
*Harvard University, Cambridge, Massachusetts**

(Received July 19, 1948)

The motion of charged particles traveling with relativistic energies in a uniform magnetic field superimposed at right angles to the electric field of a cylindrical condenser has been investigated. Expressions for the angle at which first-order focusing of a divergent beam of particles occurs and first approximations to the line breadth as well as dispersion in velocity, momentum, and energy are given.

INTRODUCTION

THE motion of charged particles traveling with non-relativistic energies in crossed electric and magnetic fields has been investigated by W. Henneberg.[1] His formulas are in a convenient form and are sufficiently accurate to be used in the design of an apparatus employing ions traveling with kinetic energies which are very much less than their proper energy. However, if these formulas are applied to systems employing particles with kinetic energies which are of the order of five percent or more of their proper energy, an error may result.

The purpose of this paper is to extend Henneberg's results to include particles with relativistic energies. The notation used here will be the same as that used by Henneberg.

EQUATIONS OF MOTION

The field configuration considered is a superposition of the electric field E of a cylindrical condenser and a homogeneous magnetic field H directed parallel to the cylinder axis. A schematic cross section of the field is shown in Fig. 1. The equations of motion will be described in terms of the cylindrical coordinates r and φ with origin at the center of curvature of the condenser and z axis along the axis of the condenser.

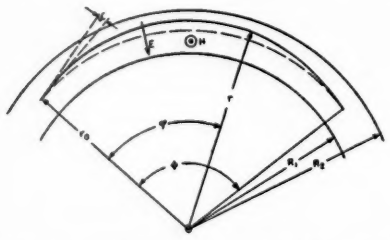

FIG. 1. A schematic representation of the field configuration considered. The positive direction of E, H, and φ are indicated.

In such a field a charged particle of relativistic mass m and charge e at r, moving with angular velocity $\omega=d\varphi/dt$ and radial velocity $\dot{r}$, will satisfy:**

$$d(m\dot{r})/dt=mr\omega^2-eE-Her\omega/c, \quad (1)$$

$$d(mr^2\omega-\tfrac{1}{2}Her^2/c)/dt=0, \quad (2)$$

$$d(mc^2)/dt=-eE\dot{r}. \quad (3)$$

The positive direction of E, H, and φ is indicated in Fig. 1.

From Eq. (1) it is seen that the electric and magnetic field strengths may be adjusted so that the electric force and the centrifugal force have a resultant which is just canceled by the radial magnetic force acting on the particle, thereby making the radial momentum constant in time. With the field strengths adjusted so that this condition is realized, a charged particle traveling initially with a velocity $v_0=r_0\omega_0$ which has no radial component will describe a circular orbit of radius r_0.

In order to satisfy this condition for circular orbits, it is clear that the ratio of the electric force to the centrifugal force may be any positive or negative number so long as the radial magnetic force is adjusted to cancel the combined electric and centrifugal forces. Because of this generality, Henneberg introduced the parameter y which he defined as follows:

$$y=(eE/mr_0\omega_0^2)_0.*** \quad (4)$$

* This work has been supported in part by Navy Contract N5 ori-76, Task Order IV, Part D.

[1] W. Henneberg, Ann. d. Physik **19**, 335 (1934).

** This consideration will be confined to particles moving in the plane $z=0$.

*** The zero subscript on an expression in parentheses indicates that the expression is evaluated at $t=0$. The zero subscript on a single symbol not in parentheses denotes the

The notation may be simplified slightly by making the following substitutions:

$$|eH/mc| = h; \quad \pm|eE/m| = \mathcal{E}/r. \tag{5}$$

($\mathcal{E}$ will be positive or negative depending on whether the electric force acting on the particle is directed inward or outward.) It is to be noted that in this form the spatial variation of E is stated explicitly.

By expanding the left member of Eq. (1) and making use of Eqs. (3) and (5), Eq. (1) becomes

$$\ddot{r} - (\mathcal{E}/r)(\dot{r}^2/c^2) = r\omega^2 - \mathcal{E}/r - hr\omega. \tag{6}$$

Integration of Eq. (2) gives

$$mr^2\omega - \tfrac{1}{2}mhr^2 = C = (mr^2\omega - \tfrac{1}{2}mhr^2)_0. \tag{7}$$

From Eq. (3) it follows that m may be expressed as a function of r alone. Then ω may be expressed as the following function of r,

$$\omega = C/mr^2 + \tfrac{1}{2}h, \tag{8}$$

and eliminated from (6) giving

$$\ddot{r} - (\mathcal{E}/r)(\dot{r}^2/c^2) = C^2/m^2r^3 - \tfrac{1}{4}h^2r - \mathcal{E}/r. \tag{9}$$

FIRST-ORDER SOLUTION: FOCUSING

Consider a source of particles located at $r=r_0$, $\varphi=0$. The field strengths are adjusted so that a particle with speed $r_0\omega_0$ will describe a circular orbit if it leaves the source with zero radial velocity. Particles which satisfy these initial conditions must by (6) satisfy

$$r_0\omega_0^2 = \mathcal{E}_0/r_0 + h_0r_0\omega_0 \tag{10}$$

as well as

$$C_0 = (m)_0r_0^2\omega_0 - \tfrac{1}{2}(mh)r_0^2. \tag{11}$$

The motion of particles which diverge initially from the circular orbit by an angle α (see Fig. 1) but have the same speed $r_0\omega_0$ may be described in terms of α and the parameters characterizing the circular orbit. To do this, the variables r and ω and the parameter C are expressed in terms of power series in α, namely:

$$\begin{aligned} r &= r_0 + \alpha r_1 + \alpha^2 r_2 + \cdots, \\ \omega &= \omega_0 + \alpha\omega_1 + \alpha^2\omega_2 + \cdots, \\ C &= C_0 + \alpha C_1 + \alpha^2 C_2 + \cdots. \end{aligned} \tag{12}$$

If α is small, the terms involving α to a power higher than the first may be neglected in Eqs. (12).

value of the quantity associated with the stable or circular orbit. The only exception is m_0 which is taken to be the symbol for the rest mass of the particle.

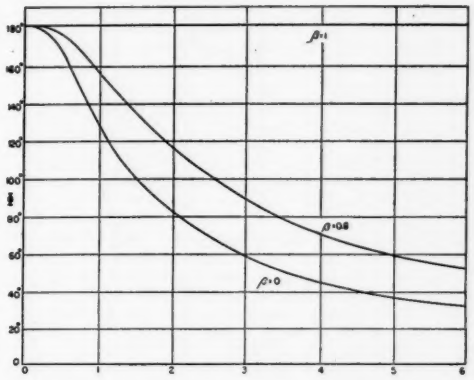

FIG. 2. A plot of the angle of focus Φ *versus* the absolute value of the field parameter y for three values of the relative speed of the particle, $\beta = r_0\omega_0/c$.

In order to find the differential equation r_1 must satisfy, terms containing powers of α higher than the first are neglected and Eq. (9) is expanded by Taylor's series. That is,

$$f(r_0 + \alpha r_1) \doteq f(r_0) + (df/dr)_0\alpha r_1.$$

Then upon equating coefficients of α,

$$\begin{aligned} \ddot{r}_1 = {} & 2C_0C_1/(m^2)_0r_0^3 - (3C^2/m^2r_0^4)_0r_1 \\ & - (2C^2/m^3r_0^3)_0(dm/dr)_0r_1 - \tfrac{1}{4}(h^2)_0r_1 \\ & - \tfrac{1}{2}(hr_0)_0(dh/dr)_0r_1 - [d(\mathcal{E}/r)/dr]_0r_1. \end{aligned} \tag{13}$$

This equation may be simplified by rewriting the expression on the right in terms of ω_0, y, and β, where $\beta = r_0\omega_0/c$. In regard to C^2 it should be noted that from Eq. (7) it follows that

$$(\omega_1)_0 = (C_1/mr^2)_0.$$

However, since only particles which have the speed $r_0\omega_0$ are being considered, it is seen that

$$\begin{aligned} (r\omega)_0 &\doteq r_0(\omega_0 + \alpha\omega_1 + \alpha^2\omega_2)_0 \\ &= r_0\omega_0\cos\alpha \doteq r_0(\omega_0 - \tfrac{1}{2}\alpha^2\omega_0). \end{aligned} \tag{14}$$

Then $(\omega_1)_0 = 0$, hence $C_1 = 0$ and $C^2 = C_0^2$ to terms of first order in α.

The simplified form of Eq. (13) is

$$\ddot{r}_1 = -[1 + y^2(1-\beta^2)]\omega_0^2r_1. \tag{15}$$

The solution of this well-known differential equation subject to the initial conditions $r_1 = 0$, $\dot{r}_1 = r_0\omega_0$ at $t = 0$ may be written at once:

$$r_1 = \frac{r_0 \sin\omega_0[1 + y^2(1-\beta^2)]^{\frac{1}{2}}t}{[1 + y^2(1-\beta^2)]^{\frac{1}{2}}}. \tag{16}$$

So, to terms of first order in α, r becomes equal to r_0 when the particle has swept through the angle

$$\varphi=\Phi=\pi[1+y^2(1-\beta^2)]^{-\frac{1}{2}}. \tag{17}$$

A plot of Φ *versus* the absolute value of y is given for three values of β in Fig. 2.

SECOND-ORDER SOLUTION: LINE BREADTH

When second-order terms are taken into account it will be found that the image of the source formed at $\varphi=\Phi$ is "smeared out" on one side or the other of r_0 by an amount which depends on α^2. The extent of the smearing out of the image is referred to as the line breadth and is denoted by B. As a first approximation of B, r_2 will be found and evaluated at $\varphi=\Phi$.

To find the differential equation r_2 must satisfy, Taylor's expansion is applied again to (9). Here

$$f(r_0+\alpha r_1+\alpha^2 r_2)\doteq f(r_0)+(df/dr)_0(\alpha r_1+\alpha^2 r_2)+\tfrac{1}{2}(d^2f/dr^2)_0(\alpha^2 r_1^2+\cdots),$$

or upon equating the coefficients of α^2,

$$\ddot{r}_2=2C_0C_2/(m^2)_0r_0^3+(\mathcal{E}/r_0)_0(\dot{r}_1^2/c^2)_0+(df/dr)_0r_2+\tfrac{1}{2}(d^2f/dr^2)_0r_1^2, \tag{18}$$

where from Eq. (15) it is seen that

$$(df/dr)_0=-[1+y^2(1-\beta^2)]\omega_0^2.$$

By differentiation and simplification,

$$(d^2f/dr^2)_0=(2\omega_0^2/r_0)[3/2+2y(1-\beta^2)+3y^2(1-\beta^2)/2-2y^3\beta^2(1-\beta^2)].$$

Then

$$\ddot{r}_2=A_0-\gamma^2r_2+A_1\sin^2\gamma t, \tag{19}$$

where

$$A_0=-\tfrac{1}{2}[1+y(1-2\beta^2)]r_0\omega_0^2,$$
$$\gamma^2=[1+y^2(1-\beta^2)]\omega_0^2,$$

and

$$A_1=\frac{3+4y+3y^2(1-\beta^2)-6y\beta^2[1+y^2(1-\beta^2)]}{2[1+y^2(1-\beta^2)]}r_0\omega_0^2.$$

Subject to the initial conditions $r_2=\dot{r}_2=0$ at $t=0$, the solution is

$$r_2=a_1\sin^2\gamma t+a_2(1-\cos\gamma t), \tag{20}$$

where

$$a_1=-r_0\frac{3+4y+3y^2(1-\beta^2)-6y\beta^2[1+y^2(1-\beta^2)]}{6[1+y^2(1-\beta^2)]^2} \tag{21}$$

and

$$a_2=r_0\frac{3+5y+3y^2(1-\beta^2)-3y^3(1-\beta^2)-6y\beta^2[1+y^2(1-\beta^2)]}{6[1+y^2(1-\beta^2)]^2}. \tag{22}$$

But now to get the line breadth it is necessary to evaluate r_2 at the time when $\varphi=\Phi$. To do this, an expression for ω_1 must be obtained. A simple way to obtain this expression is to carry out the differentiation indicated in Eq. (2). The result of this operation may be written in the form of

$$\dot{\omega}_1=-[1+y(1-\beta^2)]\omega_0\cos\gamma t.$$

Subject to the initial conditions $\omega_1=0$ for $t=0$ it is seen that

$$\omega_1=-\gamma^{-1}\omega_0^2[1+y(1-\beta^2)]\sin\gamma t.$$

Then, by integration,

$$\varphi=\omega_0 t+\alpha\frac{1+y(1-\beta^2)}{1+y^2(1-\beta^2)}(\cos\gamma t-1). \tag{23}$$

For $\varphi=\Phi$,

$$t=T=\frac{\pi}{\gamma}+\frac{2\alpha}{\omega_0}\cdot\frac{1+y(1-\beta^2)}{1+y^2(1-\beta^2)}. \tag{24}$$

Then set

$$r=r_0+B \text{ for } \varphi=\Phi, \quad t=T,$$

where B is the line breadth.

So from (20) and (24)

$$B\doteq 2\alpha^2r_0\left[\frac{a_2}{r_0}-\frac{1+y(1-\beta^2)}{1+y^2(1-\beta^2)}\right].$$

By (22) this becomes

$$B\doteq-\alpha^2r_0\frac{1+\frac{1}{3}y+y^2(1-\beta^2)+3y^3(1-\beta^2)}{[1+y^2(1-\beta^2)]^2}.\dagger$$

DISPERSION AND REDUCED DISPERSION

The line breadth is a quantity which is useful in the description of the performance of a system. Still other useful quantities are the dispersion

† The expression given in the minutes of the 1947 annual meeting (Phys. Rev. **73**, 1259 (1948)) is incorrect.

TABLE I. Expressions for the angle of focus Φ, line breadth B, velocity dispersion D_v, potential difference between the plates of the cylindrical condenser V, and the magnetic field strength H for the four field parameters most frequently used.

	Magnetic $y=0$	Electric $y=1$	Achromatic $y=-1/(1-\beta^2)$	Wein velocity filter $r_0=\pm\infty$; $r_0/y=(mc^2\beta^2/eE)_0$
Φ	π	$\frac{\pi}{\sqrt{2}}\cdot\frac{\sqrt{2}}{(2-\beta^2)^{\frac{1}{2}}}$	$\frac{\pi}{\sqrt{2}}\cdot\left(\frac{2(1-\beta^2)}{2-\beta^2}\right)^{\frac{1}{2}}$	$L=\frac{m_0c^2\beta^2\pi}{eE}\cdot\frac{1}{1-\beta^2}$ $=\pi R_H\cdot\frac{1}{(1-\beta^2)^{\frac{1}{2}}}$
B	$-\alpha^2r_0$	$\frac{-4\alpha^2r_0}{3}\cdot\frac{4-3\beta^2}{(2-\beta^2)^2}$	$\frac{\alpha^2r_0}{3}\cdot\frac{4+8\beta^2-3\beta^4}{(2-\beta^2)^2}$	$-\frac{3\alpha^2m_0c^2\beta^2}{eE}\cdot\frac{1}{(1-\beta^2)^{\frac{1}{2}}}$ $=-3\alpha^2R_H\cdot\frac{1}{1-\beta^2}$
D_v	$2r_0\cdot\frac{1}{1-\beta^2}$	$2r_0\cdot\frac{1}{1-\beta^2}$	0	$\frac{2m_0c^2\beta^2}{eE}\cdot\frac{1}{(1-\beta^2)^{\frac{1}{2}}}$ $=2R_H\cdot\frac{1}{1-\beta^2}$
V	0	$\frac{m_0c^2\beta^2}{e}\ln\frac{R_2}{R_1}\cdot\frac{1}{(1-\beta^2)^{\frac{1}{2}}}$	$\frac{m_0c^2\beta^2}{e}\ln\frac{R_2}{R_1}\cdot\frac{1}{(1-\beta^2)^{\frac{1}{2}}}$	$\frac{(R_2-R_1)m_0c^2\beta^2\pi}{eL}\cdot\frac{1}{1-\beta_2}$
H	$\frac{m_0c^2\beta}{er_0}\cdot\frac{1}{(1-\beta^2)^{\frac{1}{2}}}$	0	$\frac{m_0c^2\beta}{er_0}\cdot\frac{2-\beta^2}{(1-\beta^2)^{\frac{1}{2}}}$	$H=E/\beta$

and reduced dispersion in velocity, momentum, and energy. The expressions for the dispersion in velocity and in momentum should become equivalent in the limit of small velocities. The velocity dispersion should be equal to β^2 times the energy dispersion in the same limit.

Consider first what is meant by velocity dispersion.

A particle which leaves the source at r_0 along the tangent to the circular orbit not with velocity $v_0=r_0\omega_0$ but v_0+dv will be a distance dx from r_0 after it has swept through the angle $\varphi=\Phi$. This distance will be proportional to the fractional increment in velocity, i.e., $dx=D_vdv/v_0$. The proportionality constant D_v is called the velocity dispersion. A first approximation of D_v is obtained by setting $r=r_0+x$ and determining r to the first order, setting $\varphi=\Phi$ and comparing with $r=r_0+D_vdv/v_0$.

Setting $r=r_0+x$, $v=v_0+dv$, and applying Taylor's expansion for functions of two variables to Eq. (9) results in

$$\ddot{x}=-\gamma^2x+adv, \tag{26}$$

where

$$a=\omega_0[1+y(1-\beta^2)]/(1-\beta^2)$$

and γ^2 is as defined in connection with Eq. (19). The solution for initial condition $x=0$ at $t=0$ is

$$x=a\gamma^{-2}(1-\cos\gamma t)dv. \tag{27}$$

Then for $\varphi=\Phi$, $x=2a\gamma^{-2}dv$. Upon comparison with $r-r_0=x=D_vdv/v_0$ it is seen that a first approximation to the velocity dispersion is

$$D_v\doteq\frac{2r_0}{1-\beta^2}\cdot\frac{1+y(1-\beta^2)}{1+y^2(1-\beta^2)}. \tag{28}$$

Expressions for the momentum dispersion D_p and the energy dispersion D_m may be obtained in a manner similar to that indicated above. The momentum dispersion is defined by the following equation:

$$dx=D_pdp/p_0;$$

the energy dispersion by

$$dx=D_md(mc^2)/mc^2=D_mdm/m.$$

The resulting expressions are

$$D_p\doteq 2r_0\frac{1+y(1-\beta^2)}{1+y^2(1-\beta^2)} \tag{29}$$

and

$$D_m\doteq\frac{2r_0}{\beta^2}\cdot\frac{1+y(1-\beta^2)}{1+y^2(1-\beta^2)}. \tag{30}$$

It is interesting to note that

$$D_p^{-1}=D_m^{-1}+D_v^{-1},$$

an equality which may be obtained directly from the definition of momentum.

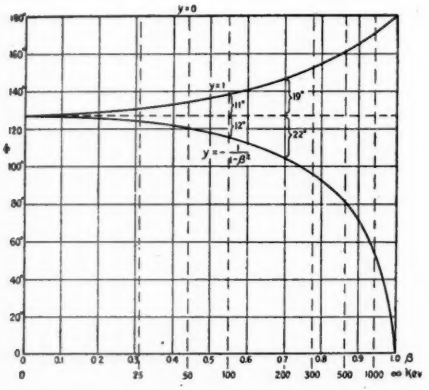

FIG. 3. A plot of the angle of focus Φ *versus* the relative speed $\beta=r_0\omega_0/c$ for three common values of the field parameter y. A kinetic energy scale for electrons is indicated along the β-axis.

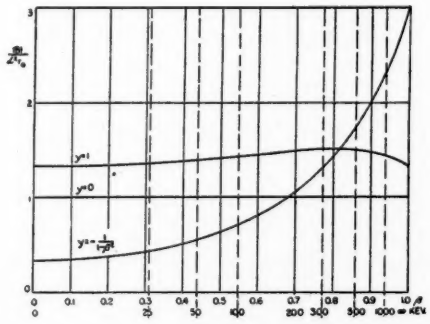

FIG. 4. A plot of the absolute value of the line breadth divided by the square of the angle of divergence and the radius of the circular orbit $|B|/\alpha^2 r_0$ *versus* the relative speed of the particle $\beta=r_0\omega_0/c$ for three common values of the field parameter y. A kinetic energy scale for electrons is indicated along the β-axis.

All three of these expressions vanish when $y=-1/(1-\beta^2)$. It can be shown that $dr_0/dv=dr_0/dp=dr_0/dm=0$ for $y=-1/(1-\beta^2)$.

The reduced dispersion δ is a quantity which serves as a better figure of merit than D or B alone. It is defined by

$$\delta=|D/B|\alpha^2.$$

This analysis indicates that a first approximation of δ_v is

$$\delta_v \doteq \frac{2}{1-\beta^2}\cdot\frac{1+y(1-\beta^2)+y^2(1-\beta^2)+y^3(1-\beta^2)^2}{1+\frac{1}{3}y+y^2(1-\beta^2)+3y^3(1-\beta^2)}.$$

The expressions for Φ, B, D_v, and δ_v reduce to those obtained by Henneberg if β is set equal to zero.

DISCUSSION OF RESULTS

It is well known that for the pure magnetic case ($y=0$) the focusing angle is equal to π independent of β, as it is here. Referring to Table I it is seen that B is also independent of β for this case. This is as it should be since in this case the mass remains unchanged over the trajectory. On the other hand, D_v should be expected to increase as β increases, since a small fractional change in velocity gives rise to an increasingly larger fractional change in mass as β increases.

The symbol V in Table I refers to the potential which must be applied across the cylindrical condenser. The general expressions for V and H are

$$V=(m_0c^2/e)(\ln R_2/R_1)[\beta^2/(1-\beta^2)^{\frac{1}{2}}]y,$$
$$H=(m_0c^2/er_0)[\beta/(1-\beta^2)^{\frac{1}{2}}](1-y).$$

Some of the expressions in this table contain a dot. That part of the expression to the left of the dot is the non-relativistic term while that to the right is the relativistic correction.

The second column of the table refers to the pure electric case ($y=1$) which was first investigated by Hughes and Rojansky.[2] The expressions for Φ and β are plotted against β in Figs. 3 and 4. Along the β coordinate the kinetic energy of electrons in kilo-electron volts is indicated.

The case for which there is both direction focusing and velocity focusing was first investigated by Bartky and Dempster.[3] This is the case for which $D_v=0$, ($y=-1/(1-\beta^2)$), which Henneberg refers to as the "achromatic" case. The expressions for Φ and B are plotted against β in Figs. 3 and 4 for this case, too.

Prior to the present calculations, Professor J. S. Schwinger has, in an unpublished note to Professor K. T. Bainbridge, calculated the relativistic expression for Φ for the achromatic case. Schwinger imposed the condition that dr_0/dv vanish. This is equivalent to the vanishing of D_v. The results obtained here are in agreement with his results. A study of Professor Schwinger's note was of great aid in the solution of the more general problem.

It should be pointed out that the power series given here converge for a limited range of values

[2] A. L. Hughes and V. Rojansky, Phys. Rev. **34**, 284 (1929).

[3] W. Bartky and A. J. Dempster, Phys. Rev. **33**, 1019 (1929).

of α. This range of α decreases in extent as $y\beta^2$ increases. When $y\beta^2$ goes to infinity the range of α goes to zero. Consequently, the expressions for Φ, B, and D for the achromatic case are not valid in the limit as $\beta \rightarrow 1$.

The expressions for the Wien velocity filter are given in the last column of the table. In a Wien velocity filter a parallel plate condenser replaces the cylindrical condenser. The length of the filter, L, i.e., the distance between source and image, may be obtained from the limit of $r_0\Phi$ as $r_0 \rightarrow \infty$, with $r_0/y = (mv^2/eE)_0$. The calculation of the relativistic value of L was also contained in the note of Schwinger which was referred to above.

The expressions for B and D_v for the Wien filter result from the same limiting process. The R_H which appears in the table stands for the radius the particle would describe if the magnetic field alone were present. The minus sign in the expression for B is included to indicate that B and D_v have opposite signs.

To Professor K. T. Bainbridge, who suggested this problem, the author is deeply indebted for valuable suggestions and aid. Henneberg's article as well as problems arising in the relativistic treatment were discussed with Professor Bainbridge and Mr. F. L. Niemann. Professor E. M. Purcell and Professor W. H. Furry have read this article and suggested several changes.

PHYSICAL REVIEW VOLUME 74, NUMBER 9 NOVEMBER 1, 1948

Contributions to the Nuclear Processes Induced in Magnesium by Polonium Alpha-Particles

A. SZALAY AND EVA CSONGOR
Institute of Physics, University of Debrecen, Debrecen, Hungary

(Received May 10, 1948)

Mg metal was bombarded in hemispherical symmetrical arrangements from the center by a strong Po source. The excitation function of the induced Al^{28} activity and of the induced γ-radiation was determined with an improved resolving power and accuracy. The absolute yields were determined carefully. Possibilities for the origin of the γ-radiation are discussed.

AS is known, Mg consists of 3 isotopes ($A = 24$, 25, 26) amounting to 77.4, 11.5 and 11.1 percent. Six possible nuclear transformations may occur in the case of the immigration of an α-particle:

1. $Mg^{24}(\alpha,p)Al^{27}$
2. $Mg^{25}(\alpha,p)Al^{28}$
3. $Mg^{26}(\alpha,p)Al^{29}$
4. $Mg^{24}(\alpha,n)Si^{27}$
5. $Mg^{25}(\alpha,n)Si^{28}$
6. $Mg^{26}(\alpha,n)Si^{29}$

and there is the possibility of the inelastic scattering of the α-particle followed by the γ-radiation of the excited Mg nucleus.

The main subject of this paper is to investigate the exact shape of the excitation function and the absolute yield of the short-living artificial radioactivity (Al^{28}), and the excitation function, quantum energy, absolute yield and origin of the γ-radiation at α-energies below 5.3 Mev.

APPARATUS

Po Preparation

The technics of Po preparations used at this Institute enabled us—by means of a volatilization method[1]—to obtain very pure Po-sources with a strength of about 10 mC or more, on a highly polished Pt-Ir disk of 3 mm diameter.

Activation Apparatus

The Po-source was located in the center of the activation apparatus and brass hemispheres of 5 cm diameter, coated on the inside with a thick pressed Mg metal plate, were placed over it (Fig. 1). Then the air was removed and CO_2 gas of suitable pressure was let in to keep the α-particles down to the energy required. The geometry

[1] A. Szalay, Zeits. f. Physik 112, 29 (1939).

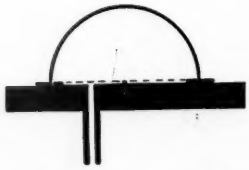

FIG. 1. Activation apparatus for Mg hemispheres bombarded from the center by Po-α-particles.

of this apparatus enabled us to make use of a solid angle of 2π and assured a very good homogeneity of the energy of the bombarding α-particles as well.

Activity Counting Equipment

The counter was a special one of hemispherical shape, developed and used by one of us years ago for the counting of weak induced activities.[1] (Fig. 2.) It was a wire-loop type counter, somewhat a transitional type between the point-counter and the G-M counter tube. Its hemispherical wall consisted of about 0.2 mm Al. Its sensitivity was carefully tested from various angles of incidence by means of a Ra-E β-gun. The hemispherical counter was situated in the middle of a lead cylinder of 4 cm thickness. The closing of the cover automatically switched on the electromagnetic counter-mechanism and started the stop-watch.

Careful determinations were made for the absorption of the electrons in the wall of the counter in the following way: Al hemispheres of the same (0.2 mm) thickness, prepared in the same way, were put as absorbing media over the hemisphere of the counter.

After finished activation (duration 6 min.) the Mg target was quickly placed on the counter and the activity was measured several times without additional absorbing hemispheres and under the same conditions, with one or two additional absorbing hemispheres. The measurements indicated that the mass absorption coefficient of the β-radiation of Al^{28} possesses under such geometrical conditions a value of $\mu=3.9\pm0.9$ cm^2/g Al. In this way the accurate correction was determined for the absorption in the wall of the counter. The value of the correction factor was 1.19. Further corrections were made for the half-life. The duration of activation and observation was numerically extrapolated back to the time of stopping of the activation and up to infinite.

RESULTS

At first it had to be decided, which of the three possible artificial radioactive nuclei are observable at so small α-energies and what is the yield of them. For this purpose, we raised the duration of the activation of the Mg targets to 30 min. The decay of the activity was observed for 35 min. and noted every minute. The decay curve showed a predominating short-living activity of Al^{28} and a weak long-living activity of Al^{29}. The activity of the long-living product was too weak to estimate its half-life exactly. It seemed to be about 7–8 min. with a probable error of ±3 min. The total yield of the long-living activity was about 20 percent of the total activity observed during 35 min., after 30 min. activation. The ratio of the intensity (number of particles/min.) of the long-living activity to the short-living one was about 8 percent at saturation activation. There is no doubt that this is the well-known Al^{29} activity of 6.7 min. half-life.[2]

We eliminated the influence of the long-living activity by means of short activation and measurement-times. In the case of the used 6-min. period for activation and for measurement as well, the long-living activity could not amount to more than 3 percent of the observed total. This error could be left out of consideration. We estimated the half-life of Al^{28} by means of ten repeated 6-min. activations with full α-energy. The activity was registered at the end of every minute for 6 min. The evaluation in the

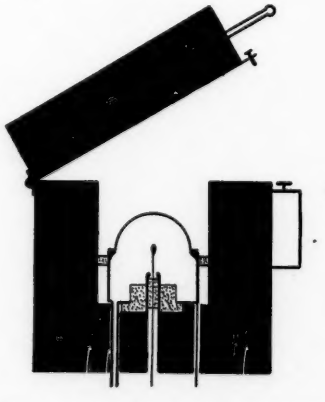

FIG. 2. Wire-loop counter for the measurement of the Al^{28} activity excited in Mg hemispheres.

[2] W. J. Henderson and R. L. Doran, Phys. Rev. 56, 123 (1939).

usual way resulted in a half-life of $T=2.07\pm0.05$ min. These measurements were carried out carefully, with a small statistical error. We state with certainty that the half-life is shorter than the 2.3 or 2.5 min. given by some earlier observers.[3,4]

THE EXCITATION FUNCTION OF THE PROCESS $Mg^{25}(\alpha,p)Al^{28}$

Measurements and considerations above showed that in the case of 6-min. activations and measurements, the observed activity can be ascribed, at least up to 97 percent, to this transmutation. The thick Mg hemispherical targets were used for the determination of the excitation curve, represented in Fig. 3. Ten repeated series of activations were made over the whole measured interval for each α-particle energy. Each point on the graph represents the sum of ten activity observations. The total activity of one activation induced by the full energy of the α-particles of the 10 mC Po-source amounted to about 600 counted particles. This gave an absolute yield (number of Al^{28} atoms/number of incident α-particles) of 1.4×10^{-7} for the natural isotope mixture and for a thick Mg target (integral yield), when corrections mentioned above and corrections for the geometrical losses are taken into account. The differential yield amounts to 0.24×10^{-7} for 5.3 Mev α-energy and for a Mg target of 1 mm air-equivalent thickness.

The ordinate of Fig. 3 shows the integral absolute yield of the process $Mg^{25}(\alpha,p)Al^{28}$ for the natural isotope mixture.

The abscissa shows the maximum ranges of the bombarding α-particles and their corresponding maximum energy, estimated by means of the graphs of Livingstone and Bethe.[5]

The excitation curve completes earlier measurements made by Chang and Szalay,[6] which were made for α-energies from 7 Mev down to 5 Mev, and which Szalay made for α-energies below 5.3 Mev.[7] It seems to show some signs of

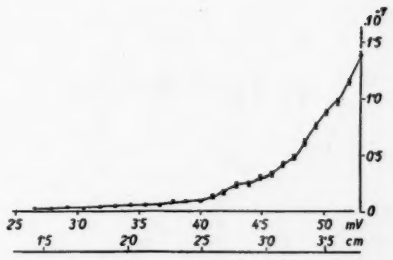

FIG. 3. The excitation function of the Al^{28} activity induced in Mg by α-particle bombardment. Abscissa: maximum range resp. energy of the α-particles; ordinate: integral absolute yield of the transmutation $Mg^{25}(\alpha,p)Al^{28}$ for a thick layer of Mg consisting of natural isotope mixture.

resonances, but the resonances are scarcely greater than the statistical errors. It seems to us to be unjustified to give some values of α-energy as resonance-energies.

INVESTIGATION OF THE GAMMA-RADIATION

It was shown by Bothe and Becker[8] that a weak γ-radiation is excited in Mg when bombarded by Po α-particles. They reported a yield of the magnitude 1 γ-quant/10^6 α-particles of maximum Po α-energy. Savel[9] investigated the excitation function, but only for 6 different α-energies, therefore the resolving power is low. He reported a quantum energy of 0.5 Mev from absorption measurements. In contradiction to his measurements Webster[10] reported a quantum energy of 5.0 Mev.

It is the task of these measurements to settle this question by employing greater accuracy.

Excitation Function

The same Po-source and Mg target of 5 cm diameter was used for the investigation of the integral γ-excitation curve. Figure 4 shows the arrangement of the target and the G-M counter-tube. The whole arrangement was surrounded by a massive lead shield of 3 cm thickness to reduce the natural effect. The G-M counter-tube consisted of 1.8 mm thick brass, had a diameter of 45 mm and a length of 88 mm.

We observed a natural effect of 2033 ± 15 impulses/hour, in addition to this came the γ-radiation of the 10 mC Po-source of 4530 ± 9

[3] C. D. Ellis and W. J. Henderson, Proc. Roy. Soc. 156, 358 (1936).
[4] L. N. Ridenour and W. J. Henderson, Phys. Rev. 52, 889 (1937).
[5] M. S. Livingstone and H. A. Bethe, Rev. Mod. Phys. 9, 266 (1937).
[6] W. Y. Chang and A. Szalay, Proc. Roy. Soc. 159, 72 (1937).
[7] A. Szalay, Naturwiss. 32, 72 (1944).
[8] W. Bothe and H. Becker, Zeits. f. Physik 66, 289 (1930).
[9] P. Savel, Ann. de physique 4, 88 (1935).
[10] H. C. Webster, Proc. Roy. Soc. 136, 428 (1932).

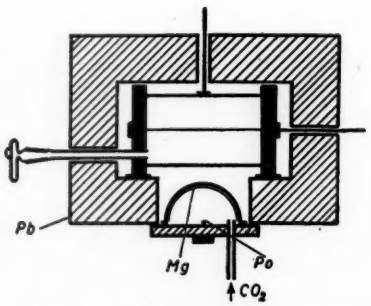

FIG. 4. Apparatus for the investigation of the excitation function of the Mg γ-radiation.

observed γ-quanta/hour. The maximum intensity of the γ-radiation, excited in the Mg target, amounted to 952 ± 45 quanta/hour, at 5.3 Mev α-energy, actually counted in the given geometrical arrangement.

Figure 5 shows the integral excitation function of the γ-radiation. It becomes observable for 4.0 Mev and then rises quickly up to higher values. The intensity is small in comparison with the natural effect, therefore the statistical errors are considerable. Resonance effects could not be stated decisively.

Absorption

Figure 6 shows the apparatus. It was the same as for the investigation of the excitation function, with the difference that a hemispherical target of 2 cm diameter was used. The stopping power of the CO_2 was not sufficient to stop the Po α-particles from bombarding the target, so a brass shutter was used, which could be moved from the outside. In this way the α-particles could be retarded from the target and so the natural effect +Po γ-radiation could be measured separately from the induced γ-radiation. The absorption measurements were carried out always at 5.3 Mev α-energy. The actual rates of counting were 2035 ± 15 quanta/hour for the natural effect, 6819 ± 42 quanta/hour for the Po-γ and 1371 ± 56 quanta/hour for Mg γ-radiation, without lead absorbents.

We combined one, two, or three lead absorbents of half cylindrical shape, with thicknesses of 2.7, 2.7, and 1.9 mm.

Figure 7 shows the results of the absorption measurements of the γ-radiation. The ordinate shows the intensity represented by the logarithm of the rate of counting ($\log I/I_0$); the abscissa shows above the actual thickness, below the "effective thickness" of the absorbing lead in cm. (The "effective lead thickness" is related to the spherical absorption coefficient μ and was estimated experimentally by the absorption of the well-known γ-radiation of ThC+C′+C″.)

For the calibration of this absorption equipment we prepared pure sources of RaC and ThC in equilibrium with their daughter products (C′ and C″ bodies). These sources were made on nickel hemispheres of exactly the same shape as the Mg target and were situated on exactly the same place.

Further we measured the absorption of the γ-radiation of the used Po source situated at the center.

Figure 7 shows the absorption of the γ-radiation induced in Mg and of the other investigated γ-radiations of Po, ThC+C′+C″ and RaC+C′+C″.

The difficulties of γ-absorption measurements, especially in cases when the very small intensity prevents the use of clear, well-defined geometrical conditions, are well known. Here we must point out some possible sources of errors in detail, and how we tried to reduce them. At first: the γ-quanta traverse the lead absorbents at various angles of incidence and for this reason it would be erroneous to use the actual thickness of the lead without any correcting factor. A "mean effective thickness" (related to the spherical absorption arrangement) must be determined experimentally. It is greater than the actual

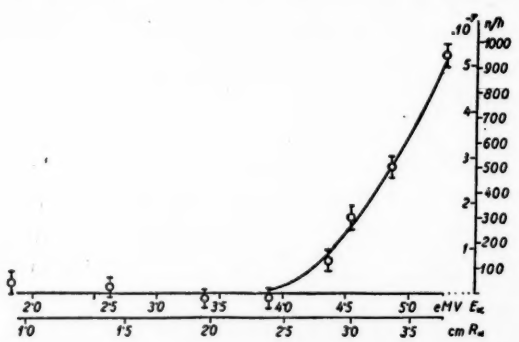

FIG. 5. Excitation function of the γ-radiation excited in a thick Mg layer by α-particles. Abscissa: maximum range resp. energy of the α-particles. Ordinates, right: rate of counting/hour; left: integral absolute yield of the γ radiation, i.e., number of γ quanta/number of incident α-particles.

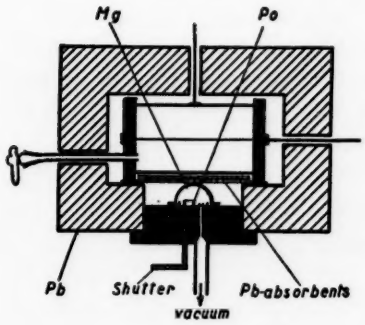

FIG. 6. Measuring equipment for the determination of the energy of the γ-radiation excited in Mg by Po-α-particles of full energy.

thickness of the lead screens. The lack of a clear geometry prevents an exact estimation of the participation of the three different components (photo-, Compton- and materialization-effects) in the total absorption coefficient μ. Disagreement of the measurements of Savel[9] and Webster[10] can be ascribed in this case certainly to the above reasons. We tried to eliminate such sources of errors by means of the calibration of the apparatus by the known γ-radiation of the natural radioactive sources of well-known lead absorption coefficient, resp. quantum energy.

The small intensity of the γ-radiation prevented the use of thicker lead absorbents. The intensity was reduced in the case of the used greatest thickness up to 63 percent for the Mg-γ, 58 percent for the ThC''-γ, 50 percent for the RaC-γ, and 43 percent for the Po-γ-radiation.

As Fig. 7 shows, the Mg γ-radiation possesses certainly a smaller absorption coefficient than the well-known γ-radiation of the ThC'', consisting of a component of overwhelming intensity of 2.65 Mev quantum energy.

We determined the effective thickness of the lead absorbents (abscissa, below) by the use of the well-known absorption coefficient for this nearby monochromatic radiation ($\mu=0.47$ cm^{-1} in Pb). In this way we obtained an absorption coefficient for the induced γ-radiation of the Mg $\mu=0.38\pm0.08$ cm^{-1} in Pb. It is remarkable that this value seems to be smaller than the smallest absorption coefficient measured for any γ-radiation in lead in the case of spherical absorption equipment. A look at Fig. 7 makes it sure that the difference of the absorption coefficient against the ThC'' γ-radiation is definitely emerging over the statistical error. The reason for the unexpectedly small value of the Mg γ-absorption coefficient must be in the reduced share of the Compton effect in the absorption, as a result of the unfavorable geometrical arrangement.

The total absorption coefficient in lead shows a flat minimum for about 3 Mev quantum energy,[11] an estimation of the quantum energy by means of lead absorption measurements is here very inaccurate. For these reasons we are unable to evaluate the quantum energy of the Mg γ-radiation with accuracy. It must possess a value somewhat greater than 3 Mev. Values of the probable error cannot be given.

Some sources of errors are eliminated in this way, because (1) the quantum energy of both radiations is nearly the same and so the shares of Compton, materialization and photo-effects are in both cases the same; and (2) the geometrical arrangement is—in both cases compared—exactly the same.

Criticism may arise by the fact that ThC+C'+C'' possesses in addition to this 2.65 Mev γ-radiation other components of 0.58 and 0.51 Mev[12], with about the same number of γ-quanta/unit time. We were unable to apply a thick lead absorbent before to make the radiation homogeneous. But measurements of v. Droste[13] showed that the sensitivity of a brass G-M counter-

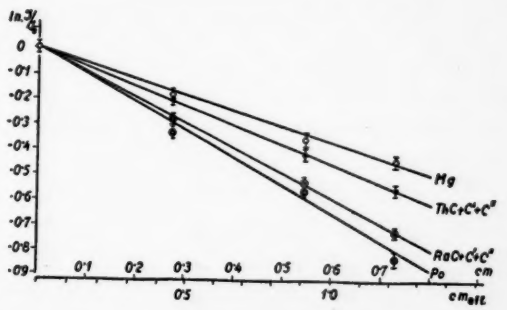

FIG. 7. Absorption of the γ-radiations in lead. Abscissa, above: actual thickness of the absorbing lead sheets; below: corrected "effective thickness" of the lead absorbents. Ordinates: logarithm of the relative decrease of the intensity of the γ radiation with *vs.* without lead absorbents for the Mg-γ. ThC+C'+C''$-\gamma$, RaC+C'+C''$-\gamma$ and for the Po$-\gamma$-radiation.

[11] Mme P. Curie *Radioactivité*, (Herman et Cie, Paris, 1935), Vol. II, Appendix 11.
[12] W. Gentner, Physik. Zeits. **36**, 836 (1937).
[13] G. v. Droste, Zeits. f. Physik **100**, 529 (1936), and **104**, 474 (1936).

tube is about 5 times smaller (0.32 percent) for 0.5 Mev quantum energy than for 2.65 Mev (1.61 percent). The very careful measurements of v. Droste showed that the practical absorption curve of this composed radiation does not differ much from the absorption curve of the filtered hard radiation, if a brass G-M counter-tube has been used for the measurement.

Recently Pollard and Alburger[14] measured the quantum energy of the γ-radiation of Mg induced by α-bombardment. They obtained a value of 3.2 ± 0.6 Mev in fairly good accordance with the value obtained above. Considering the fact that we were forced to work with sources of very low intensity and therefore under not sufficiently clear geometrical conditions, we will use in the following the value obtained by Pollard and Alburger of 3.2 Mev. (As E. Pollard kindly informed me in a private communication, Alburger's newest measurements, in the course of publication, are indicating a still higher energy of 3.8 Mev.)

MEASUREMENTS ABOUT THE ORIGIN OF THE GAMMA-RADIATION

It is well known that the electron emission of Al^{28} is followed by the emission of a γ-quant of 2.05 Mev,[15,16] the last belonging to the excited state of Si^{28}. If the induced γ-radiation observed here belonged to this process, it would show a decay period of 2.1 min. We decided this question in the following way: we measured the number of emitted γ-quanta during a period of 120 minutes in such a way that we activated the Mg target for 2 minutes, then we stopped the α-rays with the shutter. Simultaneously the counter was switched on and the γ-radiation was counted for 2 minutes. After this, the whole process of measurement was repeated 60 times periodically, so that altogether 120 minute observations of the γ-intensity could be summarized. The periodically interrupted and summarized measurements gave altogether 13,886 ±164 counts/120 min., included the natural effect+Po γ-radiation, the last two amounting to $13,714\pm162$ quanta/120 min., with closed shutter. These values above are nearly the same, within the limits of statistical errors. In the case of continuous measurements during bombardment by Po α-radiation of maximum range, the total rate of counting amounted to $16,936\pm184$ quanta/120 min. We can state with certainty that the induced γ-radiation of Mg is not identical with the γ-radiation connected with the electron emission of Al^{28}, moreover it is at least one order of magnitude more intense.

THE ABSOLUTE YIELD OF THE GAMMA-RADIATION

Knowledge of the absolute yield of the Mg γ-radiation may lead us to the decision of the question, which of the six possible nuclear processes is it connected with?

The actual measured intensity of the Mg γ-radiation was 1371 ± 56 observed γ-quanta/hour, when a hemisphere of 20 mm diameter was bombarded with the full energy of the 10.0 mC Po-source. (See geometrical arrangement in Fig. 6.)

We determined the absolute yield of the γ-radiation in the following two ways:

1st method. We estimated the geometrical angle (solid angle) of the apparatus and the absolute sensitivity of the G-M counter:

(a) an approximative calculation of the solid angle based on the maximum cross section of the G-M tube, taking the point of the solid angle into the center of gravity of the hemisphere, gave a solid angle of $0.22\cdot4\pi$.

(b) an approximative numerical integration for several zones of the hemisphere gave a total solid angle of $0.23\cdot4\pi$.

(c) another estimation based on the surface measurement of the shadow of the G-M counter projected by a point light source situated on the place of the Po source, gave a solid angle of $0.21\cdot4\pi$.

The most probable value of the solid angle is herewith $0.22\cdot4\pi$, a mean of the values above.

The absolute sensitivity of a brass G-M counter was estimated by v. Droste[13] for various wave-lengths and for the wave-length of the 2.65 Mev ThC'' γ-radiation ($\lambda=4.7$A). V. Droste estimated the sensitivity of a brass counter as 1.61 percent for the 2.65 Mev ThC'' γ-radiation.

[14] E. Pollard and D. E. Alburger, Phys. Rev. **72**, 1196 (1947).
[15] Eklund and Hole, Ark. Mat. Ast. Phys. **29A**, No. 26 (1943).
[16] J. V. Dunworth, Nature **159**, 436 (1947).

The Mg γ-radiation has an energy of about 3.2 Mev as recently estimated by Pollard and Alburger.[14] The sensitivity of a brass G-M counter can be extrapolated, by means of the measurements of v. Droste, and a sensitivity of 2 percent is to be expected for this energy. Using this value and the solid angle of our apparatus, we obtain an absolute integral yield of the Mg γ-radiation excited by full range Po-α-particles as $4.6 \cdot 10^{-7}$ γ-quanta/α-particles.

2nd method. The second way was the measurement of the absolute yield by direct comparison with a ThC'' γ-source of well-known strength. We prepared a ThC+C'+C''-source on a nickel hemisphere of the same diameter (20 mm) and have placed it in the place of the Mg hemisphere. We measured the actual number of countings/hour. The strength of the source was measured separately, by counting the number of the ThC-α-particles by a mica window counter, which was situated at the end of an evacuated tube. The activated nickel hemisphere was enclosed at the other end within the tube. The solid angle was defined by the small circular opening of the mica window counter. Successive changes in the air pressure within the tube stopped and separated the ThC-α, ThC'-α and the β-particles. In this way the number of emitted ThC-α particles could be separately determined. The number of the emitted ThC''-β-particles is the same and it is generally accepted in the literature that each ThC''-β-particle is followed by a 2.65 Mev γ-quantum. This means that a ThC+C'+C'' source is emitting nearly equal number of ThC-α particles and 2.65 Mev γ-quanta/unit time. A source of 0.9×10^{-4} mC (relating to ThC'') gave 10.5 γ-quanta/sec. in the equipment on Fig. 6.

By the numerical comparison of the ThC'' γ-radiation and the Mg γ-radiation, the error in the estimation of the solid angle is entirely eliminated and the error in the absolute sensitivity of the G-M counter is very much reduced, because only the quotient of the two sensitivities comes into the formula. Using the data of v. Droste, the sensitivity of the brass counter is expected to be 1.25 times greater for the 3.2 Mev Mg γ-radiation, than for the 2.65 Mev ThC'' γ-radiation. These numerical values give an integral absolute yield of 5.2×10^{-7} γ-quanta/full range Po-α-particles. This second way of measurement is certainly more accurate than the first.

DISCUSSION ABOUT THE ORIGIN OF THE GAMMA-RADIATION

Let us consider now the six possible processes when Mg is bombarded by α-particles.

1. $Mg^{24}(\alpha,p)Al^{27}$. The isotope mass values given by Mattauch and Flügge[17] give a mass defect of -1.96 ± 0.8 TMU; the process is herewith endoergic by -1.8 ± 0.7 Mev. Taking into account 3.2 Mev energy or more for the γ-radiation, the bombarding α-particle has to possess more than 5 Mev energy, or this process is excluded by reasons of energy. As the γ-radiation is first somewhat above 4.0 Mev α-energy observable, this possibility can be excluded certainly.

2. $Mg^{25}(\alpha,p)Al^{28}$ process was investigated carefully and our measurements show that the absolute yield of this transmutation (being 1.4×10^{-7} protons/α-particles) is definitely much smaller than that of the γ-radiation (5.2×10^{-7} γ-quanta/α-particles). The process is endoergic having a mass defect of -2.3 TMU, or -2.14 Mev calculated with the new mass value of Al^{28} of 27.99265 MU$\pm$0.7 TMU. This value is obtained by considering the recently experimentally testified fact[16] that Al^{28} emits at first a β-particle of 2.98 ± 0.18 Mev energy which is followed by a γ-quant of 2.05 Mev.[15] When we consider this fact, we obtain a new value of the mass difference between the stable Si^{28} nucleus and the Al^{28} nucleus, and so a new mass value, differing from that given by Mattauch.[17] Herewith it is excluded that the Mg γ-radiation could belong to this process.

3. $Mg^{26}(\alpha,p)Al^{29}$. We measured roughly the yield of this transmutation being even smaller than the yield of process (2). Its mass defect is about -3.3 TMU. Added to this the quantum energy of the γ-radiation, we get a minimum α-energy of 6 Mev. It is excluded by energy-conservation considerations, that the γ-radiation could belong to this process.

4. $Mg^{24}(\alpha,n)Si^{27}$, this process has a mass defect of -8.8 TMU and is definitely excluded

[17] J. Mattauch, *Kernphysikalische Tabellen* (Verlag Julius Springer, Berlin, 1942).

for Po-α-energies. It definitely does not occur even at 16 Mev α-energy.[2]

5. $Mg^{25}(\alpha,n)Si^{28}$ process is exoergic by a mass defect of $+2.31\pm0.8$ TMU. It is energetically possible that the γ-radiation could belong to this process. The question could be decided by exact experimental determination of the excitation function and the absolute yield of this transmutation.

6. $Mg^{26}(\alpha,n)Si^{29}$, this transmutation having a mass defect of -1.5 ± 0.9 TMU may be connected with the γ-radiation as well, but it is as little investigated experimentally as process (5). We are intending in the near future to carry out measurements about the yield and the excitation function of the neutron emission of Mg, when bombarded by Po-α-particles.

SUMMARY

Mg hemispheres were bombarded by a very pure Po-α-source of small diameter from the center. The excitation function of the short-living artificial radioactivity belonging to the process $Mg^{25}(\alpha,p)Al^{28}$ has been investigated (Fig. 3). The absolute yield of this transmutation has been determined very carefully. It has a value of 1.4×10^{-7} transmutations/bombarding α-particle of 5.3 Mev energy, in a thick Mg layer consisting of the natural isotope mixture of the Mg isotopes.

The excitation function of the γ-radiation, which is excited in Mg by Po-α-particles, was investigated (Fig. 5).

The absolute yield of the γ-radiation has been determined very reliably by direct comparison with the ThC''-γ-radiation of a ThC+C'+C'' preparation of exactly known strength. The absolute yield of the γ-radiation excited in a thick Mg layer of natural isotopic composition under bombardment of full energy Po-α-particles amounts to 5.2×10^{-7} γ-quanta/α-particle.

A discussion of the origin of the γ-radiation is given. Four of the six possible processes can be excluded by considerations of energy, or by the comparison of the absolute yields as well. Two remain as possible origins of the γ-radiation, $Mg^{25}(\alpha,n)Si^{28}$ being the most probable by considerations of energy.

Further investigations in these processes are intended at this Institute.

PHYSICAL REVIEW VOLUME 74, NUMBER 9 NOVEMBER 1, 1948

New Aspects of the Photon Self-Energy Problem

GREGOR WENTZEL
Institute for Nuclear Studies, University of Chicago, Chicago, Illinois
(Received June 29, 1948)

A finite but non-vanishing value for the self-energy of the photon, corresponding to a finite rest-mass, can be deduced from the new invariant formulation of quantum electrodynamics developed by Tomonaga and Schwinger, in the e^2 order approximation. The implications of this result are discussed.

INTRODUCTION

THE new development in quantum electrodynamics has led to the conviction that the anomalies of the hydrogen $2S$ level and of the magnetic moment of the electron can be explained in terms of field-dependent parts of the electronic self-energy.[1] Accordingly, it seems that the concept of electromagnetic self-energy now acquires a more than merely mathematical significance. However, the field-dependent terms can, at best, be defined as finite parts of the still diverging, total self-energy of the electron which has to be eliminated from the Hamiltonian by a formal readjustment. Therefore, there is still but little hope for a final and satisfactory solution of the self-energy problems within the framework of the conventional quantum theory of fields.

[1] J. Schwinger and V. Weisskopf, Phys. Rev. **73**, 1272 (1948); J. Schwinger, Phys. Rev. **73**, 416 (1948).

Nevertheless, just these fundamental questions ought to be examined with particular care.

Even more involved than the electron self-energy problem is that of the photon. It is well known that, according to Dirac's theory of the positron, a photon can virtually create and reabsorb electron-positron pairs, which process gives rise to a self-energy that is divergent even in Heisenberg's elaborate subtraction formalism.[2] On the other hand, Schwinger claims that, in his new formulation of quantum electrodynamics, the photon self-energy vanishes identically.[3] However, the proof which Schwinger presented in his report at the Pocono Manor Conference, March 30–April 2, 1948, is highly objectionable.* Indeed, as we wish to show, if the same method of calculation is applied as is used by Schwinger in computing the electron self-energy, the self-energy of the photon turns out to be finite but not zero, whereas other methods of calculation yield infinite values.

A non-vanishing self-energy, or rest-mass, of the photon, formally appearing in the theory, is, of course, a very undesirable feature since, even if it can be subtracted, it will destroy the gauge-invariance of the theory at least at some stage of the mathematical development, so that the electromagnetic potentials will appear as being observable quantities. Moreover, the subtraction of the lowest order self-energy terms ($\sim e^2$) will entail higher order corrections whose physical significance is rather doubtful.

THE FUNDAMENTAL EQUATIONS

The quantum theory of the electromagnetic field, as developed by Schwinger, is based on the generalized multiple-time formulation of the quantum theory of fields which was first proposed by Tomonaga.[4] Considering the electrons as specified particles $n=1, 2, \cdots$, Dirac, Fock, and Podolsky[5] introduced a state functional Ψ depending on the individual time coordinates t_n of the electrons as well as on their space and spin coordinates. In Tomonaga's theory, where all particles are described by quantized wave fields, every volume element (at x, y, z) is associated with an individual time $t(xyz)$, the function $t(xyz)$ defining a surface σ in the four-dimensional x, y, z, t space. The state functional Ψ is supposed to be a function of σ, i.e., of the function $t(xyz)$, and the Schrödinger equation determines the change of $\Psi(\sigma)$ in the event that the surface σ is displaced infinitesimally only at a particular point of the surface.

Let the surface be shifted at the point $x=(ct, x, y, z)$ over a volume $d^4x=cdtdxdydz$, and the corresponding change of $\Psi(\sigma)$ be denoted by $d^4x\partial\Psi(\sigma)/\partial\sigma(x)$, then the generalized Schrödinger equation reads:

$$ihc(\partial\Psi(\sigma)/\partial\sigma(x))=\mathcal{H}(x)\Psi(\sigma), \tag{1}$$

where $\mathcal{H}$ is the Hamiltonian density representing the interaction of electrons and the electromagnetic field:

$$\mathcal{H}(x)=-(1/c)j_\mu(x)A_\mu(x), \tag{2}$$

j_μ = electric current density produced by electrons and positrons, A_μ = electromagnetic potentials explicitly depending on space and time coordinates according to the wave equations[6]

$$(\partial^2/\partial x_\nu^2)A_\mu(x)=0, \tag{3}$$

and the invariant commutation rules

$$[A_\mu(x), A_\nu(x')]=(\hbar c/i)\delta_{\mu\nu}D(x-x'). \tag{4}$$

Both j_μ and A_μ are operators, operating on the field variables (occupation numbers) of which $\Psi(\sigma)$ is a function. In order that (1) be integrable, $\mathcal{H}(x)$ must commute with $\mathcal{H}(\bar{x})$ taken at any other point $\bar{x}$ on σ. This condition is satisfied for all spacelike surfaces (i.e., when each two surface points are spacelike to each other).

In addition, we have the supplementary conditions

$$(\partial A_\mu(x)/\partial x_\mu)\Psi(\sigma)=0, \tag{5}$$

for all points x on the surface σ. As in the Dirac-Fock-Podolsky formalism, it is convenient to require more generally

$$\Omega(x', \sigma)\Psi(\sigma)=0, \tag{6}$$

where x' is now an independent space-time point,

[2] W. Heisenberg, Zeits. f. Physik **90**, 209 (1934).
[3] J. Schwinger, Phys. Rev. (to be published).
* *Note added in proof, October 1, 1948:* Professor Schwinger kindly informed me of a new derivation of his previous result. But this new argument again involves an integration by parts which, in my opinion, is not legitimate mathematically.
[4] S. Tomonaga, Progress Theor. Phys. **1**, 27 (1946).
[5] P. A. M. Dirac, V. Fock, and B. Podolsky, Physik. Zeits. Sowjetunion **2**, 468 (1932).
[6] $x_4=ix_0=ict$. Similarly for all four-vectors.

not necessarily lying on σ, Ω being an operator reducing to $\partial A_\mu/\partial x_\mu$ for surface points, satisfying the wave equation

$$(\partial^2/\partial x_\nu'^2)\Omega(x', \sigma)=0, \quad (7)$$

and the compatability conditions

$$[\Omega(x', \sigma), \Omega(x'', \sigma)]=0, \quad (8)$$

$$ihc(\partial\Omega(x', \sigma)/\partial\sigma(x))+[\Omega(x', \sigma), \mathfrak{H}(x)]=0. \quad (9)$$

The last condition is sufficient (but not necessary) to ensure $\partial(\Omega(x', \sigma)\Psi(\sigma))/\partial\sigma(x)=0$, in agreement with (6). An operator Ω satisfying all requirements is

$$\Omega(x', \sigma)=\frac{\partial A_\mu(x')}{\partial x_\mu'}+\frac{1}{c}\int_\sigma d\sigma_\mu j_\mu(x)D(x'-x), \quad (10)$$

($d\sigma_\mu$=four-vector surface area at x: in a particular frame of reference $d\sigma_1=d\sigma_2=d\sigma_3=0$, $d\sigma_4=-idxdydz$).

The perturbation method, as applied by Schwinger, starts with a unitary transformation

$$\Psi(\sigma)=e^{-iS(\sigma)}\phi(\sigma), \quad (11)$$

$$S(\sigma)=\frac{1}{2hc}\int d^4x'\epsilon(x', \sigma)\mathfrak{H}(x'). \quad (12)$$

Here

$$\epsilon(x', \sigma)=\begin{cases}+1 \text{ for points } x' \text{ earlier than } \sigma,\\ -1 \text{ for points } x' \text{ later than } \sigma,\end{cases}$$

and the x' integration is meant to be extended over the entire four-dimensional space (between two fixed surfaces in the infinite past and the infinite future). Inserting (11), with

$$e^{-iS}=1-iS-\tfrac{1}{2}S^2+\cdots,$$

into (1), the terms linear in e cancel, because of

$$\hbar c(\partial S(\sigma)/\partial\sigma(x))=\mathfrak{H}(x),$$

and the Schrödinger equation for ϕ, up to second-order terms in e, reduces to

$$ihc(\partial\phi(\sigma)/\partial\sigma(x))=\tfrac{1}{2}i[S(\sigma), \mathfrak{H}(x)]\phi(\sigma)+\cdots. \quad (13)$$

According to (2) and (12) the new second-order Hamiltonian is

$$\frac{i}{2}[S(\sigma), \mathfrak{H}(x)]=\frac{i}{4\hbar c^3}\int d^4x'\epsilon(x', \sigma)\times[j_\mu(x')A_\mu(x'), j_\nu(x)A_\nu(x)]. \quad (14)$$

THE SELF-ENERGY OF THE PHOTON

Disregarding terms independent of the A_μ's, i.e., neglecting the commutators (4), the essential terms in (14) may be written

$$\frac{i}{4\hbar c^3}\int d^4x'\epsilon(x', \sigma)[j_\mu(x'), j_\nu(x)]A_\mu(x')A_\nu(x). \quad (15)$$

Since we want to study the energy of photons, in the absence of electrons and positrons, the operator $[j_\mu(x'), j_\nu(x)]$ may be replaced by its vacuum expectation value which is easily derived by expressing the current densities in terms of the electron wave operators:

$$\langle[j_\mu(x'), j_\nu(x)]\rangle_{\text{vac}}=4ie^2c^2\Big\{\frac{\partial\Delta(x'-x)}{\partial x_\mu}\frac{\partial\Delta_1(x'-x)}{\partial x_\nu}+\frac{\partial\Delta(x'-x)}{\partial x_\nu}\frac{\partial\Delta_1(x'-x)}{\partial x_\mu}-\delta_{\mu\nu}\Big[\frac{\partial\Delta(x'-x)}{\partial x_\lambda}\frac{\partial\Delta_1(x'-x)}{\partial x_\lambda}+\mu^2\Delta(x'-x)\Delta_1(x'-x)\Big]\Big\}, \quad (16)$$

where Δ and Δ_1 denote the two invariant delta-functions involving $\mu=mc/\hbar$, as specified below (cf. (20), (21)). Subtracting, finally, from (15), the vacuum value (no photons present), we obtain the operator corresponding to the photon self-energy density

$$\mathfrak{H}_{\text{self}}=\frac{i}{4\hbar c^3}\int d^4x'\epsilon(x', \sigma)\langle[j_\mu(x'), j_\nu(x)]\rangle_{\text{vac}}\times\{A_\mu(x')A_\nu(x)-\langle A_\mu(x')A_\nu(x)\rangle_{\text{vac}}\}. \quad (17)$$

Let us calculate the expectation value $\langle\mathfrak{H}_{\text{self}}\rangle_\kappa$ for a state in which we have only one photon of momentum $\hbar\kappa_\lambda(\kappa_\lambda^2=0)$. Then

$$\langle A_\mu(x')A_\nu(x)\rangle_\kappa-\langle A_\mu(x')A_\nu(x)\rangle_{\text{vac}}=C_{\mu\nu}(\kappa)\cos\kappa_\lambda(x_\lambda'-x_\lambda). \quad (18)$$

Hence, putting

$$x_\lambda' - x_\lambda = \xi_\lambda, \quad \text{and} \quad \epsilon(x', \sigma) = -\xi_0/|\xi_0|$$

(which is justified because the function (16) vanishes identically for space-like vectors ξ):

$$\langle \mathcal{H}_{\text{self}} \rangle_\kappa = \frac{e^2}{\hbar c} C_{\mu\nu} \int d^4\xi \cos\kappa_\lambda \xi_\lambda \cdot \frac{\xi_0}{|\xi_0|} \times \left\{ \frac{\partial \Delta(\xi)}{\partial \xi_\mu} \frac{\partial \Delta_1(\xi)}{\partial \xi_\nu} + \frac{\partial \Delta(\xi)}{\partial \xi_\nu} \frac{\partial \Delta_1(\xi)}{\partial \xi_\mu} - \delta_{\mu\nu} \left[\frac{\partial \Delta(\xi)}{\partial \xi_\lambda} \frac{\partial \Delta_1(\xi)}{\partial \xi_\lambda} + \mu^2 \Delta(\xi) \Delta_1(\xi) \right] \right\}. \quad (19)$$

If the ξ-space integration is carried out by introducing polar coordinates and integrating first over the invariant hyperboloids $\xi_\lambda^2 = \text{const.}(<0)$, the integral proves to be divergent even if the singularities of the invariant delta-functions on the light-cone ($\xi_\lambda^2 = 0$) are removed (smeared out over a narrow region). The strongest singularities are of the type

$$\left. \begin{aligned} \Delta(\xi) &= D(\xi) + \cdots = \frac{1}{2\pi} \frac{\xi_0}{|\xi_0|} \delta(\xi_\lambda^2) + \cdots, \\ \Delta_1(\xi) &= D_1(\xi) + \cdots = 1/2\pi^2 \xi_\lambda^2 + \cdots. \end{aligned} \right\} \quad (20)$$

Only by introducing integral representations of the delta-functions and carrying out the integrations in a particular order will one be able to arrive at finite values for the self-energy.

Following Schwinger's procedure in his calculation of the electron self-energy, we insert in (19)

$$\left. \begin{aligned} \Delta(\xi) &= \frac{1}{4\pi^2} \frac{\xi_0}{|\xi_0|} \int_{-\infty}^{+\infty} d\alpha \exp\left(-i\alpha \xi_\nu^2 + \frac{i\mu^2}{4\alpha} \right), \\ \Delta_1(\xi) &= \frac{i}{4\pi^2} \int_{-\infty}^{+\infty} d\beta \frac{\beta}{|\beta|} \exp\left(-i\beta \xi_\nu^2 + \frac{i\mu^2}{4\beta} \right), \end{aligned} \right\} \quad (21)$$

and integrate first over the ξ-space, while keeping α, β fixed. Observing that

$$\int d^4\xi \exp(i\gamma \xi_\nu^2) = \int d\xi_0 \exp(-i\gamma \xi_0^2) \times \prod_\kappa \int d\xi_\kappa \exp(+i\gamma \xi_\kappa^2) = \frac{i\pi^2}{\gamma |\gamma|}, \quad (22)$$

we obtain

$$\langle \mathcal{H}_{\text{self}} \rangle_\kappa = \frac{1}{16\pi^2} \frac{e^2}{\hbar c} C_{\mu\nu} \int d\alpha \int d\beta \frac{\beta}{|\beta|} \frac{1}{(\alpha+\beta)|\alpha+\beta|} \times \exp\left(\frac{i\mu^2}{4} \left(\frac{1}{\alpha} + \frac{1}{\beta} \right) \right) \cdot \left[8\alpha\beta \frac{\partial^2}{\partial \kappa_\mu \partial \kappa_\nu} - \delta_{\mu\nu} \left(4\alpha\beta \frac{\partial^2}{\partial \kappa_\lambda^2} + \mu^2 \right) \right] \exp\left[\frac{i\kappa_\lambda^2}{4(\alpha+\beta)} \right].$$

We note

$$\frac{\partial^2}{\partial \kappa_\mu \partial \kappa_\nu} \exp\left[\frac{i\kappa_\lambda^2}{4(\alpha+\beta)} \right] = \exp\left[\frac{i\kappa_\lambda^2}{4(\alpha+\beta)} \right] \times \left(\frac{i}{2(\alpha+\beta)} \delta_{\mu\nu} - \frac{1}{4(\alpha+\beta)^2} \kappa_\mu \kappa_\nu \right),$$

and here we may put $\kappa_\lambda^2 = 0$ and drop the term $\sim \kappa_\mu \kappa_\nu$[7] because $\kappa_\mu \kappa_\nu C_{\mu\nu} = 0$ on account of the supplementary condition (5) (vanishing of the longitudinal components). If we symmetrize the integrand in α and β

$$\left(\frac{\beta}{|\beta|} \rightarrow \frac{1}{2} \left(\frac{\alpha}{|\alpha|} + \frac{\beta}{|\beta|} \right) \right),$$

the result is

$$\langle \mathcal{H}_{\text{self}} \rangle_\kappa = \frac{1}{32\pi^2} \frac{e^2}{\hbar c} C_{\nu\nu} \int d\alpha \int d\beta \times \left(\frac{\alpha}{|\alpha|} + \frac{\beta}{|\beta|} \right) \frac{1}{(\alpha+\beta)|\alpha+\beta|} \times \exp\left[\frac{i\mu^2}{4} \left(\frac{1}{\alpha} + \frac{1}{\beta} \right) \right] \times \left(-\frac{4i\alpha\beta}{\alpha+\beta} - \mu^2 \right). \quad (23)$$

In order to carry out the remaining integrations, let us introduce new variables

$$\frac{\alpha-\beta}{\alpha+\beta} = y, \quad \frac{\mu^2}{4} \left(\frac{1}{\alpha} + \frac{1}{\beta} \right) = z,$$

$$\frac{d\alpha d\beta}{(\alpha+\beta)^2} = \left| \frac{dy dz}{2z} \right|, \quad \frac{\alpha}{|\alpha|} + \frac{\beta}{|\beta|} = \begin{cases} 2\dfrac{z}{|z|} & \text{for } |y|<1, \\ 0 & \text{for } |y|>1. \end{cases}$$

[7] This was also done by Schwinger in his Pocono Manor lecture, but he apparently overlooked the remaining term $\sim \delta_{\mu\nu}$.

From (23) we obtain

$$\langle \mathcal{H}_{\text{self}} \rangle_\kappa = \frac{1}{32\pi^2}\frac{e^2}{\hbar c}\mu^2 C_{\nu\nu} \times \int_{-1}^{+1} dy \int_{-\infty}^{+\infty} dz \frac{1}{|z|} e^{iz}\left(-\frac{i}{z}-1\right).$$

The imaginary part of the integrand has a singularity at $z=0(\sim \pm z^{-2})$, but since it is an odd function of z, it may be regarded as giving no contribution to the integral. Keeping only the real part,

$$\int_{-\infty}^{+\infty} \frac{dz}{|z|} e^{iz}\left(-\frac{i}{z}-1\right) = 2\int_0^\infty dz \frac{d}{dz}\left(-\frac{\sin z}{z}\right) = 2,$$

$$\langle \mathcal{H}_{\text{self}} \rangle_\kappa = \frac{1}{8\pi^2}\frac{e^2}{\hbar c}\mu^2 C_{\nu\nu}. \tag{24}$$

$C_{\mu\nu}$, as defined by (18) (with $x'=x$), is equal to the electromagnetic energy density of the photon state considered, divided by κ_0^2. Therefore, a photon of momentum $\hbar\boldsymbol{\kappa}$, having the total energy $\hbar c\kappa_0 = \hbar c|\boldsymbol{\kappa}|$ in the zero-order approximation, appears in the second-order approximation as having the energy

$$\hbar c\kappa_0\left(1+\frac{1}{8\pi^2}\frac{e^2}{\hbar c}\frac{\mu^2}{\kappa_0^2}+\cdots\right) = c\left[(\hbar|\boldsymbol{\kappa}|)^2+\frac{1}{4\pi^2}\frac{e^2}{\hbar c}(mc)^2\right]^{\frac{1}{2}}. \tag{25}$$

This corresponds to a "photon rest-mass" amounting to one electron mass divided by $(137\pi)^{\frac{1}{2}}$ (because, in the Heaviside units used here, $e^2/4\pi\hbar c = 1/137$).

ELIMINATION OF THE PHOTON SELF-ENERGY

In order to restore Maxwell's equations, one might try to replace the Hamiltonian (2) by

$$\mathcal{H}(x) = -\frac{1}{c} j_\mu(x)A_\mu(x) - \tfrac{1}{2}\gamma A_\mu^2(x),$$

and to determine the constant γ such that the new term in $\mathcal{H}$ cancels the self-energy term. If the result (24) or (25) is accepted, this would be achieved by

$$\gamma = \frac{1}{4\pi^2}\frac{e^2}{\hbar c}\mu^2.$$

However, the new Schrödinger equation would no longer be compatible with the supplementary conditions (6). In order to ensure the compatibility, it is easiest to construct the amended Hamiltonian and supplementary conditions by a unitary transformation from the old ones.

The transformation

$$\Psi(\sigma) = e^{-iU(\sigma)}\Psi'(\sigma) \tag{26}$$

leads to the new Schrödinger equation

$$i\hbar c(\partial\Psi'(\sigma)/\partial\sigma(x)) = \mathcal{H}'(x,\sigma)\Psi'(\sigma), \tag{27}$$

with

$$\mathcal{H}'(x,\sigma) = e^{iU(\sigma)}\mathcal{H}(x)e^{-iU(\sigma)} - i\hbar c e^{iU(\sigma)}\frac{\partial e^{-iU(\sigma)}}{\partial\sigma(x)}. \tag{28}$$

Defining

$$\Omega'(x',\sigma) = e^{iU(\sigma)}\Omega(x',\sigma)e^{-iU(\sigma)}, \tag{29}$$

the conditions (6) become

$$\Omega'(x',\sigma)\Psi'(\sigma) = 0, \tag{30}$$

and the compatibility requirements are, of course, fulfilled; indeed

$$[\Omega'(x',\sigma), \Omega'(x'',\sigma)] = 0,$$

and, on account of (9),

$$\frac{\partial}{\partial\sigma(x)}\{\Omega'(x',\sigma)\Psi'(\sigma)\} = \left\{\frac{\partial e^{iU(\sigma)}}{\partial\sigma(x)}e^{-iU(\sigma)} + e^{iU(\sigma)}\frac{\partial e^{-iU(\sigma)}}{\partial\sigma(x)} + \frac{1}{i\hbar c}\mathcal{H}'(x,\sigma)\right\}\Omega'(x',\sigma)\Psi'(\sigma),$$

which vanishes according to (30).

If we choose

$$U(\sigma) = \frac{\gamma}{4\hbar c}\int d^4x'\epsilon(x',\sigma)A_\mu^2(x'), \tag{31}$$

with the same meaning of the symbols as in (12),

so that

$$\hbar c\frac{\partial U(\sigma)}{\partial\sigma(x)}=\tfrac{1}{2}\gamma A_\mu^2(x),$$

and if we consider γ to be small of the second order ($\sim e^2$), the transformed Hamiltonian (28) becomes, up to third-order terms inclusively,

$$\mathfrak{H}'(x,\sigma)=\mathfrak{H}(x)-\tfrac{1}{2}\gamma A_\mu^2(x)+i[U(\sigma),\mathfrak{H}(x)]+\cdots. \quad (32)$$

The second term is the one that will be cancelled by the photon self-energy term, after the transformation (11), (12), now applied to Ψ' instead of Ψ. The first and third terms may be written

$$-(1/c)j_\mu(x)B_\mu(x), \quad (33)$$

with

$$B_\mu(x)=A_\mu(x)+i[U(\sigma),A_\mu(x)], \quad (34)$$

or, according to (4) and (31),

$$B_\mu(x)=A_\mu(x)+\tfrac{1}{2}\gamma\int d^4x'\epsilon(x',\sigma)\times A_\mu(x')D(x'-x). \quad (35)$$

Here σ is meant as a spacelike surface passing through the point x; since $D(x'-x)$ vanishes for all spacelike vectors $x'-x$, $B_\mu(x)$ is independent of σ. If x is varied, σ has to be varied accordingly. From (34) and (31) it is easily derived that $B_\mu(x)$ obeys, up to terms $\sim e^2$, the equation

$$(\partial^2/\partial x_\nu^2)B_\mu(x)=\gamma B_\mu(x); \quad (36)$$

thus $B_\mu(x)$ may be represented as a superposition of plane waves $\exp(ip_\lambda x_\lambda)$, with $p_\lambda^2=-\gamma$. (This follows also from (35), if plane waves $\exp(i\kappa_\lambda x_\lambda)$ are inserted for A_μ.) Accordingly,

$$[B_\mu(x),B_\nu(x')]=(\hbar c/i)\delta_{\mu\nu}\Delta_\gamma(x-x'), \quad (37)$$

where Δ_γ is the modified D-function obeying the differential equation (36). This result makes it clear, that the third term in $\mathfrak{H}'(32)$, as a correction to the first, reflects a wrong rest-mass of the photon. Of course, this term is again unwanted, since it would affect mainly the low frequency phenomena, and should be transformed away.

The introduction of the rest-mass term also destroys the gauge invariance. It is true that the Schrödinger equation (27) is formally gauge invariant in the sense that the change of gauge $A_\mu\rightarrow A_\mu+\partial\Lambda/\partial x_\mu$ is equivalent to a unitary transformation, so that the inverse transformation restores the Schrödinger equation in its original form. But the operators corresponding to observable quantities, such as the field strengths $\partial A_\mu/\partial x_\nu-\partial A_\nu/\partial x_\mu$, are not invariant under these transformations. One may, however, expect that in the second approximation, where Maxwell's field equations are re-established, a gauge-invariant formulation will become possible.

CONCLUSION

The results of the last section are hardly encouraging in view of higher approximations. We have tried to take the quantum theory of fields seriously, without admitting any *ad hoc* subtractions inconsistent with the principles of quantum mechanics. The outcome shows that the empirical fact, that the photon has no rest-mass, does not fit naturally into the framework of quantum electrodynamics. It seems questionable to what extent the predictions of such a theory in higher order effects are trustworthy.

Finally, it should be remembered that the pair creation of other charged particles (mesons, protons) is likely to contribute to the photon self-energy. Therefore, the phenomena involving electrons, positrons, and photons only, can hardly be expected to be quite independent, in the higher order effects, of the existence of other particles and their nature.

Small-Angle X-Ray Scattering from Amorphous Materials

GEORGE H. VINEYARD
Department of Physics, University of Missouri, Columbia, Missouri
(Received June 4, 1948)

The causes of excessive x-ray scattering at small angles from amorphous materials are discussed, and a formula is derived for the scattered intensity from a substance containing definite macroscopic regions of inhomogeneity, such as clumps of molecules, pockets, or foreign inclusions. The formula shows the effect of both macroscopic and microscopic molecular arrangements.

Some previous observations of small-angle scattering from liquid and gaseous argon are examined in the light of this theory, to see whether they may be accounted for by heterophase fluctuation phenomena. A model with small droplets of liquid included in the vapor phase, and small bubbles of vapor included in the liquid phase is considered, and in order to explain the observations a droplet radius of about 5 angstroms is found necessary. This is considered too small to be plausible, and alternative explanations on the basis of less sharply defined density fluctuations are suggested.

1. INTRODUCTION

THE scattering of x-rays from amorphous materials has long been used to derive information concerning atomic arrangements. Following the method of Zernike and Prins,[1,2] a Fourier inversion of the x-ray scattering pattern is used to find the average atomic density at distance r from any one atom in the sample. The atomic density function so derived still allows many interpretations as to the actual atomic arrangement, and occasionally other features of the scattering pattern have been taken as evidence of certain types of structure. Thus, an excess scattering at small angles is often taken as indicating subdivision of the sample into small particles. A considerable collection of theory on the effect of small particle size in producing excess small-angle scattering exists.[3] In most of this work, each particle is treated as a continuum, so that the influence of atomic arrangement is neglected. Furthermore the possibility that the particles are not truly distinct, but are merely regions of excessive or deficient atomic density, has not been adequately treated.

The present paper considers the possible causes for excess scattering at small angles from amorphous materials, and develops formulas for calculating the scattering patterns for certain classes of structures. In particular the scattering from an amorphous material containing macroscopic inhomogeneities is treated at length. As an application of these results, a study is made of the meaning of small-angle scattering observed under certain conditions from argon.

2. CONSIDERATION OF CAUSES OF SMALL-ANGLE SCATTERING

The coherent x-ray scattering from a sufficiently large sample of amorphous material whose atoms are spherically symmetric is given by the well-known formula[2]

$$I=Nf^2\left(1+\int_0^\infty 4\pi r^2(\rho-\rho_0)\frac{\sin kr}{kr}dr\right), \quad (1)$$

where I is the intensity of scattering at angle 2θ, in electron units, N is the number of atoms in the sample, f is the atomic structure factor, k is $(4\pi\sin\theta)/\lambda$, λ being the wave-length, ρ is the average density of atoms at distance r from any one atom, and ρ_0 is the over-all average density of atoms. The factor $(\rho-\rho_0)$ differs appreciably from zero only in the region $0\leqslant r\leqslant r_c$, where r_c is some correlation distance which measures the extent of the long-range order in the structure. The factor $(\sin kr)/kr$ is approximately unity for $kr\ll 1$ and therefore the value of I for all angles such that $k\ll 1/r_c$* will be very nearly

[1] F. Zernike and J. A. Prins, Zeits. f. Physik **41**, 184 (1927).
[2] N. S. Gingrich, Rev. Mod. Phys. **15**, 90 (1943).
[3] A. Guinier, *Radiocristallographie* (Dunod, Paris, France, 1945), Chap. XII.

* Except, of course, for θ within a few seconds of 0°, where the 000 scattering, not included in Eq. (1), predominates. For samples of appreciable size, this region is beyond the reach of experiment.

equal to

$$I(0)=Nf^2\left(1+\int_0^\infty 4\pi r^2(\rho-\rho_0)dr\right). \quad (2)$$

Zernike and Prins[1] have shown that

$$1+\int_0^\infty 4\pi r^2(\rho-\rho_0)dr=\langle(n-\langle n\rangle_{Av})^2\rangle_{Av}/\langle n\rangle_{Av} \quad (3)$$

where n is the number of atoms in any selected volume of the fluid whose dimensions are large compared to r_c. This fractional mean square fluctuation in n is related to the compressibility by a well-known result of statistical mechanics, so that, finally,

$$I(0)=Nf^2\frac{RT}{V}K, \quad (4)$$

where R is the gas constant, T the absolute temperature, V the molar volume, and K the isothermal compressibility. This equation is inaccurate in cases where K is anomalously large, and invalid for samples which are mixtures of different substances.

In understanding the meaning of small-angle scattering in terms of atomic arrangements, Eq. (2) will for our purposes be more useful than Eq. (4). Clearly $I(0)$ will be large in those substances for which $\rho-\rho_0$ tends to be large. We may then set ourselves the problem of inquiring what kinds of structures will lead to large values of $\int_0^\infty 4\pi r^2(\rho-\rho_0)dr$. A complete and detailed answer is not known to the writer, but two general types of structures with this property will be pointed out.

If the average density of the sample is small, one can easily characterize those arrangements which will give small-angle scattering, and such structures constitute our first type. More precisely, if $(4\pi/3)r_c^3\rho_0\ll 1$, the desired condition will obtain when $\int_0^{r_c}4\pi r^2\rho dr$ is comparable with unity or larger. Plainly this means that the atoms are arranged in clusters of some sort. A partially or completely associated gas best typifies this situation, and one easily calculates that if the N atoms of a rarefied sample are all associated in molecules of m atoms each, $I(0)=mNf^2$, which is precisely m times as large as if the N atoms were arranged entirely at random. One also easily finds that the angle at which this excess scattering ceases is given roughly by $\sin\theta=\lambda/d$, where d is the diameter of the molecule. This simple type of arrangement is of interest chiefly because it affords one simple approach to denser arrangements which would also show small-angle scattering. Thus, if the density of the associated gas is allowed to increase one would expect the small-angle effect to persist, to a diminishing extent, until the intermolecular spaces vanished completely. Another artificial, but interesting model of this type is the following: Suppose every molecule is diatomic, and that the molecular diameter d is considerably larger than the diameter of the atoms, and also larger than the average distance between neighboring molecules (imagine the molecules interpenetrate freely, although the atoms are impenetrable). Then, again,

$$1+\int_0^\infty 4\pi r^2(\rho-\rho_0)dr>0,$$

but the existence of definite clumps would hardly be apparent from an instantaneous photograph of the atomic arrangement.

A second type of structure giving small-angle scattering is one in which macroscopic inhomogeneities of any kind are present. Such inhomogeneities will cause ρ to be larger, on the whole, at $r<r_c$, than ρ_0. It is easy to see that the presence of macroscopic regions where the mean density is greater than in the surrounding regions will elevate ρ at small r in this fashion. It is not so evident, but it is equally true that the presence of regions of less than average density will also cause ρ to be larger at small r than at large r. Both of these statements may be proved in a very general way from the Zernike and Prins relation (3), since the presence of any regions of inhomogeneity in atomic density will make $\langle(n-\langle n\rangle_{Av})^2\rangle_{Av}>0$. One may learn more about the detailed situation by computing ρ in the following way: If $\sigma(x,y,z)$ is the density of atoms at x, y, z in the sample, if there are N atoms in the sample, and if r, θ, φ are polar coordinates centered at x, y, z

$$\rho(r)=\frac{1}{N}\int_{-\infty}^{\infty}\int\int\sigma(x,y,z)\langle\sigma(x+r\sin\theta\sin\varphi,\ y+r\sin\theta\cos\varphi,\ z+r\cos\theta)\rangle_{Av}dxdydz, \quad (5)$$

TABLE I. Zero-angle scattering in argon found by two different methods.

Datum point (numbered as in Eisenstein and Gingrich)	$I(0)/Nf^2$ Calculated from compressibility	$I(0)/Nf^2$ Extrapolated from Eisenstein and Gingrich x-ray measurements
1	0.2	0.11
2	0.3	0.08
4	0.43	0.22
5	1.2	1.0
6		1.2
7	5.	2.8
8	4.	2.1
9	1.9	1.5
10	1.8	1.5
11	1.2	1.0
12	1.1	1.0
13	1.2	1.1
14	1.5	1.4
15	1.1	1.04
16	1.5	1.2
17	1.8	1.6
18	2.1	1.6
19	3.6	1.9
20	1.3	1.7
21	1.5	1.1
22	2.4	1.5
23		0.3
24		0.7
25	12.	1.7
26	2.4	1.6

where the indicated averaging is over θ and φ. Suppose the sample consists of a number of distinct regions, each large compared to the interatomic correlation distance r_c, and randomly located relative to one another. Let the average atomic density in the ith region be σ_i, and the volume of this region V_i. For $r \geqslant r_c$, $\sigma(x,y,z)$ in the above formula may be taken equal to σ_i when x, y, z lies in the ith region, and one finds

$$\rho(r_c) \cong \frac{1}{N}\int_{-\infty}^{\infty}\int\int\int \sigma^2 dxdydz = \sum_i \sigma_i^2 V_i / \sum_i \sigma_i V_i.$$

However, for sufficiently large r $\rho(r)$ must equal the average atomic density $\sum_i \sigma_i V_i / \sum_i V_i$, which we call ρ_0. By algebraic manipulation one sees that the first quotient of summations above is always equal to or larger than the second quotient, the inequality prevailing whenever two or more of the regions possess unequal densities, and therefor $\rho(r_c) \geqslant \rho_0$. One may also show by further reasoning from the above constitutive formula for $\rho(r)$ that, so long as most of the sample has a uniform average density, the regions of inhomogeneity being widely spaced, $\rho(r)$ decreases monotonically with r for $r \geqslant r_c$. The value of r at which $\rho(r)$ becomes sensibly equal to ρ_0 can also be found, and turns out to be equal to the largest dimension of the largest region, in case the locations of the regions are completely random. This means that the small-angle scattering produced by such inhomogeneous regions will become negligible at scattering angles approximately such that $\sin\theta = \lambda/D$, where D is the maximum linear dimension of the region.

3. SCATTERING FROM AN AMORPHOUS SUBSTANCE CONTAINING MACROSCOPIC INHOMOGENEITIES

We will now consider in detail a structure of the type last discussed, and derive a formula for its x-ray scattering. Suppose an amorphous substance contains certain regions of macroscopic size in which the density, or kind, or arrangement of molecules is appreciably different from that in the rest of the substance, and suppose that these regions are randomly distributed throughout the material. This situation would occur, for example, if a liquid near its boiling point contained small bubbles of vapor, or if a vapor near its condensation point contained small droplets of liquid. The calculations would also apply to an emulsion of one substance with another, to a dilute suspension of colloidal particles in a liquid, and to the case where the special regions contained no molecules at all, as in a substance with occasional empty pockets or a closely packed aggregate of amorphous particles, in which there would be holes interspersed among the particles.

It is possible to calculate from Eq. (5), but it will be more convenient to start with the usual formula for the scattering from an isotropic aggregate of spherically symmetric molecules,

$$I = \sum_n \sum_m f_n f_m \frac{\sin kr_{nm}}{kr_{nm}}. \tag{6}$$

Here f_n is the structure factor of the nth molecule, and r_{nm} is the distance between the nth and mth molecules. Each summation extends over the entire aggregate. We adopt the following artifice: The sample is first imagined to be macroscopically homogeneous, and then the real sample is arrived at by subtracting all the original molecules in certain special regions and then add-

ing the clumps of molecules which actually occupy these regions.

Let the ith region of inhomogeneity be referred to as R_i, let the entire original set of molecules be called S, let the subset of S which must be removed to empty R_i be T_i, and let the set of molecules actually present in R_i be U_i. Each of the two summations in (6) may then be expanded as

$$\sum_n = \sum_S - \sum_{T_1} - \sum_{T_2} - \cdots + \sum_{U_1} + \sum_{U_2} + \cdots,$$

where $\sum_S$, for example, means summation over all molecules of the set S. Because of the distributive property of multiple summations, the double summation of (6) then expands, schematically, as follows:

$$\begin{aligned}\sum_n \sum_m = &\left(\sum_S \sum_S\right) - \left(2\sum_S \sum_{T_1} + 2\sum_S \sum_{T_2} + \cdots\right) \\ &+ \left(2\sum_S \sum_{U_1} + 2\sum_S \sum_{U_2} + \cdots\right) + \left(2\sum_{T_1} \sum_{T_2}\right. \\ &\left. + 2\sum_{T_1} \sum_{T_3} + \cdots + 2\sum_{T_2} \sum_{T_3} + \cdots\right) \\ &- \left(2\sum_{T_1} \sum_{U_1} + 2\sum_{T_2} \sum_{U_2} + \cdots\right) \\ &- 2\left(\sum_{T_1} \sum_{U_2} + \sum_{T_2} \sum_{U_1} + \sum_{T_1} \sum_{U_3} + \sum_{T_3} \sum_{U_1}\right. \\ &\left. + \sum_{T_2} \sum_{U_3} + \sum_{T_3} \sum_{U_2} + \cdots\right) + \left(2\sum_{U_1} \sum_{U_2}\right. \\ &\left. + 2\sum_{U_1} \sum_{U_3} + \cdots + 2\sum_{U_2} \sum_{U_3} + \cdots\right) \\ &+ \left(\sum_{T_1} \sum_{T_1} + \sum_{T_2} \sum_{T_2} + \cdots\right) \\ &+ \left(\sum_{U_1} \sum_{U_1} + \sum_{U_2} \sum_{U_2} + \cdots\right). \end{aligned} \quad (7)$$

The summations in (7) have been divided with parentheses into 9 groups, each of which is conveniently dealt with separately. Each of the regions R_i will be assumed to have the same size and shape. This restriction can be removed by the use of suitably averaged terms in the following development, but it does not seem worth while to complicate the reckoning to this extent. We suppose the original sample to consist of one species of molecule only, and the sets U_i to consist of one species only, possibly a different species. We assume that the regions R_i have random orientations, and occur sufficiently infrequently that they can have random locations. We adopt the following symbols.

N_S = the number of molecules in the set S
n_R = the number of regions R_i
N_T = the number of molecules in any one of the sets T_i
N_U = the number of molecules in any one of the sets U_i
f = the structure factor of the molecules in the set S
f' = the structure factor of the molecules in the sets U_i
ρ_S = the average density of other molecules at distance r from any molecule in the set S
ρ_{S0} = the limit of ρ_S at large r
ρ_T = the average density of other molecules of T_i at distance r from every molecule in the set T_i
ρ_U = the average density of other molecules of U_i at distance r from every molecule in the set U_i

It should be noted that ρ_T and ρ_U, because of the limited size of the regions R_i, not only show fluctuations at small r owing to the details of atomic arrangements, but also go to zero at a distance equal to the largest dimension of R_i. We further define a function μ related to the shape and size of the region R_i, as follows: Let a single molecule roam at random through such a region. Then μ is the average molecular density at distance r from points averaged over the entire region. For a spherical region of radius a, one easily finds

$$\begin{aligned}&\mu = (3/4\pi a^3)(r/2a-1)^2(r/4a+1) \quad 0 \leqslant r \leqslant 2a \\ &\mu = 0 \qquad\qquad\qquad\qquad\qquad\quad r > 2a. \end{aligned} \quad (8)$$

Consider the double summation of (7) applied in (6). Because of the large size of the entire sample compared to each of the inhomogeneous regions, and because of the random locations of the latter, the 3rd, 4th, 6th, and 7th parenthesized groups in (7) may be shown to contribute negligibly small amounts compared to the other groups. Each of the remaining terms may be rewritten as integrations, with the aid of the mutual density functions just defined. In rewriting the contributions of the 1st and 2nd groups, no appreciable error is caused by subtracting ρ_{S0} from ρ_S under the integral sign, for the same reasons as used in deriving Eq. (1).[1] Because of the random location of molecules in the set T_i relative to those in U_i, except that both sets are confined within R_i, the contribu-

tion of the 5th group may be rewritten:

$$-\left(2\sum_{T_1}\sum_{U_1}+2\sum_{T_2}\sum_{U_2}+\cdots\right)\left(f_n f_m \frac{\sin kr_{nm}}{kr_{nm}}\right)$$
$$=-2n_R N_T N_U f f' \int_0^\infty 4\pi r^2 \mu \frac{\sin kr}{kr} dr.$$

Collecting these terms and rearranging somewhat, one finds

$$I=(N_S-n_R N_T)f^2\left[1+\int_0^\infty 4\pi r^2(\rho_S-\rho_{S0})\frac{\sin kr}{kr}dr\right]$$
$$+n_R N_T f^2 \int_0^\infty 4\pi r^2\{(\rho_T-N_T\mu)$$
$$-(\rho_S-\rho_{S0})\}\frac{\sin kr}{kr}dr$$
$$+n_R N_U f'^2\left[1+\int_0^\infty 4\pi r^2(\rho_U-N_U\mu)\frac{\sin kr}{kr}dr\right]$$
$$+n_R(N_U f'-N_T f)^2\int_0^\infty 4\pi r^2\mu\frac{\sin kr}{kr}dr. \quad (9)$$

The meanings of these terms are straightforward. The first and third terms arise from the interferences between the molecules in the major part of the sample and between the molecules in the inhomogeneous regions, respectively, calculated as if both these sets were indefinitely large, but weighted according to the numbers of molecules present in each set. The second term will be very nearly zero because the factor in curly brackets is nearly zero, and will hereafter be neglected. The last term gives that part of the small-angle scattering coming from the size and shape of the inhomogeneous regions. Note that its coefficient is positive regardless of whether the regions contain an excess or defect of electronic density. In the case of spherical regions, where μ is given by (8), the last term of (9) becomes

$$n_R(N_U f'-N_T f)^2$$
$$\times[(3/k^3a^3)(\sin ka-ka\cos ka)]^2. \quad (10)$$

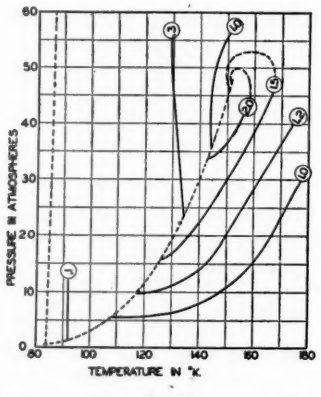

FIG. 1. Contours of constant zero angle scattering on P-T diagram. Taken from Eisenstein and Gingrich data be extrapolation. Numbers in circles are values of $I(0)/Nf^2$.

4. SMALL-ANGLE SCATTERING FROM ARGON

In a series of very careful measurements of the x-ray scattering by liquid and gaseous argon, Eisenstein and Gingrich[4] observed a very strong scattering at small angles under certain conditions of pressure and temperature, especially in the vicinity of the critical point.[5] The suggestion has been made[4] that this small-angle effect may be evidence of the formation of microscopic droplets of liquid in the vapor near its condensation point, or of tiny bubbles of vapor in the liquid near its boiling point. Such pre-transition manifestations have been assumed in several proposed theories.[6] From the results of the present calculations it is possible to make a semi-quantitative evaluation of the degree to which the argon data support or discredit such a discrete droplet model.

As a crude index of the magnitude of the small-angle scattering effects in the Eisenstein and Gingrich data, we have extrapolated their curves of scattered intensity *vs.* angle to zero angle, and taken the ratio $I(0)/Nf^2$, where $I(0)$ is the scattered intensity at zero angle (in electron units), N is the number of atoms in the sample, and f is the atomic structure factor, also at zero angle. This extrapolation, of course, is a highly inaccurate process, and the results can be expected to have little more than order of magnitude validity in cases when the small angle scattering is large. Table I lists these results,

[4] A. Eisenstein and N. S. Gingrich, Phys. Rev. **62**, 261 (1942).

[5] A similar effect had previously been observed in work by Stewart on ether and by Harvey on nitrogen: G. W. Stewart, Trans. Faraday Soc. **29**, 982 (1933); G. G. Harvey, Phys. Rev. **45**, 848 (1934).

[6] Among others, J. Frenkel, J. Chem. Phys. **7**, 200, 538 (1939); E. Brody, Physik. Zeits. **23**, 197 (1922).

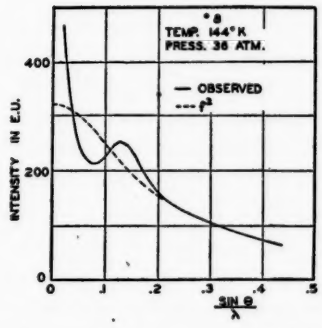

FIG. 2a. Typical scattering curve for argon, showing small-angle effect. (Eisenstein and Gingrich No. 8.)

and, for better visualization, the figures have been put in their proper places on a pressure-temperature diagram and rough contours of constant $I(0)/Nf^2$ drawn in, as shown in Fig. 1.

As a check on the experimental values of $I(0)/Nf^2$ we may use the relation of Zernike and Prins, Eq. (4), and compute $I(0)/Nf^2$ from known values of density and isothermal compressibility.[7] Extensive P-V data on gaseous argon have been given by Onnes and Crommelin,[8] and fairly good values of compressibility may be taken from the slopes of their isotherms. For the liquid, no such data exist, and the best that could be done was to utilize estimates of atomic nearest-neighbor separations from the x-ray data of Eisenstein and Gingrich. The values of $I(0)/Nf^2$ so obtained are also listed in Table I. The agreement seems fair for all points except numbers 7, 8, 19, and 25, in all of which cases the compressibility $I(0)$ is considerably too high. It seems likely that the values from compressibility are the more reliable here, for in all these cases the experimental scattering curves were rising very steeply at their small-angle limits.

From Fig. 1 it is seen that the most extreme effects are found in the vicinity of the critical point, as would naturally be expected for a fluctuation phenomenon. For a typical scattering curve from this realm, showing a marked small-angle effect, number 8 of Eisenstein and Gingrich is reproduced in Fig. 2a. One may analyze this curve under the hypothesis that the material in the sample consists of a homogeneous vapor phase containing n_R spherical droplets of liquid, all of radius a. Referring to Eqs. (9) and (10) we should expect that the observed intensity curve could be split into two components, the first component being the first three terms in (9), ascribable to small-scale atomic position correlations, and the second component being given by the last term of (9), ascribable to droplet size and density effects. A somewhat arbitrary, but highly reasonable assumption for the first part is to take it as identical with the curve of Fig. 2a except that the rising portion at small angles is omitted, the curve being extrapolated directly to zero from the bottom of the first valley. It is readily shown that both components of the intensity curve must have zero slopes at zero angle, and hence a straight horizontal extrapolation would not be unreasonable for this component. The remaining component representing droplet size effects is then readily determined. These two curves are shown in Fig. 2b, the former being labeled Large Angle Component, the latter, Small Angle Component.

From the small-angle component one can then determine the radius of the droplets by fitting Eq. (10) to it. This task is made more difficult by several factors. Firstly, only a restricted portion of the curve is available. Secondly, the division of the observed total intensity into small- and large-angle components was an inexact procedure and may have altered the shape of the small-angle component curve. Thirdly, the droplets, if present, would be expected to occur in a range of sizes, and (10) should therefore be replaced by a like term averaged over droplet sizes. It does not seem possible to take accurate

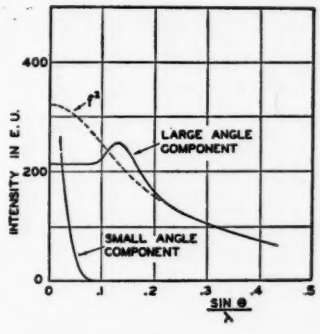

FIG. 2b. Subdivision of 2a into large-angle and small-angle components.

[7] Recently Yvon has used this Zernike and Prins relation the other way around in the effort to evaluate liquid compressibilities from their small-angle x-ray scattering: M. J. Yvon, J. de phys. et rad. 7, 201 (1946).

[8] H. K. Onnes and C. A. Crommelin, Kon. Akad. van Wetenschappen te Amsterdam, 29 Oct. 1910, p. 582.

TABLE II. Radii of droplets necessary to explain the observed small-angle scattering in argon.

Datum point	Droplet Radius, in Angstrom Units			
	By method *a*	By method *b*	By method *c*	Average of *a*, *b*, and *c*
5	5.5	6.6	6.5	6.2
6	6.4		7.8	7.1
7	5.1	7.1	6.3	6.2
8	4.5	6.5	5.2	5.4
9	5.3	5.9	6.0	5.7
10	4.9	4.9	4.1	4.6
23	7.9			7.9
24	7.2			7.2
25	5.1	7.8	6.5	6.5
26	4.5		5.2 to 7.3	5.7

account of these complications; nevertheless, even in unfavorable cases the results of simple theory should still be correct to an order of magnitude. It is not possible to fit (10) to the curve of Fig. 2b precisely with any choice of parameters. A simplest criterion of fitting, which we call method *a*, is to make the first minimum of (10) coincide with the apparent zero point in the curve. A second procedure (method *b*) is to adjust the parameters in (10) (of which there are essentially two) to secure agreement at two points on the curve. As choice of these two points, the zero angle value, determined by compressibility, and an experimental value chosen at an abscissa about midway between the extremities of the curve were taken. This choice should be as independent of the above mentioned uncertainties as any which could be made. A third procedure (method *c*) is to approximate (10) for small k by a Gauss error function and determine the droplet radius from a measurement of the slope of a plot of $\ln(I/f^2)$ *vs.* k^2.[9] This method is well known in x-ray particle size determinations.[3] Table II presents the results of the three methods for several of the Eisenstein-Gingrich patterns which showed prominent small-angle effects. The self-consistency is reasonable, and, as a best index of the radius of droplet necessary to explain the observed scattering, on the assumption that molecular arrangement actually is of this type, we may take the average of the results from the three methods. This is given in the last column of the table.

[9] The plots of $\ln(I/f^2)$ *vs.* k^2 were remarkably straight lines at small angles, except for pattern 26. For this, the range of slopes is listed.

It is at once evident from these results that the predicted droplet radii are in all cases so small that it becomes very difficult to believe that such droplets could be considered as regions of a distinct phase having anything like the properties of macroscopic amounts of material in that state. In sample number 8, for example, the droplet radius of 5.4A is little more than the nearest neighbor distance in crystalline argon (3.8A), and would be large enough to contain only 9 atoms at a density equal to that of the liquid at the same pressure and temperature.

If one knew the density of material in the droplet and vapor regions, one could also calculate the number of droplets which must occur in the sample. In the absence of better information, a first approximation would be to assume the density of the "pure" vapor to be the same as the macroscopic vapor density, and to assume the material in the droplets to be of the same density as the macroscopic liquid at the same pressure. Calculating on this assumption with sample number 8, one finds that 70 percent of the atoms in the sample would be contained in the liquid droplets, and that the liquid droplets would occupy 38 percent of the sample volume. This means, among other things, that the original assumptions for "liquid" and "vapor" densities must have been wrong, but the assumption of various densities does not radically alter these figures.

Thus, the x-ray observations could be explained by the assumption of a droplet model, but in order to do so the majority of the droplets (or bubbles) would have to be extremely small for all of the cases which can be examined from the present x-ray data, and the droplets would in many cases have to be exceedingly numerous. It is, of course, possible that radically different effects could be observed at points still closer to the critical point.

Besides the droplet atomic arrangement for explaining this small-angle scattering, many other arrangements are also conceivable, as was indicated in a previous section. All of these may be considered as various irregular ways of clumping the molecules, but it does not seem worth while to attempt to characterize any of them in further detail, or to compare the scat-

tering which they would yield with these experimental results. From the standpoint of naïve statistical mechanical theories of liquid structure, some of them seem at least equally plausible with the droplet model, particularly when the extremely small size of droplet demanded is taken into account.

The author is indebted to Professor Gingrich and Professor Eisenstein for helpful conversations.

PHYSICAL REVIEW VOLUME 74, NUMBER 9 NOVEMBER 1, 1948

A Study of Cosmic-Ray Bursts

H. S. BRIDGE, W. E. HAZEN,* B. ROSSI, AND R. W. WILLIAMS
Physics Department and Laboratory for Nuclear Science and Engineering, Massachusetts Institute of Technology, Cambridge, Massachusetts

(Received June 21, 1948)

A "fast" ionization chamber, suitable for the investigation of cosmic-ray bursts, is described. The operation of the chamber and of the associated electronic circuits is discussed. The nature of the cosmic-ray events responsible for the production of ionization bursts was studied (*a*) by observing coincidences between several ionization chambers, (*b*) by analyzing the shape of the ionization pulses, (*c*) by operating an ionization chamber inside a cloud chamber which was expanded whenever the ionization chamber recorded a pulse. The experimental results led to the following conclusions: (1) at mountain altitudes 98 percent of the ionization pulses in an unshielded chamber of the type used are produced by nuclear disintegrations, the remaining 2 percent by air showers; (2) in the nuclear disintegrations, heavily ionizing particles of sufficiently high energy are produced to cause coincidences between neighboring chambers; (3) nuclear disintegrations are produced mainly by non-ionizing rays, which are possibly neutrons, certainly not photons; (4) about 12 inches of lead is necessary to reduce the intensity of the radiation which produces nuclear disintegrations to $1/e$ times its original value.

I. INTRODUCTION

THE ionization chamber has been widely used in cosmic-ray studies, both as an *integrating instrument*, to record the average number of ion pairs per second produced by cosmic rays in a given volume of gas, and as a *pulse instrument*, to detect the sudden appearance of large "bursts" of ionization. The most common cosmic-ray phenomena which give rise to ionization bursts are (*a*) *cascade processes* (initiated by high energy electrons or photons) resulting in the production of large electron showers, (*b*) *nuclear disintegrations* resulting in the emission of one or more heavily ionizing particles, mostly protons and α-particles with energies of the order of 10^6 or 10^7 ev. Recent experiments have brought to light the existence of complex reactions in which showers and heavily ionizing particles appear simultaneously.

The advances in experimental techniques made during the war at the Los Alamos Laboratories and elsewhere have opened a wider field of application for the ionization chamber as a pulse instrument.[1] It has been shown that by using improved electronic circuits and by taking appropriate precautions to prevent electron attachment, ionization chambers can be made into detectors which are considerably faster and more sensitive than ionization chambers of the older type. It has thus become possible to use ionization chambers for a greater variety of experiments, in particular for coincidence experiments in which small resolving times are required.

Experiments on cosmic rays by means of "fast" ionization chambers were begun at the Massachusetts Institute of Technology in the spring of 1946. Preliminary reports on some of the results obtained have already been published.[2-8] The present paper discusses methods

* Now at the University of Michigan, Ann Arbor, Michigan.

[1] See "Ionization chambers and counters" by B. Rossi and H. S. Staub, Vol. 2 of the Los Alamos Technical Series, in press. This work will be referred to as R.S.
[2] H. Bridge and B. Rossi, Phys. Rev. 71, 379 (1947).
[3] H. Bridge, Phys. Rev. 72, 172 (1947).

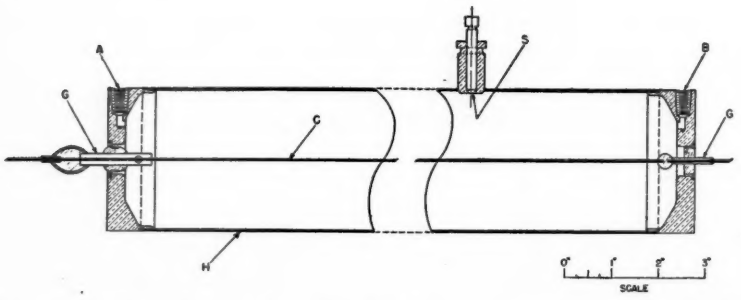

FIG. 1. The ionization chamber.

for separating the various kinds of cosmic-ray events which produce bursts in ionization chambers and describes some new results concerning cosmic-ray-induced nuclear disintegrations. These results were obtained by means of ionization chambers used both alone and in conjunction with a cloud chamber.

II. THE IONIZATION CHAMBER AND AMPLIFIER

1. Design and Electric Connections of the Chamber

All of the chambers used in our experiments were of cylindrical shape and similar in design to the chamber described in R.S., Chap. 5.4. The constructional details were somewhat modified in the course of the work and Fig. 1 represents the design which was adopted in the most recent experiments.

The outer shell H, which is also the high voltage electrode, consists of a brass tube 3 inches in outer diameter with $\frac{1}{32}$-inch walls. The collecting electrode, C, is a kovar wire, 0.025 inch in diameter and $20\frac{13}{16}$-inch effective length stretched along the axis of the brass tube. This wire is supported by the glass-kovar seals shown in the figure. The kovar cylinders, G, (guard electrodes) are grounded during operation to prevent leakage of charges from the high voltage electrode to the collecting electrode. S represents a polonium source, which is used for the calibration of the chamber. A, B are the connections for the gas filling (see below).

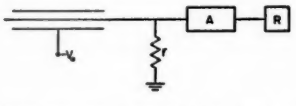

FIG. 2. Electrical connections of the ionization chamber.

The electrical connections of the chamber are schematically represented in Fig. 2. The outer shell is kept at a fixed negative voltage $-V_0$ of the order of 1500 volts. The collecting electrode is grounded through a resistor, r, and connected to the input of an electronic amplifier, A. The output of the amplifier feeds into a recorder, R, which may be either a cathode-ray oscilloscope or an electronic pulse height discriminator. The combined capacity to ground, C, of the collecting electrode, the amplifier input and the connecting leads will be called the "input capacity." The product RC will be referred to as the "input time constant."

2. Operation of the Chamber[9]

In this section we shall discuss the relationship between the number and distribution of ion pairs produced in the chamber by a given ionizing event, and the size and shape of the corresponding voltage pulse at the output of the amplifier. The chamber is filled with argon, a gas in which no electron attachment takes place, so that the negative ions are free electrons (see Section 3 below). The operation of the chamber can be described by considering it as a generator whose output current, I, depends on the ionization of the gas. The expression for I may be written as $I=I^+ + I^-$ where I^+ and I^- are given by the equations:

$$I^+ = (e/V_0)[\sum w_i^+ E_i^+]; \quad I^- = (e/V_0)[\sum w_i^- E_i^-], \tag{1}$$

In the above equations, e represents the electronic charge; V_0, the voltage difference between

[4] B. Rossi and R. W. Williams, Phys. Rev. **72**, 172(A) (1947).
[5] R. W. Williams and B. Rossi, Phys. Rev. **72**, 172(A) (1947).
[6] H. Bridge, B. Rossi, and R. W. Williams, Phys. Rev. **72**, 257 (1947).
[7] H. Bridge, W. E. Hazen, B. Rossi, Phys. Rev. **73**, 179 (1948).
[8] R. W. Williams, Phys. Rev. **73**, 1252 (1948).
[9] See reference 1, Chap. 3.

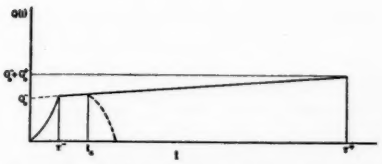

FIG. 3. Charge displaced through the ionization chamber as a function of time (schematic).

the electrodes; w_i^+, the drift velocity of a given positive ion; E_i^+, the electric field strength at the place where this ion finds itself at the time considered. The corresponding quantities for a given electron are w_i^-, E_i^-. The summations are extended to all of the ions and electrons present in the chamber. I^+ and I^- may be considered to represent the contributions of the motion of positive ions and electrons respectively, to the total intensity, I, of the ionization current.

Consider the case that N ion pairs are produced simultaneously in the chamber at the time $t=0$. An ionization current will set in and last until all ions have been collected. Under the conditions of our experiments, the drift velocity of the electrons is of the order of 10^6 cm sec.$^{-1}$, the drift velocity of positive ions is of the order of 10^3 cm sec.$^{-1}$. Therefore the electron current I^- will last for a time τ^- of the order of microseconds, while the positive ion current I^+ will last for a time τ^+ about 1000 times longer and will have a value correspondingly smaller. It follows that the charge displaced through the chamber at the end of time t, i.e., the quantity

$$Q(t)=\int_0^t I(t_1)dt_1$$

increases at first very rapidly until all electrons have been collected ($t=\tau^-$) and then much more slowly, until the collection of the positive ions is completed ($t=\tau^+$) as shown schematically by the solid line in Fig. 3.

Let us indicate with Q_0^- and Q_0^+ the total charges induced by the motion of electrons and positive ions, respectively. Integration of Eqs. (1) yields

$$\begin{aligned} Q_0^- &= -(e/V_0)[\sum_1^N V_i], \\ Q_0^+ &= (e/V_0)[\sum_1^N (V_i - V_0)], \\ Q_0 &= Q_0^+ + Q_0^- = Ne, \end{aligned} \tag{2}$$

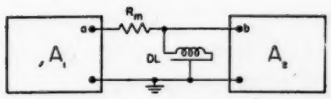

FIG. 4. Schematic diagram of "delay line clipping."

where V_i is the voltage at the place where the ith ion pair is produced. Since the charge induced by the motion of the positive ions in the time τ^- is negligible compared with the charge induced by the motion of the electrons in the same time, the value of Q at $t=\tau^-$ is practically identical with Q_0^-.

The electronic amplifiers used in our experiments were of the type described as "model 100 Amplifiers" in Vol. I of the Los Alamos Technical Series by W. C. Elmore and M. Sands, and were equipped with a "delay-line" type of low frequency rejection network (or "delay line clipping"). This device consists of a delay line DL in series with its matching resistor R_m, and is inserted between two sections A_1, A_2 of the amplifier, as shown in Fig. 4, where a is the output of the first section of the amplifier and b the input of the second section. The output impedence at point a is very small compared to the characteristic impedance of the delay line. Hence the first reflected pulse is absorbed in R_m with no further reflections. Thus, the voltage at b is the superposition of two voltage pulses; a direct pulse of the same shape as the pulse at a and a reflected pulse of opposite sign delayed by a time t_c equal to twice the delay time of the line. If the delay line has no attenuation, both of these pulses have amplitudes equal to one half the amplitude of the pulse at a. If all coupling time constants (including the input time constant, RC) are long compared with t_c, the "transient response" of an amplifier with delay line clipping is of the general type shown in Fig. 5. The transient response is here defined as the function

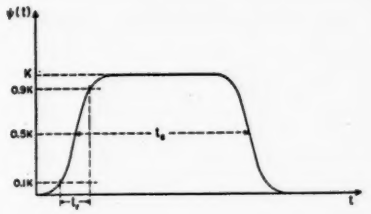

FIG. 5. Transient response of an amplifier with delay line clipping.

$\psi(t)$ which represents the output voltage obtained when a unit charge is applied instantaneously to the input at the time $t=0$. The maximum value, K, of the function $\psi(t)$ multiplied by the input capacity, C, may be defined as the "amplification" A:

$$A=KC. \tag{3}$$

The time t_r during which $\psi(t)$ rises from $0.1K$ to $0.9K$ will be referred to as the "rise time." The time t_c defined above will be referred to as the "clipping time."

The voltage at the output of the amplifier corresponding to an arbitrary current $I(t)$ at the input is given by the equation

$$V(t)=\int_{-\infty}^{t} I(t_1)\psi(t-t_1)dt_1. \tag{4}$$

In our experiments, the rise time t_r was short compared with the collection time of the electrons, τ^-, while the clipping time t_c was only slightly longer than τ^- and, therefore, was very short compared with the collection time of positive ions τ^+. Under these conditions the computation of the output voltage corresponding to an ionization burst at $t=0$ can be simplified by considering $\psi(t)$ a square wave, i.e., by taking $\psi(t)=K=$const. for $0<t<t_c$ and $\psi(t)=0$ for $t<0$ or $t>t_c$. Equation (4) then yields:

$$V(t)=K\int_0^t I(t_1)dt_1=KQ(t) \quad \text{for } t<t_c,$$
$$V(t)=K\int_{t-t_c}^{t} I(t_1)dt_1=K[Q(t)-Q(t-t_c)] \quad \text{for } t>t_c. \tag{5}$$

These equations together with Fig. 3 show that $V(t)$ reaches the value KQ_0^- at $t=\tau^-$, stays practically constant until $t=t_c$ and then decreases again, reaching zero at the time $t_c+\tau^-$, as indicated by the dotted curve in the same figure. Thus the size of the input pulse is proportional to the charge Q_0^- induced by the motion of the electrons.

The value of Q_0^- depends on the number, N, of ion pairs produced in the chamber and on the position in which these ions are produced (see Eq. (2)). For instance, if N ion pairs are produced at the same distance r from the axis of the chamber, Q_0^- has the value

$$Q_0^-=Ne[\ln(r/a)/\ln(b/a)], \tag{6}$$

where a is the radius of the wire, b the radius of the outer cylinder. If, instead, the ionization is distributed uniformly throughout the chamber we obtain:

$$Q_0^-=Ne[b^2/(b^2-a^2)-1/2\ln(b/a)] \tag{7}$$

or, for a chamber of the dimensions specified in Section II−1, $Q_0^-=0.90Ne$. Consider finally the case of a particle with constant specific ionization which traverses the chamber perpendicular to the axis, at a distance r from it. Curves giving Q_0^-/Ne *vs.* r/b are shown in Fig. 6 for different values of the ratio b/a. Ne is the total charge which would be released by a particle intersecting the axis ($r=0$) if a were equal to zero. The variation of the induced charge, Q_0^-, with increasing r shown by the curves in Fig. 6 is the result of two effects which act in opposite directions, namely, the reduction in the length of the track and the increase in its distance from the collecting electrode.

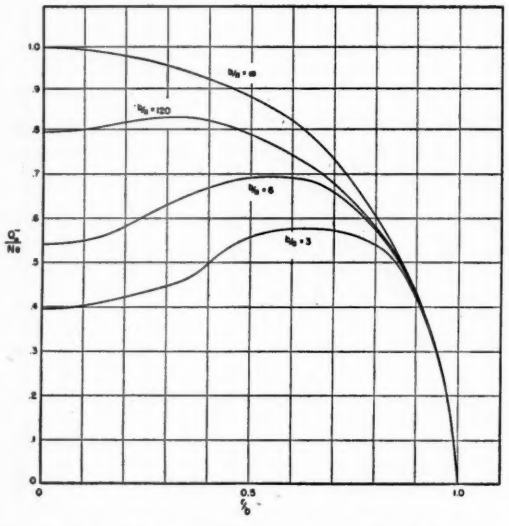

FIG. 6. Size of the electron pulse for a particle traversing the ionization chamber perpendicularly to the axis, as a function of the distance r of the track from the axis.

3. Gas Filling

An attempt was made to use mixtures of argon and CO_2 as gas filling in order to obtain

very short times of collection for electrons (see R.S., Chap. 1.4). The experience at Los Alamos has shown that chambers of a design similar to ours work satisfactorily with argon $-CO_2$ filling as detectors for γ- or β-rays (see R.S., Chap. 5.4). In testing the chambers with a source of polonium α-particles, however, it was found that the size of the pulses obtained with 5 atmospheres of argon plus 5 percent of CO_2 varied as the voltage across the chamber was changed and failed to reach saturation at the maximum voltage allowed by the design of the instrument. We believe that the reason for this behavior is columnar recombination, the influence of which is negligible in the case of lightly ionizing rays such as high energy electrons, but becomes important in the case of heavily ionizing rays such as α-particles. Since it was desirable to obtain quantitative response both for lightly ionizing and for heavily ionizing particles, and to use fairly high pressures so as to increase the sensitivity of the chamber, an effort was made to minimize columnar recombination by a more appropriate choice of the gas. It was found that pure argon with pressures up to about 7 atmospheres behaves satisfactorily in this respect and pure argon filling was thus adopted in all of our experiments. With 5 atmospheres pressure and 1000 to 2000 volts across the chamber, the time of collection of electrons was found to be approximately 7 microseconds. This time, even though considerably longer than the collection time in argon—CO_2 mixtures (see R.S., Chap. 5.4), proved adequate for most of our applications.

The filling procedure was as follows: the chamber was connected at A and B (see Fig. 1) to a purifier, consisting of an iron vessel filled with calcium metal chips, which could be heated electrically. The chamber and the purifier were first kept under vacuum for several hours with the purifier at 300°C. Then they were filled with tank argon through a dry ice trap. After closing the connection with the filling system, the gas was allowed to circulate by convection through the purifier at 300°C for 12 hours, at the end of which period the chamber was sealed off from the purifier.

4. Calibration

For the calibration of the chambers and of the amplifiers two different methods were used.

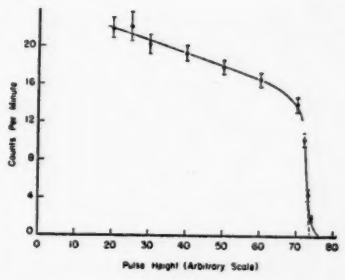

FIG. 7. Bias curve obtained with a polonium source in the chamber.

(*a*) As already mentioned, all chambers were provided with a polonium source placed near the outer wall. The polonium α-particles have an energy of 5.3 Mev and their range in argon at 5 atmospheres (the smallest pressure used in our chambers) is 0.74 cm. This range is small compared with the radius of the chamber. The α-particles brought to rest in the gas produce a number of ion pairs given by $N=5.3\times10^6/W_0$, where W_0 is the average energy to produce an ion pair, which, for argon, is equal to 26 ev. Since the range of the α-particles is small compared with the radius of the chamber, the corresponding value of Q_0^- depends only slightly on the direction of the track. It is a maximum for a track running close to the wall, in which case $Q_0^-=Ne=2.04\times10^5e$, and is 3 percent smaller than this maximum for a track perpendicular to the wall. The most convenient way to determine the maximum pulse height is to find the end point of the integral pulse height distribution, or *bias curve*, i.e., of the curve which gives the number of pulses larger than a certain size as a function of this size. As an example, the bias curve obtained with one of our ionization chambers is shown in Fig. 7. Its end point is determined by extrapolation of the linear portion of the curve, as shown in the figure. In the arbitrary scale of pulse height used, the extrapolated end point is at $P=74$. In this experiment, the voltage across the chamber was 675 volts. No appreciable change in the bias curve was observed by raising the voltage from 675 to 2000 volts. This may be taken as an indication that already at 675 volts electron recombination and attachment were negligible. In other chambers this condition was reached at a somewhat larger voltage, which, however, was never higher than 800 volts. The bias curve shown in Fig. 7 was

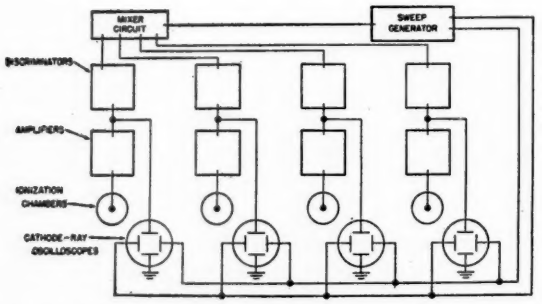

FIG. 8. Block diagram of the electronic equipment used in the coincidence experiments.

measured at sea level, where the cosmic-ray background is negligible compared with the counting rate from the polonium α-particles as shown by the fact that practically no counts are recorded at a bias slightly larger than the α-particle end point. The lack of a flat "plateau"in the bias curve is presumably explained by a background of pulses from radioactive contamination of the chamber. This background does not affect appreciably the extrapolated end point of the polonium α-particles.

(*b*) An electronic pulser was built to apply voltage pulses of known magnitude and in the shape of step functions to the high voltage electrode of the chamber. The charge Q_1 induced on the collecting electrode when the potential of the high voltage electrode is changed by a value V_1 is given by

$$Q_1 = C_1 V_1,$$

where C_1 represents the capacity between the two electrodes of the chamber. C_1 can be calculated easily if end effects are neglected. For a chamber of our type the calculated value of C_1 is 6.1 $\mu\mu$F. The extrapolated end points of the α-particle bias curve were found to be within 20 percent of the value computed from the calibration by means of artificial pulses. It is believed that the uncertainties in the energy loss per ion pair, W_0, and in the value of the interelectrode capacity, C_1, are sufficient to account for the discrepancy. In what follows, the calibration of the chambers will be based on the bias curves of the polonium α-particles. Pulse heights will be measured by the quantity $Q_0^- W_0/e$ expressed in electron-volts. This quantity represents the energy dissipated in the production of Q_0^-/e ion pairs.

FIG. 9. Photographic record of the four horizontal traces of the coincidence method. The apparatus was triggered by the large pulse appearing on the right-hand trace; two other traces show small time-coincident pulses.

III. COINCIDENCE EXPERIMENTS

1. The Principle of the Method

Ionization bursts caused by showers and by heavily ionizing particles can be separated by using several ionization chambers properly arranged and by recording the pulses of the various chambers simultaneously. Both the probability of a coincidence between the chamber pulses, and the distribution in size of the pulses when a coincidence occurs, are different depending on whether the chambers are recording showers or nuclear disintegrations.

2. The Experimental Equipment

In the coincidence experiments, four ionization chambers were used. A block diagram of the electronic equipment is shown in Fig. 8. The pulses of the individual chambers were amplified separately and brought to the deflecting plates of four cathode-ray oscilloscopes. The same pulses were also brought to four pulse height discriminators which could be adjusted to fire for signals larger than a predetermined value. The output pulses of the four discriminators were fed to a mixer circuit, which gave a pulse whenever at least one discriminator fired. This pulse was used to trigger a sweep generator, the purpose of which was to intensify the beams of the oscilloscopes (which were normally biased below cut-off) and to provide a linear horizontal sweep. The four oscilloscope screens were photographed on a continuously moving film. Figure 9 is the reproduction of a picture showing pulses of different sizes in three of the four chambers and no pulse in the fourth.

The equipment was calibrated at frequent

intervals during the experiments, both with α-particle pulses and with artificial pulses. The gain was adjusted so that the minimum detectable deflection of the oscilloscope beams corresponded to a pulse of 0.25 Mev. This size of pulse was about ten times larger than the (r.m.s.) amplifier noise. Pulses caused by electric pick-up were occasionally recorded but could be easily distinguished from ionization pulses by their oscillatory nature. They were, of course, rejected in the evaluation of the data. The speed of the sweep was 7×10^4 cm sec.$^{-1}$ and its total duration 60 microseconds. Examination of the oscilloscope records made it possible to establish the simultaneity of the pulses in the various chambers with an accuracy of 6 microseconds.

3. Separation of Bursts from Showers and Nuclear Disintegrations

The four chambers were arranged close to one another with their axes horizontal, as shown in Fig. 10. The group of chambers was enclosed in a wooden box $\frac{1}{4}$-inch thick, lined with a 0.011-inch copper sheet for electrostatic shielding. The box was placed in a wooden shack at Climax, Colorado (elevation 3500 meters, average atmospheric pressure 673 g cm^{-2}). The roof of the shack was 1.5 g cm^{-2} thick. Measurements were taken with the circuit adjusted to trigger the four sweeps whenever a pulse larger than 7.5 Mev appeared in any one of the four chambers. Such a pulse is 1.4 times the pulse produced by a polonium α-particle and consequently we may assume that only cosmic-ray events were recorded. The fact that the rate of occurrence of pulses larger than 7.5 Mev increases by a factor of about 14 between sea level and 3500 meters conclusively confirms our assumption. The results obtained in 63.1 hours of observation are summarized in Table I, and parts of these data are analyzed in Figs. 11, 12, and 13. Table I gives a classification of the pulses larger than 7.5 Mev which occurred in chamber 2 or in chamber 4 according to whether pulses larger than 0.25 Mev occurred simultaneously in none, one, two, or three of the other chambers. Curve (*a*) in Fig. 11 shows the combined integral pulse height distribution for the pulses of chamber 2 which *are not* accompanied by pulses larger than 0.25 Mev in chambers 1, 3, 4, and for the pulses of chamber 4 which *are not* accompanied by pulses larger than 0.25 Mev in chambers 1, 2, 3. Similarly, curve (*b*) in the same figure shows the combined integral pulse height distribution for the pulses of chamber 2 or chamber 4 which *are* accompanied by a pulse larger than 0.25 Mev in at least one other chamber.

TABLE I. Classification of the pulses larger than 7.5 Mev in chamber 2 (the upper chamber) and chamber 4 (the lower chamber) according to the number N of *additional* chambers in which simultaneous pulses larger than 0.25 Mev occurred.

Chamber	2				4			
N	0	1	2	3	0	1	2	3
Total counts	644	130	35	21	733	87	21	28
Counts per hour	10.2	2.06	0.55	0.33	11.6	1.38	0.33	0.44

Figure 12 is a histogram of the frequency of occurrence of various values of the mean deviation from the mean of pulse heights in events in which three chambers had observable pulses. These mean deviations have been divided by the square root of the mean, in order that events with different mean pulse heights may be com-

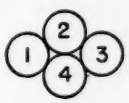

FIG. 10. First arrangement of the chambers in the coincidence experiments.

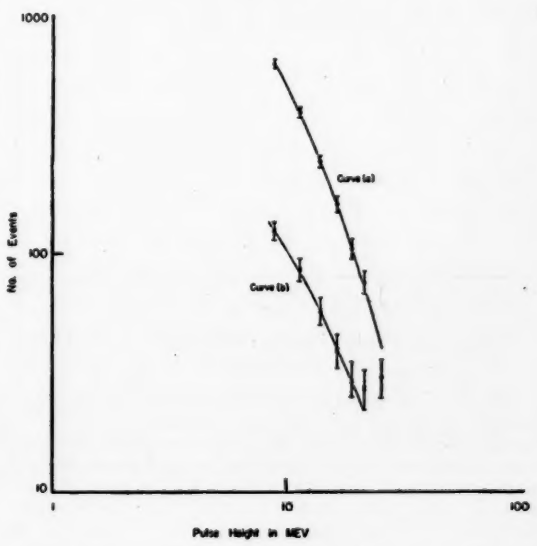

FIG. 11. Integral pulse height distributions for single pulses (curve *a*) and for coincidences (curve *b*) (time of observation 35.7 hours).

pared. The quantity plotted is therefore

$$x=\sum_{i=1}^{3}\frac{|(P)_{Av}-P_i|}{3((P)_{Av})^{\frac{1}{2}}}$$

where P_i is the pulse height in the ith chamber, and $(P)_{Av}$ is the average pulse height for the three chambers.

Figure 13 shows the same type of histogram for fourfold coincidences.[10]

In the experiment described, no heavy material was present above the chamber. This rules out the possibility that locally produced ordinary cascade showers may be partly responsible for the observed bursts. These bursts, therefore, must be produced either by large air showers or by nuclear interactions. It is reasonable to assume that an air shower should produce pulses of not very different sizes in the four thin-walled chambers used in our experiments. Direct experiments fully confirm this view, as will be shown in a separate paper by R. W. Williams. Thus any event in which at least one of the ionization chambers fails to give a detectable pulse must be interpreted as the result of nuclear interactions. Indeed it is likely that not even all of the fourfold coincidences are caused by air showers. Examination of Fig. 13 shows that the fourfold coincidences fall rather sharply into two groups, one in which the mean deviations are small, and one in which the mean deviations are large. It is natural to explain the pulses of the first group as caused by air showers, the pulses of the second group as caused by nuclear disintegrations. One thus concludes that air showers and nuclear disintegrations account, respectively, for 55 percent and 45 percent of the fourfold coincidences observed. It appears that very few of the ionization pulses observed at 3500 meters in thin-walled ionization chambers of our type are produced by air showers. The total number of pulses larger than 7.5 Mev in each chamber, regardless of whether or not detectable pulses were present in any other chamber, was 13.45 per hour. Of these, 0.3 per hour were accompanied by pulses of size comparable with their own in all of the other chambers. *Thus air showers contribute about 2 percent of the total number of pulses larger than 7.5 Mev observed in a single chamber.*

It should be noted that the relative numbers of pulses produced by air showers and by nuclear disintegrations is dependent on the dimensions of the chamber, the pressure of the gas, and the bias setting. It was found, for instance, that at 3500 meters the number of pulses larger than a certain size P produced by air showers varies as $P^{-1.7}$.[8,11] As shown in Fig. 11, the pulse height distribution for all pulses decreases more rapidly with increasing P. It thus follows that the contribution of air showers relative to that of nuclear disintegrations becomes increasingly important

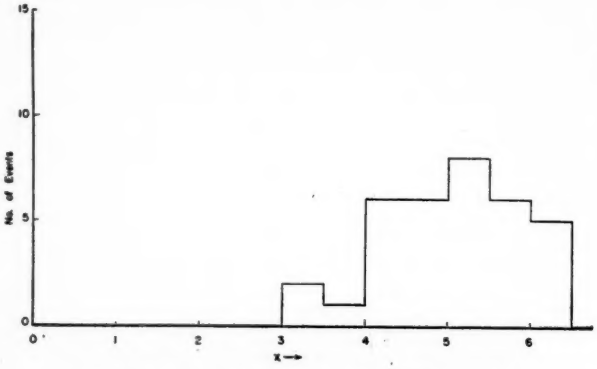

FIG. 12. Spread in pulse height for threefold coincidences.

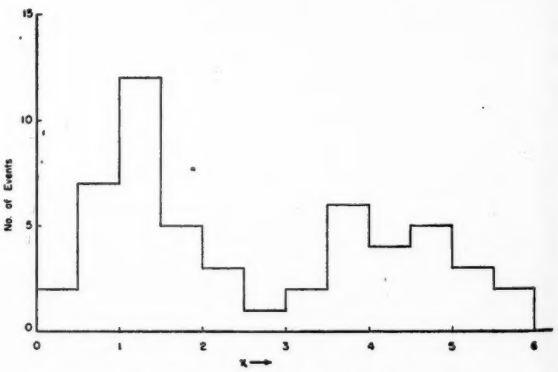

FIG. 13. Spread in pulse height for fourfold coincidences.

[10] Qualitative examination of the records shows that the fourfold events fall into two groups, "large-deviation" and "small-deviation" events. When the chambers are struck by an air shower we would expect a small mean deviation, caused mainly by the fluctuations in the number, N, of particles traversing each chamber. The distribution in number of particles may approximate a Poisson distribution, for which, if $(N)_{Av}$ is large, the mean deviations are proportional to $((N)_{Av})^{\frac{1}{2}}$. Therefore, if we divide by $((P)_{Av})^{\frac{1}{2}}$, which is proportional to $((N)_{Av})^{\frac{1}{2}}$, we will compare all air showers on the same basis, regardless of size.

[11] R. W. Williams, to be published.

as the bias energy is raised. The pulse height distribution which we observe also verifies the interpretation given for Carmichael's burst data by H. Euler.[12] Also, because of the relatively short range of the fragments from nuclear disintegrations and the large range of shower electrons, high gas pressure favors the detection of air showers. Thus Lapp,[13] whose ionization chamber had a pressure of fifty atmospheres, and who required an energy loss of several hundred Mev, reports that about 85 percent of his bursts at sea level were caused by air showers.

4. Further Results Concerning Nuclear Disintegrations

An unexpected result of our experiments was the fairly large number of coincidences between neighboring ion chambers which arise from nuclear events. It is believed that most of these events are disintegrations which take place in the wall of one chamber, and in which protons of sufficiently high energy to penetrate the walls of other chambers are produced. It may be noted that a proton must possess at least 21-Mev energy to traverse one chamber wall and 31 Mev to traverse two chamber walls. On the other hand, any proton with more than 0.25 Mev and less than 230 Mev traversing a chamber along a diameter will produce a detectable pulse. The large spread in size of the pulses simultaneously produced in two or more chambers by nuclear interactions (see Figs. 12, 13) is consistent with this interpretation.

Measurements were made of the coincidence rate between two chambers in contact as a function of their relative position. It was found that this rate is practically the same when the chambers are arranged one above the other and when they are arranged one beside the other. This result is again consistent with the above interpretation, since it is known that the heavily ionizing particles produced in nuclear interactions are distributed *approximately* at random in direction. However, the data in Table I clearly indicate a slight tendency for these particles to be projected in a downward direction. In fact, while the total counting rate for pulses larger than 7.5 Mev is very closely the same for chambers 2 and 4 (13.1 and 13.7 respectively), the fraction of such pulses accompanied by pulses in other chambers is greater for chamber 2 (upper chamber).

TABLE II. Number of coincidences in 42.2 hours between the different pairs of chambers in Fig. 14.

Chambers	Distance between axes (inches)	Coincidences in 42.2 hours
1, 2	3	66
2, 3	4½	39
3, 4	6	32
1, 3	7½	18
1, 4	13½	8

The coincidence rate was also measured as a function of the distance between chambers. For this experiment the four chambers were arranged with their axes in a horizontal plane, as shown in Fig. 14. The numbers of coincidences recorded in 42.2 hours are shown in Table II. It is seen that the number of coincidences decreases very rapidly with increasing distance. An approximate calculation shows that this number varies roughly as the average solid angle subtended by one chamber at the other, as one would expect according to our interpretation. It is possible, of course, that the rate of coincidences (1, 3) and (1, 4) might be reduced by absorption in the walls of the intervening chambers. Even though there seems to be little doubt that most of the coincidences are caused by single nuclear events, the possibility cannot be excluded that some coincidences may be produced by two or more disintegrations occurring simultaneously in different ionization chambers.

In order to obtain information on the nature of the radiation which causes the observed disintegrations, measurements were taken with the chambers arranged as shown in Fig. 10 and with lead absorbers of different thicknesses placed around them (see Fig. 15). The results obtained are summarized in Fig. 16, where the abscissa represents the thickness in g cm^{-2} of the lead

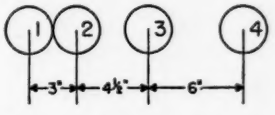

FIG. 14. Arrangement of chambers for the study of the variation of the coincidence rate with distance.

[12] H. Euler, Zeits. f. Physik 116, 73 (1940). See also J. Clay and C. G. T'Hooft, Physica 9, 251 (1944).
[13] R. E. Lapp, Phys. Rev. 69, 321 (1946).

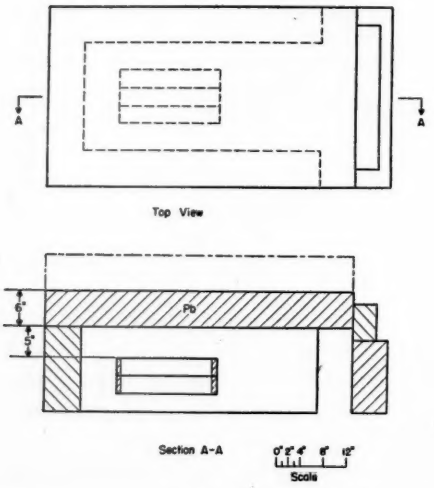

FIG. 15. Arrangement of ionization chambers and lead shields for the absorption measurements with 6 inches of lead. Dashed line in sectional view shows the additional 6 inches used for the 344 g cm^{-2} point.

absorber and the ordinate represents the corresponding transmission; i.e., the ratio N/N_0 of the counting rates with and without lead. It should be noted that in the measurements at 115 g cm^{-2} and 172 g cm^{-2} the thickness of lead on the sides was equal to that on top, while the point at 344 g cm^{-2} was obtained with only 172 g cm^{-2} on the sides.

Data for the following events were recorded: (*a*) a pulse larger than the bias energy in chamber 2 or 4 not accompanied by a pulse larger than 0.25 Mev in any other chamber; (*b*) a pulse larger than the bias energy in any chamber accompanied by pulses larger than 0.25 Mev in one or two additional chambers; (*c*) a pulse larger than the bias energy in any chamber accompanied by pulses larger than 0.25 Mev in all other chambers. The bias energy was 12.5 Mev for the point at 115 g cm^{-2} of lead, and 7.5 Mev for the other two points. Experiments showed that the pulse height distribution is not appreciably affected by the lead shielding so that the values of the transmission should be independent of bias. The events of type (*a*) observed either with or without lead are surely caused by nuclear disintegrations. Indeed, a shower from the lead may strike one of the lateral chambers (1 or 3) without striking any other chamber, but cannot strike one of the middle chambers (2 or 4) alone. The possibility that any appreciable number of showers may strike chamber 2 and be absorbed in the chamber walls, thus failing to discharge chamber 4, is ruled out by the observation that, with as well as without lead, single pulses of chambers 4 are slightly more numerous than single pulses of chamber 2 rather than the other way around (the interpretation of this slight difference has been given above). Thus the variation with increasing lead thickness of the counting rate for single pulses in chamber 2 or 4 may be considered to represent the absorption in lead of the radiation which produces nuclear disintegrations. The experimental data seem to indicate that the absorption curve has an inflection point. We feel that further experiments are necessary before this detail may be considered as established beyond any doubt and before its possible significance may be profitably discussed. Here we only wish to point out that the absorption in lead of the parent radiation is much smaller than the absorption of high-energy electrons or photons. This result, which is in agreement with qualitative data obtained by the observation of "stars" in photographic emulsions,[14] proves that electrons or photons are not the major source of nuclear disintegrations in cosmic rays. Our results are not in disagreement with the hypothesis that most of the disintegrations are produced by neutrons. The absorption curve for events of type (*b*) does not seem to

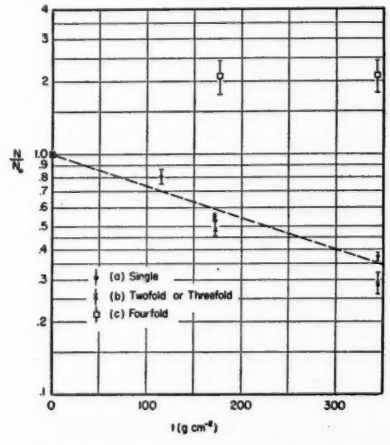

FIG. 16. Ratio of the counting rates with and without lead as a function of the lead thickness *t*. The straight line represents an exponential decrease with a mean free path of 330 g cm^{-2}.

[14] D. H. Perkins, Nature **160**, 707 (1947).

differ greatly from that for events of type (*a*). This may be construed as an indication that, also under lead, twofold and threefold coincidences, as well as single pulses, are mainly caused by nuclear disintegrations.

The number of fourfold coincidences (event *c*) is found to increase by about a factor of 2 when 172 g cm^{-2} of lead is placed above the chambers. This increase can easily be understood if electron showers capable of discharging the four chambers are produced in the lead by a penetrating radiation. This effect is known to occur.[6,7,13,15] The failure to observe a decrease in the fourfold counting rate when the lead thickness is increased from 172 to 344 g cm^{-2} is somewhat surprising in the light of other results.[16] Here again, however, we feel that more accurate experiments are needed before any conclusion can be reached.

IV. THE PULSE SHAPE METHOD

1. The Principle of the Method

Some information on the nature of the processes which give rise to bursts in ionization chambers can be obtained by examining the *shape* of the pulses. The ionization produced by a shower is fairly uniformly distributed over a large portion of the volume of the chamber, while the ionization caused by a nuclear disintegration is concentrated along the tracks of a few heavily ionizing particles. To the different distribution in space of the ionization there corresponds a different time dependence of the observed voltage pulse, $V(t)$.

It is not possible to determine theoretically the exact pulse shape corresponding to a given distribution of ionization because the dependence of the drift velocity of electrons, w^-, on the field strength E in our ionization chamber is not well known. This is due, in part, to the fact that the drift velocity of electrons in argon depends critically on the purity of the gas. However, it turns out that the shape of the function, $V(t)$, depends more critically on the distribution of the ionization than on the form of the function $w^-(E)$. This is borne out by an examination of Fig. 17. Curves *a*, *b*, *c*, in this figure were computed under the assumption of a drift velocity independent of E for the following cases: (*a*) ionization confined to an infinitesimal layer adjacent to the chamber wall; (b) ionization uniformly distributed throughout the volume of the chamber; (*c*) ionization distributed uniformly along a straight line perpendicular to and passing through the axis of the chamber. The dotted curves a', b' in the same figure represent $V(t)$ for cases (*a*) and (*b*) respectively, computed under the assumption of a drift velocity proportional to the square root of the electric field strength.[17]

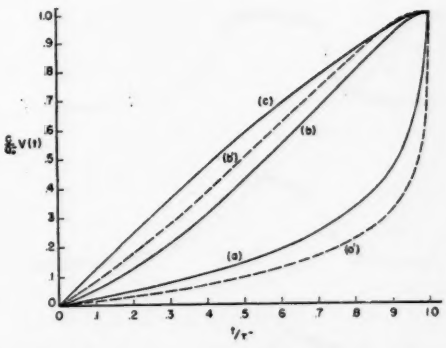

FIG. 17. Pulse shapes corresponding to different distributions of the ionization in the chamber, and to different relations between drift velocity and electric field strength.

One sees that the qualitative character of curves *a*, *a'*, and *b*, *b'* respectively is essentially the same. The shape of the curves *a*, *a'* can be easily explained by considering that, under the assumptions made, all of the electrons at a given time are at the same distance from the axis of the chamber. They are, therefore, acted upon by

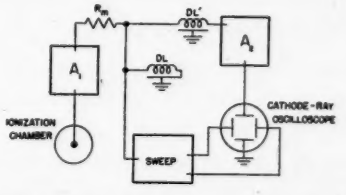

FIG. 18. Block diagram of the electronic equipment used for the analysis of pulse shapes. For significance of symbols see text and Fig. 4.

[15] W. B. Fretter, Phys. Rev. **73**, 41 (1948).
[16] H. S. Bridge, as reported by B. Rossi, Rev. Mod. Phys. **20**, 537 (1948).

[17] The actual dependence of w^- on E is complicated by the Ramsauer effect. $w^-(E)=$ const. is experimentally found to be approximately correct for large values of E, such as exist near the wire. $w^-(E)=\text{const.}\times E^{\frac{1}{2}}$ represents the drift velocity calculated under the assumptions that the mean free path for collisions is constant for all values of the agitation energy and that the energy loss of electrons is only caused by elastic collisions with the argon molecules.

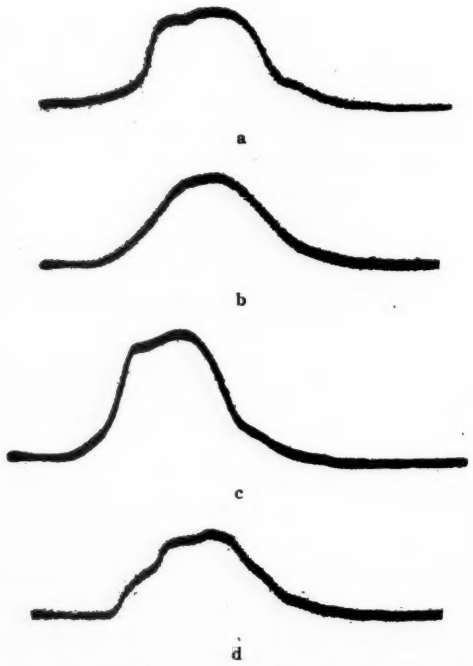

FIG. 19. Unshielded ion-chamber pulses (7500 meters). In some of the α- and ν-type pulses the negatives have been retouched so that the fast portion of the pulse rise can be reproduced satisfactorily. In all of the examples in this figure the pulses do not have an ideal flat top but show an additional rise at about $t_c/2$ which was later eliminated. (a) Pulse caused by P_0-α-particle, (b) σ-type pulse caused by an air shower, (c) α-type pulse from nuclear disintegration, (d) ν-type pulse. This example shows a distinct break presumably caused by two particles one ending close to the wall and one close to the wire.

the same field strength, E, and have the same drift velocity, $w^-(E)$, so that Eqs. (1) yield:

$$CdV/dt = NEw^-(E)/V_0, \qquad (8)$$

where N is the total number of electrons. As the electrons drift toward the wire, E increases slowly at first, then very rapidly. The slope of the function $V(t)$ increases in proportion to E if $w^-(E)$ is constant and even more rapidly if $w^-(E)$ increases with E. The reader will find it easy to understand the physical reason for the shapes of the curves b, b' and c by considering how the initial distribution of the ionization affects the rate at which electrons arrive near the wire.

2. The Experimental Arrangement

A block diagram of the electronic equipment used for the analysis of pulse shapes is shown in Fig. 18.

The pulse of the chamber is applied to the deflecting plates of the oscilloscope through a delay line, DL', inserted at a point of the amplifier where the level of the signal is of the order of one volt. The undelayed pulse is further amplified and fed to a pulse height discriminator. The signal from the discriminator triggers the circuit which provides the intensifier pulse and the linear sweep for the oscilloscope. In this way it is possible to observe the beginning of the pulse despite the small inevitable delay in starting the sweep.

The line had a delay of 8.2 microseconds and its rise time was 0.3 microsecond. The oscilloscope screen was 5 inches in diameter and the sweep speeds used ranged from 2.5×10^5 to 5×10^5 cm sec.$^{-1}$. The pulse amplifier was of the type described in II.2. Its low frequency response was determined by "delay line clipping." Clipping times, t_c, between 10 and 15 microseconds were used.

3. Experimental Tests

The instrument described in the preceding section was first used to examine the shape of the α-particle pulses from the polonium source. This, as already mentioned (see II.1), was placed on the wall of the chamber. In argon at 5 atmospheres pressure, the range of a polonium α-particle is 0.74 cm and is therefore small compared with the radius of the chamber (3.75 cm). Thus the α-particle pulses should be of the general type represented by curves a and a' in Fig. 17. The experimental results were in agreement with these conclusions. All of the α-particle pulses were found to be very nearly of the same shape, showing an initial slow rise followed by a very fast one near the end of the pulse. An example of an α-particle pulse is reproduced in Fig. 19a.

In a second experiment, pulses arising from air showers were chosen by selecting events in which three Geiger-Mueller counters arranged in a horizontal plane were discharged simultaneously with the ionization chamber. The observations were carried out at 7500 meters in a B-29 aircraft. Altogether 5 air shower pulses were recorded. They all had approximately the same shape as the sample shown in Fig. 19b, in which one clearly recognizes the general character

predicted by the theory for uniformly distributed ionization (see Fig. 17, curves b, b').

The pulses recorded with no auxiliary methods of identification had a variety of shapes, examples of which are shown in Figs. 19 and 20. A large fraction of the pulses had shapes very similar to that of an α-particle pulse (see Figs. 19c and 20b). Single heavily ionizing particles from nuclear disintegrations originating in the chamber wall and not passing close to the collecting wire probably account for most of these pulses, even though some of them may be caused by groups of short-range particles. Many examples were found of pulses showing two or more sharp "breaks" (see Fig. 19d). These correspond presumably to nuclear disintegrations which give rise to several heavily ionizing particles which stop in the gas at different distances from the wire. In some cases the slope of the pulse was greatest at the beginning and decreased gradually with increasing time (see, for instance, Fig. 20c). Comparison with Fig. 17 indicates that these pulses are probably caused by heavily ionizing particles passing near the wire. A few of the pulses observed with an unshielded chamber, and a large fraction of those observed under lead, had shapes indistinguishable from that of an air shower pulse (see Fig. 20a). It is likely, however, that not all of these pulses were actually produced by electron showers because a group of many heavily ionizing particles passing at different distances from the wire could produce a pulse practically indistinguishable from that of a shower. Further information bearing on the interpretation of pulse shapes will be presented in Part V.

For the sake of convenience, we shall adopt the following classification for the pulse shapes:

α-pulses: pulses with a single sharp break, resembling the pulses produced by the polonium α-particles.

σ-pulses: pulses with a smooth, almost linear rise, resembling those produced by air showers.

ν-pulses: pulses of all other shapes.

It must be noted that the exact boundary between σ and ν pulses is, to a certain extent, a matter of personal judgement.

Observations at 7500 meters with an unshielded chamber and with a chamber covered with 2.5 cm of lead gave the results shown in Table III.

TABLE III. Distribution of pulse shapes in an ionization chamber (a) unshielded, (b) under a 2.5-cm thick lead shield.

Pulse shape	Percent of pulses (a)	(b)
α	58	37
σ	16	44
ν	26	19

While all of the α-pulses and ν-pulses are probably produced by nuclear disintegrations, the discussion above suggests that not all of the σ-pulses are caused by showers. The pulse shape distribution in the unshielded chamber observed at 7500 meters altitude, therefore, cannot be taken as a proof that, at this altitude, the frequency of air showers relative to nuclear disintegrations is larger than 3500 meters, where it has been found to amount to 2 percent (see III.3).

V. OBSERVATIONS WITH A CLOUD CHAMBER EXPANDED BY PULSES FROM AN INTERNAL ION CHAMBER

1. The Experimental Method

In order to gain a more precise understanding of the nature of the cosmic-ray phenomena which are responsible for bursts in ionization chambers, and especially of those which give rise to coincidences between neighboring chambers, observations were made by means of a cloud chamber triggered by the pulses of an ionization

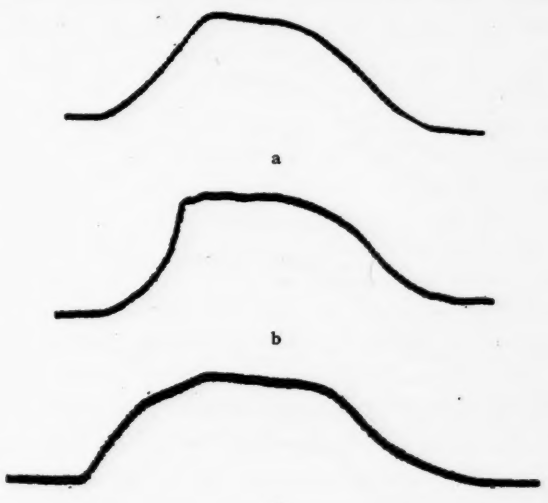

FIG. 20. Pulses from an ion chamber shielded by one inch of lead (sea level). (a) σ-type, (b) α-type, (c) ν-type showing a slope which decreases with time.

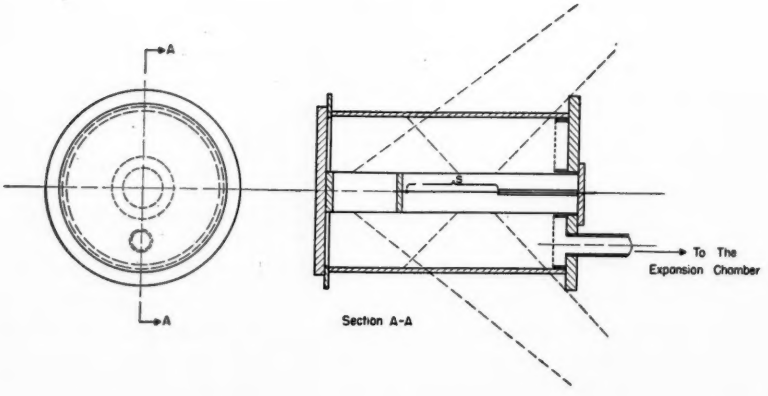

FIG. 21. Arrangement of ionization chamber inside the cloud chamber. The sensitive length of the ionization chamber wire is indicated by *S*. The approximate boundaries of the light beams are shown by the dashed lines; actually, of course, the boundaries are not sharp and it was found that heavily ionizing particles could be observed nearly anywhere in the chamber.

chamber built inside it. The diagram in Fig. 21 shows the essential features of the experimental arrangement. The ionization chamber was placed with its axis coincident with the axis of the cloud chamber. It was of the type described in Part II, except for modifications that made it suitable for insertion in the cloud chamber. The only significant modification was that one of the end plugs was seven inches from the sensitive volume whereas in the chambers of the usual type both end plugs are adjacent to the sensitive volume. The ionization chamber was 3 inches in diameter, the effective wire length was 7 inches. The walls were made of $\frac{1}{32}$-inch-thick brass and the chamber was filled with argon at 5 atmospheres pressure.

The cloud chamber followed the general design of E. J. Williams[18] in which the light scattered into the camera by the droplets is deflected through only 45 degrees. The resultant high brilliance of the droplets permits the photographic observation of a large depth of the cloud chamber. In addition, since track curvatures were not being measured, the droplet brilliance was enhanced by allowing a relatively long time for drop growth before taking the picture. Thus it proved feasible to observe the entire sensitive surface of an ionization chamber that was large enough to give a reasonable counting rate.

The expansion chamber was separated from the observation chamber in order to give free access to the terminals of the ionization chamber. It was found that, with any gas except hydrogen (i.e., with helium, argon, or air) the supersaturation threshold for formation of drops on uncharged "condensation nuclei" was as low as (helium) or lower than the threshold for condensation on charged nuclei. Hence hydrogen was used as the permanent gas. All of the information leads to the conclusion that the two large chambers and their coupling tube resulted in an oscillatory pressure wave of sufficient amplitude to produce the observed effects.

Stereoscopic photography was used to demonstrate that all of the sensitive surface of the ionization chamber was within the observable region of the cloud chamber, and for spatial reconstruction of the tracks in all events of interest.

The electrical circuits associated with the ionization chamber were of the type described in Part II. Condenser coupling from the ionization chamber to the preamplifier allowed a high (positive) voltage to be applied to the collecting wire while the outer wall of the ionization chamber remained at ground potential. The observations were made with the discriminator adjusted to select pulses larger than about 6 Mev in the ionization chamber.

The instrument described was operated both at 3050 meters (Doolittle Ranch, Colorado), and at 4300 meters (Mt. Evans, Colorado). The data were taken partly with a $\frac{1}{4}$-inch lead shield, in the shape of half a cylindrical shell, placed directly above and in contact with the ionization chamber, partly with lead plates of various thicknesses placed above the cloud chamber, partly with both lead shields, partly with neither of them. During some of the observations the pulses of the ionization chamber were recorded photographically as explained in Part IV.

[18] E. J. Williams, Proc. Roy. Soc. **A172**, 206 (1939).

This made it possible to distinguish between pulses produced by ionization bursts and by electric pick-up from other equipment or from lightning, and to correlate the shape of the pulses in the ionization chamber with the events shown by the corresponding cloud-chamber records.

Examples of cloud pictures are shown in Fig. 22. Examples of correlated cloud-chamber and ionization-chamber records are shown in Fig. 23.

2. Correlation of Ion-Chamber and Cloud-Chamber Records

The results of the observations in which the cloud-chamber and the pulse-recording equipment were operated simultaneously are summarized in Table IV. In the compilation of this

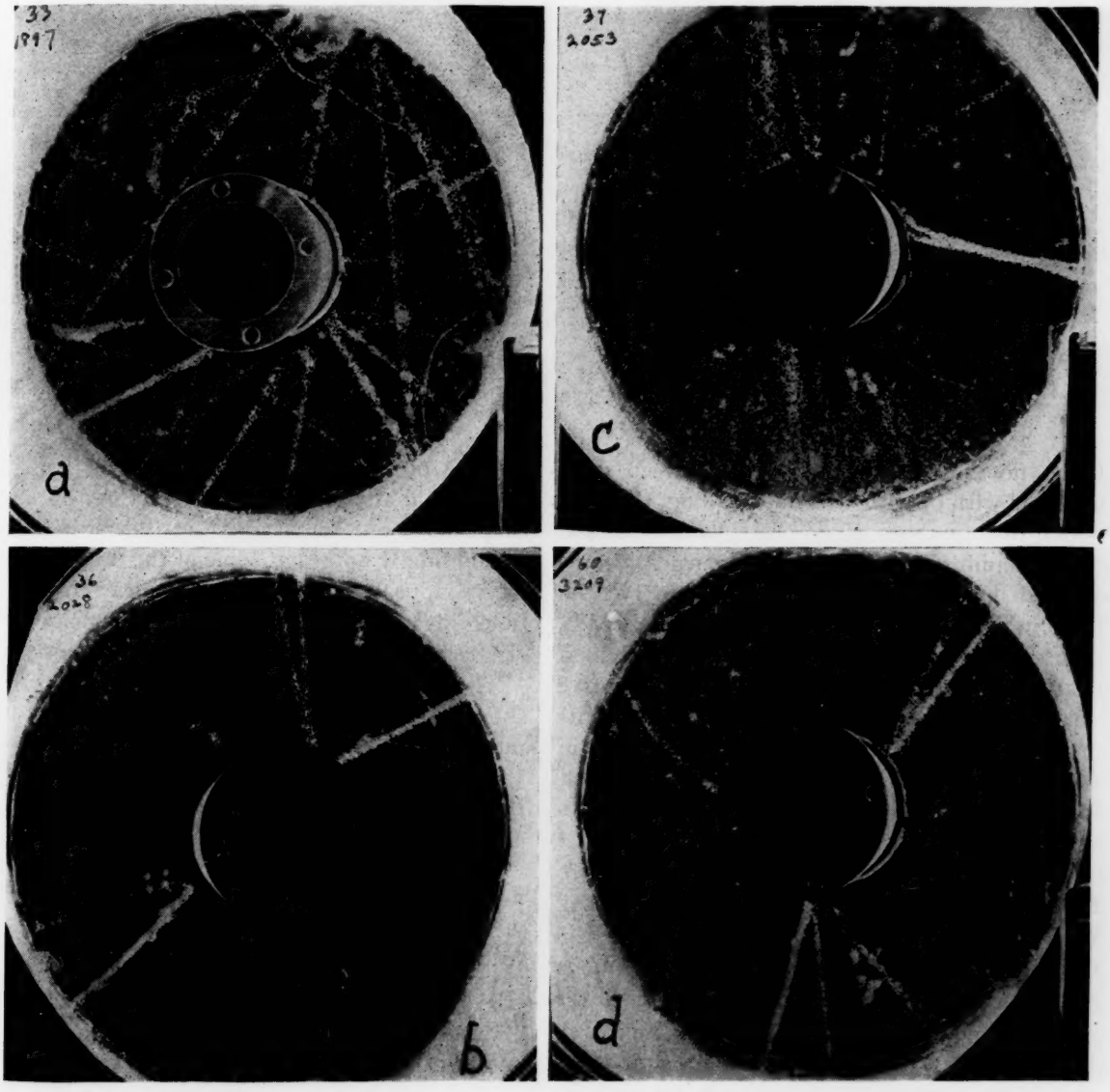

FIG. 22. Example of the cloud-chamber pictures. (a) An event in which a disintegration in the cloud-chamber wall is concurrent with a disintegration in the ionization-chamber wall. The latter may be initiated by a neutron from the former or both may be produced by neutrons from a disintegration above the apparatus. (b) A disintegration with four heavily ionizing and one lightly ionizing particles. (c) An electron shower from lead above the chamber apparently produces at least two heavy particles in a disintegration in the ionization-chamber wall. (d) A disintegration with at least seven particles appearing in the cloud chamber.

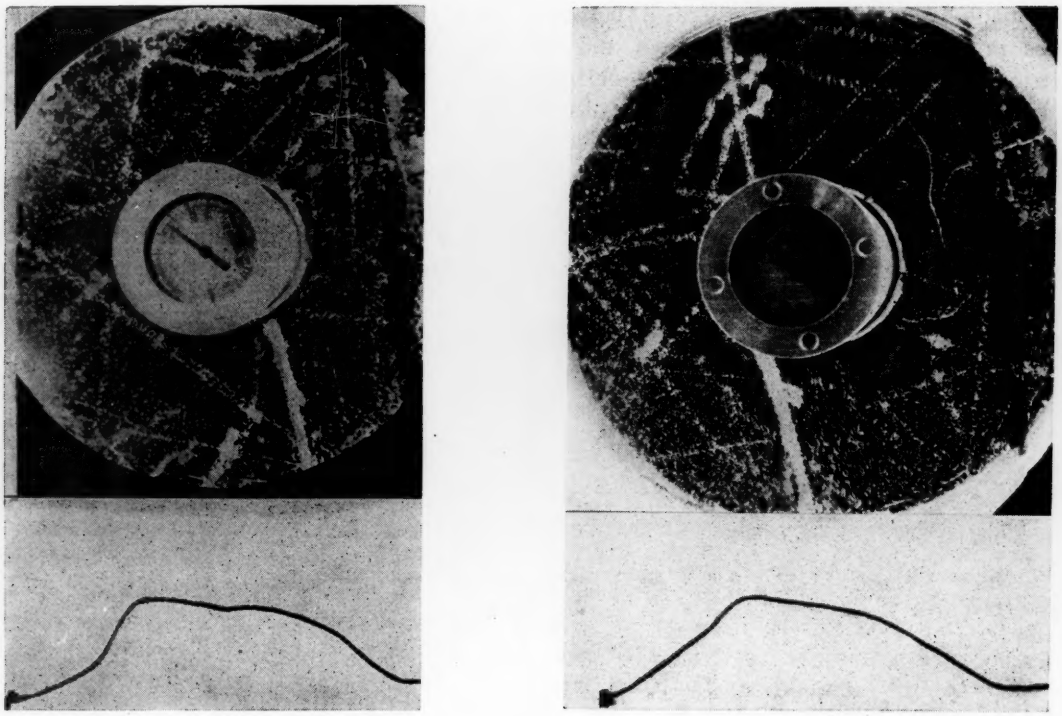

a b

table, no distinction was made between data obtained with or without lead shielding. One will notice that in about 50 percent of the cases the cloud chamber does not show any track clearly associated with the event responsible for the burst in the ionization chamber. Since, as already pointed out, the illuminated volume of the cloud chamber completely surrounded the sensitive volume of the ionization chamber, these events presumably represent nuclear disintegrations in the gas or in the wall of the ionization chamber, in which no ionizing particles capable of penetrating the chamber wall are produced.

Table IV shows that the pulses associated with the 12 pictures of electron showers were all of the σ type. Most of these showers originated in the lead shield above the cloud chamber and in some cases the shower struck near the edge of the ionization chamber (see, for instance, Fig. 23e). It thus appears that showers produce pulses of the σ type even when they do not fill a major fraction of the ionization-chamber volume with uniform ionization. Of the 86 pulses which are attributed to nuclear disintegrations either because of the lack of associated tracks or because of the appearance of heavily ionizing particles in the cloud-chamber picture, 80 have shapes of the α- or ν-type, 6 of the σ-type. One should finally note that some of the pulses of the ν-type appear to be caused by nuclear interactions in which heavily ionizing particles and electron showers are produced simultaneously.

The conclusion of this analysis is that electron showers are always recognized as such by the pulse shape but that a fraction of the order of 10 percent of the nuclear disintegrations give rise to pulses which simulate those produced by electron showers.

3. Relative Frequency of Showers and Nuclear Disintegrations Under Different Lead Shields

For this analysis, we consider all of the cloud-chamber pictures, whether or not simultaneous records of pulse shapes were obtained. The various types of events observed with different shieldings are listed in Table V. With no lead shielding, 55 pictures were obtained, of which only 3 showed electron showers and of these one showed an apparently time-associated heavy

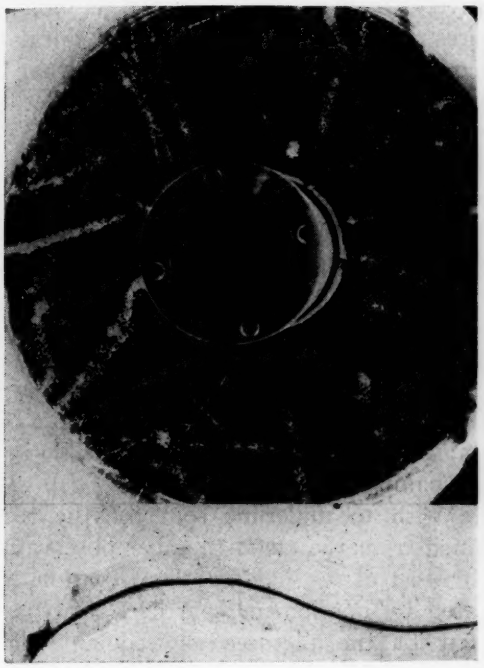

c

d

particle from the chamber wall. Table IV indicates that 42 percent of the nuclear disintegrations recorded by the ionization chamber (i.e., 36 out of 86) gives visible heavy tracks in the cloud chamber. Thus the 3-shower records must be compared with about 130 nuclear disintegrations in estimating the relative numbers of bursts produced by the two kinds of events. This comparison shows that only a very small fraction of the bursts in the unshielded ionization chamber are caused by showers, in agreement with the results obtained from the coincidence experiment described in Part III. When lead was placed either above the cloud chamber or directly on the ionization chamber, the number of elec-

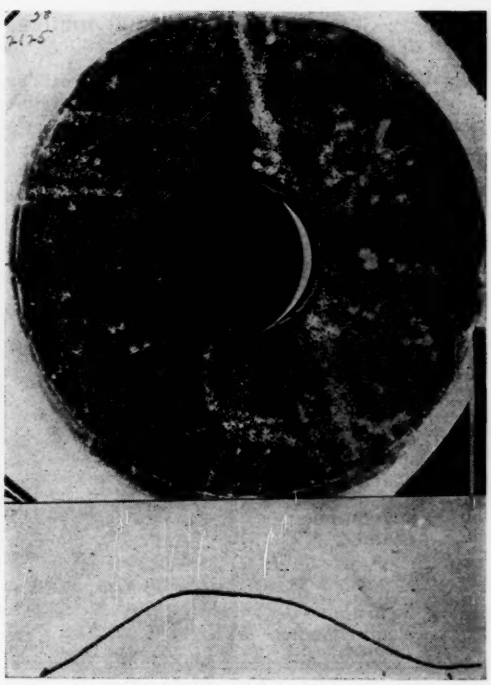

e

FIG. 23. Correlated cloud-chamber-ion-chamber records. The series (a), (b), (c) are examples in which the cloud chamber shows one or more heavily ionizing tracks from the ion chamber. They have been selected to show the greatest variation encountered in pulse shape in cases where the pulse is the result of a nuclear disintegration. Most pulses under these conditions are similar to example (a). Except for a slight break hardly visible in the reproduction, (b) would be classified as σ-type. Example (c) is a ν-type pulse the slope of which decreases with time. The cloud chamber shows 11 heavily ionizing tracks. Examples (d) and (e) show electron showers which originate in a one inch lead plate on top of the cloud chamber. It is somewhat unexpected that even when the axis of the shower is as far to the side as in (e) a σ-pulse is still obtained.

TABLE IV. Correlation of ion-chamber and cloud-chamber records, giving the number of cases in which a given type of cloud-chamber picture was associated with a given type of ionization-chamber record.

	α	ρ	σ	Total
No associated tracks	35	9	6	50
Heavy tracks from the ion chamber wall	29	7	0	36
Electron shower	0	0	12	12
Total	64	16	18	98

tron showers relative to the number of nuclear disintegrations increased markedly, as one should expect. About two-thirds of the showers observed under lead came from a single point in the lead, thus indicating that one electron or photon was responsible for the event observed in each case. In one-third of the cases there appeared to be several electrons or photons from an air shower incident upon the instrument and undergoing cascade multiplication in the lead shield.

4. Results Concerning Nuclear Disintegrations

We wish to discuss now in more detail the pictures of nuclear disintegrations. Table VI gives the distribution in size of nuclear disintegrations from the ionization-chamber wall observed at 3050 meters and 4300 meters, respectively. In the compilation of this table, the pictures obtained under various lead shields are all considered together. It appears that the character of the nuclear disintegrations does not change significantly between 3050 and 4300 meters. The results on the number-frequency distribution of disintegration particles obtained at the two altitudes have been combined and presented graphically in Fig. 24a. Figure 24b shows the corresponding frequency distribution of the events for which a simultaneous pulse shape record was available. In Fig. 24b the point at abscissa zero gives the number of events in which the ionization chamber detected a burst and no heavily ionizing track was visible in the cloud chamber.

TABLE V. Number of cloud chamber pictures showing nuclear disintegrations and electron showers under different experimental conditions.

		Event observed			
Altitude	Lead shield	Heavy tracks from ionization chamber	Shower from air	Shower from lead above cloud chamber	Shower from lead on ionization chamber
3050 m	none	21	1	—	—
3050 m	½ inch over cloud chamber	8	0	2*	—
3050 m	¼ inch on ion chamber and ½ inch on cloud chamber	1	2	1*	2
3050 m	¼ inch on ion chamber	16	0	—	3
4300 m	none	34	2*	—	—
4300 m	1 inch above cloud chamber	54	9	15*	—

* One event in each case had a slow heavy particle coming from the ionization chamber wall as well as the electron shower component.

We wish to underline some of the results obtained from the cloud-chamber observations.

(*a*) Most of the nuclear disintegrations were initiated by non-ionizing particles. Only a few percent of the pictures showed any lightly ionizing particles which could possibly be identified with the initiating particle, and some of these might actually have been produced in the disintegration. One thus concludes that nuclear absorption of negative mesons at the end of their range does not play an important role as a cause of disintegrations. The present data furnish further evidence that the non-ionizing particles which produce nuclear disintegrations are not photons, since, when lead was present above the chamber, photons would come out of the lead accompanied by electron showers (see also III.4, above).

(*b*) As already pointed out, about 42 percent of the nuclear disintegrations observed in the ionization chamber give rise to particles which appear in the corresponding cloud chamber pictures. Most of the disintegrations which give rise to ionization bursts take place within the wall of the ionization chamber and therefore the disintegration particles do not need to traverse the whole wall thickness to appear in the cloud-chamber volume. On the other hand, these particles, in general, do not come out at right angles to the surface of the ionization chamber. One thus estimates that the average range of the disintegration particles which appear in the cloud chamber is larger than the wall thickness ($\frac{1}{32}$-inch brass). A range of $\frac{1}{32}$-inch brass cor-

responds to an energy of 21 Mev for protons and to a higher energy for heavier particles. We thus conclude that almost one half of the disintegrations that give pulses larger than 6 Mev in the ionization chamber contain at least one particle of energy larger than 21 Mev. The average number of these particles with energy larger than 21 Mev is 1.8 per disintegration observed in the cloud chamber, 0.75 per disintegration observed in the ionization chamber. In the 17 pictures of nuclear disintegrations obtained with $\frac{1}{4}$ inch of lead above the ionization chamber there were 35 heavily ionizing particles observed in the cloud chamber, of which 4 came out of the ionization chamber through the lead shield. The energy of these particles, if protons, must have been greater than about 64 Mev.

(*c*) Fourteen of the 88 disintegrations observed at 4300 meters and one of the 49 observed at 3050 meters apparently showed time-associated heavy tracks passing through the gas in the cloud chamber. Time association was determined from the "width" of the tracks, which varies as $t^{\frac{1}{2}}$. From the known time rate of change of width and an estimate of $\frac{1}{2}$ mm for the accuracy of track width measurement, we obtain about $\pm 1/50$ sec. for the uncertainty in time simultaneity at a time corresponding to the chamber-triggering tracks. Thus, it seems unlikly that all of the above events can be explained as accidental coincidences of unrelated events although it is impossible to determine what fraction represents true time association from the present data. Figure 22a is an illustration of an event in which a disintegration in the ion chamber is apparently time-associated with a disintegration in the cloud-chamber wall. If one of the disintegrations was caused by a particle from the other disintegration, the connecting link, was a non-ionizing particle. It may be noted that the existence of time-associated nuclear disintegrations is strongly indicated by other observations.[19] It can be explained either by the simultaneous arrival on the instrument of several particles (neutrons?) capable of producing nuclear disintegrations, or by the production in nuclear disintegrations of secondary particles capable of producing more disintegrations. The mere existence of such effects is not surprising. Their rate of occurrence, however, when accurately known, may furnish very important clues as to the nature of the particles responsible for nuclear interactions and the order of multiplicity in their production. Experiments intended to investigate this question are in preparation.

[19] See, for example, J. Daudin, Ann. de Phys. **19**, 110 (1947); W. B. Fretter and W. E. Hazen, Phys. Rev. **70**, 230 (1946); H. Bridge and W. E. Hazen, Phys. Rev. **74**, 579 (1948).

TABLE VI. Distribution in size of the nuclear disintegrations.*

Number of particles per disintegration	Number of records at 3050 m	Number of records at 4300 m
1	27	52
2	11	21
3	6	5
4	3	3
5	2	4
6	0	0
7	0	3
Total number of particles observed	89	160
Average number of particles per disintegration observed	1.8	1.8

* This table includes some additional data obtained at 3050 meters with 4 brass plates in the cloud chamber which are not included in Tables IV and V.

5. Comparison with the Results of the Coincidence Experiment

As already noted, the cloud-chamber observations fully confirm the conclusion reached from the coincidence experiment, that, at mountain

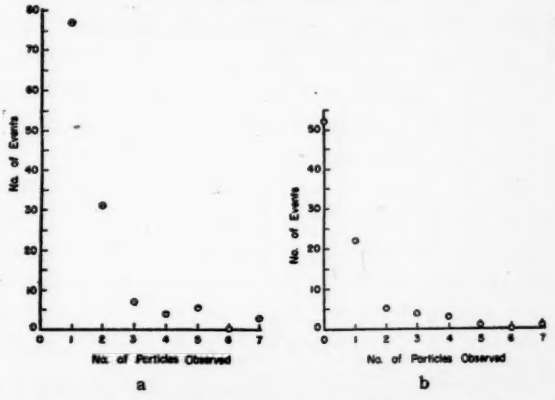

FIG. 24. (a) Number-frequency distribution for all cloud-chamber pictures in which heavily ionizing particles were observed. (b) Number-frequency distribution for cloud-chamber pictures correlated with pulse shape records. The point at zero abscissa indicates the number of events in which the ionization chamber gave a record characteristic of a nuclear disintegration and no heavily ionizing track was observed in the cloud chamber.

altitudes, all but a few percent of the ionization pulses in an unshielded chamber of our type are caused by nuclear disintegrations. These experiments also confirm the view that most of the coincidences between two neighboring chambers have the same origin, since they show that protons sufficiently energetic to traverse the chamber walls, yet sufficiently slow to ionize heavily, are produced very often in the nuclear disintegrations.

ACKNOWLEDGMENTS

The expedition at Climax was made possible by the cooperation of Mr. C. J. Abrams of the Climax Molybdenum Company and Drs. Walter Orr Roberts and John W. Evans of the Harvard College Observatory. The B-29 used for the measurements at high altitudes was provided by the U. S. Air Force. For the work at Doolittle Ranch and Mt. Evans the authors were fortunate in having the assistance of Mr. R. J. Davisson and Mr. H. Courant. Professor Mario Iona of the University of Denver greatly facilitated the work of the Doolittle Ranch-Mt. Evans expedition. Janet R. Williams assisted in analyzing much of the data.

The cloud chamber was constructed during the tenure of a Guggenheim Fellowship. The work described was supported in part by the Office of Naval Research.

PHYSICAL REVIEW VOLUME 74, NUMBER 9 NOVEMBER 1, 1948

Sea Level Latitude Effect of Cosmic Radiation*†

PETER A. MORRIS, W. F. G. SWANN, AND H. C. TAYLOR
Bartol Research Foundation of the Franklin Institute, Swarthmore, Pennsylvania

(Received June 17, 1948)

On a recent voyage from Rio de Janeiro to Boston the vertical intensity of the total and hard components of the cosmic radiation were measured with a Geiger counter telescope apparatus. For the hard component the percentage alteration from high latitudes to the magnetic equator was 5.32 ± 0.46 percent. For the soft component it was 4.46 ± 0.61 percent, and for the total radiation it was 5.04 ± 0.55 percent.

I. INTRODUCTION

PREVIOUS measurements of the sea level latitude distribution of cosmic radiation have been made chiefly with ionization chambers, although some measurements have been made with coincidence counter systems. The use of counter systems allows the determination of the effect for the soft component of the radiation either by noting the relationship between the soft component and showers produced in small thickness of lead, or by taking the differences between the intensities of the total and hard components. The extensive measurements by Compton and Turner[1] and by Gill,[2] for example, were obtained by using the ionization chamber method. Coincidence counter measurements have been made by Auger and Leprince-Ringuet,[3] Clay, Bruins and Wiersma,[4] Johnson and Read,[5] Wilson and Turner,[6] and Neher and Pickering.[7] According to Johnson,[8] the agreement between the two methods has been good, taking into account the fact that one might expect a somewhat greater latitude effect for the vertical intensities (measured by coincident counter systems) than for the integrated directional meas-

* Assisted by the Office of Naval Research with the cooperation of the National Geographic Society.

† A skeleton of the results of this investigation has been published in Phys. Rev. **72**, 1263 (1947).

[1] A. H. Compton and R. N. Turner, Phys. Rev. **51**, 1005 (1937); **52**, 799 (1937).

[2] P. S. Gill, Phys. Rev. **55**, 1151 (1939).

[3] P. Auger and L. Leprince-Ringuet, Comptes Rendus **197**, 1242 (1933); P. Auger, Nature **133**, 138 (1934).

[4] J. Clay, E. M. Bruins, and J. T. Wiersma, Physica **3**, 746 (1936).

[5] T. H. Johnson and D. N. Read, Phys. Rev. **51**, 557 (1937).

[6] V. C. Wilson and R. N. Turner, Phys. Rev. **59**, 931 (1941).

[7] H. V. Neher and W. H. Pickering, Phys. Rev. **53**, 111 (1938).

[8] T. H. Johnson, Rev. Mod. Phys. **10**, 193 (1938).

urements made with ionization chambers, because of the observed increase in latitude effect with altitude.

While agreement of previous measurements of the latitude effect for the total radiation seems good, some ambiguity, at least, is present in the experimental values for the latitude effect of the soft component. This ambiguity, as pointed out by Arley,[9] is exemplified by the conclusions of Heisenberg and Heitler in interpreting the coincident counter data of Auger and Leprince-Ringuet. Heisenberg[10] finds a ten percent latitude effect for the soft component, whereas Heitler[11] finds none.

In the light of the foregoing observations, we should like to present the measurements made by us with a system of coincident Geiger-Mueller counters on a ship voyage between Rio de Janeiro (geomagnetic latitude 12.5 degrees S) and Boston (geomagnetic latitude 53 degrees N) in the summer of 1947. The observations were made as part of the work of the National Geographic Society's expedition to South America to view the solar eclipse of May, 1947.

II. THE APPARATUS

The apparatus consisted of a system of Geiger-Mueller counter telescopes arranged in such a way that three types of events were registered—the passage of an ionizing particle through (1) a triple coincident system in which there was no absorber, (2) 8 cm of lead, and (3) 16 cm of lead. The geometry is shown schematically in Fig. 1. It will be observed that only five trays of counters were used to obtain three triple systems. This entire system of five trays was duplicated in the actual apparatus. In addition to the absorbing lead, a protective shield of one inch of lead was placed around tray number three, which tray was common to the three coincident systems. The purpose of this shield was to reduce the number of accidental counts which might arise from extensive lateral showers.

The Geiger-Mueller counters used were constructed of 0.007-inch-wall Nonex glass and

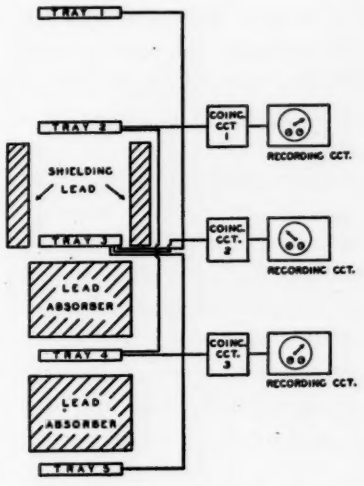

FIG. 1.

0.005-inch-wall seamless copper tubing. The copper cylinder was one cm in diameter and 10.2 cm in length. The axial wire was 0.003-inch tungsten. The counters were a non-self-quenching type filled with a mixture of argon and oxygen to a pressure of 12 cm of Hg. This mixture gave a very good plateau (the order of 200 volts or more and a slope of less than four percent per 100 volts) and a long life.

The high resistance (500 megohms) necessary for successful operation of this type of counter necessitated precautionary measures with regard to possible spurious high resistance leakage to ground in the anode circuit. For this reason the anode lead was led through a mounting tube which was imbedded in a cylinder of sulfur. This served the purpose of giving a rigid support with very good insulating properties which introduced little capacity to the circuit.

There were nine counters in each tray. They were placed side by side in the same plane so that there was considerable area between copper cylinders through which a particle could pass without being detected. For this purely geometrical reason each tray was therefore only about 77 percent efficient in detecting particles which passed through the telescope of which it was a member. From considerations of the counting rate and dead time alone of the counters, each tray would be 99.7 percent efficient. The efficiency of the triple systems was therefore about 45 percent. Since, in this investigation, we were interested only in ratios of counting rates

[9] N. Arley, Kgl. Danske Vid. Sels. Math.-Fys. Medd. **23**, No. 7.
[10] W. Heisenberg, *Vorträge über Kosmische Strahlung* (Springer-Verlag, Berlin, 1943; Dover Publications, New York, 1946).
[11] W. Heitler, Nature **140**, 235 (1937).

which were nearly the same, the low efficiency served only to lessen the total number of counts received by the apparatus and did not alter the relative counting rates at the extremeties of the latitude curves.

The effective resolving time of the coincident circuits was about 5×10^{-4} second. With this value, the accidental rate of the triple systems was about 5×10^{-5} cts/sec., or less than 0.1 percent of the true coincident rate.

The counters were operated so as to deliver a negative pulse of thirty volts or more to the grid of the associated 6AK5 amplifier tube. The arrival of a large negative pulse on the grid of this tube, which was normally conducting, reduced its plate current to essentially zero. The conventional Rossi circuit was used to establish the coincidences between trays. With the parameters indicated in the circuit diagram, Fig. 2, a triple coincidence caused a positive pulse of 20 volts or more to appear on the grid of the 2D21 thyratron, causing it to strike and therefore operate the counting register (Cyclotron Specialties Company). A double coincidence caused a pulse of only two volts or so and therefore could not overcome the nine-volt negative bias on the thyratron grid. Except for the filament and bias voltages, the other potentials in this circuit may be varied considerably with inappreciable effect on the over-all performance of the telescope. During operation all potentials were maintained within safe limits.

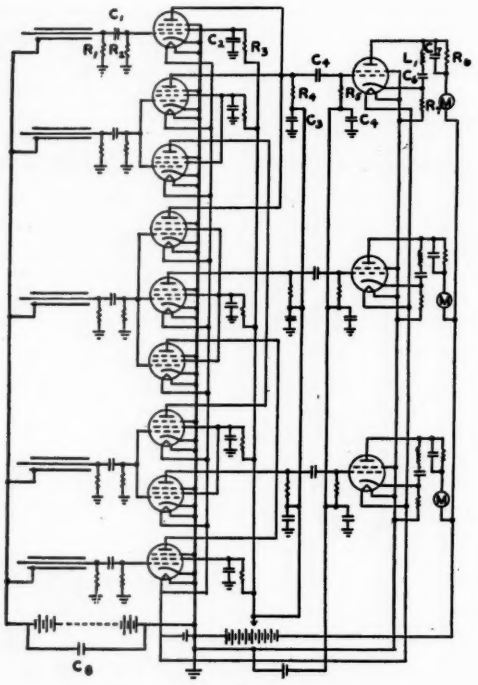

FIG. 2. Circuit diagram.

This diagram represents one-half of the entire circuit. The other half was identical. Values of the parameters were as follows: $R_1=5.10^3$, $R_2=10^6$, $R_3=10^2$, $R_4=R_5=5.10^4$, $R_6=5.10^3$, $R_7=2.10^3$; $C_1=5.10^{-12}$, $C_2=C_3=C_5=10^{-8}$, $C_4=10^{-9}$, $C_6=C_7=5.10^{-7}$, $C_8=2.10^{-6}$; $L_1=30$ mh; 2D21 plate voltage $=+180$ v, 2D21 grid bias $=-9$ v, 6AK5 plate and screen voltages $=45$ v, counter voltage $=-1000$ v.

III. RESULTS

In the discussion of the latitude effect, we shall define the latitude effect, L, in terms of the intensity, I, of the rays as measured at the magnetic equator and in the northern latitudes; i.e., $L=(I_{50}-I_0)/I_{50}$. Superscripts h and s shall refer to the hard and soft components, respectively, and no superscript indicates measurements of the total radiation. Subscripts 50 and 0 shall refer to measurements in the northern latitudes and at the magnetic equator, respectively. In addition, we shall consider that radiation which penetrates 8 or 16 cm of lead as the hard component and that radiation which is absorbed in 8 or 16 cm of lead as the soft component. It is clear that the values for the intensity of the soft component are arrived at from the difference in the values for the total and hard radiations. This method for measuring the soft component has two major drawbacks—the dissimilarity in the geometry or other characteristics of the separate coincident systems, and the increase in the value of the probable error as determined from the difference of the two measured quantities.

The observations are shown plotted in Fig. 3. In this plot the observations for the two coincident systems with the same distribution of lead are combined. In view of the large values of the statistical errors in the individual plotted points, we have combined points between 15 degrees South and 15 degrees North to obtain I_0 and points above 28 degrees North to obtain I_{50}. In this way we obtain the following values:††

†† We have also combined the data for 8 and 16 cm of lead since the two thicknesses yield practically identical results. The probable errors for the differences have been evaluated according to standard principles. See, for example, H. Margenau and G. M. Murphy, *The Mathe-*

No lead	With lead	Difference
$I_0=3.954\pm0.014$	$I_0^h=2.670\pm0.008$	$I_0^s=1.284\pm0.016$
$I_{60}=4.164\pm0.018$	$I_{60}^h=2.820\pm0.010$	$I_{60}^s=1.344\pm0.021$

Expressing L in percentages, we obtain $L=5.04\pm0.55$, $L^h=5.32\pm0.46$, $L^s=4.46\pm0.61$.

In the computation of the above values, the only errors considered have been those associated with the statistical nature of the observations. In addition to these, there were undoubtedly fluctuations in the counting rates due to magnetic disturbances and temperature and barometric variations. We were unable to obtain sufficient data to apply corrections for these effects. However, in view of the large statistical fluctuations, it is questionable if such corrections would have altered the results significantly.

It is interesting to note that the latitude effects for the total radiation and the hard component are smaller than have been reported previously. Conceivably, this could be accounted for because of different atmospheric conditions existing between Rio de Janeiro and Boston. Of greater interest, however, is the fact that our data strongly indicate the existence of a sea level latitude effect for the soft component whose magnitude is of the same order of magnitude as that for the hard and total radiation, although somewhat smaller in magnitude.

If the soft component is defined as that radiation which is absorbed in 8 cm of lead, the radiation is largely restricted, except for Auger showers, to that which is formed below one kilometer from the earth's surface, by mesotron decay and knock-on processes from the mesotron component existing near sea level, rather than pair formation having to do with primary electrons or with electrons produced near the top of the atmosphere. It is not surprising to us, therefore, to find the latitude effects of the hard and soft components of comparable magnitude.

matics of Physics and Chemistry (D. Van Nostrand Company, Inc., New York, 1943), p. 498.

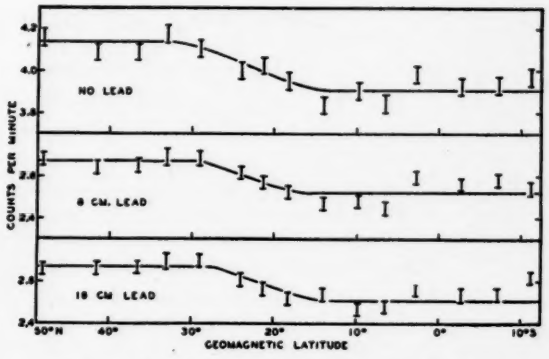

FIG. 3. Vertical coincidence rates at sea level from Rio to Boston.

IV. ACKNOWLEDGMENTS

This investigation was supported by funds from Navy contract N6ori-144 and from the National Geographic Society. The Geiger-Mueller counters were constructed by Mr. Austin G. Nester, glassblower at the Bartol Research Foundation. We wish also to acknowledge the courtesies extended to us by the Moore-MacCormack Company for permitting us to mount the apparatus aboard the S. S. Malcolm M. Stewart.

The Energy Distribution in Cosmic-Ray Showers*

JAMES A. RICHARDS, JR.** AND L. W. NORDHEIM
Duke University, Durham, North Carolina

(Received June 21, 1948)

The track length distribution $f(E)dE$ in a shower is defined as the total distance traveled by all electrons while in the energy interval dE. It is representative for the average energy distribution in a shower. The present paper obtains by numerical methods the complete functions for both electrons as well as for photons in showers of high primary energy. Calculations have been made for air and for lead, down to energies of about 4 Mev. Close approximations to the actual cross sections have been used for all energies and all physically significant processes have been included—radiation, pair production, energy loss through collision, Compton effect, and knock-on electrons. As a special result of importance we mention the high number of low-energy photons that accompany a shower, a quantity that has here been evaluated for the first time.

1. INTRODUCTION

THE well-known cascade theory of cosmic-ray showers[1] has been successfully carried through to the evaluation of total numbers of electrons and photons and their energy distribution for not too low energies. For energies around and below the so-called ionization limit (cf. below) an analytical evaluation of the energy distribution is made difficult by the complicated formulae for the probabilities of elementary processes and the incoming of additional effects, such as the Compton effect and knock-on electrons, which are usually neglected.

The first attempt to determine the number of low energy electrons in a shower is due to Arley.[2] He neglects entirely ionization losses above the critical energy and radiative effects below it, and he takes into account only those electrons in the low energy range that originate from high energy electrons which are thrown into the low range by emission of quanta. Thus, the electrons produced with small energy by quanta are omitted. The result is a serious underestimate of the number of slow electrons. The ratio of slow-to-fast electrons near the shower maximum is, according to Arley, about 1, while the actual ratio as computed in this paper is of order 3 to 4.

A more systematic treatment of the electron distribution at low energies has been given by Tamm and Belenky[3] who use simplified cross sections even in the low energy range, and a somewhat questionable mathematical approximation and by Rossi and Klapman[4] who, by a numerical method, obtain the total track length in air above energies of 10 Mev as function of the energy of a generating electron or photon.

In the present paper a numerical method is developed to obtain the track-length distribution down to low energies ($\sim$4 Mev) in showers starting with high initial energies.

In the low-energy end the nature of the material is of importance and numerical results have been obtained for air and lead. No terms of significance have been neglected, and our results should be accurate to about ± 10 percent. Our results include also the distribution of photons of low energy which has not been evaluated before.

2. THE EQUATIONS FOR THE TRACK LENGTH

The track-length distribution of a shower $f(E)dE$ is defined as the total distance traveled by all shower electrons while their energy lies between E and $E+dE$. Similarly we can define a photon track-length distribution $g(K)dK$ where we denote the photon energy by K for easy distinction. This "normal" distribution is much easier to calculate than the energy distribution as function of distance, and it has almost the same physical significance as the latter, since it

* This paper is based on a Ph.D. thesis submitted in 1942 to Duke University by Mr. Richards. Occupation with war work prevented an earlier publication of this work.

** Now at Olivet College, Olivet, Michigan.

[1] For all older work on shower theory, reference is made to the excellent summary by B. Rossi and Kenneth Greisen, Rev. Mod. Phys. **13**, 240 (1941).

[2] N. Arley, Proc. Roy. Soc. **A168**, 519 (1938).

[3] I. Tamm and S. Belenky, J. Phys. U.S.S.R. **1**, 177 (1939); Phys. Rev. **70**, 660 (1946).

[4] B. Rossi and S. J. Klapman, Phys. Rev. **61**, 414 (1942).

will be the same as the distribution at the shower maximum, and it will predominate over most of the longitudinal extension of the shower with the exception of its very early and late stages.

The following general results are known about the track-length distribution. Since all the energy in a shower is dissipated finally by ionization through electrons, the integral track-length over all energies is

$$\int_0^{E_p} f(E)dE = E_p/\beta_i, \tag{1}$$

where E_p is the primary energy and β_i the energy loss through ionization which can be considered as constant over the interesting energy range of 2 Mev to 300 Mev.

The track-length distribution has been evaluated by Nordheim and Hebb[5] in the high-energy limit where ionization losses can be neglected relative to radiation losses, and by Rossi and Greisen[1] in the next approximation, where ionization losses can be considered as small. Their result can be expressed as follows

$$f(E) = 0.437\frac{E_p}{\beta_i}\left[\frac{E}{\beta_i} + 0.818 - \frac{0.392}{(E/\beta_i)} + \cdots\right]^{-2}, \tag{2}$$

$$g(K) = 0.437 \times \frac{9}{7}\frac{E_p}{\beta_i}\left[\frac{K^2}{\beta_i^2}\left(1 + \frac{0.769}{(K/\beta_i)} + \cdots\right)\right]^{-1}. \tag{3}$$

These expressions give a good approximation down to about E and $K \sim 3\beta_i$. For lower energies, as already mentioned, the usual mathematical treatments break down, and also the cross sections for occurring processes lose their universal character.

It is to be noted that for high energies $\beta_i \ll E \ll E_p$, the distributions are proportional to $1/E^2$. We will normalize the distribution so that

$$\left.\begin{aligned} f(E) &\to 1/E^2 \\ g(K) &\to \frac{9}{7}\frac{1}{E^2} \end{aligned}\right\} \quad \text{for} \quad E \gg \beta_i.$$

The absolute number of particles produced by a primary of energy E_p is then $0.437(E_p/\beta_i)f(E)$ and correspondingly for $g(K)$.

[5] L. W. Nordheim and M. H. Hebb, Phys. Rev. **56**, 494 (1939).

In the following, we will introduce the natural units of shower theory, the critical energy, where radiation and collision losses are equal, and the unit length on which the energy loss through ionization is just this critical energy. In these units $\beta_i = 1$.

We consider the following processes: for photons, pair production and Compton effect, for electrons, radiation, ionization losses and knock-on electrons. The cross sections, as used in this paper, are summarized in the appendix. All these processes are of the type that a primary of energy E' or K' produces a secondary of energy E or K respectively.

We denote the cross sections for such a process by a function of two arguments. $\sigma(E', K)$, for instance, is the probability that an electron E' produces a quantum K and so on. Of course, $\sigma(E', K)$ is the same as $\sigma(E', E'-K)$, since the electron remains at an energy $E'-K$ after emission of the photon K. If necessary we add an index to the cross sections, for instance:

σ_r radiation by an electron,
σ_p pair production,
σ_c Compton effect,
σ_k knock-on electron.

The equations that describe the balance of all effects are then as follows

$$\int_E^\infty g(K')\sigma(K', E)dK' + \int_E^\infty f(E')\sigma(E', E)dE' - \int_0^E f(E)\sigma(E, E')dE' + \frac{d}{dE}(\beta_i f(E)) = 0, \tag{4}$$

$$\int_K^\infty f(E')\sigma(E', K)dE' + \int_K^\infty g(K')\sigma(K', K)dK' - \int_0^K g(K)\sigma(K, E')dE' - \int_0^K g(K)\sigma(K, K')dK' = 0. \tag{5}$$

The first terms describe the production of a "particle" of one kind (electron or photon) by a particle of the other kind. The next terms give the number of particles added or removed from an energy interval by processes involving energy changes. The last term in (4) takes account of the continuous energy loss by ionization for electrons.

The principal difficulty in the treatment of these equations comes from the second and third terms of Eq. (4).

$$D(E)=\int_E^\infty f(E')\sigma_r(E', E)dE' - \int_0^E f(E)\sigma_r(E, E')dE', \quad (6)$$

since it is well known that the radiation probabilities diverge for small K, i.e., $E'-E$, as $1/K$ (infra-red catastrophe). The expression (6) has, therefore to be understood as the finite limit

$$D(E)=\lim_{\epsilon=0}\left[\int_{E+\epsilon}^\infty f(E')\sigma_r(E', E)dE' - \int_0^{E-\epsilon} f(E)\sigma_r(E, E')dE'\right]. \quad (6a)$$

If the energy loss due to radiation could be considered as of continuous nature, D should be representable by an expression similar to the last term of Eq. (4), i.e.,

$$D(E)=\frac{d}{dE}[\beta_r(E)f(E)], \quad (7)$$

where $\beta_r(E)$ is the average energy loss to radiation as function of energy.

We shall now prove that Eq. (7) is in fact a sufficient approximation for our purpose.

The cross section for radiation at high energies is of the form

$$\sigma(E, E')dE'=\frac{dE'}{E-E'}S\left(\frac{E'}{E}\right), \quad (8)$$

where S is a homogeneous function of the fractional energy reduction E/E'. The total average energy loss is then

$$\beta_r=\int_0^E (E-E')\sigma(E, E')dE'=\int_0^E S\left(\frac{E'}{E}\right)dE' =E\int_0^x S(x)dx=E\int_1^\infty S\left(\frac{1}{x}\right)\frac{dx}{x^2}. \quad (9)$$

Introducing the new variable $E''=(E^2/E')$ into the second integral in Eq. (6) and renaming it afterwards again E', we obtain the transformation

$$D(E)=\int_E^\infty \left[f(E')-\frac{E}{E'}f(E)\right]S\left(\frac{E}{E'}\right)\frac{dE'}{E'-E}.$$

We know now from Eq. (2) that $f(E)$ behaves at high energies similar to $1/E^2$. Also, the discontinuity of the energy loss is most important for high energies. We can put, therefore,

$$f(E)=\frac{\varphi(E)}{E^2}; \quad \varphi(E')=\varphi(E)+(E'-E)\frac{d\varphi}{dE},$$

where φ is a slowly varying function of E for the representation of which the first term in its Taylor development is sufficient. We obtain then

$$D(E)=\left(\frac{d\varphi}{dE}-\frac{\varphi}{E}\right)\int_E^\infty S\left(\frac{E}{E'}\right)\frac{dE'}{E'^2} =\left(\frac{d\varphi}{dE}-\frac{\varphi}{E}\right)\frac{1}{E}\int_1^\infty S\left(\frac{1}{x}\right)\frac{dx}{x^2} =\frac{d}{dE}\left(\frac{\varphi}{E}\int_0^1 S(x)dx\right)=\frac{d}{dE}(\beta_r f(E)).$$

We have proved thus the substitution Eq. (7) for the limit of high energies, where the ionization losses that produce the deviation of $\varphi(E)$ from a constant are not too important. In the opposite limit of low energies radiation losses become, in any case, of lesser importance, and we are thus justified to combine D and the last term in Eq. (4) to the simple expression

$$\frac{d}{dE}[(\beta_r+\beta_i)f(E)]=\frac{d}{dE}[\beta(E)f(E)]. \quad (10)$$

This substitution has been checked for the distribution as found later in this paper, which permits a numerical evaluation of Eq. (6). The

error made by Eq. (10) turned out to be of order 8 percent for $E=1$.

It is of advantage for the further treatment to introduce the total number of new electrons produced by photons and by knock-on collisions as a separate function through the definition***

$$h(E)=\int_E^\infty g(K)\sigma(K,E)dK + \int_{2E}^\infty f(E')\sigma_k(E',E)dE'. \quad (11)$$

Equation (4) then takes the form

$$h(E)+\frac{d}{dE}[(\beta_r+\beta_i)f(E)]=0.$$

Integration of this relation between two energy values gives

$$f(E)=\frac{\beta(E_0)f(E_0)}{\beta(E)}+\frac{1}{\beta(E)}\int_E^{E_0} h(E')dE'. \quad (12)$$

We can bring Eq. (5) for the photons into a similar form

$$g(K)=\frac{1}{\sigma(K)}\left\{\int_K^\infty f(E)\sigma(E,K)dE + \int_K^\infty g(K')\sigma(K',E)dK'\right\}, \quad (13)$$

where

$$\sigma(K)=\int_0^\infty \sigma(K,E')dK', \quad (14)$$

is the total absorption coefficient for photons of energy K.

The functions $f(E)$, $g(K)$, and thus also $h(E)$ are known for sufficiently high energies, let us say above E_0, from Eqs. (2) and (3). The integral equations (11), (12), (13) permit us now to compute these functions for lower energies with the help of an iteration process.

For energies E that are not too much lower than E_0 a zero approximation for $f(E)$ will be given by

$$f_0(E)=\frac{\beta(E_0)f(E_0)}{\beta(E)}. \quad (15)$$

We find then a g_0 through

$$g_0(K)=\frac{1}{\sigma(K)}\left\{\int_{E_0}^\infty f(E')\sigma(E',K)dE' + \int_E^{E_0} f_0(E')\sigma(E',K)dE'\right\}, \quad (16)$$

and an h_0 through

$$h_0(E)=\int_{E_0}^\infty g(K)\sigma(K,E)dK + \int_E^{E_0} g_0(K)\sigma(K,E)dK. \quad (17)$$

These functions are then introduced into the right side of the full Eqs. (11) to (13) and new functions $f_0(E)+f_1(E)$, and so on, are calculated. If necessary the cycle is repeated. It has been found that this process converges rapidly. The iteration was stopped when it could be estimated that the next step would give a contribution of less than 5 percent. It was in no case necessary to go beyond an f_2.

The method is practicable since most integrations can be arranged with a variable lower limit, so that the process of integration from an E_0 to an E yields at the same time all intermediate values of the function in question.

The convergence of the method becomes less good for too low values of the final energy, since f_0 is in that case not a good approximation. The obvious remedy is, of course, to carry out the integration in steps, i.e., firstly to an energy E_1, and after evaluation of all functions to this value, to resume the process with E_1 in place of E_0.

Actual calculations have been carried out for air and lead. They will be described in the following section.

3. CALCULATIONS

a. Air

The analytical expressions for f and g (Eqs. (2), (3)) can be used for energies as low as 3 in

*** The second term in the expression for $h(E)$ represents new electrons produced in knock-on collisions. The minimum primary energy E' to produce a secondary of energy E is $2E$. The change of energy of the primary can be considered as already contained in the term for energy loss through ionization.

TABLE I. Track-length distribution in air.*

Primary Energy		$E_p \gg 3$				$E_p = 1$			
E or K	$f_{TB}(E)$	$f(E)$	$F(E)$	$g(K)$	$G(K)$	$f(E)$	$F(E)$	$g(K)$	$G(K)$
0			2.3		∞				
0.05	5.9	5.5	1.9	45	6.6	1.7	0.63	16	1.6
0.10	3.8	3.7	1.6	23	5.0	1.3	0.56	7.8	1.0
0.15	2.8	2.8	1.5	15	4.1	1.0	0.50	4.9	0.73
0.20	2.2	2.25	1.4	11	3.5	0.89	0.45	3.4	0.53
0.30	1.5	1.61	1.2	6.0	2.7	0.74	0.37	1.7	0.31
0.40	1.1	1.27	1.04	3.9	2.2	0.64	0.31	0.91	0.19
0.50	0.89	0.97	0.92	2.8	1.8	0.57	0.25	0.58	0.12
0.75	0.53	0.62	0.73	1.4	1.3	0.48	0.12	0.20	0.02
1.0	0.36	0.42	0.61	0.79	1.05	0.42		0	
1.5	0.21	0.23	0.46	0.41	0.77				
2.0	0.14	0.145	0.37	0.25	0.60				
2.5	0.10	0.100	0.31	0.16	0.51				
3.0	0.073	0.073	0.27	0.12	0.44				

* E or K = energy in units 86 Mev. In order to obtain absolute values multiply the $E_p \gg 3$ columns by $0.437 E_p$, the $E_p = 1$ column by 1.2.
$f(E)$ = track-length distribution for electrons, $f_{TB}(E)$ = track-length distribution as calculated by Tamm and Belenky.

$F(E) = \int_E^\infty f(E')dE'$.

$g(K)$ = track-length distribution for photons.

$G(K) = \int_K^\infty g(K')dK'$.

For E and $K > 3$, use Eqs. (2) and (3).

units of the shower theory. The asymptotic cross sections (A4), (A6) for complete screening are valid down to about $E = 1$. A first-iteration cycle was carried through between these energies. For the evaluation of the terms containing radiation and pair production it is only necessary to compute terms of the form

$$\int_E^\infty f(E')dE'/E'^n,$$

with $n = 0$ to 3 as functions of the lower limit, where the functions f are known from previous steps, and where high energy tails can be evaluated analytically. After carrying through the iteration for two cycles, the knock-on and Compton contributions were added. The former ones are completely negligible, while the number of Compton electrons remains small. Therefore, it was sufficient to use the integrated probability (A9) and to assume that the produced electrons have the average energy (A10).

After the functions $f(E)$ and $g(K)$ were determined down to $E = 1$, the iteration process was resumed with this new upper limit, under use of the cross sections (A5) and (A7). The Compton effect is of considerable importance in this interval and has to be recycled, and also "post-Compton" photons have to be included at lower energies. The expression for the number h of electrons produced by a photon distribution $g(K)$ through the Compton effect (compare (A8))

$$h_c(E) = B \int_{E+(mc^2/2)}^\infty \frac{g(K)}{K(K-E)} \left\{ 1 + \frac{(K-E)^2}{K^2} \right\} dK,$$

contains the lower limit also in the integrand. Thus, strictly speaking, a complete new integration would be necessary for every value of E. It was found, however, that a computation based on the assumption that all electrons produced by quanta of energy K have the same average energy, Eq. (A10) gave values of h that were in a fairly constant ratio to the true values. This was verified by carrying out the full process for the values $E = 0.3$ and 0.05, where the ratios of the complete integrals to the approximate ones were 1.2 and 1.25. For other values of E, therefore, the approximate values were calculated and corrected by multiplication with 1.23.

The results of the calculations are shown in Tables I and II which give $f(E)$, $h(E)$, and $g(K)$, and the total number of electrons above energy E, i.e., the integral

$$F(E) = \int_E^\infty f(E')dE';$$

also the total number of photons

$$G(K) = \int_K^\infty g(K')dK'.$$

The function $f(E)$ can be approximated for low energies by

$$f(E) = 2.64 \log(1/E) - 2.4, \qquad (18)$$

showing, as is to be expected, a logarithmic in-

TABLE II. Electrons produced with low energy by pair production and Compton effect (air).*

E	h_{pair}	$h_{Compton}$	h_{total}
0.05	13.9	26.5	40.4
0.10	9.4	8.3	17.7
0.15	6.7	4.1	10.8
0.20	4.9	2.3	7.2
0.30	3.1	1.00	4.1
0.40	2.2	0.58	2.8
0.50	1.65	0.35	2.00
0.75	1.00	0.11	1.11
1.00	0.70	0.06	0.76

* $h(E)dE$ = number of electrons produced in energy interval dE. Same units and normalization as in Table I.

crease for very low energy values.† The relation (18) permits an approximate evaluation of the integrated number of electrons to $E=0$. We find the contribution

$$\int_0^{0.05} f(E)dE=0.405.$$

The total track length of all electrons in air as evaluated by us is thus 2.26. The normalized value for a primary E_p is thus $0.437\times 2.26E_p=0.989E_p$. The factor is so near to the required value unity (comp. Eq. (1)) that we can be sure that no physically important effect has been omitted, and it furnishes thus a good check on our calculations.

Since for air a new cycle was started at $E=1$, it was comparatively easy to evaluate the track-length distribution produced by single primary electrons with this energy. The results are also given in Table I. In order to normalize these functions, we observe that the track length for a single electron near its initial energy should be $1/(dE/dt)=1/\beta$ or 0.5 in our case. The figures of the table should, therefore, be multiplied by $0.5/0.42=1.2$ in order to correspond to one primary electron.

b. Lead

For lead the critical energy is only 6.7 Mev. The asymptotic formulae (4), (5), are applicable to energies for which the asymptotic forms of the cross sections are valid, i.e., to about $E=10$ or ~ 67 Mev. The iteration process was therefore started from this energy on. It was possible to carry it down to $E=0.5$ or 3.4 Mev, which is nearly the same in absolute value as our lower limit for air ($E=0.05$ or 4.3 Mev). No new complications arise. It may be stated only that knock-on electrons and post-Compton photons were entirely negligible since the energy as measured in radiation units remains high for the whole range. The results are collected in Table III.

Table III. Track-length distribution of electrons and photons in lead.*

	$E_p\gg 10$			
E or K	$f(E)$	$F(E)$	$g(K)$	$G(K)$
0.5	0.90	1.02	6.4	2.8
1.0	0.43	0.71	2.0	1.8
1.5	0.26	0.54	0.89	1.16
2.0	0.17	0.43	0.49	0.83
3.0	0.089	0.30	0.21	0.51
4.0	0.054	0.23	0.11	0.37
5.0	0.036	0.18	0.072	0.28
6.0	0.025	0.152	0.048	0.22
7.0	0.018	0.130	0.032	0.18
8.0	0.014	0.114	0.022	0.15
9.0	0.011	0.102	0.016	0.13
10.0	0.0086	0.092	0.012	0.12

* Unit of E or $K=6.7$ Mev. Normalization and meaning of symbols same as in Table I.

4. DISCUSSION

In comparing air and lead we see that the electron distributions are essentially the same if expressed in their respective radiation units. The photon distributions are, however, quite different, the number of photons at half the critical energy in lead being 2.3 times the corresponding number for air. The reason for this difference lies in the smaller absorption coefficient for photons in lead for the same reduced units which increases their free path and therefore their track length. This effect does not react strongly on the electron distribution since finally all photons are reconverted into electrons.

One of the results of our calculation is the ratio of the number of quanta to the number of electrons in a shower as a function of energy and also, of course, the evaluation of the total number of photons. While at high energies the ratio of photons to electrons is 9/7, the photons are preponderant at low energies. If we consider all energies down to our lower limit of ~ 4 Mev, we find that for both air and lead there are about 3 times as many photons as electrons.

The calculations for both air and lead have about the same lower energy limit of ~ 4 Mev in absolute units. Since the total track length is given by Eq. (1) for all materials, it is possible to determine the fraction of the shower of energy less than 4 Mev. It is about $\frac{1}{6}$ for air and $\frac{1}{2}$ for lead. The fraction of the total shower above the critical energy is 27 percent for both air and lead. A further comparison can be made with the calculations of Rossi and Klapman.[4] They find for the fraction of the track length above 10 Mev in air a value $3.06/4.3=0.71$. This is in complete agreement with the value from our calculations (1.64/2.26).

† The photon distribution behaves like $(1/K)$, due to this factor in the radiation cross section, and since the probability to produce a photon with $K<E$ is approximately independent of E.

It is interesting to compare our results with the analytical formula of Tamm and Belenky.[3] This formula, normalized as ours to $1/E^2$ at high energies, can be written as follows:

$$f(E)_{\text{T.B.}}=2.3^2\left\{(1+\epsilon)e^{\epsilon}\left[-Ei(-\epsilon)-1+\frac{1+\epsilon}{\epsilon_p}e^{-(\epsilon_p-\epsilon)}\right]-(1+\epsilon)e^{\epsilon}[-Ei(-\epsilon_p)]\right\}. \quad (19)$$

The symbols have the following meaning: $\epsilon=2.3E$; $\epsilon_p=2.3E_p$, where E_p is the primary energy of the shower-producing electron in radiation units. Ei is the exponential integral according to the definition in Jahnke-Emde.[6] The values of the above function for $E_p=\infty$ (i.e., infinitely high primary energy) are also given in Table I. It is surprising how close the agreement between our values and the Tamm-Belenky function is, in spite of the neglections made in the derivation of the latter. The explanation of this behavior lies probably in the fact that the Tamm-Belenky function is so constructed that it has the correct asymptotic behavior as $1/E^2$ at high energies and that it satisfies the energy principle (Eq. (1)). These requirements already determine to a considerable extent the character of the function. However, an attempt to calculate a photon distribution by the Tamm-Belenky method would probably give rather inaccurate results. Equation (19) includes the dependence of the track-length distribution on the primary energy of the shower-producing electron. According to the preceding remarks it will be safe to use this formula if not too high an accuracy is required.

APPENDIX

Units and Cross Sections

For a complete discussion of cross sections, compare W. Heitler[7] and B. Rossi and K. Greisen.[1]

For the unit of length we take the radiation length t_0

$$\frac{1}{t_0}=\frac{4}{137}\left(\frac{e^2}{mc^2}\right)^2 NZ\bar{Z}\,\lg 183Z^{-\frac{1}{3}}, \quad (A1)$$

where N is the number of atoms per cc and $\bar{Z}=Z+1$. $\bar{Z}$ is introduced in order to include approximately the effects of the atomic electrons. The value of t_0 is 3.03×10^4 cm for air and 0.519 cm for lead.

In order to find the unit of energy β_i we equate the total energy loss by radiation

$$-\left(\frac{dE}{dt}\right)_r=E\frac{NZ\bar{Z}}{mc^2}\left(\frac{e^2}{mc^2}\right)^2\times\left(4\lg 183Z^{-\frac{1}{3}}+\frac{2}{9}\right), \quad (A2)$$

to the energy loss by collision

$$-\left(\frac{dE}{dt}\right)_{\text{coll}}=\frac{2N\pi e^4Z}{mc^2}\left[\lg\frac{E_1E_0^2}{2mc^2I^2Z}\right], \quad (A3)$$

where $I=13.5$ ev according to Bloch, and E_1, the maximum energy of secondary electrons, is taken as 10 mc^2. Secondary electrons of higher energy are introduced separately as knock-on electrons. The values for E_0 are 86 Mev for air and 6.7 Mev for lead. With these units, we obtain the following probabilities:

Pair Production

At high energies (complete screening)

$$\sigma(K,E)dE=\frac{dE}{K}2\left[1-\frac{4}{3}\frac{K}{E}+\frac{4}{3}\frac{K^2}{E^2}\right]. \quad (A4)$$

The factor 2 is introduced to include both electron and positron. At low energies, the approximation

$$\sigma(K,E)dE=\frac{dE}{K}\times 2\sigma_{\text{pair}} \quad (\text{for } E<E_0), \quad (A5)$$

is made, where σ_{pair} is the total cross section for pair production as evaluated by Heitler.[7] E_0 has been taken as 1.15 for air and 10 for lead.

Radiation by Electrons

At high energies the cross section is

$$\sigma(E,K)dK=\frac{dK}{K}\left[\frac{4}{3}-\frac{4}{3}\frac{K}{E}+\frac{K^2}{E^2}\right]. \quad (A6)$$

[6] E. Jahnke and F. Emde, *Tables of Functions* (Dover Publications, New York, 1943).
[7] W. Heitler, *Theory of Radiation* (Oxford University Press, London, 1945), 2nd ed.

At lower energies the simple interpolation formula

$$\sigma(E, K)dK = \frac{dK}{K}\left[\frac{4}{3} - \frac{4}{3}\frac{K}{E} + \frac{K^2}{EE_0}\right], \quad \text{(A7)}$$

gives an extremely satisfactory approximation as can be verified by comparison with the graphs given by Rossi and Greisen.[1]

Compton Effect

The probability for a Compton transition per unit radiation length is for $K' \gg mc^2$

$$\sigma(K, K')dK' = \frac{BdK'}{KK'}\left(1 + \frac{K'^2}{K^2}\right), \quad \text{(A8)}$$

with $B = 137\pi mc^2/4\bar{Z}\ \lg 183Z^{-\frac{1}{2}} = 0.017$ for air and 0.0265 for lead. The integrated Compton probability is

$$\sigma(K) = \frac{B}{K}\left(\lg\frac{2K}{mc^2} + \frac{1}{2}\right). \quad \text{(A9)}$$

The average energy $\bar{E}$ of an electron produced in a Compton collision with a quantum K is

$$\bar{E} = K\left[1 - \frac{4}{3}\left(\lg\frac{2K}{mc^2} + \frac{1}{2}\right)^{-1}\right]. \quad \text{(A10)}$$

The *absorption coefficient* for photons is obtained from the combination of Compton and pair production cross sections.

Knock-on Probability

$$\sigma_k(E, E') = \frac{2BdE}{E'^2}\left(1 - \frac{2E'}{E}\right), \quad \text{(A11)}$$

where B is the same as for the Compton effect.

PHYSICAL REVIEW VOLUME 74, NUMBER 9 NOVEMBER 1, 1948

Microwave Spectra of Some Linear *XYZ* Molecules

C. H. TOWNES,* A. N. HOLDEN, AND F. R. MERRITT
Bell Telephone Laboratories, Murray Hill, New Jersey

(Received June 29, 1948)

Measurements of the pure rotational spectra of a number of isotopes and vibrational states of OCS, ClCN, BrCN, and ICN near one centimeter wave-length have been made. Experimental techniques used and interpretation of the spectra of linear *XYZ* molecules are discussed. Tables include frequencies and intensities of lines and comparison with theoretical values, rotational constants B_0, rotation-vibration constants α, *l*-type doubling constants, internuclear distances, half-width parameters of lines, quadrupole coupling constants, and nuclear quadrupole moments. Agreement between experimental results and available theory is good in all cases except for the values of *l*-type doubling constants.

SINCE much of the pure rotational spectra of molecules lies in the microwave region, and since microwave techniques have been developed to give both high resolution and accurate frequency measurements, microwave spectroscopy may be expected to make a considerable contribution to the study of molecular rotational spectra.

Among the simplest of the molecules which can be studied with microwave techniques are those of the linear *XYZ* type, when their end-to-end dissymmetry is sufficient to give them an appreciable dipole moment. Their spectra are relatively simple and intense, so that they provide a good test of theory and techniques, and a good introduction into more complex types of molecules. Only brief statements of some of the more important observations on this type of spectra have so far been published. Even though microwave study of these simple linear molecules may be regarded as just well begun, it seems

* Now at Columbia University, New York, New York.

appropriate to give a more detailed account of experiments and results.

CARBON OXYSULFIDE

The spectrum produced by the linear molecule OCS is particularly simple because its more abundant isotopic types show no nuclear quadrupole effects. Nuclei of the most plentiful isotopic species $O^{16}C^{12}S^{32}$ have been known for some time to have zero spins, and since the nuclei can, therefore, take no preferred orientation in the molecule, no quadrupole effects are possible. Electron diffraction measurements had assigned distances 1.16 ± 0.02A for the O−C bond and 1.56 ± 0.03A for the C−S bond. Computation of the moment of inertia I from these internuclear distances shows that of the expected series of rotational lines of frequency $2Jh/8\pi^2I$ the one for $J=2$, or the transition from $J=1$ to $J=2$, should produce an absorption near 1.25 cm-wavelength, or in the region called "K" band for which oscillators and other microwave components are available.

Absorption due to this line was first reported by Walter and Hershberger,[1] using gas at atmospheric pressure, and the line located at 24,325.92 Mc by Dakin, Good, and Coles,[2] near the position predicted from electron diffraction results. Again because no nuclear quadrupole effects are present the Stark effect in this molecule is simple and lends itself to a very accurate determination of the OCS dipole moment. Dakin, Good, and Coles[3] measured the frequency separation between the two components into which this line is split by an electric field applied parallel to the microwave radiation and thus obtained a value 0.72 Debye unit for the OCS moment, in fair agreement with the value 0.65 determined by other methods.**

Intensity and shape of microwave absorption lines are given according to Van Vleck and Weisskopf[4,5] by the expression

$$\gamma=\frac{4\pi Nf|\mu_{ij}|^2\nu^2}{3ckT\tau}\left[\frac{1}{(\nu-\nu_0)^2+(1/2\pi\tau)^2}+\frac{1}{(\nu+\nu)^2+(1/2\pi\tau)^2}\right], \quad (1)$$

where:

- γ is the absorption coefficient in cm^{-1}, $\gamma/2$ is the loss in nepers/cm.
- N is the number of gas molecules per unit volume.
- f is the fraction of molecules in the lower state of the transition $i\rightarrow j$.
- ν_0 is the molecular resonant frequency.
- τ is the time between intermolecular collisions.
- μ_{ij} is the quantum-mechanical matrix element for the absorption transition averaged over all values of the magnetic quantum number m.
- c, k, T are the velocity of light, Boltzmann constant, and absolute temperature of the gas, respectively.

At pressures less than $\frac{1}{10}$ atmosphere the second term in brackets of expression (1) is quite negligible. The first term in brackets appears to agree well with experiment under low pressure conditions down to pressures of about 10^{-2} mm Hg, where various complicating effects may be of importance. For the rotational transition $J=J_0\rightarrow J_0+1$ of a linear molecule, $|\mu_{ij}|^2=\mu^2(J_0+1)/(2J_0+1)$, where μ is the molecular dipole moment, and

$$f=f_v\frac{(2J_0+1)\exp[-J_0(J_0+1)B/kT]}{\sum_J(2J+1)\exp[-J(J+1)B/kT]},$$

where B is the molecular rotational constant and related to the moment of inertia I by $B=h^2/8\pi^2I$. The quantity f_v is the fraction of molecules in the vibrational and electronic state under consideration—usually close to one for the lowest state. For a line occurring in the microwave region $J_0B\ll kT$ and the sum may be fairly accurately replaced by an integral so that $f=f_v(2J_0+1)B/kT$ and, neglecting the second term of (1) at low pressures,

$$\gamma=\frac{2\pi Nf_vh\mu^2\nu^2\nu_0}{3c(kT)^2\tau[(\nu-\nu_0)^2+(1/2\pi\tau)^2]}. \quad (2)$$

[1] J. E. Walter and W. D. Hershberger, J. App. Phys. 17, 814 (1946).
[2] T. W. Dakin, W. E. Good, and D. K. Coles, Phys. Rev. 71, 640 (1947).
[3] T. W. Dakin, W. E. Good, and D. K. Coles, Phys. Rev. 70, 560 (1946).
** The result of very recent measurement of dipole moment by dielectric effect [J. G. Jelatis, J. App. Phys. 19, 419 (1948)] is 0.720 ± 0.005 Debye unit. For refinement of dipole moment measurement by Stark effect, see M. W. P. Strandberg, T. Wentink, and R. Kyhl, Phys. Rev., to be published.

[4] J. H. Van Vleck and V. F. Weisskopf, Rev. Mod. Phys. 17, 227 (1945).
[5] C. H. Townes, Phys. Rev. 70, 665 (1946). Note that definitions of γ and f are slightly different in this reference from those used here.

It should be noted that this formula gives a maximum absorption coefficient (when $\nu=\nu_0$) which increases approximately as the cube of the frequency ν_0. This is one of the reasons why microwave absorption measurements in gases have been mostly made at as high frequencies as can conveniently be used.

Even after the molecular dipole moment is known, the peak intensity or value of γ when $\nu=\nu_0$ cannot be predicted because it depends on the value of τ, which usually must be determined empirically, although enough measurements have now been made to allow in some cases a rough guess at τ. The half-width, or width in frequency of the absorption line at one-half maximum, may be used as a measure of τ, since it equals $1/\pi\tau$.

The intensity and half-width of the OCS $J=1\rightarrow2$ line have been measured at a gas pressure of a fraction of a millimeter of mercury. The half-width is $(12\pm2)p$ megacycles/sec., where p is the pressure in mm Hg, and the peak absorption coefficient is $5.1\pm0.7\times10^{-5}$ cm^{-1} for a plane wave. Substituting the measured half-width into expression (2) and using the value $\mu=0.72\times10^{-18}$ e.s.u., the predicted peak absorption when $T=300°$C is $5.4\pm0.9\times10^{-5}$ cm^{-1}.

Walter and Hershberger's measurement[1] of an absorption coefficient $8\pm2\times10^{-5}$ cm^{-1} for a frequency of 24,000 Mc in OCS at atmospheric pressure is higher than this because at this pressure adjacent rotational lines $J=0\rightarrow1$, and $J=2\rightarrow3$ and others contribute appreciably to the absorption of 24,000 Mc. There is an additional small contribution from the second term of (1) at this pressure. Assuming the experimentally determined half-width of the $J=1\rightarrow2$ line is correct for the other lines and assuming expression (1) holds at atmospheric pressure, the peak absorption coefficient of the $J=1\rightarrow2$ line at low pressure may be abstracted from Walter and Hershberger's measurement as $5.6\pm2.0\times10^{-5}$ cm^{-1}.

Although most of the OCS molecules are in the ground vibrational state, an appreciable number are excited to higher vibrational states. Molecular vibrations interact slightly with the molecular rotational levels, producing small changes in the rotational constant B of the order of B^2/ω, where ω is the vibrational frequency. For molecules of the type discussed here, these effects are generally taken into account by writing the rotational frequencies as

$$\nu=2J[B_e-\alpha_1(v_1+\tfrac{1}{2})-\alpha_2(v_2+1)-\alpha_3(v_3+\tfrac{1}{2})], \quad (3)$$

where B_e is the value of the rotational constant B assuming no vibration; α_1, α_2, and α_3 are coefficients representing the change in the effective value of B due to vibration. The quantum numbers v_1, v_2, and v_3 are integers representing the degree of excitation of the three vibrational modes. Mode number two gives a contribution α_2 rather than $\alpha_2/2$ in the ground state ($v_1=v_2=v_3=0$) because it is the degenerate bending mode. In addition, interaction between rotational and vibrational motions removes the degeneracy of this bending mode. This effect is manifested most prominently in case $v_2=1$, when the level which is doubly degenerate in the absence of rotation is split by rotation into what is known as l-type doublets. The rotational frequencies are then[6]

$$\nu=2J[B_e-\alpha_1(v_1+\tfrac{1}{2})-2\alpha_2\pm q/2-\alpha_3(v_3+\tfrac{1}{2})]. \quad (4)$$

The quantities α_1, α_2, α_3 have been calculated by Nielsen.[7] Unfortunately they are primarily dependent on the generally unknown anharmonic force constants of vibration. A theoretical evaluation of q is given by Nielsen and Shaffer.[8] This q must be carefully distinguished from the q sometimes used as a measure of the molecular quadrupole field. The α's and q may be determined experimentally if rotational lines due to molecules in the ground state and various excited states can be observed. For OCS the vibrational frequencies are known so that the fraction of molecules in excited states may be calculated. The lowest vibrational frequency and hence the one most abundantly excited is the bending mode. In each of the two bending modes ($v_2=1$) there is one-thirteenth of the molecules at room temperature. Lines due to the transition $J=1\rightarrow2$ of these excited molecules have been found and are listed in Table I. From their frequencies a value minus 10.59 Mc for α_2 and 6.39 Mc for q can be obtained. This value of q does not agree exactly with Nielsen and Shaffer's theoretical evaluation,[8] nor do the values for other linear

[6] G. Herzberg, *Infrared and Raman Spectra* (D. Van Nostrand Company, Inc., New York, 1945), p. 377.
[7] A. H. Nielsen, J. Chem. Phys. 11, 160 (1943).
[8] H. H. Nielsen and W. H. Shaffer, J. Chem. Phys. 11, 140 (1943).

TABLE I. Measured OCS lines in the microwave region.

Molecule	Designation of line	Frequency in megacycles	Line used as frequency standard	Frequency interval in megacycles between standard and measured line
$O^{16}C^{12}S^{32}$	$J=1\rightarrow2$	24325.92±0.02*		
	$J=1\rightarrow2$, $v_2=1$, l_1	24355.50	$O^{16}C^{12}S^{32}$ $J=1\rightarrow2$	29.58±0.08
	$J=1\rightarrow2$, $v_2=1$, l_2	24381.07	$O^{16}C^{12}S^{32}$ $J=1\rightarrow2$, $v_2=1$, l_1	25.57±0.05
	$J=3\rightarrow4$	48651.7**		
	$J=4\rightarrow5$	60814.1**		
$O^{16}C^{12}S^{33}$	$J=1\rightarrow2$	24020.21	$O^{16}C^{12}S^{32}$ $J=1\rightarrow2$	305.71±0.04
$O^{16}C^{12}S^{34}$	$J=1\rightarrow2$	23731.33±0.03*	$O^{16}C^{12}S^{32}$ $J=1\rightarrow2$	594.63±0.04
	$J=3\rightarrow4$	47462.3**		
$O^{16}C^{13}S^{32}$	$J=1\rightarrow2$	24247.69	$O^{16}C^{12}S^{32}$ $J=1\rightarrow2$	78.23±0.05
$O^{16}C^{13}S^{34}$	$J=1\rightarrow2$	23646.92	$O^{16}C^{12}S^{34}$ $J=1\rightarrow2$	84.41±0.10
$O^{16}C^{14}S^{32}$	$J=1\rightarrow2$	24173.0±1.0***		
$O^{18}C^{12}S^{32}$	$J=1\rightarrow2$	22819.30	$N^{14}H_3$ 3,2	14.85±0.05

* Dakin, Good, and Coles, Phys. Rev. **71**, 640 (1947).
** Hillger, Strandberg, Wentink, and Kyhl, Phys. Rev. **72**, 157 (1947).
*** Arthur Roberts, Phys. Rev. **73**, 1405 (1948).

molecules measured here. This discrepancy will be discussed further below.

A number of other lines have been found which are due to isotopic species of OCS and to other transitions. All OCS lines which have been measured here or reported in the literature are listed in Table I. Lines are designated by the two values of J involved in the transition, the vibrational quantum numbers, and in the case of l-type doublets, by the symbols l_1 and l_2 which indicate, respectively, the low frequency and high frequency components of the doublet. Although the lines measured by Dakin *et al.* and Hillger *et al.* were measured by comparison with a lower frequency standard, the measurements in this laboratory consisted of measurement of intervals between the unmeasured line and some line used as a standard which was accurately known. This technique will be described below. Since for most purposes frequency intervals need to be known much more accurately than absolute frequencies, Table I lists the measured intervals and their probable errors. The previously published[9] interval $O^{16}C^{12}S^{33}-O^{16}C^{12}S^{32}$ is modified by 0.04 Mc in the table as a result of new measurements.

The $O^{16}C^{12}S^{34}$ and $O^{16}C^{12}S^{33}$ lines have been observed in normal isotopic mixtures where their abundances are 4.2 percent and 0.74 percent, respectively. Since positions of lines due to rare isotopic molecules can be rather accurately calculated if the lines due to more common isotopes are known, and since lines due to various isotopic species are generally very easily resolved, sufficient improvement in sensitivity of microwave spectroscopy should make it a useful tool in detecting the presence of rare isotopes. An improvement of a factor of about 50 in sensitivity is needed to detect the OCS^{36} line with the natural abundance. The $O^{16}C^{13}S^{32}$ and $O^{18}C^{12}S^{32}$ lines were observed in material enriched to 20 percent and 1.5 percent, respectively.

Failure to observe splitting in the rotational lines of these molecules due to nuclear quadrupole effects shows that the quadrupole couplings for C^{13}, S^{34}, and O^{18} must be less than 0.5, 1.0, and 1.0 Mc, respectively, in these molecules assuming reasonable values of spin. The significance of this failure to find quadrupole splitting will be discussed below.

It might be expected that from the very accurate moments of inertia of various isotopic species of a molecule which can be obtained with microwave spectroscopy, very accurate internuclear distances may be determined. In addition, if lines due to three isotopic species are known, it might be supposed that the two internuclear distances could be accurately determined, and, in addition, one mass ratio. Unfortunately, this is not the case because moments of inertia are determined not only by the equilibrium internuclear distances, but in addition by the values of the three α's, and these α's differ

[9] C. H. Townes, A. N. Holden, and F. R. Merritt, Phys. Rev. **72**, 513 (1947).

in value from one isotopic species to another in a way which cannot be accurately known without a rather detailed knowledge of the anharmonic force constants involved. (This variation can be seen in Table IX.) As a result, the accuracy of internuclear distance determination is usually limited to about ± 0.01A because of incomplete information about the α's, when better knowledge of these quantities would allow an accuracy better by an order of magnitude.

An illustration of these effects may be obtained by examining the simpler diatomic molecule. If the potential between the two nuclei were strictly parabolic, fluctuations in the internuclear distance taking place even in the lowest vibrational state would result in a value of B_v slightly greater than B_e, the value for the artificial case when the nuclei are at rest at the equilibrium distance. In terms of the constant α, this produces a negative contribution to α. However, generally the anharmonic force constant is large enough to increase the average distance between the nuclei when vibration is present, giving a positive contribution to α considerably larger than the harmonic contribution. Similarly in the case of triatomic linear molecules, the harmonic contributions to α_1 and α_3 are negative and to α_2 positive, but in all known cases the anharmonic terms are larger and of opposite sign so that α_1 and α_3 are positive and α_2 negative. In the case of OCS, the harmonic contribution to α_2 is approximately $+2.6$ Mc and the net value of α_2 is -10.6 Mc.

Probably in only a few polyatomic molecules will it be feasible to evaluate rigorously zero-point vibration effects, so that some estimate of the errors involved in their omission is needed. Fairly direct evidence of the size of these effects is afforded by a comparison of internuclear distances determined from various pairs of isotopic lines and collected in Table II. Since there is no reason to expect the errors to be the same when lines of two sulfur isotopes and lines of two oxygen isotopes are used to calculate the distances, the inconsistencies may be taken as a measure of the total error due to all zero-point vibrations. If no zero-point vibrations were present, the various determinations should not differ by more than 0.001A, but actual differences are as large as 0.01A.

TABLE II. OCS bond distances calculated from various isotopic pairs.*

Pair of isotopic molecules used	C–O distance	C–S distance
$O^{16}C^{12}S^{32}-O^{16}C^{12}S^{34}$	1.1647A	1.5576A
$O^{16}C^{12}S^{32}-O^{16}C^{13}S^{32}$	1.1629	1.5591
$O^{16}C^{12}S^{34}-O^{16}C^{13}S^{34}$	1.1625	1.5594
$O^{16}C^{12}S^{32}-O^{18}C^{12}S^{32}$	1.1552	1.5653

* Zero-point vibrations are neglected, producing the main discrepancies between distances obtained from various isotopic pairs. Isotopic masses are taken from Mattauch (see reference 10).

Dakin, Good, and Coles[2] have given an analysis of the various sources of error in determination of internuclear distances from the OCS^{32} and OCS^{34} lines, and decided that uncertainty in the ratio of masses of the two sulfur isotopes produced the largest error of ± 0.0047A. They omitted mention of zero-point vibration errors which appear to be larger. In addition, if one accepts the mass values for sulfur given by Mattauch,[10] the probable error due to their uncertainty is only ± 0.0016A. Hillger, Strandberg, Wentink, and Kyhl[11] give internuclear distances determined from the OCS^{32} and OCS^{34} lines to an accuracy of 0.0001A and state that uncertainties in the value of h produce the largest errors in their determination. In oral presentation of their work, however, they pointed out the difficulties due to zero-point vibrations.

Another method of demonstrating the importance of zero-point vibrations is to evaluate the difference between B_0, the effective rotational constant including the vibrations, and B_e, the hypothetical rotational constant if the atoms were all at equilibrium positions. This may be done in the case of OCS because the frequency shifts are known for isotopic change of mass of each of the three atoms. If the carbon, oxygen, and sulfur mass ratios are kept constant, but each assumed proportional to a variable m, it can be shown that B_e is inversely proportional to m and each of the α's is proportional to $m^{-\frac{1}{2}}$. Hence the sum of the α's may be evaluated from the data of Table II by calculating the change in B_0 due to the same fractional change in mass of all of the atoms simultaneously, and properly relating the change in B_0 which is not propor-

[10] J. Mattauch, *Nuclear Physics Tables* (Interscience Publishers, Inc., New York, 1946).
[11] Hillger, Strandberg, Wentink, and Kyhl, Phys. Rev 72, 157 (1947).

tional to this mass change to the sum of the α's. Thus to a good approximation

$$\frac{\alpha_1+2\alpha_2+\alpha_3}{B_0}=-\frac{8[m_om_cl_{oc}\Delta l_{oc}'+m_sm_cl_{sc}\Delta l_{sc}''+m_om_s(l_{oc}+l_{sc})(\Delta l_{oc}'+\Delta l_{sc}'+\Delta l_{oc}''+\Delta l_{sc}'')]}{m_om_cl_{oc}^2+m_sm_cl_{sc}^2+m_om_s(l_{oc}+l_{sc})^2}, \quad (5)$$

where m_o, m_c, m_s are masses of oxygen, carbon, and sulfur, respectively; l_{oc}, l_{sc}, l_{os} are distances between atoms represented by the subscripts; $\Delta l_{oc}'$ is the difference between the distance l_{oc} determined from the isotopic carbon lines and that from the isotopic oxygen lines; $\Delta l_{sc}'$ is similar to $\Delta l_{oc}'$, but refers to the distance l_{sc}; $\Delta l_{oc}''$ is the difference between the distance l_{oc} determined from the isotopic carbon line and that from the isotopic sulfur lines; $\Delta l_{sc}''$ is similar to $\Delta l_{oc}''$, but refers to the distance l_{sc}. Evaluation of expression (5) gives $\alpha_1+2\alpha_2+\alpha_3=+0.00856B_0$, or $B_e=(1+0.00428)B_0$.*** Thus the $J=1\rightarrow2$ transition is decreased approximately 104 Mc by zero-point vibrations. In the case of diatomic molecules, it may be shown that the isotopic frequency shift calculated by neglecting zero-point vibrations will be in error by a fraction $(B_e-B_0)/2B_0$. Assuming the magnitude of this error is roughly the same in the frequency difference between the $O^{16}C^{12}S^{32}$ and $O^{16}C^{12}S^{34}$ lines, an error in the OC distance of 0.0091A would be produced. This estimate is of about the same magnitude as the deviations in Table II. Thus from evaluating B_0-B_e, from the variations in Table II and from similar variations for ClCN to be found below, it appears that ±0.01A is a reasonable estimate of the error in internuclear distances to be generally expected from zero-point vibrations.

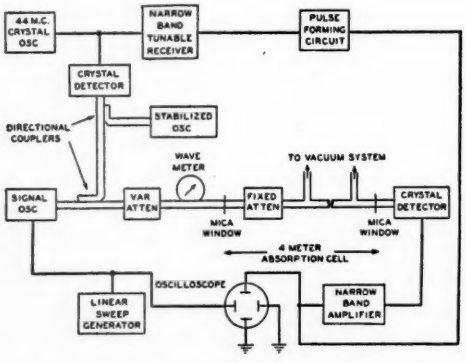

FIG. 1. System for detection and frequency measurement of absorption lines.

*** Recent measurements of α_1 [A. Roberts, private communication; C. H. Townes and S. Geschwind, Phys. Rev. 74, 626 (1948)] as 18.12 Mc, combined with this relation, allow evaluation of α_3 as 55.1 Mc.

As was noted earlier,[9] although in most cases zero-point vibrations prevent an accurate measurement of mass ratios in this type of molecule, ratios of mass differences may be fairly accurately obtained if lines for more than two isotopes of the same element are measured. Lines for $O^{16}C^{12}S^{32}$, $O^{16}C^{12}S^{33}$, and $O^{16}C^{12}S^{34}$ provide such a case. Assume that approximate internuclear distances are known so that the isotopic shift $\Delta\nu$ between two sulfur isotopes may be calculated except for an error of the order of $[(B_e-B_0)/2B]\Delta\nu$ due to zero-point vibrations. Although the exact amount of this error is unknown, it will fortunately depend in a linear way on the mass difference Δm of the sulfur isotopes except for quantities of the order $[(B_e-B_0)\Delta\nu/2B]\Delta m/m$ and less, where m is the mass of sulfur. The entire isotopic shift is also linearly dependent on Δm to a fractional accuracy of $\Delta m/m$. Consequently, the fractional error which might be introduced in obtaining the ratio of mass differences $(S^{33}-S^{32})/(S^{34}-S^{32})$ by completely neglecting zero-point vibrations is of the order

$$\left[\frac{(B_e-B_0)}{2B}\right]\frac{\Delta m}{m}\approx\frac{1}{15{,}000}.$$

If the ratio $(S^{33}-S^{32})/(S^{34}-S^{32})$ is calculated from the frequency intervals given in Table I, the result is 0.49975 ± 0.0001. This agrees poorly† with the value 0.50038 ± 0.0002 from Mattauch's tables.[10]

EXPERIMENTAL TECHNIQUES

Discussion of OCS has afforded an introduction into the type of spectra produced by linear

† Further work [C. H. Townes and S. Geschwind, Phys. Rev. 74, 626 (1948)] has shown that effects due to the S^{33} nuclear quadrupole moment increase the frequency of the OCS^{33} line observed here by 0.54 Mc. If this is taken into account, one obtains $(S^{33}-S^{32})/(S^{34}-S^{32})=0.50066\pm0.00015$, still in poor agreement with Mattauch, but in good agreement with the value 0.50060 ± 0.00005 from recent measurements of nuclear reactions by Davison (Paper P5, Washington meeting of Am. Phys. Soc., 1948).

XYZ molecules. It appears appropriate now to describe some of the apparatus and techniques used in making the measurements quoted before progressing to other more complicated spectra.

Figure 1 shows a system used for detecting absorption lines which is similar to that previously described,[5] but includes circuits for measuring line frequencies more accurately than can be done with a simple wave meter. Radiation from the signal oscillator (type 2K50 was used throughout) traverses the absorption cell and is detected by a rectifying "crystal." The resulting signal after amplification is put on the vertical plates of an oscilloscope. The oscillator is swept over a few megacycles and the sweep put on the horizontal plates of the oscilloscope so that frequency is plotted against transmission through the absorption cell by the oscilloscope trace, and absorption lines show up as vertical pips on the trace. Frequency is measured approximately by the wave meter which may be set so that its resonance likewise produces a pip on the oscilloscope. The signal oscillator was swept about twice per second, and the band width of the circuit amplifying the detected signal was narrowed as much as possible (to about 20 cycles per second) to eliminate noise without undesirably distorting pips due to absorption lines. Such a system is simple and can detect absorption lines as weak as 10^{-6} cm^{-1}, or 5×10^{-7} nepers/cm in the 4-meter absorption cell used. To obtain this sensitivity a power of about 0.1 milliwatt must be transmitted through the gas. This much power produces saturation[5,12] at low gas pressures and prevents work with very narrow lines.

Although no thorough investigation of sensitivity and sources of noise has been undertaken in these laboratories, some observations on the problem of sensitivity have been made. The systems used here for detecting absorption lines characteristically show noise and interfering effects which are approximately proportional to the microwave power used. One source of trouble is imperfect matching and consequent reflections back and forth in the cell. These reflections produce a variation in detected signal with power which can mask the variations due to absorption lines. Reflections can generally be easily reduced to the point where they produce variations of transmitted power of one percent, and with care they may be reduced by another factor of ten. Some trouble is often encountered with noise due to mechanical vibration, but this source can usually be eliminated. The random noise generally encountered can be due either to crystal noise or to noise in the signal oscillator, or both. This random noise is often many orders of magnitude above thermal noise. Noise encountered in work described here usually appeared to originate in the detecting crystal and was approximately proportional to the power absorbed by the crystal. It was found advantageous with the system described above to apply a biasing current to the crystal so that the average d.c. voltage across the crystal when it received microwave power was approximately zero. Application of this biasing current at times both increased the detected signal and decreased the random noise. Another demonstration that most of the noise originates in the crystal rather than the signal oscillator is given by the system previously described[5] which amplifies only the difference between signals from radiation which has traversed the absorption cell and a monitoring signal directly from the signal oscillator. This scheme should eliminate oscillator noise, but usually results in very little noise reduction. However, under other conditions, and with other arrangements for detecting absorption lines, oscillator noise may be of more importance. An expression for the theoretical limit of detectable absorption is given elsewhere.[13]

For some experiments a modification of the system of Fig. 1 was used which involved cutting the oscillator on and off by means of a square wave applied to the reflector electrode. This square wave was of about 2500 cycles/sec., and it was thought perhaps by detecting only a narrow band about 2500 cycles, some crystal noise might be avoided, since crystal noise is in some cases proportional to the inverse of the frequency at which noise is detected. A phase-detecting circuit, or "lock-in" amplifier, was used to amplify the detected signal and to obtain the desired narrow band about 2500 cycles. This

[12] B. Bleaney and R. P. Penrose, Proc. Phys. Soc. **60**, 83 (1948); T. A. Pond, and W. F. Cannon, Phys. Rev. **72**, 1121 (1947).

[13] C. H. Townes and S. Geschwind, J. App. Phys. **19**, 795 (1948).

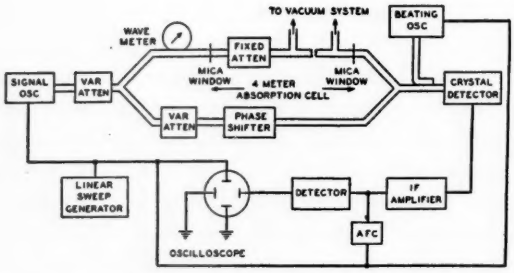

FIG. 2. Microwave spectrometer using r-f bridge and heterodyne detection.

arrangement resulted in no appreciable increase of signal to noise ratio, although it did avoid pick-up troubles due to 60 cycles and other low frequency sources.

One of the difficulties in detecting weak absorption lines is the necessity of observing small changes of a large background signal. However, there are ways of avoiding to some extent the handicap of measuring very small fractional effects. One is afforded by the Stark modulation technique described by Hughes and Wilson.[14] Another is the bridge detecting system illustrated by Fig. 2. The bridge was balanced by means of the phase adjustment and variable attenuator so that power arriving at the detecting crystal was about one-tenth of the power through either arm. An absorption line was detected as a change in this balance due to selective absorption in the absorption cell and, to a lesser extent, by phase shifts produced. This reduced the power variation at the crystal due to an absorption line by the square root of ten, but reduced the noise by about a factor of ten, so the net result was a more sensitive system. In order to detect the small amounts of power received by the crystal in this arrangement, heterodyne detection was used with a 60-Mc I.F. amplifier and an automatic frequency control (A.F.C.) circuit to maintain the beating oscillator exactly 60 Mc from the sweeping signal oscillator. Another reason for setting up this heterodyne system was to provide detection of lines with very small amounts of energy flowing through the absorption cell so as to avoid saturation and obtain very narrow lines. In some cases where high resolution was desired, power flowing through the absorption cell was reduced to about one microwatt. The sensitivity of this system was such that the OCS^{33} line could just be detected in the normal isotopic mixture at room temperature with 4 meters of absorption cell. Since S^{33} has an abundance of 0.74 percent this represents an absorption coefficient of 4.5×10^{-7} cm^{-1} or 2.2×10^{-7} nepers/cm. Probably better balancing would afford some additional improvement. This system has the advantage of good sensitivity, and of obtaining very narrow lines. However, it is very slow and awkward to use for searching because considerable adjustment is needed at each frequency in order to obtain optimum sensitivity.

In order to study the change in relative intensity of lines with change in temperature, and in order to boost the intensity of some weak lines, a thermally insulated metal trough was built around the absorption cell of the bridge detecting system. Hot water or refrigerant could be put in the trough to vary the temperature of the absorption cell from near 100°C to liquid nitrogen temperatures. Formula (2) shows that the intensity of a rotational line in the microwave region increases rapidly with decreasing temperature. For fixed N, the half-width may be expected to be proportional to $(T)^{\frac{1}{2}}$, so that the absorption coefficient is generally proportional to $1/T^{5/2}$. At dry ice temperature, which proved to be a convenient working point, intensities of ground-state lines were in fact found to be about three times greater than at room temperature. For some of the weak isotopic OCS lines, the temperature was decreased to about 125°K, where the intensity is ten times greater than at room temperature, in order to look for the possibility of weak lines split from the main line by nuclear quadrupole effects.

Frequency measurements to an accuracy of two to five megacycles may be obtained with the frequency meter shown in Fig. 1. More accurate measurements of frequency differences between lines was accomplished by using the stabilized 1-cm oscillator and a 44-Mc quartz crystal oscillator shown in this same figure. If the signal oscillator, the stabilized oscillator, and the crystal oscillator are all fed into a detecting crystal, the same beat frequency is obtained for any two signal oscillator frequencies separated by an integral multiple of 44 Mc. If the receiver is tunable

[14] R. H. Hughes and E. B. Wilson, Phys. Rev. **71**, 562 (1947).

over a range of 22 Mc, it may be set so that a main beat frequency is received for any frequency of the signal oscillator, and this beat note imposed on the oscilloscope so that it coincides with the peak of an absorption line over which the signal oscillator sweeps. If the receiver is accurately calibrated, similar settings on two different absorption lines allow an accurate determination of the difference in their frequencies. This system is capable of good accuracy in measuring frequency differences, and the equipment needed is somewhat less than that required by other accurate measuring systems.[15] If the oscillator is well stabilized to eliminate difficulties with drift, the main limitations in accuracy are errors in judging the center of an absorption line. This does not provide a direct measurement of absolute frequency, but absolute frequencies can generally be obtained with more accuracy than needed by setting on one of the accurately determined ammonia lines. In the case of OCS, most of the lines were thus referred to the well measured $O^{16}C^{12}S^{32}$ line.

The oscillator was stabilized part of the time on an ammonia line by the circuit shown in Fig. 3, and part of the time by a similar circuit on a standard transmission-type wave meter.

An ammonia line is split into Stark components by the application of a constant electric field. In addition, a small a.c. field of a convenient frequency such as 10,000 cycles is applied to change the frequency of each component sinusoidally by about 0.1 Mc. A microwave signal is transmitted through the ammonia. If its frequency is approximately equal to the frequency of one of the Stark components, then its intensity at the detecting crystal will be modulated by the varying Stark field. If the oscillator frequency is higher than the average position of the Stark component, a 10,000-cycle signal of one phase will be received by the crystal; if it is lower, a similar signal of opposite phase is detected. Thus a phase-detecting circuit or "lock-in" amplifier into which the crystal signal is fed will produce a signal of one sign if the oscillator frequency is higher than the line, and of the opposite sign if the oscillator frequency is lower, providing the usual discriminator curve needed to feed back into the frequency-determining electrode of the oscillator in order to achieve stabilization. This system is particularly suited for stabilization on a gas absorption line since no part of the microwave circuit varies in synchronism with the varying Stark field except the absorption lines, and, consequently, spurious effects due to other parts of the microwave circuit are eliminated. The effectiveness of this circuit was judged by comparing the beat note produced in the frequency-measuring circuit described above with a gas absorption line over periods of several hours. No detectable variation or drift was found, which indicates that stabilization was better than about 0.05 Mc. This same type of circuit was also used with a standard frequency meter as the frequency-determining element rather than ammonia. In this case, instead of varying the frequency of peak absorption of the meter, a small signal was put on the oscillator to vary its frequency ± 0.05 Mc. Of course a beat note for frequency measurement 0.1 Mc wide was then produced, but its width proved to be no handicap. In contrast to the case where ammonia was used for stabilization, some trouble was encountered while using the frequency meter with frequency drifts of the order of 0.1 Mc. These were probably caused by temperature and atmospheric changes which shifted the resonant frequency of the cavity. A temperature change of only 1°C was sufficient to produce a 0.1-Mc shift in resonant frequency of the cavity.

Intensities and half-widths of lines were measured in an apparatus of the type shown in Fig. 1. The deflection of the oscilloscope trace varies in an approximately linear way with absorption in the wave guide. In order to measure the half-

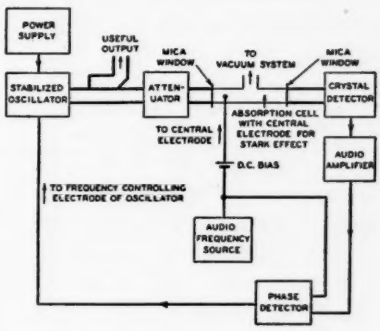

FIG. 3. Circuit for stabilizing a microwave oscillator on the frequency of a gas absorption line.

[15] W. E. Good and D. K. Coles, Phys. Rev. **72**, 157 (1947).

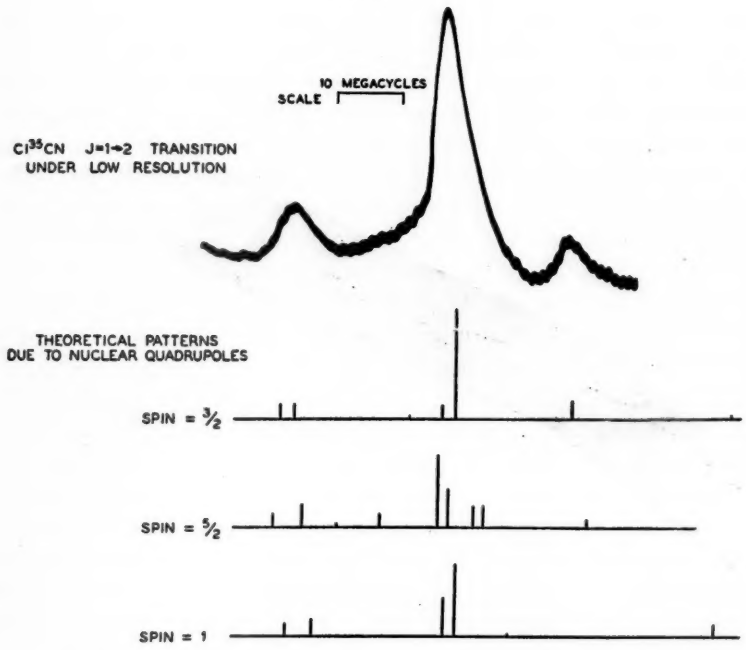

FIG. 4. Spectrum of $Cl^{35}CN$ $J=1\rightarrow2$ transition under low dispersion and comparison with quadrupole patterns for several values of nuclear spin.

width of an absorption line, gas pressure was adjusted to obtain a convenient width such as 5 Mc, and frequency markers set at the half-height points on either side of the pip seen on the oscilloscope.

Intensities were measured by comparing the size of pip produced by the resonance of a frequency meter with that produced by the gas absorption line. The fraction of power absorbed by the frequency meter was determined by measuring the rectified crystal currents with the meter set first on and then away from the oscillator frequency. In addition, absorption due to the frequency meter was determined by comparing its effect on crystal current with that of a calibrated attenuator. This type of measurement appears to have an accuracy of about ±20 percent, and with care might be made as accurate as ±10 percent.

CYANOGEN CHLORIDE

The $J=1\rightarrow2$ line of ClCN shows many of the same characteristics as that due to OCS, but is considerably more complex because both the chlorine and nitrogen nuclei possess electric quadrupole moments. The major lines of the $Cl^{35}CN$ $J=1\rightarrow2$ transition are shown under low resolution in Fig. 4. The satellite lines seen in Fig. 4 are not due to molecules in excited vibrational states. This was demonstrated by comparing their intensities relative to the main line at room temperature and at $-78°C$. Relative intensities for the two temperatures were found to be the same within ±20 percent, whereas the population of the lowest energy excited state should have decreased at the lower temperature by a factor of about 2.5. The $Cl^{37}CN$ $J=1\rightarrow2$ transition shows a similar pattern, but with the satellites separated by about 25 percent less than is the case for $Cl^{35}CN$, showing that these lines depend strongly on the nature of the chlorine nucleus. Two types of nuclear effects may be expected to cause splitting of rotational molecular lines, and have been studied in other molecules by Rabi and his associates. They are nuclear magnetic dipole interactions which give energies dependent on the cosine of the angle between nuclear spin I and molecular rotational momentum J, and nuclear electric quadrupole moments giving energies dependent on the square of this cosine. The magnetic dipole interactions are generally very small in molecules because most molecules are in $^1\Sigma$-states, and in addition the pattern to be expected is quite different from the spectrum obtained. The splitting due to a single nucleus coupled to molecular rotation of a linear molecule by electric quadrupole effects may be obtained from the basic work of Casimir.

Relative intensities and positions of the various components are readily obtained from published tables. Calculation of these quantities has been discussed in some detail in an earlier paper.[16] Plots of patterns to be expected from a $J=1\rightarrow 2$ transition assuming quadrupole interactions for a nucleus of spin 5/2, 3/2, or 1 are shown in Fig. 4 and compared with the observed $Cl^{35}CN$ spectrum. These hyperfine patterns are quite specific with respect to both the nuclear spin I and the rotational transition $J\rightarrow J+1$. The spin of N^{14} is well known to be 1, and the spins of Cl^{35} and Cl^{37} have been measured from band spectra as 5/2. The carbon, having spin zero, can contribute no quadrupole effects. It may be seen that the pattern for a spin 3/2 best fits the observed spectrum. However, more resolution is plainly needed to resolve all of the expected structure. In addition, since both N and Cl are contributing to the pattern, it is necessary to compute expected patterns when two nuclei in the same molecule show quadrupole coupling.

The case of two nuclear quadrupole couplings of arbitrary relative magnitude was solved by Bardeen, and has been described in a form convenient for calculation of spectra.[16] With this theory, it was found possible to fit very well and in detail the $Cl^{35}CN^{14}$ spectrum observed under high resolution with the heterodyne detecting system described above.[17] This fit is shown in Fig. 5. It is necessary to assume that Cl^{35} has a spin of 3/2 as indicated by the low resolution

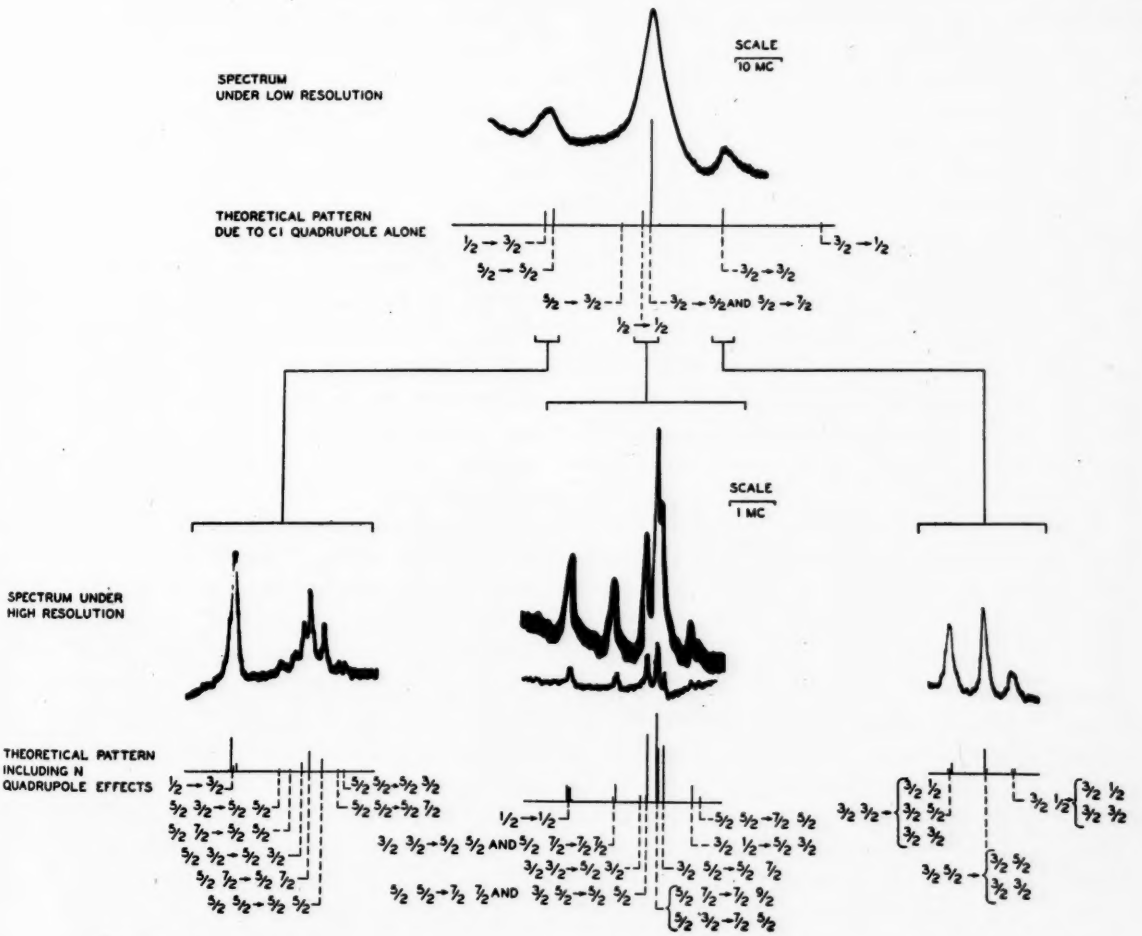

FIG. 5. Spectrum of $Cl^{35}CN$ $J=1\rightarrow 2$ transition with both low and high dispersion and comparison with theoretical pattern assuming spin of Cl^{35} is 3/2.

[16] J. Bardeen and C. H. Townes, Phys. Rev. **73**, 97 (1948).
[17] Townes, Holden, Bardeen, and Merritt, Phys. Rev. **71**, 644 (1947).

results. In this molecule, the quadrupole coupling, $eQ(\partial^2 V/\partial z^2)$, for chlorine 35 is found to be minus 83.2 megacycles and much larger than that of the nitrogen 14, which is minus 3.63 megacycles. This is the reason the major lines of the spectrum give the appearance of a pattern due to a nucleus of spin 3/2, these major lines being finely split by the effects of the nitrogen nuclear quadrupole. Lines are designated in Fig. 5 first by the final and initial values of F_1, the quantum number for the vector sum of I_1 and J, and then by final and initial values of F, the quantum number for the vector sum of I_1, I_2, and J. Here I_1 is the spin of the Cl nucleus, I_2 the spin of the nitrogen nucleus. Thus a line 5/2 7/2→7/2 9/2 indicates a transition $F_1=5/2 \rightarrow 7/2$ and $F=7/2 \rightarrow 9/2$. If only one number is given in final or initial states, it is the value of F_1. F_1 has a definite value only as a first approximation, but it is a sufficiently good quantum number for identifying the lines. Every one of the lines due to chlorine splitting have been observed, including the weak 3/2→1/2 and 5/2→3/2. The weakest line, 5/2→3/2, was also observed to split into three components due to the nitrogen quadrupole in accordance with theory, but no photograph of these lines is available for inclusion in Fig. 5. Agreement between the measured spectrum and the theoretical spectrum is so extensive and detailed, assuming that Cl^{35} has a spin of 3/2, that we may be sure this is the correct spin rather than the previously determined value of 5/2.

A good illustration of the resolving power of the technique used is also afforded by Fig. 5. The central group of lines is shown under high dispersion with two different gas pressures. In the lowest spectrum, the gas pressure is least (about 2×10^{-4} mm Hg) and the highest resolution is obtained, although at this low pressure various effects have decreased the line strengths. Saturation has changed the relative intensities of some of the components in the lowest spectrum. The two rather strong lines 5/2 3/2→7/2 5/2 and 3/2 5/2→5/2 7/2 are separated by only 140 kilocycles, but are shown completely resolved. In the right-hand group of lines, showing how the 3/2→3/2 line is split by the N quadrupole, the small line on the right is flat on the top. This indicates that the two components 3/2 1/2 →3/2 1/2 and 3/2 1/2→3/2 3/2 are almost, but not quite, resolved. Their theoretical separation is 70 kilocycles. Doppler effect and collision with the walls of the K-band guide (10.7 mm×4.3 mm cross section) should produce half-widths of about 35 and 10 kilocycles, respectively, at the gas temperature (−78°C) used for the photographs, so that actual resolving power misses the theoretical limit by a factor of two. The limit on resolution is probably partly due to saturation effects which produce a broadening of the lines and a decrease in intensity. Power transmitted through the ClCN gas in K-band guide for highest resolution was about 1.5 microwatts, which might be expected to produce noticeable saturation effects at a gas pressure of about 5×10^{-4} mm Hg, where the half-width due to intermolecular collisions should be approximately 25 kilocycles. An additional limitation on resolution, and probably an important one in the experiments here, is the fact that both signal and beat oscillators are not truly monochromatic. If care is taken to insure a very narrow frequency band produced by the oscillators, and somewhat smaller transmitted power is used, it seems reasonable to expect that resolution limited primarily by Doppler effect can be achieved, or about twice that obtained in these experiments.

As in the case for OCS, ClCN molecules excited to the first level of the bending vibrational mode are fairly abundant at room temperature, including about one-quarter of the total molecules. The lines produced by the molecules are split by l-type doubling as in the case of OCS, and in addition by nuclear quadrupole effects. The quadrupole pattern for these molecules excited to the bending vibrational mode is radically different from the pattern produced by molecules in the ground state. Because of the degeneracy of the excited bending mode, the molecules behave essentially like symmetric tops with unit angular momentum around the molecular axis. Quadrupole interactions are correspondingly modified. Assuming a spin of 3/2 and the same value of quadrupole coupling found for the ground state, the expected splitting has been calculated and is compared with excited state lines found in Table III. These lines are designated in a notation similar to that used for Fig. 5, but in addition vibrational states must be indi-

cated. This is done by specifying the value of the vibrational quantum number which is not zero, e.g., $v_2=1$, and indicating each of the l-type doublets separately. The arbitrary label l_1 has been used for the low frequency component of the doublet and l_2 for the high frequency component. All lines which can be expected from the splitting due to Cl for these excited states are found except those corresponding to the transitions $5/2\rightarrow3/2$ and $3/2\rightarrow1/2$, which are weaker than the weakest of the other lines by a factor of three. Intensities given for the excited state lines in Table III assume room temperature (298°K) conditions. In one case two lines coincide closely and are not resolved. These lines were not examined under high resolution so that no splitting due to the nitrogen quadrupole was observed.

In fitting the excited state lines, one obtains values for the rotational constant $\alpha_2=-16.39$ Mc and the l-type doubling constant $q=7.50$ Mc. Thus corresponding lines of the two l-type doublets are separated by 30.00 Mc. The value for this splitting published earlier[9] is incorrect by 5 Mc because of an error in transcribing the data.

All observed lines of the $J=1\rightarrow2$ transition of $Cl^{35}C^{12}N^{14}$ are listed in Table III. Some of these lines were measured as described above and their frequencies obtained by reference to the nearby $N^{14}H_3$ 3,3 line. Differences between these measurements and the theoretical values, assuming the values of quadrupole coupling constants, α_2, and q given above and a value $B_0=5970.820$, are of the order of 0.1 Mc and probably represent experimental errors. That agreement between theory and both position and relative intensity of the lines is good at least among any one group can be seen by comparison of the reproduction of oscilloscope sweeps in Fig. 5 and the theoretical spectra immediately below the sweeps. Measured values are given in Table III only for those lines which were measured by superposing a frequency-measuring pip on the line, but all lines observed agree well with expectations as shown in Fig. 5.

The $Cl^{37}CN$ $J=1\rightarrow2$ transition was found to have just the same pattern as shown by $Cl^{35}CN$, giving a spin of 3/2 to Cl^{37} as well as Cl^{35}. The three main groups of lines ($F_1=1/2\rightarrow3/2$ and $5/2\rightarrow5/2$, $F_1=1/2\rightarrow1/2$, $3/2\rightarrow5/2$, and $5/2\rightarrow7/2$, and $F_1=3/2\rightarrow3/2$) were examined under high resolution and all lines found to correspond to the $Cl^{35}CN$ lines except that a few were too weak to detect, since Cl^{37} has an abundance one-third that of Cl^{35}. Only the measured lines are listed in Table IV, and compared with theoretical values using a value $B_0=5847.26$ and taking quadrupole coupling constants ($eQ(\partial^2V/\partial z^2)$) minus 65.7 Mc for Cl^{37} and minus 3.63 Mc for N^{14} as before.

The quadrupole coupling constants of Cl^{35}, Cl^{37}, and N^{14} in this molecule agree well with those reported earlier from less accurate data.[17]

TABLE III. Observed lines of the $Cl^{35}C^{12}N^{14}$ $J=1\rightarrow2$ transition.

Line designation	Measured frequency in megacycles	Theoretical frequency in megacycles	Theoretical intensity relative to strongest line
1/2→3/2	23862.57	23862.47	0.32
5/2 3/2→5/2 5/2		23863.46	0.012
5/2 7/2→5/2 5/2		23863.77	0.013
5/2 3/2→5/2 3/2		23864.00	0.066
5/2 7/2→5/2 7/2		23864.18	0.14
5/2 5/2→5/2 5/2		23864.52	0.092
5/2 5/2→5/2 7/2		23864.93	0.013
5/2 5/2→5/2 3/2		23865.07	0.012
5/2 3/2→3/2 1/2 5/2 3/2→3/2 3/2 5/2 3/2→3/2 5/2		23878.60	0.0087
5/2 7/2→3/2 5/2		23878.93	0.017
5/2 5/2→3/2 3/2 5/2 5/2→3/2 5/2		23879.74	0.013
1/2→1/2	23883.30	23883.28	0.32
5/2 7/2→7/2 7/2 3/2 3/2→5/2 5/2		23884.22	0.28
3/2 3/2→5/2 3/2		23884.76	0.044
3/2 5/2→5/2 5/2 5/2 5/2→7/2 7/2		23884.91	0.57
5/2 7/2→7/2 9/2 5/2 3/2→7/2 5/2	23885.16	23885.16	1.00
3/2 5/2→5/2 7/2		23885.31	0.36
3/2 1/2→5/2 3/2		23886.03	0.14
5/2 5/2→7/2 5/2		23886.24	0.047
3/2 3/2→3/2 1/2 3/2 3/2→3/2 5/2 3/2 3/2→3/2 3/2	23899.59	23899.42	0.14
3/2 5/2→3/2 5/2 3/2 5/2→3/2 3/2	23900.20	23900.09	0.21
3/2 1/2→3/2 1/2 3/2 1/2→3/2 3/2		23900.67	0.070
$v_2=1$, l_1, 3/2→5/2	23917.9	23918.1	0.18
3/2→1/2	23920.91	23920.79	0.066
$v_2=1$, l_1, 3/2→3/2	23925.5	23925.5	0.091
$v_2=1$, l_1, 5/2→5/2	23928.7	23928.5	0.075
$v_2=1$, l_1, 5/2→7/2	23928.6	23938.9	0.37
$v_2=1$, l_1, 1/2→3/2	23944.4	23944.2	0.067
$v_2=1$, l_2, 3/2→5/2	23948.2	23948.1	0.18
$v_2=1$, l_1, 1/2→1/2 $v_2=1$, l_2, 3/2→3/2	23954.5	23955.1	0.16
$v_2=1$, l_2, 5/2→5/2	23958.4	23958.5	0.075
$v_2=1$, l_2, 5/2→7/2	23968.6	23968.9	0.37
$v_2=1$, l_2, 1/2→3/2	23974.4	23974.2	0.067
$v_2=1$, l_2, 1/2→1/2	23984.6	23984.6	0.067

TABLE IV. Measured lines of the $Cl^{37}C^{12}N^{14}$ $J=1\rightarrow 2$ transition.

Line designation	Measured frequency in megacycles	Theoretical frequency in megacycles
1/2 3/2→3/2 5/2	23372.72	23372.60
1/2→1/2	23389.00	23389.04
3/2 3/2→5/2 5/2	23389.61	23389.58
5/2 7/2→7/2 9/2 5/2 3/2→7/2 5/2	23390.53	23390.53
3/2 5/2→3/2 5/2	23402.47	23402.38

The strongest group of lines ($F_1=1/2\rightarrow 1/2$, $F_1=3/2\rightarrow 5/2$, and $F_1=5/2\rightarrow 7/2$) of the isotopic molecules $Cl^{35}C^{13}N^{14}$ and $C^{37}C^{13}N^{14}$ were also observed in ClCN enriched in C^{13} to 20 percent. The patterns appeared identical with those of the same molecules containing C^{12}, which is to be expected since the C^{13} can show no quadrupole effects if its spin is 1/2 as found by Jenkins.[18] Intervals between the strongest lines (sum of 5/2 7/2→7/2 9/2 and 5/2 3/2→7/2 5/2) of the various isotopic species of ClCN were measured in order to obtain the isotopic shifts. The intervals found are listed in Table V. As previously discussed in the case of OCS, zero-point vibrations limit the accuracy with which internuclear distances can be determined, but distances computed from three pairs of isotopic molecules by neglecting zero-point vibrations are given in Table V.

Intensity and half-width of the strongest group of lines due to $Cl^{35}C^{12}N^{14}$ were measured at pressures high enough to make the half-width several times the maximum splitting. The intensity was found to be $8.0\pm 1\times 10^{-5}$ cm^{-1} or $4.0\pm 0.5\times 10^{-5}$ nepers/cm for a plain wave, and the half-width (total width at half-maximum intensity) equivalent to 50 ± 8 Mc at a gas pressure of 1 mm Hg. The dipole moment of ClCN has apparently not been measured. If expression (2) is used to evaluate the dipole moment from this intensity measurement, the value 2.66 ± 0.25 Debye units is obtained. Since BrCN and ICN have values 2.94 and 3.71 Debye units, respectively,[19] this value for ClCN appears to be reasonable.

[18] F. A. Jenkins, Phys. Rev. **72**, 169 (1947).
[19] L. G. Wesson, *Tables of Electric Dipole Moments* (Laboratory of Insulation Research, M.I.T. 1947), pp. 15 and 17.

TABLE V. Frequency differences between various isotopic species of ClCN and computed internuclear distances neglecting zero-point vibrations.*

Isotopic species compared	Measured interval between strongest lines (5/2 7/2→7/2 9/2) in megacycles	Computed internuclear distances assuming no zero-point vibrations Cl−C	C−N
$Cl^{35}C^{12}N^{14}$, $Cl^{37}C^{12}N^{14}$	494.63 ± 0.05	1.6238	1.1700
$Cl^{35}C^{13}N^{14}$, $Cl^{37}C^{13}N^{14}$	500.67 ± 0.10	1.6246	1.1691
$Cl^{35}C^{12}N^{14}$, $Cl^{35}C^{13}N^{14}$	124.18 ± 0.05	1.6315	1.1599

* Isotopic masses are from Mattauch (see reference 10).

CYANOGEN BROMIDE

The transition $J=2\rightarrow 3$ of cyanogen bromide produces a spectrum near the same frequency as that due to the $J=1\rightarrow 2$ transition of cyanogen chloride. The two spectra are similar in many respects, both involving halogens of spin 3/2 whose large quadrupole couplings produce the main lines of the spectrum. These main lines are split more finely in both cases by the smaller N^{14} quadrupole coupling. All of the lines found for this transition which are produced by splitting due to quadrupole moments of the two bromine isotopes are listed in Table VI and compared with theory. In most cases these lines were not examined under high resolution. The splitting due to the N^{14} quadrupole moment may of course shift the center of gravity of the line and, therefore, its neglect can cause discrepancies between measured frequencies and theoretically computed frequencies. However, in most cases this shift is less than 0.1 Mc. Resolution of one of the lines and evaluation of the size of the N^{14} coupling will be discussed below. Lines in Table VI are designated in a way similar to that used in Table III. Since the splitting due to N^{14} is ignored, however, only values of F_1 are given, that is the angular momentum in units of $h/2\pi$ resulting from the vector addition of J and the angular momentum I of a bromine nucleus. In addition the bromine isotope responsible for each line is indicated as part of the line designation, since there is appreciable overlap of the spectra of the two isotopes.

Assuming quadrupole couplings†† plus 573.5 Mc for Br^{81} and plus 686.5 Mc for Br^{79}, lines of the ground vibrational state may be fairly accurately fitted by using Casimir's expression[16] for

†† Values of quadrupole coupling constants given by the authors in reference 17 are somewhat in error due to an oversight, and are not the values which give the theoretical fit for the BrCN spectrum shown there.

quadrupole interaction energy

$$-eQ\frac{\partial^2 V}{\partial z^2}\frac{\frac{3}{4}C(C+1)-I(I+1)J(J+1)}{2I(2I-1)(2J-1)(2J+3)}.$$

However, there are deviations from this fit for both isotopes. These deviations are due primarily to the fact that the bromines have such a large quadrupole coupling that first-order perturbation

TABLE VI. Lines due to $J=2\rightarrow3$ transition of BrCN.

Designation of line	Measured frequency in megacycles	Theoretical frequency including only first-order effects of bromine quadrupole	Difference in megacycles	Correction due to second-order effects of bromine quadrupole	Measured intensity relative to strongest line	Theoretical relative intensity
81 3/2→3/2	24465.33	24465.87	+0.54	+0.66	0.05	0.065
81 $v_1=1$ 5/2→7/2, 7/2→9/2	24506.75	24506.37	−0.38	−0.05	0.15	0.15
81 5/2→5/2	24507.38	24506.84	−0.54	−0.65		
81 $v_1=1$ 1/2→3/2, 3/2→5/2	24541.18	24541.87	+0.69	+0.16		0.025
81 5/2→7/2, 7/2→9/2	24573.86	24573.75	−0.05	−0.05	1.0	0.98
79 3/2→3/2	24583.00	24583.87	+0.87	+0.97	0.1	0.066
81 1/2→3/2, 3/2→5/2	24608.92	24609.25	+0.33	+0.16	0.4	0.42
81 $v_2=1, l_1$ 1/2→3/2, 7/2→9/2	24622.93	24622.90	−0.03		0.1	0.12
79 5/2→5/2	24633.71	24632.88	−0.83	−0.94	0.1	0.086
81 $v_2=1, l_2$ 1/2→3/2, 7/2→9/2	24645.82	24645.97	+0.15		0.1	0.18
79 $v_1=1$ 5/2→7/2, 7/2→9/2		24644.94				
81 $v_2=1, l_1$ 3/2→3/2, 5/2→7/2	24658.89	24658.94	+0.05		0.1	0.11
81 $v_2=1, l_2$ 3/2→5/2, 5/2→7/2	24682.13	24682.01	−0.10		0.1	0.11
79 $v_1=1$ 1/2→3/2, 3/2→5/2	24687.11	24687.36	+0.25	+0.25		0.025
79 5/2→7/2, 7/2→9/2	24713.05	24712.97	−0.08	−0.08	1.0	1.00
81 7/2→7/2	24717.19	24717.13	−0.06	−0.17		0.066
79 1/2→3/2, 3/2→5/2	24755.22	24755.47	+0.25	+0.21	0.4	0.43
79 $v_2=1, l_1$ 1/2→3/2, 7/2→9/2	24760.76	24760.31	−0.45		0.1	0.13
79 $v_2=1, l_2$ 1/2→3/2, 7/2→9/2	24784.02	24783.78	−0.24		0.1	0.13
79 $v_2=1, l_1$ 3/2→5/2, 5/2→7/2	24803.00	24803.46	+0.46		0.1	0.11
79 $v_2=1, l_2$ 3/2→5/2, 5/2→7/2	24826.70	24826.93	+0.23		0.1	0.11
79 7/2→7/2	24884.57	24884.59	+0.02	−0.25	0.05	0.066

theory is not sufficiently accurate, and the value of J in either upper or lower state of the transition is not truly constant. Bardeen has calculated the matrix elements necessary to evaluate the second-order corrections. These have been published and the theoretical corrections derived from them shown to fit well the somewhat larger second-order effects in ICN.[20] The second-order terms are proportional to $(eqQ)^2/B_0$, so they differ by about 40 percent for the two bromine isotopes. A comparison of the second-order corrections and deviations from the first-order theory displayed in Table VI shows that the deviations are primarily due to this cause. The remaining discrepancies are of the order of 0.1 Mc and probably due to shifts produced by the N^{14} quadrupole moment and to experimental error. Experimental relative intensities listed in the table are those originally published[21] before these lines were understood and analyzed. The relative intensity measurements have not been refined or measurements made on the new lines because in all cases so far tested, experimental relative intensities agree within the accuracy of measurement with theoretical values, and theoretical values are probably much more accurate and reliable.

Lines due to BrCN molecules excited to the bending vibrational mode have been found and exhibit l-type doubling as described above with the l-type doubling constant $q=3.912$ Mc and 3.845 Mc for $Br^{79}CN$ and $Br^{81}CN$, respectively. The value of α_2 is minus 11.49 Mc for both $Br^{79}CN$ and $Br^{81}CN$. The lines are split by quadrupole effects into the pattern characteristic of a symmetric top with $K=1$. The four strong components produced by the Br quadrupole for each isotope approximately coincide in pairs, giving two lines which predominate in the quadrupole pattern of each l-type doublet. Lines produced by molecules in this excited state are listed in Table VI and compared with theory. As a verification that the lines so identified were produced by molecules in an excited vibrational state, intensities of the lines at 24622.93 Mc and 24645.82 Mc were compared with intensity of the ground-state line at 24633.71 Mc for temperatures -40°C and $+85$°C. This temperature variation gives a computed change in the relative intensity of ground-state lines to those in the first excited bending mode of 2.2, which was confirmed by observation.

One of the stretching vibrational frequencies, ν_1, is also low enough to allow observation of some of its stronger lines at room temperature. The quadrupole pattern for this excited state is identical with that of the ground state assuming the quantity $\partial^2 V/\partial z^2$ is not appreciably changed, and intensity of corresponding lines are in the ratio 1:16.5 because of the Boltzmann factor. For $Br^{81}CN$ the two strongest lines due to this excited state were found and are listed in Table VI. The stronger almost coincides with the $5/2 \rightarrow 5/2$ line of the ground state. Only one of the lines due to the same excited state of $Br^{79}CN$ is given in Table VI, the other strong line being masked by the line at 24645.82 Mc which approximately coincides with it. The separation of the two strong lines of $Br^{81}CN$ excited to this stretching mode is somewhat smaller than that for the corresponding ground state lines, indicating perhaps a small difference in the value of $\partial^2 V/\partial z^2$ for the two cases. The difference is not, however, larger than might be accounted for by error in measurement of these weak lines. The molecular constant α_1 obtained from measurement of these excited state lines is 11.36 Mc and 11.23 Mc, respectively, for $Br^{79}CN$ and $Br^{81}CN$.

The $J=3 \rightarrow 4$ transition of BrCN has been studied by Gordy, Smith, Smith, and Ring.[22] They found and identified lines due to molecules excited to the low frequency stretching mode, ν_1, and as well as can be judged from their published plot of lines, the value of α_1 obtained from their measurements would agree with ours. In addition, a number of lines due to molecules excited to the first bending mode are shown in their plot, but these were not identified.

So far in this discussion, splitting of the BrCN lines by the N^{14} quadrupole has been neglected. The measurements given in Table VI were made under conditions of moderately low resolution,

[20] J. Bardeen and C. H. Townes, Phys. Rev. **73**, 627 (1948).

[21] C. H. Townes, A. N. Holden, and F. R. Merritt, Phys. Rev. **71**, 64 (1947).

[22] Gordy, Smith, Smith, and Ring, Phys. Rev. **72**, 259 (1947). Cf. also further measurements by Gordy *et al.* [Smith, Ring, Smith, and Gordy, Phys. Rev. **74**, 370 (1948)] which have appeared after this writing.

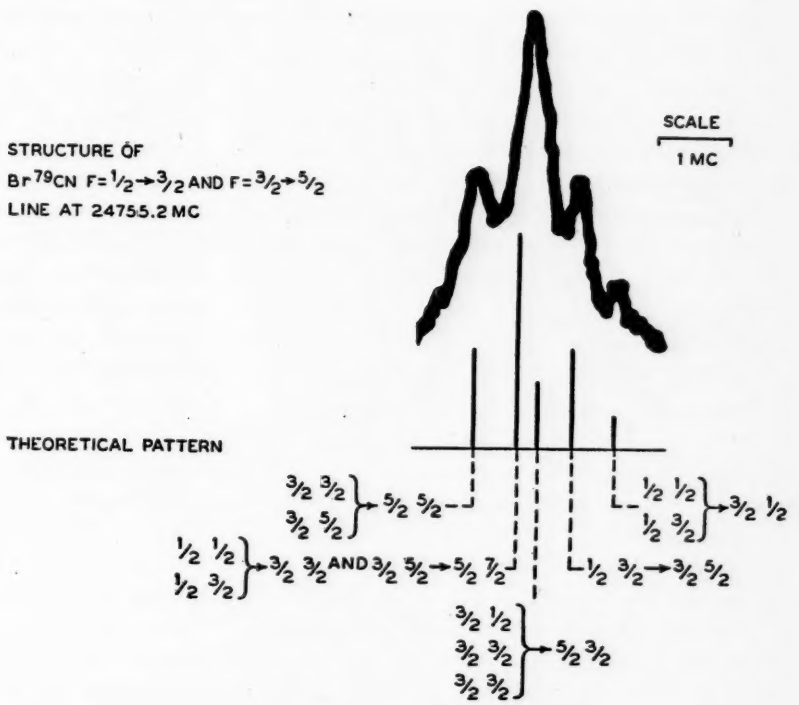

FIG. 6. Structure of $Br^{79}CN$ $J=2\rightarrow3$, $F=1/2\rightarrow3/2$, and $F=3/2\rightarrow5/2$ transitions.

and hence probably measure the center of gravity of the group of lines produced in each case by the nitrogen quadrupole. Figure 6 shows one of these groups under somewhat higher resolution. This is a composite of patterns of the lines $1/2\rightarrow3/2$ and $3/2\rightarrow5/2$ of $Br^{79}CN$ which should coincide exactly, assuming no nitrogen quadrupole moment and only first-order bromine quadrupole effects. Second-order bromine quadrupole effects separate the two lines by 0.76 Mc, and the nitrogen quadrupole moment splits each into several components, resulting in the theoretical pattern shown in Fig. 6. Because the second-order effects in $Br^{81}CN$ are about 40 percent less than those for $Br^{79}CN$, the appearance of the group of lines due to the transitions $1/2\rightarrow3/2$ and $3/2\rightarrow5/2$ of $Br^{81}CN$ is somewhat different. From the measurements of separations of various components of the group of lines shown in Fig. 6 and a comparison with the theoretical pattern computed in a way similar to that used for ClCN, the value of the N^{14} quadrupole coupling in this molecule may be determined as minus 3.83 Mc. The difference between this value and the value minus 3.63 Mc found for ClCN is not much larger than the sum of expected experimental errors in each, but it is thought to be significant.

Values of B_0 used to compute theoretical frequencies in Table VI are 4120.19 Mc and 4096.76 Mc, respectively, for $Br^{79}CN$ and $Br^{81}CN$. From these, internuclear distances may be computed as 1.158A for the C−N distance, and 1.790A for the Br−C distance. This computation again neglects the effect of zero-point vibrations, and as a consequence, the difference between the C−N distance obtained for BrCN, and that obtained for ClCN (see Table V) may not be significant.

Intensity and half-width of the $Br^{81}CN$ $5/2\rightarrow7/2$ and $7/2\rightarrow9/2$ line were measured at room temperature. The peak intensity was found to be $6.0\pm1\times10^{-5}$ cm^{-1} for a plane wave and the half-width equivalent to 42 ± 6 Mc for one-mm Hg gas pressure. Taking the value 2.94 Debye units[19] for the dipole moment of BrCN and using the measured half-width, expression (2) gives a theoretical intensity of $7.2\pm1\times10^{-5}$ cm^{-1}.

CYANOGEN IODIDE

A pure rotation transition of ICN was first reported by Gordy, Smith, Smith, and Ring,[22] who measured the $J=4\rightarrow5$ transition and gave a value 260×10^{-40} g cm^2 for the moment of inertia and 2070 ± 20 Mc for the quadrupole coupling. In

TABLE VII. Lines due to $J=3\rightarrow4$ transition of ICN.

Designation of line	Measured frequency in megacycles	Theoretical frequency including first- and second-order effects of iodine quadrupole	Theoretical intensity relative to $11/2\rightarrow13/2$ line
$v_2=2$, $l=2$			
$11/2\rightarrow13/2$	26046.32	26046.21	0.088
$5/2\rightarrow5/2$	25991.92	25991.58	0.14
$3/2\rightarrow3/2$	25969.58	25969.55	0.092
$7/2\rightarrow7/2$	25954.36	25954.24	0.16
$v_2=1$, l_2			
$11/2\rightarrow13/2$	25927.66	25927.79	0.21
$v_2=1$, l_1			
$11/2\rightarrow13/2$	25906.28	25906.29	0.21
$v_2=1$, l_2			
$9/2\rightarrow11/2$	25893.73	25893.56	0.16
$v_2=1$, l_1			
$9/2\rightarrow11/2$	25872.24	25872.06	0.16
$v_2=1$, l_2			
$7/2\rightarrow9/2$	25850.78	25850.48	0.12
$9/2\rightarrow11/2$	25837.64	25837.71	0.76
$v_2=1$, l_1			
$7/2\rightarrow9/2$	25829.31	25828.98	0.12
$11/2\rightarrow13/2$	25823.08	25823.08	1.00
$v_2=1$, l_1			
$3/2\rightarrow5/2$	25815.34	25815.55	0.058
$v_2=1$, l_1			
$5/2\rightarrow7/2$	25802.92	25803.34	0.085
$9/2\rightarrow9/2$	25789.85	25789.88	0.15
$7/2\rightarrow9/2$	25783.50	25783.56	0.56
$v_1=1$			
$9/2\rightarrow11/2$	25763.23	25763.06	0.076
$1/2\rightarrow3/2$	25752.65	25752.73	0.18
$v_1=1$			
$11/2\rightarrow13/2$	25748.18	25748.43	0.10
$5/2\rightarrow7/2$	25728.77	25728.73	0.40
$3/2\rightarrow5/2$	25711.50	25711.53	0.28
$11/2\rightarrow11/2$	25393.87	25393.69	0.097

terms of the quadrupole coupling constant as defined here, their value is 2588 ± 25 Mc. The value of B obtained from a moment of inertia 260×10^{-40} g cm^2 is 3230 Mc. The $J=3\rightarrow4$ transmission has been measured here with more accuracy than that obtained by earlier measurements, and the various components have been somewhat more thoroughly analyzed. Values of the molecular constants found here are consistent with those given by Gordy, Smith, Smith, and Ring, except that the value of quadrupole coupling constant obtained is considerably outside of their quoted experimental error.††† This may be due to the presence of second-order effects which were not recognized in these early measurements.‡ Table VII lists the measured line frequencies and the theoretical frequencies and relative intensities. Rather rough relative intensity measurements which were made agreed with the theoretical values listed in the table.

As in the case of BrCN, the further line splitting due to the N^{14} quadrupole is ignored in ICN, the lines having been measured under relatively low resolution conditions. Their positions may be shifted in some cases as much as 0.1 Mc by effects of the nitrogen nucleus, but since this is about the accuracy of measurement, these shifts have not been taken into account. In some cases rather large shifts are contributed by second-order effects because of the large size of the iodine quadrupole coupling. A more detailed statement of these second-order effects has been given elsewhere.[20] The two lines of the ground state $7/2\rightarrow9/2$ and $9/2\rightarrow9/2$ should coincide so far as first-order effects of the iodine quadrupole are concerned. Actually they are separated by 6.35 megacycles due to second-order effects. The separation between the two intense lines $11/2\rightarrow11/2$ and $11/2\rightarrow13/2$ is very large (429.21 Mc) and allows a rather accurate determination of the iodine quadrupole coupling constant, minus 2420 Mc.

A considerable number of lines due to molecules in the excited bending mode ($v_2=1$) are listed in Table VII. The value of α_2 obtained is minus 9.501 Mc and the l-type doubling constant q equals 2.688 Mc. Second-order quadrupole effects are again in evidence and are somewhat larger than for the ground state because non-zero matrix elements exist between rotational states with J values differing by only one as well as those for J values differing by two which occur in the ground state case.

One line is listed which is due to molecules doubly excited in the bending mode ($v_2=2$). In this case, the theory of Nielsen and Shaffer[8] shows that the three degenerate levels with $v_2=2$ form two states for which the angular momentum l about the molecular axis is $2\hbar$, and one state with this angular momentum equal to zero. The l-type doubling for the two states with $l=2$ is less by a factor B/ω_2 than the doubling when $l=1$, and hence is not observed. The strongest line due to this excited vibrational state, $v_2=2$, is therefore the transition $11/2\rightarrow13/2$ when $l=2$, and its measured position agrees well with that predicted

††† Very recent measurements by Gordy *et al.* [A. G. Smith, H. Ring, W. V. Smith, and W. Gordy, Phys. Rev. **74**, 370 (1948)] show very good agreement with results presented here.

‡ Cf. O. R. Gilliam, H. D. Edwards, and W. Gordy, Phys. Rev. **73**, 635 (1948).

by using the molecular constants determined from other states. Second-order quadrupole effects must again be taken into account. Several weak lines between 25,800 Mc and 26,000 Mc were found which coincide approximately with other transitions of molecules in the states $v_2=2$, $l=2$, and $v_2=2$, $l=0$, but these were not accurately measured and hence are not included in Table VII.

Peak intensity of the strongest line (11/2 $\rightarrow$13/2) was measured at room temperature and found to be $8.7\pm1\times10^{-5}$ cm^{-1}. Half-width of this same line was 4.0 ± 0.6 Mc when the gas was in equilibrium with a trap at zero degrees centigrade. From the measurements of Ketelaar and Kruger[23] this would represent a vapor pressure of 0.10 mm Hg, so that the half-width at one mm Hg pressure would be 40 ± 6 Mc. Unfortunately, ICN attacked the mercury in a McCleod gauge so rapidly that no direct measurement of vapor pressure could be made. Using a value of 3.72 Debye units for the dipole moment, expression (2) gives a theoretical peak intensity $10\pm1.4\times10^{-5}$ cm^{-1}.

Since only one isotopic variety of ICN was measured, the two internuclear distances cannot be determined from the microwave measurements on this molecule alone. If the value 1.158A found above for BrCN is taken as the C$-$N distance, then the I$-$C distance may be determined as 1.995A.

PREPARATION OF SUBSTANCES MEASURED

The OCS used in this work was prepared by the acid hydrolysis of aqueous alkali thiocyanate.[24] In the case of OC^{13}S, 5 g KCN of 21.4 atom percent C^{13}, obtained from the Eastman Kodak Company, was converted to thiocyanate by dissolving it in a freshly boiled mixture of 3 g sulfur and 10 cc distilled water and maintaining the solution at 60°C under an atmosphere of nitrogen for two days with occasional agitation. The resulting solution was cooled to 0°C and poured rapidly into a mixture at 0°C of 100 g H_2SO_4 and 50 cc H_2O. The mixture was allowed to warm slowly to 40°C over three hours with occasional agitation, the OCS slowly evolved being bubbled through 15 cc of a 30 percent NaOH solution cooled to 0°C, and condensed in a trap cooled with dry ice—acetonic mixture. In the case of O^{18}CS, the thiocyanate solution consisted of 7 g NH_4SCN dissolved in 5 cc of H_2O of 1.5 atom percent O^{18} obtained from the Atomic Energy Commission, and the acid solution was prepared by saturating 15 cc of the same water, cooled to -15°C with an ice-salt mixture, with HCl obtained by slowly dropping 100 g concentrated H_2SO_4 on 60 g NaCl moistened with ordinary water. The remainder of the procedure was the same, ordinary water being used for the NaOH solution.

The ClCN was prepared[25] by the action of Cl_2 on KCN in the presence of Zn^{++}. In the case of ClC^{13}N, 5 g of the same KCN as was used for the preparation of OC^{13}S, and 5 g of $ZnSO_4\cdot7\,H_2O$, were dissolved in 25 cc H_2O, and through the solution cooled to 0°C was passed a slow stream of Cl_2 from a commercial cylinder. When the solution was saturated with Cl_2, it was slowly warmed to 40°, a very slow stream of Cl_2 being maintained, and the evolved ClCN was passed over anhydrous $CaCl_2$ and collected in a U-tube cooled to -10°C with an ice-salt mixture.

The ICN was prepared by the method of Comastri[26] as described in Chemical Abstracts.

The BrCN was purchased from the Eastman Kodak Company.

SUMMARY

The microwave measurements described above allow determination of a number of molecular and nuclear quantities. Many of these are summarized in Tables VIII to XI.

Although line widths may eventually give considerable information about intermolecular forces, half-widths have been investigated here primarily with a view to checking theoretical intensities and to provide some basis for estimation of line intensities in the microwave region. Line half-widths (total widths at half-maximum absorption) are listed in Table VIII for a number of molecules. For the linear molecules there appears to be a rough correlation between line

[23] J. A. A. Ketelaar and S. Kruger, Rec. Trav. Chim. **62**, 550 (1943).

[24] See, e.g., A. Stock, W. Siecke, and E. Pohland, Ber. d. D. chem. Ges. **57**, 719 (1924).

[25] See, e.g., A. Klemenc and G. Wagner, Zeits. f. anorg. allgem. Chemie **235**, 427 (1938).

[26] H. T. Comastri, Anales Asoc. Quim. Argentina **27**, 45 (1939); Chem. Abs. **33**, 6743 (1939).

TABLE VIII. Measured half-width (total width at half-maximum intensity) of lines near 1 cm wave-length.

Molecule	Dipole moment in debye units	Frequency of line in megacycles	Half-width at pressure of 1 mm Hg
ICl^{35}*	approx. 0.65	27337	11±2
$O^{16}C^{12}S^{32}$	0.72	24526	12±2
$Cl^{35}C^{12}N^{14}$	approx. 2.5	23885	50±8
$Br^{81}C^{12}N^{14}$	2.94	24574	42±6
$I\ C^{12}N^{14}$	3.71	25823	40±6
$N^{14}H_3$**	1.45	23870	59±2
H_2O***	1.84	22235	14±3

* C. H. Townes, B. D. Wright, and F. R. Merritt, Phys. Rev. **73**, 1334 (1946).
** C. H. Townes, Phys. Rev. **70**, 665 (1946); B. Bleaney and R. P. Penrose, Proc. Roy. Soc. **189**, 358 (1947).
*** C. H. Townes and F. R. Merritt, Phys. Rev. **70**, 558 (1946).

width and dipole moment of the molecule. The line widths for ammonia and water are included, however, to show that other types of molecules show wide deviations from this behavior. The 3,3-line of ammonia, which has a dipole of moderate size, displays the largest half-width, whereas water, with a somewhat larger dipole moment, produces a line in the microwave region with an exceptionally small half-width. Using the half-widths determined here, intensities of lines measured correspond within experimental error (about 20 percent) to the theoretical expectations.

Molecular rotational constants for the molecules OCS, ClCN, BrCN, and ICN are given in Table IX. The last column in this table gives a value of the *l*-type doubling constant q obtained from the theory of Nielsen and Shaffer.[8] The result given in their paper as noted earlier[9] involved a numerical error of a factor of two, so that their theoretical value of q is actually $2B/\omega_2$.‡‡ A distinct and consistent disagreement between the theoretical and experimental values of q are shown by the table. There appears to be remarkable uniformity in the values of α_1 and α_2 found for these molecules, which is somewhat surprising considering the dependence of the α's on anharmonic force constants.

Internuclear distances determined are listed in Table X. In several cases these distances are averages of the values obtained from various pairs of isotopes. Uncertainties in these distances as discussed above are primarily due to the effects of zero-point vibration, which are rather difficult to determine completely. An accuracy near 0.001A rather than 0.01A in these distances could generally be obtained if the zero-point vibration effects could be determined.

Various nuclear quadrupole coupling constants $[eQ(\partial^2V/\partial z^2)$ or $eqQ]$ obtained from the present measurements are given in Table XI, as well as estimates of $\partial^2V/\partial z^2$ and Q derived from these values. The basis on which $\partial^2V/\partial z^2$ is obtained has been previously discussed.[27] The quadrupole moment evaluated by this method for Cl^{35} agrees reasonably well with the value $-7.9\pm0.2\times10^{-26}$ cm^2 recently obtained from molecular-beam measurements on atomic chlorine.[28] The quadru-

TABLE IX. Molecular rotational constants. (All quantities are expressed in megacycles.)

Molecule	B_0	α_1	α_2	α_3	q (*l*-type doubling constant)	Theoretical value of q
$O^{16}C^{12}S^{32}$	6081.480±0.005*	18.12±0.06[a,c]	−10.59±0.02	55.1	6.393±0.013	4.70
$O^{16}C^{12}S^{33}$	6004.918±0.02					
$O^{16}C^{12}S^{34}$	5932.843±0.01		−10.37±0.06[a]		6.07±0.06[a]	
$O^{16}C^{13}S^{32}$	6061.923±0.015					
$O^{16}C^{13}S^{34}$	5911.730±0.03					
$O^{16}C^{14}S^{32}$	6043.25 ±0.25[b]		−9.4 0.3[b]		6.7±0.1[b]	
$O^{18}C^{12}S^{32}$	5704.825±0.015					
$Cl^{35}C^{12}N^{14}$	5970.820±0.02		−16.39±0.02		7.500±0.015	5.98
$Cl^{37}C^{12}N^{14}$	5847.260±0.02					
$Cl^{35}C^{13}N^{14}$	5939.775±0.03					
$Cl^{37}C^{13}N^{14}$	5814.705±0.03					
$Br^{79}C^{12}N^{14}$	4120.190±0.02	11.36±0.05	−11.49±0.02		3.912±0.02	3.07
$Br^{81}C^{12}N^{14}$	4096.760±0.02	11.23±0.05	−11.49±0.02		3.845±0.02	
$I^{127}C^{12}N^{14}$	3225.527±0.02	9.33±0.02	−9.501±0.01		2.688±0.01	2.16

* B_e=6107.5.
[a] C. H. Townes and S. Geschwind, Phys. Rev. **74**, 626 (1948).
[b] Arthur Roberts, Phys. Rev. **73**, 1405 (1948).
[c] Arthur Roberts, private communication.

‡‡ Professor Nielsen has kindly confirmed by private communication that this is the correct result of his theoretical treatment.

[27] C. H. Townes, Phys. Rev. **71**, 909 (1947).
[28] L. Davis, B. T. Feld, C. W. Zabel, and J. R. Zacharias, Phys. Rev. **73**, 525 (1948).

TABLE X. Internuclear distances. These are effective distances in ground vibrational state, and error in each is probably less than 0.01A. The I−C distance in ICN is obtained by assuming 1.158 for the C−N distance; for other molecules both distances are determined by use of isotopic pairs of moments of inertia.

Molecule	Nuclei	Distance in angstroms
OCS	O−C	1.161
OCS	C−S	1.561
ClCN	Cl−C	1.629
ClCN	C−N	1.163
BrCN	Br−C	1.790
BrCN	C−N	1.158
ICN	I−C	1.995

TABLE XI. Quadrupole coupling constants and values of Q.

Molecule	Nucleus	Quadrupole coupling constant $[eqQ=e(\partial^2V/\partial z^2)Q]$ in megacycles	Atomic orbital approximation to $\partial^2V/\partial z^2$ in e.s.u.	Nuclear quadrupole moments Q in units 10^{-24} cm^2
OCS	S^{33}	−28.5 ±0.7*	$\sim 7\times10^{15}$	~ -0.05
OCS	S^{34}	<1	$\sim 7\times10^{15}$	<0.002
OCS	O^{18}	<1	$\sim 3\times10^{15}$	<0.004
ClCN	Cl^{35}	−83.2 ±0.5	17×10^{15}	−0.066
ClCN	Cl^{37}	−65.7 ±0.5	17×10^{15}	−0.052
BrCN	Br^{79}	686.5 ±0.5	34×10^{15}	0.28
BrCN	Br^{81}	573.5 ±0.5	34×10^{15}	0.23
ClCN	N^{14}	−3.63±0.1	$\sim -3\times10^{15}$	~0.02
BrCN	N^{14}	−3.83±0.08		
ICN	N^{14}	−3.80**		
ICN	I^{127}	−2420±1	45×10^{15}	−0.75

* C. H. Townes and S. Geschwind, Phys. Rev. **74**, 626 (1948).
** Smith, Ring, Smith, and Gordy, Phys. Rev. **73**, 633 (1948).

pole moment given here for iodine is somewhat larger than the value -0.45 ± 0.15 obtained from atomic spectra. A comparison of the various quadrupole coupling constants obtained by microwave spectroscopy for N^{14} in various molecules appears to give good evidence that the nitrogen bonds show considerable $s-p$ hybridization, and it is on this basis that the value of $\partial^2V/\partial z^2$ is obtained from Table XI. Although nitrogen is not an atom heavy enough to provide a favorable case for the application of the atomic orbital approximation, it is believed that at least the sign and approximate magnitude of the nitrogen quadrupole moment have been correctly obtained. Similarly, in the case of S^{33}, the character of the C−S band is quite uncertain, but the sign and approximate magnitude of the S^{33} quadrupole moment given here should be correct. It is expected that evaluation of $\partial^2V/\partial z^2$ will be discussed more fully in a later paper.

No quadrupole splitting was observed for the molecules $O^{18}C^{12}S^{32}$ or $O^{16}C^{12}S^{34}$, and in these cases the upper limit to the value of the quadrupole coupling constant which would have produced a noticeable splitting is given in Table XI. Since both oxygen and sulfur in this molecule have an incomplete shell of penetrating electrons, the value of $\partial^2V/\partial z^2$ may be expected to be rather large, so that the failure to observe quadrupole splitting indicates that the nuclear quadrupole moments of O^{18}, S^{34} are very small. This is evidence that the spins of O^{18} and S^{34} are zero, since spins of either 0 or 1/2 necessitate zero quadrupole moments. If, for example, S^{34} had a spin of one or two, a quadrupole coupling constant of approximately the same size as for the chlorine nuclei or for S^{33} might be expected, instead of a coupling constant less than one-thirtieth as large. However, more measurements of quadrupole moments and coupling constants must be made before one can be sure that small values are unlikely even with spins greater than one-half.

No interactions of the type $c\mathbf{I}\cdot\mathbf{J}$ due to coupling between the nuclear magnetic moment and a molecular field were observed, but interactions of this type as small as those reported by Nierenberg and Ramsey[29] in the alkali halides may be present and undetected.

ACKNOWLEDGMENT

The authors wish to express their appreciation for the interest and assistance of many members of the Bell Telephone Laboratories, and in particular of Dr. S. O. Morgan, Dr. J. Bardeen, and Mr. W. H. Hewitt.

[29] W. A. Nierenberg and N. F. Ramsey, Phys. Rev. **72**, 1075 (1947).

PHYSICAL REVIEW VOLUME 74, NUMBER 9 NOVEMBER 1, 1948

Electrostrictive Effect in Barium Titanate Ceramics

W. P. MASON
Bell Telephone Laboratories, Murray Hill, New Jersey
(Received June 24, 1948)

When a direct current bias is applied to a multicrystalline barium titanate ceramic, an alternating voltage can excite resonances in the ceramic. Four modes of motion have been excited—a longitudinal mode at right angles to the applied field, a radial mode of a circular plate at right angles to the applied field, a thickness longitudinal mode, and a thickness shear mode. The first three are excited when the a.c. field is applied in the same direction as the d.c. polarization, but the fourth is excited when the a.c. field is at right angles to the d.c. polarization. The amount of motion is larger than in magnetostrictive materials, and it appears that barium titanate may be an important electromechanical transducing element.

All of these modes can be accounted for on the basis of a second-order electrostrictive effect. Two electrostrictive constants are involved and these have been evaluated as

$$Q_{12} = -2.15 \times 10^{-12} (\text{cm}^4/(\text{statcoulombs})^2);$$
$$Q_{11} = +6.9 \times 10^{-12} (\text{cm}^4/(\text{statcoulombs})^2).$$

Using these constants, the measured electromechanical coupling factors for the four modes are evaluated, and these compare well with the calculated values.

A theoretical explanation of this effect is given which depends on the fact that when a given domain becomes ferro-electric it loses its cubic structure and becomes tetragonal. In this process it expands one percent along the tetragonal axis and contracts one-half percent along the other two axes. In the ceramic piece all directions for the tetragonal axis are equally probable, but an applied field can cause the domains in the direction of the field to grow at the expense of domains perpendicular to the field. This growth is accompanied by an increase in the thickness of the crystal and a decrease in radial dimensions. The measured ratio of 3 to 1, compared to the 2 to 1 ratio observed by x-rays for a single crystal, is accounted for by the nature of the ceramic material which does not join up for all grains. This does not prevent the ceramic from increasing in thickness but does cut down the radial contraction.

Experimental measurements of the electrostrictive effect are given, and it is shown that the displacement is proportional to the square or products of the electric displacements in the ceramic.

I. INTRODUCTION

WHEN an electric field or electric displacement is applied or generated in a solid dielectric, a change in shape occurs which is proportional to the square of the voltage or electrical displacement. Electrostrictive effects are usually very feeble compared to first-order piezoelectric effects that occur in many crystalline materials. However, in the case of the ferro-electric materials rochelle salt and barium titanate, electrostrictive effects[1,2] may be quite large and are of considerable interest. The thickness expansion is about as large as can be obtained by the direct piezoelectric effect in rochelle salt and is somewhat larger than can be obtained with magnetostrictive materials. Furthermore, the variations of the properties of barium titanate with temperature are not nearly as large as for rochelle salt. Hence such materials may be of use for various types of transducers. If the alternating variations are small compared to the d.c. polarization, a remanent polarization is sufficient to keep the device operative. However, for the largest displacements or voltages, the remanent polarization may become discharged and it is necessary to put on a steady d.c. biasing voltage to make the device operative.

[1] In the present paper, a strain that is proportional to the square or product of two fields or electric displacements is called an electrostrictive strain. This is contrary in some cases to a usage started by Mueller, who calls the square term a "quadratic piezoelectric effect" when it depends on a strain caused by a spontaneous polarization or an applied field acting on a piezoelectric constant. On this definition the strain in rochelle salt that is proportional to the square of the electric displacement would be a "quadratic piezoelectric effect" because it depends on the orthorhombic crystal becoming monoclinic in the ferro-electric region and generating new piezoelectric constants which give a strain proportional to the spontaneous polarization times the applied electric displacement. The electrostrictive effect in barium titanate is not of this type (see reference 2) and is in every way the analog of a magnetostrictive effect in a ferromagnetic material.

[2] W. P. Mason, Phys. Rev. **73**, 1398 (1948).

II. METHODS FOR MEASURING THE FUNDAMENTAL CONSTANTS

When a constant voltage bias is applied to a multicrystalline barium titanate ceramic, an alternating voltage can excite resonances in the ceramic. There are four effects that have been measured. These are a radial vibration of a disk

of the material,[3] a length vibration of a bar cut from such a disk, a thickness vibration in the direction of the applied field,[4] and a thickness shear mode.[5] The first three motions are excited when the d.c. field is applied in the same direction as the a.c. field, while the fourth is excited when the d.c. polarization is at right angles to the a.c. field. Since, if there are two sets of plates at right angles to each other, the a.c. field cannot be made uniform through its direction of application, this mode has to be excited by exciting a remanent polarization by the d.c. field and then taking off the plating in this direction. In fact for all of these modes the d.c. biasing voltage can be applied and then taken off and the device will still operate by means of the remanent polarization.

A typical method for measuring such resonances is shown by Fig. 1. Here a source of high voltage, such as a high voltage transformer and rectifying tube, with the output connected through high resistances, is put directly on the ceramic piece, while the a.c. voltage is applied through two 4-microfarad condensers in series. At the resonant frequencies of the ceramic, which are usually above 100 kilocycles, the impedances of the condensers are less than 1 ohm while the shunt impedance of the high voltage source being 10 megohms is much higher than the impedance of the ceramic. Hence by this method one obtains a measure of the electrical impedance of the ceramic and can determine the effect of putting a high electrical bias on it.

If one measures the impedance of a freshly made ceramic on which no electrical bias has been placed, the impedance is that of a condenser and no resonances can be excited. However, if one puts a bias of 30,000 volts per centimeter on the ceramic disk of the material, for example, having the dimensions

$$\text{radius } a=2.5 \text{ cm}; \quad \text{thickness } t=0.025 \text{ cm}, \quad (1)$$

Fig. 2 shows a measurement of the resonant and antiresonant frequencies as a function of the applied voltage, as the voltage bias is decreased to $-30{,}000$ volts per cm. Upon reversing the

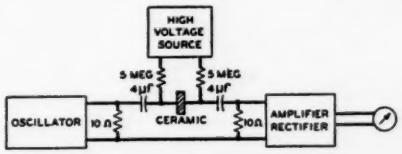

FIG. 1. Measuring circuit for studying resonances and electromechanical coupling factors in barium titanate ceramics.

direction of the bias the ascending curves shown are obtained. It is obvious that we are dealing with a hysteretic material for which the previous history determines the response. Since the electric displacement follows a similar hysteresis curve when plotted against the voltage, it is obvious that the response is determined by the electric displacement rather than the electric field. When the field is reduced to zero a polarization remains and this determines the resonant and antiresonant frequencies of the material.

From the data of Fig. 2 and the measured dielectric constant shown by Fig. 3, one can calculate the electromechanical coupling (which determines the percentage of energy stored in mechanical form to the total input electrical energy), the electrostrictive constant, and the value of the elastic constant controlling the radial vibrations. The method for deriving the fundamental elastic, electrostrictive, and electromechanical coupling constants for radial vibrations is discussed in the appendix. It is shown that the resonant frequency for a material having a Poisson's ratio 0.27, which is near that for

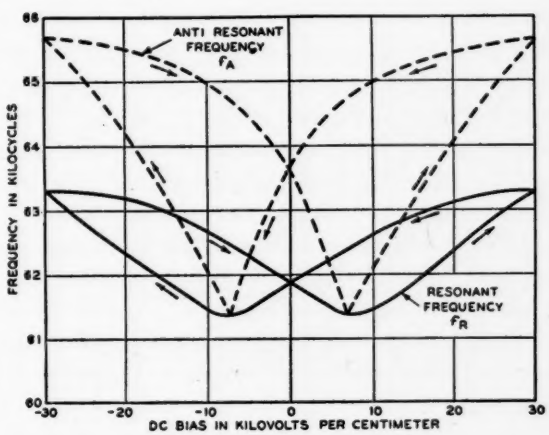

FIG. 2. Resonant and antiresonant frequencies as a function of the biasing voltage for a disk 5 centimeters in diameter.

[3] Shepard Roberts, Phys. Rev. **71**, 890–895 (1947).
[4] W. P. Mason, Phys. Rev. **72**, 869 (1947).
[5] W. L. Cherry, Jr. and Robert Adler, Phys. Rev. **72**, 981 (1947).

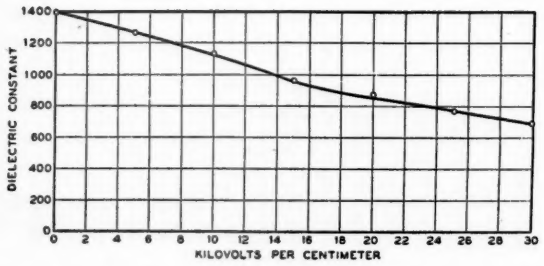

FIG. 3. Dielectric constant at room temperature as a function of the biasing voltage.

barium titanate, is given by the equation

$$f_R=\frac{2.03}{2\pi a}\left(\frac{Y_0}{\rho(1-\sigma^2)}\right)^{\frac{1}{2}}, \tag{2}$$

where a is the radius, Y_0=Young's modulus, ρ=density, and σ-Poisson's ratio. In the disk whose data are given by Fig. 2, $a=2.5$ cm, $\rho=5.5$, and $\sigma=0.27$. Hence the value of Young's modulus for zero biasing field is 1.12×10^{12} dyne/cm^2. The value of Young's modulus is increased slightly with bias, being 1.18×10^{12} at 30,000 volts per centimeter.

It is shown in the appendix that the electromechanical coupling factor k is determined in terms of the separation of resonance and antiresonance frequency, Δf, the resonant frequency f_R, the first root R, of the frequency determining equation, i.e., $R_1=2.03$, and the value of Poisson's ratio by the equation

$$k^2=\frac{\Delta f}{f_R}\left[\frac{R_1^2-(1-\sigma^2)}{1+\sigma}+\cdots\right]. \tag{3}$$

For $\sigma=0.27$, the value of the factor multiplying $\Delta f/f_R$ is equal to 2.51. Hence from the data of Fig. 2, the electromechanical coupling factor can be calculated and is shown plotted by Fig. 4. It follows a regular hysteresis loop, indicating that the remanent polarization is annulled when the voltage gradient is about 7500 volts per cm negative. For a smaller initial polarizing field, the coercive field is less.

These results indicate that for an applied d.c. voltage, since the strain is proportional to the square of the electric displacement, if we plot it against the field, the characteristic butterfly loop of a hysteretic material will result as shown by Fig. 5. Actual d.c. measurements with a bimorph unit with the field applied to only one side give values which follow this type of curve very well. The calculated constant comes very close to that measured by a.c. measurements as discussed in the next section.

Similar a.c. measurements have been made for the thickness longitudinal mode, the thickness shear mode, and the longitudinal length mode, and the coupling factors are shown plotted by Fig. 4. The frequency constant for the longitudinal thickness mode for a zero bias is 2550 kilocycle-millimeters. From this one obtains the elastic constant from the formula

$$f=(1/2t)[(\lambda+2\mu)/\rho]^{\frac{1}{2}} \tag{4}$$

as

$$(\lambda+2\mu)=1.42\times10^{12}\ \text{dynes/cm}^2. \tag{5}$$

This and the value of Young's modulus

$$Y_0=1.13\times10^{12}\ \text{dynes/cm}^2$$
$$=\mu(3\lambda+2\mu)/(\lambda+\mu) \tag{6}$$

allow one to solve for the two Lame' elastic constants. These are

$$\lambda=5.2\times10^{11}\ \text{dynes/cm}^2;$$
$$\mu=4.5\times10^{11}\ \text{dynes/cm}^2, \tag{7}$$

and from these the values of Poisson's ratio is

$$\sigma=\lambda/2(\lambda+\mu)=0.27 \tag{8}$$

as quoted above.

To obtain the thickness shear mode, one has to polarize the ceramic in one direction and then remove the plating. An a.c. field perpendicular to this will generate a thickness shear mode with a coupling shown by the single point of Fig. 4.

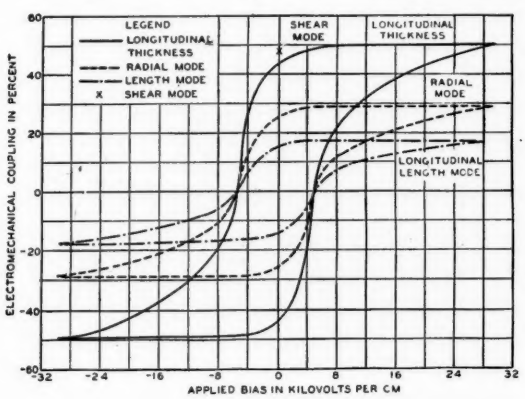

FIG. 4. Electromechanical coupling factors for four modes of motion.

III. PHENOMENOLOGICAL THEORY OF ELECTROSTRICTIVE EFFECT IN BARIUM TITANATE CERAMICS

Since in a barium titanate ceramic any crystal symmetry is lost by the distribution of crystal axes in all directions, any first-order piezoelectric effects are annulled and all the modes of motion must be due to second-order electrostrictive effects. In the experiments of Section II it was shown that the electromechanical coupling was determined by the electric displacement rather than the electric field, so that we take as the independent variable the stresses and the electric displacements. All the measurements were made under adiabatic conditions so that all constants can be considered as adiabatic.

In terms of a tensor notation the internal energy residing in the body can be expressed in the form

$$dU=T_{ij}dS_{ij}+E_m\frac{dD_m}{4\pi}+TdS, \qquad \begin{matrix} i,j=1,2,3 \\ m=1,2,3 \end{matrix} \tag{9}$$

where T_{ij} are the six stress components, S_{ij} the six strain components, E_m the fields, and D_m the electric displacements, T the absolute temperature, and S the entropy. The strain components are defined in the usual tensor form

$$S_{ij}=\frac{1}{2}\left(\frac{\partial u_i}{\partial x_j}+\frac{\partial u_j}{\partial x_i}\right), \tag{10}$$

where u_i are the displacements along the x_i axes. In order to avoid using the factor $1/4\pi$, we made the substitution

$$\delta_m=D_m/4\pi. \tag{11}$$

δ_m is then measured in statcoulombs per square centimeter.

For the present purpose, since we are going to take T_{ij}, δ_m, and S as the fundamental variables, we introduce a potential H_1, called the elastic enthalpy, defined by the equation

$$H_1=U-S_{ij}T_{ij}. \tag{12}$$

Hence

$$dH_1=-S_{ij}dT_{ij}+E_md\delta_m+TdS, \tag{13}$$

and

$$S_{ij}=-\partial H_1/\partial T_{ij};\quad E_m=\partial H_1/\partial\delta_m;\quad T=\partial H_1/\partial S. \tag{14}$$

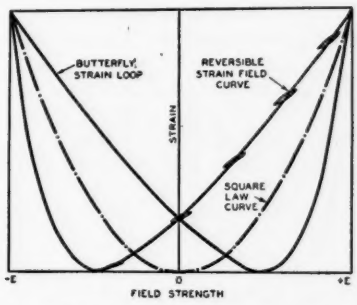

FIG. 5. Strain field relations.

Since for adiabatic conditions S does not vary, the dependent variables of interest, S_{ij} and E_m, can be written in the form

$$S_{ij}(T_{kl},\delta_n);\quad E_m(T_{kl},\delta_n). \tag{15}$$

Expanding these functions about the position of zero strain and zero electric field, we have up to second-order terms

$$S_{ij}=\frac{\partial S_{ij}}{\partial T_{kl}}dT_{kl}+\frac{\partial S_{ij}}{\partial\delta_n}d\delta_n+\frac{1}{2!}\left[\frac{\partial^2 S_{ij}}{\partial T_{kl}\partial T_{qr}}dT_{kl}dT_{qr}+2\frac{\partial^2 S_{ij}}{\partial T_{kl}\partial\delta_n}dT_{kl}d\delta_n+\frac{\partial^2 S_{ij}}{\partial\delta_n\partial\delta_o}d\delta_nd\delta_o\right]+\cdots$$

$$E_m=\frac{\partial E_m}{\partial T_{kl}}dT_{kl}+\frac{\partial E_m}{\partial\delta_n}d\delta_n+\frac{1}{2!}\left[\frac{\partial E_m}{\partial T_{kl}\partial T_{qr}}dT_{kl}dT_{qr}+2\frac{\partial^2 E_m}{\partial T_{kl}\partial\delta_n}dT_{kl}d\delta_n+\frac{\partial^2 E_m}{\partial\delta_n\partial\delta_o}d\delta_nd\delta_o\right]+\cdots. \tag{16}$$

For the present purpose some of these partial derivates can be set equal to zero. Since there is no direct piezoelectric effect on account of the uniform distribution of the crystals in all directions

$$\frac{\partial S_{ij}}{\partial\delta_n}=-\frac{\partial^2 H_1}{\partial\delta_n\partial T_{ij}}=-\frac{\partial^2 H_1}{\partial T_{ij}\partial\delta_n}=-\frac{\partial E_m}{\partial T_{ij}}=0. \tag{17}$$

Furthermore the ceramic can be described as soft electrically but not mechanically. Hence not much change in the elastic constants with stress will occur and $\partial^2 S_{ij}/\partial T_{kl}\partial T_{qr}=0$. There is a slight change of elastic constants with electric displacement as shown by Fig. 2, but it is small

TABLE I. Terms not ruled out by symmetry in the isotropic case.

	δ_1^2	$\delta_1\delta_2$	$\delta_2\delta_1$	$\delta_1\delta_3$	δ_2^2	$\delta_3\delta_1$	$\delta_2\delta_3$	$\delta_3\delta_2$	δ_3^2
S_{11}	Q_{1111}	0	0	0	Q_{1122}	0	0	0	Q_{1122}
S_{12}	0	$Q_{1111}-Q_{1122}$	$Q_{1111}-Q_{1122}$	0	0	0	0	0	0
S_{21}	0	$Q_{1111}-Q_{1122}$	$Q_{1111}-Q_{1122}$	0	0	0	0	0	0
S_{13}	0	0	0	$Q_{1111}-Q_{1122}$	0	$Q_{1111}-Q_{1122}$	0	0	0
S_{22}	Q_{1122}	0	0	0	Q_{1111}	0	0	0	Q_{1122}
S_{31}	0	0	0	$Q_{1111}-Q_{1122}$	0	$Q_{1111}-Q_{1122}$	0	0	0
S_{23}	0	0	0	0	0	0	$Q_{1111}-Q_{1122}$	$Q_{1111}-Q_{1122}$	0
S_{32}	0	0	0	0	0	0	$Q_{1111}-Q_{1122}$	$Q_{1111}-Q_{1122}$	0
S_{33}	Q_{1122}	0	0	0	Q_{1122}	0	0	0	Q_{1111}

and is neglected here. Hence we can set

$$\frac{\partial^2 S_{ij}}{\partial T_{kl}\partial\delta_n}=-\frac{\partial^3 H_1}{\partial T_{kl}\partial\delta_n\partial T_{ij}}=-\frac{\partial^3 H_1}{\partial T_{ij}\partial T_{kl}\partial\delta_n}$$

$$=-\frac{\partial E_m}{\partial T_{ij}\partial T_{kl}}=0. \quad (18)$$

This leaves only three second-order partial derivatives, two of which are related, and these we designate as

$$\frac{\partial^2 S_{ij}}{\partial\delta_n\partial\delta_o}=-\frac{\partial^3 H_1}{\partial\delta_n\partial\delta_o\partial T_{ij}}=-\frac{\partial^3 H_1}{\partial T_{ij}\partial\delta_n\partial\delta_o}$$

$$=-\frac{\partial^2 E_m}{\partial T_{ij}\partial\delta_n}=2Q_{ij\,no}; \quad (19)$$

$$\frac{\partial^2 E_m}{\partial\delta_n\partial\delta_o}=O_{mno}.$$

The two remaining first-order derivatives of Eq. (16) determine the elastic compliances and dielectric impermeabilities according to the equations

$$\frac{\partial S_{ij}}{\partial T_{kl}}=s^D{}_{ijkl}; \quad \frac{\partial E_m}{\partial\delta_n}=\beta^T{}_{mn}, \quad (20)$$

where $s^D{}_{ijkl}$ are the elastic compliance constants measured at constant electric displacement and $\beta^T{}_{mn}$ are the dielectric "impermeability" constants (inverse of dielectric constants) measured at constant stress. For the most general case there are 21 components of $s^D{}_{ijkl}$ and 6 of the impermeability constants. For the isotropic case considered here, symmetry conditions insure that there are only two elastic compliances and one dielectric impermeability. For the most general case there are 36 components of the electrostrictive tensor $Q_{ij\ no}$ and 27 for the correction O_{mno} to the dielectric constant. For the isotropic condition, the off diagonal term of the type

$$Q_{1122}=\frac{\partial^2 S_{11}}{\partial\delta_2{}^2} \quad \text{and} \quad Q_{2211}=\frac{\partial^2 S_{22}}{\partial\delta_1{}^2} \quad (21)$$

are obviously equal since the expansion along x_1 for an electric field along x_2 is equal to an expansion along x_2 for a field along x_1. Hence the tensor is symmetrical and has the same number of components as the fourth rank elastic compliance tensor $s^D{}_{ijkl}$. For the isotropic case symmetry rules out all terms except those shown by Table I. The terms on the left are the strains generated by the products of the electric displacements shown by the top column. Since $S_{ij}=S_{ji}$ and $\delta_i\delta_j=\delta_j\delta_i$, three columns and three rows are redundant. The fourth rank tensor for the elastic compliances will have the same terms with Q_{1111} replaced by s_{1111} and Q_{1122} replaced by s_{1122}. For the top variable line $\delta_1{}^2$ is replaced by T_{11}, $\delta_1\delta_2$ by T_{12}, etc.

To simplify the method of writing these equations, the usual one-index matrix symbols are used for the stresses and strains and the usual two-index compliance, electrostrictive, and impermeability constants are used; the electro-

strictive equations become

$$
\begin{aligned}
S_1&=s_{11}{}^D T_1+s_{12}{}^D(T_2+T_3)+Q_{11}\delta_1{}^2+Q_{12}[\delta_2{}^2+\delta_3{}^2]\\
S_2&=s_{12}{}^D[T_1+T_3]+s_{11}{}^D T_2+Q_{11}\delta_2{}^2+Q_{12}[\delta_1{}^2+\delta_3{}^2]\\
S_3&=s_{12}{}^D[T_1+T_2]+s_{11}{}^D T_3+Q_{11}\delta_3{}^2+Q_{12}[\delta_1{}^2+\delta_2{}^2]\\
S_{12}&=\frac{S_6}{2}=(s_{11}{}^D-s_{12}{}^D)T_6+(Q_{11}-Q_{12})\delta_1\delta_2\\
S_{13}&=\frac{S_5}{2}=(s_{11}{}^D-s_{12}{}^D)T_5+(Q_{11}-Q_{12})\delta_1\delta_3\\
S_{23}&=\frac{S_4}{2}=(s_{11}{}^D-s_{12}{}^D)T_4+(Q_{11}-Q_{12})\delta_2\delta_3\\
E_1&=\delta_1[4\pi\beta_{11}{}^T+O_{11}\delta_1]-2[Q_{11}[\delta_1T_1+\delta_2T_6+\delta_3T_5]+Q_{12}[\delta_1(T_2+T_3)-(T_6\delta_2+T_5\delta_3)]]\\
E_2&=\delta_2[4\pi\beta_{11}{}^T+O_{11}\delta_2]-2[Q_{11}[\delta_2T_2+\delta_1T_6+\delta_3T_4]+Q_{12}[\delta_2(T_1+T_3)-(\delta_1T_6+\delta_3T_4)]]\\
E_3&=\delta_3[4\pi\beta_{11}{}^T+O_{11}\delta_3]-2[Q_{11}[\delta_3T_3+\delta_1T_5+\delta_2T_4]+Q_{12}[\delta_3(T_1+T_2)-(\delta_1T_5+\delta_2T_4)]]
\end{aligned}
\tag{22}
$$

In this equation an extra term O_{11} has been added to represent the decrease in dielectric constant with applied field, which as shown by Fig. 3 is considerable.[6] Over a temperature range, the complex dielectric constant varies[7] as shown by Fig. 6. The equations for the various modes can be derived from Eqs. (22).

The simplest mode to consider is a longitudinal mode for a long thin bar generated by a field perpendicular to the length. If we take the thickness as lying along z while the length is along x, the equations reduce to

$$
\begin{aligned}
S_1&=s_{11}{}^D T_1+Q_{12}\delta_3{}^2;\\
E_3&=\delta_3[4\pi\beta_{11}{}^T+O_{11}\delta_3]-2Q_{12}\delta_3T_1.
\end{aligned}
\tag{23}
$$

For the case of interest here δ_3 consists of a part δ_{30} due to an applied field or a remanent polarization plus an alternating component due to an applied a.c. voltage. As far as the alternating components go we can write these two equations as

$$
\begin{aligned}
S_1&=s_{11}{}^D T_1+Q_{12}[2\delta_{30}\delta_3];\\
E_3&=\delta_3[4\pi\beta_{11}{}^T+O_{11}\delta_{30}]-2Q_{12}\delta_{30}T_1.
\end{aligned}
\tag{24}
$$

To reduce this equation to the standard form[8] used in solving piezoelectric crystals, we have to express the stress T_1 in terms of the strain S_1 and field E_3. By eliminating δ_3 the alternating part of the electric displacement from the last equation and substituting in the first part of Eqs. (24) we have

$$
\begin{aligned}
T_1&=\frac{S_1}{s_{11}{}^E}-\frac{2Q_{12}\delta_{30}E_3}{(4\pi\beta_{11}{}^T+O_{11}\delta_{30})s_{11}{}^E};\\
\delta_3&=\frac{E_3}{4\pi\beta_{11}S_1+O_{11}\delta_{30}}+\frac{2Q_{12}\delta_{30}S_1}{s_{11}{}^D[4\pi\beta_{11}S_1+O_{11}\delta_{30}]},
\end{aligned}
\tag{25}
$$

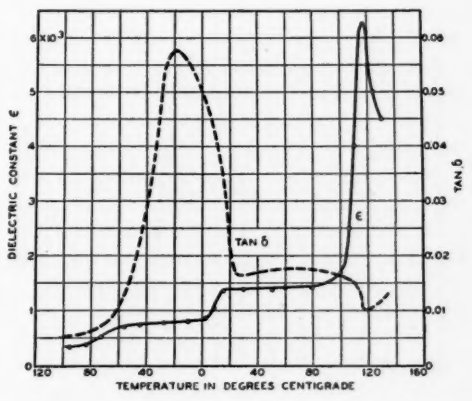

FIG. 6. Dielectric constant for zero bias as a function of the temperature.

[6] This measurement was made by Gordon Danielson of the Bell Telephone Laboratories.

[7] A. Von Hippel, R. G. Breckinridge, F. G. Chesley, and Lazlo Tisza, Ind. Eng. Chem. **38**, 1097 (1946).

[8] See, for example, W. P. Mason, Phys. Rev. **70**, 705 (1946).

where

$$s_{11}^D = s_{11}^E[1-k^2] \text{ where } k^2 = \frac{4Q_{12}^2\delta_{30}^2}{[4\pi\beta_{11}^T + O_{11}\delta_{30}]s_{11}^E}.$$

$$4\pi\beta_{11}^{S_1} + O_{11}\delta_{30} = 4\pi\beta_{11}^T + O_{11}\delta_{30} - \frac{4Q_{12}^2\delta_{30}^2}{s_{11}^D}$$

$$= (4\pi\beta_{11}^T + O_{11}\delta_{30})(1-k^2).$$

Substituting the last relation in the last of Eqs. (25), the two equations become

$$T_1 = \frac{S_1}{s_{11}^E} - \frac{2Q_{12}\delta_{30}E_3}{(4\pi\beta_{11}^T + O_{11}\delta_{30})s_{11}^E};$$

$$\delta_3 = \frac{E_3}{4\pi\beta_{11}^{S_1} + O_{11}\delta_{30}} + \frac{2Q_{12}\delta_{30}S_1}{s_{11}^E[4\pi\beta_{11}^T + O_{11}\delta_{30}]}. \quad (26)$$

These have the same form as the piezoelectric equations (37) of reference (8), and hence the same considerations exist if we set the equivalent piezoelectric constant equal to

$$d_{31}' = \frac{2Q_{12}\delta_{30}}{4\pi\beta_{11}^T + O_{11}\delta_{30}}. \quad (27)$$

This can be evaluated as in the piezoelectric case by measuring the resonant and antiresonant frequencies of the device, the dielectric constant, and the density. The coupling is given by Eq. (50) of reference (8).

$$k^2 = \frac{\pi^2}{4}\frac{\Delta f}{f_R}\left[1 + \frac{(4-\pi^2)}{4}\frac{\Delta f}{f_R} + \cdots\right], \quad (28)$$

while the piezoelectric constant is given by

$$d_{31}' = \frac{2Q_{12}\delta_{30}}{4\pi\beta_{11}^T + O_{11}\delta_{30}} = k\left(\frac{s_{11}^E}{4\pi\beta_{11}^T + O_{11}\delta_{30}}\right)^{\frac{1}{2}},$$

or

$$Q_{12} = \frac{k}{2\delta_{30}}(s_{11}^E(4\pi\beta_{11}^T + O_{11}\delta_{30}))^{\frac{1}{2}}. \quad (29)$$

Measurements have been made for the coupling of a long thin bar as a function of the applied voltage, and the results are shown by Fig. 4. The frequency constant for such a bar is 2.28×10^5 kc cm. With a density of 5.5 this corresponds to a compliance constant (inverse of Young's modulus) of 0.88×10^{-12}. The dielectric constant as a function of voltage is given in Fig. 3. Hence one can calculate the value of Q_{12}, and the value is approximately

$$Q_{12} = -2.15\times10^{-12} \text{ in c.g.s. units.}$$

The negative sign is obtained from expansion measurements which show that the bar contracts in length when a voltage is applied normal to the length.

The same constant Q_{12} drives the radial mode of a disk, but since this requires a transformation to cylindrical coordinates, the equations are discussed in the appendix. It is there shown that the coupling is $(2/(1-\sigma))^{\frac{1}{2}}$ times as large as that for the longitudinal mode. This agrees well with the experimental curve of Fig. 4.

The coupling for the thickness mode is also shown by Fig. 4. The effective piezoelectric constant for a thickness mode can be evaluated from Eq. (22) by setting $S_1 = S_2 = 0$, since no sidewise motion occurs, and solving for T_3 and δ_3 in terms of S_3 and E_3. The resulting equations are

$$T_3 = S_3c_{11}^E - \frac{2\delta_{30}[Q_{11} - (2s_{12}^D/s_{11}^D + s_{12}^D)Q_{12}]c_{11}^E}{4\pi\beta_{11}^T + O_{11}\delta_{30}}E_3;$$

$$\delta_3 = \frac{E_3}{4\pi\beta_{11}^{S_3} + O_{11}\delta_{30}} + \frac{2c_{11}^E[Q_{11} - (2s_{12}^D/s_{11}^D + s_{12}^D)Q_{12}]\delta_{30}S_3}{[4\pi\beta_{11}^T + O_{11}\delta_{30}]}, \quad (30)$$

where

$$c_{11}^E = \frac{c_{11}^D}{1-k^2};$$

$$k^2 = \frac{4\delta_{30}^2[Q_{11} - (2s_{12}^DQ_{12}/s_{11}^D + s_{12}^D)]^2c_{11}^E}{4\pi\beta_{11}^T + O_{11}\delta_{30}},$$

and

$$4\pi\beta_{11}^{S_3} + O_{11}\delta_{30} = (4\pi\beta_{11}^T + O_{11}\delta_{30})(1-k^2).$$

Hence the equivalent piezoelectric constant for this case is

$$d_{33}' = \frac{2[Q_{11} - (2s_{12}^D/s_{11}^D + s_{12}^D)Q_{12}]\delta_{30}}{4\pi\beta_{11}^T + O_{11}\delta_{30}}. \quad (31)$$

From the coupling measurements of Fig. 4 one

finds that

$$Q_{11}-\frac{2s_{12}^{D}}{s_{11}^{D}+s_{12}^{D}}Q_{12}=5.3\times10^{-12}. \quad (32)$$

Since s_{11} and s_{12} are given in terms of the c elastic constants by

$$s_{11}=\frac{c_{11}+c_{12}}{c_{11}(c_{11}+c_{12})-2c_{12}^{2}}=\frac{\lambda+\mu}{\mu(3\lambda+2\mu)};$$
$$s_{12}=\frac{-c_{12}}{c_{11}(c_{11}+c_{12})-2c_{12}^{2}}=\frac{-\lambda}{2\mu(3\lambda+2\mu)}, \quad (33)$$

we have from the Lamé elastic constants of Eq. (7)

$$s_{11}=0.88\times10^{-12};\quad s_{12}=-0.236\times10^{-12}. \quad (34)$$

Hence the value of Q_{11} becomes

$$Q_{11}=+6.9\times10^{-12} \quad (35)$$

which is of opposite sign and about 3 times as large as Q_{12}.

The fourth mode of motion that can be generated in a rectangular bar is the thickness shear mode which occurs when the alternating voltage is applied at right angles to the d.c. electric displacement. This mode was tested by taking a bar 5 cm long, 0.5 cm wide, and 0.25 cm thick, applying a voltage of 30,000 volts per cm and using the remanent polarization generated for this case. Since it is difficult to establish an electric displacement along the 0.5-cm direction with plates normal to the large faces, these were dissolved off and the a.c. field applied along the width (0.5-cm direction). The frequency of the measured resonance was 566 kilocycles, which agrees well with the shear elastic constant of Eq. (7). The coupling for the shear mode is higher than that for the thickness longitudinal mode. This is what one expects from Eqs. (22), sixth equation, from which one obtains the equation for a shear mode

$$T_4=S_4\mu^{E}-\frac{2(Q_{11}-Q_{12})\delta_{30}\mu^{E}}{4\pi\beta_{11}^{T}+O_{11}\delta_{30}}E_2,$$
$$\delta_2=\frac{E_2}{4\pi\beta_{11}^{S}+O_{11}\delta_{30}}-\frac{2(Q_{11}-Q_{12})\delta_{30}\mu^{E}}{4\pi\beta_{11}^{T}+O_{11}\delta_{30}}S_4, \quad (36)$$

where

$$\mu^{E}=\frac{c_{11}^{E}-c_{12}^{E}}{2}=\left(\frac{c_{11}^{D}-c_{12}^{D}}{2}\right)(1-k^2);$$
$$k^2=\frac{4(Q_{11}-Q_{12})^2\delta_{30}\mu^{E}}{4\pi\beta_{11}^{T}+O_{11}\delta_{30}}.$$

Inserting the values given previously for Q_{11}, Q_{12}, μ, and δ_{30} (i.e., a remanent polarization equal to 0.85 times that for a 30,000-volt/cm field), one obtains a coupling of 48 percent which agrees well with experiment. Hence the phenomenological theory accounts quantitatively for all the modes of motion observed, and allows one to measure the electrostrictive, elastic, and dielectric constants pertaining to the ceramic.

IV. THEORETICAL EXPLANATION OF EFFECT

The ratio of about 2 to 1 between the thickness effect, and the fact that the radial effect is a contraction, allows one to obtain a mechanism for this effect. Barium titanate above 120°C has a cubic structure, having the form shown by Fig. 7. Here eight barium atoms form the corners of the cube. Since each barium atom is shared between eight adjacent cells, this gives a total of one barium atom per cell. Six oxygen atoms occupy the face-centered position on the six sides, and since each is shared between two adjacent cells, this represents a total of three oxygen atoms per cell. Since the titanium atom is much smaller than the other atoms, it is relatively free to move between them.

As the temperature is lowered below 120°C, the titanium atom moves from the center to one of the six positions near the six oxygen atoms. Since the cell was neutral when the titanium was in the center, a dipole moment is introduced by

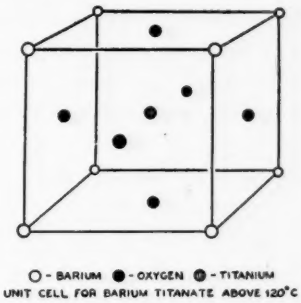

FIG. 7. Unit cell for barium titanate above 120°C.

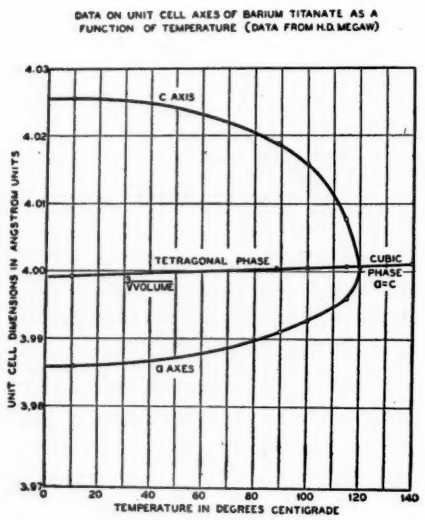

FIG. 8. Unit cell dimensions as a function of the temperature.

the motion of the titanium and the cell acquires a permanent dipole; the domain in which the cell is situated becomes ferro-electric.

When the crystal becomes ferro-electric, the cubic form is lost and the crystal becomes tetragonal with the axis in the direction of the titanium motion 1 percent longer than the other two axes. Figure 8 shows the cell dimensions as a function of temperature, as determined by Miss McGaw.[9] Along the ferro-electric axis the cell dimension increases from 4.0A to 4.026A, at room temperature, while the other two axes decrease from 4.0A to 3.86A. The total volume of the unit cell remains unchanged for the crystal, but the axial ratio has changed to 1.01.

For a polycrystalline material the dominant mechanism for producing the electrostrictive effect is the following. As the ceramic material is prepared, all domains (which can exist below 120°C) are equally distributed in all directions and no residual polarization can occur. The effect of a large d.c. field is to change the direction of polarity so that more domains are lined up in the direction of the field rather than in other directions. This change in the direction of a domain occurs not by physically changing the orientation but rather in changing the direction of the ferro-electric axis from one of the six oxygens to another of the six. When the field is taken off, the local field caused by the lining up of the domains remains and is sufficient to keep a large share of the domains lined up. Now when domains are lined up in the direction of the field, the plate expands in this direction by $\frac{2}{3}$ percent times the percentage of domains whose direction of polarization is changed. At the same time the radial dimensions contract. For the crystal, x-ray measurements show that the sidewise contraction is half as much as the thickness expansion. However, for the ceramic, since $-Q_{12}/Q_{11}=2.15/6.9=0.31$, the amount of sidewise contraction is less and a volume electrostrictive effect exists. This is probably due to the fact that the crystal domains are not bonded at all points, and a contraction of domains can occur without causing a corresponding contraction in the body, whereas an expansion along the c axis carries the material with it whether it is bonded at all points or not. The two effects—the thickness effect and the radial effect—are both of a considerable magnitude.

When a small a.c. field is applied in the presence of a d.c. field or remanent polarization, the following process probably occurs. The a.c. field in itself is too small to reverse any complete domain, but it can cause molecules on the common planes of differently directed domains to change from one domain to another and hence cause one domain to grow at the expense of other domains. If the a.c. field is opposed to the d.c. field, some molecules of the domains directed along the thickness will be lost to other domains directed in different directions and the crystal will become thinner. When the a.c. field is added to the d.c. field, these molecules and more too will be directed in the direction of the field and the plate becomes thicker. Since the change in molecule direction will, in general, lag the applied field, a large dielectric hysteresis occurs just as for rochelle salt, and the mechanical resonances have a poor Q. The radial vibration is accounted for by the contraction of the domains in directions perpendicular to the ferro-electric axis, and this process should generate a radial motion about half as large as the thickness motion, which agrees with experiment.

The value of the total increase in thickness, about 5 to 7 parts in 10^4 for 30,000 volts per cm applied gives a method for estimating the

[9] H. D. McGaw, Proc. Roy. Soc. **189**, 261–283 (April, 1947).

number of domains lined up by the d.c. field. Since the plate could expand by $\frac{2}{3}$ percent if all the domains were lined up, the percent lined up is

$$\frac{5 \text{ to } 7\times10^{-4}}{6.6\times10^{-3}}=7.6 \text{ to } 10.6 \text{ percent} \quad (37)$$

over the average value for an isotropic condition.

APPENDIX

Equation for an Electrostrictive Material in Cylindrical Coordinates

To obtain the equations of motion for a cylindrical plate, Eqs. (22) for rectangular coordinates have to be transformed to cylindrical coordinates. In cylindrical coordinates the variables are the radius vector r, the angle θ, and the dimension along the cylinder designated by z. In terms of the x, y, z rectangular coordinates

$$r^2=x^2+y^2; \quad \tan\theta=y/x; \quad z=z. \quad (38)$$

The direction cosines between the r, θ, and z directions and the x, y, and z directions are then

	x	y	z
r	$\cos\theta$	$\sin\theta$	0
θ	$-\sin\theta$	$\cos\theta$	0
z	0	0	1

(39)

Making use of the formula for the transformation of a tensor from one coordinate system to another,

$$T_{a,b}=\frac{\partial x_a}{\partial x_k}\frac{\partial x_b}{\partial x_l}T_{kl}, \quad (40)$$

letting a, b refer to r, θ, and z and noting that $\partial x_a/\partial x_k$ are the direction cosines of Eq. (39), the stress tensor becomes in cylindrical coordinates

$$\begin{aligned}
T_{rr}&=\cos^2\theta\, T_{11}+2\sin\theta\cos\theta\, T_{12}+\sin^2\theta\, T_{22},\\
T_{\theta\theta}&=\sin^2\theta\, T_{11}-2\sin\theta\cos\theta\, T_{12}+\cos^2\theta\, T_{22},\\
T_{r\theta}&=\sin\theta\cos\theta\,[T_{22}-T_{11}]+[\cos^2\theta-\sin^2\theta]T_{12},\\
T_{rz}&=\cos\theta\, T_{13}+\sin\theta\, T_{23},\\
T_{\theta z}&=-\sin\theta\, T_{13}+\cos\theta\, T_{23},\\
T_{zz}&=T_{33}.
\end{aligned} \quad (41)$$

The strain tensor transforms in a similar manner.

Conversely, the rectangular stress and strain components are related to the cylindrical components by equations of the type

$$S_{ij}=\frac{\partial x_i}{\partial x_a}\frac{\partial x_j}{\partial x_b}S_{ab}, \quad (42)$$

and

$$\begin{aligned}
S_{11}&=\cos^2\theta\, S_{rr}-2\sin\theta\cos\theta\, S_{r\theta}+\sin^2\theta\, S_{\theta\theta},\\
S_{22}&=\sin^2\theta\, S_{rr}+2\sin\theta\cos\theta\, S_{r\theta}+\cos^2\theta\, S_{\theta\theta},\\
S_{33}&=S_{zz},\\
S_{12}&=\sin\theta\cos\theta\,(S_{rr}-S_{\theta\theta})+(\cos^2\theta-\sin^2\theta)S_{r\theta},\\
S_{13}&=\cos\theta\, S_{rz}-\sin\theta\, S_{\theta z},\\
S_{23}&=\sin\theta\, S_{rz}+\cos\theta\, S_{\theta z}.
\end{aligned} \quad (43)$$

In solving the equations of motion it is necessary to know the values of the strains in terms of the displacements in the r, θ, and z directions. Denoting these by

$$u_r, \; u_\theta, \text{ and } u_z, \quad (44)$$

Love[10] has shown that the strain components are given by

$$\begin{aligned}
&S_{rr}=\frac{\partial u_r}{\partial r}; \quad S_{\theta\theta}=\frac{1}{r}\frac{\partial u_\theta}{\partial\theta}+\frac{u_r}{r}; \quad S_{zz}=\frac{\partial u_z}{\partial z}\\
&S_{r\theta}=\frac{\partial u_\theta}{\partial r}-\frac{u_\theta}{r}+\frac{1}{r}\frac{\partial u_r}{\partial\theta}; \quad S_{rz}=\frac{\partial u_r}{\partial z}+\frac{\partial u_z}{\partial r}; \quad S_{\theta z}=\frac{1}{r}\frac{\partial u_z}{\partial\theta}+\frac{\partial u_\theta}{\partial z}.
\end{aligned} \quad (45)$$

[10] Love, *Theory of Elasticity* (Cambridge University Press, London, 1934), fourth edition, p. 56.

The other necessary equations are the Newton's law equations transformed into cylindrical coordinates. From Love's[11] *Theory of Elasticity*, these are

$$\begin{aligned}
\rho\ddot{u}_r &= \frac{\partial T_{rr}}{\partial r}+\frac{1}{r}\frac{\partial T_{r\theta}}{\partial \theta}+\frac{\partial T_{rz}}{\partial z}+\left(\frac{T_{rr}-T_{\theta\theta}}{r}\right),\\
\rho\ddot{u}_\theta &= \frac{\partial T_{r\theta}}{\partial r}+\frac{1}{r}\frac{\partial T_{\theta\theta}}{\partial \theta}+\frac{\partial T_{\theta z}}{\partial z}+\frac{2T_{r\theta}}{r},\\
\rho\ddot{u}_z &= \frac{\partial T_{rz}}{\partial r}+\frac{1}{r}\frac{\partial T_{\theta z}}{\partial \theta}+\frac{\partial T_{zz}}{\partial z}+\frac{T_{rz}}{r}.
\end{aligned} \tag{46}$$

These equations give enough relations to solve the case of the electrostrictive disk of barium titanate in radial vibration. Equations (22) give the electrostrictive and elastic equations in rectangular coordinates. Transferring these to cylindrical coordinates by means of the tensor relations of Eqs. (41) and (43), we find

$$\begin{aligned}
S_{rr} &= s_{11}^{D}T_{rr}+s_{12}^{D}(T_{\theta\theta}+T_{zz})+Q_{11}\delta_r^2+Q_{12}[\delta_\theta^2+\delta_z^2],\\
S_{\theta\theta} &= s_{12}^{D}[T_{rr}+T_{rz}]+s_{11}^{D}T_{\theta\theta}+Q_{12}(\delta_r^2+\delta_z^2)+Q_{11}\delta_\theta^2,\\
S_{zz} &= s_{11}^{D}T_{zz}+s_{12}^{D}[T_{rr}+T_{\theta\theta}]+Q_{11}\delta_z^2+Q_{12}[\delta_r^2+\delta_\theta^2],\\
S_{rz} &= (s_{11}^{D}-s_{12}^{D})T_{rz}+(Q_{11}-Q_{12})\delta_r\delta_z,\\
S_{r\theta} &= (s_{11}^{D}-s_{12}^{D})T_{r\theta}+(Q_{11}-Q_{12})\delta_r\delta_\theta,\\
S_{\theta z} &= (s_{11}^{D}-s_{12}^{D})T_{\theta z}+(Q_{11}-Q_{12})\delta_\theta\delta_z,
\end{aligned} \tag{47}$$

where δ_r, δ_θ, δ_z are the electric displacements divided by 4π for the r, θ, and z directions. The electric relations become

$$\begin{aligned}
E_r &= \delta_r[4\pi\beta_{11}^{T}+O_{11}\delta_r]-2[Q_{11}(\delta_rT_{rr}+\delta_\theta T_{r\theta}+\delta_zT_{rz})+Q_{12}[\delta_r(T_{\theta\theta}+T_{zz})-(\delta_\theta T_{r\theta}+\delta_zT_{rz})]],\\
E_\theta &= \delta_\theta[4\pi\beta_{11}^{T}+O_{11}\delta_\theta]-2[Q_{11}(\delta_\theta T_{\theta\theta}+\delta_rT_{r\theta}+\delta_zT_{\theta z})+Q_{12}[\delta_\theta(T_{rr}+T_{zz})-(\delta_rT_{r\theta}+\delta_zT_{\theta z})]],\\
E_z &= \delta_z[4\pi\beta_{11}^{T}+O_{11}\delta_z]-2[Q_{11}(\delta_zT_{zz}+\delta_rT_{rz}+\delta_\theta T_{\theta z})+Q_{12}[\delta_z(T_{rr}+T_{\theta\theta})-(\delta_rT_{rz}+\delta_\theta T_{\theta z})]].
\end{aligned} \tag{48}$$

For the radially vibrating disk

$$u_\theta = 0, \tag{49}$$

and we have also

$$T_{\theta z} = T_{r\theta} = 0. \tag{50}$$

We assume that the thickness along z is very small compared to the wave-length. Since the stresses on the surface are zero and the thickness very small, we can set

$$T_{zz} = T_{rz} = 0. \tag{51}$$

These are the same assumptions as those made for a longitudinal long thin bar discussed in Eqs. (23) to (29) and hence the results are comparable. Since a field is applied only along the z direction, $\delta_r = \delta_\theta = 0$. The remaining equations then become

$$\begin{aligned}
S_{rr} &= s_{11}^{D}T_{rr}+s_{12}^{D}T_{\theta\theta}+Q_{12}\delta_z^2,\\
S_{\theta\theta} &= s_{12}^{D}T_{rr}+s_{11}^{D}T_{\theta\theta}+Q_{12}\delta_z^2,\\
E_z &= \delta_z[4\pi\beta_{11}^{T}+O_{11}\delta_z]-2Q_{12}\delta_z[T_{rr}+T_{\theta\theta}].
\end{aligned} \tag{52}$$

[11] See reference 10, p. 90.

To insert in the equation of motion (46) we need to have the stresses expressed in terms of the strains, and for the electrical boundary conditions it is better to use the fields rather than the electric displacements. Furthermore, for small alternating fields superposed on a large d.c. electric displacement, which may be caused by an applied field or a remanent polarization, we can replace δ_z by

$$\delta_z = \delta_{z0}+\delta_z e^{j\omega t}, \tag{53}$$

where δ_{z0} is the steady electric displacement if a field is applied or the remanent polarization P_0 if the field is taken off. Then solving these three equations simultaneously, the alternating components of stress, strain, and displacement are

given by the equations

$$T_{rr}=\left[\frac{s_{11}^E}{s_{11}^{E^2}-s_{12}^{E^2}}\right]S_{rr}-\left[\frac{s_{12}^E}{s_{11}^{E^2}-s_{12}^{E^2}}\right]S_{\theta\theta}-\frac{2Q_{12}\delta z_0 E_z}{(4\pi\beta_{11}^T+O_{11}\delta z_0)(s_{11}^E+s_{12}^E)},$$

$$T_{\theta\theta}=\left[\frac{s_{11}^E}{s_{11}^{E^2}-s_{12}^{E^2}}\right]S_{\theta\theta}-\left[\frac{s_{12}^E}{s_{11}^{E^2}-s_{12}^{E^2}}\right]S_{rr}-\frac{2Q_{12}\delta z_0 E_z}{(4\pi\beta_{11}^T+O_{11}\delta z_0)(s_{11}^E+s_{12}^E)},$$

$$\delta_z=\frac{E_z}{4\pi\beta_{11}^T+O_{11}\delta z_0}+\frac{2Q_{12}\delta z_0}{4\pi\beta_{11}^T+O_{11}\delta z_0}[T_{rr}+T_{\theta\theta}], \tag{54}$$

where

$$s_{11}^E=\frac{s_{11}^D}{1-k_l^2};\quad s_{12}^E=\frac{s_{12}^D}{1-\dfrac{s_{11}^D}{s_{12}^D}k_l^2};\quad k_l^2=\frac{4Q_{12}^2\delta z_0^2}{(4\pi\beta_{11}^T+O_{11}\delta z_0)s_{11}^E}.$$

k_l is the electromechanical coupling factor for a longitudinal mode given by Eq. (25). We note that since $1/s_{11}^E=Y_0^E$, the Young's modulus, and $-s_{12}^E/s_{11}^E=\sigma$, the Poisson ratio, that the first two equations of (54) can be simplified to

$$T_{rr}=\left(\frac{Y_0^E}{1-\sigma^2}\right)[S_{rr}+\sigma S_{\theta\theta}]-\frac{2Q_{12}\delta z_0 E_z Y_0^E}{(4\pi\beta_{11}^T+O_{11}\delta z_0)(1-\sigma)},$$

$$T_{\theta\theta}=\left(\frac{Y_0^E}{1-\sigma^2}\right)[S_{\theta\theta}+\sigma S_{rr}]-\frac{2Q_{12}\delta z_0 E_z Y_0^E}{(4\pi\beta_{11}^T+O_{11}\delta z_0)(1-\sigma)}. \tag{55}$$

Now noting that since the plating on the surface is an equipotential surface, E_z is not a function of r, then when Eqs. (55) are inserted in the equation of motion, (46), and the relations for a radial motion

$$S_{rr}=\frac{\partial u_r}{\partial r};\quad S_{\theta\theta}=\frac{u_r}{r} \tag{56}$$

are used, the equation of motion becomes

$$\frac{Y_0^E}{1-\sigma^2}\left[\frac{\partial^2 u_r}{\partial r^2}+\frac{1}{r}\frac{\partial u_r}{\partial r}-\frac{u_r}{r^2}\right]=\rho\frac{\partial^2 u_r}{dt^2}=-\omega^2\rho u_r. \tag{57}$$

The last term results for simple harmonic motion.

Since this is a Bessel's equation of the first order, a solution is

$$u_r=AJ_1\left(\frac{\omega r}{v}\right),\quad \text{where}\quad v=\frac{Y_0^E}{(1-\sigma^2)\rho}. \tag{58}$$

No Bessel's function of the second kind is required since the displacement u_r vanishes at the center of the disk. At the boundary when $r=a$ the radius of the disk, the stress $T_{rr}=0$. From (55) we have

$$0=\frac{Y_0^E A}{1-\sigma^2}\left[\frac{\omega}{v}J_0\left(\frac{\omega a}{v}\right)-\frac{(1-\sigma)J_1(\omega a/v)}{a}\right]-\frac{2Q_{12}\delta z_0 E_z Y_0^E}{(4\pi\beta_{11}^T+O_{11}\delta z_0)(1-\sigma)}. \tag{59}$$

Hence

$$A=\frac{2Q_{12}\delta z_0 E_z(1+\sigma)}{[4\pi\beta_{11}^T+O_{11}\delta z_0]\left[\dfrac{\omega}{v}J_0\left(\dfrac{\omega a}{v}\right)-\dfrac{(1-\sigma)J_1(\omega a/v)}{a}\right]}. \tag{60}$$

From this data we can evaluate the stresses T_{rr} and $T_{\theta\theta}$ as

$$T_{rr}=-\frac{2Q_{12}\delta_{z0}Y_0^E E_z}{(4\pi\beta_{11}^T+O_{11}\delta_{z0})(1-\sigma)}\left[1-\left[\frac{\frac{\omega}{v}J_0\left(\frac{\omega r}{v}\right)-\frac{(1-\sigma)J_1(\omega r/v)}{r}}{\frac{\omega}{v}J_0\left(\frac{\omega a}{v}\right)-\frac{(1-\sigma)J_1(\omega a/v)}{a}}\right]\right],$$

$$T_{\theta\theta}=-\frac{2Q_{12}\delta_{z0}E_z Y_0^E}{(4\pi\beta_{11}^T+O_{11}\delta_{z0})(1-\sigma)}\left[1-\left[\frac{\frac{\sigma\omega}{v}J_0\left(\frac{\omega r}{v}\right)+\frac{(1-\sigma)J_1(\omega r/v)}{r}}{\frac{\omega}{v}J_0\left(\frac{\omega a}{v}\right)-\frac{(1-\sigma)J_1(\omega a/v)}{a}}\right]\right]. \tag{61}$$

The next step in the solution is to obtain the electrical impedance by a.c. methods. This can be obtained by substituting the values of T_{rr} and $T_{\theta\theta}$ in the last of Eqs. (54) and integrating over the surface of the crystal. Since the value of δ_z at the surface is equal to the surface charge this will evaluate the total charge Q and we have

$$Q=\int_0^{2\pi}d\theta\int_0^a\delta_z r dr=\frac{E_z\pi a^2}{(4\pi\beta_{11}^T+O_{11}\delta_{z0})}+\frac{2Q_{12}\delta_{z0}}{(4\pi\beta_{11}^T+O_{11}\delta_{z0})}\int_0^{2\pi}d\theta\int_0^a r[T_{rr}+T_{\theta\theta}]dr. \tag{62}$$

Introducing the value of T_{rr} and $T_{\theta\theta}$ from Eq. (61) this integral becomes

$$Q=\frac{E_z\pi a^2}{(4\pi\beta_{11}^T+O_{11}\delta_{z0})}\left[1-\frac{8Q_{12}\delta_{z0}Y_0^E}{(4\pi\beta_{11}^T+O_{11}\delta_{z0})(1-\sigma)}\left[1-\frac{(1+\sigma)\int_0^a\frac{\omega}{v}r J_0(\omega r/v)dr}{a^2\left(\frac{\omega}{v}J_0(\omega a/v)-\left(\frac{1-\sigma}{a}\right)J_1(\omega a/v)\right)}\right]\right]. \tag{63}$$

Performing the integration and employing the substitution

$$\frac{1}{(4\pi\beta_{11}^T+O_{11}\delta_{z0})}\left[1-\frac{8Q_{12}^2\delta_{z0}^2Y_0^E}{(4\pi\beta_{11}^T+O_{11}\delta_{z0})(1-\sigma)}\right]=\frac{1}{4\pi\beta_{11}^{RC}+O_{11}\delta_{z0}}, \tag{64}$$

where β_{11}^{RC} is the radially clamped impermeability constant, i.e., the impermeability when the plate is prevented from moving radially, we have

$$Q=\frac{E_z\pi a^2}{(4\pi\beta_{11}^{RC}+O_{11}\delta_{z0})}\left[1+\frac{k^2}{(1-k^2)}\frac{(1+\sigma)J_1(\omega a/v)}{(\omega a/v)J_0(\omega a/v)-(1-\sigma)J_1(\omega a/v)}\right], \tag{65}$$

where the coefficient of coupling for a radial mode becomes

$$k_r^2=\frac{8Q_{12}^2\delta_{z0}^2Y_0^E}{(4\pi\beta_{11}^T+O_{11}\delta_{z0})(1-\sigma)}. \tag{66}$$

Comparing this with the longitudinal mode, given by Eq. (25), we see that the radial mode has a higher coupling by the factor

$$(2/1-\sigma)^{\frac{1}{2}}. \tag{67}$$

Since the admittance of the plate is equal to the current into the plate divided by the voltage across

the plate, and for simple harmonic motion

$$i=dQ/dt=j\omega Q, \tag{68}$$

the impedance of the electrostrictive plate is given by

$$\frac{1}{Z}=\frac{i}{E}=\frac{j\omega\pi a^2}{(4\pi\beta_{11}{}^{RC}+O_{11}\delta_{z0})l_t}\left[1+\frac{k^2}{1-k^2}\frac{(1+\sigma)J_1(\omega a/v)}{(\omega a/v)J_0(\omega a/v)-(1-\sigma)J_1(\omega a/v)}\right]. \tag{69}$$

The resonant frequency occurs when

$$(\omega a/v)J_0(\omega a/v)-(1-\sigma)J_1(\omega a/v)=0. \tag{70}$$

For a value of $\sigma=0.27$ found from the elastic measurements, this equation has the lowest root

$$(\omega a/v)=2.03=R_1. \tag{71}$$

Hence the frequency is given by the equation

$$f_R=(2.03/2\pi a)(Y_0{}^E/\rho(1-\sigma^2))^{\frac{1}{2}}. \tag{72}$$

The antiresonant frequency occurs when the expression in brackets in Eq. (69) reduces to zero. This occurs at a frequency somewhat above the resonant frequency. To determine the frequency separation Δf, between resonance and antiresonance, we develop the function $J_0(\omega a/v)$ and $J_1(\omega a/v)$ in a MacLaurin's series about the root R_1. This gives

$$\begin{aligned}J_0(\omega a/v)&=J_0(R_1)+\frac{\partial}{\partial f}[J_0(\omega a/v)]_{(\omega a/v)=R_1}\Delta f+\cdots\\&=J_0(R_1)-\frac{2\pi a}{v}J_1(R_1)\Delta f+\cdots,\\J_1(\omega a/v)&=J_1(R_1)+\frac{\partial}{\partial f}[J_1(\omega a/v)]_{(\omega a/v)=R_1}\Delta f+\cdots\\&=J_1(R_1)+\frac{2\pi a}{v}\left[J_0(R_1)-\frac{J_1(R_1)}{R_1}\right]\Delta f+\cdots.\end{aligned} \tag{73}$$

Inserting these values in Eq. (69) and setting the numerator equal to zero, the frequency separation Δf becomes

$$\frac{\Delta f}{f_R}=\frac{(k^2/(1-k^2))(1+\sigma)}{R_1{}^2-(1-\sigma^2)}. \tag{74}$$

Hence solving for the coupling factor k^2, we find to a first approximation

$$k^2=\frac{\Delta f}{f_R}\left[\frac{R_1{}^2-(1-\sigma^2)}{1+\sigma}\right]. \tag{75}$$

For $\sigma=0.27$ the value of the factor multiplying $\Delta f/f_R$ is equal to 2.51. Comparing this to the factor for a longitudinal crystal given by Eq. (28), which is $\pi^2/4=2.47$, it is seen that the same equations are very nearly applicable. By using Eq. (75) the coupling can be evaluated by measuring the separation of resonant and antiresonant frequencies and the frequency f_R. The resonant frequency and the density give the elastic constant by employing Eq. (72). From the measured value of k_r, the measured value of the dielectric constant, which is the inverse of

$$\epsilon_{11}=\frac{1}{\beta_{11}{}^T+\dfrac{O_{11}\delta_{z0}}{4\pi}}, \tag{76}$$

one can determine $Q_{12}\delta_{z0}$ from Eq. (66). By taking a known value of field for which ϵ_{11} has been measured, δ_{z0} is determined by the equation

$$\delta_{z0}=\frac{E_z}{(4\pi\beta_{11}{}^T+O_{11}\delta_{z0})}=\frac{E_z\epsilon_{11}}{4\pi}.$$

By observing how the coupling varies around a hysteresis loop, one can evaluate the remanent polarization.

Heat Transfer in Liquid Helium II by Internal Convection†

F. LONDON AND P. R. ZILSEL
Duke University, Durham, North Carolina

(Received July 12, 1948)

The heat transfer in liquid helium II by internal convection is calculated on the basis of Tisza's two-fluid model. One arrives at the following differential equation for the heat current density, $\mathbf{q}$:

$$\text{curl curl}\mathbf{q} = -\Lambda \,\text{grad}T.$$

Here T = temperature, $\Lambda = (\rho s)^2 T/\eta_n$ is a numerical constant depending on temperature and pressure only (ρs = entropy density and η_n = the viscosity of the "normal" fluid). Comparison with the measurements of the heat transfer in very fine slits by Keesom and co-workers shows only partial agreement. It appears that the heat conductivity of helium II in narrow slits, even in the limit of very small flow, cannot be described by the usual laminary flow solutions of hydrodynamics within the two fluid model, even if one introduces further assumptions such as viscous slip and an Ohm's law type resistance.

I. INTRODUCTION

THE measurements of heat transfer in liquid helium II published recently by Keesom and Duyckaerts,[1] Mellink,[2] and Meyer and Mellink,[3] have shown that in extremely fine capillaries or slits (diameter 0.15–19μ) and for sufficiently small heat input *the transported heat becomes proportional to the temperature difference.* According to previous measurements it appeared that the heat current is proportional to $(\text{grad}T)^{\frac{1}{3}}$ (Keesom[4]). It now appears that this cube root dependence on the temperature gradient is restricted to heat flow in wider capillaries and to larger currents. The new results are of interest insofar as for the first time they seem to give qualitative support to general ideas promoted by Tisza[5] and H. London[6] interpreting the enormous heat conductivity in liquid helium II by a mechanism of "internal convection." This mechanism implies a heat current proportional to $\text{grad}T$. Since this result seemed to be in contradiction to every available experimental evidence so far the theory had never been developed in detail. It might now appear desirable to compare the theoretical expectations with the new experimental data.

According to the view in question, liquid helium II is described as consisting of two mutually interpenetrating fluids having densities ρ_n and ρ_s, respectively. The "normal" fluid (n) carries almost all the entropy of helium II and has ordinary viscosity, whereas the "superfluid" (s) has no viscosity and negligible entropy ($\eta_s = 0$, $s_s \simeq 0$). In first approximation the two fluids are considered as uncoupled, the macroscopic motion of each being described by its own hydrodynamic velocity field $\mathbf{v}_n$ and $\mathbf{v}_s$, respectively.

The "two-fluid" model was originally derived from the idea[7] that the condensation mechanism shown by an ideal Bose-Einstein gas might be responsible for the transition from helium I to helium II at the λ-point. The Bose-Einstein condensation exhibits the unique example of a system of two mutually interpenetrating phases one of which has zero entropy. However, the model in question may, of course, be employed without going into the details of any molecular theory. As a *macroscopic model* it has proved capable of accounting for a number of the peculiar properties of liquid helium II.

It leads to a very simple solution of the apparent paradox that viscosity experiments performed with superfluid helium flowing through

† The work reported here was carried out under Contract N7onr-455 with the Office of Naval Research.

[1] W. H. Keesom and G. Duyckaerts, Physica **13**, 153 (1947), (referred to in text as K and D).

[2] J. H. Mellink, Physica **13**, 180 (1947).

[3] L. Meyer and J. H. Mellink, Physica **13**, 197 (1947), (referred to in text as M and M).

[4] W. H. Keesom, *Helium* (Elsevier Publishing Company, Inc., Amsterdam, 1942).

[5] L. Tisza, Nature **141**, 913 (1938); Comptes Rendus **207**, 1186 (1938); J. de phys. et rad. **1**, 165, 350 (1940); Phys. Rev. **72**, 838 (1948).

[6] H. London, Proc. Roy. Soc. **A171**, 484 (1939).

[7] F. London, Nature **141**, 643 (1938); Phys. Rev. **54**, 947 (1938).

thin capillaries gave no measurable viscosity at all (Kapitza,[8] Allen and Misener[9]) while experiments using a rotating disk immersed in superfluid helium showed a quite normal viscosity of the same order as that of ordinary liquid helium I (Keesom and MacWood[10]).

It was further possible on the basis of this model to give an interpretation of the so-called fountain (or thermo-hydrodynamical) effect as caused by an essentially reversible mechanism of the type of the thermo-electric effects.[5,6] More precisely, the model of Tisza implies that two containers filled with liquid helium II and connected with each other by extremely fine capillaries will be in equilibrium, if a temperature difference ΔT maintained between the containers is accompanied by a pressure difference,

$$\Delta p = \rho s \Delta T, \tag{1}$$

where s = entropy per gram, and ρ = density of liquid helium II. This "thermo-hydrodynamical pressure difference" has subsequently been quantitatively confirmed by the measurements of Kapitza[11] and of Keesom and co-workers.[1,2,3]

Going beyond this result, Tisza inferred from the same model the possibility of a peculiar form of wave motion in liquid helium II in which temperature and entropy density perform periodic fluctuations, quite analogous to the pressure and density fluctuations in ordinary sound. These "temperature waves" represent density waves of ρ_n and ρ_s separately with a phase difference of 180° to each other so that $\rho_n + \rho_s$ is approximately constant. The same mechanism was again derived by Landau[12] who called it "second sound." The phenomenon was subsequently observed by Peshkov[13] and later by Lane and co-workers.[14] These authors found very close agreement between the measured and the theoretically predicted dependence on temperature of the propagation velocity of these temperature waves. Especially these experiments furnish a very sharp test of the validity of the general assumptions which are at the basis of the model under discussion.

However, the second sound waves are not able to transfer much entropy since they propagate nothing but the mechanical energy of their excitation which is extremely small, while the entropy density undergoes only periodic local fluctuations. Thus the second sound is not directly responsible for the "heat superconductivity" in liquid helium.

If one has a capillary or a fine slit connecting two vessels of liquid helium and maintains a temperature difference between them and thus also has a pressure difference according to (1), the normal fluid will not be entirely immobilized by its viscosity. A stationary state will be reached when a certain circulation of the two fluids is established: Superfluid carried by the thermo-hydrodynamic force will go from the cooler to the warmer container. There it will be excited into the normal fluid state, in which state the excess helium will return with viscous flow to the cooler container. Here its excess heat content will be carried away by the thermostat and the excited normal fluid will fall back again into the superfluid state. As only the normal fluid is supposed to carry entropy, a stationary heat flow will be established carrying heat from the warmer to the cooler container. This is the mechanism of heat transfer[5,6] which we shall call "internal convection" and which we are going to discuss in greater detail in the present paper.

II. THE DIFFERENTIAL EQUATIONS OF INTERNAL CONVECTION

The differential equations by which the model of the two mutually interpenetrating fluids has been described are still somewhat uncertain. In particular, the experimentally observed existence of something like an upper limit for the superflow has not yet found a satisfactory mathematical description within the theory. However, in the limit of small deviations from equilibrium, that is, if one neglects all except linear terms in the velocities $\mathbf{v}_n$ and $\mathbf{v}_s$ and in the derivatives of the other quantities entering into the equations, Tisza's assumptions definitely lead to the following set of equations:[12]

[8] P. Kapitza, Nature **141**, 74 (1938).
[9] J. F. Allen and A. D. Misener, Nature **141**, 75 (1938).
[10] W. H. Keesom and G. E. MacWood, Physica **5**, 737 (1939); **8**, 65 (1941).
[11] P. Kapitza, J. Phys. USSR **5**, 59 (1941).
[12] L. Landau, J. Phys. USSR **5**, 71 (1941).
[13] V. Peshkov, J. Phys. USSR **8**, 381 (1944); **10**, 389 (1946).
[14] C. T. Lane, H. Fairbank, H. Schultz, and W. Fairbank, Phys. Rev. **70**, 431 (1946); **71**, 600 (1947).

Conservation of mass:

$$\partial(\rho_n+\rho_s)/\partial t=-\mathrm{div}(\rho_n\mathbf{v}_n+\rho_s\mathbf{v}_s); \quad (2)$$

conservation of momentum:

$$\partial(\rho_s\mathbf{v}_s+\rho_n\mathbf{v}_n)/\partial t=-\mathrm{grad}p -\eta_n(\mathrm{curl\ curl}\mathbf{v}_n-4/3\ \mathrm{grad\ div}\mathbf{v}_n), \quad (3)$$

where η_n is the coefficient of viscosity of the normal component and p is the pressure.

Conservation of entropy:

$$\partial(\rho s)/\partial t=-\mathrm{div}(\rho s\mathbf{v}_n). \quad (4)$$

It should be noted that in Eq. (4) terms have been omitted which would express an irreversible increase in entropy such as that due to the dissipation of kinetic energy caused by the viscosity of the normal component, since such terms are quadratic in the velocities.

Finally:

$$\partial\mathbf{v}_s/\partial t=-\rho^{-1}\,\mathrm{grad}p+s\,\mathrm{grad}T. \quad (5)$$

The derivation of Eq. (5) implies some assumptions which might still appear very much open to argument. We will not enter here into such a discussion but rather take Eqs. (2), (3), (4), and (5) as the presumably simplest expression of the thermo-hydrodynamics of liquid helium II for small velocities. In particular Eqs. (3) and (4) express the assumption that viscosity and entropy are only attributed to the normal component. Equation (5) generalizes the equilibrium condition (1), making a very far-reaching step by attributing a thermo-hydrodynamical force to every volume element of the liquid in which a temperature gradient is being maintained. It is this Eq. (5) which is responsible for the appearance of temperature waves in the theory.

By subtracting ρ times (5) from (3) one obtains:

$$\rho_n\partial(\mathbf{v}_s-\mathbf{v}_n)/\partial t=\rho s\,\mathrm{grad}T +(\eta_n/\rho sT)(\mathrm{curl\ curl}\mathbf{q}-4/3\ \mathrm{grad\ div}\mathbf{q}), \quad (6)$$

similarly, Eq. (2) minus s^{-1} times Eq. (4) gives

$$\rho_s\,\mathrm{div}(\mathbf{v}_s-\mathbf{v}_n)=\rho\dot{s}/s =\rho/s\left[\left(\frac{\partial s}{\partial T}\right)_p\dot{T}+\left(\frac{\partial s}{\partial p}\right)_T\dot{p}\right]. \quad (7)$$

In (6) we have written $\mathbf{q}$ for the heat current density vector

$$\mathbf{q}=\rho sT\mathbf{v}_n. \quad (8)$$

Eliminating $\mathbf{v}_s-\mathbf{v}_n$ from (6) and (7) we obtain the wave equation of the temperature waves of Tisza and Landau plus an attenuation term:

$$-\frac{\rho_n}{\rho_s}\frac{\partial(1/s)}{\partial T}\ddot{T}=\mathrm{div\ grad}\left[T-\frac{4}{3}\frac{\eta_n}{\rho}\frac{\partial(1/s)}{\partial T}\dot{T}\right]. \quad (9)$$

Here we have omitted the term $(\partial s/\partial p)_T\dot{p}$ which entails a coupling between the temperature waves and the pressure (ordinary sound) waves. This is very small since $(\partial s/\partial p)_T=-(\partial V/\partial T)_p$ is very small for liquid helium II.

In case that *conditions of stationary heat transfer* are reached, we have to go back to Eq. (6). Since under those conditions $\mathrm{div}\mathbf{q}=0$, we obtain:

$$\Lambda\,\mathrm{grad}T=-\mathrm{curl\ curl}\mathbf{q}, \quad (10)$$

where

$$\Lambda=(\rho s)^2T/\eta_n \quad (11)$$

is a new characteristic coefficient.

Equation (10) replaces the usual equation

$$K\,\mathrm{grad}T=-\mathbf{q}$$

of ordinary heat conductivity. One might call (10) the differential equation of "heat superconductivity" or, more appropriately, of "internal heat convection." It expresses quantitatively the idea of H. London and Tisza that entropy is being transferred by a movement of the two phases relative to each other.

Whereas in ordinary heat conductivity

$$\mathrm{curl}\mathbf{q}=0,$$

as follows directly from the usual heat conduction equation, we see that according to (10) a temperature gradient can be maintained in helium II only if $\mathrm{curl}\mathbf{q}\neq0$. This is a consequence of the fact that in the present form of the theory the only resistance to internal convection at small velocities is the viscosity of the normal phase.

The *boundary conditions* derive from those of the normal phase.[15]

$$v_{n\parallel}=0; \quad \rho sTv_{n\perp}=-K_a(\mathrm{grad}T)_{\perp\ \mathrm{solid}},$$

where K_a is the heat conductivity of the adja-

[15] L. Landau, J. Phys. USSR 8, 1 (1944).

cent medium. This means

$$q_{\parallel}=0; \quad q_{\perp}=-K_s(\mathrm{grad}T)_{\perp \text{ solid}}.$$

For a *slit of width d* one obtains as solution the parabolic current distribution of laminary viscous flow over the cross section $(-\frac{1}{2}d\leqslant x\leqslant\frac{1}{2}d)$ of the slit in the form

$$\mathbf{q}=\tfrac{3}{2}\bar{\mathbf{q}}(1-4x^2/d^2),$$

where $\bar{\mathbf{q}}$ is the mean value of q taken over the cross section of the slit. Hence

$$\Lambda\,\mathrm{grad}T=-12\bar{q}/d^2 \qquad (12)$$

and accordingly the mean "heat conductivity" is given by

$$\bar{K}=\bar{q}/|\mathrm{grad}T|=\Lambda d^2/12=(\rho s)^2Td^2/12\eta_n. \qquad (13)$$

Similarly for a circular capillary of radius R one calculates as mean heat conductivity

$$\bar{q}/|\mathrm{grad}T|=\Lambda R^2/8.$$

The entropy density of helium between 1°K and the λ-point can be approximately represented by the empirical formula

$$\rho s=0.72\times10^{-3}T^{5.6}\ \text{cal deg.}^{-1}\ \text{cm}^{-3}$$
$$=3\times10^{4}T^{5.6}\ \text{erg deg.}^{-1}\ \text{cm.}^{-3}$$

The viscosity measurements of Keesom and MacWood by the oscillating disk method actually determine the product $\rho_n\eta_n$; if one assumes that $\rho_n\sim s$, as is suggested by general arguments, it follows that η_n is roughly constant between 1°K and the λ-point and about equal to the viscosity of liquid helium I, that is, of the order $\eta_n\simeq2\times10^{-5}$[g cm^{-1} sec.$^{-1}$]. With these values one obtains for the mean heat conductivity (13) of the slit of width d:

$$\bar{K}\simeq0.9\times10^{5}T^{12.2}d^2[\text{cal deg}^{-1}\ \text{cm}^{-1}\ \text{sec}^{-1}]. \qquad (13')$$

For comparison we give the heat conductivity of ordinary helium I at 3.3°K:

$$K_{\mathrm{HeI}}=6\times10^{-5}[\text{cal deg.}^{-1}\ \text{cm}^{-1}\ \text{sec.}^{-1}].$$

Accordingly even in a slit of only 10μ diameter the "mean heat conductivity" of liquid helium II at 2°K would be 10^7 times larger than that of helium I.

III. COMPARISON WITH EXPERIMENT AND DISCUSSION

a. Critical Velocity

In comparing the "mean heat conductivity" given by Eq. (13′) with the experimental data[1,2,3] one must take care to confine oneself to the region of presumable validity of the linear theory, i.e., to the region of sufficiently small heat currents where $\bar{\mathbf{q}}$ is proportional to grad$T$. In the narrowest slits ($d<.75\mu$) no deviations from the linear law are observed within the range of the given data (grad$T\simeq10^{-2}$ deg. cm^{-1}). As the width d of the slit increases, deviations appear first at temperatures close to the λ-point until, for $d>10\mu$, no linear dependence of $\bar{\mathbf{q}}$ on grad$T$ is observed even at the lowest temperatures ($T\simeq1.1$°K) and for the smallest measured temperature gradients. The values of $\bar{q}$ at which the deviations begin in the various experiments can be determined from the given data only very approximately. But it appears that the limiting feature is a critical velocity of the superflow $\mathbf{v}_s$ and not perhaps turbulence of the normal flow $\mathbf{v}_n$, as one might think. From Eq. (8) and the condition of no net flow

$$\rho_n\mathbf{v}_n+\rho_s\mathbf{v}_s=0,$$

one has

$$\bar{\mathbf{q}}=\rho sT\bar{\mathbf{v}}_n=-\rho sT\frac{\rho_s}{\rho_n}\bar{\mathbf{v}}_s\sim-T(T_\lambda^{5.6}-T^{5.6})\bar{\mathbf{v}}_s \qquad (14)$$

where $T_\lambda=2.19$°K is the temperature at the λ-point.

Within the limits of accuracy of their determination from the experimental data the values of v_s (critical) obtained with the aid of (14) are *independent of the temperature*. They depend on the width d of the slit approximately as d^{-1}.

Typical examples of the determination of $\bar{v}_sd$ (critical) from the experimental data are collected in Table I. The column headed $\bar{q}\times d$ gives the mean heat current density multiplied by the width of the slit. In a slit of given width d and at a given temperature T the region of validity of a linear law is determined by the proportionality of $\bar{q}\times d$ to the temperature difference ΔT, that is by $\bar{q}\times d/\Delta T=$constant. The braces in Table II indicate the experimental limits within which in each case the proportionality of q to ΔT comes to an end. When $\bar{q}\times d/\Delta T$

TABLE I. Limits of the linear region; determination of critical velocities.

$d\times10^4$ cm	T °K	$\bar{q}d\times10^6$ cal/cm sec	$(\bar{q}d/\Delta T)\times10^3$ cal/cm sec. deg.	$\bar{v}_s d\times10^3$ cm²/sec.	R_n
0.75	2.097	4.03	8.5	1.45	2.3
	2.097	4.16	8.5	1.5	2.4
	2.097	6.65	7.7	2.4	3.9
1.15	1.989	2.2	8.2	0.5	1.4
	1.989	6.5	8.2	1.3	4.0
	1.989	8.9	7.9	1.8	5.4
	2.170	0.57	11.4	0.9	0.3
	2.170	1.04	10.4	1.7	0.6
	2.170	1.64	10.2	2.6	1.0
1.75	1.960	0.58	11.0	0.1	0.15
	1.960	3.34	11.0	0.63	0.8
	1.960	6.6	10.5	1.3	1.7
	1.960	9.4	10.3	1.8	2.4
	1.960	16.4	9.9	3.0	4.1
9.3	1.586	3.9	15.8	0.5	1.2
	1.586	12.6	15.8	1.6	3.9
	1.586	30.4	9.5	3.9	9.4
	1.807	5.8	72	0.8	1.8
	1.807	10.1	72	1.4	2.7
	1.807	25.1	67	3.6	6.8
	1.807	35.7	38	5.1	9.7
	1.962	6.1	190	1.2	1.5
	1.962	14.9	177	2.8	3.7
	1.962	31.1	133	5.8	7.8

begins to decrease the critical velocity has been exceeded. $R_n=\rho_n\bar{v}_n d/\eta_n$ is the Reynolds number for the "normal" flow. One sees from the table that in every case R_n is smaller by orders of magnitude than the value $\sim10^3$ at which turbulence may be expected to set in; thus the observed deviations from linear dependence of $\bar{q}$ on grad$T$ cannot be ascribed to turbulent flow of the viscous normal phase.

The product $d\times\bar{v}_s$ (critical) is seen to be of the order of magnitude

$$d\times\bar{v}_s(\text{critical})\simeq10^{-3}\ \text{cm}^2\ \text{sec.}^{-1}.$$

This is in agreement with the values obtained from Kapitza's experiments;[11] it is about 10 times larger than the values found by Daunt and Mendelssohn[16] for the transfer velocity in the supra-surface film.*

The d^{-1} dependence of $\bar{v}_s$ (critical) accounts for the fact that no region of linear dependence of $\bar{q}$ on grad$T$ has been observed in capillaries wider than 10μ. By virtue of the factor multiplying $\bar{\mathbf{v}}_s$ in (14) the critical value of $\bar{q}$ for a slit of given d approaches zero as the temperature approaches the λ-point. Thus for $T\rightarrow T_\lambda$ a linear formula can give no more than the slope $\partial\bar{q}/\partial|\text{grad}T|$ at grad$T=0$. This explains the fact that in capillaries of intermediate width $(1-10\mu)$ a region of linear dependence of $\bar{q}$ on grad$T$ is observed at low temperatures, whereas at temperatures close to the λ-point deviations from the linear law tend to occur even for the smallest measured values of grad$T$.

For the same reason, experimental curves of $\bar{q}$ *versus* T for given values of grad$T$—curves which show a maximum in the conductivity between 1.9° and 2.0° and then a rapid decrease as $T\rightarrow T_\lambda$—are misleading, since for any finite value of $|\text{grad}T|$ the critical velocity is inevitably exceeded if one goes sufficiently near the λ-point. This situation is exemplified in Fig. 1 which shows a typical experimental curve of $\bar{q}$ *versus* T for constant $|\text{grad}T|$ (heavy curve). The broken line is the corresponding curve of $\bar{q}$ (critical) as given by Eq. (14) with $d\times\bar{v}_s(\text{critical})=10^{-3}$ cm²/sec. One sees that the critical velocity is exceeded already at a temperature below the maximum of $\bar{q}$. This is quite generally the case.

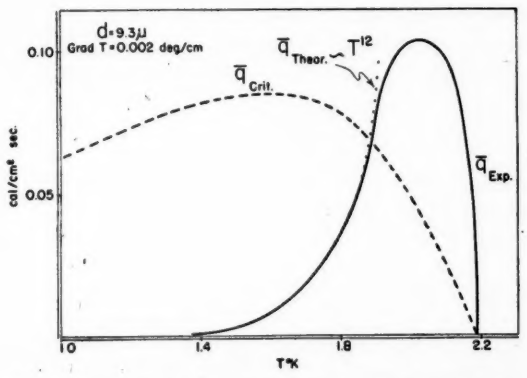

FIG. 1. Experimental heat current density $\bar{q}_{exp}$ as a function of the temperature T for constant temperature gradient (heavy curve); the curve plotted refers to a slit of width $d=9.3\times10^{-4}$ cm and to grad$T=0.002$ deg./cm. The broken curve gives the critical value of $\bar{q}$ as a function of T for a slit of the same width. The maximum in the experimental curve, as well as its decrease as the temperature approaches the λ-point, occurs in the region where $\bar{q}_{exp}>\bar{q}_{critical}$, i.e., outside the region of validity of the linear theory.

[16] J. G. Daunt and K. Mendelssohn, Proc. Roy. Soc. **A170**, 423 (1939); also: A. Bijl, J. de Boer, and A. Michels, Physica **8**, 655 (1941).

* *Note added in proof:* According to K. R. Atkins, Nature **85**, 925 (1948) the supra-surface film also has a considerably larger critical velocity in the presence of a temperature difference.

Hence one cannot expect to explain the decrease of $\bar{q}$ towards the λ-point by the present theory.

b. Linear Region: Experimental Values of $\bar{K}$

Representative values of the mean heat conductivity $\bar{K}_{\text{exp.}}=\bar{q}/|\text{grad}T|$ in the linear region are given in Table II. They were calculated from the experimental data of Meyer and Mellink (M and M) and Keesom and Duyckaerts (K and D). The corresponding theoretical values, $\bar{K}_{\text{theor.}}$, are given by Eq. (13′). In Table II L is the length of each slit; $\bar{K}_{\text{exp.}}/\bar{K}_{\text{theor.}}$ gives the ratio of the experimental to the theoretical value of the mean conductivity. The last column roughly gives the power of variation of $\bar{K}_{\text{exp}}$ with T.

The accuracy of some of the quantities entering into the tables might be somewhat doubtful, the greatest uncertainty probably coming from the determination of the width d of the slit in the various experiments. The widths were determined from optical interference measurements and from measurements of gas flow through the slits. Even granting the accuracy of those determinations (Meyer and Mellink estimate the probable error at 20 percent) they can only give the *average* width over the slit; the actual width may vary considerably in different parts of the slit. Since the mean heat conductivity depends rather strongly on the width, this is a source of considerable error. Another, though probably minor, source of error is the corrections applied to the observed heat flows to take account of losses of various kinds. From Table II one sees that the values of $\bar{K}_{\text{exp}}$ from Meyer and Mellink are consistently higher than those from Keesom and Duickaerts. M and M indicate that they had considerable difficulty in attaining a stationary state in their experiments, so that one might suspect that their measurements were not really made under stationary conditions and that this is the cause of the discrepancy between the two sets of data. The only other explanation one could think of is that this strange discrepancy has something to do with the length of the slits, those of M and M being less than half as long as those of K and D. Such an explanation does not seem very likely, however: "end effects" should be expected to be due to Bernoulli terms which have been neglected in the linear hydrodynamic equations. Since such terms are quadratic in the velocities of flow one would expect that if "end effects" are important they would destroy the proportionality between $\bar{q}$ and $|\text{grad}T|$.

TABLE II. Comparison of experimental and theoretical values of the mean heat conductivity.

	T(°K)	$\bar{K}_{\text{exp}}$ (cal/deg. cm sec.)	$\bar{K}_{\text{theor}}$ (cal/deg. cm sec.)	$\bar{K}_{\text{exp}}/\bar{K}_{\text{theor}}$	$\frac{\Delta\ln(\bar{K}_{\text{exp}})}{\Delta\ln(T)}$
$L=0.248$ cm	1.586	4.45	22	0.20	
$d=9.3\times10^{-4}$ cm	1.807	18.7	103	0.18	11.0
(K and D)	1.962	43.5	295	0.15	10.3
$L=0.275$ cm	1.223	0.066	0.032	2.05	
$d=1.75\times10^{-4}$ cm	1.476	0.61	0.32	1.92	11.9
(K and D)	1.705	3.5	1.86	1.88	12.1
	1.960	17.2	10.2	1.69	11.5
$L=0.275$ cm	1.799	5.35	1.55	3.45	
$d=1.15\times10^{-4}$ cm	1.989	17.1	5.28	3.25	11.6
(K and D)	2.170	24	15.5	1.55	3.9
$L=0.1$ cm	1.411	1.05	0.060	17.5	
$d=1.0\times10^{-4}$ cm	1.802	12.4	1.19	10.4	10.1
(M and M)	1.948	21.4	3.06	7.0	7.3
	2.159	31	10.8	2.9	3.6
$L=0.275$ cm	1.403	0.39	0.031	12.5	
$d=0.75\times10^{-4}$ cm	1.600	1.85	0.156	11.8	11.8
(K and D)	2.097	30.2	4.3	7.0	10.3
$L=0.1$ cm	1.086	0.124	0.0006	202	
$d=0.5\times10^{-4}$ cm	1.274	0.277	0.0043	64	5.0
(M and M)	1.315	0.354	0.0064	55	8.3
	1.659	2.48	0.108	23	8.3
$L=0.1$ cm	1.226	0.25	0.00097	260	
$d=0.3\times10^{-4}$ cm	1.358	0.48	0.0034	140	6.4
(M and M)	1.558	1.35	0.018	75	7.5
	1.652	1.92	0.0365	54	6.0

Altogether it appears that the listed values of $\bar{K}_{\text{exp.}}/\bar{K}_{\text{theor.}}$ may be expected to be uncertain by as much as a factor of 2 one way or the other. In spite of this the data indicate quite clearly the general dependence of $\bar{K}$ on the temperature and the width of the slit.

c. Temperature Dependence

Except in the two narrowest slits ($d=0.3$ and 0.5μ)** *the theoretical $T^{12\cdot2}$ dependence agrees rather*

** M and M have also made measurements in still narrower slits (0.15 and 0.2μ), but those measurements were made by a non-stationary method and therefore have not been used in the present analysis.

well with the experimental data up to about 1.9°; the fit is somewhat better with $d(\log\bar{K})/d(\log T) \simeq 11.5$. This may be accounted for theoretically if one assumes $\eta_n \sim T^{0.5}$, as is the case in an ideal gas and in liquid helium I,*** instead of taking η_n = constant as was done in deriving Eq. (13′). When T approaches the λ-point $\bar{K}$ as a function of T levels off very definitely, but in no case has an actual maximum been observed. (Note that K is, of course, understood as function of T always in the limit $|\text{grad}T| \to 0$.)

In the narrowest slits the dependence on temperature is rather as T^7 or T^8 up to the highest temperatures at which measurements have been made ($T \simeq 1.7°$). No data are available on whether there is a leveling off at higher temperatures in this case also.

d. Absolute Value of $\bar{K}$ and Dependence on Width of Slit

A glance at the last column in Table II shows that the ratio of the observed to the theoretically predicted mean heat conductivity varies in order of magnitude from 10^2 in the narrowest slits to 10^{-1} in the widest. This looks rather discouraging; but it should be pointed out that except for its proportionality to d^2, which obviously does not fit the facts, the formula (13), based on the idea of heat transfer by internal convection, comes much closer to the experimental data than would a formula based on the usual type of heat conduction by "diffusion of energy." The latter mechanism would give a heat conductivity approximately independent of the temperature and of the order of that in helium I, that is too small by a factor of about 10^{-5} to 10^{-7}.

Actually there is an increase of the mean conductivity with d in the wider slits ($d \gtrsim 10^{-4}$ cm), but it is not nearly as strong as d^2. In the narrowest slits the conductivity seems to be approximately independent of d.

*** As has been pointed out by Tisza (see reference 5), the small density of liquid helium and the temperature dependence of the viscosity of helium I make it appear likely that in contrast to all other liquids the viscosity of liquid helium is of the "kinetic" type usually found in gases. In this case one would expect

$$\eta_n \simeq \rho_n l_n \bar{u}_n,$$

where l_n is the mean free path and $\bar{u}_n$ the mean thermal velocity of the "normal" particles. The product $\rho_n l_n$ should be approximately temperature-independent and $\bar{u}_n \simeq T^4$

IV. ATTEMPTS TO ACCOUNT FOR THE DISCREPANCIES

The discrepancies between the observed values of $\bar{K}$ and the predictions of the theory as given by Eq. (13′) are essentially of two types: (*a*) *In the narrowest slits the observed values of the heat current density are some hundred times larger than those predicted by the theory.* (*b*) *In the widest slits in which a linear dependence of* $\bar{q}$ *on* grad$T$ *has been observed the heat currents are actually less than expected from the theory; furthermore at temperatures close to the* λ*-point the conductivity increases with temperature much more slowly than the theory predicts.*

To account for these discrepancies, one may attempt to generalize in two respects the equations by which internal convection has been described in Sec. 2 of this paper.

Item (*a*) points to a larger conductivity for the narrowest slits than is given by the theory. Since it appears impossible to get rid of the normal viscosity by manipulating the differential equations, one may conclude that the boundary condition $v_{n\parallel} = 0$ is too stringent. One may introduce a slip of the normal flow velocity v_n along the wall of the slit by replacing the boundary condition $v_{n\parallel} = 0$ by

$$v_{n\parallel} = -a\partial v_{n\parallel}/\partial N, \tag{15}$$

where N is the outward normal to the boundary of the slit. The quantity a in (15) is of the dimension of a length and should be of the order of the mean free path of the particles in the normal phase. From the experimental value of the viscosity one estimates for the mean free path at the λ-point

$$l_n \simeq 10^{-7} \text{ cm} (T = T_\lambda),$$

so that one should expect

$$a \simeq l_n \simeq 10^{-7}(\rho/\rho_n) \simeq 10^{-7}(T_\lambda/T)^{5.6} \text{ cm}.$$

Item (*b*) indicates the presence of a resistance to internal convection in addition to the viscosity of the normal fluid. This additional resistance becomes significant for wider slits. One may try empirically to account for this discrepancy by formally introducing an Ohm's law type of resistance into the Eq. (6) describing the relative motion of the two phases. This

means that we replace Eq. (10) by

$$-\text{grad}T=\Lambda^{-1}(\text{curl curl}\mathbf{q}+\beta^2\mathbf{q}) \quad (16)$$

the function $\beta(T)$ to be determined empirically.

Band and Meyer[17] have recently fitted the heat conductivity in a wider capillary by assuming a resistance to the relative motion of the two phases equivalent to a term like the supplementary one in Eq. (16). However, since they were using data from the region of cube root dependence of q on $|\text{grad}T|$, their resistance is a function not only of T but also of q itself (proportional to q^2). Furthermore, they completely neglect the viscous resistance of the normal phase, using *only* the Ohm's law type of resistance; thus in their formula the heat conductivity is independent of the width of the capillary. Because of its proportionality to q^2 the resistance proposed by Band and Meyer cannot be applicable to the linear region. At any rate it appears hopeless to try to understand the laws of motion of the two-phase model of helium II in the region of supra-critical velocities as long as one cannot account satisfactorily for the small heat currents.

Using (16) and the boundary condition (15) the stationary solution becomes

$$\mathbf{q}=\Lambda\beta^{-2}\,\text{grad}T\left[\frac{\cosh\beta x}{\cosh(\beta d/2)+a\beta\sinh(\beta d/2)}-1\right], \quad (17)$$

and one obtains for the mean heat current density:

$$\bar{q}=\Lambda\beta^{-2}|\text{grad}T|\left[\frac{\xi^{-1}\sinh\xi}{\cosh\xi+a\beta\sinh\xi}-1\right], \quad (18)$$

where we have put $\beta d/2=\xi$. Expanding this expression into powers of ξ we obtain as heat conductivity for slits of small width d:

$$\bar{q}/|\text{grad}T|=\Lambda\beta^{-2}[a\beta\xi+(\tfrac{1}{3}-a^2\beta^2)\xi^2+\cdots]$$
$$=\frac{\Lambda d^2}{12}[1+6a/d-3a^2\beta^2+\cdots].$$

One sees that the new assumptions amount to a correction by a factor

$$[1+6a/d-3a^2\beta^2+\cdots] \quad (19)$$

in the formula (13′) for the mean heat conductivity. If one takes a and $\beta(T)$ independent of d, as they ought to be if they are to have any reasonable physical meaning, one sees that a correction factor of the type (19) will not suffice to bring (13′) into agreement with the experimental data: The expression (18) for the mean heat conductivity still increases too fast with d; in particular for very narrow slits it is proportional to d rather than independent of d as the experimental data (of Table II) seem to indicate.

It is interesting to note that quite formally Eq. (18) is able to account for the T^7 dependence of $\bar{K}$ in the narrowest slits where one can presumably neglect the term proportional to d^2 compared to $6ad$. One can fit the data fairly well by setting

$$a\simeq 3\cdot 10^{-3}T^{-5.5}\text{ cm},$$

which has the right temperature dependence for the mean free path of the normal phase particles. However for two reasons this is not likely to have physical significance: First, the mean free path would be larger than the width of the slit; in that case, however, the whole hydrodynamic description of the flow would break down. Second, the mean free path implied by a slip of this magnitude is some hundred times larger than the mean free path corresponding to the experimental value of the viscosity as determined in the rotating disk experiments of Keesom and MacWood.[10] On the other hand it should be pointed out that there is no *direct* experimental evidence to exclude a slip of this magnitude: It is true that Keesom and MacWood failed to detect any measurable slip in their experiments. However, within the experimental accuracy of their measurements a slip of the magnitude in question here could not have been observed.

V. CONCLUSIONS

From the above discussion it appears that the present data on the heat flow in helium II in narrow slits cannot satisfactorily be described by the usual laminary flow solutions of the two-fluids hydrodynamics even with the additional assumptions of viscous slip and an Ohm's law type resistance. On the other hand, since our discussion was aimed at the limiting case of small

[17] W. Band and L. Meyer, Phys. Rev. **73**, 226 (1948).

velocities, when $\mathbf{v}_n$ is proportional to grad$T$, one cannot have recourse to assuming complications by turbulent flow either.

It is, of course, possible that the whole concept of the two-fluid hydrodynamics loses its validity when dissipative processes are considered. However, in view of the achievements of the theory in general, it appears unwarranted to go so far, and one will expect that, at least in the limit of very small velocities, the theory should be competent to account also for dissipative processes.

It might be pointed out that the critical values of $v_s d$ obtained from the present data, as well as those from Kapitza's flow experiments, are some ten times larger than those observed in connection with the supra-surface film (Daunt and Mendelssohn), the latter being of the order of $h/4\pi m \simeq 10^{-4}$. Hence it might be argued that the applicability of the theory is restricted to still smaller velocities, i.e., still smaller heat currents than the ones used in the experiments under discussion. This does not appear to be a valid argument since for most slits the observed heat conductivity is *larger* than that predicted by the theory. One cannot think of any perturbation mechanism which would lead to a *decrease* of the resistance with *increasing* flow velocity. At any rate it would be desirable to extend the measurements to still smaller heat currents.

It seems that in order to account for the present experimental data in terms of the general two-fluid theory some features of the theory must be revised. There appear to be two possibilities for doing this:

(1) One may have to abandon the idea of attributing an ordinary hydrodynamic viscosity to the normal phase of helium II. This would not be very satisfactory, since it is precisely the assumption that the normal phase has viscosity while the superfluid phase has none which in Tisza's theory explains some of the most striking properties of helium II (rotating disk experiments *versus* superfluid flow in narrow capillaries).

Or (2) one may have to assume that in the case of stationary flow through narrow slits the normal phase of the liquid helium II does not touch the wall of the slit at all, but that there is a film of pure superfluid next to the wall. This alternative is at any rate preferable to the first one. Allen and Misener[18] were led to a similar picture from their investigations of viscous flow of helium II in narrow capillaries ("sub-surface film"). This assumption would mean that there are large variations in the densities of the two phases over the width of the slit when stationary flow is being maintained.

This possibility is rather difficult to investigate quantitatively at the present time, since one does not know the correct hydrodynamic equations for the two-phase model if one cannot consider ρ_n and ρ_s as approximately constant.

One cannot entirely exclude the possibility that the phenomena may be describable in terms of end effects: Terms of the type grad(v_s^2), which have been neglected in the linear equations, may become large at the ends of the slit. It would appear that since such terms are quadratic in the velocities they cannot be important in the limit of small velocities, that is, in the region of proportionality of $\mathbf{v}_s$ and $\mathbf{v}_n$ to grad$T$. But it could be that the distance within which $\mathbf{v}_s$ and $\mathbf{v}_n$ reach the values they assume within the slit, is itself proportional to $\mathbf{v}_s$, so that grad(v_s^2) would actually be linear in $\mathbf{v}_s$. However, also this possibility cannot be investigated quantitatively without further refinement of the hydrodynamics of the model.

[18] J. F. Allen and A. D. Misener, Proc. Roy. Soc. **A172**, 467 (1939).

PHYSICAL REVIEW VOLUME 74, NUMBER 9 NOVEMBER 1, 1948

Some Observable Effects of the Quantum-Mechanical Fluctuations of the Electromagnetic Field

THEODORE A. WELTON*
Department of Physics, Massachusetts Institute of Technology, Cambridge, Massachusetts

(Received June 4, 1948)

An intuitive explanation is given for the electromagnetic shift of energy levels by calculating the mean square amplitude of oscillation of an electron coupled to the zero-point fluctuations of the electromagnetic field. The resulting disturbance of the charge and current density of the electron gives rise to various observable effects which can be estimated in a simple classical fashion. The effects treated are the Lamb shift, the correction to the g-factor for the orbital and spin angular momenta of the electron, and the correction to the Compton scattering cross section at low energies. A simple explanation is also given for the peculiar ultraviolet divergence noticed by Pauli and Fierz in their treatment of the infra-red paradox.

I. INTRODUCTION

IT has been pointed out by Bethe[1] that the displacement of the $2S$ level of hydrogen observed by Lamb and Retherford,[2] can be simply explained as a shift in the energy of the atom arising from its interaction with the radiation field. In order to obtain this result, it is necessary to subtract from the usual infinite result an infinite energy which is essentially the electromagnetic self-energy of the electron. The residual energy shift gives the experimental result, after the introduction of a plausible cut-off in the integral over quantum energies. It is the purpose of this note to point out the existence of a simple picture of the origin of this residual finite level shift which is capable of extension to other phenomena in which virtual emission and absorption of quanta gives rise to formal divergences. In many cases it yields a simple understanding of the phenomenon and, in addition, a semiquantitative calculation of the magnitude of the effect.

Since Bethe's subtraction removes the classical electromagnetic self-energy, the remaining physically significant energy must be thought of as arising from the purely quantum-mechanical aspects of the system. The quantization of the radiation field manifests itself qualitatively through the existence of fluctuating field strengths in empty space, and it is therefore natural to inquire into the effects produced on mechanical systems by these fluctuations. The most obvious effect is the spontaneous emission of radiation from atoms in excited states. This phenomenon can be thought of as forced emission taking place under the action of the fluctuating field. Another effect which is equally simple is the existence of a fluctuation in position of a free electron. This may be thought of as a Brownian motion of the electron in equilibrium with a hohlraum, which motion persists when the temperature is reduced to absolute zero. It may be expected that this fluctuation in position will disturb the charge and current distribution arising from an electron in an atom, and hence give rise to observable effects. Weisskopf[3] has pointed out that the interaction of this fluctuation with the field which produces it gives a natural explanation for a part of the infinite self-energy of the free electron. In this paper we shall assume that the position fluctuation is a real concept, while we shall think of the energy of interaction between the field and particle fluctuations as having no physical reality. We propose to give a discussion of these effects which is as nearly intuitive as possible, postponing any attempts at formal justification to the last part of this paper.

II. THE MEAN SQUARE FLUCTUATION IN POSITION OF A FREE ELECTRON

Our starting point is the observation that the quantum-mechanical zero-point variation of the radiation field in empty space gives rise to fluctuating electric and magnetic fields whose mean square values at a point in space are given by the

* Now at the Randal Morgan Laboratory of Physics, University of Pennsylvania, Philadelphia, Pennsylvania.

[1] H. A. Bethe, Phys. Rev. **72**, 339 (1947).

[2] W. E. Lamb, Jr. and R. C. Retherford, Phys. Rev. **72**, 241 (1947).

[3] V. F. Weisskopf, Phys. Rev. **56**, 72 (1939).

well-known relation

$$\langle E^2\rangle_{Av}=\langle B^2\rangle_{Av}=\frac{2\hbar c}{\pi}\int_0^\infty k^3dk. \tag{1}$$

In this equation the variable k refers to the wave number of a quantum, and the contribution to the mean square fluctuation arising from frequencies in the range cdk is therefore explicitly displayed. Equation (1) can be simply derived by ascribing to every normal mode of the radiation field an energy which is just the zero-point energy for an oscillator with the frequency of the normal mode. The total energy can be written either as the volume integral of the ordinary electromagnetic energy density or as a sum over normal modes, and Eq. (1) merely states the equality of these two forms.

It will now be assumed that an otherwise free electron is acted on by these fluctuating fields. The electron will be assumed to move with nonrelativistic velocities so that if $\mathbf{q}$ is its position vector, the equation of motion is

$$m(d^2\mathbf{q}/dt^2)=e\mathbf{E}. \tag{2}$$

The vector $\mathbf{E}$ is the fluctuating field specified by (1). Since Eq. (2) is linear, we can regard it as a classical equation for the quantum-mechanical expectation value of $\mathbf{q}$. For a given harmonic component of $\mathbf{E}$ the solution of (2) is obvious. We perform this integration, find the resulting value of $\langle q^2\rangle_{Av}$, and sum over frequencies using (1). We then obtain a quantity $\langle(\Delta q)^2\rangle_{Av}$, defined as the mean square fluctuation in position of a free electron

$$\langle(\Delta q)^2\rangle_{Av}=\frac{2}{\pi}\frac{e^2}{\hbar c}\left(\frac{\hbar}{mc}\right)^2\int_{k_0}^{\kappa}\frac{dk}{k}. \tag{3}$$

The upper and lower limits of integration are infinity and zero if the preceding assumptions are literally adhered to. The divergence at the upper limit of the integral in (3) is certainly fictitious since the equation of motion (2) neglects the spatial dependence of a given Fourier component of the electromagnetic field. This spatial dependence would give rise to a longitudinal recoil of the electron in addition to the transverse oscillation which we have included. This recoil will become important for light with a wavelength shorter than the Compton wave-length of the electron. We therefore assume that the upper limit is given by

$$\kappa=mc/\hbar. \tag{4}$$

This assumption will be further supported in the last section of this paper.

The lower limit is strictly zero, and for a free electron we therefore have the result that the mean square fluctuation in position is infinite. It should, however, be remembered that the divergence arises from very large, but very slow low frequency fluctuations. These contributions will be suppressed by the presence of any sort of binding, and the lower limit k_0 will be determined in every case from consideration of the details of the electronic motion. This point will be discussed more carefully in a later section.

III. THE LAMB SHIFT

The magnitude of this mean square fluctuation in position will be very small for any reasonable k_0, but an observable effect will arise when the electron moves in a potential with a large curvature. This can easily be seen in the following way. Consider the motion of an electron in a static field of force specified by a potential energy $V(\mathbf{q})$. The coordinates of the electron consist of a part which varies smoothly in time with the orbital frequency plus a part which fluctuates randomly in time. We designate the smooth part by $\mathbf{q}$ and the random part by $\Delta\mathbf{q}$. The instantaneous potential energy is then given by

$$V(\mathbf{q}+\Delta\mathbf{q})=[1+\Delta\mathbf{q}\cdot\nabla+\tfrac{1}{2}(\Delta\mathbf{q}\cdot\nabla)^2+\cdots]V(\mathbf{q}). \tag{5}$$

The effective potential energy in which the particle moves will just be the average of (5) over all values of $\Delta\mathbf{q}$. Remembering that $\Delta\mathbf{q}$ has an isotropic spatial distribution, we obtain

$$\langle V(\mathbf{q}+\Delta\mathbf{q})\rangle_{Av}=[1+\tfrac{1}{6}\langle(\Delta q)^2\rangle_{Av}\nabla^2+\cdots]V(\mathbf{q}). \tag{6}$$

We thus see that the existence of the position fluctuation of the electron will effectively modify the potential in which it moves by the addition of a term proportional to the Laplacian of the potential energy. This correction will suffice if ∇^2V is sufficiently small, but in general it must be remembered that the effective potential energy is to be obtained from the original potential energy by the application of an integral operator

with a displacement kernel, which is just the distribution function for $\Delta\mathbf{q}$. This point will be amplified in a later section.

Now consider the perturbation of the levels of the hydrogen atom caused by this modification of the potential energy. We take for $V(\mathbf{q})$ the static potential of the nucleus

$$V(\mathbf{q}) = -\frac{e^2}{r}. \tag{7}$$

The expansion (6) does not converge for this potential, but for the time being it will be assumed that the first correction term in (6) is sufficient, the justification being left until later. We obtain the correction to the potential energy by combining (3), (4), and (6)

$$\Delta V(\mathbf{q}) = \frac{4e^2}{3}\frac{e^2}{\hbar c}\left(\frac{\hbar}{mc}\right)^2 \log\frac{mc^2}{\hbar c k_0}\delta(\mathbf{q}). \tag{8}$$

The correction to the energy of a stationary state of the atom with wave function $\psi(\mathbf{q})$ will be

$$\Delta E = \frac{4e^2}{3}\frac{e^2}{\hbar c}\left(\frac{\hbar}{mc}\right)^2 \log\frac{mc^2}{\hbar c k_0}|\psi(0)|^2. \tag{9}$$

This expression will be recognized as identical with the expression derived by Bethe for the level shift. The quantity hck_0 should clearly be taken equal to the average excitation energy (17.8 Rydbergs) introduced by Bethe,[1] in order to obtain approximate agreement with the experimental result of Lamb. This value for the lower cut-off occurring in the integral over quanta seems implausibly large from the arguments advanced thus far, but it will later be shown by a simple argument to be very reasonable.

It should be noted in passing that from the nature of the effect the sign of the energy shift is clear, it being obvious that the fluctuation in position must always act to weaken the effect of the potential energy.

We must now discuss the validity of the seemingly inadmissible omission of powers of the Laplacian higher than the first from the expansion (6). Suppose that the probability of finding the instantaneous fluctuation $\Delta\mathbf{q}$ in the volume element $d\Delta\mathbf{q}$ is

$$P(\Delta\mathbf{q})d\Delta\mathbf{q}. \tag{10}$$

Returning to the derivation of (6), we can write

$$\langle V(\mathbf{q}+\Delta\mathbf{q})\rangle_{Av} = \int d\Delta\mathbf{q} P(\Delta\mathbf{q})\, V(\mathbf{q}+\Delta\mathbf{q}). \tag{11}$$

We are actually interested in the integral over-all space of the product of (11) with $|\psi(\mathbf{q})|^2$, in finding an energy shift

$$\int d\mathbf{q}|\psi(\mathbf{q})|^2\langle V(\mathbf{q}+\Delta\mathbf{q})\rangle_{Av} = \int d\mathbf{q}\int d\Delta\mathbf{q} P(\Delta\mathbf{q})\, V(\mathbf{q}+\Delta\mathbf{q})|\psi(\mathbf{q})|^2. \tag{12}$$

Taking $\Delta\mathbf{q}$ and $\mathbf{q}' = \mathbf{q}+\Delta\mathbf{q}$ as variables of integration we obtain for this average

$$\int d\mathbf{q}' V(\mathbf{q}')\int d\Delta\mathbf{q} P(\Delta\mathbf{q})|\psi(\mathbf{q}'-\Delta\mathbf{q})|^2. \tag{13}$$

We then see that by requiring only the weak condition that $|\psi(\mathbf{q})|^2$ does not have too large a curvature we can obtain for (13)

$$\int d\mathbf{q} V(\mathbf{q})\{|\psi(\mathbf{q})|^2 + \tfrac{1}{6}\langle(\Delta\mathbf{q})^2\rangle_{Av}\nabla^2|\psi(\mathbf{q})|^2\} = \int d\mathbf{q}|\psi(\mathbf{q})|^2\{1+\tfrac{1}{6}\langle(\Delta q)^2\rangle_{Av}\nabla^2\} V(\mathbf{q}). \tag{14}$$

The second line is obtained by an obvious integration by parts. The second term represents the correction to the energy of the system and gives a result identical with that previously obtained.

IV. LOW ENERGY COMPTON SCATTERING

The general picture thus far developed can be used to give valuable insight into many interesting phenomena. We shall examine briefly several simple processes involving the interaction of electrons and radiation. In each case, the first non-vanishing approximation to the energy, or the second non-vanishing approximation to the transition probability will diverge if calculated on the usual theory. The preceding arguments concerning the Lamb shift strongly indicate that the physically real and finite parts of these divergences will always manifest themselves as a spreading out of the electronic charge and current by the fluctuation in position previously calculated.

As the simplest example of a phenomenon in which the position fluctuation modifies a transition probability, we consider the non-relativistic Compton scattering. For simplicity, we consider the effect to be completely classical, since this must give the correct non-relativistic answer. A free electron executes a steady forced oscillation under the action of the incident light wave and emits a scattered light wave of the same frequency. The effect of the position fluctuation is twofold. The electron behaves now like a distributed charge with a mean square radius $\langle(\Delta q)^2\rangle_{Av}$. It therefore interacts less strongly with the incident wave and radiates a weaker scattered wave. To find the magnitude of this reduction in the interaction between the electron and a light wave, we merely consider the change in the phase factor for the wave introduced by the averaging over the position fluctuation of the electron. This yields

$$\begin{aligned}\langle \exp i\mathbf{k}\cdot(\mathbf{q}+\Delta\mathbf{q})\rangle_{Av} &= \exp i\mathbf{k}\cdot\mathbf{q}\langle[1+i\mathbf{k}\cdot\Delta\mathbf{q} \\ &\quad -\tfrac{1}{2}(\mathbf{k}\cdot\Delta\mathbf{q})^2+\cdots]\rangle_{Av} \\ &= \exp i\mathbf{k}\cdot\mathbf{q}[1-\tfrac{1}{6}k^2\langle(\Delta q)^2\rangle_{Av}], \quad (15)\end{aligned}$$

where $\langle\ \rangle_{Av}$ indicates an average over the position fluctuation. The correction, as in the case of the Lamb shift, involves the product of the mean square position fluctuation with the Laplacian of the space function describing the interaction. We see that the amplitude of oscillation and the amplitude of the scattered wave will each suffer a fractional reduction equal to

$$\tfrac{1}{6}k^2\langle(\Delta q)^2\rangle_{Av}. \quad (16)$$

The resultant reduction will be twice as large and the reduction in the scattered intensity or cross section will be twice as large again, so that for the fractional change in cross section, we have

$$\begin{aligned}\frac{\Delta\sigma}{\sigma} &= -\tfrac{2}{3}k^2\langle(\Delta q)^2\rangle_{Av} \\ &= -\frac{4}{3\pi}\frac{e^2}{\hbar c}\left(\frac{\hbar k}{mc}\right)^2\log\frac{mc}{\hbar k_0}. \quad (17)\end{aligned}$$

We argue that the angular distribution will remain unchanged, since the scattering retains its dipole character.

There remains the problem of determining the lower cut-off k_0. We observe that frequencies of fluctuation higher than the frequency of the light wave will effectively spread out the scattering charge, while frequencies below this limit will only displace the scattering charge bodily in a random fashion. We therefore place $k_0=k$ and obtain

$$\frac{\Delta\sigma}{\sigma} = -\frac{4}{3\pi}\frac{e^2}{\hbar c}\left(\frac{\hbar k}{mc}\right)^2\log\frac{mc}{\hbar k}. \quad (18)$$

We see that the correction goes to zero strongly at low frequencies, and that for quanta of two-hundred kilovolts energy, where the formula (18) is probably still adequate, the fractional decrease becomes about one part in two thousand. The increase with energy indicated in (18) cannot be expected to continue much farther, so that an experimental verification of the result (18) seems out of the question.

V. THE INTERACTION BETWEEN A SPIN AND A MAGNETIC FIELD

A further interesting illustration of the utility of the viewpoint of this paper, as well as a useful example of its limitations, can be found in the effect on the Zeeman splitting of an atomic level produced by the interaction of the electron with the radiation field. In this case, fluctuations of the radiation field change the effective potential energy of interaction between the external magnetic field and the spin and orbital magnetic moments of the electron. A simple calculation of the effect can be given by a method analogous to the one previously used. Consider a simple system which consists of an angular momentum with an associated magnetic moment. For definiteness we take the system to be an electron spin which is free except for the action of the fluctuations of the radiation field. Let $(\hbar/2)\boldsymbol{\sigma}$ be the angular momentum operator for the spin. Then the equation of motion for $\boldsymbol{\sigma}$ is

$$\frac{\partial\boldsymbol{\sigma}}{\partial t} = \frac{e}{mc}\mathbf{B}\times\boldsymbol{\sigma}, \quad (19)$$

where $\mathbf{B}$ is the instantaneous magnetic field intensity arising from the field fluctuations. If we consider thee quation of motion for the quantum-mechanical expectation of $\boldsymbol{\sigma}$, we obtain the same equation, but with $\boldsymbol{\sigma}$ interpreted as a unit classical vector.

We solve Eq. (19) by making use of the fact that for vanishing e, $\boldsymbol{\sigma}$ is fixed in direction. We call the fluctuating correction to this fixed vector $\Delta\boldsymbol{\sigma}$ and obtain

$$\Delta\boldsymbol{\sigma}=\frac{e}{mc}\mathbf{B}\times\boldsymbol{\sigma}, \tag{20}$$

where $\boldsymbol{\sigma}$ is constant in time. We follow the same procedure used for obtaining $\langle(\Delta q)^2\rangle_{Av}$ in the first section of this paper. This yields

$$\langle(\Delta\sigma)^2\rangle_{Av}=\sigma^2\frac{e^2}{\hbar c}\frac{2}{\pi}\left(\frac{\hbar}{mc}\right)^2\int_0^\kappa k\,dk, \tag{21}$$

where $\langle(\Delta\sigma)^2\rangle_{Av}$ is the mean square fluctuation in the unit spin vector. The upper limit of the integral has been made κ rather than infinity, but the question of evaluating κ will be deferred for the moment.

We define the mean square angle of fluctuation $\langle(\Delta\theta)^2\rangle_{Av}$

$$\langle(\Delta\theta)^2\rangle_{Av}=\frac{\langle(\Delta\sigma)^2\rangle_{Av}}{\sigma^2}=\frac{2}{\pi}\frac{e^2}{\hbar c}\left(\frac{\hbar}{mc}\right)^2\frac{\kappa^2}{2}. \tag{22}$$

Now, as in the case of the Lamb shift, we find the effect of this fluctuation on the potential energy of the spin in a magnetic field. This energy is, if the external magnetic field has magnitude B and is in the Z direction,

$$\frac{e\hbar}{2mc}\sigma_z B=\frac{e\hbar B}{2mc}|\sigma|\cos\theta, \tag{23}$$

where θ is the angle between the spin direction and the z axis. We see that the fluctuations merely affect the average value of $\cos\theta$. This effect can easily be found by the use of some simple spherical trigonometry. Let $\bar{\theta}$ be the angle between the z axis and the average spin direction. Let θ be the angle between the instantaneous spin vector and the z axis. Let $\Delta\theta$ and ϕ be the colatitude and azimuth angles of the instantaneous spin vector with respect to the average spin vector. The effect of the fluctuations will then be to replace $\cos\theta$ in (23) by $\langle\cos\theta\rangle_{Av}$, where the brackets indicate an average over the fluctuations of the spin vector. We have

$$\langle\cos\theta\rangle_{Av}=\langle\cos\bar{\theta}\cos\Delta\theta+\sin\bar{\theta}\sin\Delta\theta\cos\phi\rangle_{Av}. \tag{24}$$

The indicated average is easily performed by remembering that the average of $\cos\phi$ must vanish because of the isotropy of the fluctuation. Furthermore, $\Delta\theta$ will be assumed small so that $\cos\Delta\theta$ is well represented by the first two terms in its series expansion. We obtain

$$\begin{aligned}\langle\cos\theta\rangle_{Av}&=\cos\bar{\theta}[1-\tfrac{1}{2}\langle(\Delta\theta)^2\rangle_{Av}]\\&=\cos\bar{\theta}\left[1-\frac{e^2}{2\pi\hbar c}\left(\frac{\hbar\kappa}{mc}\right)^2\right].\end{aligned} \tag{25}$$

We then see that the correction to the orientation energy of the spin consists in a reduction in the magnitude of the energy proportional to the energy itself. It is therefore convenient to think of the effect of the interaction with the radiation field as consisting of an alteration of the magnetic moment, μ, associated with the spin. We have

$$\frac{\Delta\mu}{\mu}=-\frac{e^2}{2\pi\hbar c}\left(\frac{\hbar\kappa}{mc}\right)^2. \tag{26}$$

In this case the lower cut-off in the integral over quanta is unimportant, since no contribution arises from small values of k. The magnitude of the effect is, however, correspondingly more sensitive to the value of the upper cut-off. We first consider the case where the magnetic moment μ is associated with the orbital angular momentum of an electron in an atom. Here the upper cut-off is supplied in a natural fashion by the fact that Eq. (19) is valid only for magnetic fields with wave-lengths so long that there is no serious retardation over a distance of the order of the atomic radius. We therefore set

$$\kappa=1/a=(e^2/\hbar c)(mc/\hbar), \tag{27}$$

where a is an average orbital radius for a valence electron, taken to be equal to the Bohr radius. Equation (26) then becomes

$$(\Delta\mu/\mu)=-(1/2\pi)(e^2/\hbar c)^3, \tag{28}$$

so that for an orbital moment, the effect under consideration is completely negligible.

The situation is different if we consider the case of the intrinsic magnetic moment of the electron. Here it must be assumed that the moment can be concentrated to a radius equal roughly to the Compton wave-length of the electron, since a wave packet consisting of positive energy states only and possessing a definite spin can be made to occupy a volume of this radius. Under these conditions, quanta with wave num-

bers higher than $mc/\hbar$ will not act coherently on the spin and we have κ equal to the reciprocal Compton wave-length. Hence, for a spin, Eq. (26) becomes

$$\Delta\mu/\mu = -e^2/2\pi\hbar c, \tag{29}$$

where the exact numerical factor is, of course, not to be taken too seriously. Unfortunately, although the magnitude of the correction seems, from recent molecular beam experiments,[4] to be nearly correct, the sign of the effect should be reversed. This unsatisfactory result of our qualitative considerations is probably to be ascribed to our complete neglect of the relativistic nature of the electron spin. By a careful relativistic calculation, Schwinger[5] has recently shown that the correct sign will indeed follow from a reasonable theory. The effective reduction in the moment which is indicated by our simple non-relativistic theory seems to be more than compensated by an effective increase in the moment which arises, according to Schwinger, from the magnetic interaction of the electron with the filled negative energy states of the vacuum.

VI. QUANTUM-MECHANICAL TREATMENT OF $\langle(\Delta q)^2\rangle_{Av}$ AND JUSTIFICATION OF THE LOWER CUT-OFF

We shall now attempt to give a more formal justification for some of the assertions thus far made, and in particular we propose to give a rigorous quantum-mechanical meaning to the quantity $\langle(\Delta q)^2\rangle_{Av}$, which has thus far been rather loosely treated in an almost purely classical fashion.

We begin by writing the Hamiltonian for an electron moving non-relativistically under the influence of an electrostatic field and the radiation field. We neglect retardation in the interaction between the electron and the radiation field, and assume unit quantization volume for the field

$$H=\frac{p^2}{2m}+V(q)+\sum_k a_k^+ a_k \hbar ck - \frac{e}{mc}\sum_k\left(\frac{2\pi\hbar c}{k}\right)^{\frac{1}{2}}(e_k\cdot p)(a_k+a_k^+). \tag{30}$$

Here p and q are the vector momentum and coordinate of the electron, $V(q)$ is the electrostatic potential energy, a_k^+ and a_k are the usual occupation operators for a normal mode of the field with wave number k, and e_k is a unit vector in the direction of polarization of the quantum. The term in the square of the vector potential has been omitted since it does not affect the Lamb shift.

The Hamiltonian (30) has been carefully studied by Pauli and Fierz[6] in connection with the resolution of the infra-red paradox, and we follow their treatment, in its essentials. We first rewrite (30) by completing the square indicated by the last two terms

$$H=\frac{p^2}{2m}+V(\mathbf{q})+\sum_k\left[a_k^+-\frac{e}{mc}\left(\frac{2\pi}{\hbar ck^3}\right)^{\frac{1}{2}}\mathbf{e}_k\cdot\mathbf{p}\right]\times\left[a_k-\frac{e}{mc}\left(\frac{2\pi}{\hbar ck^3}\right)^{\frac{1}{2}}\mathbf{e}_k\cdot\mathbf{p}\right]\hbar ck - \frac{e^2}{m^2c^2}\sum_k\frac{2\pi}{k^2}(\mathbf{e}_k\cdot\mathbf{p})^2. \tag{31}$$

The last term, which has been added to complete the square, is just Bethe's subtraction term, as can be seen by replacing the sum by an integral

$$\frac{e^2}{m^2c^2}\sum_k\frac{2\pi}{k^2}(\mathbf{e}_k\cdot\mathbf{p})^2=\frac{2e^2}{3\pi}\frac{p^2}{m^2c^2}\int_0^\infty dk. \tag{32}$$

We now adopt the point of view that the Hamiltonian (30) is incorrect and should be modified by the addition of the explicitly divergent term (32). The resulting theory should then be free from all divergences of classical origin. We write the Hamiltonian as

$$H=\frac{p^2}{2m}+V(\mathbf{q})+\sum_k A_k^+ A_k\hbar ck, \tag{33}$$

with A_k and A_k^+ defined by

$$A_k=a_k-\frac{e}{mc}\left(\frac{2\pi}{\hbar ck^3}\right)^{\frac{1}{2}}\mathbf{e}_k\cdot\mathbf{p}, \qquad A_k^+=a_k^+-\frac{e}{mc}\left(\frac{2\pi}{\hbar ck^3}\right)^{\frac{1}{2}}\mathbf{e}_k\cdot\mathbf{p}. \tag{34}$$

[4] J. E. Nafe, E. B. Nelson, and I. I. Rabi, Phys. Rev. **71**, 914 (1947); D. E. Nagle, R. S. Julian, and J. R. Zacharias, Phys. Rev. **72**, 971 (1947); P. Kusch and H. M. Foley, Phys. Rev. **72**, 1256 (1947).

[5] J. Schwinger, Phys. Rev. **73**, 416 (1948).

[6] W. Pauli and M. Fierz, Nuovo Cimento **15**, 167 (1938).

If we define new variables P and Q by

$$\mathbf{P}=\mathbf{p},$$
$$\mathbf{Q}=\mathbf{q}+\frac{ie}{mc}\sum_k\left(\frac{2\pi\hbar}{ck^3}\right)^{\frac{1}{2}}\mathbf{e}_k(a_k-a_k^+), \tag{35}$$

we see that the capitalized variables are related to the small variables by a contact transformation. We write the Hamiltonian in terms of the new variables, replacing capital letters by small letters

$$H=\frac{p^2}{2m}+V\left(\mathbf{q}-\frac{ie}{mc}\sum_k\left(\frac{2\pi\hbar}{ck^3}\right)^{\frac{1}{2}}\mathbf{e}_k(a_k-a_k^+)\right)+\sum_k a_k^+a_k\hbar ck. \tag{36}$$

It is finally convenient to change to field variables which are the real coordinates and momenta of harmonic oscillators. We thus obtain

$$H=\frac{p^2}{2m}+V(\mathbf{q}+\Delta\mathbf{q})+\sum_k\tfrac{1}{2}(P_k^2+c^2k^2Q_k^2), \tag{37}$$[7]

with

$$\Delta\mathbf{q}=\frac{e}{mc}(4\pi)^{\frac{1}{2}}\sum_k\mathbf{e}_k\frac{Q_k}{k}. \tag{38}$$

The general character of the consequences of this Hamiltonian is easy to deduce. We assume that for all quanta with frequencies above k_0, the corresponding radiation oscillators execute their unperturbed motion. Quanta below this cut-off will be arbitrarily excluded for the time being, and it will be further assumed, in order to avoid the necessity of discussing the infra-red paradox, that the limit k_0 is placed sufficiently high that no quanta can be emitted. The effect of the second term in (37) will then be only to produce elastic deflections of the electron. We see that in a calculation of the probability of such a deflection, by the use of the Born approximation, the potential energy term in (37) is effectively replaced by its average over the coordinates of all the radiation oscillators. This average can be easily calculated by considering the Fourier transform of $V(\mathbf{q})$. We take

$$V(\mathbf{q})=\int d\boldsymbol{\lambda}U(\boldsymbol{\lambda})\exp i\boldsymbol{\lambda}\cdot\mathbf{q},$$
$$V(\mathbf{q}+\Delta\mathbf{q})=\int d\boldsymbol{\lambda}U(\boldsymbol{\lambda})\exp i\boldsymbol{\lambda}\cdot\mathbf{q}\times\prod_k\exp\left(\frac{ie}{mc}(4\pi)^{\frac{1}{2}}(\mathbf{e}_k\cdot\boldsymbol{\lambda})\frac{Q_k}{k}\right). \tag{39}$$

To obtain the effective potential energy, we must average the product at the end of the integrand over the unperturbed Gaussian wave functions for the ground states of the radiation oscillators. The integrals are easily done, yielding

$$\begin{aligned}\langle V(\mathbf{q}+\Delta\mathbf{q})\rangle_{Av}&=\int d\boldsymbol{\lambda}U(\boldsymbol{\lambda})\exp i\boldsymbol{\lambda}\cdot\mathbf{q}\times\prod_k\exp\left(-\pi(\mathbf{e}_k\cdot\boldsymbol{\lambda})^2\frac{e^2}{\hbar c}\left(\frac{\hbar}{mc}\right)^2\frac{1}{k^3}\right)\\&=\int d\boldsymbol{\lambda}U(\boldsymbol{\lambda})\exp i\boldsymbol{\lambda}\cdot\mathbf{q}\times\exp\left(-\frac{1}{3\pi}\frac{e^2}{\hbar c}\left(\frac{\hbar}{mc}\right)^2\times\int_{k_0}^{\kappa}\frac{dk}{k}\lambda^2\right).\end{aligned} \tag{40}$$

This expression can now be rewritten in several interesting ways

$$\begin{aligned}\langle V(\mathbf{q}+\Delta\mathbf{q})\rangle_{Av}&=\int d\boldsymbol{\lambda}U(\boldsymbol{\lambda})\exp i\boldsymbol{\lambda}\cdot\mathbf{q}\times\exp-\tfrac{1}{6}\lambda^2\langle(\Delta q)^2\rangle_{Av}\\&=\exp(\tfrac{1}{6}\langle(\Delta q)^2\rangle_{Av}\nabla^2)\,V(\mathbf{q}).\end{aligned} \tag{41}$$

The differential operator appearing in (41) is in reality an integral operator which can easily be written explicitly as

$$\langle V(\mathbf{q}+\Delta\mathbf{q})\rangle_{Av}=\left[\frac{3}{2\pi\langle(\Delta q)^2\rangle_{Av}}\right]^{\frac{1}{2}}\int d\mathbf{q}'V(\mathbf{q}')\times\exp\left(-\frac{3|\mathbf{q}-\mathbf{q}'|^2}{2\langle(\Delta q)^2\rangle_{Av}}\right). \tag{42}$$

The displacement kernel occurring in (42) is clearly just the distribution function for the quantity $\Delta\mathbf{q}$, previously assumed in Eq. (11). It is interesting to consider from our present point

[7] A similar transformation of the Hamiltonian seems to have been used by H. A. Kramers (unpublished).

of view the somewhat unexpected results encountered by Pauli and Fierz in their treatment of the infra-red paradox by means of the Hamiltonian (37). They found that the correction of order e^2 to the elastic scattering of a particle by the potential V diverged if no upper cut-off were made in the sum over quanta. They were able to show, however, that if the correction were calculated exactly from the approximate Hamiltonian, the elastic scattering cross section became identically zero, even though no quanta could actually be emitted. Both results were difficult to understand at the time because the removal of the electromagnetic self-energy had presumably rendered the theory convergent. We now see that the residual divergence is just that occurring at the upper limit of the integral over quanta in our expression for the mean square fluctuation in position of the electron. To the order e^2, the resulting infinite position fluctuation will give rise to an infinite correction to the scattering potential and therefore to the cross section. On the other hand, the integral operator (42) really has the effect of reducing the potential to zero if $\langle(\Delta q)^2\rangle_{Av}$ is taken to be infinite. This gives zero scattering cross section in an exact calculation. Both difficulties will clearly be removed, as indicated in the last section of this paper, by the inclusion of recoil, which gives an automatic upper cut-off. It is, of course, necessary, as has been pointed out by Lewis,[8] to make the appropriate subtraction for the electromagnetic self-energy just as has been assumed in obtaining the Hamiltonian (37).

We now turn to the consideration of the significance of the lower cut-off k_0. From the Hamiltonian (37), we can immediately arrive at a formal justification for our earlier intuitive arguments. We consider, for simplicity, the ground state of the system, which for vanishing e goes over into a state whose wave function is the product of the ground state wave function of the atom with the ground state wave functions for all the radiation oscillators. In order to obtain the Lamb shift for this state, we must calculate the energy change to the order e^2 produced by the term added to $\mathbf{q}$ in the argument of the potential energy. This can easily be done and leads in fact just to Bethe's result for the energy shift, as it must. For our purposes, however, we observe that the radiation oscillators can be divided into those with frequencies higher than the characteristic frequency of the electronic motion and those with lower frequencies. The high frequency oscillators are not particularly affected by the coupling with the electron, and the part of the energy shift arising from them is to be considered as that due to averaging the potential energy over the unperturbed ground state wave functions of these oscillators. The low frequency oscillators are, according to the original form of the Hamiltonian, to be thought of as driven by the electronic motion rather than the reverse.

To demonstrate the correctness of this viewpoint, we make a Taylor expansion of the potential energy to the order e^2 and write the terms which appear as perturbations

$$V(\mathbf{q}+\Delta\mathbf{q})-V(\mathbf{q}) = \frac{e}{mc}(4\pi)^{\frac{1}{2}}\sum_k \frac{1}{k}Q_k(\mathbf{e}_k\cdot\nabla)V(\mathbf{q}) + \frac{1}{2}\left(\frac{e}{mc}\right)^2 4\pi\Big[\sum_k Q_k(\mathbf{e}_k\cdot\nabla)\Big]^2 V(\mathbf{q}). \quad (43)$$

The energy correction to the order e^2 can be obtained by considering the effect of the first term on the right-hand side of (43) in the second order of the perturbation theory and the second term in the first order. We obtain

$$\Delta E = 4\pi\left(\frac{e}{mc}\right)^2\sum_k\sum_n \frac{\hbar}{2ck^3}\frac{|(0|e_k\cdot\nabla V|n)|^2}{E_0-E_n-\hbar ck} + \tfrac{1}{2}4\pi\left(\frac{e}{mc}\right)^2\sum_k\frac{\hbar}{2ck^3}(0|(e_k\cdot\nabla)^2V|0), \quad (44)$$

where the index n refers to the nth atomic state, and the unperturbed atomic state is denoted by the index 0. We then replace the sums over radiation oscillators by integrals and do the integrals over the angles of k and the sum over polarization directions. The resulting expression is

$$\Delta E = \frac{1}{3\pi}\frac{e^2}{\hbar c}\left(\frac{\hbar}{mc}\right)^2\int_0^\kappa\frac{dk}{k}\Big\{(0|\nabla^2V|0) + 2\sum_n\frac{(0|\nabla V|n)\cdot(n|\nabla V|0)}{E_0-E_n-\hbar ck}\Big\}. \quad (45)$$

The first term in (45) is immediately recognizable as the energy shift which would be ob-

[8] H. W. Lewis, Phys. Rev. **73**, 173 (1948).

tained by our original semiclassical argument if the position fluctuation were taken to be that for a free electron. The assumption of course is always to be made that the formally infinite upper limit of integration is in reality the reciprocal Compton wave-length. The second term can be given a simple interpretation by studying its behavior for small and large values of k. We first assume that $hck \ll |E_0 - E_1|$, where E_1 is the energy of the lowest intermediate atomic state that occurs in the sum over n. We can then expand the integrand of the second term in powers of k

$$2\sum_n \frac{(0|\nabla V|n)\cdot(n|\nabla V|0)}{E_0 - E_n - \hbar ck} = 2\sum_n (0|\nabla V|n)\cdot(n|\nabla V|0)\left\{\frac{1}{E_0 - E_n} + \frac{2\hbar ck}{(E_0 - E_n)^2} + 0(k^2)\right\}. \quad (46)$$

The first two terms in (46) can be simplified by the use of the equations of motion and the commutation relations. We obtain

$$2\sum_n \frac{(0|\nabla V|n)\cdot(n|\nabla V|0)}{E_0 - E_n - \hbar ck} = -(0|\nabla^2 V|0) + \frac{2ck}{\hbar}(0|p^2|0) + 0(k^2). \quad (47)$$

We then see that the apparent logarithmic divergence at the lower limit of the integral in (45) is removed. The largest surviving contribution to the integrand for low frequency quanta is just the low frequency contribution to the classical electromagnetic self-energy. This cancellation will approximately persist until the series expansion used in Eq. (46) becomes poorly convergent, that is until the quantum frequency becomes comparable with the orbital frequency of the electron. For frequencies higher than this the situation will become quite complicated until the quantum energy becomes larger than the highest energy effectively occurring in the sum over intermediate atomic states. For quantum energies so high that the sum in the second term of (45) effectively converges before the denominator begins to differ much from hck, we see that the importance of this term in comparison with the first term decreases with increasing k. As a result of this limiting behavior of the second term for small k and large k, it is convenient to represent the energy shift by the expression

$$\Delta E = \frac{1}{3\pi}\frac{e^2}{\hbar c}\left(\frac{\hbar}{mc}\right)^2 \int_{k_0}^{\kappa} \frac{dk}{k}(0|\nabla^2 V|0), \quad (48)$$

where the lower limit k_0 is adjusted to give the correct value for (45).

This effective lower cut-off can apparently be evaluated only by doing the indicated sum, but a useful general property can easily be deduced. For a harmonic oscillator, the sum over states reduces to a single term. The atomic energy difference occurring in this term is just that corresponding to the orbital frequency of the electron; the transition between the two limiting types of behavior for the sum takes place for a quantum frequency equal to the orbital frequency, and ck_0 will therefore be very close to the orbital frequency.

This simple behavior holds only for a harmonic oscillator. As the potential becomes more concentrated near the center (approaching the Coulomb potential, for example), the matrix elements of ∇V appearing in the sum over states will become important for states lying higher and higher above the unperturbed atomic state. The first terms in the sum will always have energy differences corresponding to the orbital frequency of the electron, but the first terms become relatively less and less important as we approach the Coulomb potential. The quantity k_0, which marks the transition between the two limiting forms for the sum, will accordingly rise higher and higher above the orbital frequency. A careful evaluation of the effective lower cut-off for the case of the $2S$ level of hydrogen gives, according to Bethe,[1] a value of 17.8 Rydbergs or approximately twenty times the orbital frequency. This seemingly high value is now not surprising in view of the foregoing arguments.

VII. JUSTIFICATION OF THE UPPER CUT-OFF

In this section we shall attempt to give a quantum-mechanical derivation of the expression for the mean square fluctuation in position. We shall include the effect of retardation but not the effect of relativity. In this way, the existence of the

upper cut-off in the integral over quantum energies will be given some formal support. We assume the complete non-relativistic Hamiltonian for a spinless charged particle coupled to the radiation field, but otherwise free

$$H=\frac{p^2}{2m}+\sum_k a_k^+ a_k \hbar ck + \frac{e}{mc}\sum_k \left(\frac{2\pi\hbar c}{kV}\right)^{\frac{1}{2}} (\mathbf{e}_k\cdot\mathbf{p}) \times (a_k \exp i\mathbf{k}\cdot\mathbf{q}+a_k^+ \exp -i\mathbf{k}\cdot\mathbf{q}) + \frac{e^2}{2mc^2}\left[\sum_k \left(\frac{2\pi\hbar c}{kV}\right)^{\frac{1}{2}} \mathbf{e}_k \times (a_k \exp i\mathbf{k}\cdot\mathbf{q}+a_k^+ \exp -i\mathbf{k}\cdot\mathbf{q})\right]^2. \quad (49)$$

In analogy with the semiclassical derivation given in the first part of this paper, we assume an electron at rest and calculate its motion in the first approximation under the action of the coupling with the field. The unperturbed wave functions for the problem are

$$\frac{\exp(i\mathbf{P}\cdot\mathbf{q})}{(V)^{\frac{1}{2}}}(\mathbf{k}_1, \mathbf{k}_2, \cdots), \quad (50)$$

where $\mathbf{P}$ is the wave vector for the wave function of a free electron with definite momentum and $(k_1, k_2, \cdots)$ is the wave function for the radiation field with the indicated quanta present. The zero-order wave function has no quanta present and has in it a range of electron momenta, so that the position of the electron can be approximately given. We have

$$\psi=\sum_P A_P \frac{\exp(i\mathbf{P}\cdot\mathbf{q})}{(V)^{\frac{1}{2}}}(\cdots). \quad (51)$$

The electron density, averaging over the coordinates of the radiation oscillators, is

$$\langle|\psi|^2\rangle_{Av}=\sum_P\sum_{P'} A_{P'}^* A_P \frac{\exp(i(\mathbf{P}-\mathbf{P}')\cdot\mathbf{q})}{V}. \quad (52)$$

We now assume that the coupling between the electron and the radiation field is turned on. Each wave function occurring in the sum (51) will be perturbed, and the electron density (52) will be accordingly altered. We proceed to calculate the perturbed density to the order e^2. The third term in our Hamiltonian will enter to the first order in the correction to the wave function. It cannot enter to the second order, since this would either lead back to the zero-order wave function, or to one referring to two quanta, which is orthogonal to the zero-order function and will therefore give no contribution in the averaging over the radiation field coordinates. The last term in the Hamiltonian gives no contribution for the same reason. It is interesting to note that any subtraction term added to the Hamiltonian to render the theory convergent will give no contribution for the same reason again. A second-order correction to the wave function does, however, arise from the renormalization necessitated by the first-order correction.

The wave function referring to definite electron momentum becomes

$$\frac{\exp i\mathbf{P}\cdot\mathbf{q}}{(V)^{\frac{1}{2}}}(\cdots)+\frac{e\hbar}{mc}\sum_k \left(\frac{2\pi\hbar c}{kV}\right)^{\frac{1}{2}} \frac{(\mathbf{e}_k\cdot\mathbf{P})}{E_P-E_{P-k}-\hbar ck} \times \frac{\exp(i(\mathbf{P}-\mathbf{k})\cdot\mathbf{q})}{(V)^{\frac{1}{2}}}(\mathbf{k})-\frac{e^2\hbar^2}{2m^2c^2}\sum_k \frac{2\pi\hbar c}{kV} \times \frac{(\mathbf{e}_k\cdot\mathbf{P})^2}{(E_P-E_{P-k}-\hbar ck)^2}\frac{\exp(i\mathbf{P}\cdot\mathbf{q})}{(V)^{\frac{1}{2}}}(\cdots). \quad (53)$$

The averaged electron density then becomes

$$\langle|\psi|^2\rangle_{Av}=\sum_P\sum_{P'} A_{P'}^* A_P \frac{\exp(i(\mathbf{P}-\mathbf{P}')\cdot\mathbf{q})}{V} \times\left\{1-\frac{e^2\hbar^2}{2m^2c^2}\sum_k \frac{2\pi\hbar c}{kV}\left(\frac{\mathbf{e}_k\cdot\mathbf{P}}{E_P-E_{P-k}-\hbar ck} -\frac{\mathbf{e}_k\cdot\mathbf{P}'}{E_{P'}-E_{P'-k}-\hbar ck}\right)^2\right\}. \quad (54)$$

We now assume that P and P' are always small compared with the reciprocal Compton wavelength. The energy denominators become

$$E_P-E_{P-k}-\hbar ck=\frac{\hbar^2P^2}{2m}-\frac{\hbar^2(\mathbf{P}-\mathbf{k})^2}{2m}-\hbar ck = -\hbar ck\left(1+\frac{\hbar k}{2mc}-\frac{\hbar\mathbf{k}\cdot\mathbf{P}}{mck}\right). \quad (55)$$

The last term in (55) is always very small compared with the first term, so we shall ignore it. The electron density becomes, changing the sum

to an integral and doing the sum over polarizations and the integration over angles,

$$\langle|\psi|^2\rangle_{Av}=\sum_P\sum_{P'}A_{P'}{}^*A_P\frac{\exp(i(\mathbf{P}-\mathbf{P}')\cdot\mathbf{q})}{V}$$
$$\times\left\{1-\frac{1}{3\pi}\frac{e^2}{\hbar c}\left(\frac{\hbar}{mc}\right)^2(\mathbf{P}-\mathbf{P}')^2\right.$$
$$\left.\times\int_0^\infty\frac{dk}{k\left(1+\frac{\hbar k}{2mc}\right)^2}\right\}. \quad (56)$$

This can be rewritten in a more transparent form

$$\langle|\psi|^2\rangle_{Av}=\left\{1+\frac{2}{\pi}\frac{e^2}{\hbar c}\left(\frac{\hbar}{mc}\right)^2\right.$$
$$\left.\times\int_0^\infty\frac{dk}{k\left(1+\frac{\hbar k}{2mc}\right)^2}-\tfrac{1}{6}\nabla^2\right\}$$
$$\times\sum_P\sum_{P'}A_{P'}{}^*A_P\frac{\exp(i(\mathbf{P}-\mathbf{P}')\cdot\mathbf{q})}{V}. \quad (57)$$

From this we see that the effect of the coupling between electron and radiation field is to spread out the electron density function, the mean square spreading distance being

$$\langle(\Delta q)^2\rangle_{Av}=\frac{2}{\pi}\frac{e^2}{\hbar c}\left(\frac{\hbar}{mc}\right)^2\int_0^\infty\frac{dk}{k\left(1+\frac{k}{2\kappa}\right)^2}$$
$$=\frac{2}{\pi}\frac{e^2}{\hbar c}\left(\frac{\hbar}{mc}\right)^2\left\{\int_{k_0}^\infty\frac{dk}{k\left(1+\frac{k}{2\kappa}\right)^2}\right.$$
$$\left.+\int_0^{k_0}\frac{dk}{k\left(1+\frac{k}{2\kappa}\right)^2}\right\}. \quad (58)$$

We make our usual assumption that only frequencies above some lower cut-off k_0 are effective when the electron is bound, and therefore omit the second term in (58). The integral over k can be performed without difficulty, yielding

$$\langle(\Delta q)^2\rangle_{Av}=\frac{2}{\pi}\frac{e^2}{\hbar c}\left(\frac{\hbar}{mc}\right)^2\log\frac{2\kappa}{\epsilon k_0}, \quad (59)$$

where ϵ is the base of the natural logarithms. We therefore see that the inclusion of the retardation leads to an upper cut-off which is about three quarters of the crude value (κ) originally assumed.[9]

The derivation just given has some attractive features. It gives a convergent result for the physically meaningful part of the reaction of the field on the electron, without the necessity of subtracting two infinite terms. The result (59) suffers, however, from the obvious disadvantage that a non-relativistic Hamiltonian was used to obtain convergence in a region where the non-relativistic assumption is clearly seriously in error. It would seem to be of the greatest interest to apply the method just used to the calculation of $\langle(\Delta q)^2\rangle_{Av}$ in the hole theory. Such a procedure is seen to be scarcely unambiguous, although it is apparently again possible to obtain the physically interesting results without the introduction of the usual subtraction terms. It is hoped that this point can be treated in detail in a later paper.

VIII. ACKNOWLEDGMENT

The author desires to express his sincere appreciation for the encouragement and helpful criticism given him by Professor V. F. Weisskopf. The work here reported was supported in part by the Office of Naval Research.

[9] W. E. Lamb has pointed out (unpublished) that the inclusion of recoil in a non-relativistic calculation of the line shift in hydrogen gives a convergent result.

PHYSICAL REVIEW VOLUME 74, NUMBER 9 NOVEMBER 1, 1948

The Dipolar Broadening of Magnetic Resonance Lines in Crystals

J. H. VAN VLECK
Harvard University, Cambridge, Massachusetts
(Received July 6, 1948)

In regular crystals, the width of the absorption lines arising from the magnetic moment of the electron or nucleus is caused primarily by the interaction between the magnetic dipoles. It is prohibitively difficult to determine the precise shape of the absorption line theoretically, but the invariance of the diagonal sum in quantum mechanics permits the calculation of the second moment of the frequency deviation, and hence the r.m.s. line breadth. The latter agrees excellently with the observations of Pake and Purcell on the magnetic absorption of the F nucleus in CaF_2, both in absolute magnitude, and in the dependence on the direction between the magnetic field and the principal cubic axes. The fourth moment was also computed to examine how good an approximation is the conventional assumption of a Gaussian shape. As long as no exchange is present (the nuclear case) the Gaussian model is moderately good. For the 100 direction in a cubic crystal, the theoretical ratio of root mean fourth to root mean square breadth is 1.25. Pake and Purcell's measurements yield 1.24. A Gaussian model would require 1.32. The theory is extended to include crystals with two kinds of spin moments (two types of nuclei, or simultaneous nuclear and electronic spin). Coupling between unlike moments is less effective (by a factor $\frac{3}{5}$ in the r.m.s. width) than that between like in broadening the lines.

In the paramagnetic absorption caused by electronic spin, it is imperative to include the effect of exchange coupling. This interaction does not contribute to the second moment, but greatly increases the fourth. As a result, the lines are peaked much more sharply than one would compute from the second moment with the Gaussian model for line shape. This "exchange narrowing" explains why microwave paramagnetic absorption lines are much narrower than one first conjectures from the amount of dipolar coupling.

The theoretical calculations are given in Sections II–IV. The final sections V–VI give the comparison with the experiments of Pake and Purcell, and with the model of Bloembergen, Purcell, and Pound, for r-f absorption in liquids.

I. INTRODUCTION

THE present paper[1] deals with the broadening of the absorption lines of crystals by dipolar interaction, with emphasis primarily on the r-f and microwave regions. The theory is much better tested by measurements in these domains than at ordinary optical wave-lengths since with the latter the line broadening is exceedingly small compared to the proper frequency and also it may not be safe to neglect, as we do, the influence of Doppler and radiation broadening.

We shall deal exclusively with media in which the atoms are regularly spaced, i.e., with crystals. The material may, however, be either a single crystal or a powder. The broadening which we consider is caused essentially by the magnetostatic interaction of the atomic dipoles, and is hence "adiabatic" in character. The mechanism is thus quite different from that in gases, where non-adiabatic collisions are the main factor, as shown in the theory of Bloembergen, Purcell, and Pound.[2]

We shall assume throughout that the moments responsible for the absorption are magnetic, and arise from spin, be it nuclear or electronic. The influence of the crystalline electric field will be neglected, and the material will be supposed non-ferromagnetic. This procedure is well warranted in experiments on nuclear resonance absorption. The effect of the crystalline Stark effect on the absorption by electronic spin will be examined in a later paper. In another article the theory will be extended to the ferromagnetic case to provide a microscopic derivation of the Kittel formula for the resonance frequency.

The energy terms attributable to magnetic spin-spin interaction and to application of the external constant magnetic field will be called, respectively, the dipolar and Zeeman energies. We believe that these names are less ambiguous than the word magnetic, which can relate to either term according to the usage of the author. It will be supposed throughout that the applied field is sufficiently large that the dipolar interaction is small compared to the Zeeman member. This condition is fulfilled at the field strengths used in most experiments on resonance absorp-

[1] A preliminary account of the present paper was given at the 1947 Chicago meeting of the American Physical Society. For abstract see Phys. Rev. **73**, 1229 (1948).
[2] N. Bloembergen, E. M. Purcell, and R. V. Pound, Phys. Rev. **73**, 679 (1948).

tion at the Larmor frequency. The resonance wave-lengths are ordinarily in the r-f or microwave region according as the spin is nuclear or electronic. In a later article, Miss Wright will extend the theory to the case of non-resonant absorption at very low frequencies such as are used in the Dutch experiments on paramagnetic relaxation.

An important feature of the present paper is the inclusion of exchange interaction. Except for the exclusion of ferromagnetism, no restriction need be made on the size of the exchange coupling in our calculations, as it commutes in matrix multiplication with the Zeeman term, so that both energies can be simultaneously diagonal.

The mathematical theory will be developed in Sections II, III, and IV. Comparison with experiment will be made in Section V, and readers not interested in theoretical calculations may wish to proceed directly to this section. In Section VI a qualitative comparison will be made with the theory of Bloembergen, Pound, and Purcell on relaxation phenomena in gases or liquids.

II. CALCULATION OF THE MEAN SQUARE ABSORPTION FREQUENCY

We shall suppose that the constant magnetic field H is applied in the z direction, and that the oscillating field whose absorption is being studied is along the x axis. Because of the dipolar interaction, the absorption is not strictly monochromatic at the frequency $Hg\beta/h$, and the present paper attempts to estimate the amount of the diffusion. Here and elsewhere, β denotes the Bohr magneton, nuclear or electronic as the case may be, and g is the corresponding Landé factor.

The Hamiltonian matrix is

$$\mathcal{H}=Hg\beta\Sigma_j S_{zj}+\Sigma_{k>j}\tilde{A}_{jk}\mathbf{S}_j\cdot\mathbf{S}_k+g^2\beta^2\Sigma_{k>j}[r_{jk}^{-3}(\mathbf{S}_j\cdot\mathbf{S}_k)-3r_{jk}^{-5}(\mathbf{r}_{jk}\cdot\mathbf{S}_j)(\mathbf{r}_{jk}\cdot\mathbf{S}_k)]. \tag{1}$$

Here the first, second, and third members are, respectively, the Zeeman, exchange, and dipolar energies. The symbol S_{zj} denotes the z matrix-component of the spin angular momentum (electronic or nuclear) of atom j, measured in multiples of the quantum unit $h/2\pi$. All atoms are assumed to have the same g-factor, and same spin quantum number S. This restriction will, however, be removed in Section IV. We make the usual assumption that the exchange coupling can be calculated on the basis that the atoms are effectively in S states, so that the exchange term has the isotropic form proportional to the scalar product of the two spins. If each atom has z electrons not in complete shells, and if these electrons are treated as equivalent, then the constant of proportionality in the second member of (1) is connected[3] with the usual exchange integral J_{jk} by the relation $\tilde{A}_{jk}=-2z^2J_{jk}$. The exchange interaction is present only in the electronic, and not in the nuclear case since the orbital exchange energy is correlated by the exclusion principle with the alignment of electronic rather than nuclear spin.

For our purposes it is advantageous to use a system of quantization in which the z component of spin is diagonal. In order to exhibit more clearly the effects of this quantization, we write scalar products such as $\mathbf{r}_{jk}\cdot\mathbf{S}_j$ in the explicit form $r_{jk}(\alpha_{jk}S_{xj}+\beta_{jk}S_{yj}+\gamma_{jk}S_{zj})$, where α_{jk}, β_{jk}, γ_{jk} are the direction cosines of $\mathbf{r}_{jk}$ relative to the x,y,z axes. When this is done, Eq. (1) becomes

$$\begin{aligned}\mathcal{H}=Hg\beta\Sigma_j S_{zj}+\Sigma_{k>j}\tilde{A}_{jk}\mathbf{S}_j\cdot\mathbf{S}_k+\Sigma_{k>j}g^2\beta^2r_{jk}^{-3}\{&\mathbf{S}_j\cdot\mathbf{S}_k-3\gamma_{jk}{}^2S_{zj}S_{zk}-\tfrac{3}{4}(\alpha_{jk}{}^2+\beta_{jk}{}^2)(S_{j+}S_{k-}+S_{j-}S_{k+})\}\\
+\big[\Sigma_{k>j}g^2\beta^2r_{jk}^{-3}\{&-\tfrac{3}{4}(\alpha_{jk}{}^2-\beta_{jk}{}^2)(S_{j+}S_{k+}+S_{j-}S_{k-})+\tfrac{3}{2}i\alpha_{jk}\beta_{jk}(S_{j+}S_{k+}-S_{j-}S_{k-})\\
&-\tfrac{3}{2}\gamma_{jk}(\alpha_{jk}-i\beta_{jk})(S_{j+}S_{zk}+S_{zj}S_{k+})-\tfrac{3}{2}\gamma_{jk}(\alpha_{jk}+i\beta_{jk})(S_{j-}S_{zk}+S_{zj}S_{k-})\}\big].\end{aligned} \tag{2}$$

Here we have used the abbreviations S_{j+}, S_{j-} for the combinations $S_{xj}+iS_{yj}$, $S_{xj}-iS_{yj}$ which are introduced in order to simplify the selection rules. Namely, the selection rules for S_{j+}, S_{j-} are, respectively, $\Delta M_j=+1$, $\Delta M_j=-1$ and hence are sharper than those $\Delta M_j=\pm1$ for S_{xj} or S_{yj}. Here M_j is the magnetic quantum number for atom j, supposed individually space quantized relative to the z axis. We shall use the letter M for the total magnetic quantum number $\Sigma_j M_j$.

[3] For a discussion of the dependence of exchange energy on spin alignment, see, for instance, J. H. Van Vleck, *The Theory of Electric and Magnetic Susceptibilities* (Oxford University Press, 1932), p. 316 ff.

Were it not for the portion of (2) inclosed in heavy brackets, the z component of total angular momentum, i.e., $\Sigma_j S_{zj}$, would be a constant of the motion, and would be specified by the usual total magnetic quantum number M. The x component of magnetic moment would then conform rigorously to the selection rule $\Delta M = \pm 1$, and the absorption would be entirely in the vicinity of the Larmor frequency $g\beta H/h$. The inclusion of the bracketed part of (2) introduces matrix elements in the Hamiltonian function of the type $\Delta M = \pm 1, \pm 2$. The addition of these elements makes the selection rule $\Delta M = \pm 1$ for the x component of moment cease to be rigorous. As a result, transitions of the form $\Delta M = 0, \pm 2, \pm 3$ are allowed, corresponding to changes in Zeeman energy amounting to 0, $2g\beta H$, $3g\beta H$. (Still larger changes in M are allowed if the perturbation calculation is carried further, but the intensity is so low as to be negligible.) The subsidiary lines whose frequencies are near 0, $2g\beta H/h$, $3g\beta H/h$ are not those of interest to us, and so we shall henceforth drop the bracketed part of (2). This omission is not to be regarded as merely a simplification. Retention of the omitted part of (2) would, in fact, be completely erroneous in the ensuing computation of various mean powers of the frequencies by the commutator method. If the commutator with the complete Hamiltonian were used, we would include the contribution of the lines centering about 0, $2g\beta H/h$, $3g\beta H/h$ as well. Then we could not use the departure of the mean square frequency from $g^2\beta^2H^2/h^2$ as a measure of the mean square line breadth of the main line. The subsidiary lines are, to be sure, much fainter than the primary Larmor component, but differ so much from the latter in frequency that their contribution to the mean square frequency deviation is of the same order as the mean square breadth of the dominant line. The situation is illustrated schematically in Fig. 1.[4]

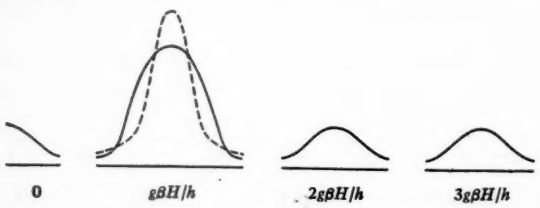

FIG. 1. Schematic illustration of main and subsidiary absorption lines. The dashed curve indicates how the shape of the main line is distorted by exchange coupling.

Let the letter n denote the characteristic values of the expression (2), exclusive of the bracketed part, which is henceforth supposed omitted. Also let $(S_x)_{nn'}$ be the matrix element of $S_x = \Sigma_j S_{xj}$ which connects the states n and n'. The corresponding frequency is, of course, $\nu_{nn'} = (\mathcal{H}_n - \mathcal{H}_{n'})/h$. Then by definition the mean square absorption frequency, i.e., the frequency computed by weighting each fine-structure component with the associated squared amplitude, is

$$\langle \nu^2 \rangle_{Av} = \frac{\Sigma_{n,n'} \{ \nu_{nn'}{}^2 | (S_x)_{nn'} |^2 \}}{\Sigma_{n,n'} | (S_x)_{nn'} |^2}. \tag{3}$$

The trick is now to note that both the numerator and denominator of (3) can be expressed as diagonal sums. If the notation Tr be used for the trace or diagonal sum, then (3) can be written as

$$\langle \nu^2 \rangle_{Av} = -\mathrm{Tr}[\mathcal{H}S_x - S_x\mathcal{H}]^2/h^2\mathrm{Tr}(S_x)^2. \tag{4}$$

The great advantage of (4), which provides the standard method for computing mean square frequencies, is that the invariance of the diagonal sum makes it unnecessary to know the individual characteristic values $\mathcal{H}_n$. Instead the diagonal sum can be computed in an arbitrary system of quantization, most conveniently one in which each spin is individually space-quantized. It would, of course, be hopeless to try and compute the various characteristic values $\mathcal{H}_n$, since the number of them is comparable with the number of atoms composing the crystal. Rigorously, these characteristic values form a discrete rather than continuous manifold. When, however, there are 10^{20} or so fine-structure components to a line, it has effectively a continuous structure, as sketched in Fig. 1.

The retained part of (2) can be written as

$$\mathcal{H} = Hg\beta\Sigma_j S_{zj} + \Sigma_{k>j} A_{jk} \mathbf{S}_j \cdot \mathbf{S}_k + \Sigma_{k>j} B_{jk} S_{zj} \cdot S_{zk}, \tag{5}$$

[4] A sketch similar to Fig. 1, except for the exchange modification, is given by L. J. F. Broer in his thesis, Amsterdam, 1945, and also in Physica 10, 801 (1943). Broer discusses the orders of magnitude of the intensities and breadths of the main and subsidiary lines, but does not essay a quantitative calculation of the r.m.s. width.

with

$$A_{jk}=\tilde{A}_{jk}+g^2\beta^2 r_{jk}^{-3}[\tfrac{3}{2}\gamma_{jk}^2-\tfrac{1}{2}],\quad B_{jk}=-3g^2\beta^2 r_{jk}^{-3}[\tfrac{3}{2}\gamma_{jk}^2-\tfrac{1}{2}]. \tag{6}$$

The reader should be careful to distinguish between the symbols $\tilde{A}_{jk}$ and A_{jk}. Both appear as coefficients of the scalar product $\mathbf{S}_j\cdot\mathbf{S}_k$, but $\tilde{A}_{jk}$ embodies the effect of exchange alone, whereas A_{jk} also contains a dipolar contribution. The distinction can perhaps be remembered most easily by thinking of the wavy line as indicative of the transposition involved in exchange. Any coefficient without this line above it does not arise solely in virtue of exchange coupling. All B coefficients are purely dipolar in origin.

The scalar product $\mathbf{S}_j\cdot\mathbf{S}_k$ commutes with $S_x=\Sigma_j S_{xj}$. Hence the second member of (5) has no influence on $\langle\nu^2\rangle_{Av}$. As a result we can conclude that exchange has no effect on the mean square absorption frequency.

We can evaluate traces in (4) with the aid of the familiar commutation and trace relations, *viz.*,

$$S_{xj}S_{yk}-S_{yk}S_{xj}=\delta_{jk}S_{zj}i,\quad \mathrm{Tr}S_{zj}^2=\tfrac{1}{3}S(S+1)(2S+1)^N,\quad \mathrm{Tr}S_{zj}=0, \tag{7}$$

where S is the spin quantum number of an individual atom. The traces over the different atoms can be computed independently. Thus

$$\mathrm{Tr}S_{xj}S_{xk}=\mathrm{Tr}S_{xj}=\mathrm{Tr}S_{xk}=0(j\neq k),\quad \text{etc.}$$

Proceeding in this fashion, we find that

$$\mathrm{Tr}(S_x)^2=\tfrac{1}{3}NS(S+1)(2S+1)^N, \tag{8}$$

$$\begin{gathered}\mathcal{H}S_x-S_x\mathcal{H}=Hg\beta i\Sigma_j S_{yj}+i\Sigma_{k>j}B_{jk}(S_{yj}S_{zk}+S_{yk}S_{zj}),\\ -\mathrm{Tr}(\mathcal{H}S_x-S_x\mathcal{H})^2/(2S+1)^N=\tfrac{1}{3}Ng^2\beta^2H^2S(S+1)+(2/9)S^2(S+1)^2\Sigma_{k>j}B_{jk}^2,\end{gathered} \tag{9}$$

where N is the total number of atoms in the crystal.

One can easily convince oneself that the line structure (apart, of course, from the usual powers of ν) is symmetrical about a center located at the Larmor frequency $Hg\beta/h$. This statement can be proved from the fact that to every characteristic value of the expression (5), there is another one wherein the Zeeman energy is reversed in sign, but in which the dipolar and exchange energy is unaltered. Hence every fine-structure component on the high frequency side of $Hg\beta/h$ has a mirror image on the other side, with the same line strength, since the transition probability is unaffected by consistent reversal of the sign of the magnetic quantum number. Thus it follows from (4), (8), and (9) that the mean square deviation of the frequency from the Larmor value is

$$\langle\Delta\nu^2\rangle_{Av}=\langle(\nu-g\beta H/h)^2\rangle_{Av}=\langle\nu^2\rangle_{Av}-g^2\beta^2H^2/h^2=\tfrac{1}{3}S(S+1)h^{-2}\Sigma_k B_{jk}^2, \tag{10}$$

with B_{jk} defined as in (6). We suppose all atoms similarly situated, so that the sum at the end of (10) is independent of j.

If the crystal has cubic symmetry, it is found that when the definition (6) of the B_{jk} is used, the expression (10) becomes

$$\langle\Delta\nu^2\rangle_{Av}=\tfrac{3}{5}g^4\beta^4h^{-2}[a+b(\lambda_1^4+\lambda_2^4+\lambda_3^4)]S(S+1), \tag{11}$$

where λ_1, λ_2, λ_3 are the direction cosines of the applied field H relative to the principal cubic axes X, Y, Z. The constants a, b are independent of λ_1, λ_2, λ_3, and have the values

$$a=\Sigma_k r_{jk}^{-6}[7-9(\mu_{jk}^4+\nu_{jk}^4+\xi_{jk}^4)],\quad b=\Sigma_k r_{jk}^{-6}[-9+15(\mu_{jk}^4+\nu_{jk}^4+\xi^4)]. \tag{12}$$

Here μ_{jk}, ν_{jk}, ξ_{jk} are the direction cosines of $\mathbf{r}_{jk}$ relative to the X, Y, Z axes. For a simple cubic lattice, the sums over k are readily computed, and (11) becomes

$$\langle\Delta\nu^2\rangle_{Av}=36.8g^4\beta^4h^{-2}d^{-6}[\tfrac{1}{3}S(S+1)][(\lambda_1^4+\lambda_2^4+\lambda_3^4)-0.187]. \tag{13}$$

Here d is the spin-lattice constant, i.e., the distance between neighboring magnetic atoms located on a simple cubic grating. (Our constant d need not be the same as the conventional lattice constant, since there may be intervening atoms devoid of spin which are irrelevant for our problem.)

With a powder, rather than single crystal, we can replace the powers of the direction cosines by their averages over a sphere, and then (11) reduces to

$$\langle\Delta\nu^2\rangle_{Av}=\tfrac{3}{5}g^4\beta^4h^{-2}S(S+1)\Sigma_k r_{jk}^{-6}. \tag{14}$$

It may be noted that the value $\langle\Delta\nu^2\rangle_{Av}$ is larger by a factor $(\frac{3}{2})^2$ than it would have been had we computed this quantity in a naive fashion by erroneously assuming that because of the Larmor precession only the z component of moment of each atom is effective in the interatomic coupling. In other words, if we had assumed that the effective dipolar part of (2) was $\Sigma_{k>j}g^2\beta^2r_{jk}^{-3}(1-3\gamma_{jk}^2)S_{zj}S_{zk}$, the values of the constants a and b in (11) would be 4/9 as great as given by (12). This fact has already been demonstrated by Bloembergen, Pound, and Purcell.[2] When only the z components of moment are retained, the calculation becomes particularly simple, as it is then essentially magnetostatic rather than quantum-mechanical. Unfortunately the higher moments, say $\langle\Delta\nu^n\rangle_{Av}$, cannot, in general, be correctly obtained by multiplying the results obtained with the simplified model by a factor $(\frac{3}{2})^n$.

Our formula (14) for the mean square frequency deviation in an isotropic medium or powder is exactly 3/10 as large as the corresponding expression which Waller[5] derived for the mean square frequency in the absence of any external field. Waller used the same method as ours, except that in the numerator of (4) he took the commutator of S_x with the complete Hamiltonian function (1) or (2), inclusive of the bracketed terms. In his case, the inclusion of the bracketed terms was, of course, appropriate, since without the external field the separation into different frequency bands in accordance with the harmonic of the Larmor frequency is no longer relevant. By a very slight extension of Waller's calculation, it can be proved that in an applied field of arbitrary strength, the mean square frequency, inclusive of all lines, is equal to $g^2\beta^2H^2h^{-2}+10\langle\Delta\nu^2\rangle_{Av}/3$, where $\langle\Delta\nu^2\rangle_{Av}$ is given by (14). In strong fields, the subsidiary lines, of frequencies approximately 0, $2\beta H/k$, $3\beta H/h$, make a contribution $7\langle\Delta\nu^2\rangle_{Av}/3$ to this mean square. This contribution is independent of H because in strong fields, as Broer[4] has noted, the amplitudes of the "forbidden" lines are inversely proportional to H, whereas the frequencies are approximately linear in H. In weak fields there is, of course, no essential distinction between the main lines and the subsidiaries or harmonics.

The usual assumption is that the frequencies have a Gaussian distribution

$$f(\nu)=[1/2\pi\langle\nu^2\rangle_{Av}]^{\frac{1}{2}}\exp[-(\nu-g\beta H/h)^2/2\langle\Delta\nu^2\rangle_{Av}]. \tag{15}$$

Then the full "half-width," i.e., twice the deviation in frequency from the central value at which the intensity has dropped to half its maximum, is

$$\Delta\nu_{\frac{1}{2}}=2(\log\sqrt{2})^{\frac{1}{2}}\sqrt{2}[\langle\Delta\nu^2\rangle_{Av}]^{\frac{1}{2}}=2.35[\langle\Delta\nu^2\rangle_{Av}]^{\frac{1}{2}},\quad \Delta\nu_{\text{m.sl.}}=2[\langle\Delta\nu^2\rangle_{Av}]^{\frac{1}{2}}. \tag{16}$$

We also include in (16) the formula for the frequency separation $\Delta\nu_{\text{m.sl.}}$ of the two points of maximum slope $(df/d\nu)_{\max}$ in the absorption curve.

One of the main points to be made in the present paper is that extreme caution must be exercised in using (15). A good idea as to the applicability of (15) may be formed by reckoning out the fourth moment, as we shall do in the next section, and examining whether it comes at all near to being equal to $3[\langle\Delta\nu^2\rangle_{Av}]^2$, as (15) would require. We shall see that if exchange forces are important, (15) is necessarily far from the truth. On the other hand, in the case of nuclear resonance, where exchange does not enter, the error involved in (15) is not so serious.

[5] I. Waller, Zeits. f. Physik **79**, 380 (1932).

III. CALCULATION OF THE MEAN FOURTH POWER OF THE FREQUENCY

We now proceed to the more difficult calculation of the fourth moment. The standard formula,[6] analogous to (4), for the mean fourth power of the frequency is

$$h^4\langle\nu^4\rangle_{Av}=\mathrm{Tr}[\mathcal{H}U-U\mathcal{H}]^2/\mathrm{Tr}(S_z)^2, \tag{17}$$

where U equals $\mathcal{H}S_z-S_z\mathcal{H}$ and in our case is given by (9). Using the commutation rules (7) one finds

$$\mathcal{H}U-U\mathcal{H}=+H^2g^2\beta^2\Sigma_jS_{xj}+\Sigma_{k>j}\{[jk]+[kj]\}+\Sigma_{l>k>j}\{[jkl]+[klj]+[ljk]\}, \tag{18}$$

where

$$[jk]=2Hg\beta B_{jk}S_{xj}S_{zk}+B_{jk}{}^2S_{xj}S_{zk}{}^2+A_{jk}B_{jk}[-S_{zj}S_{xk}S_{zk}+S_{yk}S_{yj}S_{xj}-S_{yj}{}^2S_{xk}+S_{xj}S_{zk}{}^2],$$
$$[jkl]=2B_{jk}B_{kl}S_{zj}S_{xk}S_{zl}+[-B_{jl}A_{jk}+B_{kl}A_{jk}-B_{jl}A_{kl}+B_{jk}A_{kl}][S_{zj}S_{xk}S_{zl}-S_{yj}S_{xk}S_{yl}],$$

with $A_{jk}=A_{kj}$, $B_{jk}=B_{kj}$ defined as in (6).

Since the frequencies are symmetrically distributed about a centroid $g\beta H/h$, the relation $\langle\nu^4\rangle_{Av}=\langle(g\beta Hh^{-1}+\Delta\nu)^4\rangle_{Av}$ gives

$$\langle\Delta\nu^4\rangle_{Av}=\langle\nu^4\rangle_{Av}-6H^2g^2\beta^2h^{-2}\langle\Delta\nu^2\rangle_{Av}-H^4g^4\beta^4h^{-4}. \tag{19}$$

In order to work out the trace in (17), it is necessary to use, besides (7), relations such as

$$\mathrm{Tr}S_{zj}{}^3=\mathrm{Tr}S_{zj}{}^2S_{yj}=0,\quad \mathrm{Tr}S_{xj}S_{yj}S_{zj}=\tfrac{1}{6}iS(S+1)(2S+1)^N,$$
$$\mathrm{Tr}S_{zj}{}^4=\tfrac{1}{5}[S^2(S+1)^2-\tfrac{1}{3}S(S+1)](2S+1)^N,\quad \mathrm{Tr}S_{xj}{}^2S_{yj}{}^2=\tfrac{1}{5}[\tfrac{1}{3}S^2(S+1)^2+\tfrac{1}{6}S(S+1)](2S+1)^N. \tag{20}$$

With the aid of the preceding formulas, it is finally found that

$$\begin{aligned}h^4\langle\Delta\nu^4\rangle_{Av}=N^{-1}\Sigma_{j,k,l\neq}&[3B_{jk}{}^2B_{jl}{}^2+2A_{jk}{}^2(B_{jl}-B_{kl})^2+2A_{jk}A_{kl}(B_{jl}-B_{jk})(B_{jl}-B_{kl})\\&+2A_{jk}B_{jk}(B_{jl}-B_{kl})^2][\tfrac{1}{3}S(S+1)]^2+2N^{-1}\Sigma_{k>j}\{B_{jk}{}^4\cdot\tfrac{1}{5}[S^2(S+1)^2-\tfrac{1}{3}S(S+1)]\\&+2B_{jk}{}^3A_{jk}\cdot\tfrac{1}{5}[\tfrac{2}{3}S^2(S+1)^2-\tfrac{1}{2}S(S+1)]+\tfrac{1}{2}B_{jk}{}^2A_{jk}{}^2[\tfrac{4}{5}S^2(S+1)^2-\tfrac{3}{5}S(S+1)]\}.\end{aligned} \tag{21}$$

Here the notation $j, k, l\neq$ means that none of the indices are to be equal. There are thus six times as many terms in the triple sum in (21) as in the type $l>k>j$ employed in (18). The $\neq$ convention makes it possible to write (21) more compactly than otherwise. In (18), however, it was desirable to use the $>$ rather than $\neq$ scheme in order to exhibit clearly the fact that terms differing by simple permutations must be added before rather than after squaring.

An interesting check on the arithmetical correctness of (21) is that all terms involving the A's cancel if $S=\frac{1}{2}$ and if, in addition, all the B_{jk}, etc., are formally given a value B independent of the subscripts. Under these restrictions, simple general considerations show that the exchange terms (i.e., those proportional to A_{jk}) should have no effect on the spectrum. Namely, the exchange energy $\Sigma_{k>j}\tilde{A}_{jk}\mathbf{S}_j\cdot\mathbf{S}_k$ (or equally well the energy $\Sigma_{k>j}A_{jk}\mathbf{S}_j\cdot\mathbf{S}_k$ defined by (6), which contains in addition a dipolar contribution) commutes with Σ_jS_{zj} or Σ_jS_{xj}, and hence with the Zeeman energy, as well as with the dipole moment responsible for the absorption. This energy also commutes with the remaining dipolar Hamiltonian

$$B\Sigma_{k>j}S_{zj}S_{zk}=\tfrac{1}{2}B[(\Sigma_jS_{zj})^2-\Sigma_jS_{zj}{}^2],$$

if $S=\frac{1}{2}$, for then $S_{zj}{}^2$ has the unique value $\frac{1}{4}$, making the term $\Sigma_jS_{zj}{}^2$ merely an additive constant. Hence the exchange energy can be diagonalized without affecting in any way the matrix elements relevant to our absorption problem, and should hence not be involved in the moments of any order. As soon as B_{jk} depends on the subscripts, this statement is no longer true, for then the exchange energy does not commute with the dipolar part of the Hamiltonian.

The fact that (21) contains terms of the form A^2B^2 and AB^3, rather than just B^4, shows that the exchange (i.e., $\tilde{A}$) terms influence the fourth moment, even though they do not enter in the second moment. This behavior is possible only if the absorption tapers off less sharply in the wings than the

[6] Compare, for instance, I. Waller, Zeits. f. Physik 79, 381 (1932).

Gaussian distribution would predict, but at the same time is peaked more sharply in the immediate vicinity of the center of the line, so that the original value of the mean square is unaltered. The half-width, and also the width between the points of maximum slope, is then smaller than given by (16). A rough, schematic illustration of the situation is given in Fig. 1; here the solid and dashed curves are, respectively, exclusive and inclusive of the effect of exchange coupling. It is thus not surprising that experimentally (see Section V) the absorption lines caused by electronic spin are often sharper than one would predict from dipolar interaction alone. Just how much the "exchange narrowing" amounts to cannot be inferred just from the second and fourth moments alone, since a detailed theory of the line shape which we do not have at present would be necessary. We shall allude to this question briefly in Section VI.

Explicit Computation of the Fourth Moment for a Simple Cubic Lattice. In order to evaluate (21) more explicitly, we shall assume a simple cubic grating, since this is the simplest to calculate, as well as one of the commonest to occur. We shall, for the present, neglect terms of the type $\tilde{A}B^3$, and also the purely dipolar contribution to the fourth moment, as sums of the type $\tilde{A}B^3$ or B^4 will be small compared with those of the $\tilde{A}^2B^2$ variety if exchange is preponderant. When this order of approximation is made, we can replace A_{jk} by $\tilde{A}_{jk}$ (cf. Eq. (6)), thus making the A terms arise entirely from exchange. We shall make the usual assumption that the exchange coefficients $\tilde{A}_{jk}$ are negligible except between neighboring atoms, and have a constant value $\tilde{A}$ when j is a neighbor of k. We shall furthermore disregard the dipolar terms connecting atoms separated by distances greater than $2d$, where d is the grating spacing. The resulting error amounts to only a very few percent, since the sums converge rapidly. The distance occurs to the inverse sixth power in expressions of the type $\tilde{A}^2B^2$, inasmuch as $B\sim r^{-3}$. Furthermore in (21) the great bulk of the long-range terms in $\tilde{A}^2B^2$, i.e., those in the triple sum, involve only the difference of the B's sharing the same terminal atom, and then the convergence is even better, since $(B_{jl}-B_{kl})^2\sim r_{jl}^{-4}$ as $r_{jl}\to\infty$, if k is a neighbor of j. In calculating grating sums, it is highly advantageous to have only such differences involved, and it is for this reason that we have grouped the terms in the way that we have in (21).

When the summations in (21) are explicitly performed with the simplifications mentioned in the preceding paragraph, it is found that

$$h^4\langle\Delta\nu^4\rangle_{Av}=4.9\times10^2g^4\beta^4d^{-6}\tilde{A}^2[\tfrac{1}{3}S(S+1)]^2[\lambda_1^4+\lambda_2^4+\lambda_3^4-0.187]$$
$$+\tfrac{1}{4}g^4\beta^4d^{-6}\tilde{A}^2[\tfrac{4}{5}S^2(S+1)^2-\tfrac{3}{5}S(S+1)]\cdot81[\lambda_1^4+\lambda_2^4+\lambda_3^4-\tfrac{1}{3}], \quad (22)$$

where d is the spin-lattice constant, i.e., the distance between neighboring magnetic atoms.

If the Gaussian assumption (15) were valid, the value of $\langle\Delta\nu^4\rangle_{Av}$ would be $3[\langle\Delta\nu^2\rangle_{Av}]^2$. The formula for $\langle\Delta\nu^2\rangle_{Av}$ is given in (13). Hence

$$\frac{\langle\Delta\nu^4\rangle_{Av}}{3[\langle\Delta\nu^2\rangle_{Av}]^2}=\frac{0.12\tilde{A}^2}{g^4\beta^4d^{-6}}[\lambda_1^4+\lambda_2^4+\lambda_3^4-0.187]^{-1}. \quad (23)$$

In calculating this ratio, we have omitted the contribution of the second line of (22), which is smaller than the first and which vanishes entirely if $S=\frac{1}{2}$. The value of $\tilde{A}$ at which the ratio (23) equals unity is a measure of amount of exchange coupling required to distort the shape of the line appreciably. (In this connection it should be remembered that the numerator of (23) omits the purely dipolar contributions which alone are sufficient to give a ratio about unity.) Simple dimensional examination of (21) shows that this critical value of $\tilde{A}$ is given by a formula of the type $\tilde{A}=cg^2\beta^2/d^3$, where c is a dimensionless constant. From (23) it is seen that the value of c will depend on direction. When the field H is along the 100 axis (X axis), c equals 2.6, while for the 111 direction c becomes 1.1. The phenomenon of "exchange narrowing" should hence be somewhat more pronounced for the 111 than the 100 application of the field, but the resulting anisotropy in the line shape is probably not large. (Incidentally, it appears to be purely an accident that the subtractive constant is 0.187 in both (13) and the first line of (22).)

We have tacitly supposed that dipolar interaction alone does not cause significant departures from the Gaussian distribution. This assumption may be tested by calculating the fourth moment by means of (21) with omission of all but dipolar terms. In this connection, it should be noted that in (21) the dipolar coupling not only enters through the B constants, but also through the A's, since by (6) the value of A_{jk} is $-\frac{1}{3}B_{jk}$ when there is no exchange. Thus it is no longer allowable to neglect all the A_{jk} except those joining neighboring atoms, although such terms have a distinctly dominant effect. When A_{jk} is replaced by $-\frac{1}{3}B_{jk}$, the expression (21) can be written

$$\langle\Delta\nu^4\rangle_{Av}=\{3(\Sigma_k B_{jk}^2)^2-\tfrac{1}{3}N^{-1}\Sigma_{jkl\neq}B_{jk}^2(B_{jl}-B_{kl})^2-\tfrac{1}{5}\Sigma_k B_{jk}^4[8+\tfrac{3}{2}(S^2+S)^{-1}]\}\{\tfrac{1}{3}S(S+1)\}^2. \quad (24)$$

If only the first right-hand member were present, the fourth moment would have precisely the Gaussian value. Even for a simple cubic lattice, explicit evaluation of (24) would be laborious for an arbitrary angle between the applied field and the principal axes; also the angular dependence in the resulting analytical formula would be cumbersome, involving the direction cosines to the eighth rather than fourth power as in (22). We have therefore calculated (24) for a simple cubic lattice for the special case that H is directed along the 100 axis. Then we find that (24) becomes

$$\langle\Delta\nu^4\rangle_{Av}=3[\langle\Delta\nu^2\rangle_{Av}]^2[1-0.160-0.021(S^2+S)^{-1}]. \quad (25)$$

If $S=\frac{1}{2}$, Eq. (25) yields a root mean fourth deviation $[\langle\Delta\nu^4\rangle_{Av}]^{\frac{1}{4}}$, which is 1.25 times the root mean square $[\langle\Delta\nu^2\rangle_{Av}]^{\frac{1}{2}}$. With a Gaussian distribution, the ratio would be 1.32 instead of 1.25. The departures from Gaussian form caused by pure dipolar interaction are thus not great. They tend to blunt the absorption curve, rather than peak it more sharply as the exchange corrections do. For a rectangular shaped curve, the ratio would be 1.16.

Rough numerical examination of (24) for the case that H is along the 111 direction indicates that for this orientation the departures from the Gaussian form are smaller than for the 100. The ratio of the root mean fourth to root mean square deviation is about 1.30.

If exchange effects are present, and if H is directed along the 100 axis, the fourth moment is the sum of the expressions (22) and (24), with $\lambda_1=1$, $\lambda_2=\lambda_3=0$ in (22). The existence of terms of the form $\tilde{A}B^3$ when (6) is substituted in (21) implies that this additivity is not rigorous. However, the contribution of the terms of structure $\tilde{A}B^3$ turns out to be small, and may be considered zero within the accuracy to which we have evaluated the grating sums.

IV. CALCULATION FOR A CRYSTAL WITH TWO MAGNETIC INGREDIENTS

It is not difficult to extend the analysis to a grating which contains two different types of atoms, having, respectively, g-factors g and g', also spins S and S'. This situation arises when the crystal contains two species of atoms, both with nuclear (or both with electronic) spin. A further example of particular interest is encountered when a small percentage of atoms with electronic spin is added to a crystal whose nuclear resonance is being studied.

With two ingredients, it is necessary to distinguish which type of atom is active in the resonance. Without loss of generality we can assume that the atoms with unprimed spin are responsible for the absorption at the wave-length being utilized. It is supposed throughout the present section that the two g-factors are sufficiently different so that the resonances for the two varieties of atoms do not overlap. This condition is abundantly fulfilled when one of the spins is nuclear and the other electronic. In applying our formulas, the same definition of the magneton β must be used for both ingredients; hence g will be different by a factor of the order 10^3 for the nuclear and electronic constituents. If both spins are nuclear, their g-factors will in general differ, so that our calculations are applicable. It is not necessary that the spin quantum numbers S and S' be unlike. If both spins are electronic, both g and g' are presumably nearly 2, though there can be deviations from the ideal value 2 because of spin-orbit interaction. Then one must be careful to see whether g and g' differ sufficiently to separate the two resonances and make the present calculation relevant. The separation can, of course, be increased by augmenting the applied magnetic field. A limiting case which we do

not calculate, but which might ultimately prove of interest, and which could be treated by the general mathematical methods of the present paper, is that of atoms with identical g-factors but unlike spin quantum numbers. The general case in which the difference between the two Larmor frequencies is comparable with the dipolar broadening would present an intricate mathematical problem.

We shall throughout use primed and unprimed letters to distinguish the two varieties of atoms. Since the unprimed component is responsible for the resonance, the x component of moment S_x to be used in (4) or (17) involves only the summation $\Sigma_j S_{xj}$ over the unprimed atoms. A point particularly to be emphasized is that in constructing the Hamiltonian function $\mathcal{H}$, it is essential to exclude matrix elements of the type $\Delta M_j=+1$, $\Delta M_{k'}=-1$, or $\Delta M_j=-1$, $\Delta M_{k'}=+1$. Here M_j, $M_{k'}$ denote the magnetic quantum numbers appropriate to separate spatial quantization of atoms j and k', respectively. The effect of such elements would be to create a subsidiary absorption line at a Zeeman frequency $(2g-g')\beta H/h'$, and also to modify very slightly the irrelevant absorption at $g'\beta H/h$ due primarily to the primed system. These elements should thus be excluded, just as the heavily bracketed part of (2) was dropped in Section II to avoid inclusion of the subsidiary lines in Fig. 1. Generalized to the present problem, Fig. 1 would contain two main lines of frequency $g\beta H/h$, $g'\beta H/h$ respectively, and a variety of minor ones, of frequency $(2g-g')\beta H/h$, $2g\beta H/h$, $(g+g')\beta H/h$, etc. We are essaying the calculation of the width of the main line at $g\beta H/h$.

In virtue of the remarks made in the preceding paragraph, parts of the Hamiltonian function having factors of the form $(S_{xj}+iS_{yj})(S_{xk'}-iS_{yk'})=S_{j+}S_{k-}$ or $S_{j-}S_{k+}$ should be omitted, although they must be retained when both letters are primed, or both unprimed. In a scalar product such as $\mathbf{S}_j\cdot\mathbf{S}_{k'}=S_{xj}S_{xk'}+S_{yj}S_{yk'}+S_{zj}S_{zk'}$ only the term $S_{zj}S_{zk'}$ is relevant. Hence, when one letter is primed and the other unprimed, even more of the dipolar terms should be discarded than those bracketed in (2). The effective exchange and dipolar potential coupling together two unlike atoms j,k' is thus $C_{jk'}S_{zj}S_{zk'}$ where

$$C_{jk'}=\tilde{A}_{jk'}+(1-3\gamma_{jk'}{}^2)gg'\beta^2r_{jk'}{}^{-3}. \tag{26}$$

The total Hamiltonian to be employed in place of (5) is

$$\mathcal{H}=Hg\beta(\Sigma_j S_{zj}+\Sigma_{j'}S_{zj'})+\Sigma_{k>j}(A_{jk}\mathbf{S}_j\cdot\mathbf{S}_k+B_{jk}S_{zj}S_{zk}) \\ +\Sigma_{k'>j'}(A_{j'k'}\mathbf{S}_{j'}\cdot\mathbf{S}_{k'}+B_{j'k'}S_{zj'}S_{zk'})+\Sigma_{j,k'}C_{jk'}S_{zj}S_{zk'}. \tag{27}$$

Here $A_{j'k'}$, $B_{j'k'}$ are to be understood defined as in (6) except for the addition of primes. The commutator $U=\mathcal{H}S_x-S_x\mathcal{H}$ is given by the expression

$$U=ig\beta H\Sigma_j S_{yj}+i\Sigma_{k>j}B_{jk}(S_{yj}S_{zk}+S_{yk}S_{zj})+i\Sigma_{j,k'}C_{jk'}S_{yj}S_{zk'},$$

which replaces (9). One finds that

$$\mathcal{H}U-U\mathcal{H}=(\mathcal{H}U-U\mathcal{H})_0+\Sigma_{l'}\Sigma_{k>j}\{2C_{jl'}B_{jk}S_{xj}S_{zk}S_{zl'}+2C_{kl'}B_{jk}S_{xk}S_{zj}S_{zl'} \\ +A_{jk}(C_{jl'}-C_{kl'})(-S_{zj}S_{xk}S_{zl'}+S_{xj}S_{zk}S_{zl'})\} \\ +\Sigma_j\Sigma_{l'>k'}\{A_{k'l'}(C_{jk'}-C_{jl'})(S_{yj}S_{yk'}S_{xl'}-S_{yj}S_{xk'}S_{yl'})+2C_{jk'}C_{jl'}S_{xj}S_{zk'}S_{zl'}\}+\Sigma_{j,k'}C_{jk'}{}^2S_{xj'}S_{zk'}{}^2,$$

where $(\mathcal{H}U-U\mathcal{H})_0$ denotes the value which would result were there no primed atoms, and which is given by the right side of (18).

The same procedure that was used previously, based on Eqs. (4), (17), and (19), can now be employed to calculate the second and fourth moments. The following expressions are finally obtained for the mean square and mean fourth power frequency deviation:

$$\langle\Delta\nu^2\rangle_{Av}=\tfrac{1}{3}S(S+1)h^{-2}\Sigma_k B_{jk}{}^2+\tfrac{1}{3}S'(S'+1)h^{-2}\Sigma_{k'}C_{jk'}{}^2, \tag{28}$$

$$h^4\langle\Delta\nu^4\rangle_{Av}=h^4[\langle\Delta\nu^4\rangle_{Av}]_0+N^{-1}[\tfrac{1}{3}S(S+1)][\tfrac{1}{3}S'(S'+1)]\Sigma_{l'}\Sigma_{k>j}\{6B_{jk}{}^2(C_{jl'}{}^2+C_{kl'}{}^2) \\ +2A_{jk}{}^2(C_{jl'}-C_{kl'})^2+4B_{jk}A_{jk}(C_{jl'}-C_{kl'})^2\}+N^{-1}\Sigma_j\Sigma_{l'>k'}[2A_{k'l'}{}^2(C_{jk'}-C_{jl'})^2 \\ +6C_{jk'}{}^2C_{jl'}{}^2][\tfrac{1}{3}S'(S'+1)]^2+N^{-1}\Sigma_{j,k'}C_{jk'}{}^4\cdot\tfrac{1}{5}[S'(S'+1)-\tfrac{1}{3}]S'(S'+1). \tag{29}$$

Here N is the number of unprimed atoms, and $h^4[\langle \nu^4 \rangle_{Av}]_0$ denotes the right side of (21), or in other words the mean fourth power deviation which would result were the coupling to the primed system completely absent. The expression (29) would have the value corresponding to the Gaussian hypothesis only if we could omit from (29) all terms except the two with factor 6, also from (21) all terms except that with factor 3, and if, in addition, we could disregard the exclusion of equal indices, replacing a sum of the type $\Sigma_a \Sigma_{c>b}$ by $\frac{1}{2}\Sigma_{a,b,c}$, etc. Actually, of course, these conditions are not fulfilled.

The results (28) and (29) doubtless appear rather formidable, but have several interesting implications, which we shall now summarize.

(a) All other things being equal, dipolar coupling between unlike atoms is less effective than that between like ones in broadening the lines. This prediction follows from the fact that the mean square broadening (28) involves the coefficients B_{jk} and C_{jk} symmetrically, along with the fact that the definition (6) of B_{jk} involves a factor $\frac{3}{2}$ not contained in the dipolar part of the expression (26) defining C_{jk}. Hence the contributions of like atoms to the mean square are enhanced by a factor 9/4 as compared with those of unlike ones, apart from any allowances for diversity in magnitude of the g-factor or of the spin quantum number. This greater effectiveness of coupling between like atoms has its physical origin in resonance, and is expressed mathematically by the irrelevance of more terms of the Hamiltonian when the atoms are unlike.

(b) Exchange interaction between unlike atoms tends to broaden absorption lines. This prediction is a consequence of the fact that the definition (26) of C_{jk} includes a term involving the exchange coefficient $\tilde{A}_{jk}$, whereas that (6) of B_{jk} does not. Hence exchange coupling between dissimilar atoms, unlike that between similar ones, contributes to the mean square broadening (28). This diversity in behavior has arisen because $\tilde{A}_{jk}\mathbf{S}_j \cdot \mathbf{S}_k$ commutes in matrix multiplication with the x component of moment $S_x = \Sigma_k S_{xk}$, whereas $\tilde{A}_{jk'} S_{xj} S_{xk'}$ does not.

(c) Both dipolar and exchange interactions between atoms of the primed system contribute to the fourth, but not to the second moment. This one sees from the presence in (29), but absence in (28), of terms containing $A_{j'k'}$. The definition (6) of $A_{j'k'}$ includes both dipolar and exchange members. Hence there will be a narrowing effect and deviations from the Gaussian structure, in case either the exchange or dipolar interaction between the primed atoms is sufficiently large compared to the dipolar coupling between unprimed atoms, and also to both the exchange and dipolar interactions between unlike atoms.

(d) Exchange interaction between the unprimed atoms does not contribute to the second moment, but enhances the fourth moment, even if the dipolar broadening is caused primarily by interplay between unlike rather than exclusively unprimed atoms, i.e., by the addition of "foreign atoms." This statement expresses the presence in (29) of terms of the form $A_{jk}^2 C_{jl'}^2$, which will be more important than those of the form $A_{jk}^2 B_{jl}^2$ in (21), if $\Sigma_{k'} C_{jk'}^2 \gg \Sigma_k B_{jk}^2$.

A distinction should be noted between effects (a), (b) and (c), (d). Namely, (a), (b) are both operative on the mean square, and do not necessarily imply that the Gaussian assumption is a bad one. On the other hand, (c), (d) involve mechanisms influencing only the fourth and higher moments, and hence are consequential only if there are significant deviations from the Gaussian distribution.

Exchange integrals involving nuclear spins are presumably negligible. Hence only item (a) is of interest in experiments on nuclear resonance in materials devoid of any electronically paramagnetic atoms. A possible, but infrequently occurring exception is that the dipolar mechanism in (c) might make the broadening smaller than one would compute from (a) with the Gaussian hypothesis if the nuclei of the "foreign" atoms, i.e., those of the primed system not responsible for the resonance, are numerous and also have g-factors or spins materially greater than those of the primary (unprimed) atoms. Effect (b) of consequence only if both components have electronic spin.

Items (a) and (c) are of particular interest in case experiments are made on the broadening of nuclear resonance lines by the addition of a relatively small number of foreign atoms with electronic spin. Then g'/g is of the order 10^3,

TABLE I. Calculated and observed r.m.s. frequency deviations in CaF_2.*

Direction	$\Delta\nu_2$(calc.)	$\Delta\nu_2$(calc.)	$\Delta\nu_2$(obs.)
100	14.4 kc	3.60 gauss	3.68±0.20 gauss
110	10.0	2.24	2.25±0.20
111	6.1	1.53	1.77±0.20

* The experimental measurements are by Pake and Purcell.

and Eq. (28) shows that, as one would guess, the foreign atoms will begin to influence the width of the absorption line when they are about 10^{-6} as abundant as the atoms responsible for the nuclear resonance. The broadening influence of the impurity will, however, be somewhat smaller than one would expect by simple extension of the formulas for a one-component system. In the first place, as already mentioned, the diversity in the definitions (6) and (26) of B_{jk} and C_{jk} diminishes the second or foreign part of (28) by a factor 4/9 compared to what one would expect by extrapolation of the first part. Far more important, however, is the fact that, as soon as the impurity becomes abundant enough to influence the line shape, the dipolar, not to mention the exchange, coupling between the foreign atoms enhances the fourth moment very materially, and hence makes the effective line-breadth considerably less than one would calculate from the mean square with the Gaussian hypothesis. One's first reaction is perhaps that any dipolar interaction between the foreign atoms is a higher order effect because of their unabundance. We have seen that only a small amount of paramagnetic impurity is needed to influence the mean square breadth of the nuclear resonance. Inspection of the structure of (29), however, shows that the dipolar coupling between the foreign or primed atoms yields contributions to the fourth moment of the order $(N'/N)^2g^2g'^6/d^{12}$, as compared with terms of the order $(N'/N)^2g^4g'^4/d^{12}$ from the square of the contribution of the foreign atoms to the mean square. (Mathematically, this statement is a consequence of appearance of terms of the form $A_{k'l'}{}^2C_{jk'}{}^2$ coordinately with those of the form $C_{jk'}{}^2C_{jl'}{}^2$ in the sum of type $\Sigma_j\Sigma_{l'>k'}$ in (29), and by definitions (6) and (28) one has $|A_{k'l'}|\sim(g'/g)|C_{jk'}|$ if $\tilde{A}_{k'l'}=0$.) The dipolar interaction between the impurity atoms hence necessarily makes the line shape non-Gaussian if they are abundant enough to be the main broadening agency.

V. COMPARISON WITH EXPERIMENT

As yet, the experimental data available to test our theory are rather meager. However, the rapid development of radiofrequency and microwave spectroscopy leads us to expect greatly enhanced evidence in the future.

Diamagnetic Crystals with One Type of Nuclear Spin. The simplest case theoretically is that of a crystal with a single variety of nuclear spin, and devoid of any electronic paramagnetism. Since we have assumed throughout that the influence of the crystalline field is negligible, it is essential that the nuclei be devoid of quadrupole moments unless the field is cubic. Otherwise a significant part of the broadening may be caused by the interaction of the quadrupole moment with the crystalline electric field. (A crystalline field which is of cubic symmetry will not, however, interact with a nuclear quadrupole moment.)

If there are no quadrupolar complications, the broadening of the resonance line should be due solely to the dipolar coupling between the nuclear spins, inasmuch as exchange forces involving nuclear spins are negligible. The mean square deviation of the frequency from its central value should then be computable from (13).

Calcium fluoride is a crystal *par excellence* for testing the theory of pure dipolar broadening mentioned in the preceding paragraph. The only spin is that of the fluorine nucleus, and the fluorine nuclei are arranged in a simple cubic lattice. Furthermore, the spin of the F nucleus is $\frac{1}{2}$, so that there can be no complications arising from quadrupole moments. The nuclear resonance absorption by a single crystal of CaF_2 has been measured by Purcell, Bloembergen, and Pound.[7]

The directional effects are most simply tested in a preliminary way by study of the variation of the peak absorption at the center of the line when the orientation of the magnetic field relative to the principal axes of the crystal is changed. The peak is easier to measure than the breadth,

[7] E. M. Purcell, N. Bloembergen, and R. V. Pound, Phys. Rev. 70, 988 (1946).

and exhibits the salient features of the directional trends. With the Gaussian assumption (15), the peak absorption should be inversely proportional to the r.m.s. line breadth, and so should have an angular factor which is the square root of the reciprocal of that given in (13). The angular dependence calculated on this basis when the magnetic field is rotated through various positions in the 110 plane is shown by the dashed line in Fig. 2, taken from the paper by Purcell, Bloembergen, and Pound. The measured peak absorption is shown by the solid line. The constant of proportionality is determined so as to give agreement in the 001 direction.

On the whole, the accord between theory and experiment in Fig. 2 is satisfying. Exact agreement cannot be expected, since the Gaussian assumption on which the theoretical curve is predicated is not rigorous. Since, experimentally, only the relative rather than absolute values of the peak absorption are known, measurements of the type shown in Fig. 2 do not provide a test of the calculated absolute magnitude of the line breadth.

In order to examine the absolute value of the width, and in order to study its directional dependence in a refined fashion not contingent on the Gaussian hypothesis, the r.m.s. width has recently been directly determined experimentally for three angles by Pake and Purcell.[8] The ingenious technique which they employed is described in the following paper; it involves a quite accurate determination of the line shape, so that the various points on the absorption curve can be weighted in accord with their r.m.s. frequency deviation and integrated. The comparison of theory and experiment is given in Table I. In making this comparison we follow the customary practice of expressing the frequency in terms of the magnetic field which will produce a Zeeman shift equal to the frequency interval in question. We also, however, include the values of the theoretical line widths in kilocycles. The abbreviated notation $\Delta\nu_n$, used in Table I and the ensuing discussion, has the significance $\Delta\nu_n = (\langle\Delta\nu^n\rangle_{Av})^{1/n}$.

Pake and Purcell have pushed the comparison of theory and experiment a step further by measuring the root mean fourth frequency deviation for the 100 direction. The observed value of the ratio $\Delta\nu_4/\Delta\nu_2$ is 1.24; our theory gives 1.25. The rectangular, triangular, and Gaussian approximations to the line shape would yield ratios 1.158, 1.245 and 1.316.

The agreement is certainly gratifying, especially when it is recalled that no undetermined constants are involved. Still, the good accord cannot be regarded as too much of a surprise, for, theoretically, in an ideal crystal one cannot envisage any important mechanism for broadening other than the dipolar one, whose moments we calculate rigorously. We believe that our example of CaF_2 is the first case of a substance, either solid or gaseous, where it has been possible to make an unambiguous comparison of a theoretical and observed line breadth with a high degree of accuracy.

It is to be emphasized that in Table I we compared the theoretical value of the r.m.s. frequency deviation with the same quantity observed experimentally, and not with half the frequency difference between the points of maximum slope in the absorption curve. For a Gaussian curve, $\frac{1}{2}\Delta\nu_{\text{m.sl.}}$ and $\Delta\nu_2$ would be identical. The observed values of $\frac{1}{2}\Delta\nu_{\text{m.sl.}}$, *viz.*, 4.4, 3.5, and 2.4 gauss for the 100, 110, and 111 directions are considerably higher than $\Delta\nu_2$. This fact shows that the Gaussian model is not an accurate one. In the 100 direction, the ratio $\frac{1}{2}\Delta\nu_{\text{m.sl.}}/\Delta\nu_2$ is 1.22. This value is reasonable; it

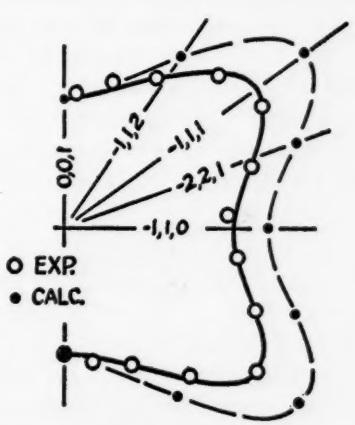

FIG. 2. Peak absorption intensity as a function of direction in a CaF_2 crystal. The solid curve gives the measurements of Purcell, Bloembergen, and Pound. The dashed curve is calculated from the theoretical r.m.s. breadth, under the assumption that the lines are Gaussian.

[8] G. Pake and E. M. Purcell, Phys. Rev. **74**, 1184 (1948).

is a little nearer the ratio 1.0 for a Gaussian shape than that 1.73 for a rectangular one. The ratio $\Delta\nu_4/\Delta\nu_2$ of root mean fourth to root mean square frequency deviation was likewise intermediate between the Gaussian and rectangular models, but somewhat closer to the former.

We saw in Section III that the deviations of the fourth moment from the Gaussian value should be smaller for the 111 than the 100 direction. It is tempting to examine whether this fact will explain the somewhat different angular variation of the peak intensity in Fig. 2 than that provided by the Gaussian model. The corrections calculated on this basis, however, operate in the wrong direction. A rectangle has a value of peak intensity lower by a factor $(\pi/6)^{\frac{1}{2}}$ than that for a Gaussian curve of the same $\Delta\nu_2$. Thus the greater deviations from the Gaussian shape in the 100 direction would tend to increase, relatively, the prongs of the dotted curve in Fig. 2 in the 111 orientation. Dr. Pake tells us that probably the discrepancy in Fig. 2 is to be explained in terms of the fact that the crystal is not ideal. The mean square frequency deviation is considerably smaller for the 111 direction than for other nearly adjacent orientations, and the peak absorption higher. Hence, if the crystal is not perfectly cut, what one thinks is the 111 axis is not really this, but a sort of mixture of nearby directions. As a result, the measured value of $\Delta\nu_2$ for supposedly the 111 axis may be too high, and the peak absorption too low, in accord with the trend in Table I and Fig. 2. The estimates of experimental error in Table I relate to the uncertainty in the integration to obtain the root mean deviation; they do not include any error caused by crystal imperfections. The good agreement for the 111 and 110 directions suggests that the error attendant to the integration has been overestimated. The existence of crystalline imperfections does not immediately explain why the ratio $\frac{1}{2}\Delta\nu_{\text{m.sl.}}/\Delta\nu_2$ actually has a value (1.36) for 111 greater than that (1.22) for 100. The closer validity of the Gaussian model, which gives unit ratio, for the 111 direction would offhand suggest that even with crystal imperfections a trend should be expected which is the reverse of the observed. However, the value of $\Delta\nu_{\text{m.sl.}}$ is sensitive to small perturbations, and the maximum slope of the curve may well come from a spurious wing contributed by a microcrystal not perfectly aligned.

Diamagnetic Crystals with Two Types of Nuclear Spins. In paragraph (a) of Section IV it was pointed out that, because of less resonance, dipolar coupling between nuclei of unequal g-factors is less effective in broadening the lines than the corresponding dipolar interaction between like nuclei of comparable magnetic moment (more accurately, of magnetic moment equal to the geometric mean of that of the two dissimilar components). Unpublished work of G. Pake on the fluorine resonance in KHF_2 confirms this prediction. The second moment has not been measured with as high precision as in CaF_2. However, his data show clearly that without the theoretical reduction factor 4/9 caused by the dissimilarity of the moments in the H-F interactions, the calculated second moment would be much too high to agree with observation. (X-ray measurements do not fix the positions of the H atoms, but chemical and other evidence indicates that they are on lines connecting F nuclei; if H is midway on an F$-$F line the calculated moment is too high without the reduction factor; it is increased further if the proton is not at the midpoint but instead resonates between two unsymmetrical locations.)

Nuclear Resonance in Crystals with Paramagnetic Impurities. If atoms with electron spin are added to an otherwise diamagnetic crystal, but not to so great an extent that electronic absorption masks the nuclear, then the nuclear resonance lines should be widened. However, the discussion at the end of Section IV shows that the action of both the exchange and dipolar forces connecting electronic spins make the effective half-width much smaller than that calculated from the second moment on the assumption of a Gaussian distribution. Unfortunately, no adequate data are yet available to test the theory on this subject. Bloembergen, Purcell, and Pound do indeed find that the widening of nuclear resonance lines in diamagnetic *liquids* by the addition of paramagnetic ions is smaller than the Gaussian model would lead one to expect. These authors, however, show that this behavior is explicable on the grounds that the paramagnetic ions migrate rapidly in the liquid, thus

diminishing the coherence and effectiveness of the dipolar forces coupling together nuclear and electronic spins. Thus there are two alternative mechanisms, both of which appear adequate to explain why paramagnetic impurities are not more potent in widening nuclear resonance lines in liquids. Probably the Bloembergen-Purcell-Pound migration effect is the dominant factor, for reasons to be discussed near the end of Section VI. The migration mechanism would not be relevant if the measurements were made on crystals rather than liquids, and so experiments are obviously desirable on nuclear resonance of crystals with paramagnetic atoms substituted for diamagnetic in a small percentage of the lattice points.

Absorption Arising from Electronic Spin in Paramagnetic Crystals. A number of experiments[9,10] have been performed by now at various laboratories on resonance absorption by electron spin in paramagnetic crystals. In several instances, the line breadth is considerably smaller than one would calculate from dipolar broadening alone if one makes the Gaussian hypothesis and so uses Eqs. (14) and (16). Some examples are given in Table II. These discrepancies are, we believe, to be attributed to the phenomenon of "exchange narrowing," of which the theory was developed in Section III. We there showed that exchange interactions between atoms with electron spins makes the mean fourth power frequency deviation considerably larger than one would calculate with the Gaussian hypothesis from the mean square broadening caused by dipolar interaction, and that consequently the lines are more peaked and so effectively narrower than one would at first expect.

In connection with Table II it should be noted that part of the line broadening may originate in other causes than the dipolar mechanism. In particular, the crystalline Stark effect has a widening action in manganous salts, as does anisotropy in the g-factor in the cupric salts, whose effect we shall discuss elsewhere.[11] The broadening caused by this anisotropy is proportional to the magnitude of the applied field, and hence can be reduced by using rather low resonant frequencies. Hence in an endeavor to eliminate as much as possible all but dipolar broadening, we give in Table II the half-breadths for copper furnished by the measurements of Zavoisky[9] at 200 cm, rather than the larger ones yielded by the data of Cummerow and Haliday,[10] also Arnold and Kip,[12] at about 3 cm.

TABLE II. Approximate observed values of the width between the points of half the maximum absorption, contrasted with the values calculated from dipolar coupling under the assumption that the curve has a Gaussian shape.

	$\Delta\nu_{\frac{1}{2}}$ Observed*	$\Delta\nu_{\frac{1}{2}}$ Calculated
$CuCl_2 \cdot 2H_2O$	125 gauss	750 gauss
$CuSO_4 5H_2O$	175	475
$MnSO_4 4H_2O$	400	1500
$MnSO_4$	300	3500

* See references 9 and 10.

When it is taken into account that other factors besides dipolar coupling may be responsible for some of the line width, the need of invoking the exchange effect to reduce the dipolar broadening becomes even more patent.

An additional piece of evidence may be mentioned in favor of the basic correctness of our model of "exchange narrowing." Exchange forces are relatively short-range, and so should be an effective factor only in materials with a fairly high concentration of magnetic ions. Actually, only in such compounds do the measured line widths prove conspicuously lower than those computed under the assumption of a Gaussian distribution. Glaring discrepancies such as those reported in Table II do not appear for the alums, with their many water molecules of hydration. Also, in Table II, the anhydrous salt $MnSO_4$ shows the greatest disparity between experiment and the Gaussian theory. Precisely this behavior is to be expected, since with no waters of coordination the paramagnetic ions will be closer together, and the "exchange narrowing" consequently greater.

Non-Resonant Paramagnetic Absorption at Low Frequencies. A number of experiments have been performed in Holland by Gorter and others[13] on

[9] E. Zavoisky, J. Phys. U.S.S.R. **10**, 170, 197 (1945).
[10] R. L. Cummerow, D. Haliday, and G. E. Moore, Phys. Rev. **70**, 433 (1946), **72**, 1233 (1947).
[11] For preliminary abstract see Phys. Rev. **73**, 1249 (1948).
[12] R. D. Arnold and A. F. Kip, Phys. Rev. to be published; abstract in **73**, 1247 (1948).
[13] For a survey of this subject, and references, see Gorter's book, *Paramagnetic Relaxation* (Elsevier Publishing Company, Inc., Amsterdam and New York, 1947).

absorption at low frequencies, either in the absence of a magnetic field, or in a weak field comparable with the dipolar interaction. Here again there is evidence for "exchange narrowing" inasmuch as in magnetically concentrated materials the line breadth turns out less than that calculated by a Gaussian treatment of the dipolar effect. This subject has been briefly discussed in a letter to the editor by Gorter and the writer,[14] and we shall not pursue it here since the present paper aims to treat primarily resonant absorption wherein the Zeeman frequency is much greater than the line width. The adaptation of the mathematical methods used in the present paper to the non-resonant, low frequency case will be made in a future paper by Miss Wright.

VI. RELATION TO THE RELAXATION THEORY OF BLOEMBERGEN, POUND, AND PURCELL

A very interesting explanation of nuclear absorption and relaxation phenomena in gases, liquids, or in solids with molecular rotation has been presented by Bloembergen, Pound, and Purcell.[2] These authors point out that the migrations of atoms in fluids change the distances between spins and also the orientations of the axes connecting them. In molecular solids collisions alter the orientations of the molecular axes and hence of spin-spin axes if the molecule involves more than one spin. All these factors spoil the coherency of the action between the different electron spins, and so make the perturbing effect of the dipolar coupling in broadening the lines less than one would compute from the Gaussian model. As Gorter[14] has noted, the mechanism presented in the present paper has considerable analogy to that employed by Bloembergen, Pound and Purcell, provided that in our case we regard the coherency as spoiled by spin waves rather than collisions or migrations. It is well known that exchange, as well as dipole interaction, has the effect of making the spatial components of individual spins cease to be constants of the motion, and gives rise to a continual turning over of spins, which can be envisaged as waves of spin reversal being propagated through the crystal. Bloch showed that at low temperatures this wave picture can be taken literally; at higher temperatures, the term "spin wave" is to be construed only in a generalized sense as meaning that the spins are in a constant state of upheaval because of the exchange forces. It is for this reason that exchange narrows the lines.

The calculation of the fourth moment can be given in rather general terms so as to apply to fluids. We shall show that the results of Bloembergen, Pound, and Purcell,[2] can be interpreted in terms of our moment criteria. Let q symbolize the coordinates other than spin variables which are involved in the dipolar potential. The q's then specify the orientation of the line joining two dipoles, and their distance of separation. The complete Hamiltonian function of the mechanical system will include a portion $\mathcal{H}_2$ which commutes with the total spin moment responsible for the resonance, but which does not commute with the q's. For example, $\mathcal{H}_2$ might be the intermolecular coupling which reorientates molecules at collisions, or even simply the translational kinetic energy associated with the migrations of ions. Then a sort of relaxation time for a variable q may be defined by

$$\frac{1}{\tau_c^2}=\frac{\mathrm{Tr}[\mathcal{H}_2 q-q\mathcal{H}_2]^2}{-h^2\mathrm{Tr}q^2}. \tag{30}$$

This quantity τ_c is essentially the same as that which Bloembergen, Pound, and Purcell denote by the same letter. If $\mathcal{H}_2$ is large compared with the dipolar part of the Hamiltonian, or, more precisely, if $1/\tau_c^2 \gg \langle\Delta\nu^2\rangle_{Av}$, then the mean fourth power deviation as calculated from (17) and (19) will be of the order

$$\langle\Delta\nu^4\rangle_{Av}=\langle\Delta\nu^2\rangle_{Av}/\tau_c^2. \tag{31}$$

According to the theory of Bloembergen, Pound, and Purcell, the half-width will be materially lower than $[\langle\Delta\nu^2\rangle_{Av}]^{\frac{1}{2}}$ if $1/\tau_c^2 \gg \langle\Delta\nu^2\rangle_{Av}$. Inspection of (31) shows that this is precisely the condition that the fourth moment appreciably exceed the Gaussian value $3[\langle\Delta\nu^2\rangle_{Av}]^2$. Both approaches, i.e., the relaxation and moment methods, thus agree as to the conditions under which narrowing phenomena should appear.

Instead of thus applying moments to fluids, one can, vice versa, try to adapt qualitatively the relaxation theory to spin waves in crystals. In

[14] C. J. Gorter and J. H. Van Vleck, Phys. Rev. 72, 1128 (1947).

this fashion one can obtain an estimate of the order of magnitude of the half-width when exchange narrowing is important—something we could not do by the method of moments. According to the theory of Bloembergen, Pound, and Purcell, the half-width is of the order $\tau_c\langle\Delta\nu^2\rangle_{Av}$ if $1/\tau_c^2 \gg \langle\Delta\nu^2\rangle_{Av}$. As applied to our problem of spin interaction, the variables q must be considered as including functions of the spin coordinates, and the Hamiltonian $\mathcal{H}_2$ symbolizes the exchange energy. The relaxation time for the spin waves furnished by (30) is then of the order $h/\tilde{A}$, where $\tilde{A}$ is the exchange integral. Analogy to the relaxation theory thus suggests that the effective half-width is of the order $h\langle\Delta\nu^2\rangle_{Av}/\tilde{A}$. Too much reliance, especially quantitatively, should not be placed on this estimate, as it is derived in a rather superficial way, and conveys little more information than one might conjecture from dimensional considerations.

The action of the spin waves associated with exchange forces only influences energy transfers internal to the spin system, and so does not help in securing thermal equilibrium between this system and the rest of the universe. In this respect there is a difference between the adaptation of the relaxation theory to the spin system, and its original use in connection with atomic migrations. With the latter, energy balance is secured by energy transfer between the spin system and the translations or rotations of atoms or molecules, which thus serve as a thermostat if the relaxation time τ_1 for this transfer is sufficiently short. If τ_c is small enough to permit applicability of (31), $1/\pi\tau_1$ should be comparable with the half-width $\Delta\nu_{\frac{1}{2}}$ of the absorption line and of the order $\langle\Delta\nu^2\rangle_{Av}\tau_c$. In the experiments of Bloembergen, Pound, and Purcell on nuclear resonance in liquids with paramagnetic impurities, it is found that $\Delta\nu_{\frac{1}{2}}$ as measured by direct observation of the line width is very nearly equal to $1/\pi\tau_1$ when τ_1 is determined by measurements of incipient saturation or departures from thermal equilibrium caused by use of excessive power. This fact suggests that the narrowing of nuclear resonance lines in liquids is caused primarily by migration effects, for one would expect to have $1/\tau_1 \ll \Delta\nu_{\frac{1}{2}}$ if the narrowing were due mainly to dipolar or exchange coupling between paramagnetic ions as suggested in paragraph (c) of Section IV. In monatomic crystals, on the other hand, $1/\tau_1$ is millions of times smaller than $\Delta\nu_{\frac{1}{2}}$, and then our adiabatic calculation of the line breadth is well warranted.

In closing, it should be stressed once more that the theory of dipolar broadening of resonance lines in crystalline solids as developed in the present paper is entirely an adiabatic one, regardless of whether there are modulations by exchange forces. Our calculations thus throw no light on the mechanism which keeps the spin system in thermal equilibrium with the rest of the universe in crystals.

The writer is much indebted to Professors C. J. Gorter and E. M. Purcell for stimulating discussions. Also he wishes particularly to thank Dr. George Pake for his interest and cooperation in testing experimentally the predictions regarding the various moments.

Line Shapes in Nuclear Paramagnetism

G. E. PAKE*† AND E. M. PURCELL
Lyman Laboratory of Physics, Harvard University, Cambridge, Massachusetts

(Received July 6, 1948)

This note discusses briefly several methods of describing the width and shape of the resonances characteristic of nuclear paramagnetism. Use of the so-called moments of the shape function is illustrated by an experimental determination of a root mean square line width which is in substantial agreement with a calculation by Van Vleck. The solutions of the Bloch equations, which lead to the Lorentz shape function traditional in the theory of radiation- and collision-broadened lines, are compared with susceptibility curves based on a Gauss absorption curve. A significant difference between the two dispersion curves serves as a criterion for determining whether or not either of these two shapes closely approximates to a given experimental curve, and experimental examples of each are given.

For comparison of shape functions, several well-known specializations of the Kronig-Kramers relations are employed. The collection of these formulae may incidentally prove convenient and useful to those engaged in studies of nuclear paramagnetism.

INTRODUCTION

WHEN a sample containing nuclear magnetic moments is immersed in a constant magnetic field $\mathbf{H}_0$, energy may be absorbed from a radiofrequency magnetic field which is perpendicular to $\mathbf{H}_0$ and has a frequency near the nuclear Larmor frequency. The rate of absorption is proportional to the imaginary component of the nuclear magnetic susceptibility $\chi=\chi'-i\chi''$. The dependence of χ'' on frequency ν is given by the shape function $g(\nu)$, defined as follows:[1]

$$\left.\begin{aligned}\chi''(\nu)&=\pi\chi_0\nu_0 g(\nu)\\ \int_0^\infty g(\nu)d\nu&=1\\ T_2&=\tfrac{1}{2}[g(\nu)]_{\text{Max.}}\end{aligned}\right\}. \qquad (1)$$

Here $\chi_0=N\mu^2(3kT)^{-1}(I+1)/I$ is the static nuclear susceptibility and $\nu_0=(\mu H_0)/(Ih)$ is the resonant frequency for a nucleus with spin I and magnetic moment $\mu=g\beta I$, g being the nuclear g-factor and β the nuclear magneton. For a given shape function, the line width is proportional to $1/T_2$. If $\chi''(\nu)$ is known, $\chi'(\nu)$ is given by the first of the Kronig-Kramers relations:

$$\left.\begin{aligned}\chi'(\nu)-\chi'(\infty)&=\frac{2}{\pi}\int_0^\infty\frac{\nu'\chi''(\nu')d\nu'}{\nu'^2-\nu^2}\\ \chi''(\nu)&=-\frac{2\nu}{\pi}\int_0^\infty\frac{\chi'(\nu')-\chi'(\infty)}{\nu'^2-\nu^2}d\nu'.\end{aligned}\right\}. \qquad (2)$$

These formulae were originally derived for the electric susceptibility.[2] Gorter and Kronig[3] later pointed out their validity for magnetism, and they are easily shown to apply to a large class of complex quantities used in the analysis of physics and engineering problems.[4]

In Eq. (2), as well as in Eqs. (3), (4), and (5) which follow, the Cauchy principal value is to be understood, that is, if $f(\nu')$ has a singularity at $\nu'=\nu$, then

$$\int_0^\infty f(\nu')d\nu'=\lim_{\delta\to 0}\left[\int_0^{\nu-\delta}f(\nu')d\nu'+\int_{\nu+\delta}^\infty f(\nu')d\nu'\right].$$

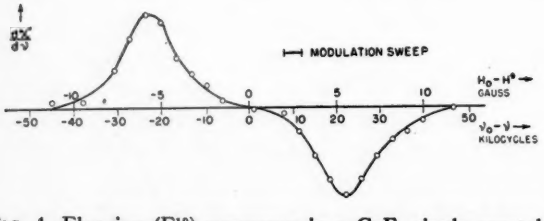

FIG. 1. Fluorine (F^{19}) resonance in a CaF_2 single crystal. $\mathbf{H}_0$ along [100]; $H^*=6824.2$ gauss, $\nu=27.33$ Mc.

* Predoctoral Fellow of the National Research Council.
† Now at Washington University, St. Louis, Missouri.
[1] N. Bloembergen, E. M. Purcell, and R. V. Pound, Phys. Rev. **73**, 679 (1948).
[2] R. de L. Kronig, J. Opt. Soc. Am. **12**, 547 (1926); H. A. Kramers, Atti del Congresso Internationale dei Fisici, Como, Vol. 2, 545 (1927). Compare also Radiation Laboratory Report 735 by J. H. Van Vleck, or Vol. 13, Radiation Laboratory Series (McGraw-Hill), Chap. 8.
[3] C. J. Gorter and R. de L. Kronig, Physica **3**, 1009 (1936).
[4] H. W. Bode, *Network Analysis and Feedback Amplifier Design* (D. Van Nostrand and Company, New York, 1945), Chap. XIV.

SPECIAL FORMS OF THE KRONIG-KRAMERS RELATIONS

Both $\chi'(\nu)$ and $\chi''(\nu)$ for nuclear resonances are effectively zero except in a small frequency interval, usually no more than 200 kilocycles even for solids, about the resonant frequency ν_0 of at least several megacycles. The approximations $\nu'/(\nu'+\nu)\cong\frac{1}{2}$ and $\nu/(\nu'+\nu)\cong\frac{1}{2}$ therefore allow

$$\left.\begin{aligned}\chi'(\nu)&=\frac{1}{\pi}\int_0^\infty\frac{\chi''(\nu')d\nu'}{\nu'-\nu},\\ \chi''(\nu)&=-\frac{1}{\pi}\int_0^\infty\frac{\chi'(\nu')d\nu'}{\nu'-\nu}.\end{aligned}\right\}. \tag{3}$$

Placing $\nu'=\nu_0+\Delta\nu'$ and $\nu=\nu_0+\Delta\nu$ yields

$$\left.\begin{aligned}\chi'(\nu_0+\Delta\nu)&=\frac{1}{\pi}\int_{-\infty}^\infty\frac{\chi''(\Delta\nu')d(\Delta\nu')}{\Delta\nu'-\Delta\nu},\\ \chi''(\nu_0+\Delta\nu)&=-\frac{1}{\pi}\int_{-\infty}^\infty\frac{\chi'(\Delta\nu')d(\Delta\nu')}{\Delta\nu'-\Delta\nu}.\end{aligned}\right\}. \tag{4}$$

Extension of the lower limit from $-\nu_0$ to $-\infty$ adds negligibly to the integrals in view of the narrowness of the resonance. Formulae (4) are more conveniently applied to nuclear susceptibilities than the more general relations (2). Placing $(\nu'/\nu)-1\cong(\nu'-\nu)/\nu_0$ and using $\chi'(0)\ll\chi'(\nu_0)$ after partial integration of Eq. (3) yields

$$\left.\begin{aligned}\chi'(\nu)&=\frac{1}{\pi}\int_0^\infty\frac{d\chi''(\nu')}{d\nu'}\log\left|\frac{\nu_0}{\nu'-\nu}\right|d\nu',\\ \chi''(\nu)&=-\frac{1}{\pi}\int_0^\infty\frac{d\chi'(\nu')}{d\nu'}\log\left|\frac{\nu_0}{\nu'-\nu}\right|d\nu'.\end{aligned}\right\}. \tag{5}$$

The modulation type of apparatus developed by Purcell, Pound, and their co-workers[1,5] may be adjusted to measure quantities directly proportional to either of the derivatives involved in Eq. (5). If the available apparatus measures directly the derivative of but one part of the nuclear susceptibility, the relations (5) offer the most direct means of obtaining the other part. The form of the integrals in Eqs. (5), each of which has a logarithmic singularity in its integrand, also makes evident the qualitative similarity between one part of the susceptibility and the derivative of the other part.

[5] R. V. Pound, E. M. Purcell, and H. C. Torrey, Phys. Rev. 69, 681 (1946).

TABLE I. Root mean second moments of the F^{19} absorption line in a single crystal of CaF_2 for three directions of magnetic field in the crystal.

H_0 direction	Experiment	Theory of Van Vleck
100	3.68±0.20 gauss	3.60 gauss
110	2.25±0.20	2.24
111	1.77±0.20	1.53

THE MOMENTS OF THE SHAPE FUNCTION

In the preceding paper, Van Vleck finds expressions for the second and fourth moments of the shape function $g(\nu)$, the $(2n)$th moment being defined as

$$\langle(\Delta\nu)^{2n}\rangle_{Av}=\int_0^\infty g(\nu)(\Delta\nu)^{2n}d\nu. \tag{6}$$

In particular, Van Vleck obtains the second moment in terms of the direction cosines of the magnetic field $\mathbf{H}_0$ with respect to the principal axes of a simple cubic lattice, and he calculates the fourth moment for $\mathbf{H}_0$ along the 100 axis.

The simple cubic lattice of F^{19} nuclei in crystalline CaF_2 offers opportunity for an experimental check of these calculations. The dependence of peak signal strength on magnetic field direction in this crystal has been examined by Purcell, Bloembergen, and Pound.[6] In the present experiments, a cylindrical specimen about 1 cm in diameter and 2.5 cm long was cut from a single crystal of fluorite, the cylindrical axis lying along the 110 crystal direction. The crystal was inserted into the r-f coil of the permanent magnet apparatus described elsewhere,[7] and the derivative of the F^{19} absorption line was plotted for several directions of $\mathbf{H}_0$ in the crystal. One of these experimental curves is reproduced in Fig. 1, the magnetic field being along 100. The second moment may be found directly from this curve by performing a partial integration on the right member of Eq. (6) and recalling that $g(\nu)$ vanishes except in a small frequency interval about ν_0:

$$\langle(\Delta\nu)^{2n}\rangle_{Av}=-\frac{1}{2n+1}\int_0^\infty(\Delta\nu)^{2n+1}\frac{dg(\nu)}{d\nu}d\nu. \tag{7}$$

[6] E. M. Purcell, N. Bloembergen, and R. V. Pound, Phys. Rev. 70, 988 (1946).

[7] G. E. Pake, J. Chem. Phys. 16, 327 (1948).

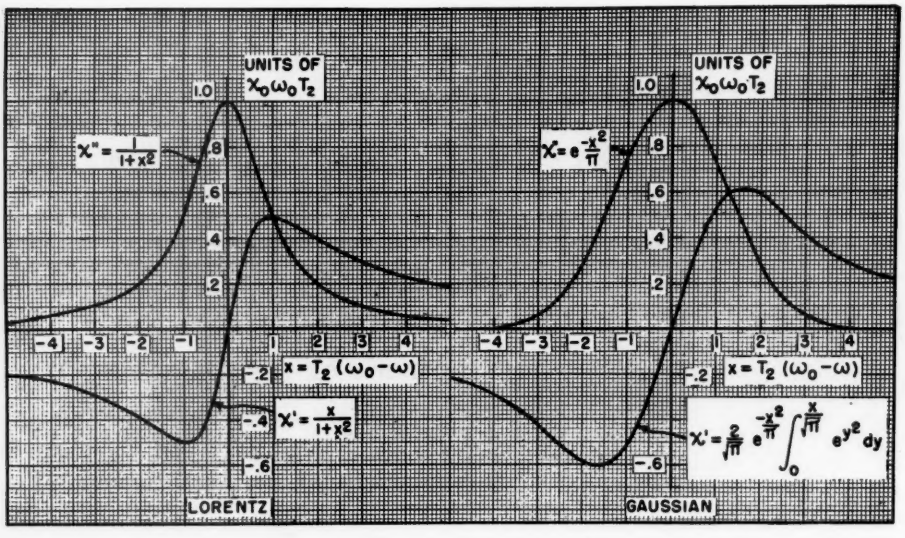

FIG. 2. Nuclear susceptibilities, $\chi=\chi'-i\chi''$.

Root mean square line widths (measured in units of magnetic field rather than frequency) were evaluated numerically using Eq. (7) and curves such as that of Fig. 1 for three directions of $\mathbf{H}_0$ in the CaF_2 crystal. The experimental results are listed in Table I, along with the corresponding values calculated by Van Vleck. The failure of the theoretical width for 111 to fall within the limits of error should not cause undue concern, inasmuch as the relatively large power of $\Delta\nu$ in the integrand of Eq. (7) accentuates the effect on a narrow line of spurious broadening introduced by crystal imperfections or by small errors in crystal orientation.

Figure 1 can be used in a similar way to evaluate the fourth moment, with the result $\langle(\Delta H)^4\rangle_{Av}^{\frac{1}{4}}=4.56\pm0.20$ gauss. Inasmuch as a considerable part of the error quoted arises from magnetic field calibration, it is perhaps more instructive to consider the ratio $\langle(\Delta H)^4\rangle_{Av}^{\frac{1}{4}}/\langle(\Delta H)^2\rangle_{Av}^{\frac{1}{2}}$; the experimental value is 1.24 ± 0.02, compared with 1.25 given by theory.

COMPARISON OF LORENTZ AND GAUSSIAN LINE SHAPES

Bloch[8] has obtained a system of differential equations satisfied by the expectation value of the nuclear magnetization which lead to the Lorentz shape function traditional in the theory of radiation- and collision-broadened spectral lines. For r-f magnetic fields sufficiently weak to preclude saturation, the Bloch susceptibilities are

$$\left.\begin{aligned}\chi''(\omega)&=\chi_0\omega_0T_2\frac{1}{1+T_2^2(\omega_0-\omega)^2},\\ \chi'(\omega)&=\chi_0\omega_0T_2\frac{T_2(\omega_0-\omega)}{1+T_2^2(\omega_0-\omega)^2},\end{aligned}\right\}\tag{8}$$

where $\omega=2\pi\nu$ is the angular frequency. These susceptibilities are consistent with the Kronig-Kramers relations and with the definitions of Eq. (1).

In attempting to determine line shape by the diagonal sum method, Broer[9] finds a general expression for the $(2n)$th moment:

$$\langle(\Delta\nu)^{2n}\rangle_{Av}=\frac{\mathrm{Tr}\left[\frac{d^n}{dt^n}S_x\right]^2}{(2\pi)^{2n}\,\mathrm{Tr}[S_x]^2}.\tag{9}$$

Although the shape function would, in principle, be determined by its moments, the highest thus far calculated is the fourth, which Van Vleck obtains in the preceding paper. The practical difficulties in evaluating the higher moments force Broer to follow Heisenberg's theory of ferromagnetism by assuming that $g(\nu)$ is proportional to a Gauss function, $\exp[-\alpha(\Delta\nu)^2]$. Equation (1) requires such an absorption curve to have the form

$$\chi''(\omega)=\chi_0\omega_0T_2\exp[-T_2^2(\omega_0-\omega)^2/\pi].\tag{10}$$

[8] F. Bloch, Phys. Rev. **70**, 460 (1946).

[9] L. J. F. Broer, Physica **10**, 801 (1943).

From Eq. (10) and the first of Eqs. (4) one finds after considerable manipulation that

$$\chi'(\omega)=\chi_0\omega_0T_2\cdot 2\pi^{-\frac{1}{2}}F(\pi^{-\frac{1}{2}}T_2(\omega_0-\omega)), \quad (11)$$

where

$$F(x)=e^{-x^2}\int_0^x e^{y^2}dy. \quad (12)$$

Both Lorentz and Gaussian formulae for $\chi'(\omega)$ should and do reduce to χ_0 at $\omega=0$. To verify this for Eq. (11), one may use $dF/dx=1-2xF$ and the fact that dF/dx is vanishingly small at great distances in frequency from ω_0, in particular, at $\omega=0$.

Both Lorentz and Gaussian shape functions may be linked with idealized physical models, the first of which relies solely on the broadening introduced by oscillatory local field components at the Larmor frequency. By this means neighboring nuclei limit the lifetime of a given nuclear spin state by inducing transitions from it, and mathematical analysis closely parallel to that for collision broadening of ordinary spectral lines[10] would lead to the Lorentz shape function. Such a picture, however, ignores local field static components,** which disperse the resonance values of the large constant magnetic field and which provide the broadening mechanism of the second model: The effective static local field at an absorbing nucleus depends upon the positive or negative excess of its near neighbors with spins aligned in the positive $\mathbf{H}_0$ direction. Spins throughout the sample are assumed to be randomly parallel or antiparallel to $\mathbf{H}_0$ (I is taken $\frac{1}{2}$ for simplicity), and, in the limit of large numbers of near neighbors clustered about each absorbing nucleus, this excess number becomes distributed among the absorbing nuclei according to a Gauss function. The effective local field of the model is essentially proportional to this distribution. Although these models evidently represent much-simplified approximations to reality, they identify the two shape functions, Lorentz and Gaussian, with physical pictures which, however incomplete, may prove helpful until the detailed theory is cast into a form more amenable to calculation.

Figure 2 compares, as functions of $x=T_2(\omega_0-\omega)$, the Lorentz curves of Eq. (8) with the Gaussian curves of Eqs. (10) and (11). Values of the function $F(x)$, which arises in heat-flow problems, are taken from a tabulation by Miller and Gordon.[11] The derivatives of these curves are plotted in Fig. 3, corresponding to the quantities measured directly by experiment. From Figs. 2 and 3, one

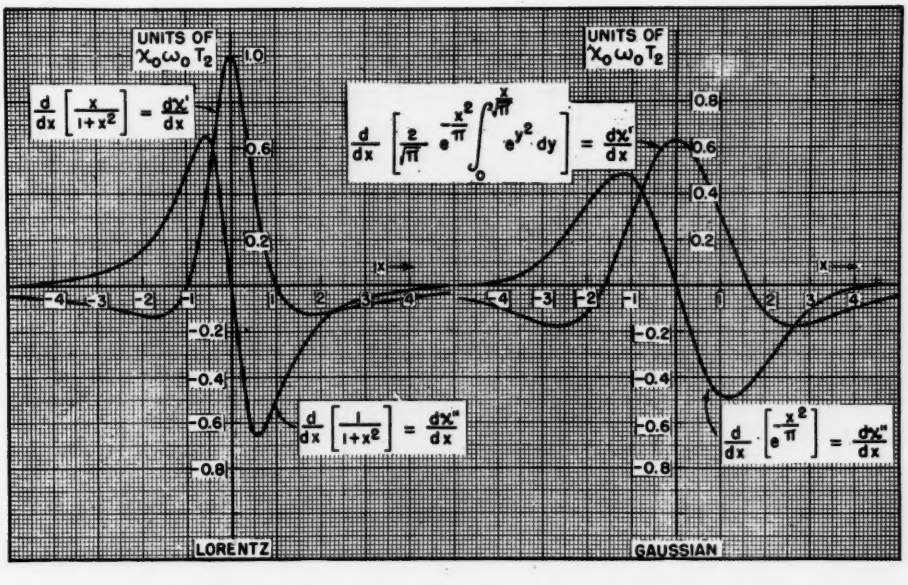

FIG. 3. Derivatives of nuclear susceptibilities, $x=T_2(\omega_0-\omega)$.

[10] J. H. Van Vleck and V. F. Weisskopf, Rev. Mod. Phys. **17**, 227 (1945).

** In Reference 1, pp. 695 and 696, the dipole-dipole Hamiltonian is written in a form which displays terms corresponding to static and Larmor frequency local fields.

[11] W. L. Miller and A. R. Gordon, J. Phys. Chem. **35**, 2875 (1931).

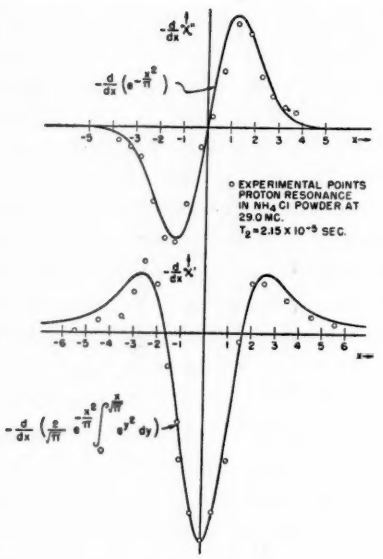

FIG. 4. Negative derivatives of nuclear susceptibilities, $\chi=\chi'-i\chi''$; $x=T_2(\omega_0-\omega)$.

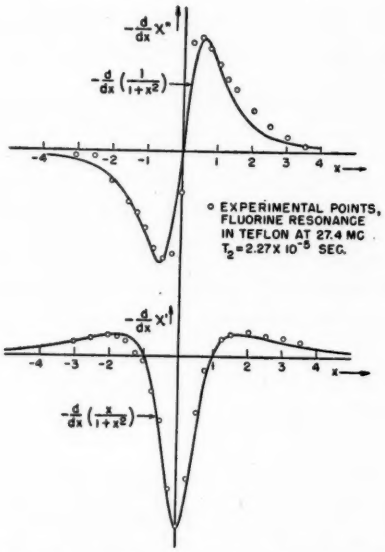

FIG. 5. Negative derivatives of nuclear susceptibilities, $\chi=\chi'-i\chi''$; $x=T_2(\omega_0-\omega)$.

can relate any experimental width measure to $1/T_2$. The Lorentz and Gaussian curves differ most significantly in the ratio R of the large maximum of $d\chi'/dx$ to either small minimum: R(Lorentz) = 8:1 and R(Gauss) = 3.5:1. Application of this criterion to an experimental dispersion curve indicates which shape function, if either, seems likely to fit the data.

Figures 4 and 5 show experimental nuclear susceptibilities, measured with the permanent magnet apparatus, which approximate to these two shape functions. The F^{19} resonance in polytetrafluoroethylene (Teflon) at room temperature fits the Bloch curves reasonably well, whereas the proton resonance in NH_4Cl powder at room temperature has $R=3.3$ and more nearly resembles the Gaussian curves. It should be borne in mind that many substances, especially crystals in which "frozen-in" nuclei determine line width and shape, may possess a shape function differing markedly from the two simple ones considered here. Figure 1, for example, does not resemble closely either absorption curve derivative in Fig. 3; the proton dispersion curve for $(NH_4)_2SO_4$ powder has $R=2.5$, and pronounced fine structure has been observed in hydrated crystals.[7]

Facilities for the experimental work here reported, including the large permanent magnet, were provided through a Frederick Gardner Cottrell Special Grant-in-Aid from the Research Corporation.

Letters to the Editor

PUBLICATION of brief reports of important discoveries in physics may be secured by addressing them to this department. The closing date for this department is five weeks prior to the date of issue. No proof will be sent to the authors. The Board of Editors does not hold itself responsible for the opinions expressed by the correspondents. Communications should not exceed 600 words in length.

High Energy Spallation and Fission Products of Uranium

P. R. O'CONNOR* AND G. T. SEABORG
Department of Chemistry and Radiation Laboratory, University of California, Berkeley, California
September 13, 1948

WE have bombarded natural uranium with 380-Mev helium ions in the Berkeley 184-inch cyclotron in order to study the distribution in yield to the radioactive products. After each of the irradiations, amounting to some 25 in number, the metallic uranium (2-cm×0.5-cm area and 0.1-cm thickness) was dissolved, and the yield in weighed chemical reactions of each of several isotopes was determined by means of counting experiments using a thin-window, bell-jar type Geiger-Mueller counter under conditions of known counting efficiency. Corrections were made for self-absorption, and for absorption by air and the mica window; back-scattering was insignificant in comparison with other factors. Conventional alpha-particle counters and an alpha-pulse analyzer[1] were used for the alpha-emitters. The yield for each isotope was determined relative to a standard isotope, the 12.8-day Ba^{140}, in order to compensate for the day-to-day variation in intensity of the helium ion beam. The results show what appears to be a continuous yield of radioactive products for the entire range of elements from the uranium region down to elements in the vicinity of atomic number 25. A plot of relative yield *vs.* the mass number of the radioactive products is shown in Fig. 1. The total cross section for the fission reaction (estimated from the area under the fission part of the curve) amounts to about 2×10^{-24} cm², but this value must be considered to be a very rough one, because of the unknown intensity of the helium ion beam. The errors indicated on this curve are estimated probable errors, arising from counting statistics, chemical operations, and correction factors applied.

There are several points of interest in connection with this distribution curve. The yield curve probably results from two essentially different types of reactions. Spallation reactions probably account for the products from the region of uranium down to those in the neighborhood of mass number 180–200, while the remainder of the curve is accounted for by the fission process. Isotopes with mass numbers 180–200 are more likely spallation products than fission products, and the small differences in yield in this region are not significant because of the low levels of radioactivity produced. Not shown on the curve are a number of alpha-emitting isotopes with mass number in the neighborhood of 210 which were observed to be present in relatively high yield; these are believed to be products of alpha-emitting radioactive chains[2] originating from heavier isotopes which are found in higher yield as can be seen from the curve.

The distribution of fission products seems to show only a single peak in the region of maximum yield. These results are of course very much in contrast with the yield curve for slow neutron fission of U^{235} with its very characteristic two peaks and deep valley in between.[3] This is not unexpected in view of the previously observed increased relative yield of fission products resulting from symmetrical cleavage as the energy of the bombarding particle is increased.[4–7] This single maximum is somewhat similar to that observed by Goeckermann and Perlman[8] in the fission of bismuth with 190-Mev deuterons, although the maximum, of course, occurs at a higher mass number. The data indicate, but are not sufficiently accurate to prove, that the maximum in the curve occurs at a mass number definitely less than one-half that of the initial compound nucleus formed in the reaction as is the case for bismuth fission, and thus it cannot be said with certainty whether fission is preceded by the emission of a number of neutrons as in the mechanism proposed by Goeckermann and Perlman. Since uranium can undergo fission as the result of small excitation energy, it is probable that some

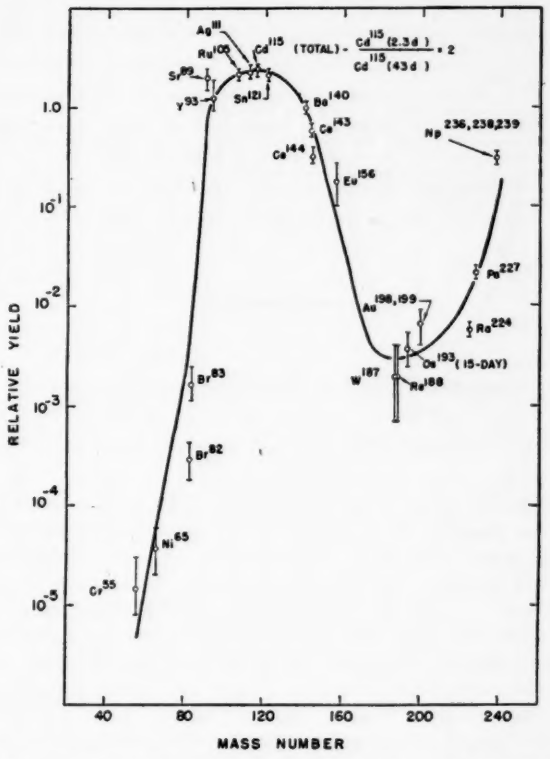

FIG. 1. Relative yield curve for products from 380-Mev helium ion bombardment of uranium.

of the fission results from reactions in which only a fraction of the total energy of the helium ion is utilized to form a fissioning compound nucleus of mass around 240, a mechanism similar to that of slow neutron fission results. Thus a number of mechanisms may prevail ranging from this one to that in which a number of neutrons are emitted before the fission process, giving rise to symmetrical cleavage as the most probable process, with the latter mechanism perhaps predominating in view of the shape of the distribution curve.

The fission yield curve definitely extends to higher and lower mass numbers than is the case for the fission of uranium with lower energy particles. At the low energy end the products down to the region of atomic number about 27 seem definitely to be fission products, but the source of the $_{24}Cr^{55}$ is doubtful in that the uranium may have contained sufficient iron impurity to account for the small yield of this isotope. It may be noted that if there are fission products with mass number as low as about 55 it should be expected that there be heavy fission products extending up to about mass number 180, and hence joining with the region of spallation products.

We would like to acknowledge the help of Mr. R. L. Folger in some of the chemical experiments and the cooperation of Mr. D. C. Sewell and Mr. J. T. Vale and the members of the 184-inch cyclotron group. This work was performed under the auspices of the Atomic Energy Commission.

* Present address: Department of Chemistry, University of Minnesota, Minneapolis, Minnesota.

[1] See, e.g., A. Ghiorso, A. H. Jaffey, and H. P. Robinson, "An alpha-pulse analyzer apparatus," Plutonium Project Record, **14B**, 17.3 (1948) (to be issued).
[2] A. Ghiorso, W. W. Meinke, and G. T. Seaborg, Phys. Rev. **74**, 695 (1948).
[3] "Nuclei formed in fission," Plutonium Project, J. Am. Chem. Soc. **68**, 2411 (1946); Rev. Mod. Phys. **18**, 513 (1946).
[4] Y. Nishina, K. Kimura, T. Yasaki, and M. Ikawa, Nature **146**, 24 (1940); Phys. Rev. **58**, 660 (1940); **59**, 323 (1941); **59**, 667 (1941).
[5] E. Segrè and G. T. Seaborg, Phys. Rev. **59**, 212 (1941).
[6] A. S. Newton, Phys. Rev. (in press).
[7] A. Turkevich, presented at meeting of A.A.A.S. in Chicago (December, 1947).
[8] R. H. Goeckermann and I. Perlman, Phys. Rev. **73**, 1127 (1948).

Cross Section for the Reaction $C^{12}(\gamma,n)C^{11}$

J. L. Lawson and M. L. Perlman*
Research Laboratory, General Electric Company, Schenectady, New York
September 22, 1948

PURE graphite has been irradiated by x-rays from the betatron operating at 50 and 98 Mev at measured quantum intensities. The number of (γ,n) processes occurring per unit time was determined by observation of the C^{11} activity with a calibrated Geiger-Müller counter.

The quantum intensity was determined for both 50- and 98-Mev betatron operation first by calibrating an ionization chamber monitor at low level with an absolute x-ray spectrum analyzer designed by one of the authors,[1] and second by a careful measurement of the relative ion chamber response from the low level operation to the high levels used in the C^{12} bombardment. While this second calibration step seems simple and straightforward, it was found somewhat difficult because of the large intensity range covered (about 10^5), the desired accuracy (about 5 percent), and the fluctuating nature of the betatron x-ray beam. The spectrum analyzer, used to calibrate the ion chamber at low level in terms of the absolute quantum intensity, counts electron-positron pairs ejected from a thin target of chosen material and weight. This analyzer first uses a collimator which defines a beam aperture and, by means of a magnetic field region, clears the beam of charged particles. A pair-forming target, magnetic field, and Geiger-counter array then serves to register electron and positron events; finally, an analyzing circuit registers electron-positron events of given total energy, which is, therefore, essentially the pair spectrum. This instrument at present registers pairs in energy channels 15 Mev in width; the number of quanta in each energy channel is obtained from the pair data, the pair-forming target thickness, and the cross section for pair production. This last cross section is now known theoretically and experimentally.[1]

The spectrographic graphite powder irradiated was held in an aluminum mount in a layer of uniform thickness and known area. The mount was accurately positioned so that the graphite layer subtended exactly the same part of the beam subtended by the pair radiator.

After irradiation for a known time at nearly constant and known intensity, all the powder was formed into a pellet of standard geometry; the subsequent decay of the 20-minute C^{11} activity was followed. The geometry, counting arrangements, and correction methods for absorption, self-absorption, and back-scattering were the same as those used for studies of relative yields x-ray induced nuclear reactions.[2] After the counting measurements were completed, the graphite was weighed and the target thickness calculated. The activity was calculated to saturation bombardment, and it was corrected for the geometrical efficiency of the end-window counter. This efficiency (34 percent of the total solid angle) was determined with the aid of a thin weighed U_3O_8 deposit—the UX_2 beta-rays of which were counted through an absorber sufficiently thick to remove the soft UX_1 radiations.

Results of the measurements are shown in Table I. The numbers in column II are calculated by dividing the number of pairs per minute in the 15-Mev wide band (centered at 30 Mev) by the width, and then dividing by the cross section for pair production at 30 Mev and also by the pair-forming target thickness. The quantity, σ, shown in the fourth column is essentially the ratio of column III to column II and represents the product of cross section by the level width of the γ-n reaction,

Table I.

I X-ray energy (Mev)	II No. of quanta/ Mev minute (at 30 Mev)	III No. of (γ,n) processes/min. mg atom cm^{-2}	IV $\sigma=\frac{\text{III}}{\text{II}\times 6.02\times 10^{20}}$
98	4.74×10^7	4220	1.48×10^{-25} Mev cm^2
98	4.74×10^7	4220	1.48×10^{-25} Mev cm^2
50	1.24×10^7	1090	1.46×10^{-25} Mev cm^2

providing the level is at approximately 30 Mev. The uncertainty in the absolute cross section is estimated to be ±20 percent; however, the comparison of cross sections at 50 and 98 Mev is probably good to 5 percent.

The fact that the cross sections based on the intensity at 30 Mev are the same with both 50-Mev and 98-Mev x-rays shows that quanta above 50 Mev in energy do not contribute appreciably to the (γ,n) process on C^{12}. It is worth pointing out that this conclusion is independent of absolute pair production cross section, efficiency of pair counting, and corrections applied to the counting data for the C^{11}. It is probable that this conclusion applies to (γ,n) reactions generally, in view of the fact that relative yields for these at 50 Mev and at 100 Mev follow the same trend.[2]

A theory to account for some of the observations on x-ray induced nuclear relations has been put forward by M. Goldhaber and E. Teller.[3] A cross section of about 1-Mev barn is predicted for the reaction $Cu^{63}(\gamma,n)Cu^{62}$. The $Cu^{63}(\gamma,n)$ cross section can be deduced from the measured $C^{12}(\gamma,n)$ cross section by use of the reaction resonance energy,[4] the relative yields of the two reactions,[2] and the relative quantum intensities at the two resonance energies. The result obtained in this way is 1.5-Mev barns.

* Present address: Department of Chemistry, University of Wyoming, Laramie, Wyoming.
[1] J. L. Lawson, to be published.
[2] M. L. Perlman and G. Friedlander, Phys. Rev. **74**, 442 (1948).
[3] M. Goldhaber and E. Teller, Phys. Rev. **74**, 1046 (1948). We are indebted to Professor Goldhaber for making these results known to us before publication.
[4] G. C. Baldwin and G. S. Klaiber, Phys. Rev. **73**, 1156 (1948).

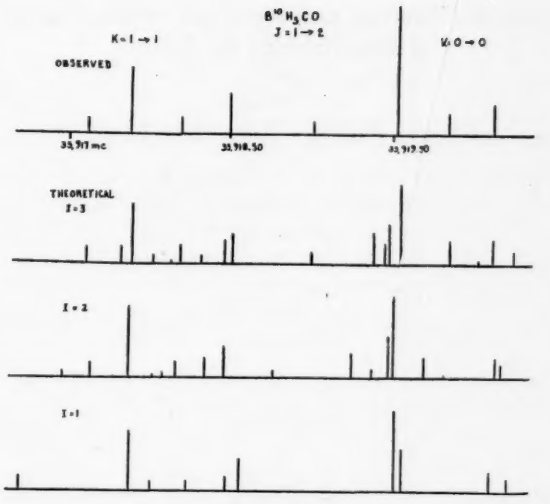

FIG. 1. Comparison of observed hyperfine structure of the $J=1\rightarrow2$ transition of $B^{10}H_3CO$ with that predicted for different assumed spin values of B^{10}.

Nuclear Spins and Quadrupole Moments of B^{10} and B^{11}

WALTER GORDY AND HAROLD RING*
*Department of Physics, Duke University,** Durham, North Carolina*
AND
ANTON B. BURG
*Department of Chemistry, University of Southern California,*** Los Angeles, California*
September 14, 1948

FROM microwave absorption measurements on pure rotational transitions of borine carbonyl, the nuclear spin of B^{10} has been determined as 3 and that of B^{11} as $\frac{3}{2}$. Figure 1 shows a comparison of the observed and calculated hyperfine structure for the $J=1\rightarrow2$ transition of $B^{10}H_3CO$. Insofar as the spectrum could be resolved, there is good agreement between the observed spectrum and that calculated with $I=3$. The values of 1 and 2 can definitely be eliminated, and, of course, a zero value is eliminated by the fact that a hyperfine structure exists. The value of 3 is also substantiated by the fact that broad lines were observed where groups of unresolvable lines were predicted. Likewise, there is good agreement between the observed hyperfine structure of $B^{11}H_3CO$ and that calculated with $I=\frac{3}{2}$. (See Fig. 2.) The theoretical hyperfine structures calculated for other spin values but not shown here are not in agreement with observation.

The nuclear quadrupole coupling, $eQ(\partial^2V)/(\partial z^2)$, for B^{10} is -3.30 ± 0.10 and that for B^{11} is -1.55 ± 0.08. Thus the quadrupole moments of the two boron isotopes are of the same sign, and that of B^{10} is 2.13 times that of B^{11}.

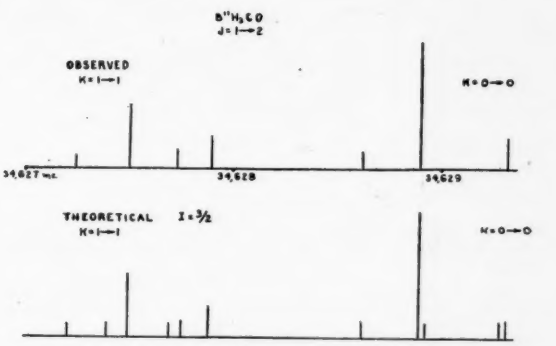

FIG. 2. Comparison of observed hyperfine structure of the $J=1\rightarrow2$ transition of $B^{11}H_3CO$ with that predicted for a B^{11} spin of 3/2.

The symmetric-top configuration for borine carbonyl has been proved, though the bond orbitals of the boron are not tetrahedral. As may be expected from its chemical instability, the molecule is easily distorted by centrifugal forces. Because of these distortions the $K=1$ lines of the $J=1\rightarrow2$ transition occur at lower frequencies than do the $K=0$ lines: 1.34 mc for $B^{10}H_3CO$ and 1.50 mc for $B^{11}H_3CO$.

Further details, including data on other transitions, will be given in a later report.

* Frederick Gardner Cottrell Fellow.
** The research at this university was supported by a grant-in-aid from the Research Corporation.
*** The work at this University was supported through a contract with the Office of Naval Research.

Erratum: Thermal Consequences of the Capture of Neutrinos by the Earth

[Phys. Rev. 74, 621 (1948)]

A. E. BENFIELD
Department of Engineering Sciences and Applied Physics, Harvard University, Cambridge, Massachusetts

THE Editor regrets that two mistakes were made in printing the above-named Letter to the Editor.

(i) The second sentence of the first paragraph should read, "He argues that neutrinos originating at the center of the *sun* would produce a maximum heating effect in the earth. . . ." The word *sum* was mistakenly printed for *sun*.

(ii) The denominator of the first term of Eq. (1) should be $6k$, not 61.

A Search for Gamma-Rays from He^6 and F^{18}

WILLIAM J. KNOX
Radiation Laboratory, Department of Physics, University of California, Berkeley, California

September 17, 1948

THE series of beta-active nuclei He^6, Be^{10}, C^{14}, F^{18}, Na^{22}, etc., has created much discussion because some of its members show allowed transitions while others are forbidden. It seemed possible that the allowed cases might represent transitions to excited states; if so, a consistent rule would govern the transitions to the ground states. However, the results given below seem to exclude this explanation, unless the unlikely assumption of a very low energy gamma-ray is made.

Absorption measurements on F^{18} have shown a penetrating radiation which has the expected annihilation radiation energy of about 0.5 Mev. In order to exclude further the possibility of a true gamma-ray of about 0.5-Mev energy, which would not be detected by half-thickness measurements, absorption curves on F^{18} and C^{11} have been compared to see if the ratio of positrons to photons is the same. C^{11} is assumed to have no gamma-ray, since the upper energy limit of its positron spectrum[1] corresponds very closely to both the mass difference[2] and the computed Coulomb energy difference[1] between B^{11} and C^{11}, and the spectrum is apparently simple. The C^{11} and F^{18} on which the measurements were made were produced by $(n,2n)$ reactions on polystyrene foils and LiF using 90-Mev neutrons produced by the 184-inch cyclotron. The shorter-lived activities (O^{15}, N^{13}, C^{11}) were allowed to decay out of the F^{18} samples before making measurements. The ratio of the number of counts coming from the sample when surrounded by 400 mg/cm² of Al to the number of beta-counts extrapolated to zero absorber was observed to be 0.011 for C^{11} and 0.010 for F^{18}, both values with a probable error of about ten percent. These values are consistent with the known counting efficiency for annihilation radiation of the Geiger tubes used. There is no evidence from these measurements that there is a nuclear gamma-ray associated with F^{18}.

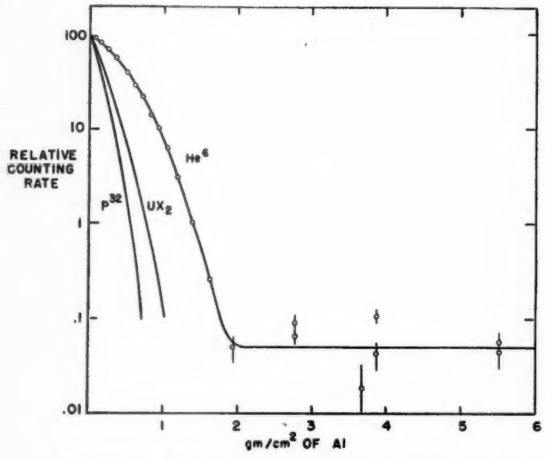

FIG. 1. Absorption of He^6 betas in aluminum and comparison curves on P^{32} and UX_2.

He^6 was obtained by bombarding powdered Be in a brass vessel with 11-Mev neutrons produced by the 60-inch cyclotron. For the purpose of identification the half-life was measured on an automatic photographic short half-life measuring apparatus,[3] and five determinations gave a value of 0.82 ± 0.06 second in agreement with previously reported values.[4,5] For absorption measurements a continuous flow method was used in which the He^6 was swept from the vessel with helium, filtered through a fine glass wool plug, and transported through about 85 ft. of $\frac{3}{16}$-in. tubing to the cyclotron control room, where background radiation was low enough to make measurements while the cyclotron was operating. An end window Geiger tube suspended above a graphite block and surrounded by a lead shield was used for counting. The He^6 was swept through a chamber in the graphite block which was covered by a 1.5-mil Al window situated directly beneath the Geiger tube. In this manner essentially all of the He^6 beta-particles emitted in the vicinity of the counter, with the exception of those actually counted, were absorbed in carbon, thus minimizing bremsstrahlung. Flat aluminum absorbers were interposed between the counting tube and the gas chamber, and counting was done with the cyclotron operating at a constant level and with the He flowing at a constant rate. Under these operating conditions the reproducibility of a monitoring count using some standard amount of absorber was within ± four percent for a given set of measurements. The absorption curve obtained is reproduced in Fig. 1, together with comparison curves taken under similar conditions of geometry and absorber arrangement on samples of P^{32} and UX_2. The initial portion of the curve was obtained with a zero absorber counting rate of about 10,000 c.p.m. while the final portion was obtained with about five times this intensity. Coincidence corrections were made and all points were normalized to 100 at zero absorber. Probable errors due to counting are shown on the lowest points. The amount of radiation penetrating more than 2 g/cm² of absorber is about 0.05 percent of the total number of counts, which is the magnitude expected due to production of bremsstrahlung. Hence, it is concluded that there is no gamma-ray associated with the disintegration of He^6 unless it is of very low

energy (<100 kev) or of low intensity (< ten percent of disintegrations if gamma-ray were of 1 Mev). Further comparison of the He^6 curve with the P^{32} and UX_2 curves gives ranges of 1.85 and 1.88 g/cm² of aluminum, respectively. This corresponds to a maximum energy of 3.7 Mev, using the range-energy relationship $E_{max}=1.85R+0.245$,[6] with an estimated possible error of ±0.2 Mev. This value for the energy is in close agreement with previously reported values.[4,5]

Appreciation is expressed to Professor E. M. McMillan for suggesting this problem. This paper is based on work performed under the auspices of the Atomic Energy Commission in connection with the Radiation Laboratory, University of California, Berkeley, California.

[1] Delsasso, White, Barkas, and Creutz, Phys. Rev. **58**, 586 (1940).
[2] Haxby, Shoupp, Stephens, and Wells, Phys. Rev. **58**, 1035 (1940).
[3] T. M. Putnam, to be published.
[4] Bjerge and Brøstrom, Kgl. Danske Vid. Sels. Math.-Fys. Medd. 16, No. 8 (1938).
[5] H. S. Sommers, Jr. and R. Sherr, Phys. Rev. **69**, 21 (1946).
[6] L. E. Glendenin, Nucleonics **2**, No. 1 (Jan. 1948).

The Nuclear Spin and Magnetic Moment of Na^{22} *

LUTHER DAVIS, JR.
Research Laboratory of Electronics, Massachusetts Institute of Technology, Cambridge, Massachusetts
September 13, 1948

THE atomic beam magnetic resonance method,[1] as used by Zacharias[2] to determine the nuclear spin and magnetic moment of K^{40}, has been modified to permit similar observations to be made with radioactive nuclei having considerably shorter half-lives. These modifications involve the use of a mass spectrometer for separating the Na^{22} peaks from the large background of Na^{23} and a beryllium copper multistage electron multiplier[3,4] for detecting the Na^{22}. The source of atoms for the beam is a monel metal oven with an exit canal long compared with its width, designed so as to conserve radioactive material. A sample of NaN_3 containing 330 microcuries of Na^{22} (3×10^{-9} mole) in a dilution of one part in 10^4 of $Na^{23}N_3$ was placed in the oven. Decomposition occurs at 320°C, providing an atomic sodium beam. A 16-hour run was sufficient for all present determinations and required the evaporation of only 4×10^{-10} mole of Na^{22} out of the oven. The beam intensity of Na^{22} was naturally small, a few thousand atoms/sec., and the radiofrequency transition intensities were less than 100 atoms/sec.

Two types of transitions were observed, first at low frequency with $\Delta m_f=\pm1$ and $\Delta F=0$. These permit direct comparison of g_F for Na^{22}, with g_F for Na^{23}. For an unexcited alkali atom, $F=I+\frac{1}{2}$, and the spin of the Na^{22} is obtained as soon as a transition is observed at the mass position 22 of the mass spectrograph.

Search was made for resonances with the homogeneous field (as determined by the Na^{23} transition) and radiofrequency set for transitions corresponding to $I=0$, 1, 2, 3, 4, 5, and 6, and with the mass spectrometer set for 22. Resonances were observed only for spin 3 at mass 22.

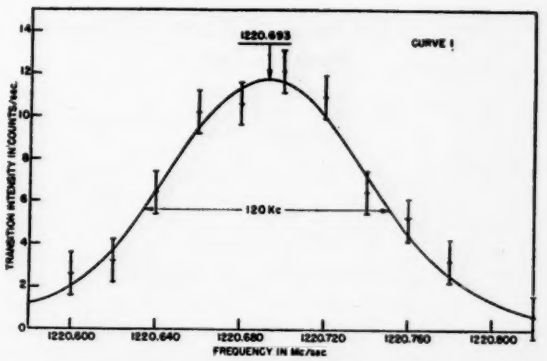

FIG. 1. Transition intensity *vs.* frequency of oscillating field for the two Na^{22} lines $F=7/2$, $M_f=\pm1/2\leftrightarrow F=5/2$, $M_f=\pm1/2$ at a field of 6.17 gauss. One count/sec. is equivalent to about 7 atoms/sec.

These peaks faded out for mass numbers $22\frac{1}{2}$ and $21\frac{1}{2}$ and could not possibly have been a spurious effect from the more abundant Na^{23}. These low frequency resonances were followed as the magnetic field was increased to permit an evaluation of the h.f.s. $\Delta\nu$ of Na^{22}. The second type of transition can then be made in which $\Delta F=\pm1$. Curve 1 shows the result of an experiment in which a $\Delta F=\pm1$ transition was made in almost zero field.

The results show that the spin of Na^{22} is 3 in units of $h/2\pi$, and its h.f.s. $\Delta\nu$ is 1220.64 ± 0.04 mgc/sec. By comparison with the value of the nuclear magnetic moment of Na^{23}, given by Millman and Kusch,[5] we obtain for Na^{22}, 1.746 ± 0.003 nuclear magnetons. The sign of this nuclear moment was also shown to be positive in just the way that was used by Zacharias on K^{40}.

Good, Peaslee, and Deutsch[6] report that the disintegration of Na^{22} goes by 100 percent positron emission to an excited state of Ne^{22}, and they conclude also that the spin of this excited state differs from that of Na^{22} by at most one unit. The spin of Ne^{22*} is therefore either 2, 3, or 4. Further unpublished data by Professor Deutsch indicate that the effective half-life for the possible transition to the ground state of Ne^{22} is at least 5000 years, consistent with a spin change of three units.

I am greatly indebted to Dr. E. T. Clarke who prepared the Na^{22} by a $Mg^{24}(d,\alpha)Na^{22}$ reaction in the M. I. T. cyclotron, to Professor J. W. Irvine, Jr., for the separation[7] of the Na^{22} from the cyclotron target and for the conversion of the $Na^{22}Cl$ to $Na^{22}N_3$, to Dr. Darragh Nagle for the design and construction of the molecular beam apparatus adapted for use in this experiment, and to Professor J. R. Zacharias who suggested the problem and some of the methods, and with whom constant discussions of the problems involved led to the successful conclusion of this experiment.

* This work has been supported in part by the Signal Corps, the Air Materiel Command, and the Office of Naval Research.
[1] P. Kusch, S. Millman, and I. I. Rabi, Phys. Rev. **57**, 765 (1940).
[2] J. R. Zacharias, Phys. Rev. **61**, 270 (1942).
[3] J. S. Allen, Phys. Rev. **55**, 967 (1939).
[4] Hin Lew, *Hyperfine Structure of Aluminum by Atomic Beam Method* (M. I. T. thesis, 1948).
[5] S. Millman and P. Kusch, Phys. Rev. **58**, 438 (1940).
[6] W. M. Good, D. Peaslee, and M. Deutsch, Phys. Rev. **69**, 813 (1946).
[7] J. W. Irvine, Jr. and E. T. Clarke, J. Chem. Phys. **16**, 686 (1948).

Note on the Spins of Nuclei of Mass Number Ten

M. GOLDHABER*
*Brookhaven National Laboratory,** Upton, Long Island, New York*
September 13, 1948

THREE nuclei of mass number ten are known: Be^{10}, B^{10}, and C^{10}. B^{10} is stable and is assumed to have a nuclear spin $I=1$, like the other stable nuclei (D^2, Li^6, and N^{14}) which are "self-conjugate" (having an odd number of protons and an equal number of neutrons). Be^{10} decays to B^{10} with the emission of β-rays with a maximum energy $E=0.56$ Mev and a half-life $T=(2.5-2.9)\times10^6$ years.[1] This lifetime is approximately 10^9–10^{10} times longer than would be expected for an allowed transition. The apparently similar transition $He^6 \xrightarrow{\beta} Li^6$ ($E=3.7$ Mev, $T=0.8$ sec.) is allowed. Many attempts have been made to explain the long life of Be^{10}, which has proved to be an outstanding difficulty for β-ray theory. The following alternative assumptions have usually been made: Assumption (a)—Though even-even nuclei have as a rule the spin $I=0$, Be^{10} is an exception and has the spin $I=4$. The transition from Be^{10} to B^{10} would then involve a spin change $\Delta I=3$ which would make the long lifetime reasonable. Assumption (b)—The spin of Be^{10}, like that of other even-even nuclei, is $I=0$, but the β-transition, $I=0\rightarrow I=1$, is forbidden because of a selection rule which does not operate in the case of the transition $He^6\rightarrow Li^6$.

Both assumptions are not very satisfactory. Following the discovery by Davis[2] that Na^{22} (a "self-conjugate" nucleus) has the spin $I=3$ and a magnetic moment $\mu=1.746$, it seems worth while to discuss the following assumption: Assumption (c)—The spin of B^{10} is not $I=1$, as hitherto assumed, but $I=3$.

Some of the consequences of assumption (c) are the following:

(1) From the g-value 0.598, measured by Millman, Kusch, and Rabi,[3] a value for the magnetic moment of B^{10} $\mu=1.794$ would follow.

(2) From a formula due to Sachs[4] it can be shown that the measured g-value is compatible with a $^3D_3$ state for B^{10}, with only a slight admixture of higher states. According to Feenberg and Phillips,[5] a system of five protons and five neutrons is rather unique in having in the Hartree approximation two degenerate ^3D states, as well as a ^3F and a ^3G state near the ground state, which might all contribute to an $I=3$ state.

(3) The spin of Be^{10} could be assumed to be $I=0$, as for other even-even nuclei, and the β-transition would be highly forbidden because $\Delta I=3$.

(4) Similarly, C^{10} could be assumed to have $I=0$. Sherr, Muether, and White[6] have shown that this nucleus decays to an excited state of B^{10}. The transition to the ground state of B^{10} would be highly forbidden because $\Delta I=3$.

(5) In the reaction $B^{10}+D^2\rightarrow Be^8+He^4$, Be^8 is usually found in its excited state of $\sim$3 Mev,[7] which has on good grounds been identified as a D-state.[8] This would be difficult to understand if the spin of B^{10} were $I=1$ rather than $I=3$.

Many other nuclear reactions involving B^{10} might be worth discussing in the light of the assumption made about its spin, but such a discussion might better await a direct measurement of this quantity, which is now being attempted in the Nuclear Moments Laboratory here.

* University of Illinois.
** Research carried out at Brookhaven National Laboratory under the auspices of the Atomic Energy Commission.
[1] E. M. McMillan, Phys. Rev. **72**, 591 (1947); D. J. Hughes, C. Eggler, and C. M. Huddleston, Phys. Rev. **71**, 269 (1947).
[2] Luther Davis, Jr., Phys. Rev. **74**, 1193 (1948). I wish to thank Dr. Zacharias and Mr. Davis for informing me of this result before publication.
[3] S. Millman, P. Kusch, and I. I. Rabi, Phys. Rev. **56**, 165 (1939).
[4] R. G. Sachs, Phys. Rev. **69**, 611 (1946).
[5] E. Feenberg and M. Phillips, Phys. Rev. **51**, 597 (1937).
[6] R. Sherr, H. R. Muether, and M. G. White, Bull. Am. Phys. Soc. **23**, No. 3, 45 (1948).
[7] J. D. Cockcroft and W. B. Lewis, Proc. Roy. Soc. **154**, 246 (1936); P. I. Dee and C. W. Gilbert, Phys. Rev. **154**, 279 (1936).
[8] See W. F. Hornyak and T. Lauritsen, Rev. Mod. Phys. **20**, 191 (1948).

Microwave Absorption Line Frequencies of Methyl Alcohol and their Stark Effect

DONALD K. COLES
Westinghouse Research Laboratories, East Pittsburgh, Pennsylvania
September 16, 1948

THE CH_3OH molecule presents an interesting problem for analysis because of the internal rotation of the OH bond around the axis of the OCH_3 group. Hershberger and Turkevitch[1] and Dailey[2] have reported altogether about twenty-five microwave absorption lines for methyl alcohol, including eight lines which appear to form a converging series.

The first "line" of this series has now been resolved into three distinct lines, and more accurate frequency measurements have been made on the first nine members of the series. The first-order Stark effect of these lines, observed first by Dailey, has now been studied in detail. The absorption lines were split with low electric fields (0.5 to 50 volts per cm), observations being made with the electric field of the microwave parallel to the static electric field, so that the Stark quantum number M does not change during a microwave-induced transition.

For modulation purposes a much smaller electric field (0.1 to 1.0 volts per cm) was superimposed on the static electric field. Different frequencies of alternation were used, from 50 kc to 400 kc, and the crystal current amplifier was usually tuned to the frequency of the alternating field. It is worth remarking that a non-zero value of the static electric field must be used with this method of tuning. Otherwise, the Stark pattern for the second half of the cycle will be identical with that for the first half of the cycle, and no modulation will be observed.

The Stark components of each line were spaced almost uniformly, and the outer components were most intense. This means that the quantum number J does not change during a transition, and that the number of components on each side of the pattern is equal to J. The values of J thus determined and the line frequencies are listed below.

TABLE I.

J	Frequency (megacycles)	Stark coefficient A (mc per e.s.u.)
2	24,934.38	145
3	24,928.70	155
4	24,933.47	168
5	24,959.08	185
6	25,018.14	207
7	25,124.88	230
8	25,294.41	257
9	25,541.43	291
10	25,878.18	324

The frequency shifts of the Stark components from the center of the pattern were found to be rather accurately proportional to the electric field E and the Stark component quantum number M. The Stark coefficient tabulated in Table I is the coefficient A in the equation

$$\nu_{JM}=A(ME/J^2+J). \quad (1)$$

Although the coefficient A depended only slightly on M and E, it was found to depend greatly on J.

Recent calculations by Dennison and Burkhard[3] provide a series of lines starting with $J=2$, which can be closely fitted to the observed frequencies. Their preliminary calculations were based on a special model of an asymmetric-top with hindered internal rotation. Such a model, however, seems inadequate to explain the observed dependence of the Stark coefficients on J.

The Stark effect measurements are rather well represented by the formula

$$\Delta\nu(\text{sec.}^{-1})=\frac{E(\text{e.s.u.})}{h}\left[\frac{M}{(J^2+J)^{\frac{1}{2}}}\times\frac{0.895\times10^{-18}}{(J^2+J)^{\frac{1}{2}}}+0.0113\times10^{-18}(J^2+J)^{\frac{1}{2}}\right]. \quad (2)$$

In Eq. (2) the quantity 0.895×10^{-18} is presumably the value in e.s.u. of the electric dipole moment parallel to the axis of symmetry. From this and a generally accepted value for the total dipole moment, we find the value 1.41×10^{-18} e.s.u. for the component of the dipole moment perpendicular to the symmetry axis.

From Eq. (2) one may deduce a value for the change (during a transition) of the internal direction cosine to be associated with this component of the dipole moment. This value is approimately $0.0080(J^2+J)^{\frac{1}{2}}$.

[1] W. D. Hershberger and J. Turkevitch, Phys. Rev. **71**, 554 (1947).
[2] B. P. Dailey, Phys. Rev. **72**, 84 (1947).
[3] D. M. Dennison and D. G. Burkhard, Symposium on Molecular Structure and Spectroscopy, Ohio State University (June 1948).

Alpha-Ray Spectra of RaC and RaC′

W. Y. CHANG
Palmer Physical Laboratory, Princeton University, Princeton, New Jersey
August 27, 1948

TABLE I. Alpha-ray spectra of RaC and RaC′.

Element	Alpha-energy Mev	Relative integral intensity
RaC		
RaC′α_0	7.683 (ref.)	10^6
α_0	5.517±0.02	160
α_1	5.466±0.02	200
α_2	5.333±0.02	70
RaC′		
α_0	7.683 (ref.)	10^6
α_2	9.080±0.015	30

BEFORE the cyclotron magnet of the alpha-ray spectrograph* was returned to the cyclotron group, a few plates were exposed to the alpha-particles from several natural radioactive sources, still using the track method of detection. Examination of the plates has been mostly done during the past few months. The following is a summary of the results obtained for RaC and RaC′. The results for RdTh, ThC, and ThC′ will be presented in the following note. We must say that several cases, especially those concerned with the weak lines, need further study with stronger sources.

Sources of radon deposit were prepared in the following usual manner. Radon gas of about 150 m.c. was introduced by means of a mercury pump into the vacuum of a glass tube, which contained a nickel cylinder with a platinum wire at the center. The radon gas was condensed onto the wire with liquid air outside. The wire was negatively charged at about 250 v relative to the cylinder. After about five hours the wire was removed, washed with alcohol, and heated in vacuum to about 400°C. When exposure of the plates was started in the spectrograph, RaA had practically died out, leaving mainly RaC and RaC′ as the alpha-ray sources on the wire.

To study the region on the high energy side of the RaC′ line, the magnetic field was increased so that the RaC′ line was near to the low energy end of the plate (about 19 cm long) but still on the plate. Examination of the plate was extended up to a region of about 11.5 Mev. Only one line at 9.080 Mev has been found. The intensity and energy of this line can nicely be identified with the third long-range line as found by Rutherford and his co-workers. The other lines do not show up on the plate, presumably because the source was too weak; the peak value of this line as found in the present case is not more than 20 times the general background. We feel that, in order to study these extremely weak long-range lines, the general background must be reduced to less than 1 in 10^6 of the main line. This background was presumably due to such scattering that the scattered particles produced tracks on the plate parallel to the true tracks of the particles which had come directly from the source.

For the study of the region on the low energy side of the RaC′ line, the magnetic field was adjusted so that the RaC′ line was near to the high energy end of the plate. A region covering approximately 4.8–6.0 Mev was examined. Three or four lines have been found in an interval of about 0.5 Mev (see the curve). The energies of the first two lines are in good agreement with the α_1 and α_2 of RaC as found by Rutherford and his co-workers. The third one is weaker, and the fourth one (if true) is still weaker and very broad. The intensity of each line is roughly 1 in 10^4 of the intensity of the RaC′ line (for better values see

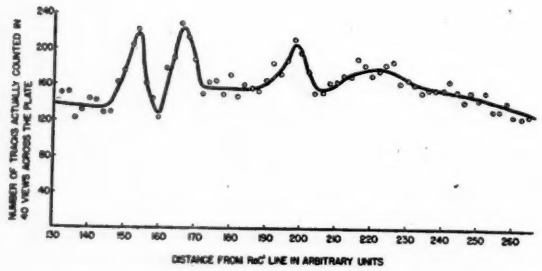
NUMBER OF TRACKS ACTUALLY COUNTED IN 40 VIEWS ACROSS THE PLATE
240
200
160
120
80
40
130 140 150 160 170 180 190 200 210 220 230 240 250 260
DISTANCE FROM RaC' LINE IN ARBITRARY UNITS

FIG. 1. Energy distribution of RaC alpha-particles.

Table I). We did not measure the energy and intensity of the last (broad) line. The distribution curve was approximately checked with a weaker source. It would be still desirable to repeat the experiments with stronger sources.

We should like to thank Miss Sophia Wysienska and Mrs. Allen Fry for their invaluable help in examining the plates.

*W. Y. Chang, Phys. Rev. **69**, 60 (1946).

Alpha-Ray Spectra of RdTh, ThC, and ThC′

W. Y. CHANG AND T. COOR
Palmer Physical Laboratory, Princeton University, Princeton, New Jersey
August 27, 1948

A MESOTHORIUM source[1] of about 6 m.c. was dissolved in about 15 cc of 1N HCl and heated gently. A solution of 6 mg $ZrCl_2$ was then added to it. Finally, NH_4OH was gradually added to the above solution until all $Zr(OH)_2$ (as carrier for $RdTh(OH)_2$) was precipitated (no excess of NH_4OH). The precipitate was then dissolved in about 10 cc of $\frac{1}{10}N$ HCl. Electrolysis of this last solution took place between two platinium wires as the electrodes and at a voltage of about 5 volts. A source prepared in this way was rich in RdTh containing some ThB, ThC, and ThC′. A source rich in ThC and ThC′ was also prepared from the above filtrate by electrolysis, which was first allowed to stand for a few days for ThB to grow. If this filtrate is made acidic, electrolysis will deposit the active products but not ThX (if alkaline, ThX will be out on the electrode but not the active deposit).[2]

The alpha-ray spectrograph which was mentioned in the preceding note was used here also for the following experiments. Each plate exposed to a source prepared by the first method has had the RdTh lines and the ThC lines on the same plate when the magnetic field was properly adjusted. Here the RdTh lines were very strong. The ThC lines were so weak that the weak lines are missing, and the tracks of the two strong lines are countable. RdTh α_0 line has been used as the reference line for calculating the energies of the other groups. It is seen from Table I that the relative intensities and energies of these lines agree well with the values obtained by other investigations.

TABLE I. Alpha-Ray Spectra of RdTh, ThC, and ThC′.

Element	Alpha-energy Mev	Relative integral intensity
RdTh	5.420 (ref.)	30
α_0	5.354±0.02	8
α_1		
ThC		
RdThα_0	5.420 (ref.)	
α_1	6.113±0.02	9
α_2	6.074±0.02	30
ThC′		
α_0	8.778 (ref.)	10^6
α_2	10.553±0.01	250

The region on the high energy side of the ThC′ line was examined from two plates, one obtained from a source prepared by the first method and the other by the second method. Unfortunately, the source from the second method was not much stronger than that from the first method. So in both cases we have not found the weak long-range line, but the values from the two plates for the strong line are practically equal. Examination was extended up to about 11.5 Mev.

As shown in the table, the energies and intensities obtained here and in the preceding note of the known lines are in close agreement with the values of the other workers.[3] However, our average values (without relativistic correction) of the group energies are all slightly larger.

The low energy regions of RaC′, RdTh, and ThC′ were examined thoroughly, down to about 2 Mev below the main line in each case. We have found no weak lines in RaC′ and ThC′ but some evidence of weak lines in RdTh. In the case of RdTh there seems to be a series of little humps, which occurred, in general, consistently when the examination was repeated. However, the peak values of these humps are not much larger than the statistical fluctuation; they are even less prominent than those found in Ra.[4] Therefore, one cannot draw any definite conclusion yet until the experiment is repeated further.

In the low energy region of ThC′, there appear two prominent lines, one at 7.663 Mev and the other at 6.891 Mev, being, respectively, roughly 1 in 300 and 1 in 700 of the ThC′ line intensity. We feel that they are due to contamination. The first line may be due to RaC′, though we could not find the Ra line from a plate which was exposed to a source prepared in the same way. The second line may be due to actinon, though the energy seems to be higher than the previous value, the difference being larger than the experimental error.

Recently Wadey[5] has made an investigation of the Po alpha-particles. He has finally found that the weak lines, which we found before, were not apparent in his experiment, but that the distribution in the neighborhood of the main line was affected considerably when different materials were used for the support. He explains, therefore, the Po weak lines as due to diffusion of Po atoms into the support and interaction with the crystals of the metal. The explanation is very interesting. In this connection it

may be worth while to mention that in our previous case a source prepared by condensing Po onto a palladium rod gave similar results to those on nickel strips. In any case, it is important to make a systematic experimental study starting with a support of very low atomic number.

We should like to thank Miss Sophia Wysienska and Mrs. Allen Fry for their invaluable help in examining the plates.

[1] We are thankful to Dr. M. Blau, then of the Canadian Radium Uranium Company for lending us the mesothorium source.
[2] F. Soddy, *Chemistry of Radioactive Elements* (1914), Part 2, second edition; E. Rutherford, *Radioactive Substances and Their Radiations* (1913); O. Hahn, *Applied Radioactivity* (1936).
[3] The results up to 1935 are collected in F. Rasetti's book, *Elements of Nuclear Physics* (1936).
[4] W. Y. Chang, Phys. Rev. **70**, 632 (1946).
[5] To appear in Phys. Rev. One of us would like to thank Dr. W. G. Wadey for letting him read the manuscript before publication.

Further Data Concerning the Variation of Penetrating Showers with Altitude*

JOHN TINLOT
Department of Physics and Laboratory of Nuclear Science and Engineering, Massachusetts Institute of Technology, Cambridge, Massachusetts
September 20, 1948

ADDITIONAL data have been obtained confirming the preliminary results recently published[1] concerning the altitude variation of the penetrating showers. It is now clear that the frequency of these showers varies exponentially with atmospheric depth from sea level to an altitude of 30,000 feet, the highest altitude investigated. The information obtained in the recent measurements also makes it possible to estimate the relative importance of penetrating showers which are, and those which are not, accompanied by atmospheric showers.

The detector of penetrating showers is described in the communication cited. Briefly, it consists of five trays of four Geiger-Mueller counters arranged in a block of lead as sketched in the inset of Fig. 1. Multiple coincident counter discharges of certain kinds are interpreted as detecting the passage of penetrating showers; these "events" are referred to by symbols of the type $A_\alpha B_\beta \cdots$, signifying simultaneous discharge of α- or more counters in tray A, β- or more counters in tray B, etc. During the experiments discussed here, an "extension" tray F was placed four inches to the side of the block of lead, at the level of the upper surface. This was used in conjunction with the detectors to investigate the correlation with atmospheric showers. The equipment in this form was operated at altitudes of 300 feet (Lexington, Massachusetts), 9500 feet (Doolittle Ranch, Colorado), and 14,300 feet (Mt. Evans, Colorado).

All of the events listed in the previous communication were recorded, in addition to events of the type $A_1B_2C_2F_\eta$, where $\eta = 1, 2, 3,$ or 4.

The complete set of data giving the frequencies of the events $A_1B_1C_1D_1$, $A_2B_2C_2$, $A_1B_2C_2$, and $A_2B_2C_1$ at seven different altitudes is reproduced in the graph. The event $A_2B_2C_2$ is believed to be least affected by spurious effects and thus to represent closely the occurrence of penetrating showers at all altitudes. The experimental points for this event lie on an exponential curve within the experimental error at all points. The exponential curve chosen by the method of least mean square errors to give the best fit yields an absorption thickness of 118 ± 2 g cm^{-2}. As can be seen from the figure, the events $A_1B_2C_2$ and $A_2B_2C_1$ also follow the exponentials with the same absorption thickness down to the pressure 725 g cm^{-2} (9500 feet).

Information obtained with the extension tray is shown in Table I. Most significant is that the rate for the event $A_2B_2C_2F_1$ is at all altitudes 10 percent or less than the rate for $A_2B_2C_2$. This clearly shows that the great majority of the events recorded by the penetrating shower detector are not accompanied by dense atmospheric showers. This finding disagrees with that of Janossy and Broadbent[2] who concluded that at sea level about one-half of the penetrating showers are accompanied by atmospheric showers. It is evident, however, that the geometry of the detecting apparatus places a strong bias on the type of shower recorded.

It is interesting to note that at 14,000 feet the event $A_2B_2C_2F_4$ is about one-half as frequent as the event $A_2B_2C_2F_1$, while the frequencies of the events $A_2B_2C_2F_2$ and $A_2B_2C_2F_3$ are intermediate in value. Thus the atmospheric showers which accompany the passage of a penetrating shower through the detector appear to have a high

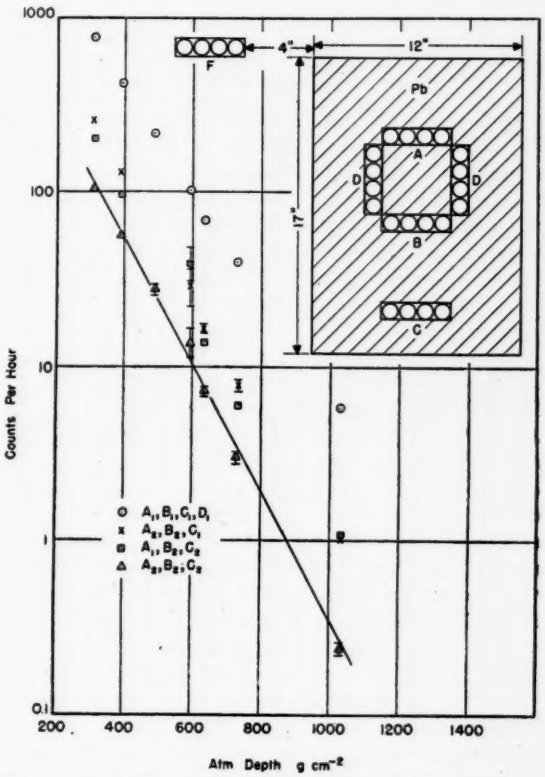

FIG. 1. Complete set of data giving the frequency of the events $A_1B_1C_1D_1$, $A_2B_2C_1$, $A_1B_2C_2$, and $A_2B_2C_2$ at seven different altitudes.

TABLE I.

Altitude (feet)	Pressure (g cm^{-2})	Time (hour)	$A_1B_1C_2$ (counts)	$A_1B_1C_2F_1$ (counts)	$A_2B_2C_2$ (counts)	$A_2B_2C_2F_1$ (counts)	$A_2B_2C_2F_2$ (counts)	$A_2B_2C_2F_3$ (counts)	$A_2B_2C_2F_4$ (counts)
250	1030	308 113.5	309	16	25	3			
9500	725	58			174	17	12	10	6
14,000	625	41.5			293	15	10	9	8

density. The area of each counter is 67.5 cm². If one assumed that all of the showers striking tray *F* had the same average density, one would calculate this density as being about 220 particles per square meter.

The facilities for the work at Mt. Evans were provided by the Inter-University High Altitude Laboratory.

* Assisted by the joint program of the Office of Naval Research and the Atomic Energy Commission.

[1] J. Tinlot, Phys. Rev. **73**, 1476 (1948).
[2] D. Broadbent and L. Janossy, Proc. Roy. Soc. **A192**, 364 (1948).

Development of Thick Emulsions by a Two-Bath Method*

M. BLAU
Columbia University, New York, New York
AND
J. A. DE FELICE
Brookhaven National Laboratory, Upton, Long Island, New York
September 13, 1948

THE increased use of thick emulsions in nuclear physics has made it desirable to find a satisfactory technique of uniformly developing them. Dilworth, Occhialini, and Payne[1] have described the so-called temperature development method. We are using an alternate method of development on Ilford, C2, 200 u plates, which is probably applicable to even thicker emulsions. The results we have obtained to date might be helpful to others who are using these emulsions.

The method we adapted for our purpose is essentially that described by Crabtree *et al.*[2] which was used for the uniform development of large quantities of motion picture film. In this method the developer is divided into two baths. The first bath contains the developing agent, part of the sodium sulfite and the potassium bromide, but no alkali. The second bath contains all the necessary constituents of an ordinary developer plus an additional amount of alkali. In the first bath the developer diffuses into the emulsion. However, the rate of development is very low because of the lack of alkali. In the second bath the actual development takes place because of the presence of the alkali. It was necessary to add developing agent to the second bath, because not enough can be absorbed from the first bath.

After trying various combinations of the constituents and different times of development we find the following procedure to give the best results.

Step 1: Soak in water for 10 min.
Step 2: Solution *A* for 30 min. (slight agitation).
Step 3: Solution *B* for 30 min. (no agitation).
Step 4: 2 percent acetic acid 15 min. (agitation).
Step 5: Fix in *F*-5 at 74°F with constant agitations 6–8 hours.
Step 6: Wash in running water 2 hours.

Solution A:

Elon	1.1 g.
Na_2SO_3	24.0 g.
Hydroquinone	4.4 g.
KBr	2.0 g.
H_2O to make	2000 cc

Solution B:

Stock *D*-19	400 cc
H_2O	1600 cc
Additional Na_2CO_3	16 g.

For different batches of the same emulsion, slight adjustments of the developing times and the composition of the solutions may be necessary. The temperatures of the solutions in the Steps 1–4 were all kept constant at 68°F. The temperature of the fixer could also be kept at 68°F. However, it was increased to 74°F to shorten the fixing time.

Because the temperature is kept constant the danger of reticulation is avoided. None of our plates showed any sign of reticulation. Proton tracks in the emulsion had their normal grain density while the background fog was very low. The plates appeared to be uniformly developed throughout the emulsion.

* This document is based on work performed under Subcontract S-62 of Contract AT-30-2-GEN-16 for Brookhaven National Laboratory at Columbia University.
[1] C. C. Dilworth, G. P. S. Occhialini, and R. H. Payne, Nature **162**, 102 (1948).
[2] Crabtree, Parker, and Russel, Soc. Mot. Pic. ENO, VO RR **21**, 21 (1933).

Thermonuclear Reactions in the Expanding Universe

R. A. ALPHER AND R. HERMAN
Applied Physics Laboratory, The Johns Hopkins University, Silver Spring, Maryland*
AND
G. A. GAMOW
The George Washington University, Washington, D. C.
September 15, 1948

IT has been shown in previous work[1–3] that the observed relative abundances of the elements can be explained satisfactorily by consideration of the building up of nuclei by successive neutron captures during the early stages of the expanding universe. Because of the radioactivity of the neutron, and also because neutrons are used in forming the elements, the building up process must have been completed essentially in a time of the order of several neutron decay periods, i.e., about 10^3–10^4 sec. It should be noted that following the essential completion of the main element forming process, the temperature prevailing

in the expanding universe was still high. Consequently, one should expect changes in the relative abundances of the lighter elements as a result of thermonuclear reactions of these nuclei with protons. While these thermonuclear reactions must have proceeded during the element forming stage, their rates were negligible by comparison with those of neutron capture reactions. Examination of the relative abundance data suggests that the abnormally low abundances of certain of the light elements, such as lithium, beryllium, and boron, resulted from thermonuclear destruction of these nuclei with the concomitant formation of additional helium. In contradistinction to the other light elements, these are found to have large cross sections for proton reactions.[4]

On the basis of the foregoing discussion it may be shown that for certain of the light elements the difference between the present relative abundance and the abundance computed according to the neutron capture process is consistent with known thermonuclear reaction rates and cosmological information afforded by the neutron capture process. The well-known formula for the rate of thermonuclear reactions gives the number of processes per gram per second as[4,5]

$$p=5.3\times10^{25}\rho x_1x_2\Gamma\phi\tau^2e^{-\tau}\ \mathrm{g}^{-1}\ \mathrm{sec.}^{-1}, \tag{1}$$

where ρ is the total density of matter, x_1 and x_2 the concentrations by weight of the nuclei involved in the reaction, $\Gamma/\hbar$ the probability of the reaction in sec.$^{-1}$ after penetration, ϕ a function of the nuclear parameters, and

$$\tau=\alpha T^{-1/3}, \tag{1a}$$

where T is given in units of 10^6°K. The time dependence of temperature and density[6] of matter in the expanding universe, consistent with the conditions required by the neutron capture process, has been shown to be [7,8]

$$T=2.14\times10^{10}t^{-1/2}\text{°K}, \tag{2a}$$

and

$$\rho=7.2\times10^{-3}t^{-3/2}\ \mathrm{g\ cm}^{-3}. \tag{2b}$$

Using Eqs. (1) and (2) in

$$\frac{d[\ln x_2]}{dt}=-pm_2, \tag{3}$$

where m_2 is the mass of the nuclear species 2, with the concentration by weight of protons assumed constant, $x_1=0.5$, we obtain

$$\ln R=A[I(t_0)-I(t)], \tag{4}$$

where R is the ratio of the observed relative abundance to that computed by the neutron capture theory,[1-3]

$$A=-2.96\times10^{21}m_2x_1\Gamma\phi\alpha^2, \tag{5a}$$

$$I(t)=t^{-1/6}\exp(-Bt^{1/6})+BEi(-Bt^{1/6}), \tag{5b}$$

and $B=3.60\times10^{-2}\alpha$. In Eqs. (5), t_0 represents the time at which the proton reactions became important, and t represents the current epoch. The quantities Γ, ϕ, and α are given by Bethe[4] for a number of reactions. The quantity α is $(20)^{1/3}$ times the value of τ tabulated by Bethe for $T=20\times10^6$°K.

Applying Eqs. (5) to the reactions of Li, Be, and B with protons, we find that in order to explain the present extremely low relative abundances of these elements by thermonuclear destruction one must assume that the process became important at about $t_0\sim10^3$ sec. This value of t_0 is of the correct order of magnitude for the time at which the neutron capture process became unimportant.

The same analysis applied to other light elements, such as F^{19}, which also have rather low abundances compared to their computed values, yields a similar result. On the other hand, the elements involved in the carbon-nitrogen cycle reactions do not show any appreciable depletion because of thermonuclear reactions in the expanding universe. For example, in the case of N^{14} the assumption that $t_0\sim10^3$ sec. leads to the result that up to the present epoch the abundance of this nuclear species would have been reduced by only one part per million.

* A portion of the work described in this paper was supported by the Bureau of Ordnance, U. S. Navy, under Contract NOrd-7386.

[1] R. A. Alpher, H. A. Bethe, and G. A. Gamow, Phys. Rev. **73**, 803 (1948).
[2] R. A. Alpher, Phys. Rev. (in press).
[3] R. A. Alpher and R. C. Herman, Phys. Rev. (in press).
[4] H. A. Bethe, Phys. Rev. **55**, 434 (1939).
[5] G. A. Gamow and E. Teller, Phys. Rev. **53**, 608 (1938).
[6] We wish to point out that Eq. (2b) gives the time dependence of matter density in an expanding universe controlled by radiation. It is believed that the error involved in employing this relation up to the present epoch is not large.
[7] G. A. Gamow, Phys. Rev. **74**, 505 (1948).
[8] G. A. Gamow, Nature, in press.

On the Total Half-Life Period of K^{40}

T. GRÅF
L. Meitner Laboratory of Nuclear Physics, Stockholm, Sweden
September 10, 1948

IN connection with the recent determination[1] of the β-decay constant of K^{40}, which yielded $\lambda_\beta=(0.505\pm0.055)\times10^{-9}$ year^{-1}, with a corresponding β-decay period $T_\beta=(13.7\pm1.5)\times10^8$ years, an attempt was made to revise the branching ratio λ_e/λ_β, where λ_e is the decay constant for electron capture, as obtained by Bleuler and Gabriel,[2] in order to allow for the effect of back-scattering. With the corrected branching ratio (1.8 ± 0.5) an approximate value of $(5\pm1.5)\times10^8$ years was computed for the total half-life T.

At present a more accurate value of T may be calculated by combining the above value of λ_β with Ahrens and Evans'[3] recent Ca^{40}/K^{40} ratio in lepidolites, which became available after the mailing date of the author's notes.[1,4] Since in these minerals, of age $t=2.1\times10^9$ years, an excess

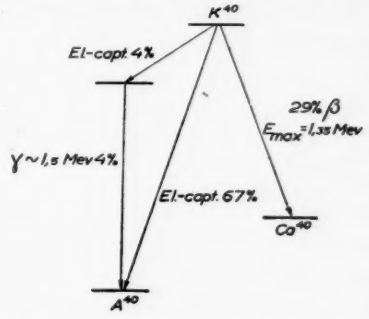

FIG. 1. Decay scheme of K^{40} with relative branching intensities.

of Ca^{40} was found, corresponding to a mean value of 11 for the ratio of radiogenic Ca^{40}/K^{40}, from the relation $Ca^{40}/K^{40}=(\lambda_\beta/\lambda)[\exp(\lambda t)-1]$ one obtains readily for the total decay constant $\lambda=\lambda_e+\lambda_\beta=(1.74\pm0.22)\times10^{-9}$ year^{-1}, and for $T=(4.0\pm0.5)\times10^{9}$ years. Hence, $\lambda_e=(1.235\pm0.22)\times10^{-9}$ year^{-1} and $\lambda_e/\lambda_\beta=2.45\pm0.50$. Figure 1 shows the resulting decay scheme for K^{40}. The limits of T account for an incertitude of 25 percent in the value of Ca^{40}/K^{40} and for a probable error of 1.2×10^{8} years in the value of t. The coincidence with the approximate figure of 4×10^{8} years suggested by Thompson and Rowlands[5] is fortuitous, since these authors assumed larger values for both $\lambda_e/\lambda_\beta(\sim3)$ and $T_\beta(16\times10^{8}$ years[6]).

Ahrens and Evans themselves deduced $(4.5\pm0.5)\times10^{8}$ years from their Ca^{40}/K^{40} ratio. They used a λ_β value obtained by raising by 50 percent Mühlhoff's[6] value and by reducing Bleuler and Gabriel's by an amount corresponding to an estimated scattering of 50 percent. Thus, a value of 10.6×10^{8} years was obtained for the β-decay period. However, as pointed out previously,[1] Bleuler and Gabriel made no comparison but, instead, an absolute determination of λ_β from the observed counting rate. Since reflection through the whole surface of the brass source mount in their experiments may reach 60 percent,[7] it may, when not allowed for, together with the low value of 90 percent assumed for the counter efficiency (instead of unity), enhance the value found for λ_β by a factor $1.60/0.90=1.78$, or even more. On the other hand, in Mühlhoff's comparison between K^{40} and uranium, differences in back-scattering could account only for a small fraction of the proposed correction.

The latest conclusions[4] on the geophysical significance of potassium may remain essentially unchanged, in particular the value of $(22\pm3)\times10^{-6}$ cal. per year per gram, given for the present heat production of potassium. However, the estimates[3,4] concerning the heat output of potassium in the past appear to be rather conservative. In fact, with the new value of the total half-life the heat produced by potassium 2×10^{9} years ago appears to be 3 times, and 3.35×10^{9} years ago—at the origin of the earth[8]—36 times larger than that generated at present by the total amount of radioactivity in the earth's crust.

Furthermore, when assuming, following Suess,[9] that the K^{40} content originally present in potassium was of the same magnitude as that of Lu^{176} in lutetium ($\sim$3 percent), it may be concluded that the "age" of potassium, and of the other elements, cannot be significantly higher than the age of the earth, and is probably less than 4×10^{9} years.

[1] T. Gráf, "On the half-life of K^{40}," Phys. Rev. **74**, 831 (1948).
[2] E. Bleuler and M. Gabriel, Helv. Phys. Acta **20**, 67 (1947).
[3] L. H. Ahrens and R. D. Evans, Phys. Rev. **74**, 279 (1948).
[4] T. Gráf, "Significance of the radioactivity of K^{40} in geophysics," Phys. Rev. **74**, 831 (1948).
[5] F. C. Thompson and S. Rowlands, Nature **152**, 103 (1943).
[6] W. Mühlhoff, Ann. d. Physik **7**, 205 (1930).
[7] T. Gráf (work to be published).
[8] A. Holmes, Nature **159**, 127 (1947).
[9] H. E. Suess, Phys. Rev. **73**, 1209 (1948).

Proceedings of the American Physical Society

Minutes of the Meeting at Washington, April 29 to May 1, 1948

THE 285th meeting of the American Physical Society, being the 1948 Spring Meeting, was held at Washington, D. C., on Thursday, Friday, and Saturday, April 29, 30, and May 1, 1948. In respect of the number of contributed papers (231) this was by over 20 percent the largest meeting of our history. Whether it was also the largest in respect to attendance will never be known; the registration was only 1450 (against more than 1700 at the previous New York meeting), but the wide dispersion of the sessions may have discouraged many of our members from coming to the one building where a registration desk was installed. This was the Lisner Auditorium of George Washington University: we held sessions also in two rooms of the Hall of Government of that University, in the National Academy of Sciences, in the new East-Building lecture room of the National Bureau of Standards, and in the auditoriums of the Departments of Commerce and Interior. Deep gratitude is due the authorities of these institutions and the Local Committee, headed as last year by Professor T. B. Brown; special thanks are owed Mrs. L. Marton who took charge of the distribution of tickets to the dinner and other gatherings, to Mr. Hugh Odishaw of the National Bureau of Standards who provided for the staffing for the registration desk, to Mrs. F. G. Brickwedde for arranging a reception by Mrs. Truman for visiting ladies—and to whatever controlled the weather, not sultry in the least but exceptionally delightful.

The most extensive group of invited papers composed the Symposium on Radiofrequency and Microwave Spectroscopy, held under the joint sponsorship of the U. S. Navy and the American Physical Society (the idea originated with E. R. Piore) and extending over three sessions. Another group of invited papers provided by the National Bureau of Standards consisted of six by members of its staff on basic physical measurements effected at that institution.

A Symposium on Computing Machines included papers by Howard Aiken, R. L. Snyder, and W. J. Eckert. E. M. McMillan and E. Segrè spoke of recent work at the Radiation Laboratory in Berkeley, W. Heitler on theories of meson production, E. A. Johnson on magnetization of ancient glacial varves, and two invited papers were provided by the Division of Electron Physics. Two of our most distinguished members attained the age of eighty in this year of 1948: R. A. Millikan gave an address "Why My Stork Chose 1868" and R. W. Wood an after-dinner speech. The two hundred and thirty-one contributed papers were distributed among twenty-two sessions. Abstracts of these and titles of the invited papers are printed hereinafter. Post-deadline papers by J. W. DuMond and J. M. Richardson were given by authorization of the Council under the authority conferred upon it by a recent amendment of the by-laws of the Society.

The banquet of the Society was held on Thursday evening in the Grand Ballroom of the Mayflower Hotel, President Oppenheimer presiding; the attendance was nearly 400. His Majesty's Ambassador, Lord Inverchapel, presented the Duddell Medal with accompanying scroll and check, which the Physical Society of London had awarded to R. J. Van de Graaff. R. W. Wood delighted the assembly with the after-dinner speech mentioned above, and five physicists and mathematicians (Carl Beck, Thomas Carroll, Duncan Harkin, Alan Shapley, and Alan Waterman) brought the evening to its culmination by rendering for us the Schumann piano quintet.

The Council met on Saturday afternoon, and began its proceedings by electing to Membership no fewer than three hundred and five candidates (their names are appended) and to Fellowship Maurice Desirant. By mail ballot the Council had recently elected to Honorary Membership six distinguished foreign physicists: Louis de Broglie, James Chadwick, P. A. M. Dirac, H. A.

Kramers, Max von Laue, and Arnold Sommerfeld. J. A. Bearden and E. U. Condon were nominated to the National Research Council as representatives of the American Physical Society on the Division of Physical Sciences thereof, to serve until June 30, 1951. Ten sets of Physical Review and Reviews of Modern Physics, extending over the war years and until June 30, 1948, have been donated to Japanese institutions of learning; it is intended to confer a similar gift on German institutions. The organization of our publications is modified in the following manner. J. T. Tate, the elected Managing Editor of all of the publications of the Society, continues in this role; he acquires the title of Editor of the Physical Review (reporting to himself as Managing Editor), and J. W. Buchta is appointed Editor of the Reviews of Modern Physics (reporting to Tate as Managing Editor). Six additional members of the Board of Editors (over and above the ten elected members) are to be appointed for staggered terms by the President of the Society. The sixteen members of the Board of Editors are then to be distributed into panels, one to be concerned primarily with the Physical Review and the other primarily with the Reviews of Modern Physics.

The Society has lost through death James C. Biddle, Leonard E. Miller, Raymond E. Reinhart, and Alva W. Smith.

It is announced with great satisfaction that the 1948 Membership List of the American Physical Society is actually in press.

Elected to Membership: Melvin W. Aarons, Frank L. Adelman, Frank J. Allen, Gabriel Allen, W. D. Allen, John W. Anderegg, Donald A. Anderson, Philip W. Anderson, Calvin G. Andre, Yngve Axner, Donald Hart Baker, Ewart M. Baldwin, Robert M. Baer, Domenick Barbiere, Ian G. Barbour, Paul Henry Barrett, Albert A'len Bartlett, Leonard Becker, Benjamin Bederson, Marcel Benoit, John Robert Beyster, Lawrence C. Biedenharn, Jr., Arthur Trew Biehl, John A. Bjorkland, Wade Blocker, Franklin C. Bobb, Robert Bouchez, William Robert Bradford, Judith Bregman, Leo Broussard, Alfred B. Brown, Jr., John E. Brugger, Oscar Bunemann, Benedict Carlat, E. Thomas Casellini, Dwight A. Caswell, Tsung Sui Chang, Ruth K. Cheney, George Chertock, William Jeffries Childs, Eugene Lent Church, Edward Hawthorne Clark, Fred J. Clark, John F. Clark, Jr., Marshall R. Cleland, Matthew Conrad, Rodney L. Cool, Streatfield H. Cox, Jr., Lawrence H. Crandon, C. T. H. Crawford, John Norris Crawford, Pierre Cuer, J. Warren Culp, George L. Cunningham, Jr., Stanley J. Czyzak, Milton Dank, Morris Darnowsky, Harry Davis, Robert B. Day, David L. Dexter, J. W. T. Dobbs, Jr., Hugh L. Donley, Angelo Drigo, Mae A. Driscoll, Walter F. Dudziak, Donal Baker Duncan, Richard P. Durbin, William T. Dyall, Freeman J. Dyson, Frank S. Eadie, Richard R. Eggleston, Geoffrey Gunther Eichholz, Mortimer M. Elkind, Cavid Ener, Frederic John Eppling, Kenneth W. Erickson, Harold W. Euker, Herman Farber, Robert E. Fearon, Melvin I. Ferentz, Wade Lanford Fite, Robert M. Frank, Marvin J. Freiser, Francois N. Frenkiel, Robert H. Frickel, Marvin Harold Friedman, Sidney Friedrich, Edward Allan Frieman, Guy C. Fromm, Robert A. Frosch, John H. Gardner, I. E. Garrick, Richard Paul Gaunt, Frank C. Gibson, Otis R. Gilliam, Barbara M. Girdwood, Leonard Glatt, Leonard M. Goldman, Jacob H. Goldstein, William Livingston Gordon, S. R. Govindarajan, Rodney E. Grantham, Lowell Greenbery, Don J. Grove, Walter R. Guild, James Warren Hadley, Richard R. Haefner, William Marsland Hall, J. J. S. Hamilton, Swegn D. Hamren, Stanley S. Hanna, C. Austin Haulman, George W. Hees, James Ransom Heirtzler, Victor P. Henri, Gilman A. Hill, Oskar Hirzel, Bartow Hodge, Robert Bronson Holden, George T. Holmes, David W. Hone, E. Irl Howell, Richard H. Huddlestone, R. P. Hudson, John L. Hult, H. W. Ibser, John Ise, Jr., William B. Ittner, III, Edwin T. Jaynes, Leticia Mazzia Kahrilas, Walter Robert Keagy, Jr., Raymond L. Kelly, Robert Warner Kenney, George S. Kenny, William J. Knox, Irving L. Kofsky, Theodore Kohane, Alfred T. Kornfield, Samuel Koslov, William A. S. Lamb, George F. Lanzl, Ezra B. Larsen, Cesare Mansueto Giulio Lattes, Samuel Lattimore, Roger B. Lazarus, Cecil E. Leith, Jr., Alan M. Liebschutz, Morris Liebson, Bernard R. Linden, G. R. Lomanitz, Harvey C. Losow, Jerold M. Lowenstein, Leland J. Luft, Harold Carter Lukens, S. T. Ma, William Warren Managan, Bernard Margolis, Graham Wallace Marks, W. G. Marley, Leona Woods Marshall, David George Edwardes Martin, Robert L. Martin, Julius Marx, Jesse Marymont, Richard W. Mattoon, Charles William Mautz, Dean Augustus McCown, John Lawrence McHale, Jr., J. Rand McNally, Jr., Sister Marie Gertrude McNeil, Duane Torrance McRuer, J. Lawrence Meem, Jr., Harry W. Mergler, Lother Meyer, Daniel Weber Miller, Clark B. Millikan, Theodore Mischel, C. D. Moak, Harold A. Moore, Samuel P. Morgan, Jr., Kennard Harold Morganstern, Leonard Muldawer, N. K. Mundle, Rev. Walter A. Murtaugh, O.P., John P. Nielsen. A. Wilson Nolle, Carrol R. Nisewanger, Rollin Hosmer Norris, Henry Pierre Noyes, Yves Nubar, Brian O'Brien, Jr., Louis Shreve Osborne, William J. Otting, Jr., Carl F. J. Overhage, Peter Edward Pashler, H. W. Peng, John Virgil Pennington, Alfred Morris Perry, Jr., Mary W. Peters, Albert G. Petschek, William G. Pfann, Anne N. Phillips, Donald D. Phillips, George Lawson Pickard, Arthur Gustav Pieper, Sidney Platt, Ralph H. Plumlee, Franklin Pollock, Frank Press, Luther E. Preuss, D. C. Ralph, Maurice Rattray, Jr., Robert H. Rediker, Robert Resnick, Stephen E. Reynolds, Wilson Richard, Leonard M. Rieser, Jr., Florence Robertson, Eugene Sant Robinson, Edward Rollinson, Arnold Rosen, Burt M. Rosenbaum,

Marshall Nicholas Rosenbluth, Daniel Rosenthal, Marcel Rouault, Irving Rowe, Jose Maria Rubiato, William Rubinson, Malvin A. Ruderman, Albert Sevier Sabin, Arthur Sard, S. A. Schaaf, Robert Schafroth, Robert D. Schamberger, Edwin J. Schillinger, Jr., Albert Isadore Schindler, Roland W. Schmitt, Robert H. Schuler, Silvan S. Schweber, Robert H. Sehnert, Leo Seidlitz, Bryce Seligman, Richard B. Setlow, Pat Shao, Philip Shapiro, A. H. Shapley, Roy S. Sharpe, Frank C. Shoemaker, Seymour Shwiller, Virginia V. Sides, Richard A. Silverman, John Arol Simpson, David R. Smith, Joseph E. Smith, S. Ruven Smith, Bertrand W. Squier, Jr., Kenneth Jack Standley, Martin C. Steele, James S. Stewart, Bertram Stiller, William A. Stirrat, Richard G. Stoudenheimer, Joel Strandberg, Warren F. Stubbins, William H. Surber, Jr., Leonard I. Swern, Lewis P. Tabor, Samuel I. Taimuty, Francis K. Tallmadge, Charles Edwin Teeter, Jr., James Michael Templeman, Fred H. Tenney, Michel Ter-Pogossian, George R. Thurman, Yu Ting, Jarvis Todd, Dominic S. Toffolo, John Roger Triplett, Gardiner Luttrell Tucker, T. E. Turner, Winfield W. Tyler, Francis E. Van Bergen, Mario Verde, Donald Wahl, Earle Horace Warner, Albert B. Weaver, Irving R. Weingarten, David E. Weiss, Ephraim Weiss, Jerald A. Weiss, Max T. Weiss, Gregor Wentzel, Robert J. Wickham, Thomas A. Wiggins, Lawrence Wilets, Harvey B. Willard, Donald K. Winslow, George P. Wood, Cecil Sherman Woodbrey, Lester L. Woodward, Wayne E. Wright, Victor H. Yngve, Charles F. Yost, Louis Zernow, Bruno John Zwolinski.

KARL K. DARROW, *Secretary*
American Physical Society
Columbia University
New York 27, New York

Symposium on Radiofrequency and Microwave Spectroscopy

Outline of the Topics of the Symposium. K. K. DARROW, *Bell Telephone Laboratories.*

Fine Structure of the Hydrogen Atom by a Microwave Method. W. E. LAMB, JR., *Columbia University.*

Intrinsic Magnetic Moment of the Electron. POLYCARP KUSCH, *Columbia University.*

Hyperfine Structure of Hydrogen and Deuterium. JOHN NAFE, *Columbia University.*

Molecular-Beam Experiments with Chlorine. J. R. ZACHARIAS, *Massachusetts Institute of Technology.*

A High Precision Determination of the Ratio of the Nuclear Magnetic Moments of Proton and Neutron. HANS STAUB, *Stanford University.*

The Structure of Nuclear Resonance Absorption Lines in Crystals. R. V. POUND, *Harvard University.*

Nuclear Magnetic Resonance Experiments at the Massachusetts Institute of Technology. FRANCIS BITTER, *Massachusetts Institute of Technology.*

Nuclear Magnetic Moments of Hydrogen 3 and Helium 3. H. L. ANDERSON, *Argonne National Laboratory.*

Microwave Resonance Absorption in Paramagnetic Salts. P. R. WEISS, *Rutgers University.*

Microwave Resonance Absorption in Ferromagnetic Materials. CHARLES KITTEL, *Bell Telephone Laboratories.*

Precision Measurement of Molecular Rotation Frequencies. D. K. COLES, *Westinghouse Electric Corporation.*

Rotational Spectra of Linear Molecules. M. W. P. STRANDBERG, *Massachusetts Institute of Technology.*

Nuclear Properties Determined from Microwave Spectroscopy. C. H. TOWNES, *Columbia University.*

Use of Microwave Spectroscopy for Studies of Molecular Structure. E. BRIGHT WILSON, *Harvard University.*

Invited Papers on Basic Physical Measurements at the National Bureau of Standards

Intercomparisons of the Standard Meter. L. V. JUDSON, *National Bureau of Standards.*

Spectrum Lines of Hg 108 as Standards of Length. W. F. MEGGERS, *National Bureau of Standards.*

The Absolute Electrical Units. F. B. SILSBEE, *National Bureau of Standards.*

Proposed Revision of the International Temperature Scale. H. F. STIMSON, *National Bureau of Standards.*

Radioactivity and Neutron Standards. L. F. CURTISS, *National Bureau of Standards.*

Microwave Frequency Standards. H. LYONS, *National Bureau of Standards.*

Invited Papers on Computing Machines

Computing Machines. HOWARD AIKEN, *Harvard University.*

Status of Large-Scale Computing Devices in the United States. R. L. SNYDER, *University of Pennsylvania.*

The IBM Selective Sequence Electronic Calculator. W. J. ECKERT, *International Business Machines.*

Invited Papers of the Division of Electron Physics

Pulsed Emission Correlated with Low Temperature Direct Current Emission Properties of Certain Oxide-Coated Cathodes. R. L. MCCORMACK, J. CARDELL, *Raytheon,* AND W. B. NOTTINGHAM, *Massachusetts Institute of Technology.*

Conductivity Induced in Thin Insulating Films by Electron Bombardment. L. PENSAK, *RCA Laboratories.*

Other Invited Papers

Theory of Meson Production. W. HEITLER, *Dublin Institute for Advanced Studies.*

Magnetization of Ancient Glacial Varves. E. A. JOHNSON, *Department of Terrestrial Magnetism.*

A1. A Survey of Recent Work at the Radiation Laboratory in Berkeley. E. M. MCMILLAN, *University of California, Berkeley.*

Why My Stork Chose 1868. R. A. MILLIKAN, *California Institute of Technology.*

A2. Experiments on High Energy Neutron-Proton Scattering. EMILIO SEGRÈ, *University of California, Berkeley.*

Invited Papers

A1. A Survey of Recent Work at the Radiation Laboratory in Berkeley. E. M. MCMILLAN, *University of California, Berkeley.*

A2. Experiments on High-Energy Neutron-Proton Scattering. EMILIO SEGRÈ, *University of California, Berkeley.*

B1. Magnetization of Ancient Glacial Varves. E. A. JOHNSON, *Department of Terrestrial Magnetism.*

EA1. Why My Stork Chose 1868. R. A. MILLIKAN, *California Institute of Technology.*

S12. Theory of Meson Production. W. HEITLER, *Dublin Institute for Advanced Studies.*

Basic Physical Measurements at the National Bureau of Standards

R1. Intercomparisons of the Standard Meter. L. V. JUDSON.

R2. Spectrum Lines of Hg 198 as Standards of Length. W. F. MEGGERS.

R3. The Absolute Electrical Units. F. B. SILSBEE.

R4. Proposed Revision of the International Temperature Scale. H. F. STIMSON.

R5. Radioactivity and Neutron Standards. L. F. CURTISS.

R6. Microwave Frequency Standards. H. LYONS.

Division of Electron Physics

U1. Pulsed Emission Correlated with Low Temperature Direct-Current Emission Properties of Certain Oxide-Coated Cathodes. R. L. MCCORMACK AND J. CARDELL, *Raytheon,* and W. B. NOTTINGHAM, *Massachusetts Institute of Technology.*

U2. Conductivity Induced in Thin Insulating Films by Electron Bombardment. L. PENSAK, *RCA Laboratories.*

Computing Machines

W1. Computing Machines. HOWARD AIKEN, *Harvard University.*

W2. Status of Large Scale Computing Devices in the United States. R. L. SNYDER, *University of Pennsylvania.*

W3. The IBM Selective Sequence Electronic Calculator. W. J. ECKERT, *International Business Machines.*

Symposium on Radiofrequency and Microwave Spectroscopy

M1. Outline of the Topics of the Symposium. K. K. DARROW, *Bell Telephone Laboratories.*

M2. Fine Structure of the Hydrogen Atom by a Microwave Method. W. E. LAMB, *Columbia University.*

M3. Intrinsic Magnetic Moment of the Electron. P. KUSCH, *Columbia University.*

M4. Hyperfine Structure of Hydrogen and Deuterium. JOHN NAFE, *Columbia University.*

N1. Molecular Beam Experiments with Chlorine. J. R. ZACHARIAS, *Massachusetts Institute of Technology.*

N2. A High-Precision Determination of the Ratio of the Nuclear Magnetic Moments of Proton and Neutron. HANS STAUB, *Stanford University.*

N3. The Structure of Nuclear Resonance Absorption Lines in Crystals. R. V. POUND, *Harvard University.*

N4. Nuclear Magnetic Resonance Experiments at the Massachusetts Institute of Technology. FRANCIS BITTER, *Massachusetts Institute of Technology.*

N5. Nuclear Magnetic Moments of Hydrogen 3 and Helium 3. H. L. ANDERSON, *Argonne National Laboratory.*

V1. Microwave Resonance Absorption in Paramagnetic Salts. P. R. WEISS, *Rutgers University.*

V2. Microwave Resonance Absorption in Ferromagnetic Materials. CHARLES KITTEL, *Bell Telephone Laboratories.*

V3. Precision Measurement of Molecular Rotation Frequencies. D. K. COLES, *Westinghouse Electric Corporation.*

V4. Rotational Spectra of Linear Molecules. M. W. P. STRANDBERG, *Massachusetts Institute of Technology.*

V5. Nuclear Properties Determined from Microwave Spectroscopy. C. H. TOWNES, *Columbia University.*

V6. Use of Microwave Spectroscopy for Studies of Molecular Structure. E. BRIGHT WILSON, *Harvard University.*

Contributed Papers on Nuclear Scattering

A3. Proton-Proton Scattering: 2.4 to 3.5 Mev. J. M. BLAIR, WILLIAM SLEATOR, JR., GEORGE FREIER, E. E. LAMPI, AND J. H. WILLIAMS, *University of Minnesota.**—The experiments on the differential cross section for proton-proton scattering reported at a previous meeting[1] have been completed, extending the measurements to higher energies. The dimensions of the apparatus, the current collection system, etc. have been recalibrated, and considering the probable errors in these measurements and the internal consistancy of the scattering data, it is believed that the probable errors in the absolute cross sections are 1.6 percent. At the lowest energy where these measurements overlap those of Herb[2] our values deviate from theirs, in the region from 20° to 45°, by ½ percent. Proton-proton cross section per unit solid angle (in barns) angles given in laboratory system, energies in Mev:

energy	8°	10°	12.5°	15°	17.5°	20°	25°	30°	35°	40°	45°
2.43	8.12	3.09	1.35	.804	.631	.564	.528	.528	.503	.475	.443
3.05	5.03	2.01	.969	.631	.539	.494	483	.469	.450	.425	.402
3.26	4.47	1.79	.869	.605	.513	.479	.473	.450	.441	.410	.380
3.50	3.72	1.55	.778	.548	.474	.463	.442	.428	.418	.397	.366

* The research described in this abstract was supported in part by the Office of Naval Research.

[1] Sleator, Blair, Lampi, and Williams, Bull. Am. Phys. Soc. Jan. 1948, p. 9.

[2] Herb, Kerst, Parkinson, and Plain, Phys. Rev. **55**, 998 (1939).

A4. Analysis of Proton-Proton Scattering.—CHARLES L. CRITCHFIELD, *University of Minnesoat.*—The experimental results of Blair, Sleator and Williams on the scattering of protons in hydrogen have been analyzed. Provisional values of the *S*-wave "phase-shifts" K_0, due to nuclear forces, as determined from the scattering observed in the range of laboratory angles, 20 to 45 degrees, are shown in Table I. Small deviations from the formula for the differential cross section that includes only the *S*-wave anomaly occur at small angles of scattering and will be discussed with reference to uncertainties in corrections, relativistic effects and possible *P*-wave effects.

TABLE I.

Energy	2.432	3.047	3.259	3.501	Mev
K_0	48.6	51.0	51.8	52.4	degrees

A5. On the Neutron-Proton Force.—JOHN M. BLATT, *M.I.T.*—Neutron-proton scattering experiments[1] below 10 Mev were analyzed using Schwinger's theory[2] which describes the force phenomenologically by the scattering length a[3] which it causes, and by its *effective range* r (depending both upon the wellrange and welldepth). a_t and r_t (triplet state) are related through the deuteron binding energy; a_s and r_s are independent. Scattering data give two relations between r_t and r_s. Unfortunately these two relations overlap completely, so one can't find either r_t or r_s. The coherent scattering amplitude $f=2(0.75a_t+0.25a_s)$ and the epithermal cross section determine r_t uniquely. f is measured by neutron scattering from parahydrogen[4] and hydrogen-containing crystals.[5] The crystal measurement contradicts the parahydrogen measurement and the scattering data. The parahydrogen measurement and the scattering data contradict the hypothesis of the charge independence of nuclear forces in a given spin-state. A redetermination of f is strongly recommended.

[1] C. L. Bailey *et al.*, Phys. Rev. **70**, 583 (1946). D. Frisch, Phys. Rev. **70**, 589 (1946).
[2] J. Schwinger, unpublished.
[3] E. Fermi and L. Marshall, Phys. Rev. **71**, 66 (1947).
[4] R. B. Sutton *et al.*, Phys. Rev. **72**, 1147 (1947).
[5] G. C. Shull *et al.*, Phys. Rev. **73**, 262 (1948).

A6. Elastic Scattering of Protons by Aluminum in the Neighborhood of the 985 Kev Resonance. R. S. BENDER,* F. C. SHOEMAKER, S. G. KAUFMANN, AND G. M. B. BOURICIUS, *University of Wisconsin.*—According to the Breit-Wigner theory of nuclear resonances, there should be an anomalous variation of the cross section for elastic scattering of protons in the neighborhood of a resonance level. To observe this effect, the energy spread of the proton beam and the absorption thickness of the target should approximate the resonance width, less than 300 volts for the 985 kev aluminum level. The Wisconsin pressure generator and electrostatic analyzer[1] were used to obtain protons of the desired mean energy and energy spread. The targets were made by evaporating aluminum onto a pure carbon block. Since carbon nucleii are lighter than those of aluminum, protons elastically scattered by the aluminum have higher energy. A magnetic analyzer thus allowed only those protons scattered by aluminum to enter the proportional counter. The scattering angle was 165°. Runs were taken, counting both protons and gamma radiation, with different target thicknesses and beam spreads. The general form of the anomaly agrees with the theory, but the analysis of the data is as yet incomplete.

* Now at the University of Pittsburgh.
[1] R. E. Warren, J. L. Powell, and R. G. Herb, Rev. Sci. Inst. **18**, 559 (1947).

A7. A New Method of Studying Nuclear Energy Levels.* H. W. FULBRIGHT AND R. R. BUSH, *Princeton University.*—A technique has been developed for performing scattering experiments inside the dee chamber of the Princeton

35-inch single-dee synchro-cyclotron. A small scattering camera which rests on the floor of the chamber supports the scattering foil. The foil is a narrow vertical strip which intercepts the undeflected beam. Those particles scattered slightly downward follow helical paths of small pitch; some of them pass through a vertical slit and strike a horizontal photographic plate. The energy of the particle which produces a given track in the plate can be deduced from the position of the track, the strength of the magnetic field, and the geometry of the camera. Actually, distinct lines easily seen by the unaided eye are obtained from elastically and inelastically scattered protons with exposure times of about thirty minutes. The sharpness of the lines shows that the energy spread of the cyclotron beam at any of the radii used is probably less than 0.1 Mev. A wide range of incident energies and scattering angles has been covered by placing the camera in different positions. Results obtained will be described in the following paper.

* This work was supported in part by Navy contract.

A8. Nuclear Energy Levels from Inelastic Scattering of Protons.* R. R. BUSH AND H. W. FULBRIGHT, *Princeton University.* By means of the method just described, protons of 6.7, 10.5, and 17.0 Mev have been scattered from magnesium, aluminum, and iron. Natural magnesium which is 77.4 percent Mg^{24} showed levels at 1.2, 1.7, 2.7, 4.6, 6.0, 8.1, and 9.2 Mev above the ground state. These energy values are believed to be accurate within ±0.3 Mev, except those at 2.7 and 9.2 Mev which are within ±0.5 Mev. The 2.7 Mev line is weak; the others are approximately as intense as the elastic line for large scattering angles. The 4.6 and 6.0 Mev lines show a marked variation of intensity with scattering angle. Possible alternate reactions involving the emission of deuterons and alpha-particles were considered and ruled out. The fact that Mg^{25} and Mg^{26} are low in abundance suggests that all the levels listed, except possibly that at 2.7 Mev, are levels of Mg^{24}. Results obtained from aluminum and iron will also be discussed.

* This work was supported in part by Navy contract.

A9. Neutron Helium Resonance Scattering. L. EISENBUD, *Brookhaven National Laboratory.*—An analysis of the data of Hall and Koontz* on the angular distribution of neutrons scattered by He for neutron energies between 0.8 and 1.6 Mev has been undertaken to determine the character of the levels of He^5. The analysis was made in terms of a generalized one level formula.** If it is assumed that the scattering is largely due to the presence of a $P_{1/2}$ and a $P_{3/2}$ level, the data requires that the $P_{3/2}$ level be at about 1.2 Mev, and the $P_{1/2}$ at about 1.6. This order of the levels is difficult to understand on theoretical grounds. Moreover the constants required for the fit to the data lead to the conclusion that the *distribution* of $P_{1/2}$ levels is quite different from that of $P_{3/2}$ levels and this throws doubt on the validity of the description obtained. The general behavior of the angular distribution functions may also be explained on the assumption of a low lying $P_{1/2}$ level (<0.5 Mev), a $P_{3/2}$ level at 1.2 Mev and an $S_{1/2}$ level at about 1.6 Mev. This order of levels seems more satisfactory on the basis of internal consistency but leads to difficulty in connection with the proton, helium scattering. Research carried out at the Brookhaven National Laboratory under the auspices of the Atomic Energy Commission.

* T. A. Hall and P. G. Koontz, Phys. Rev. **72**, 196 (1947).
** E. P. Wigner and L. Eisenbud, Phys. Rev. **72**, 29 (1947).

Ferromagnetism and Photoconductivity

B2. Effect of Surface Treatment on Complex Permeability. G. T. RADO, M. MALOOF, AND H. ROSENBLATT, *Naval Research Laboratory.*—Using the method previously described[1] the complex permeability ($\mu=\mu_1-i\mu_2$) of iron and nickel as a function of a polarizing magnetic field (H_0) was measured at 200 mc/sec. and at 975 mc/sec. In agreement with our previous observations[2,3] the high frequency permeability is nearly constant for polarizing fields below the knee of the magnetization curve. For sufficiently large H_0, moreover, μ_1 agrees with the static incremental permeability (μ_{stat}) measured on the same sample which was used for the high frequency tests. Iron and nickel differ both in the character of the dispersion and in the effect of surface treatments on μ. For untreated nickel, unlike untreated iron, the value of H_0 necessary to reduce μ_1 to unity is much larger than that required for static saturation. If, however, the surface is polished and the sample subsequently reannealed, the above mentioned agreement between μ_1 and μ_{stat} is obtained. The results will be discussed in terms of the mechanisms of magnetization underlying the various theories of ferromagnetic dispersion.

[1] M. H. Johnson, G. T. Rado, M. Maloof, Phys. Rev. **71**, 472(A) (1947).
[2] G. T. Rado, M. H. Johnson, M. Maloof, Phys. Rev. **71**, 472 (A) (1947).
[3] M. H. Johnson, G. T. Rado, M. Maloof, Phys. Rev. **71**, 322 (1947).

B3. Barkhausen Noise in Ferromagnetic Electrical Circuit Elements. R. T. BEYER AND J. A. KRUMHANSL, *Brown University.*—The voltages induced by Barkhausen effects in the ferromagnetic core materials of electrical circuit elements are treated as random processes. It is assumed that statistical behaviors throughout the core are identical, furthermore, that all domains have the same magnetic moment and are oriented either parallel or antiparallel to the core axis. Average values and mean square fluctuations of induced voltages, together with a description of the noise spectrum are obtained. Application is made to the calculation of the limiting sensitivity of magnetic amplifiers.[1] In this connection some theory of operation of magnetic amplifiers is presented. For the case considered, it is assumed that the signal windings of the magnetic amplifier transformers are not loaded appreciably, so that the resulting calculation refers to open circuit noise.

[1] H. S. Sack, R. T. Beyer, G. H. Miller, and J. W. Trischka, Proc. I.R.E. **35**, 1375 (1947).

B4. Theory of the Ferromagnetism of Simple Tetragonal Arrays. CHARLES KITTEL, *Bell Telephone Laboratories.*—The theory of the ferromagnetic properties of three-

dimensional tetragonal lattices is of particular interest because the two limiting cases are believed to be essentially non-ferromagnetic. Let J_a, J_c denote the exchange integrals between nearest neighbors along the a and c axes, respectively; when $J_a/J_c \gg 1$ the lattice may be considered as a series of independent plane lattices, while $J_a/J_c \ll 1$ represents independent linear chains. A quantum-mechanical spin-wave treatment shows that the Bloch expression for the magnetization of a simple cubic lattice $I_s/I_0=1-0.117(kT/J)^{\frac{1}{2}}$ becomes $1-[0.117(kT)^{\frac{1}{2}}/J_c^{\frac{1}{2}}J_a]$ in the tetragonal case, so that qualitatively it appears that the Curie temperature may perhaps be proportional to $J_a^{\frac{1}{2}}J_c^{\frac{1}{2}}$ or, in the rhombic case, $J_a^{\frac{1}{2}}J_b^{\frac{1}{2}}J_c^{\frac{1}{2}}$. For a *simple* hexagonal lattice $I_s/I_0=1-[0.068(kT)^{\frac{1}{2}}/J_c^{\frac{1}{2}}J_a]$; similar structures occur in several ferromagnetic manganese compounds and in several magnetically-concentrated salts of the iron group which show some ferromagnetic features at low temperatures.[1] The above expressions suppose that the J's are positive; anisotropy effects are considered separately.

[1] B. H. Schultz, Thesis, Leyden, 1940.

B5. Double Transmission and Depolarization of Neutons. M. BURGY, D. J. HUGHES, AND J. WALLACE, *Argonne National Laboratory.*—As described in earlier reports the production of polarized neutrons was measured by means of the "single transmission effect" which is the relative increase in transmission of an iron block when magnetized. The single transmission effect is simply related to the amount of polarization in the transmitted beam. Recently a series of measurements have been made concerning "double transmission effects" and depolarization of neutron beams. The measurements are made by passing a neutron beam through two blocks of iron, the first block acting as the polarizer, the second as the analyzer. The change in intensity of the transmitted beam with reversal of magnetization in the analyzer is called the double transmission effect. The large effects predicted by theory have been obtained but only when the fields between the magnets are carefully adjusted so that the neutron spin alignment is maintained. Depolarization of neutron beams by unmagnetized iron has been measured by placing thin sheets (of the order of 10^{-3} cm in thickness) of various iron samples between the magnets. The depolarization results give the domain sizes directly and domains ranging from 10^{-3} cm to 7×10^{-5} cm (the latter in severely cold worked material) have been observed.

B6. Neutron Polarization. J. STEINBERGER AND G. C. WICK.—In view of the discrepancy existing between experimental results[1] and theoretical predictions[2] on the polarization cross section p of iron for neutrons, a critical revision has been made of various factors: (a) the coherent nuclear cross section of Fe is about 50 percent larger than previously assumed, (b) the form factor for the d shell may also be larger, especially for Bragg reflections of higher order, (c) while the decrease in the Bragg scattering due to thermal agitation (Debye-Waller factor) has been taken into account, the inelastic diffuse scattering that accompanies it has been neglected so far, although it gives a non-negligible polarization effect.[3] Finally: (d) the assumption that the microcrystals are oriented at random is unjustified in cold rolled materials. When all these corrections are taken into account, the conclusion is reached that there is no serious evidence of any disagreement between theory and experiment.

[1] D. J. Hughes, Bul. Am. Phys. Soc. **22**, 18 (1947).
[2] O. Halpern, M. Hamermesh, and M. H. Johnson Phys. Rev. **59**, 981 (1941); M. Hamermesh, Phys. Rev. **61**, 17 (1942).
[3] O. Halpern, Phys. Rev. **72**, 260 (1947).

B7. The Spectral Emissivity of Iron and Cobalt. H. B. WAHLIN AND HARRY KNOP, *University of Wisconsin.*—The variation of the spectral emissivity for λ6690A has been determined as a function of the temperature. Sharp changes have been found in iron at the A_3 and A_4 points, and a less sharp change between these two points. In cobalt a change has been found at the Curie point. An iron-cobalt alloy also shows changes.

B8. The Photoconductivity of Silver Chloride and Thallium Bromide in the Visible and Near Infra-Red.* WALLACE C. CALDWELL** AND LLOYD P. SMITH, *Cornell University.*—The photoconductivity of silver chloride and thallium bromide crystals increases as the light wave-length decreases from 1.0 to 0.35 micron. Below saturation voltage the photoconductivity of either crystal can be enhanced by exposure to ultraviolet light. Photoconductivity measurements on silver chloride after annealing the crystal in air shows some structure at 0.39 micron. After annealing the crystal in a chlorine atmosphere this structure nearly disappears. Enhancement of photoconductivity by ultraviolet is less for the chlorinated sample. When silver specks are formed in silver chloride, a broad photoconductivity band develops the onset of which is at 0.95 micron. Thallium bromide annealed in air has a sharp photoconductivity peak at 0.44 micron. Possible *mechanisms* for the above effects will be discussed.

* Work partially supported under a contract with the Office of Nava Research.
** National Research Council Predoctoral Fellow. Now at Iowa State College.

B9. Effects of Chlorine and Sulphur on Photoconductivity in Silver Chloride.* FLOYD R. BANKS, JR., *Polytechnic Research and Development Company.*—Silver chloride crystals have been tempered for various times in atmospheres of chlorine and sulphur, and annealed at the rate of 18°C per hour. The effect of chlorine is to suppress greatly the photoconductivity in silver chloride. Thus, samples heated at 430°C for 50 hours in chlorine (760 mm pressure at room temperature) have a photoelectric response in the spectral region surveyed (0.38 to 2 microns) approximately one-thousandth of that for silver chloride tempered in air at the same temperature for 24 hours and annealed at the same rate. Silver chloride heated in evacuated containers with varying amounts of sulphur (from 0.05 percent to about 100 percent by weight), tempered at 430°C for three hours and annealed, shows a photoelectric response analogous to silver sulphide. Peak photoelectric currents of about 0.1 microamperes at approximately 1.2 electron volts are obtained. Silver chloride tempered at 430°C for various times in evacuated

containers and annealed has increased low temperature dark conductivity (compared with samples tempered in air) and reduced (by about 200) photoelectric response.

* Supported by the Office of Naval Research.

Atomic Spectra and X-Rays

C1. Forbidden Lines in O II. L. H. ALLER, *University of Indiana*, C. W. UFFORD, *University of Pennsylvania*, AND J. H. VAN VLECK, *Harvard University.*—Among the strongest and most frequently observed of the forbidden lines found in the gaseous nebulae are the λ3726.16 and λ3728.91 lines of O II corresponding to the $^4S_{3/2}-{}^2D_{3/2}$ and $^4S_{3/2}-{}^2D_{5/2}$ transitions in the ground p^3 configuration. The widespread appearance of this radiation would suggest that a knowledge of the physical parameters characterizing its production (e.g. transition probabilities) might be useful in deciphering the character of the nebulous regions in which it appears in our own and other galaxies. If the electron density is so high that the collisional de-excitations of the upper level are much more frequent than radiative de-excitations, the population of the upper level follows Boltzmann's formula. Then measures of the intensity of the lines together with a knowledge of the electron temperature and the transition probabilities would give us the number of ionized oxygen atoms. For comparison with the theoretical calculations, including spin-spin interaction in addition to intermediate coupling, the ratio of the transition probabilities was measured photometrically in a number of planetary nebulae. The average measured value of the ratio was 0.49 as compared with a theoretical value of 0.58.

C2. The Zeeman Effect of Gold. J. B. GREEN, *Naval Ordnance Laboratory*, AND HOWARD N. MAXWELL, *Kalamazoo College.*—The Zeeman spectrum of gold has been photographed from 2400A to 6500A at a field strength of about 36,000 gauss. Patterns from some 28 classified lines for Au I were measured, about half of which were obtained with much better resolution than that of Symons and Daley. The calculated g values indicate that gold obeys an intermediate type of coupling rather than LS. The patterns for λλ5837, 4437, 4315 indicate these lines belong to Au I rather than Au II as given by Rao. Many of the Au II patterns were unresolved, but λ2990 has a pattern belonging to $\Delta J=0$. Sawyer and Platt have classified it as either $\Delta J=1$ or $\Delta J=0$. λ5726 classified as Au I by Sawyer and Platt has a well resolved pattern with $g=1.803$ for $J=1$ and 1.352 for $J=2$. term. The lines λλ5354, 5380, 5427 are members of the same multiplet and result from transitions between $J=2$, 1, 0 and the level $J=1$ whose g value is 1.780. λ5719 is a $J=2$ to $J=1$ transition with $g=1.744$ for $J=1$ term. The wave-lengths of a number of unclassified lines appearing on the plates have been measured on the assumption that the lines belong to gold.

C3. A Self-Consistent Field for Ca XIII. W. H. DAVIS, A. O. WILLIAMS, JR., AND R. T. BEYER, *Brown University.*—Edlen has identified certain spectrum lines in the sun's corona as the result of transitions in highly stripped calcium ions.[1] A self-consistent field for one of these ions, Ca XIII, has been computed without exchange or relativistic corrections, with the intention of investigating these transitions. The calculations converge rapidly because of the large excess of nuclear charge. The degree of self-consistency attained is at least as good as that specified by Hartree. The state examined is $(1s)^2(2s)^2(2p)^4$; an "excited" state $(1s)^2(2s)(2p)^5$ has also worked out to the same precision. A first approximation to the transition energy between these two (*not* the corona line in question) is 510,000 cm^{-1}, to be compared with experimental values of 594,000 and 618,000 cm^{-1}. Since this value is only the difference between Hartree energy parameters, not between actual energy levels, it is naturally not very good. Calculations of the s.c.f. with exchange and of energy levels are in progress.

[1] Edlen, B. Month. Not. Roy. Astron. Soc. **105**, 323 (1945).

C4. Aurora Spectra Showing Broad Hydrogen Lines. C. W. GARTLEIN, *Cornell University.*—The best spectra of the aurora taken since 1939 with the two prism spectrograph having camera lens 10 cm focal length and $F/1.65$ aperture show lines within 2 to 5A of the positions of $H\alpha$, $H\beta$, and $H\gamma$. All of the lines are approximately 5A broad. Using large scale microphotometer tracings the lines can be separated from the various bands of nitrogen, and the identification as hydrogen lines seems established since no other origin will give these lines as the spectrograms show them. Many spectra taken on the time sequence spectrograph, aperture $F/.8$, show that these lines appear most strongly preceding and during an outburst of aurora. This is in support of Eckersley's theory of ionosphere disturbances. Thus, there is evidence to indicate that the hydrogen is of solar origin and a primary cause of some aurora outbursts and magnetic storms. Spectrographs of high light power and greater dispersion should be used in further studies.

* Research done as part of National Geographic Society—Cornell University Study of Aurora.

C5. A Prospective Means for Studying the Solar and Coronal Spectra in the Vacuum Ultraviolet. J. E. MACK, *University of Wisconsin.*—The great strides made recently in extending the known solar spectrum into the neighborhood of 50,000 cm^{-1} with the aid of rocket-borne spectrographs naturally lead to speculations on the possible extension of the solar and coronal spectra into the vacuum region. There can be little doubt that interesting structure exists there.[1] The only dispersive instrument that has been used for vacuum spectroscopy is the reflection grating; the focal property of the curved mirror is especially useful in gathering light from weak laboratory sources. The sun, with its great intensity, makes quite a different problem, especially in view of the serious incoherent scattering of visible light from the surface, which limits the usefulness of the solar record even at longer wave-lengths. A transmission grating, even with the disadvantage of requiring slit collimation instead of focusing, appears to be a promising alternative. Consideration has been given to the

design and construction problem for a grating 1 mm square traversed by between 200 and 1000 wires.

[1] I. S. Shklovsky, Astronomical Journal of the Soviet Union **22**, 249 (1945).

C6. Low Angle Scattering of Colloidal Solutions. PETER G. BERGMANN, *Syracuse University.*—In analogy to the diffraction patterns of liquids, the low angle pattern of colloidally dispersed matter must depend on both particle size and particle distribution. The effect of the distribution will be appreciable whenever particle size and distance between neighbors are of the same order of magnitude, in other words in highly concentrated solutions. If the colloidal particles are all alike in size and shape, then the intensity of the diffraction pattern at each point will be the product of the form function of the particles and the Fourier transform of the particle distribution. An experimental determination of the latter function is then possible, at least in principle. The case of a size and shape distribution will also be discussed.

C7. The Interpretation of Small Angle X-Ray Scattering Observed from Argon. GEORGE H. VINEYARD, *University of Missouri.*—Measurements of the x-ray scattering from argon[1] at many different pressures and temperatures have shown an unexpectedly large scattering at small angles from both liquid and vapor in the neighborhood of the critical point. It has been suggested that this may be due to pre-transition phenomena such as the formation of minute droplets of liquid in the vapor, when near the condensation point, and the reverse for liquid near its boiling point.[1] By means of a relation due to Zernike and Prins between the scattering at very small angles and the mean square density fluctuations of a substance, the scattering at essentially zero angle can be computed. The small angle scattering to be expected from droplets of one phase immersed in another is also computed. From these results and the present data on argon an estimate of the size and frequency of occurrence of droplets is made, and it is found that the droplet would have to contain so few atoms that its characterization as a distinct phase is probably meaningless. Preferable models of the apparent atomic arrangement are discussed.

[1] A. Eisenstein and Gingrich, Phys. Rev. **62**, 261 (1942).

C8. Determination of h/e by X-Rays. GUENTER SCHWARZ AND J. A. BEARDEN, *Johns Hopkins University.*—New measurements have been made on the high frequency limit of the continuous x-ray spectrum near 8000 and 10,000 volts. In most of the work sealed-off x-ray tubes with Cu and W targets were used. Our present measurements are characterized by a highly stabilized source of high voltage and a double crystal spectrometer with crystals of theoretical resolving power. The resulting isochromats rise sharply and considerably more detail is present in the structure near the high frequency limit than was noted in our earlier measurements.[1] In one series of experiments a W target was maintained at a temperature above 1300°C in order to eliminate possible effects due to surface contaminations. If we apply the work function correction the values of h/e determined from all of our experiments lie within the range from 1.3783 to 1.3787 $\times 10^{-17}$ erg sec./e.s.u. If the second derivative method had been used in determining the limit in our earlier measurements[1] the average value of h/e would have been 1.3786 $\times 10^{-17}$, is excellent agreement with our present determination.

[1] J. A. Bearden and G. Schwarz, Phys. Rev. **59**, 934(A) (1941).

C9. Bioelectric Potentials as an Index of X-ray Action. A. A. BLESS, *University of Florida.*—Romanoff and Bless[1,2] have investigated the variation of the biolectric potential of the avian blastoderm and also the variation of the size of the blastoderm as a function of x-ray dosage, and have found that these variations follow the same pattern. A number of investigators have found a direct correlation between the magnitude of the potential and the vital activity of the organism. Recent results obtained in this laboratory show that the functional relations between the effects of x-rays on the vital activity of corn seeds and the effects of the same rays on the bioelectric potential are similar. It seems very reasonable to conclude that the biological effects of x-rays at least, if not of all types of radiation, may be traced through the variations of the electrical potentials of the material. This provides in many cases very rapid and reliable means of measuring the biological action of the rays without introducing new variables which is the case when the growth of organisms is used as a measure of biological effects.

[1] A. L. Romanoff and A. A. Bless, Proc. Nat. Acad. Sci., **8**, 306 (1942).
[2] A. A. Bless and A. L. Romanoff, J. Cell. and Comp. Physiol., **21**, 117 (1943).

Precision Spectroscopy of Nuclear Gamma-Rays with a Focussing Curved Quartz Crystal. J. W. M. DUMOND, DAVID LIND, AND B. B. WATSON, *California Institute of Technology.*

Gases at Microwave Frequencies; Magnetic Resonance

D1. Electrical Breakdown between Coaxial Cylinders at Microwave Frequencies.* MELVIN A. HERLIN AND SANBORN C. BROWN, *Massachusetts Institute of Technology.*—The proposed criterion for breakdown of a low pressure gas at microwave frequencies is that the ionization rate equal the diffusion rate for electrons.† This principle has been applied to compute the breakdown of air in coaxial cylinders using ionization rate data obtained from breakdown experiments between parallel plates. Agreement between computed and measured curves supports the validity of the above criterion for breakdown. The method of computation is illustrative of the general problem of computing breakdown voltages for tubes of arbitrary shape and field configuration using ionization rates obtained from parallel plate, uniform field breakdown.

* This work has been supported in part by the Signal Corps, the Air Materiel Command, and O.N.R.
† Melvin A. Herlin and Sanborn C. Brown, Bull. Am. Phys. Soc. **23**, 13 (1948).

D2. A Method of Measuring the Complex Conductivity of an Ionized Gas at Microwave Frequencies.* EDGAR EVERHART AND SANBORN C. BROWN, *Massachusetts Institute of Technology.*—The complex conductivity of an ionized gas, σ_c, is defined as the ratio of the electron current density to the electric field. It does not include the displacement conductivity, $j\omega\epsilon_0$. In order to measure σ_c, a high frequency discharge is created between parallel plates. By microwave impedance methods one can measure the admittance of the discharge. The admittance is expressible in terms of an integral over σ_c'. According to existing theories σ_c is proportional to the electron concentration, which is itself a sinusoidal function of position between the parallel plates. It is possible to compute the admittance of a discharge as a function of electron concentration. These computed curves have the same qualitative form as those obtained experimentally. A characteristic of both theory and experiment is that the susceptance of the discharge goes through zero and changes sign at sufficiently high values of electron concentration.

* This work has been supported in part by the Signal Corps, the Air Materiel Command, and O.N.R.

D3. Measurements of the Complex Dielectric Constant of Gases at Microwaves. HAROLD LYONS, GEORGE BIRNBAUM, AND S. J. KRYDER, *National Bureau of Standards.*—A method for the measurement of the complex dielectric constant of gases and vapors has been developed in the microwave range. A frequency-modulated signal is simultaneously applied to two resonant cavities and their response curves presented on a cathode-ray tube. The cavities are adjusted to have the same resonance frequency, with one cavity evacuated. Gas is then admitted to the evacuated cavity causing its resonance frequency to shift. The difference in resonance frequency is measured by aligning two frequency markers, which appear as intensified spots on the CRT, on top of each resonance curve. The loss angle is measured by determining the cavity Q-shift by aligning the frequency markers at the half-power points of the resonance curve. Results obtained for $(\epsilon-1)\times10^4$ at approximately 9000 Mc/sec. at NTP are: helium -0.710 ± 0.009, $CO_2-9.88\pm0.02$, $N_2-5.87\pm0.02$, $O_2-5.32\pm0.02$, Air -5.77 ± 0.01. Values for water vapor, and its dipole moment, were checked. The dielectric constant and loss angle of ammonia was found. The susceptibility of ammonia was not linear with pressure as would be expected from collision broadening of the ammonia absorption line. The resonant cavity method, when the proper mode is used, is insensitive to adsorption of vapors on the walls of the cavity.

D4. A Comparison of the g Value of the Electron in Hydrogen and Deuterium. EDWARD B. NELSON AND JOHN E. NAFE, *Columbia University.*—The ratio of the h.f.s. separation of the ground state of H to that of D is less than the theoretical value by 0.017 percent. The ratio, $(g_J)_H/(g_J)_D$, of the atomic g-factor of the $^2S_{\frac{1}{2}}$ state in H to that of D, has been measured in the search for an effect which might explain the discrepancy. The frequencies f_H, of the transition $(1, 0\leftrightarrow1, -1)$ in H. and f_D, of the transition $(3/2, -1/2\leftrightarrow3/2, -3/2)$ in D, were observed in the same magnetic field by the atomic-beam magnetic resonance method and the ratio $(g_J)_H/(g_J)_D$ was computed from the Breit-Rabi[1] formula. The principal uncertainty is caused by the drift of the magnetic field. The average of thirty-six observations in four runs in which f_H and f_D were measured alternately is $(g_J)_H/(g_J)_D=1.000004\pm0.000025$. The average of three runs in which the two resonances were observed simultaneously is $(g_J)_H/(g_J)_D=0.999991\pm0.000010$. The uncertainty indicated in each result is the mean deviation of the residuals. We conclude that the atomic g-factors of H and D differ by less than ±0.001 percent.

[1] G. Breit and I. I. Rabi, Phys. Rev. 38, 2082 (1931).

D5. A Precision Magnetic Field Stabilizer.* H. S. SOMMERS, JR., P. R. WEISS, AND W. HALPERN, *Rutgers University.*—The work at Rutgers University on measurements of nuclear magnetic moments by resonance absorption requires precision control of the field of a large electromagnet. A pilot model electronic current stabilizer for a ½-kw magnet has been built and tested. This unit monitors the current by the drop in a standard resistor in series with the magnet. The difference between this voltage and a preset potentiometer voltage is converted to a.c. in a Brown synchronous vibrator. The amplified difference signal is converted back to d.c. in a detector which maintains the sign of the original d.c. signal, and is used to drive the power amplifier which excites the magnet. The power amplifier is a low noise, broad-band unit with ½-kw output, made from a commercial mg set by addition of electronic feedback.** This unit keeps the current fluctuations to a ratio of less than 5×10^{-6} peak to peak d.c. for all frequencies higher than 1/min. No measurements were made on the longer period drift. The loop requires ½-sec. to correct a step change of 0.02 percent and 2 sec. to correct a step of 1 percent.

* This work supported by O.N.R. and the Rutgers University Research Council.

** H. S. Sommers, Jr., and P. R. Weiss, W. Halpern, Bul. Am. Phys. Soc. 23, No. 2, Abstract E-1 (1948).

D6. Paramagnetic Resonance Absorption in Single Crystals of Chrome Alum and in Aqueous Solutions of Manganous Salts.* DAVID HALLIDAY AND JOHN WHEATLEY, *University of Pittsburgh.*—Paramagnetic resonance measurements at 9375 mc/sec. on single crystals of $CrNH_4(SO_4)_2\cdot12H_2O$ have recently been reported by Weiss, Whitmer, Jen-Sen Hsiang, and Torrey[1] and interpreted by them to yield a splitting of the lowest level of Cr^{+++}, due to crystalline Stark effects, of 0.15 ± 0.01 cm^{-1}. We have made measurements on both this salt and $CrK(SO_4)_2\cdot12H_2O$ for two crystalline orientations at room temperature. Resonance absorption for the latter salt has been studied at 90°K also. For the crystal orientation used by Weiss, etc. two independent values of the splitting may be determined for each salt; for the second crystal orientation a third splitting value may be determined, using a theory due to Kittel. The mean splittings are approximately:

$CrNH_4(SO_4)_2\cdot12H_2O$	0.13 cm^{-1}	25°C
$CrK(SO_4)_2\cdot12H_2O$	0.12 cm^{-1}	25°C
$CrK(SO_4)_2\cdot12H_2O$	0.17 cm^{-1}	90°K

Paramagnetic resonance absorption has also been observed for aqueous solutions of manganous salts contained in a thin-walled capillary placed along the axis of a TE_{001} mode cavity[2] resonating at 9375 mc/sec.

* Assisted by ONR.
[1] P. R. Weiss, C. A. Whitmer, H. C. Torrey, and Jen-Sen Hsiang, Phys. Rev. 72, 975 (1947).
[2] C. H. Collie, J. B. Hasted, and D. M. Ritson, Proc. Phys. Soc. 60, 71 (1948).

D7. Paramagnetic Resonance Absorption Line Shapes for Single Crystals of $CuSO_4 \cdot 5H_2O$.* JOHN WHEATLEY AND DAVID HALLIDAY, *University of Pittsburgh* AND J. H. VAN VLECK, *Harvard University*.—Paramagnetic resonance absorption in single crystals of $CuSO_4 \cdot 5H_2O$ at frequencies near 9375 mc/sec. has been studied as a function of the steady external magnetic field and of the orientation of the crystal. As rotation axes (*a*) the magnetic axes of the crystal and (*b*) one of the two perpendicular microscopic tetragonal axes have been used. The high frequency field and the rotation axis were both perpendicular to the steady field. The variation with orientation of the effective *g* factor, reported by Arnold and Kip[1] and interpreted by one of us[2] in terms of exchange coupling between Cu^{++} ions, has been confirmed. A variation of absorption line breadth with orientation has been found, the narrowest and broadest lines having widths at half-amplitude of 75 and 220 oersteds. An approximate theory for this effect, based on the assumption that the exchange energy is a function only of the total spin, will be presented. Finally, a study of the shapes of absorption curves has been made which offers general confirmation of the theory of exchange narrowing recently presented by Gorter and Van Vleck.[3]

* Assisted by ONR.
[1] Arnold and Kip, Bull. Am. Phys. Soc. 23, No. 2, F5 (1948).
[2] J. H. Van Vleck, Bull. Amer. Phys. Soc. 23, No. 2, G8 (1948).
[3] C. J. Gorter and J. H. Van Vleck, Phys. Rev. 72, 1129 (1947).

D8. Microwave Resonance Absorption in Potassium Chrome Alum.* R. T. WEIDNER, P. R. WEISS, AND C. A. WHITMER, *Rutgers University*.—The paramagnetic resonance absorption in single crystals of potassium chrome alum has been measured at a frequency of 9375 mc/sec. The measurements were made with three different orientations of the crystalline axes with respect to the d.c. magnetic field. These orientations were: the d.c. field perpendicular to (*a*) the 111-face, (*b*) the 100-face, (*c*) the 110-face. Crystals of this salt diluted with aluminum potassium alum were also measured in these same orientations. The absorption patterns show that dilution decreases the Stark splitting of the ground state of the chrome ion. In addition, there is a marked decrease in the absorption peaks of the diluted salt compared to those of the undiluted salt.

* This work has been supported by the Rutgers Research Council, the Research Corporation, and the U. S. Navy.

D9. Microwave Resonance Absorption in Ferromagnetic Semiconductors. WILLIAM H. HEWITT, JR., *Bell Telephone Laboratories*.—The high resistivity of ferrites suggests that measurements of ferromagnetic resonance absorption may be of particular interest. The absorption effect is expected to be large in comparison with that in conducting ferromagnetic materials, because the greater skin depth permits a relatively larger volume of the specimen to absorb. Measurements were made at 23958 megacycles with a thin plane specimen of zinc-manganese ferrite $(ZnO)(MnO) \cdot 2Fe_2O_3$ fitted across the wave guide. It has a resistivity of 2350 ohm-cm, initial permeability of 1700 at 1000 cycles, and saturation magnetization M_s of 200. The input impedance looking into the specimen was determined as a function of the applied magnetic field when the sample was backed first by a short and then by a quarter wave-length section. With this data, the real and imaginary parts of both the permeability and the dielectric constant were separated. Using[1] $\omega_0 = \gamma(BH)^{\frac{1}{2}}$ where $\gamma = ge/2mc$ and H(corrected for demagnetization) is the field strength when $j\mu_2$ is maximum we find a *g* value of 2.12. With a small sphere of a similar ferrite with a higher resistivity (4.2×10^4 ohm-cm) a *g* value of 2.16 is obtained using $\omega_0 = \gamma H$.

[1] C. Kittel, Phys. Rev. 73, 155 (1948).

D10. The Electric Quadrupole Moments of the Chlorine Nuclei.* LUTHER DAVIS, JR. AND CARROLL W. ZABEL, *Massachusetts Institute of Technology*.—The hyperfine structures of the $^2P_{3/2}$ ground state of Cl^{35} and Cl^{37} have been determined by the atomic-beam magnetic resonance method. For both isotopes, $I = J = 3/2$, there are four energy levels at zero magnetic field, corresponding to $F = 0$, 1, 2, and 3, given by the relation $W = a(C/2) + (b'/24)C(C+1) + c[C^3 + 4C^2 + 4(C/5)]$ where $C = F(F+1) - I(I+1) - J(J+1)$, a is the magnetic dipole, b' the electric quadrupole, and c the magnetic octupole interaction constant. The measurement of the separations between adjacent levels, $a - b' + 153.1c$, $2a - b' + 54.2c$, $3a + b' + 171.3c$, allows the determination of the interaction constants a, b', and c.

$a_{35} = 205.288 \pm 0.030$ Mc, $a_{37} = 170.686 \pm 0.030$ Mc,
$b'_{35} = 55.347 \pm 0.070$ Mc, $b'_{37} = 43.256 \pm 0.070$ Mc,
$c_{35} = 380 \pm 500$ c.p.s. $c_{37} = 20 \pm 500$ c.p.s.

After including small relativity corrections the electric quadrupole moments calculated from the ratio b'/a are $Q_{35} = -(7.921 \pm 0.05) \times 10^{-26}$ cm², and $Q_{37} = -(6.189 \pm 0.05) \times 10^{-26}$ cm². An unusual method was used to observe the $F = 1$ to $F = 0$ transition. The refocused beam intensity, due to transitions between $F = 1$ and $F = 2$, was diminished by superimposing a second oscillating field corresponding to the transition from $F = 1$ to $F = 0$.

* This work has been supported in part by the Signal Corps, the Air Materiel Command, and O.N.R.

D11. A Recording Microwave Refractometer. GEORGE BIRNBAUM, *National Bureau of Standards* (*Introduced by Harold Lyons*).—This instrument can measure and continuously record the dielectric constant (or index of refraction) of low loss gases, liquids, and solids. A sawtooth frequency-modulated signal is simultaneously applied to two cavity resonators, one used as a reference cavity, the other to contain the dielectric sample. The output of the cavity resonators yield resonance responses which are amplified in separate channels. These resonance responses are sharpened and applied to a trigger tube which is turned on by one pulse and turned off by the other. The

average output current of the trigger tube is metered. For a linearly frequency-modulated output from the microwave oscillator, the trigger-tube output current is proportional to the frequency difference between the two cavities. It appears possible with some refinements to detect a very small change in frequency of 1 part in 10^8. The output of the circuit is made to drive a recording meter and is thus capable of following rapid changes in index of refraction. Modifications are possible which will allow recording of the absorption coefficient or loss angle of dielectrics. The instrument should lend itself to microwave propagation measurements.

Theoretical Physics

E1. A Special Property of the Electron's Gyromagnetic Ratio. JOSEPH W. WEINBERG, *University of Minnesota.*—Theoretical cross sections for electromagnetic processes at high energies for charged particles of spin $h/4\pi$ and magnetic moment $g(eh/4\pi mc)$ are largely proportional to powers of $(g-1)^2E^2$,[1] and are markedly reduced when, as for the electron, $g=1$. This is explained by the classical picture of a charge e, of magnetic moment M, which, in a rest system, $(v=0,\ c=1)$, obeys $dv/dt=(e/m)E$, $dM/dt=g(e/m)M\times H$. Relativity requires the existence of an electric moment $P=M\times v$, which vanishes in a rest system, but has a finite rate independent of g. Acceleration of the moments produces magnetic and electric dipole radiation, whose destructive interference cancels the dominant contribution when $g=1$. This accounts for those features of the quantum cross sections properly ascribed to radiation. Additional g-sensitivity due to the deflection process can be inferred from the quantum picture of momentum transfer as mediated by photons. The classical spectrum has been investigated for the case of impact radiation in a Coulomb field, where the moments are submitted to sudden changes $\delta P=M\times\delta v$, $\delta M=gM\times[\delta v\times v]$. Modified and reinterpreted by the correspondence principle, the result agrees quantitatively with the field-theory cross section for radiation after deflection through $\delta v/v$, divided by the corresponding elastic scattering cross section.

[1] W. Pauli, Jr., Rev. Mod. Phys. 13, 203 (1941).

E2. An Invariant Quantum Electrodynamics. JULIAN SCHWINGER, *Harvard University.*—In order to isolate the divergent aspects of current quantum electrodynamics[1] in a manner that is Lorentz- and gauge-invariant, it is necessary to employ a formulation of the theory that preserves these invariant features at all stages. This has been achieved by a field theory generalization of Dirac's many-time formalism for particles interacting with the electromagnetic field, in which infinitesimal spatial volume elements play the role of particles. An appropriate canonical transformation enables one to exhibit the self-energy modifications of electron and photon properties, which, for the electron, correspond to the addition of an invariant, though divergent, electromagnetic mass. Self-energy effects for the photon vanish identically, in contrast with previous theories. The radiative corrections to the interaction energy of an electron with an external field are obtained in properly covariant form. In particular, we confirm the additional spin magnetic moment, $\delta\mu/\mu=(1/2\pi)(e^2/\hbar c)$, obtained previously from a non-invariant formulation.

[1] J. Schwinger, Phys. Rev. 73, 415 (1948).

E3. Variational Principles for Diffraction Problems. HAROLD LEVINE AND JULIAN SCHWINGER, *Harvard University.*—The diffraction of a scalar plane wave by an aperture in a plane screen is described in terms of two variational principles. An important role is assumed by the amplitude of the diffracted spherical wave at large distances from the aperture. For a boundary condition which requires that the wave function vanish on the screen, explicit expressions for the amplitude are obtained, which have the property of being stationary with respect to variations relative to the correct values of (1) the wave functions in the aperture, and (2) the discontinuities in the normal derivative of the wave functions at the screen, arising from a pair of incident waves. In addition, these expressions are independent of the scale of the wave functions. From the detailed application to a problem for which exact results are available,[1] it appears that when combined with suitable trial functions, the variational principles provide approximate, yet accurate expressions over a wide range of frequencies for the diffracted amplitude and transmission cross section. The formulation is extended to the diffraction of an electromagnetic plane wave, with the assumption of a perfectly conducting screen.

[1] C. J. Bouwkamp, "Theoretical and numerical calculation of diffraction by a circular aperture," Dissertation (In Dutch), Groningen, 1941.

E4. A Relativistic Cut-Off for Quantum electrodynamics. R. P. FEYNMAN, *Cornell University.*—According to Lienard and Wiechert, the classical electromagnetic potentials at one point depend on the charges and currents at another point at a distance r at a time earlier by $t=r/c$. The influence is proportional to the retarded part of the Dirac delta-function of the square of the four-dimensional interval $S^2=t^2-r^2/c^2$. We replace this delta-function by a finite arbitrary function of S^2 of very small width a^2. When the corresponding alteration is made in quantum mechanics, quantities which previously were infinite turn out finite. The self-energy of a free electron behaves as a change in mass. The change depends logarithmically on a. The electromagnetic correction to a scattering cross section and the self-energy of a bound electron also depend logarithmically on a. When expressed, however, in terms of the corrected mass of the free electron, these quantities are not sensitive to a and remain finite as a approaches zero. They then agree with the results of Bethe, Weisskopf, Lewis, and the theory of Schwinger,* except for terms corresponding to polarization of the vacuum. These terms are not made convergent by the above procedure. The procedure is relativistically invariant.

* See, for example, Bull. Am. Phys. Soc. 23, No. 2, Z-8, Z-9, Z-10 (1948); also H. W. Lewis, Phys. Rev. 73, 173 (1948).

E5. Boundary Conditions as Relativistic Interaction. MARCOS MOSHINSKY AND E. P. WIGNER.—The simplest type of relativistic interaction between two particles, which

necessarily leads to convergent results, can best be formulated in an eight-dimensional configuration space-time. Both time derivatives of the wave function are given by the corresponding free particle equation at all points in configuration space, and it is postulated that the wave function be regular everywhere except at the points where the space-time coordinates of the particles coincide. At these points, the wave function can have a singularity. It then turns out that the relativistic invariance and the conservation law of probability determine the singularity up to a constant: For two Klein-Gordon particles this singularity gives rise to a scattering cross section $4\pi a^2/(1+k^2a^2)$; where a is the constant in question and k the wave number of the relative motion of the two particles. Other types of interaction can be formulated in Fock space, the simplest ones being the disintegration of one particle into two (and the reverse process), and the transformation of two particles into two particles of different masses, etc. In this last case the difference of the squares of the two masses must be the same before and after collision. The apparent impossibility of incorporating the ideas of the "hole theory" into low dimensional configuration spaces makes it unlikely that these considerations will enable one to avoid introducing functionals.

E6. On the Integral Equations of Motion. ELLIOT T. BENEDIKT, *North American Aviation.*—The equations of motion for a particle and for a general mechanical system will be set up in integral form. A solution of the above equations by an iteration process will be discussed for the case of a particle moving under the combined action of a time-dependent and a position-dependent conservative force. The above procedures will be applied to the case of a particle moving in a central Newtonian field, under the action of a (finite) time-dependent force.

E7. Statistical Error in Transmission Measurements. M. E. ROSE AND M. M. SHAPIRO, *Clinton National Laboratory.*—In certain exponential absorption experiments it is important to achieve minimum statistical error in a limited time or to minimize the counting time required to measure the absorption coefficient with a preassigned accuracy. The conditions required to attain these ends, i.e., the geometry for optimum transmission and the optimum apportionment of counting times among the incident and transmitted beams and background, have been investigated for a wide range of relative backgrounds (10^{-3} to 10^{2}) and for two geometries: (1) beam area fixed, absorber thickness alone is varied; (2) beam area and absorber thickness are both disposable parameters, while the total amount of absorber intercepting the beam remains fixed. In both cases the flux density and background rate are assumed constant. The optimum transmissions are shown to be, in general, considerably small than those commonly used in absorption experiments. Thus, for case (1), a useful rule is to employ a transmission of about 0.1 for low backgrounds, 0.2 for moderate backgrounds, and 0.3 for high backgrounds. The following have also been determined: (*a*) minimum statistical error for a given total counting time; (*b*) statistical error and the best distribution of counting times for non-optimum geometry; (*c*) sensitivity of the accuracy or total counting time to deviations from optimum transmission.

E8. Symmetry Properties of Ψ-functions. G. J. YEVICK, *Stevens Institute of Technology.*—The Young symmetry operator[1] proves to be a simple but powerful tool in the analysis of the n-body problem in quantum mechanics. For Ψ-functions with symmetries other than completely symmetric (Einstein-Bose statistics) or completely antisymmetric (Fermi-Dirac statistics), Wigner has suggested that it may be possible to construct the interaction between a collection of non-mutually interacting particles and the particles which create or destroy them, in such a manner that the first collection is automatically forced into the desired symmetry. It appears that this can be done with the aid of the Young symmetry operator. The full consequences of such a procedure have not yet been worked out. In order to apply such a method—especially for the involved problem of second quantization—a complete analysis of the symmetry properties of the Ψ-functions for a fixed number of particles has been carried out. In addition to the Young symmetry operator, the Laplace identity relations for determinants provide the general solution to such an analysis.

[1] See E. G. Weyl, *Group Theory and Quantum Mechanics*, Chapter V.

E9. Irreversibility and Quantum Mechanics.* L. TISZA, *Massachusetts Institute of Technology.*—The formalism of quantum mechanics is symmetric with respect to future and past, whereas in thermodynamics the increase in entropy marks an asymmetry. The numerous attempts at reconciling the two points of view seem not quite satisfactory. Some progress has been achieved on the following lines: the increase in entropy is a consequence of the destruction of phase relations connected with the limitations of the observer dealing with molecular systems. These limitations are in addition to those inherent in quantum mechanics and can be expressed as follows: (1) Only such macroscopic operations and measurements are feasible which may be expressed in the Hilbert space of a single particle and which affect all similar particles identically. (2) The *principle of thermal uncertainty* states that a completely closed system is an inadmissible idealization, since the system must interact at least with the walls and other devices by which it is shielded from the surroundings. The resulting "thermal noise" is essential for the increase in entropy, which would be impossible if the temporal behavior of the system were determined by a rigorously constant Hamiltonian operator. The situation is analogous to that in communication where the information contained in the signal is decreased only because of noise.

* This work has been supported in part by the Signal Corps, The Air Materiel Command, and the O.N.R.

E10. Note on the General Properties of S Matrices. T. S. CHANG, *Carnegie Institute of Technology* (*Introduced by F. Seitz*).—The general properties of S matrices are re-

examined. First, we show that the equation $S\dagger S=1$ expressing the unitariness of the S matrix is not true in general, and must be modified by the introduction of a non-positive-definite weight w. This corresponds to the fact that there are negative probability densities in the relativistic theory of elementary particles. Next, S is determined in terms of wave matrices Ψ representing outgoing and incoming scattered waves (plus incident waves), and the commutability between S and the Hamiltonian (if any) is discussed. Next, a difficulty connected with the description of the discrete states by the wave matrices at $S=0$ and at pure imaginary values of the magnitude of the momentum is pointed out. Finally, with S assumed to transform in a Lorentz transformation as Ψ should, the wave matrices Ψ in the S matrix theory are shown to transform only approximately correctly in the x representation (i.e., they transform correctly only after the neglect of terms 0 (γ^{-2}), γ being the distance between the scatterer and the scattered particle).

On a Coarse-Grained Density in Phase Space and Its Relation to Transport Phenomena. J. M. RICHARDSON, *Bell Telephone Laboratories.*

Cosmic Rays

EA2. Directional Distribution of the Total Cosmic Radiation at Atmospheric Heights up to 10-cm Hg at Princeton.* JOHN WINCKLER, *Princeton University.*—The intensity distribution of cosmic-ray particles as a function of zenith and azimuth was measured by unshielded Geiger counters carried by balloons. Four threefold telescopes directed in the vertical, horizontal, and at 30° and 60° zenith angles, were used. Additional counters registered air showers. Pressure, temperature, orientation, and cosmic-ray events were transmitted to a ground recording station by a 15-channel radio telemetering system.

A preliminary analysis of the data indicates the following facts:

(a) The sea level $\cos^2\theta$ dependence on zenith angle θ is modified near 10-cm Hg to a more isotropic distribution, in which the horizontal intensity is 20 percent of the vertical and the intensity at $\theta=60°$ is 50 percent (showers excluded).
(b) Within the statistical accuracy of the data there is no certain azimuthal effect at any zenith angle.
(c) Total air showers are 10 percent of the vertical intensity. Showers accompany in equal numbers coincidences at $\theta=0$, 30°, and 60°, and in smaller numbers at $\theta=90°$.
(d) The vertical intensity-altitude curve agrees with the results of Pfotzer.

It is planned to continue the experiments at higher altitudes ($\approx$1-cm Hg) using lead filters and more efficient shower protection.

* This work was performed under contract with the Office of Naval Research.

EA3. East-West Asymmetry, Zenith Angle Dependence, and Flux Measurements of Cosmic Rays up to 36,000 Feet.* JAMES F. JENKINS, JR., *Johns Hopkins University.*—The counting rates of counter telescopes with 0, 2, 8, and 10 cm of Pb were measured in B-29 aircraft at Inyokern, California (43° N geomagnetic latitude) from 2250 to 36,000 feet. For the hard telescopes (8- and 10-cm Pb) the data were taken at 0° and 45° off the vertical and at north, east, south, and west geographical directions in the 45° position. For the soft telescopes (0- and 2-cm Pb) the data were taken only in the vertical position. The counting rates of two pairs of G-M tubes were also measured at these altitudes—one pair under 2-cm Pb and the other under no Pb. Asymmetries of west over east in the order of 10 percent were observed at altitudes greater than 20,000 feet for penetrating particles. In this same altitude range, showers showed a west to east asymmetry of from 3 percent to 18 percent. From a consideration of the two points, (0° and 45°) at each altitude, on the zenith angle curve, it is seen that if a $\cos^n\theta$ relationship is assumed, that $n=2$ up to 18,000 feet, and then falls off toward $n=0$, the value at 36,000 feet being $n\sim1$. This is in accordance with the findings of Swann.[1]

* This work has been made possible by the support of the Navy Bureau of Ordnance.
[1] W. F. G. Swann, Rev. Mod. Phys. 11, 242 (1939).

EA4. Density Spectrum and Latitude Dependence of Extensive Air Showers at Sea Level.* S. F. SINGER, *Johns Hopkins University.*—An arrangement of four closely spaced trays, each containing ten Geiger counters, was used to investigate the particle density spectrum of extensive air showers (Auger showers). The measurements were carried out in Silver Spring, Maryland (geomagnetic latitude 50°), and in the Canadian Arctic ($\lambda=80°$ to 90°). In both cases the material above the counters was 0.6 g/cm² of wood. Master coincidences were formed between the *parallel* outputs of three counter trays (A, B, and C) and subsidiary coincidences between the master coincidence pulse and the *individual* Geiger counters in two trays (A and D). This served to speed up the process of data taking and also gives information about the structure of showers. No latitude dependence was found over the range of densities which could be resolved by the apparatus. The method of computation of a power law spectrum for particle densities, also correlations with a shielded ion chamber, and the theoretical implications of the results will be discussed.

* This work has been made possible by the support of the Navy Bureau of Ordnance.

EA5. Neutron Densities in the Atmosphere as a Function of Latitude and Altitude.* J. A. SIMPSON, JR., *University of Chicago.*—The densities of neutrons with energies greater than 0.3 ev were measured in aircraft using boron trifluoride proportional counters. It may be shown that these measurements correspond to free space measurements. The total vertical intensity of charged particles traversing 5 g/cm² and the vertical intensity of mesons traversing 20 cm of lead were also measured at the same time. The factor of increase of neutron density between 0° and 53° N magnetic latitude is much greater than the

corresponding latitude factors for the total vertical intensity or for the so-called "soft" vertical intensity. At 45-cm Hg pressure the factor for neutrons is 2.3±0.1; at 30-cm Hg it is 2.8±0.1; at 20.0-cm Hg it is 3.3±0.2; and at 15.0-cm Hg it is 3.5±0.2. The total exponential absorption of the neutron producing radiations corresponds to: 192±8 g/cm² at 0° and 19° N; 181±7 g/cm² at 40° N; 160±7 g/cm² at 53° N. All measurements were made between pressure altitudes of 10^4 and 3.7×10^4 feet. Some measurements of neutron production in aluminum and lead have been made. The results and interpretation of the above data will be discussed.

* A portion of this work was supported by the Office of Naval Research.

EA6. A Possible Circulation of Cosmic-Ray Helium Particles Around the Earth.* W. F. G. SWANN, *Bartol Research Foundation.*—Chandrashekhar Aiya found a sudden drop in cosmic-ray intensity at 21 cm of lead thickness at an altitude of 3110 feet on the magnetic equator. W. F. G. Swann and P. A. Morris found a similar drop at 22 cm of lead at Bocayuva at an altitude of 2300 feet near the magnetic equator, but found no such drop at Swarthmore, Pennsylvania.

A drop of the kind cited indicates a sharp peak in the spectral energy distribution curve at the top of the atmosphere, the peak occurring at an energy necessary for mesotrons to penetrate to the point of observation and through the thickness of lead concerned. Such a peak invites the assumption of heavy nuclear particles circumscribing the earth at the magnetic equator and breaking up into mesotrons. It is shown that a single ionized helium primary with energy such as to enable it to circulate around and near the earth at the equator would, on breaking up into 40 mesotrons, endow each mesotron with an energy of 1.2×10^9 ev. The mesotron energy necessary to penetrate at Bocayuva and through the 20 cm of lead is 1.3×10^9 ev.

* Assisted by the Office of Naval Research and by the National Geographic Society.

EA7. Rocket Borne Cloud Chamber I. S. E. GOLIAN, C. Y. JOHNSON, AND M. KUDER, *Naval Research Laboratory.*—A cloud chamber of 6-inch diameter was sent aloft in a V-2 rocket launched on January 22. The chamber contained argon at 2-atmospheres pressure and 2 lead plates of 1-cm thickness. Expansions were made every 25 seconds without counter control. Twelve photographs were taken at high altitude. A description of the apparatus and of some of the photographs will be given.

EA8. Rocket Borne Cloud Chamber II. G. J. PERLOW, E. KRAUSE, AND C. SCHROEDER, *Naval Research Laboratory.*—Additional analysis of the photographs of the previous abstract will be given. Particular emphasis will be placed on the results of counter experiments made in other rocket flights.

Neutrons

F1. Diffusion of Neutrons without Change in Energy in a Medium with Anisotropic Scattering. M. A. GREENFIELD, *North American Aviation.*—Using Mark's[1] method of solving the transport equation for diffusing neutrons with anisotropic scattering, the writer has considered the case for a semi-infinite absorbing medium containing sources. It is shown that the neutron density has a spatial dependence as $e^{K_0 z}$ where K_0, reciprocal of the diffusion length, is given by:

$$\frac{1}{2l_aK_0}\ln\frac{1+K_0l}{1-K_0l}=\frac{1+(3b/l_al_cK_0^2)}{1+(3b/l_lK_0^2)},$$

l, l_a, l_c, b are, respectively, the total, scattering, capture mean free paths and the average cosine of the scattering angle. If b is 0, the expression reduces to one given by Placzek.[2] In the case treated by Mark, the neutron density gradient is essentially constant a few mean free paths from the boundary; a constant gradient suffices to supply neutrons leaking out at the boundary. For an absorbing medium the density gradient increases away from the boundary to supply the absorption load as well as the leakage neutrons.

[1] J. C. Mark, "Milne's problem for anisotropic scattering," Nat. Research Council of Canada, 1947.
[2] G. Placzek and G. M. Volkoff, "Notes on diffusion of neutrons without change in energy," Nat. Research Council of Canada, 1943.

F2. Neutron Diffusion in Shielding Materials.* P. C. GUGELOT AND M. G. WHITE, *Princeton University.*—Neutron absorption experiments have been carried out to obtain information on the shielding qualities of different concrete blocks of 46×46×46 cm. A steel tube of 7.5-cm diameter through the center of the block and parallel to the neutron beam could be filled with concrete slabs of 5.3-cm thickness. Silver foils with or without Cd absorbers were placed between the slabs and activated by neutrons from 18-Mev protons on Be. A G.M. counter placed between the slabs gave information on the ionizing radiation inside the block. The following mixtures have been investigated. The half-value thickness (D_{Ag} in cm) at $d=20$ cm for the 2.3-min Ag activity excited by thermal neutrons and the half-thickness (D_C in cm) for the counter at $d=20$ cm were:

Mixture	gr H_2O/cm³	gr Fe/cm³	Density	D_{Ag}	D_C
Concrete	0.20	—	2.35	9.5	13.3
Concrete+1.2% Pyrex	0.14	—	2.39	8.5	13.3
Cement+limonite ore	0.49	0.93	2.63	4.8	9.0
Cement+limonite+Fe	0.35	3.23	4.41	4.5	7.9
Cement+limonite+Fe +1% Pyrex	0.45	2.26	3.60	4.9	7.7
Cement+magnetite	0.21	1.93	3.78	8.2	9.0
Water	1.00	—	1.00	6.0	14.8

* Supported in part by Navy contract.

F3. Depolarization of Neutrons during Diffusion. S. BOROWITZ, *New York University.*—Following a recent suggestion[1] we consider the cumulative effect of several depolarizing collisions as a possible method for investigating the spin dependence of nuclear forces, when the scattering amplitudes are almost equal. Specifically, we examine the following situation: a plane monochromatic beam of polarized, thermal neutrons is incident normally on a semi-infinite slab of material of finite thickness, which scatters the neutrons isotropically and elastically.

We wish to calculate the polarization of the transmitted beam. The transport equations for the neutrons of each polarization lead to a coupled system of integro-differential equations which reduce to a pair of equations of the Wiener-Hopf type. The equations are solved approximately by a method originated by G. C. Wick.[2] The first approximation is equivalent to considering the process a diffusion; the higher approximations, which converge rapidly, correct for the non-spherical distribution of the neutron density. The results indicate that conditions for performing an experiment are favorable. For a thickness of scatterer of 10 mean free paths, one obtains considerable depolarization for reasonable values of the scattering amplitudes. Using a pile as a neutron source, the intensity is not reduced beyond what is easily measured.

[1] M. Hamermesh and J. Schwinger, Phys. Rev. **69**, 145 (1946).
[2] G. C. Wick, Zeits. f. Physik **121**, 702 (1943).

F4. Inelastic Scattering of Fast Neutrons. L. SZILARD, S. BERNSTEIN, B. FELD, AND J. ASHKIN, *University of Chicago.*—Measurements of inelastic scattering effects of Ra$-\alpha-$Be and Ra$-\alpha-$B neutrons in Fe, Pb, and Bi have been made. A U^{238} fission threshold detector was used. The method consisted in measuring the fission counting rate in the detector with and without the spherical scatterer surrounding the source. From the decrease in the counting rate caused by the presence of the scatterer, values of the cross section for inelastic scattering to below the U^{238} fission threshold were calculated for several assumed values of the elastic scattering cross section. For example, if the elastic scattering cross section is taken equal to zero, the inelastic scattering cross sections in barns are as follows:

	Ra$-\alpha-$Be neutrons	Ra$-\alpha-$B neutrons
Fe	1.0	0.8
Pb	1.2	0.9
Bi	1.5	1.1

F5. The Recently Improved Slow Neutron Velocity Spectrometer with Some of the Results Obtained. W. W. HAVENS, JR., L. J. RAINWATER, C. S. WU, AND J. R. DUNNING, *Columbia University.*—The Columbia University slow neutron velocity spectrometer system[1] has been improved by using a 1-mc crystal oscillator to provide the fundamental timing. This permits cyclotron and detector "on times" of 2, 4, 8, 16, etc. microseconds. Total cycle periods of 1024 or 8192 μsec. are used, depending on whether or not Cd filters can be used. Using 2 μsec. "on-times" and a 6-meter path length gives a total effective resolution width <1 μsec./meter. Since a time of flight of 0.72 μsec./meter corresponds to a neutron energy of 10,000 ev, it is now possible to observe strong neutron resonance levels above 1000 ev as sharp deep dips on a curve of slow neutron transmission *vs.* time of flight. Results will be shown for Al, Zn, Cr, and NaBr, showing strong neutron resonance levels above 1000 ev. This document is based on work performed for the Atomic Energy Commission.

[1] J. Rainwater and W. W. Havens, Jr., Phys. Rev. **70**, 136 and 154 (1946); Rainwater, Havens, Wu, and Dunning, *ibid.* **71**, 65 (1947); Havens, Wu, Rainwater, and Meaker, *ibid.* **71**, 165 (1947); Wu, Rainwater, and Havens, *ibid.* **71**, 174 (1947).

F6. Neutron Scattering Resonances in Elements from Scandium to Arsenic. S. P. HARRIS AND A. S. LANGSDORF, JR., *Argonne National Laboratory.*—Since the discovery of the predominantly scattering character of the resonance in Mn for 300-ev neutrons, a search for similar resonances has been made using an annular BF_3 proportional counter as described in a published report on the scattering character of the 115-ev Co resonance. This apparatus permits observation of resonance scattering up to a few thousand ev. We have observed similar resonance scattering effects in Cu, Ga, and indications of such resonances in Sc, V, and As. The latter three are difficult to measure because the presumed resonances are above 1000 ev where the sensitivity of detection is low. The resonance in Cu is probably in the region of 500 to 1000 ev. In the case of Ga, both isotopes seem to have such resonances, and both in the range 100 to 500 ev. All the above are odd atomic number elements. Among even atomic number elements resonance scattering effects are consistently weaker, being practically unobservable in Fe and Ni, and small but observable in Ti and Cr. In Zn the resonance effect seems clear-cut. It is possible that the observed resonance scattering effects in these even atomic number elements are ascribable to the odd mass number isotopes of low abundance. Since none of these can be activated, enriched isotopes will have to be used to confirm this supposition.

F7. Total Neutron Cross Sections of Compounds with Different Crystalline Structures. LESTER WINSBERG, DAVID MENEGHETTI, AND S. S. SIDHU,* *Argonne National Laboratory.*—The total neutron cross sections of polycrystalline compounds such as close-packed hexagonal ZnO, body-centered cubic TlBr, and face-centered cubic CaO were determined with the Argonne neutron velocity selector[1] and neutron crystal spectrometer[2] in the energy region of 0.001 to 1.0 electron volts. The curves of cross section as a function of neutron energy were resolved as a sum of absorption, coherent scattering, and incoherent scattering cross sections. These curves contain cross-section peaks, which are due to coherent scattering from various crystalline planes. The positions of the peaks come at neutron wave-lengths which satisfy the relation, $n\lambda = 2d$, where n is the order of the reflection and d is the interplanar distance. These diffraction effects are similar to those obtained with x-rays. The cross sections calculated by means of Eqs. (4) and (6) in reference 3 were compared with the experimentally obtained curves.[3] The change in the phase of the neutron wave on scattering by Zn and Ca is the same as that for O, which is in agreement with the work of Fermi and Marshall, and for Tl is the same as for Br. The free-atom scattering cross section of Ca determined from these data is 2.5 ± 0.5 barns, based on a value of 4.1 barns for 0. The corresponding scattering amplitude for Ca is $0.46 \pm 0.05 \times 10^{-12}$ cm. These values for Ca are much less than any previously reported.

* On leave from the University of Pittsburgh.
[1] T. Brill and H. V. Lichtenberger, Phys. Rev. **72**, 585 (1947).
[2] W. H. Zinn, Phys. Rev. **71**, 752 (1947).
[3] E. Fermi, W. J. Sturm, and R. G. Sachs, Phys. Rev. **71**, 589 (1947).

F8. Oscillatory Method for Measuring Neutron Cross Sections by the Effect on the Reactivity of a Chain-

Reacting Pile. ALEXANDER LANGSDORF, JR., *Argonne National Laboratory.*—An increase in sensitivity by a factor of about 20 over the already described static control rod method[1] has been achieved by oscillating samples in and out by the Argonne heavy water pile (at one cycle per 20 seconds). The a.c. ripple in ion current from a BF_3 chamber in the pile is measured by a galvanometer circuit. Emphasis has been placed upon measuring resonance absorption, $\int \sigma_a dE/E$, of samples oscillating in a cadmium tube. One then measures capture, slowing down and scattering effects. The scattering may almost be eliminated, slowing down calculated, and $\int \sigma_a dE/E$ determined except for some light elements. Total pile cross sections are measured by removing the Cd sleeve. Then absorption as small as by Bi ($\sim 0.05 \times 10^{-24}$ cm^2 including impurities) may be measured to a few percent in spite of 200 times greater σ_s, using a 1000-g sample.

[1] H. L. Anderson, E. Fermi, A. Wattenberg, G. L. Weil, and W. H. Zinn, Phys. Rev. 72, 16 (1947).

F9. Delayed Emission of Neutrons from the Decay of N^{17}. N. KNABLE, E. O. LAWRENCE, C. E. LEITH, B. J. MOYER, AND R. L. THORNTON, *University of California, Berkeley.*—The bombardment of oxygen and elements immediately above it in atomic number with 195-Mev deuterons is observed to yield a delayed emission of neutrons decaying with a half-life of slightly over four seconds. Measurements of the decay periods, with a BF_3 proportional counter corrected for resolving time, for target elements from oxygen through chlorine gave a single half-life of 4.14 ± 0.04 seconds. Observations of the intensity of gamma-radiation, together with the magnitude of the yield of delayed neutrons, precluded an explanation in terms of $\gamma - n$ reactions. Bombardments of various elements by deuterons, protons, and neutrons indicated that the active isotope responsible for the decay period leading to the neutron emitter must have $Z \leq 8$ and $A - Z = 10$. Subsequent experiments by Alvarez[1] definitely assigned the effect to a nitrogen isotope, identifying N^{17} as the nucleus which carries the phenomenon. Results of a general search through the periodic table for such effects will be reported. Complex decay curves for delayed neutrons from Ce, Gd, Pt, Au, Hg, Tl, Pb, and Bi will be shown. This work was performed under the auspices of the Atomic Energy Commission.

[1] See abstract F11.

F10. Production of N^{17} by Deuteron Bombardment.* W. W. CHUPP AND E. M. MCMILLAN, *University of California, Berkeley.*—The nucleus N^{17} offers a unique opportunity for studying many-particle reactions among the light elements, since its specific property of giving 4.13-sec. delayed neutrons allows it to be easily distinguished. We have examined the yield of delayed neutrons from a number of substances bombarded by an external beam of 195-Mev deuterons from the 184-inch cyclotron. The beam passed through a monitor consisting of a thin LiF crystal and then through a thin sample of known surface density; after 30 seconds of exposure the sample was allowed to fall into a sensitive re-entrant BF_3 chamber and the monitor was pulled alongside a BF_3 counter, and then simultaneous counts were taken for 30 seconds. The chambers were heavily shielded by paraffin to reduce background. Two kinds of measurements were taken: (1) comparisons of the relative yields per atom and (2) excitation curves as the deuterons were slowed down by copper absorbers between monitor and sample. The relative yields per atom show a roughly exponential decrease with the number of particles emitted, as indicated:

O not incl. O^{16}	F	Na	Mg	Al	Si	P	S	Cl	K
100,000	8400	2600	840	840	230	230	70	78	25

The excitation curves are monotonic with energy and show thresholds increasing with Z.

* This work was performed under the auspices of the Atomic Energy Commission.

F11. Properties of the 4-Second Neutron Emitter of Low Z. LUIS W. ALVAREZ, *University of California, Berkeley.*—A gas flow method has been used to show that a nitrogen isotope is responsible for the delay. The number of neutrons in the active nucleus is known from the work of Lawrence and Moyer, so the complete identification is N^{17}. In support of the Bohr-Wheeler hypothesis, "neutron-β" coincidences have been observed. The neutrons themselves are not detected, but instead, the recoiling O^{16} nuclei are observed in an atmospheric pressure proportional counter, through which passes a stream of He carrying the N^{17}. The pulse size distribution of the recoils gives directly the differential neutron distribution and this is observed to be very broad. Preliminary results show a maximum at zero energy, with a tail extending to more than 2 Mev. Its shape is probably due to the fifth power law of β-decay, in which case it is not the true neutron width. Preliminary absorption measurements of the β-rays in coincidence with the neutrons indicate an upper limit of 3.7 ± 0.4 Mev. With the improved apparatus now in use, it should be possible to determine the neutron spectrum accurately and look for the expected variation of β-ray upper limit with neutron energy. This work was sponsored by the Atomic Energy Commission.

F12. On the Radioactive Decay of the Neutron. ARTHUR H. SNELL AND L. C. MILLER, *Clinton National Laboratories.*—A collimated beam of neutrons, three inches in diameter, emerges from the nuclear reactor and passes axially through a thin-walled, aluminum, evacuated cylindrical tank. A transverse magnetic field behind the thin entrance window cleans the beam of secondary electrons. Inside the vacuum, axially arranged, an open-sided cylindrical electrode is held at +4000 volts with respect to ground. Opposite the open side a smoothed graphite plate is held at −4400 volts. The field between these electrodes accelerates and focuses protons which may result from decay of neutrons, so that they pass through a $2\frac{1}{4} \times 1\frac{5}{8}$ inch aperture in the center of the graphite plate, and strike the first dynode of a secondary electron multiplier. The first dynode is specially enlarged so as to cover the aperture. Readings are taken (1) with and without a thin B^{10} shutter

in the neutron beam; (2) with and without a thin foil over the multiplier aperture; (3) with and without the accelerating voltage. In a total counting rate of about 300 per min., about 100 are sensitive to operations (1), (2), and (3). In the absence of the accelerating field or with the foil (2) in, operation (1) does not change the counting rate. Assuming all of the 100 c.p.m. to be due to decay protons, preliminary estimates of the collecting and counting efficiency (10 percent) and of the number of neutrons in the sample (4×10^4) give for the neutron a half-life of about 30 minutes. It is at present much safer however to say that the neutron half-life must exceed 15 minutes. Coincidences are presently being sought between the disintegration betas and the collected protons.

Solid-State Physics Including Semi-Conductors

G1. Work Function and Semiconductors at High Temperatures. P. H. MILLER, JR. AND J. J. MARKHAM, *University of Pennsylvania.*—Bardeen's[1] theory of surface states has been extended to include the influence of the intrinsic electrons and holes at high temperatures on the behavior of the potential barrier near the surface of a semiconductor. Because of the high density of electrons and holes at very high temperature, the barrier potential must be very small and not influenced by the surface states (assumed density 10^{14} cm^{-2} volt^{-1}). Smith and Miller[2] found that work functions of N and P type silicon are independent of temperature and are approximately the same. This was interpreted as indicating that the height to which the surface states are filled is the same for both N and P type material but not necessarily at a point half-way between the filled and unfilled bands. The extended theory shows that this point is about halfway between the two bands.

[1] J. Bardeen, Phys. Rev. **71**, 720 (1947).
[2] A. H. Smith and P. H. Miller, Jr., Bull. Am. Phys. Soc. **23**, No. 2, p. 25.

G2. Hall Effect in Tellurium Measured by a.c. Method.* VIRGIL E. BOTTOM, *Purdue University.*—In order to eliminate the contribution from the Ettingshausen effect an a.c. method for measuring the Hall effect has been developed. Frequencies used have been between 1000 and 10,000 cycles per second, since in this range the Hall effect has been found to be independent of frequency. The circuit allows the measurement of both high and low resistivity samples and the Hall e.m.f. may be observed directly on the screen of an oscilloscope. Thus upon heating the sample it is possible to follow visually the change in the number of electrons as a function of temperature as determined from the Hall effect. Applied to various samples of tellurium, both commercial and especially purified, it has been found that the Hall effect is positive between the temperatures 20° and 400°C, with a slope indicating an activation energy in agreement with the value reported[1] for tellurium films.

* This work has been supported by Signal Corps contract.
[1] Wayne Scanlon and K. Lark-Horovitz, Phys. Rev. **72**, 530 (1947).

G3. Dependence of Resistivity of Germanium on Electric Field.* RALPH BRAY, *Purdue University.*—High resistivity ($\rho\sim1$ ohm-cm) germanium samples, macroscopically uniform, are ohmic only up to fields of the order of 100 v/cm;[1] the critical field, E_c, above which the resistivity decreases, and the functional relation between the resistivity and field, $\rho(E)$, vary from sample to sample. Constant current pulses of 5-microsecond duration are used, thereby eliminating heating effects, and also determining the time constant for the field effect ($\sim10^{-7}$ sec.). Studies of the temperature dependence with both p and n type samples show that the maximum in the field effect occurs at a temperature corresponding to the transition from impurity to intrinsic conduction; the field effect diminishes rapidly on either side of the maximum. E_c and $\rho(E)$ are also temperature dependent. Secondary field effects with much longer time constants and giving first increasing and then decreasing resistivity with increasing field become important at the higher temperatures. To determine how far the field changes the number of carriers or their mobility, Hall effect measurements using these pulses have been started.

* Supported by Signal Corps.
[1] R. Bray, K. Lark-Horovitz, and R. N. Smith, Phys. Rev. **72**, 53 (1947).

G4. Electronic States in Almost Periodic Systems. HUBERT M. JAMES, *Purdue University.*—The effects on electronic states in crystals of local disturbances (impurity atoms or local charge distributions; termination of the crystal at free surfaces) have heretofore usually been discussed by a fusion of particle and wave concepts. Many results thus obtained are open to criticism. A complete wave-mechanical analysis of such systems has therefore been made in the one-dimensional case. If the perturbing potential varies slowly, the wave functions are almost periodic functions with the period of the crystal potential, modulated by multiplying factors which are solutions of wave equations for effective potentials not in general identical with the perturbing potential. This analysis shows that the exclusion principle has in the past been improperly applied in discussing impurity states of crystals. It also makes possible a reliable qualitative discussion of impurity and surface states. Local depressions of potential may cause one or more trapping states to occur below each electronic band; a local rise in potential produces similar states above the bands. Localized surface states may occur with energies above or below the electronic bands; the electrons are trapped on the surface by image forces acting in conjunction with the perfectly reflecting crystal.

G5. Electrical Breakdown in LiF below Room Temperature. J. W. DAVISSON, *Naval Research Laboratory.*—Evidence will be presented to show that the star patterns formed by dielectric breakdown in LiF,[1] which lie at an azimuth of 12° at room temperature, do not reduce azimuth in a continuous manner with decrease of temperature. Statistical counting of the paths shows that only discrete orientations are permitted in this temperature range. This behavior further supports the notion that the star patterns do not represent merely an average direction

formed by competative breakdown in the [110] and [111] directions. The general problem of breakdown will be summarized.

[1] Phys. Rev. 73, (1948).

G6. The Change in the Electrical Resistance Produced by Cold-Work. J. S. KOEHLER, *Carnegie Institute of Technology.*—Experimentally the electrical resistance of most metals increases by a few percent when they are cold-worked at room temperature. The present calculations are designed to decide whether this increase in the electrical resistance can be correlated with the increase in the density of dislocations which occurs during cold-work. The changes which take place in the dislocation density can be calculated from the changes in the yield stress. The dislocation contribution to the electrical resistance can be calculated if the relaxation time t associated with dislocation scattering is known. The first step in obtaining t is the calculation of the matrix element $V(kk')$ which gives the probability per unit time that a free electron of wave number k makes a transition to wave number k' as a result of the perturbation of the crystal lattice produced by the introduction of the dislocations. This matrix element is then used in the usual Bloch integral equation which determines t. The results obtained are that: The relaxation time t depends on the relative orientation of the electric field which produces the current and the dislocations. This directional dependence of the added resistance can be seen to be qualitatively reasonable. The calculated additional resistance introduced by cold-working copper at room temperature is 0.4 percent. Possible reasons for the discrepancy will be discussed (supported by O.N.R.).

G7. Measurement of Secondary Emission of Insulators at Low Primary Energies. PAUL K. WEIMER, *Radio Corporation of America.*—Published data on the secondary emission of insulators at primary energies of less than 20 volts are meager.[1] Experimental difficulties caused by charging of the test surface and poor alignment of the incident beam are encountered. An experimental method based on the electron optical techniques used in television camera tubes[2] has been developed. The sample is scanned by the primary beam and the returning electrons passed into an electron multiplier. The output signal is fed into a television viewing tube, providing a visual means of aligning and centering the beam. A pulsing technique with a saw-tooth voltage on the sample maintains charge equilibrium and permits the study of thick samples. The curve of secondary emission *vs.* primary energy is presented directly on an oscilloscope screen in a form convenient for study of fine structure in the curve. Measurements have been made on glass, silica, and various metals. One measurement on G.8 glass gave a ratio at 2-volts primary energy of 0.7 which was reduced to 0.3 on evaporation of a layer of silver too thin to be conducting.

[1] G. Maurer, Zeits. f. Physik 118, 122 (1941).
[2] A. Rose, P. K. Weimer, and H. B. Law, Proc. I.R.E. 34, 424 (1946).

G8. Production and Tests of Metal Single Crystal Surfaces.* H. E. FARNSWORTH, *Brown University.*—A summary is given of various methods of etching metal crystal surfaces so as to obtain a geometrical boundary parallel to a given set of planes for investigations in surface physics and chemistry. When some crystals are etched chemically under conditions favorable to the production of the desired surface, a thin polycrystalline layer is deposited on the surface during the process. In some cases this layer is soluble in certain solutions and hence may be dissolved, or it may be removed by heat treatment in vacuum. Recent tests on the etching of a silver crystal by the method of electrolytic polish indicate that in this case this layer is not removed by subsequent thermal treatment. Tests by optical and electron diffraction methods are described.

* A part of this work was assisted by the Office of Naval Research.

G9. Sintering Process Study by Electron Micrography. H. CHRISTENSEN AND C. J. CALBICK, *Bell Telephone Laboratories.*—Thin flakes of nickel-manganese oxide originally composed of two interdispersed particle size ranges were studied by means of silica replicas of their free surfaces. These flakes were heated to selected temperatures in the sintering range 720° to 1300°C, then rapidly cooled. Below about 900°C the micrographs show incorporation of smaller particles into larger ones. From 900°C to 1200°C, the larger grains continue to grow with development of a terraced surface structure. Above 1200° the simple terraced structure tends to break down into a double terraced structure. Sometimes the terraces continue across a grain boundary, undergoing a sharp change in direction because of the change in crystallographic orientation. The height of one terrace above another is in the range 10^{-6} to 2×10^{-5} cm. These phenomena are not inconsistent with Frenkel's views[1] that surface tension is responsible for viscous flow of material from smaller particles to adjacent larger particles and also that surface flow can occur in a "two-dimensional" gas phase.

[1] J. Frenkel, J. Phys. U.S.S.R. 9, 385, 392 (1945).

G10. Stress Relaxation by Interstitial Atomic Diffusion in Tantalum. T'ING-SUI KÊ, *University of Chicago.*—In a preceding report,[1] it was shown that the internal friction peaks observed in tantalum containing small amounts of C and O are caused by the stress—induced preferential distributions of C or O among the interstices in tantalum. In order to further elucidate this viewpoint, the relaxation strength associated with these relaxations has been determined by rigidity and stress relaxation measurements in torsion covering a wide range of temperature. When the reciprocal of relaxation strength is plotted against absolute temperature, the graph is a straight line through the origin. This linear relationship agrees with that predicted by theory, assuming a model of stress-induced preferential distribution. The finding that the extrapolated line passes through absolute zero shows that the interaction between solute atoms is negligibly small. This implies that the critical temperature for self-induced preferential distributions of solute atoms is close to absolute zero in the present case.

[1] T. S. Kê, Bull. Am. Phys. Soc. (December 1947).

G11. A Theoretical Approach to the Strength of Materials Under Cyclic Loading. EDWARD SAIBEL, *Carnegie Institute of Technology*.—In a previous paper* the author has derived a theoretical relationship between the time it takes a material to fracture under a steady load and the applied stress. This derivation, based on the Eyring theory of reaction rates, considered the breaking of bonds between ions or atoms as the product of the reaction and took into account in an approximate manner the effect on the remaining system of the net product of the reaction. This work is extended to the cyclic loading of a material and an approximate relationship of the form $s=A-BT(\log N-C)$ is found; where s is the stress amplitude, N is the number of cycles to fracture, T is the absolute temperature, and A, B, and C are constants characteristic of the material.

* Edward Saibel, J. Chem. Phys. **15**, 760 (1947).

G12. Adsorption of Mercury by Activated Carbon. R. C. MASON, *Westinghouse Research Laboratories*.—The early observations of Coolidge[1] on the adsorption of mercury vapor by activated carbon have been confirmed by extensive experiments on adsorption between −5°C and 100°C. A special ion gauge was used to measure the vapor density, and the amount of mercury adsorbed was determined by direct weighing. The density of mercury atoms in equilibrium with the adsorbed phase could be represented by

$$n=Dw\epsilon^{-Q/RT},$$

where n is the number of atoms per cm³, w is the weight of mercury adsorbed in milligrams per gram of carbon, and Q is the differential heat of adsorption. For a number of different carbons, Q was found to be approximately 10,000 calories per mole, and D to be of the magnitude of 10^{21}.

From the kinetics of the adsorption, some conclusions about the nature of adsorption and the structure of the carbon may be drawn.

[1] J. Am. Chem. Soc. **49**, 1949 (1927).

More or Less Thermal; Mass-Spectra of Ions

H1. Redefinition of the Thermodynamic Scale of Temperatures. F. G. BRICKWEDDE, *National Bureau of Standards*.—In 1939 Giauque urged that we proceed to redefine the number scale of the present thermodynamic temperature scale as recommended by Joule and Thomson. The new number scale would be determined by assigning a number to the temperature (T_0) of the ice point (ordinary freezing point or triple point) on the absolute scale (scale on which the lowest possible temperature is 0°). By assigning to the ice point the present best value (~273.16) on the present Kelvin scale, the newly defined and presently used thermodynamic scale would be the same, to within the present accuracy, of the best gas thermometer measurements. The steam point (100°C) would be reduced to the status of other secondary thermometric fixed points. The new definition would fix the number difference (~273.16°) between the absolute (or new Kelvin) and centigrade scales. Fixing by definition the numerical value ($1/T_0$) of the temperature coefficient of volume and pressure changes of the *ideal* gas (now an empirical constant) had other advantages: (1) the accuracy of temperature determinations with gas thermometers would be improved, and (2) the necessity would be removed of recomputing (by methods not agreed upon) previously determined temperatures whenever a different empirical value is used for the fundamental temperature coefficient of the ideal gas.

H2. The Viscosity of D_2O and of H_2O from 5° to 125°C.* R. C. HARDY AND R. L. COTTINGTON, *National Bureau of Standards (Introduced by F. G. Brickwedde)*.—Measurements of the absolute viscosity of D_2O of 99.5 percent purity and of H_2O were made over the temperature range 5° to 125°C. The work also included determinations of the density of D_2O over the temperature range 90° to 125°C. Values for the viscosity and density of 100 percent D_2O with 0.7-atom percent excess O^{18} were obtained by linear extrapolation. A Bingham variable pressure viscometer was used in the range 5° to 95°C. This instrument was calibrated with water at 20°C using the value 1.005 centipoise for the viscosity of water at this temperature. A modification of the Ostwald viscometer, with equal air pressure applied to both limbs to prevent boiling, was used at the higher temperatures. This instrument was calibrated with water at several temperatures using viscosity values determined with the Bingham instrument. The ratio of the viscosity of D_2O to that of ordinary water at the same temperature was found to be 1.3052 at 5°C. This ratio decreased at a diminishing rate with an increase in temperature to a value of 1.1456 at 125°C.

* This work supported in part by Atomic Energy Commission.

H3. Heats of Vaporization of Uranium Hexafluoride. J. F. MASI, *National Bureau of Standards (Introduced by F. G. Brickwedde)*.—Measurements of heats of vaporization of uranium hexafluoride have been made from 4° to 90°C to complete the work on thermodynamic properties of this important substance. A heavy-walled copper vaporization chamber, nickel-plated on the inside, was enclosed in a vacuum jacket which was surrounded with a bath maintained within 0.002°C of any desired temperature. The temperature of the emergent vapor was obtained from a nickel resistance thermometer on the exit tube. The apparatus was tested by obtaining the heat of vaporization of water at 60° and 95°C; the results obtained were scattered uniformly about the values given by Osborne, Stimson, and Ginnings,[1] with a spread of about 0.3 percent at 60° and 0.1 percent at 95°. The heats of vaporization of UF_6 were measured at seven temperatures from 4°C to the triple point (64.05°C) and at four temperatures above the triple point. Six samples of UF_6 were used, all from the same original source and all purified in the same manner. The experimental heats of vaporization had a precision of ±0.5 percent for the solid and about ±1.0 percent for the liquid. There is agreement, within experimental error, with values calculated from the vapor pressure equation of Crist and Weinstock (to be published in J. Chem. Phys.), except at temperatures below 35°C.

[1] N. S. Osborne, H. F. Stimson, and D. C. Ginnings, *J. Res. Nat. Bur. Standards*, **23**, 197–260 (1939).

H4. The Vapor Pressure of O_2 from the Triple Point to the Critical Point. HAROLD J. HOGE, *National Bureau of Standards.*—The vapor pressure of O_2 has been measured over the entire liquid range. Low pressures were measured with a mercury manometer, intermediate and high pressures with a piston gage. Temperatures were measured with a platinum resistance thermometer. Vapor pressures in the neighborhood of the normal boiling point agree rather well with previously accepted values. At high pressures the data are somewhat lower than the 1914 values of Onnes, Dorsman, and Holst. Part of the disagreement is probably due to a difference in temperature scales. The triple point temperature was found to be 54.363°K. A calorimetric method was used to determine the critical temperature and to show whether or not the equilibrium chamber contained both liquid and vapor. If either phase disappears, the heat capacity drops sharply. Hence so long as the heat capacity remains high there are two phases in the equilibrium chamber and vapor-pressure measurements may be made. The highest temperature at which the drop in heat capacity occurs was found by varying the quantity of material in the apparatus. This temperature, about 154.5°K, is the critical temperature as calorimetrically determined.

H5. A Photoelectric Pyrometer for the Measurement of Luminous Flame Temperatures. J. A. SANDERSON, J. A. CURCIO, AND DOROTHY V. ESTES, *Naval Research Laboratory.*—A photoelectric pyrometer has been developed for the measurement of flame temperatures by a method suggested by Hottel and Broughton.[1] By means of a photomultiplier tube, RCA 1-P22, covered with an interference filter transmitting a spectral band 140A wide at λ5520A, radiant intensities of luminous gas-oxygen flames were measured first against a dark background and then with a mirror of reflectivity R so placed behind the flame that radiation was retrodirected, thus, in effect, increasing the flame thickness. The photo-cell filter system was calibrated with radiation from a ribbon filament tungsten lamp at known temperatures. Application of Wien's and Kirchoff's radiation laws provided a relation between photo-cell currents and true flame temperature. Flame temperatures determined by this method were about 10 to 15 percent lower than temperatures obtained by line reversal, presumably because the latter method gave a result for the hottest part of the flame, while the pyrometer gave a result for the integrated radiation emitted by the entire thickness of the flame. Typical temperatures of a gas-oxygen torch were: pyrometer 1758°K; line reversal 1945°K.

[1] H. C. Hottel and F. P. Broughton, Ind. and Eng. Chem. Anal. Ed. 4, 166 (1932).

H6. Measurement of Gas Temperatures in the Exhaust Flames of Rocket Motors by Spectroscopic Methods. I. H. M. STRONG AND F. P. BUNDY, *General Electric.*—In measuring the temperature of the exhaust gases of a rocket motor, it is necessary to use a physical optical method that does not disturb the flow of the gases. Because of the hazardous nature of the combustion, all observations must be made by remote control. An apparatus is described for measuring the temperature by the sodium line reversal method. A wide range of temperatures for the comparison radiator is provided by illuminating an optical wedge with a tungsten arc and focusing its image on the slit of the spectrograph. Reversal occurs on the wedge image at a place where the temperatures of the comparison radiator and the flame are equal. The results are recorded photographically in the spectrograph. The optical parts are all mounted on a rigid framework which is shock mounted inside of a protective box. All necessary settings are made through the use of solenoids. The effect of the complex flame structure, the width of the sodium line, and the resolving power of the spectrograph on the measurement of temperature will be discussed.

H7. Measurement of Gas Pressures in the Exhaust Flames of Rocket Motors by Spectroscopic Methods. II. F. P. BUNDY, A. B. GREGG, AND H. M. STRONG, *General Electric.*—The gases from rocket motors emerge from the exhaust nozzle at supersonic speed. The boundary conditions inside and just outside the nozzle usually cause a series of stationary shocks in the flame which are commonly known as "shock diamonds." Methods have been developed for measuring the temperatures and pressures in different parts of the flame structure by optical means which do not require any mechanical disturbance of the gas flow. This paper describes the method used for measuring the pressures. It is based upon the shift of wavelength of the sodium D-line radiation toward the red caused by the influence of the foreign gas molecules of the flame. This red shift effect is proportional to $pT^{-\frac{1}{2}}$, and depends upon the perturbing gas. The small shift of wavelength is measured from the change in diameter of the fringes of a Fabry-Perot interferometer. The effect has been calibrated by use of a special pressure flame chamber in the laboratory. The gas pressures at different places in a typical rocket flame are found to range from 0.8 atmospheres up to 2.5 atmospheres.

H8. Determination of Detonation Temperatures in High Explosives.[1] R. L. BOYER.[2]—Theoretical evaluation of the high pressures and temperatures of the detonation wave in solid explosives has been based on experimental values of the rates of detonation at various loading densities and an assumed form of the equation of state. The calculated temperatures vary with the loading density, and depend upon the particular assumptions made in the equation of state. An experimental method has been developed to determine detonation temperatures. The radiant energy emitted by the detonating explosive is readily detected for narrow spectral ranges by sensitive phototubes and the time record of the radiation is obtained by photographing the sweep trace of a cathode-ray oscilloscope with the phototube circuits connected to the vertical deflection plates. Preliminary results are given for the detonation temperatures of pentaerythritol tetranitrate powders at several loading densities which indicate a decrease in

detonation temperature with increasing loading density in agreement with predictions based on the Kistiakowsky-Wilson equation of state.

[1] This research is part of the work being done at the Bureau of Mines, supported by the Office of Naval Research.
[2] Physicist, Explosives Research Section, Bureau of Mines, Pittsburgh, Pa.

H9. Radio Frequency Mass Spectrometer. WILLARD H. BENNETT, *National Bureau of Standards.*—Studies of the origins of negative ions are made difficult by the fact that dissociation cross sections for such ions are generally much larger than atomic and molecular ionization cross sections because the electron attachment energies for negative ions are generally small. To separate and identify negative ions, it is essential that the negative ions be required to travel a much shorter distance than the particles have to travel in the familiar kinds of mass spectrometers using magnetic resolution of beams. A six-electrode tube with cylindrical symmetry has been developed, in which an adjustable radio frequency is applied to the second grid. A mass resolution is obtained which is adequate for many kinds of negative ion studies. By extending the method to two stages in a nine-electrode tube, either with cylindrical or parallel plane electrodes, and applying the radio frequency to two of the grids, a higher order mass resolution is obtained which is generally usable in the mass spectrometry of positive ions, and in ionization studies as well as in the present negative ion investigations.

H10. Ionization Efficiency Curves from Mass Spectrometer Data. S. N. FONER, A. KOSSIAKOFF AND F. T. MCCLURE, *Johns Hopkins University.*—A theoretical treatment is developed which provides a method of eliminating the effect of the thermal spread of electrons on the appearance potential curves obtained with a mass spectrometer. Thus it is possible to derive the ionization efficiency curves from the appearance potential curves without *a priori* assumptions regarding the nature of the former. The relationship between these curves is given by $P(V)=I(V)-2kTI'(V)+k^2T^2I''(V)$, where $P(V)$ is proportional to the ionization efficiency for electrons of energy V, $I(V)$ is the ion current obtained with an accelerating voltage V, primes indicate differentiation, and the other symbols have their usual significance. Other experimental influences affecting the observed appearance potential curves are discussed. The application of the methods is illustrated with experimental data on several of the rare gases.

H11. The Appearance Potential of Metastable Ions in Some Hydrocarbon Gases. R. E. FOX, A. LANGER, AND J. A. HIPPLE,* *Westinghouse Research Laboratories.*—The study of hydrocarbon spectra in a mass spectrometer has shown several diffuse peaks which have been attributed to metastable ions. These ions presumably are in an excited state, and it has been shown that they spontaneously dissociate during transit through the mass spectrometer tube with a half-life of about 10^{-6} seconds. A study of the appearance potential of some of these metastable peaks has been made in order to determine if any measurable excess energy is associated with the metastable condition. If no excess energy is involved, then the appearance potential of the metastable ion should agree with that of the parent ion in the dissociation process. The appearance potentials of peaks in the butanes, butenes and 1,3 butadiene were measured and the results will be presented which indicate that in most of the cases studied an excess energy of about 2 ev above the ionization level is required for the metastable state.

* Now located at National Bureau of Standards.

H12. Metastable Transitions in Mass Spectra of Hydrocarbons. EVELYN G. BLOOM, FRED L. MOHLER, J. H. LENGEL AND C. E. WISE, *National Bureau of Standards.*—Mass spectra of hydrocarbons show mass peaks of the parent ion and nearly all possible dissociation products and, in addition, small wide peaks at non-integral mass numbers which have been ascribed to ions which undergo dissociation after they have passed through the ion accelerating field. The apparent mass of these ions m_a is given by the relation $m_a=m_f^2/m_i$ where m_f is the final mass and m_i the initial mass.[1] In a systematic survey of 56 saturated and unsaturated hydrocarbons, 362 metastable transitions have been identified.[2] There are 32 different transitions involving loss of masses 2, 15, 16, 26, 27, 28, 29, 30, 42, and 44. Loss of mass 2 is by far the most common transition. The losses of masses 15 (CH_3), 29 (C_2H_5), and 30 (C_2H_6) come only from the parent molecule ions.

[1] Hipple, Fox and Condon, Phys. Rev. 69, 347 (1946).
[2] American Petroleum Inst. Catalog of Mass Spectral Data.

H13. Analysis of Solids by the Mass Spectrometer. W. M. HICKAM, *Westinghouse Research Laboratories* (*Introduced by R. C. Mason*).—Solid samples of known weight introduced into the mass spectrometer tube are completely vaporized in a furnace. The resulting molecular beam is subjected to electron bombardment where the observed ion current for a given mass to charge ratio is a measure of the evaporation rate for that particular element. The integral of the ion current with respect to time is found to be proportional to the amount of the element present. Applying this method to the investigation of impurities in copper, sensitivity of one part impurity per million parts copper has been obtained on Sb, Se, As, and Ag when using two milligram samples. The high vapor pressure of these elements as compared to copper at the furnace temperature provide rapid vaporization and the resulting high sensitivity.

Theoretical and Experimental Nuclear Physics

I1. Some Deuteron Variational Methods. WILLIAM RARITA, *Brooklyn College and Massachusetts Institute of Technology.*—We report some methods of calculating accurately the depths of different shape potentials of the deuteron for non-central forces. Starting with a square well we know the radial S and D wave functions u and w out-

side the well. Inside the range of interaction we assume a general expansion in terms of modes. These modes for u and w we take to be Bessel functions of order one-half and five-halves, respectively. The wave-lengths of these modes are determined by requiring the continuity of the logarithmic derivative. By using the variational principle for one mode and then two such modes we get 0.95 and 0.99 of the full binding energy. With an exponential times a power of the interparticle distance as our modes, we decided to relax the joining condition so as to require only continuity at the potential edge. The results for the square well were gratifying. For a meson potential, as the convergence seemed slow, we resorted to an iteration procedure lately developed by Feshbach and Schwinger to improve our initial three mode solution. A promising start was also made on the triton problem in which the wave function was allowed to have a discontinuous second derivative over a certain boundary.

I2. Comparison of Recent Methods in the Theory of Nuclear Reactions. T. TEICHMANN, *Princeton University.*—A comparison has been made of the resonance formula recently derived by a simple method by Feshbach, Peaslee, and Weisskopf[1] and the more general results on the same subject obtained by Wigner and Eisenbud.[2] In the treatment of reference 1 all processes other than scattering are lumped together as "absorption" and characterized by a single complex parameter; this parameter, as well as the phases, etc., is assumed to be a smooth function of the energy. As a consequence of these assumptions the absorption cross section goes to zero between each pair of resonances. According to the results of reference 2, this can only occur if the ratio of the partial widths corresponding to the emission of different γ-quanta, etc., is the same for all resonances. Mathematically speaking, this is due to the fact that a two-alternative process, for instance, is characterized in general by three real parameters which are simple functions of the energy, while only two such functions are used in reference 1. While these particular consequences of reference 1 must be regarded as doubtful, the order of magnitude of the scattering cross section is correct, and that of the neutron width seems to be in reasonable agreement with experimental results, at any rate within a factor of 5.

[1] Feshbach, Peaslee, and Weisskopf, Phys. Rev. **71**, 147 (1947).
[2] E. P. Wigner, Phys. Rev. **70**, 606 (1946); E. P. Wigner and L. Eisenbud, Phys. Rev. **72**, 29 (1947).

I3. On Tensor Forces and the Variation-Iteration Method. H. FESHBACH, *Massachusetts Institute of Technology* AND J. EISENSTEIN AND J. SCHWINGER, *Harvard University.*—A complete exploration of the phenomenological theory of the deuteron employing a non-central forces has been hampered by the absence of a satisfactory method for the calculation of force constants for shapes other than the square well. In the present paper, the variation-iteration[1] method has been applied successfully to this problem. Given the shapes of the central and non-central forces, the well depths of each, V_0 and γV_0, respectively, are determined by the binding energy and quadrupole moment of the deuteron. A variational integral is constructed for V_0, γ being kept constant. There is a complication provided by the non-positive definiteness of the operators. Nevertheless, one can determine upper and lower bounds for V_0. The meson well shape has been used; the central force has the range r_0 determined by proton-proton scattering. The range of the non-central force was varied from r_0 to $2r_0$. V_0 was determined to one part in a thousand. V_0 decreases rapidly γ increases correspondingly with decreasing range of the non-central force. The changes are much sharper than those in the corresponding square well case. Other well shapes are being investigated.

[1] J. Schwinger, Phys. Rev. **72**, 742 (1947).

I4. Exchange Currents in Nuclei. R. G. SACHS, *University of Wisconsin.*—Recent measurements[1] of the magnetic moment of He^3 indicate[2] the existence of exchange currents in nuclei as suggested by Villars.[3] Villars successfully considered the exchange moment produced by a charge-bearing meson field which is known not to give a good account of nuclear forces. An attempt is made to avoid this difficulty by considering the phenomenological exchange forces as a starting point. It is found that an exchange current must be introduced to establish the equation of continuity for the current and charge density produced by the protons. This exchange current is substantially the same as that obtained by Siegert[4] on the assumption of a special type of charge-bearing field. Application to H^3 and He^3 indicates that the corresponding exchange moment is too small to account for the observed moments. This theory is expected to be somewhat more limited than a field theory since it takes no account of the detailed structure of nucleons.

[1] H. L. Anderson and A. Novick, private communication.
[2] R. G. Sachs, Bull. Am. Phys. Soc. **22**, 9 (1947).
[3] F. Villars, Phys. Rev. **72**, 256 (1947), Helv. Physica Acta **20**, 476 (1947).
[4] A. F. Siegert, Phys. Rev. **52**, 787 (1937).

I5. $d-p$ and $d-n$ Cross Sections. D. C. PEASLEE, *Massachusetts Institute of Technology.*—On the basis of a very simple model it is made plausible that the Oppenheimer-Phillips or stripping process is responsible for practically the entire observed $d-p$ cross section at any bombarding energy E_d. This is indicated by agreement between the few available quantitative $d-p$ excitation curves—for Na^{24}, Co^{59}, Cu^{63}, Br^{81}, and Bi^{209}—and computed curves, assuming that only the stripping process is effective. The observed decline of the excitation curves with increasing E_d at energies above the barrier height of the target nucleus is interpreted as the result of effective $d-n$ competition in which the excited nucleus re-emits the neutron acquired in the $d-p$ stripping process. Comparison of the observed cross section magnitudes with the calculated values involves specifying as a nuclear parameter the average "sticking probability" ξ of an elementary particle. It is expected that the $d-n$ excitation curves are also predominantly due to the stripping process for incident energies $E_d \gtrsim 10$ Mev. Comparison of the $d-p$ and $d-n$ stripping processes indicates that the observed ratio σ_{dp}/σ_{dn} will exceed unity at all energies E_d comparable with or below the target Coulomb barrier and may approach the limit $\sigma_{dp}/\sigma_{dn} \to \xi_n/\xi_p \approx 1$ as $E_d \to \infty$.

I6. Interference Effects in Angular Correlations. D. S. LING* AND D. L. FALKOFF,** *University of Michigan.*—The selection rules for nuclear transitions allow the simultaneous emission of radiation of different orders. Between such allowed radiations there exists the possibility of interference effects in the angular distribution and total intensity of the radiation. Most important is the simultaneous emission of electric 2^l and magnetic 2^{l-1} pole radiation since their intensities can be of the same order. We find that for a single transition there is no interference either in the total radiation or in its angular distribution. However, in cascade transitions, interference effects can radically alter the angular correlation. For example, for $\gamma-\gamma$ correlation with the first transition pure dipole and the second a mixture of electric quadrupole and magnetic dipole and with the angular momentum of successive states $J+1$, J, and $J-1$, the correlation is:

$$W(\theta)=1+\frac{28+3(J-1)(J-5)\alpha^2+84(J-1)\alpha}{364+(J-1)(55J+61)\alpha^2-28(J-1)\alpha}\cos^2\theta.$$

α^2 is essentially the ratio of quadrupole to dipole intensity. The terms involving α arise from interference.

* Rackham Pre-Doctoral Fellow.
** National Research Council Fellow.

I7. Preliminary Results of a He^6 Neutrino Experiment.* JAMES S. ALLEN, H. R. PANETH, AND A. H. MORRISH, *University of Chicago.*—An intense source of He^6 has been developed through the use of the Be^9 (n, α) He^6 reaction. The source consists of one pound of beryllium powder in a metal can placed near the target of the University of Chicago cyclotron. The He^6 gas is swept out of the powder by alcohol vapor and carried through a pipe line to the recoil chamber. The nuclear recoils resulting from the disintegration of He^6 are detected by means of an electron multiplier tube and the β-rays by an end-window Geiger counter. The energy spectrum of the recoils is studied by recording coincidences between the two detectors as a function of the retarding potential between a set of grids in the path of the recoils. The recoil spectrum observed for 180° coincidences has a maximum energy of approximately 1400 ev. The shape of the spectrum suggests that the angular correlation between the electron and neutrino follows a $(1-\beta\cos\theta)$ law. An investigation of the effect of the geometry of the apparatus upon the shape of the spectrum is being made.

* This research was supported by the Office of Naval Research.

I8. Proposed Nuclear Reactions Involving Polarized Protons. LINCOLN WOLFENSTEIN, *University of Chicago.*—Calculations have been made on several proposed methods for producing and using polarized beams of protons. Methods of production include (a) the (n, p) reactions of N^{14} and He^3, using polarized thermal neutrons, and (b) the resonant scattering of protons from helium.[1] The method (b) will produce higher energies and intensities but is possible only if a P resonance is actually involved. The percentage polarization depends on the ratio of the $^2P_{3/2}-^2P_{1/2}$ splitting to the resonance width, a 45 percent polarization corresponding to a ratio as small as 0.1. The following reactions employing polarized protons were considered: (1) $Li^7+p\rightarrow 2He^4$ and (2) proton-proton scattering. In general, the effect on a reaction of using protons (or neutrons) polarized perpendicular to their axis of incidence is to introduce a left-right asymmetry in the outgoing intensity. Thus, in case (1) the polarization introduces an appreciable term $C\sin\theta\cos\theta\sin\phi$ in the angular distribution of the alpha-particles. For the proton-proton case, the polarization effect is very small, less than 1 percent for energies up to 2.5 Mev. Finally, polarization is shown to persist in the slowing down of protons.

[1] Compare J. Schwinger, Phys. Rev. **69**, 681 (1946).

I9. Nuclear Magnetic Moments and Meson Exchange. P. MORRISON, *Cornell University.*—Villars[1] has emphasized the importance of the contribution to the magnetic moments of nuclei made by the exchange of mesons between nucleons. Attempts to explain the observed magnetic moment of the triton by considering only the spin and orbital moments of the nucleons[2] require the use of wave functions with large admixtures of high orbital states. It seems probable that the difference between proton and triton magnetic moment includes an exchange contribution. We ask how far the form of meson theory adopted affects the exchange magnetic moment for light nuclei. For nuclear states in which there is no orbital angular momentum, these statements hold for quite general forms of meson-nucleon coupling: (a) The exchange current contribution to the magnetic moment of deuteron and alpha particle is strictly zero, but is finite for the case of the nuclei of mass three, and (b) the sum of the magnetic moments of triton and He^3 is equal to the magnetic moment of the deuteron. These conclusions follow from symmetry arguments alone for any meson-nuclear coupling in which positive and negative mesons are coupled to nucleons with equal strength. The sign and magnitude of the exchange effect in either H^3 or He^3 depends on the form of coupling, but the details of the wave function can affect even the sign of the result. Orbital motion will produce additional effects.

[1] F. Villars, Phys. Rev. **72**, 256(L) (1947).
[2] R. G. Sachs, Bull. Am. Phys. Soc. **22**, 9 (1947).

I10. Polarization Effects in Ionization Loss of Fast Particles.* FRANK L. HEREFORD, *Bartol Research Foundation.*—The effect of the polarization properties of a medium on the ionization energy loss of fast charged particles (suggested by W. F. G. Swann) has been investigated theoretically by Fermi and recently by Halpern and Hall.[1] Whereas previously published curves predict an appreciable effect only at energies of about 20 m_0c^2 and higher, Halpern and Hall indicate that in the case of 1-Mev electrons traversing carbon, the reduction in loss caused by polarization is approximately 8 percent. By measuring the relative stopping powers of carbon and H_2O with a double coincidence train of thin wall (0.035 g/cm²) counters, this reduction has been confirmed. The observed stopping power ratio, S_{H_2O}/S_c, was 1.18±.02 compared with 1.16 (Halpern-Hall) and 1.08 (Bethe-Bloch). Scattering difficulties were minimized by choosing equal thicknesses (in radiation lengths) of carbon and H_2O for com-

parison. This effects equal scattering[2] in the specimens without seriously altering the energy distribution of the particles suffering loss. It is this fortuitously favorable situation in the case of carbon and H_2O which makes the experiment feasible.

* Assisted by the Office of Naval Research.
[1] O. Halpern and H. Hall, Phys. Rev. 73, 477 (1948).
[2] B. Rossi and K. Greisen, Rev. Mod. Phys. 13, 264 (1941).

I11. Variation of He^3/He^4 Abundance Ratio in Natural Sources of Helium. L. T. ALDRICH AND ALFRED O. NIER, *University of Minnesota.*—As an extension of the mass spectrometer work reported earlier,[1] an investigation of the He^3/He^4 ratio in helium obtained from radioactive ores, beryl crystals, and natural gas has been undertaken. No He^3 peak was observed in any of the five radioactive samples studied and if He^3 exists in these, the He^3/He^4 ratio is less than 0.3×10^{-7}. The He^3/He^4 ratios in seven beryl samples varied from 0.5 to 10.5×10^{-7}. Samples from four natural gas wells in the vicinity of Amarillo, Texas gave He^3/He^4 ratios of 0.6, 1.4, 1.4, and 2.0×10^{-7}, respectively. These values are to be compared with ratios of 1.4 and 12.0×10^{-7} found for commercially obtained well and atmospheric helium, respectively. The precision of measurement in all this work was such as to leave no doubt that significant differences in He^3 concentration exist.

[1] L. T. Aldrich and A. O. Nier, Phys. Rev. 70, 983 (1946).

I12. Packing Fraction Measurements of the Heavy Elements. A. J. DEMPSTER, *Argonne National Laboratory.*—The resolving power of the double focusing mass spectrograph previously used for comparing the masses of the isotopes of the heavy elements has been increased about ten times. The ions are produced by electron ionization of the vapor of the metal or volatile metallic compounds using 1000 volt electrons. Ions with high multiple charges are produced with sufficient intensity in this manner.* A new electrode arrangement for accelerating and focusing the ions has been adapted for use with 15,000-volt accelerating potentials. The resolution obtained will be illustrated by photographs of the mass spectra of zinc showing $_{64}Zn^{+4}$, O^+, NH_2^+, and CH_4^+ ions at mass 16, and $_{68}Zn^{+4}$, OH^+, and NH_3^+ ions at mass 17. From these comparisons mass values may be found for the zinc isotopes which give preliminary packing fractions of -7.68×10^{-4} for Zn^{64} and -7.64×10^{-4} for Zn^{68}.

* A. E. Shaw, Phys. Rev. (in press).

I13. Ranges in Air and Mass Identification of Plutonium Fission Fragments. S. KATCOFF, J. A. MISKEL, AND C. W. STANLEY, *Los Alamos.*—Determinations were made of the mean and extrapolated ranges in air of plutonium fission fragments for twenty individual masses between 83 and 157. Collimated fission fragments passing through air at 120 or 140-mm pressure were deposited, after being stopped by the air, on a series of 14 thin lacquer films. These were analyzed radiochemically for individual fission products. The corrected activities were plotted against distance traversed by the fragments, yielding differential range curves whose widths of half-maximum were 11.7±1.3 percent, independent of fragment mass. The activities found beyond each distance were plotted against distance giving integral range curves. Mean and extrapolated ranges were derived from these. In the light group the extrapolated ranges decrease from 2.90 cm (15°C and 760 mm) for mass 83 to 2.25 cm for mass 117; in the heavy group they decrease from 2.25 cm for mass 127 to 1.95 cm for mass 157. From the range-mass curve drawn for well-known masses, definite assignments of 92, 93, and 132 were given to 3.5-hr. Y, 10-hr. Y, and 77-hr. Te, respectively. Highly probable assignments of 94 and 134 were given to 20-min. Y and 54-min. I, respectively.

I14. Stopping of Fission Fragments. W. M. GOOD, E. O. WOLLAN, AND W. A. STRAUSER, *Oak Ridge National Laboratory.*—A study is being made of the range in air and other gases of the fission fragments which are responsible for the 4.5-sec., 22-sec., and 55-sec. delayed neutron activities. The apparatus consists of a special gas tight chamber ("rabbit") which contains a fission foil, a collector button, a gas sealing button, and a filling valve. This rabbit is sent in and out of the Clinton pile in a pneumatic tube, and the catcher button is automatically removed from the assembly on exit from the pile and sent into a counter assembly where the delayed neutron activity is counted as a function of time after irradiation and of the gas pressure in the rabbit. The apparatus will be described in detail. To date results have been obtained on the range in air of the above-mentioned fission fragments from both U^{235} and U^{233}. These results are listed in Table I.

TABLE I.

	4.5 sec.	22 sec.	55 sec.
235	3.13±0.03 mg/cm air	2.33±0.02	3.19±0.03
233	3.16±0.03	2.33±0.02	3.16±0.03

Reactions of Transmutation

J1. The Ratio of Deuterium to Beryllium Photo-Disintegration Thresholds. BERNARD WALDMAN AND WALTER C. MILLER, *University of Notre Dame.*—We have measured the ratio of the deuterium to beryllium photodisintegration thresholds. Electrons, accelerated in a pressure electrostatic generator, were used to produce x-rays in a thick gold target. The neutrons were detected with a boron trifluoride proportional counter, a fast pulse amplifier, and a synchroscope. The electron energy was measured by a null type generating voltmeter. An off-balance voltage of one kilovolt could be detected. The observed ratio is 1.338±0.004. This measurement assumes the linearity of the generating voltmeter. Our ratio is consistent with the results quoted in Stephens summary.[1] No attempt has been made to calibrate the voltmeter on an absolute scale. This research was supported by the Office of Naval Research.

[1] W. E. Stephens, Rev. Mod. Phys. 19, 19 (1947).

J2. On the Angular Distribution of Protons from the Photo-Disintegration of the Deuteron.[1] W. M. WOODWARD[2] AND I. HALPERN, *Massachusetts Institute of Tech-*

nology.—The new pressure electrostatic generator at M.I.T. is used as a source of γ-rays (up to 3 Mev) to investigate the photo-disintegration of the deuteron. The protons from the reaction are detected by means of three proportional counters, connected in coincidence and anti-coincidence, which are mounted on a radius through the deuteron target and can be rotated about it. The arrangement permits measuring simultaneously the range and direction of the disintegration protons. The deuteron target and the counters are housed in a single chamber and deuterium gas serves both as the source of deuterons and as the counter gas. This eliminates any windows which would stop low energy protons and makes it possible to work down to within 200 kv of the threshold. The principal experimental difficulty was detecting the low energy protons in the presence of the large γ-ray background from the generator. The proper choice of counter design, and of electron target for the production of γ-rays, plus an optimum amount of lead, make this possible. Very preliminary results yield rough agreement with the theory of Bethe and Peierls at 2.6 and 2.75 Mev.

[1] Work assisted in part by Office of Naval Research.
[2] Now at Cornell University, Ithaca, New York.

J3. Photoelectric Production of Protons in Nuclei. E. D. COURANT, *Cornell University.*—Recent experiments[1] show that the ratio of (γ, p) to (γ, n) cross sections in medium nuclei with 17-Mev γ-rays is considerably higher than is to be expected from the statistical theory.[2] This may be explained by noting that, instead of interacting with the nucleus as a whole and forming a compound nucleus, the γ-ray may be absorbed by dipole interaction with a single proton, which is ejected immediately. The cross section for this process may be small compared to that for the formation of a compound nucleus, but large compared to that for the emission of a proton from the compound nucleus. The cross section has been estimated by regarding the nucleus as a Fermi gas and using the theory of the surface photoelectric effect in metals.[3] It is found that this model yields (γp) cross sections of the right order of magnitude to account for the experiments. More accurate calculations are in progress.

[1] Hirzel and Wäffler, Helv. Phys. Acta **20**, 373 (1947).
[2] Weisskopf and Ewing, Phys. Rev. **57**, 472 (1940).
[3] Mitchell, Proc. Roy. Soc. **146A**, 442 (1934).

J4. Angular Distributions of Neutrons from (d, n) Reactions. C. E. FALK, E. CREUTZ, AND F. SEITZ, *Carnegie Institute of Technology.*—Using threshold detectors and 15-Mev deuterons from the University of Pittsburgh cyclotron, angular distributions of neutron groups from about 7 to 25 Mev from various targets have been observed. A large excess of neutrons is found in the forward direction of the incident deuteron beam. This observation is in general agreement with the work of Roberts and Abelson[1] who found large ratios of the neutron yields at 0° to those at 90°. The half-widths of our angular distributions as measured with threshold detectors can be roughly explained in the case of a copper target by using a modified Boltzmann energy distribution of the nuclear particles in conjunction with the evaporation theory and allowing for the recoil of the compound nucleus. In the case of a lithium target, however, the forward peaks of all energy groups observed seem to be too narrow (about 30° at half maximum) to be explained by a spherically symmetric neutron distribution in the center of mass system.

[1] R. B. Roberts and P. H. Abelson, Phys. Rev. **72**, 76 (1947).

J5. Magnetic Analysis of Disintegration Products. W. W. BUECHNER, R. J. VAN DE GRAAFF, E. N. STRAIT, C. G. STERGIOPOULOS, AND A. SPERDUTO, *Massachusetts Institute of Technology.*—An annular magnet of the Cockcroft type[1] has been constructed and employed to investigate certain reactions produced by protons and deuterons from an electrostatic accelerator. The apparatus is used to study particles emitted at 90° to the incident beam. The region of uniform magnetic field is 70 cm in diameter and 5 cm wide. The field strength is determined by a null method, natural alpha-particle groups being used for calibration. When the incident protons or deuterons are elastically scattered by thin gold foils, a sharp peak is obtained on the Eastman NTA plates used for detection, thus providing a precise measure of the voltage of the accelerator. Bombardment of thin targets of the light elements yields sharp peaks of protons and alpha-particles, groups differing in energy by one percent being clearly resolved. When somewhat thicker targets are used, the peaks broaden, the breadth affording a measure of the target thickness so that absolute thin-target cross sections may be obtained. This work was supported in part by the Office of Naval Research.

[1] Cockcroft, J. Sci. Inst. **10**, 71 (1933).

J6. Energy Relations in the $Be^9(d,\alpha)Li^7$ Reaction. E. N. STRAIT, C. G. STERGIOPOULOS, A. SPERDUTO, AND W. W. BUECHNER, *Massachusetts Institute of Technology.*—The analyzing magnet described in the preceding abstract has been used to study the alpha-particles from the $Be^9(d,\alpha)Li^7$ reaction. The energy of the incident deuterons was adjusted to a value (1.5 Mev) such that the alpha-particles had an energy of about 5.2 Mev. This made it possible to compare their deflection directly with that of the 5.30 Mev group from polonium. The two alpha-groups, corresponding to the formation of Li^7 in the ground and an excited level appear on the same photographic plate as the polonium group, making possible a (direct) measure of the energy difference between these two levels. This is found to be 490 ± 10 kev, in good agreement with the results of Graves.[1] The protons from $Be^9(d,p)Be^{10}$ also appear on this plate. Measurements are in progress using the same procedure on the protons from $Li^6(d,p)Li^7$. This work was supported in part by the Office of Naval Research.

[1] E. R. Graves, Phys. Rev. **57**, 855 (1940).

J7. Energy and Angle Variation of $Li^6(d,\alpha)\alpha$. N. P. HEYDENBURG, C. M. HUDSON,* D. R. INGLIS,† AND W. D. WHITEHEAD, JR., *Department of Terrestrial Magnetism.*—The yield curve of the reaction $Li^6(d,\alpha)\alpha$ is observed to have a sharp maximum at $\frac{3}{4}$ Mev, followed by a broad minimum before rising rapidly between 3 and 3.5 Mev, the highest bombarding energy employed. The angular distribution may be expressed in the form $1+A\cos^2\theta+B\cos^4\theta$.

The coefficient A rises from a low value at $\frac{3}{4}$ Mev to a maximum slightly above unity at 2 Mev, then drops to $\frac{3}{4}$ at 3 Mev. The $\cos^4$ term is absent up to 1.5 Mev and makes a small positive contribution at higher bombarding energies.

* Office of the Chief of Ordnance, War Department.
† Johns Hopkins University.

J8. Theory of the Lithium-Two-Alpha Reactions. D. R. INGLIS, *The Johns Hopkins University.*—Recent measurements[1] of the angular distribution of the reaction $Li^7(p,\alpha)\alpha$ show that the intensity varies with angle as $1+A\cos^2\theta+B\cos^4\theta$. The odd parity of Li^7 and the even alphas permit only odd protons. The earlier treatment[2] of entering p-waves which accounts for the term in $\cos^2\theta$ is extended to include entering f-waves and yields a formula for B containing the same resonance denominator as does A. A fit with experiment is obtained with certain matrix elements treated as arbitrary parameters. The p-wave entering at low energies permits assymmetry, but a node in the numerator of A due to fortuitous properties of the compound states brings about symmetry at the lowest energy observed. In the reaction $Li^6(d,\alpha)\alpha$ the asymmetry disappears at low energy in a more natural way, because of the relative impenetrability of the barrier of the even Li^6 nucleus for d as compared with s waves. For a similar reason in $\cos^4\theta$ enters with a higher power of the relative penetrability in the Li^6 reaction than it does in the Li^7 reaction (and it is, indeed, observed[3] to be much less prominent in the former).

[1] Heydenburg, Hudson, Inglis, and Whitehead, Phys. Rev. 73, 216 (1948).
[2] Critchfield and Teller, Phys. Rev. 65, 10 (1941).
[3] Preceding abstract.

J9. Deuteron Bombardment of Boron and Fluorine.* E. L. HUDSPETH AND C. P. SWANN, *Bartol Research Foundation.*—The yield of gamma-rays from boron and from fluorine has been observed as a function of the energy of the bombarding deuterons. The deuteron energy was varied from about 300 to 1200 kev. The yield of gamma-rays from each element rises smoothly, with no indication of any pronounced resonances which cannot be ascribed to carbon contamination. A more thorough investigation is proceeding. The yield of protons from the bombardment by deuterons of a MnF_2 target has also been measured. The beta-ray activity induced in the target through the formation of F^{20} was observed, and this activity is proportional to the proton yield. It was found that the cross section for the reaction at 1.3 Mev is $(1.2\pm0.6)\times10^{-26}$ cm^2; this value was obtained by using a target of about 20-kilovolt thickness. The cross section is about one-third of this value at 900 kilovolts and approximately three times this value at 1.6 Mev. These data are also being extended.

* Assisted by the Office of Naval Research.

J10. Resonances in the Disintegration of Carbon by Deuterons.* T. W. BONNER, J. E. EVANS, J. C. HARRIS, AND G. C. PHILLIPS, *Rice Institute.*—Observations were made on the number of neutrons, gamma-rays, and radioactive N^{13} atoms formed when carbon is bombarded by fast deuterons. The deuterons were detected by recoil protons in a proportional counter. Neutrons were counted which proceeded in the same direction as the deuterons. Resonances at 870 and 1270 kev were obtained in the yield of gamma-radiation, neutrons, and radioactive N^{13}. A pronounced resonance at 1120 kev was observed for gamma-radiation and radioactive N^{13}, but there was only a slight indication of this resonance for neutrons in the forward direction. Since the yield of N^{13} is a measure of the total number of neutrons, this shows that the intensity of neutrons is asymmetrical. Experiments show that the resonance for gamma-radiation at 1417 kev is slightly assymetrical and its half-width is 7 less than kev. Studies were made on the yield of neutrons in the forward direction in the neighborhood of 1417 kev, but no evidence was found for a resonance.

* This work was supported by the Office of Naval Research.

Fluid Dynamics and Ultrasonics

K1. Effect of Length of Capillary on Capillary Rise of Polar Liquids. GEORGE ANTONOFF, *Fordham University.*—Capillary rise is sometimes affected by the length of capillary above meniscus in it. For example, in an aqueous layer benzene-water capillary rise increases with the length of the tube until a kind of saturation is reached. The true value is obtained from the author's law,

$$\gamma_{12}=\gamma_1-\gamma_2$$

where γ_{12} is the interfacial tension, γ_1 is the S. T. (Surface Tension) of the benzene layer, and γ_2 is S. T. of aqueous layer, where the difficulty arises. Its value can be calculated as follows:

$$\gamma_2=\gamma_1-\gamma_{12}.$$

The capillary rise with no or little tube above gives lower values. Above a certain length it gives higher values. Thus, other than Laplacean forces operate, and their range is measured in cm. Glass below the meniscus pulls downwards. That above pulls upwards. The value of S. T. is in between and cannot be computed from capillary rise. These effects are connected with the polar character of substances used.

K2. Intensity as a Factor in Precision Measurements in Ultrasonics. J. A. FITZPATRICK, THOMAS KANKOVSKY, AND WILLIAM J. THALER, *Catholic University of America,** (*Introduced by J. C. Hubbard*).—E. Schreuer[1] has shown that exact measurements of ultrasonic velocity in liquids by means of the Hiedemann method of visibility have a dependence upon intensity which is attributed to a development of a temperature gradient in the sound wave. This implies the necessity of stating the intensity in connection with a measurement of velocity by this method. Work in progress by optical and electromechanical methods, particularly by ultrasonic interferometry, shows that intensities necessary for the latter are much less and that velocity measurements of high precision, both in liquids

and gases, may be made with the ultrasonic interferometer at intensities far below any which can affect the precision of the result.

* Supported by the Office of Naval Research.
[1] E. Schreuer, Akustische Zeits. 4, 215 (1939).

K3. Ultrasonic Velocity in Liquid Halides. ALFRED WEISSLER, *Naval Research Laboratory.*—In order to investigate further the relation between molecular structure and the velocity of sound in liquids, measurements of sound velocity in ten liquid halides at 30° were made with a 3-Mc ultrasonic interferometer. Included were the tetrachlorides of carbon, silicon, titanium, germanium, and tin, which are of interest because their molecules may be considered as approximately spherical. The velocities observed range from about 750 to 1000 meters/second. Neither the velocity nor the adiabatic compressibility varies monotonically with the atomic number of the central atom. However, the computed ratio of specific heats is practically constant for all five tetrachlorides, as expected from their similar structures and degrees of freedom. The other halides studied were those of the phosphorus-arsenic family. Of the ten liquids, silicon tetrachloride has the highest adiabatic compressibility, in agreement with its known low internal pressure.

K4. Supersonic Absorption in Resonant Liquid Column with a Free Face. JOSEPH L. HUNTER, *John Carroll University.*—When standing waves of sound occur in liquid columns, nodal (excess) pressures of zero indicate perfect reflection and zero attenuation in the liquid. Departures from this condition are a function of attenuation and reflection constants. Experimentally, a measurement of nodal pressure may be made by loading a piezoelectric crystal with a liquid column and driving it at its response frequency. The crystal serves the dual purpose of sonic generator and pressure-measuring device. This method was used by Hubbard for measuring absorption in gases and by Fox and Hunter in liquids. It has been found that great simplification occurs if (1) only critical column lengths are considered (2) a free boundary is used as the reflecting face. It may be shown that the effect of the loaded crystal on the electrical circuit is approximately that of a pure resistance connected between the leads to the crystal, and the magnitude of absorption of supersonic waves in the liquid may be readily evaluated when the magnitude of this equivalent resistance is known. Measurements in high viscosity liquids have given absorption values close to those predicted from viscosity considerations.

K5. Concentration of Ultrasonic Beams by Curved Reflectors. F. E. FOX AND V. GRIFFING, *Catholic University of America.*—For the study of cavitation in liquids it is necessary to produce high intensity sound waves within the liquid, while avoiding cavitation at the sound source. With ultrasonic waves, a concave reflector can be used for this purpose. Elementary considerations indicate that 70–80 percent of the power in a plane sound wave beam of diameter D can be concentrated into a beam of diameter $d \simeq \lambda f D^{-1}$ in the focal region of a concave spherical reflector of focal length f, where the wave-length is λ. Using focal lengths 3–4 cm and sound in water with frequencies of 2–4 Mc, a gain (i.e., ratio of intensity in the focal region to that in the plane wave) of 30–60 might be expected. Experiments indicate that gains of this order of magnitude can be obtained. A horizontal beam of moderate intensity strikes the concave reflector which is so tilted that the reflected beam is approximately vertical. With the water surface $2f$ above the reflector, the radiation pressure of the beam striking the surface raises a mound of water about a millimeter high with an area about that of the sound source. As the water level is lowered, the area of the mound decreases and the height increases. When the surface approaches the focal region, the water is lifted out of the surface and thrown in a thin stream in an arc 10 to 15 cm high. At a critical level the water is ejected as a fine spray. Clouds are formed in which the droplets have radii smaller than 10^{-3} cm.

K6. Rigorous Expansions of the Acoustic Radiation Field of a Vibrating Piston in a Baffle.* PAUL M. MARCUS, *Massachusetts Institute of Technology.*—Several new expansions of the field of a vibrating piston in a baffle have been found which are useful for calculations at large values of ka ($k = 2\pi/$wave-length, $a =$radius of piston). These supplement the Backhaus-Stenzel expansions in spherical wave functions which converge well for $ka \leqslant 10$. New, useful recurrence relations and formulas are obtained for the Backhaus coefficients. An expansion in powers of $1/kR$ converges well at any ka for large enough kR. The first term is the familiar asymptotic form of the field

$$[J_1(ka \sin\theta)/ka \sin\theta][\exp[ikR]/kR].$$

The derivation, based on the King integral, also gives the expansion in powers of $1/kR$ of any wave function expressible as a Sommerfeld-type integral. Rearrangement gives a series whose first term is Lommel's formula for Fresnel diffraction through a circular hole. Several expansions are based on Schoch's formula for the field as a cylindrical beam of sound (geometrical optics limit) plus a line integral diffraction correction which is small for large ka.

* This work has been supported in part by the Signal Corps, the Air Materiel Command, and O.N.R.

K7. A Method for the Instantaneous Measurement of Velocity and Temperature in High Speed Air Flow. DOUGLAS MARLOW, C. R. NISEWANGER, AND W. M. CADY, *Inyokern.*—Some preliminary experiments have been conducted to determine the feasibility of direcly measuring shock wave temperatures and particle velocities by means of a train of ultrasonic waves projected across the shock tube of a spark shadowgraph, normal to the direction of propagation of the shock front. The spark shadowgraph is an instrument which consists of a tube along which shock waves are propagated and which has a transparent section through which the shock may be photographed by means of the light from a synchronized high intensity spark discharge lasting about one microsecond. The wave train is generated by a 344-kc x cut quartz crystal mounted with its top surface flush with the bottom surface of the shock tube. The top surface of the latter is covered with felt to

absorb the beam and prevent a standing wave pattern. Various forms of distortion of the ultrasonic wave fronts during and after the passage of the shock may be observed, from which the temperature and particle velocity may be deduced. For example, those waves which have left the crystal before the arrival of the shock are tilted and blown downstream as a group, those which are emitted during the passage of the shock over the crystal are displaced progressively farther downstream (as one proceeds away from the crystal surface) and bent, while those which are emitted after the passage of the shock remain straight and parallel to the crystal but are staggered echelon fashion as in the previous case. From measurements of the various angles and displacements involved one can find the temperature and streaming velocity.

K8. A Supersonic, Intermittent, Movable Wind Tunnel for Optical Studies.* R. LADENBURG, C. C. VAN VOORHIS, AND J. WINCKLER, *Palmer Physical Laboratory.*—A novel kind of supersonic wind tunnel will be described, which runs for times between a few tenths of a second and four seconds. It is used for shadow, schlieren, and interferometric studies. A pressure tank of 250 cubic feet, filled through a compressor line with dry air up to 150 lb./in.^{2}, discharges through a pressure-operated gate valve into a Laval nozzle, a diffuser, and a second tank connected to a high speed vacuum pump. The Reynolds number in the working section (cross section $3\times3''$) can be varied in the ratio 100:1. The Mach number of the present nozzle is 2.3, but much higher Mach numbers will be used also. The light source is a magnesium spark of about 0.2 microsecond duration which, with suitable interference filters, gives at least 50 interference fringes in the blue. The flow around two-dimensional and axially symmetric models and the density, temperature, and velocity profiles in supersonic boundary layers are to be studied by schlieren photography and by interferometry, using a Mach interferometer with 5″ glass plates. This instrument is shock free, supported in a fixed position, but the pressure tank with attached nozzle can be rolled back and forth on tracks so that the various parts of the nozzle may be investigated optically.

* This work is carried out under contract with the Office of Naval Research.

K9. Interferometric Analysis of Two-Dimensional Supersonic Flow Through Small Channels.* D. BERSHADER AND R. LADENBURG, *Princeton University.*—The study by interferometry of the expansion of air from a pressure tank into the atmosphere through a channel of rectangular cross section has been made possible by using plane parallel glass plates for a pair of opposite walls of the channel. Two such channels were used, each about one centimeter in width and two centimeters in depth, one being a divergent channel (half-angle = 4.0°), and the other a Laval nozzle for $M = 1.7$. Results obtained for the potential flow give good agreement with theory as well as with independent measurements of Mach angles on schlieren pictures and shadowgrams. Detailed density measurements have also been made on the turbulent boundary layers along the walls. From these measurements it has been possible to calculate, on the basis of certain assumptions, boundary layer profiles of temperature and velocity.

* This work was done under a contract with the Office of Naval Research.

K10. A Pneumatic Flow Type Pressure Controller. W. A. WILDHACK, *National Bureau of Standards.*—The constancy of flow through a nozzle for which the downstream pressure is less than 0.528 of the upstream pressure is used to obtain a variable, accurately controlled, reduced pressure independent of variations of the suction source. A small flow of air is drawn through a variable restriction in series with a nozzle, by a suction pump. The pressure in the line between the variable restriction and the nozzle depends only on the adjustment of the restriction and is independent of variations of suctions downstream of the nozzle, as long as they are less than 0.528 of the controlled pressure. The device requires a flow of only 1 l.p.m. and can be used as a pilot to operate large valves controlling the pressures in large chambers.

K11. A Linear-Resistance Flowmeter. A. S. IBERALL AND W. A. WILDHACK, *National Bureau of Standards.*—A linear-resistance flowmeter has been developed for general laboratory and instrument applications. It consists of a porous plug of fibrous material, usually glass, with a pressure-measuring device to indicate the pressure drop across the plug, which is proportional to the flow. Since the flow is essentially laminar, the resistance occurs only because of the viscosity of the fluid metered, and it is independent of the density, except for corrections necessitated by molecular effusion at lower pressures. Thus, this type of flowmeter is useful in indicating the volume, or ambient, flow at various pressures. The correction for the effect of temperature on the viscosity of air, for example, is 0.3 per cent per °C. Performance equations based on hydrodynamic drag are found to be more valid for high porosity packs of fibrous materials than those based on the hydraulic radius concept. Formulas and charts are presented to permit design for maximum flows of 10^{-3} to 10^{3} l.p.m., with pressure differences of 10^{-2} to 10^{2} cm of water at full scale.

K12. A Hydrodynamic Problem: The Flapping Wavemaker. E. H. KENNARD, *David Taylor Model Basin.*—Waves of definite frequency can be generated by a boundary executing small displacements from a vertical plane P. The mathematical problem thus presented is interesting because the moving boundary extends in the direction of the subsidiary vertical space variable, whereas propagation occurs horizontally. In the absence of gravity, the motion of the water can be represented by a sheet of sources on P, reflected in the plane S of the free surface to preserve the boundary condition there. The water raised above S by this motion during each successive element of time can be treated as an "initial elevation" and represented in the usual way as a Fourier integral of harmonic oscillations, with reflection in P to preserve the boundary condition there. After a start from rest, the whole motion

ultimately becomes periodic. If the horizontal displacement of the boundary at a depth y below the free surface is $\xi=\xi_0 f(y)\sin\omega t$, the amplitude of the waves of wavelength λ generated at a distance in deep water is $(4\pi\xi_0/\lambda)\times\int_0^\infty e^{-2\pi y/\lambda}f(y)dy$. The solution is easily modified for shallow water.

K13. Application of the Image Converter Tube as Electronic Stroboscope.* GEORGE H. MARKSTEIN, *Cornell Aeronautical Laboratory.*—In the course of work on periodical flow disturbances in flames it appeared desirable to observe the infra-red radiation of the flame gases stroboscopically. It was found that the infra-red image converter tube[1] 1P25 could be operated as a stroboscope by applying rectangular voltage pulses to one or several of the electrodes in such a way that the image was blanked except for a short part of the cycle. Apart from allowing stroboscopic observation in the infra-red, the device offers advantages over mechanical stroboscopes, owing to the absence of inertia, which enables synchronization even with phenomena which are not strictly periodical; the frequency range of operation appears to be limited only by the time constants of the associated circuits. Applications of the device to combustion studies will be shown.

* Work supported by the Bureau of Aeronautics and the Office of Naval Research.

[1] G. A. Morton and L. E. Flory, R.C.A. Rev. 7, 385 (1946).

K14. On the Calculation of Steady Diabatic Flows. B. L. HICKS, *Ballistic Research Laboratories.*—The direct problem amounts to determination of a flow pattern for given boundary conditions and distribution of heat sources q. Experience with almost uniform flows[1a] and with flows derivable from a potential function[1b] ($\bar{V}=\bar{N}(g(N)RT)^{\frac{1}{2}}$, $\bar{N}=\nabla\varphi_N$) suggests that the inverse problem may be more generally tractable. In the direct problem q need not be restricted. In the inverse problem, the Crocco vector $\bar{W}=u\vec{i}+v\vec{j}$ must satisfy an integrability condition[1c] which, for uniplanar flow in the incompressible approximation, becomes $2(v_x-u_y)(u_x+v_y)+v(u_{xx}-u_{yy})+(v_{xx}-v_{yy})u=0$. An experimentally realized low speed flow $\bar{W}(x,y)$ can only fail to satisfy this equation where transient, viscous, or mixing phenomena are appreciable, if the specific heat of the fluid is constant. A new formulation of diabatic flow theory can then be based on (i) specification of $u(x,y)$ in an appropriate region; (ii) specification of v, v_x and v_y on appropriate (partial) boundaries of this region; (iii) solution of the hyperbolic equation for v; and (iv) computation of the $q(x,y)$ necessary to effect this flow. Radial and vortex flows can be calculated completely and will be used to illustrate some of these remarks.

[1] B. L. Hicks, (a) Phys. Rev. 73, (1948); (b) B.R.L. Rep. No. 633, May 1947; (c) Quar. App. Math. Jul. (1948).

K15. Relativistic Rankine-Hugoniot Equations. A. H. TAUB, *University of Illinois.*—In Part I of this paper the stress energy tensor and the mean velocity vector of a simple gas are expressed in terms of the Maxwell-Boltzmann distribution function. The rest density ρ^0, pressure, p, and internal energy per unit rest mass ϵ are defined in terms of invariants formed from these tensor quantities. It is shown that ϵ cannot be an arbitrary function of p and ρ^0 but must satisfy a certain inequality. Thus $\epsilon=(1/\gamma-1)\times p/\rho^0$ for $\gamma>5/3$ is impossible. It is known that if ϵ is given by this relation and $\gamma>2$, then sound velocity in the medium may be greater than that of light in vacuum. This difficulty is now removed by the inequality mentioned above. In Part II of this paper the relativistic form of the Rankine-Hugoniot equations are derived and it is shown that, as a consequence of the inequality mentioned earlier, the shock wave velocity is always less than that of light in vacuum.

Diverse Topics

L1. REAC: Direct Current Analog Computer.* H. BELOCK, E. BROMBERG, S. FIFER, U. MANFREDI, R. MCCOY, AND H. ZAGOR, *Reeves Instrument Corporation.*—REAC (Reeves Electronic Analog Computer) is an electronic analog computer employing direct current computing elements and servos for the solution of initial valued non-linear total differential equations. The basic component of the REAC is a direct current amplifier, and each standard REAC has a total of 20 direct current amplifiers consisting of seven integrating amplifiers, seven inverting amplifiers, and six summing amplifiers. The servos make it possible to carry out multiplications of variable quantities, to perform resolution of vectors, and to introduce arbitrary non-linear functions. Thus each standard REAC can solve differential equations up to the seventh order. However, several REACs can be connected together to increase the capacity of the equipment where higher order problems are involved. Solutions are recorded on a six-channel recorder providing graphical presentation of the effect of changing one or all of the parameters of the problem being solved. Insertion of problems on REAC is carried out by plugging of telephone cords to bays on the front of the cabinet so as to connect the input and output circuits of each amplifier in any desired manner. In order to permit continuously adjustable coefficients, 24 micropots with micrometer dials are provided. The over-all accuracy of REAC is limited by the resistors, capacitors, and drift in the power supplies. A REAC prototype has been in operation for over a year on Navy problems. Solutions of some differential equations will be shown.

* Developed under Contract, Office of Naval Research.

L2. High Speed X-Ray Motion Pictures.* C. M. SLACK, L. F. EHRKE, C. ZAVALES, D. DICKSON, AND R. G. YOUNG, *Westinghouse Lamp Division.*—A system has been developed capable of making up to 150 radiographs in one second. A special hot cathode tube is energized by a pulse transformer circuit to give x-ray pulses of 10 microseconds duration. An alternate excitation method is a choke charging voltage doubling circuit using a trigger tube. The short exposure time permits the use of continuously moving film without blur in the radiographs. Either the indirect method of photographing a fluorescent screen on motion picture film in a camera such as the General Radio oscilloscope camera, or the direct method using specially cut strip film passing over a revolving fluorescent drum may be used. In the latter case, the radiographs may be studied

individually or may be photographed on motion picture film for projection as a movie. The system has been developed primarily for studying the burning of rocket propellants but should find wide application in medical and industrial fields.

* Supported by Bureau of Ordnance, Navy Department.

L3. A Small Generating Voltmeter and Generating Electrometer.* S. E. REYNOLDS AND E. J. WORKMAN, *New Mexico School of Mines.*—The authors describe a small, combination generating voltmeter and generating electrometer which is adaptable to many laboratory uses. Principles previously used by Workman and Holzer[1] have been employed in the construction of an instrument, one and one-half inches in diameter and five inches long. This unit contains a six-volt motor (1/10 watt), a rotating sector, and a subminiature vacuum tube, the grid of which is actuated by contact to the rotating sector. When the rotating sector is alternately exposed and covered in an electric field, the grid control circuit has a sensitivity of approximately 1/20 volt per volt per centimeter of field. The normal plate current is approximately ½ milliampere and may be ink-recorded directly. In another application, an insulated quadrant electrode is presented in close proximity to the rotating sector in which case the instrument becomes an indicating or recording electrostatic voltmeter or electrometer. In this case the grid control voltage may be of the order of one volt per volt on the electrode. Power consumption on the complete unit including amplifier is less than 2/10 watts. Applications of these instruments are discussed.

* The research described in this abstract was supported in part by the War Department Signal Corps.

[1] E. J. Workman and R. E. Holzer, "Recording generating voltmeter for lightning studies," Phys. Rev. **55**, 606(A) (1939).

L4. A Wide Range Field Control System for a Magnetic Spectrograph.* E. P. TOMLINSON, *Princeton University.*—A 20-cm radius of curvature double-focusing magnetic spectrograph of the type developed by Svartholm and Siegbahn[1] is being built. For this instrument a control system has been constructed by which the field of a large electromagnet may be set and held to better than 0.1 percent at any desired value between some 10 and 2000 gauss. The basic element of the system is a monitoring coil rotated in the field at 1800 r.p.m. by a synchronous motor. The resulting 30-cycle voltage, taken from the coil through slip rings, is compared in a potentiometer circuit with a fixed 30-cycle reference voltage. This reference voltage is generated by a permanent magnet rotating, on the same shaft with the monitor coil, inside a fixed coil. Electronic circuits then control the current of the electromagnet so that essentially a null output is maintained from the potentiometer. The final stage of the current control circuit consists of six 6AS7 tubes in parallel, giving a maximum of 1.5 amperes. Four shunts, in addition to the tubes, give the necessary total current range of 0 to 5 amperes.

* This work was supported in part by Navy contract.

[1] N. Svartholm and K. Siegbahn, Arkiv. f. Mat., Ast. och Fysik **33**, No. 21 (1946).

L5. Extremals of Impedance Elements in Wave Guide Equivalent Circuits.* ROBERT M. WHITMER, *Rensselaer Polytechnic Institute.*—Dr. J. S. Schwinger, in unpublished M.I.T. Radiation Laboratory work, has shown that by basing the analysis alternatively on the transverse electric and transverse magnetic fields, one may obtain upper and lower limits to the values of diagonal impedance elements. In the present work it is shown that, at least in some cases, the same procedure also gives limiting values of the squares of the errors in the off-diagonal elements. Unlike the case for the diagonal terms, the signs can be obtained only by numerical calculation.

* This work was done during the war, in the M.I.T. Radiation Laboratory.

L6. Dipole, Quadrupole, and Octupole Field and Search Coils Using Loops and Solenoids. M. W. GARRETT, *Swarthmore College.*—Symmetrical systems of coaxial circular loops designed for nearly uniform central magnetic field (Helmholtz, Maxwell, and McKeehan) produce ideal dipole fields at remote points, to the same approximation. As search coils measuring flux density, they respond only to the axial component of central field. Systems designed for uniform central gradient produce remote quadrupole fields, and measure as search coils the central gradient. Octupole and higher order remote fields correspond to systems producing second- and higher order central fields. Again, flux changes through these various systems measure dipole, quadrupole, or octupole moments of magnets or coils suddenly removed from the central region, while mutual inductance formulas for two such systems assume a primitive form. Systems of coaxial solenoids exhibit slightly modified properties. New types and individual solutions are proposed. For example, when all coils lie on a single sphere, application of recurrence formulas for Legendre polynomials permits calculation of new systems and correlation of known ones. New types employ coaxial solenoids or loops in odd or even number, include dipole quadrupole and octupole systems, may eliminate seven or more terms from the series expansion, and probably have analogues of cylindrical geometry. Solenoid forms are related to Brown's fluxball. Lyle's principle minimizes errors of finite cross section.

L7. The Diffraction Pattern of Electromagnetic Waves in the Planes of Apertures. C. L. ANDREWS, *General Electric Company.*—Measurements were made of the intensities of diffraction patterns in the planes of rectangular and circular apertures and in the planes of equivalent hoops and rods. Whether the apertures were in perfectly reflecting screens or in perfectly absorbing screens, the sharpest diffraction patterns were always in the planes of the apertures themselves. The use of equivalent hoops and rods leads to the alternate explanation of diffraction as a combination of a geometrically propagated wave with wavelets from the edges of the apertures. This treatment of diffraction as an edge effect provides the simplest means of explaining the diffraction pattern in the plane of the screen as well as behind and in front of the screen.

L8. Electrical Activity as Related to Thunderstorm Cell Growth. E. J. WORKMAN AND S. E. REYNOLDS,* *New Mexico School of Mines.*—The internal structure of a series

of thunderstorms, which occurred near Albuquerque, New Mexico, during the summer of 1947, was observed by 3-cm radar. The initial appearance, subsequent growth of the radar echo-producing centers, and the time sequences involved in their development were related to the electrical activity of the storm as indicated by potential gradient change recorders. Data on twelve storm cell studies fit into a consistent pattern. The top of the earliest radar return occurred at about the 22,000 foot level (−10°C isotherm). The subsequent upward growth of the radar return was at the average rate of 850 feet per minute with a range of 450 to 1600 feet per minute. After reaching a height of approximately 31,000 feet (−28°C isotherm) the top of the radar return descended at a rate approximately equal to the rate of ascent. The initiation of electrical activity was nearly synchronous with the maximum height of the return producing area. The electrical activity increased with the descent of the top of the radar picture. In general, the electrical activity ceased when the top of the cell had lowered to approximately 24,000 feet or to about the −13°C isotherm.

* Supported by War Department Signal Corps.

L9. The Source of the Solar Magnetic Field. JAMES W. FOLLIN, JR., *Institute for Advanced Study and Princeton University.*—Recent work of Elsasser[1] has shown that the fluid motion strongly couples the various magnetic modes of a conducting sphere. The reverse coupling, required to form a regenerative system, is not as simple. It is proposed that this coupling results from the Hall effect. The resultant differential equations are non-linear and have non-zero equilibrium solutions, at least one of which is stable. In particular there is an axially symmetric solution which is stable against symmetric perturbation, but its stability against tilting of the dipole axis has not been determined. The sign of the field is determined indirectly from the current carriers (electrons) and appears to have the right magnitude and direction. The energy required to maintain the current distribution generating the field is derived from the variation of angular velocity with radius and latitude. Schwarzschild[2] has shown recently that this velocity distribution is a result of the additional energy flow caused by the effect of centrifugal force on density. Hence, this mechanism may be adequate to explain the solar magnetic field.

[1] W. M. Elsasser, Phys. Rev. **69**, 106 (1946); **70**, 202 (1946); and **72**, 821 (1947).
[2] Schwarzschild, Astrophys. J. **106**, 427 (1947).

L10. Cathode Spark Velocities in $CuSO_4$ Solutions. HUGH F. HENRY, *University of Georgia.*—The velocity of the cathode spark produced in $CuSO_4$ solutions under application of impulsive potentials of 25 kv and 30 kv has been investigated for interelectrode gaps of 10 mm to 80 mm and for solution concentrations between 0.0020*N* and 0.0600*N*. The method used has been previously described for anode spark velocity measurements.[1] Velocities of 100–500 m/sec. have been determined. The average value for 25 kv is 235 m/sec. while the average for 30 kv is 190 m/sec. Empirically, the results indicate that the spark velocity is inversely proportional to the square root of the interelectrode gap but is directly proportional to some function of the solution normality. The average potential existing across the electrodes when the spark ceases its extension into the liquid was computed to be 15.6 kv. This value is close to that obtained for the anode spark under similar conditions.[2]

[1] H. F. Henry, Phys. Rev. **69**, 693 (1946).
[2] H. F. Henry, Phys. Rev. **72**, 184 (1947).

L11. The Refractive Index of Several Hydrocarbons in the Near Ultraviolet Wave-Length Region. JAMES L. LAUER,* *University of Pennsylvania.*—Index of refraction measurements were carried out with twenty-one liquid hydrocarbons, paraffinic, naphthenic, olefinic, and aromatic, in their respective transparent regions between 220 and 420 millimicrons, both at 20° and at 25°C, to an average accuracy and precision of ±0.0002 in refractive index. The data for each compound were fitted to an empirical equation relating frequency and index and from these the constants in the Sellmeier-Drude equation were calculated wherever possible. Interesting variations in these constants were observed for compounds of related structures. The instrument used for the measurements was the same as the one described in an earlier article.[1]

* Present address: Sun Oil Company, Norwood, Pennsylvania.
[1] James L. Lauer and P. H. Miller, Jr., J. Opt. Soc. Am. **37**, 664–668 (1947).

Reactions of Transmutation

P1. Corrections to Range Data. R. F. HUMPHREYS AND H. T. MOTZ, *Yale University.**—The interpretation of the ranges of particles emitted in an induced nuclear reaction has been considered in some detail by Livingston and Bethe.[1] They have calculated corrections due to target thickness, angle spread (for 90° observation), and range straggling that must be applied to observed extrapolated ranges to obtain mean ranges and energies. In the present work there is added to these corrections the effects of primary beam inhomogeneity, the level sensitivity of the proportional counter, and the variation of electrical counter depth. It is shown that the common practice of "peaking" a counter may introduce an appreciable shift of the extrapolated ranges caused both by shift in counter depth and by change in the observed group shape. The width of observed groups may be altered considerably by the counting level as well as by the beam inhomogeneity. To a good approximation these effects are predictable. They are shown to be range dependent and vary from reaction to reaction. Their relative magnitudes for both 90° and 0° observation are discussed.

* Assisted by the Office of Naval Research.
[1] Livingston and Bethe, Rev. Mod. Phys. **9**, 245 (1937).

P2. The $Na^{23}(\alpha p)Mg^{26}$ Reaction. H. T. MOTZ AND R. F. HUMPHREYS, *Yale University.*—The corrections discussed in the above abstract have been applied to the $Na^{23}(\alpha p)Mg^{26}$ reaction for 0° observation. Thin sodium targets have been bombarded with 7-Mev alpha-particles from the cyclotron. Four groups were observed, the second of which is only barely resolved from the ground state and

has not been previously reported. The beam energy and inhomogeneity has been measured by a proportional counter calibrated with ThC′ alphas. The extrapolated ranges of the proton groups have been corrected for the effect of beam inhomogeneity, angle spread, range straggling, counter "peaking," and counter depth. The corrections are of the magnitude of 5 cm for the 88 cm end group. The Q values obtained are 1.44, 1.12, −0.30, and −1.3 Mev. Gamma-ray absorption measurements[1] are in agreement with the transition from the third excited level. The ground state Q differs by 0.5 Mev from the value reported in early work, but is consistent with the reactions $Mg^{25}(d\alpha)Na^{23}$ and $Mg^{25}(dp)Mg^{26}$ studied in this laboratory. Using the Na^{23} mass reported by this laboratory[2] a new Mg^{26} mass is found to be 25.99133±0.0003 Mu.

* Assisted by the Office of Naval Research.
[1] David E. Alburger, Bull. Am. Phys. Soc. **23**, 9 (1948).
[2] Elder, Motz, and Davison, Phys. Rev. **71**, 917 (1947).

P3. The $Al^{27}(dn)$ Reaction. R. A. PECK, JR., *Yale University.**—A thin aluminum target has been bombarded with 3.6-Mev deuterons and the energy distribution of the evolved neutrons studied, following a conventional microphotographic procedure.

* Supported by the Office of Naval Research.

P4. Energy Levels of Al 28 and Mg 25. E. POLLARD, V. L. SAILOR, AND L. D. WYLY, *Yale University.**—Al 28 can be formed by the dp reaction on Al 27. Attempts to resolve the proton structure into groups in the past have been unsuccessful.[1] This indicates an unusually close level spacing. Recent work by Seagondollar and Barschall indicates that neutron scattering by Al 27 shows fluctuations in cross section which correspond to levels in Al 28 about 70 kv apart. These are at an excitation of 7 Mev. Observation of protons from a thin layer of Al bombarded by deuterons shows the presence of 20 levels between 0 and 6.5-Mev excitation. These levels occur in five fairly definite groups, one near the ground state, which appears to be either a doublet or a triplet, and each of the others at approximately 1.3-Mev separation. The separation of the individual levels, as far as they are at present resolved, is approximately 250 kv. This is definitely less than usually observed. The maximum Q value for the above reaction is 5.64 Mev. Alpha-particles occurring in three groups of Q values 7.05, 6.38, and 5.70 Mev are observed corresponding to the ground state and two excited states of Mg 25. Additional group structure may be present.

* Assisted by the Office of Naval Research.
[1] H. L. Schultz, W. L. Davidson, and L. Ott, Phys. Rev. **58**, 1043 (1940).

P5. Recent Results of Investigation of Reaction S(dp). PERRY W. DAVISON, *Yale University.**—Further investigation of the proton groups from the deuteron bombardment of sulphur has disclosed the presence of a low intensity long range group with a Q of 8.8±0.1 Mev. It is believed that this group corresponds to the ground state of S^{34} from the reaction $S^{33}(dp)S^{34}$. However, this assignment is not definite being based on this group's intensity relative to what is thought to be the ground state group of S^{33}, Q=6.48 Mev. This ratio of intensities is about 1:100 and the relative concentrations of S^{33} and S^{32} is 1:130. Assuming this assignment the following mass differences, in mass units, are obtained: $S^{33}-S^{32}$, 0.99965 ±0.00005; $S^{34}-S^{33}$, 0.9972±0.0001; $S^{34}-S^{32}$, 1.9969 ±0.0002. Four of the groups previously reported and assigned to S^{33} have been found to be double. This may possibly be caused by overlapping of the S^{33} and S^{35} patterns. The definite assignment as to isotope in this study will have to wait until separated isotopes are available.

* Assisted by the Office of Naval Research.

P6. Measurement of Short Range Nuclear Recoils from Disintegrations of the Light Elements. S. K. ALLISON, H. V. ARGO, W. R. ARNOLD, L. DEL ROSARIO, H. A. WILCOX, AND C. N. YANG, *University of Chicago.*—An energy selection of the disintegration particles from beryllium and deuterium (D_2O ice) targets under 200–400 kv proton and deuteron bombardment has been accomplished with a cylindrical electrostatic deflector. The particles emerging from the deflector are detected by an Allen electron multiplier tube.* The absence of any foil or window between the target and the detector makes is possible to observe all particles with energies below an upper limit zW_{max} where z is the number of electronic charges on the fragment and W_{max} is an upper limit defined essentially by the geometry of the deflector and the high voltage it will tolerate. In our work W_{max} is close to 1 Mev. From the reactions $Be^9(p,\alpha)Li^6$ and $Be^9(p,d)Be^8$ one observes scattered protons, disintegration α's and d's and the lithium particles, the latter appearing in three states of ionization. Unfortunately, in the present state of our experiments interference from the scattered protons prevents observation of the α's from Be^8. Scattered deuterons, He^3 and H^3 particles from the (d,d) reactions are observed. The He^3 particles indicate a provisional Q of 3.35±0.05 Mev for $D(d,n)He^3$, agreeing with Bonner's 1941 value** of 3.31±0.03 Mev obtained from the ranges of protons recoiling from the neutrons. Experiments are being continued.

* The preparation of electron multiplier tubes for these experiments has been accomplished with the aid of funds from the Office of Naval Research.
** T. W. Bonnner, Phys. Rev. **59**, 237 (1941).

P7. Threshold and Resonances in the $C^{14}(pn)$ Reaction.* W. E. SHOUPP AND B. JENNINGS, *Westinghouse Research Laboratories.*—The threshold energy required to induce the (pn) reaction in C^{14} has been measured to be E_t=.662 ±.003 Mev. This reaction is the inverse of the $N^{14}(np)$

process studied by Hughes and Eggler[1] and their observed reaction energy $Q_{np}=.597\pm.009$ Mev may be compared[2] with the negative of the reaction energy $Q_{pn}=-.617\pm.002$ Mev observed here. The errors assigned do not include errors in the absolute voltage scale that may amount to as much as 1 percent. Two resonances in the process have also been observed at proton energies of 1.135 and $1.28\pm.004$ Mev respectively. These energy levels of the compound nucleus N^{15} may be correlated with the two lowest states previously observed in the $N^{14}(np)$ reactions.[3,4]

* This work performed under contract with Office of Naval Research.
[1] Hughes and Eggler, Bull. Am. Phys. Soc. 23, 10 (1947).
[2] Stephens, Rev. Sci. Inst., 19, 22 (1947).
[3] Barshall and Battat, Phys. Rev. 70, 245 (1946).
[4] Huber and Stebler, Phys. Rev. 73, 89 (1948).

P8. The $N^{14}(n,p)$ Reaction and the Proton Range-Energy Curve. W. FRANZEN, I. C. CORNOG AND W. E. STEPHENS, *University of Pennsylvania.*—The range of protons emitted in the slow neutron disintegration of nitrogen has been measured in a cloud-chamber to be 1.00 cm of air, in agreement with other observers. The energy of this proton (561 kev as deduced from the extrapolated end-point of the C^{14} beta-spectrum and the n-H mass difference) establishes a point on the proton range-energy curve. This point agrees well with Bethe's 1937 curve,[1] but deviates considerably from his later curve.[2] It is pointed out that other points can be established on the proton range-energy curve in this region by data on reaction cycles involving (a) other slow neutron (n,p) reactions [$He^3(n,p)$, $B^{10}(n,p)$, $Cl^{35}(n,p)$, $Sc^{45}(n,p)$] and the extrapolated end-points of the beta-spectra of the product nuclei; (b) protons emitted in $D^2(\gamma,n)$ and the energy of the gamma-ray (ThC″, Na^{24}); (c) H^3 nuclei emitted in $He^3(n,p)H^3$ and $Li^6(n,\alpha)H^3$ (in these cases proton ranges can be computed from the H^3 ranges with small error). Existing data on these types of experiments will be compared with published range-energy curves to point out agreements, discrepancies and possibilities for further measurements.

[1] Livingston and Bethe, Rev. Mod. Phys. 9, 268 (1937).
[2] H. A. Bethe, Phys. Rev. 53, 313 (1938).

P9. Thin Target (α,n) Cross Sections of Be, Mg, and Al.* I. HALPERN,** *Los Alamos Scientific Laboratory.*—The (α,n) cross sections for beryllium, magnesium, and aluminum were measured as a function of alpha-energy up to the full energy of polonium alphas. The cross sections were determined by counting the neutrons released in the reactions in a graphite block with a slow-neutron counter. The energy response of the counting apparatus was reasonably "flat." The disintegration chamber was of spherical geometry with the source at the center. Energies of alphas incident on the surrounding target were determined by the pressure of the stopping gas in the chamber. The target and source thicknesses were such that the energy resolution was of the order of 10 percent. The lowest resonance in beryllium occurs at 1.6 Mev. The cross section at the peak is .13 barns and rises to .4 barns at 5 Mev. The aluminum and magnesium cross sections are smaller by a factor of about twenty, and no resonances can be identified with certainty.

* The information contained herein will appear in Division V of the National Nuclear Energy Series (Manhattan Project Technical Section) as part of the contribution of the Los Alamos Laboratory.
** Now at Massachusetts Institute of Technology.

Cryogenics

Q1. Superconducting Noise and Rectification. DONALD H. ANDREWS, *Johns Hopkins University.**—Using a superconducting bolometer of CbN, measurements have been made of the background noise for 18 values of the current between 0 and 42 ma. Temperature was varied slowly over the transition range between 15° and 16°K and simultaneous tracings made with two recording potentiometers of the d.c. resistance of the bolometer and of the amplified and rectified noise potential. For low current the noise was greatest in the superconducting state and for high current in the normal state. As temperature varied, there were many peaks of noise, the pattern varying strikingly with current. At high currents the peaks were associated with breaks in the d.c. resistance curve. The pattern of rectification at radio frequency showed similar variations with different values of imposed d.c. The magnitude of rectified signal was greatest for r.-f. between 0.2 and 1.2 mc. and between 50 and 110 mc. Rectification was at a maximum for r.-f. modulated between 300 and 700 c.p.s. and fell off sharply above 1200 c.p.s. Reversing the direction of d.c. changed both the magnitude and temperature pattern of rectification.

* This research was carried out under a basic research contract with the Physics Division, Office of Naval Research, U. S. Navy.

Q2. A Recent Study of the Infra-Red Sensitivity of Superconducting Bolometers.* NELSON FUSON, *Johns Hopkins University.*—25 columbium nitride superconducting bolometers have been studied for sensitivity and noise characteristics. These bolometers were irradiated with a wide band of 360 c.p.s. square wave modulated, infrared radiation of about $\frac{1}{10}$ microwatt mm² intensity. The bolometer response was amplified by a matching input transformer and wide band amplifier such that the combined gain was 5×10^6. Time constants ranging from 0.8 to 17.0 milliseconds were measured for the last 12 bolometers studied. The minimum detectable power of these latter bolometers range from 0.3 to 300×10^{-10} watt when calculated under the reference conditions suggested by Jones.** Comparisons are given between these superconducting bolometers and other infra-red detectors described in the literature.

* This work has been supported by the Rockfeller Foundation.
** R. Clark Jones, J. Opt. Soc. Am., 37, 879 (1947).

Q3. Surface Impedance of Tin at 24000 mc/sec.* E. MAXWELL, P. M. MARCUS, AND J. C. SLATER, *M.I.T.*—The surface resistance of white tin has been measured at 24000 mc/sec. from 300°K to 4°K and in the superconducting state from 4° to 2°K. It is found, in agreement

with other experimenters[1] that the surface resistance approaches an asymptotic value at low temperatures independent of the d.c. resistivity. At 4°K the apparent a.c. resistivity is 60 times the d.c. value. The general form of the variation roughly follows the (unpublished) theory[2] of E. H. Sondheimer and A. E. H. Reuter of Cambridge. By fitting the experimental data to the theoretical curve one can calculate an approximate value for the number of free electrons per atom. We find a value of 0.2. The theory can be extended to the superconducting case by adding another term for the super-current. It is then possible to obtain the variation with temperature of the static penetration depth λ, of the superconductor, by making assumptions about the change in the number of normal electrons below the transition temperature. The curve obtained agrees approximately with other determinations and we find a value of 7×10^{-6} at 2°K.

* This work has been supported in part by the Signal Corps, Air Materiel Command and O.N.R.

[1] London, H., Proc. Royal Soc., **A176**, 522 (1940); Pippard, A.B., Proc. Roy. Soc. **A191**, 371 (1947); Garrison, J.B., Ph.D. thesis, M.I.T., 1947.

[2] Private communication to Prof. J. C. Slater.

Q4. On Temperature Dependence of Penetration Depth in Superconductors. JULES DE LAUNAY AND M. C. STEELE, *Naval Research Laboratory.*—Using the Gorter-Casimir thermodynamic theory of superconductivity, the form of the Sommerfeld relation for the specific heat of electrons, the form of the acceleration theory for the penetration depth, λ, and the parabola relationship for the threshold magnetic fields, it is found that the variation of λ with temperature T is given by $\lambda/\lambda_0=[1-(T/T_c)^6]^{-\frac{1}{2}}$, where λ_0 is the penetration depth at 0°K, and T_c is the transition temperature for no applied magnetic field. Comparison with experiments on mercury and tin shows good agreement. Absolute values for the penetration depth of these elements are calculated from the experimental results by using the derived equation.

Q5. De Haas-van Alphen Effect in Zinc. L. ONSAGER AND J. E. ROBINSON, *Yale University.*—Blackman's theory[1,2] of the de Haas-van Alphen Effect is applied to data obtained by S. G. Sydoriak[3] for Zn at 4.2°K. Agreement with theory for fields up to 3 kilogauss is good for the spacing of the oscillations of the magnetic moment, less certain for the envelope shape. Data for higher fields is incomplete. The data for Zn can be accounted for in terms of one zone of hexagonal symmetry containing about 8×10^{-6} electrons per atom, these electrons having a chemical potential $E_0\sim.02$ ev, longitudinal effective mass $m_{||}\sim20m_0$, and transverse effective mass $m_\perp\sim.01m_0$. As implicitly required for the application of Blackman's theory, the computed specific heat of the de Haas-van Alphen zone is small compared to the measured electronic specific heat.

[1] M. Blackman, Proc. Roy. Soc. (A), **166**, 1 (1938).
[2] D. Shoenberg, Proc. Roy. Soc. (A), **170**, 341 (1939).
[3] S. G. Sydoriak, Bull. Am. Phys. Soc., **23**, No. 2, p. 15.

Q6. Characteristics of Liquid Air as a Low Temperature Bath. LESTER I. BOCKSTAHLER AND HARMON PLUMB, *Northwestern University.*—Baths of liquid air, pure oxygen, and commercial nitrogen were studied under the usual laboratory operating conditions. The temperature and oxygen content of each bath was determined at regular time intervals as the liquid evaporated (a) freely under atmospheric pressure, (b) rapidly at reduced pressure, (c) rapidly upon the introduction of an immersion heater. Temperatures were read by means of a platinum-resistance thermometer. The percent oxygen content was computed from density measurements made by the usual Jolly balance method—weighing an aluminum cylinder in air, water and in the liquid in turn. The comparative behavior of each liquid sample is shown by time-temperature graphs. Freshly prepared liquid air may vary as much as twenty percent in oxygen content depending on the method of liquefaction. Results of the oxygen-nitrogen composition are in good agreement with the values found by Dodge and Dunbar[1] using varying mixtures of pure oxygen and nitrogen.

[1] J. Am. Chem. Soc. **49**, 591 (1927).

Q7. The Effect of Relaxation on the Theory of Second Sound in Helium II. WILLIAM BAND AND LOTHAR MEYER, *University of Chicago.*—Following the idea that propagation of second sound implies a lack of internal equilibrium, the equations for the two-velocity field model of liquid helium II[1] are generalized. Expressions follow for $V_{s\infty}$, $V_{n\infty}$ and V_{s0}, V_{n0}, respectively the velocities of propagation of second sound and normal sound at infinite frequency (no relaxation) and zero frequency (complete thermal equilibrium or full relaxation). At zero frequency the second sound reduces to thermal diffusion (V_{s0} imaginary). Normal sound undergoes a sharp Einstein dispersion and absorption at the lambda temperature (for generally used frequencies) in agreement with attenuation measurements.[3] The theory is used to compute σ the fraction of normal particles from thermodynamic and second sound velocity data,[4] and the energy per normal particle is obtained from σ and the experimental data on total heat content.

[1] W. Band and L. Meyer, Phys. Rev. **73**, 226 (1948).
[2] L. D. Landau, J. Phys. U.S.S.R. **5**, 71 (1941); **11**, 91 (1947); L. Tisza, Phys. Rev. **72**, 838 (1947).
[3] J. R. Pellam and C. F. Squire, Phys. Rev. **72**, 1245 (1947).
[4] V. P. Peshkov, J. Phys. U.S.S.R. **8**, 381 (1944); **10**, 389 (1946); C. T. Lane, H. Fairbank and W. Fairbank, Phys. Rev. **71**, 9 (1947).

Q8. Relaxation and Heat Conductivity in Liquid Helium II. LOTHAR MEYER AND WILLIAM BAND, *University of Chicago.*—The equation for thermal diffusion derived above[1] agrees with the relaxation equation used previously[2] if the second sound velocity is corrected to zero frequency. The relaxation time τ is calculated to a higher accuracy. The peculiar property of the heat current in being proportional to the cube root of the temperature gradient can be phenomenologically reduced to the relation $u_s^2\tau_s=J$, where u_s is the velocity of the superfluid balancing the mass flow of normal particles transporting the energy. τ_s is a relaxation time derived from τ by the conditions for frequency balance. J is a simple function of temperature only, approaching $h/m\pi$ at temperatures below 1°K. The

equations lead to a qualitative understanding of the reduction of thermal conductivity by mass flow.[3]

[1] Meyer and Band: preceeding abstract.
[2] Band and Meyer, Phys. Rev. **73**, 226 (1948).
[3] Kapitza, P., J. Phys. U.S.S.R. **4**, 181 (1941).

Q9. Approximate Methods in Momentum Space. M. DRESDEN, *University of Kansas.*—A theoretical discussion of the properties of liquid He II should be based on the properties of the (non-relativistic) quantum mechanical many-body problem. Since it has been conjectured that at low temperatures there exists some kind of order in momentum space,[1] it has seemed worth while to obtain methods which will approximate the momentum wave function directly. This wave function satisfies an integral equation of the Hopf-Wiener type. It is possible using the conventional integral equation methods to obtain a sequence of functions the limit of which is the exact wave function in momentum space. Fourier inversion of the members of the sequence gives then an approximating sequence for the wave functions in coordinate space. Each member of this sequence can be expressed in terms of integrals over the potential energy function. The first approximation to this coordinate wave function, describes particles in essentially a constant field (some averaged field)—the next approximation utilizes more details of the potential energy function. Similar methods can be used to obtain the eigenvalues—in particular some information about the lowest eigenvalue and the lowest wave function can be obtained.

[1] F. London, Rev. Mod. Phys. **17**, 310 (1945).

Mesons Natural and Artificial

S1. Production of Mesons by the 184-inch Berkeley Cyclotron. Part I. Experimental Arrangement.* EUGENE GARDNER AND C. M. G. LATTES, *University of California, Berkeley.*—We have observed tracks which we believe to be due to mesons in photographic plates placed near a target bombarded by 380-Mev alpha particles. The plates used were Ilford Nuclear Research Plates, type C.2. The identification of the particles responsible for the tracks was first made on the basis of the appearance of the tracks; they show the same type of scattering and variation of grain density with residual range found in cosmic-ray meson tracks by Lattes, Occhialini, and Powell,[1] and about two-thirds of them produce observable stars at the end of their range. For a 10-minute exposure in the cyclotron, about 50 meson tracks are found along the 3-inch edge of a photographic plate. Carbon, beryllium, copper, and uranium have been used so far as target materials, and all are found to give mesons. When a carbon target was bombarded with 300-Mev alpha particles, mesons were found but with reduced yield.

* This paper is based on work performed with the support of the Atomic Energy Commission.
[1] C. M. G. Lattes, G. P. S. Occhialini, and C. F. Powell, Nature **160**, 453, 486 (1947).

S2. Production of Mesons by the 184-inch Berkeley Cyclotron. Part II. Mass Determination.* C. M. G. LATTES AND EUGENE GARDNER, *University of California, Berkeley.*—The mass of the mesons produced by the 184-inch Berkeley cyclotron has been determined by measuring the bending in the magnetic field and the range in emulsion. The radius of curvature of the trajectory is found by measuring the distance from the target to the point at which the meson enters the emulsion and the angle which the track makes with the edge of the plate. From the first 50 meson tracks measured we find a mass of 313 ± 16 electron masses. It is highly probable that these mesons are the heavy mesons described by Lattes, Occhialini, and Powell.[1] The mass determination which we have made was done with apparatus intended only for survey work, and some of the error is associated with lack of precision of location of the photographic plates. There was an aluminum foil of thickness 0.001 inch in front of the plates. It is thought that much better accuracy will be possible with better apparatus and a thinner foil.

* This paper is based on work performed with the support of the Atomic Energy Commission.
[1] C. M. G. Lattes, G. P. S. Occhialini, and C. F. Powell, Proc. Roy. Soc. (in press).

S3. Search for Photons from Stopped Mesons. ORESTE PICCIONI, *Massachusetts Institute of Technology.*—The main purpose of this research was to investigate whether the rest energy of negative (normal) mesons, captured in Fe, is released in the form of light. At the same time a check has been made on the possibility that photons are emitted together with electrons, in the decay process of positive mesons stopped in Fe. The apparatus consists of a vertical telescope for collimating a beam of penetrating particles in an iron plate (absorber). By means of anti-coincidence counters, events were selected corresponding to particles stopped in the absorber. For those events a picture was taken of a scope indicating which one of a group of counters H was discharged. The counters H were disposed at one side of the absorber, and from the picture it was possible to determine whether a photon coming from the iron was converted in a lead plate. The results rule out the assumption that one (or more) photon of energy 30 Mev (or more) accompanies the stopping of each negative meson. The same results indicate as well that the decay process of positive mesons does not involve emission of high energy photons. This is in agreement with a recent works of R. Sard and co-worker, and of B. Pontecorvo and co-worker. In the hypothesis of a neutral meson emitted in the process involving the disappearance of a negative meson, a lower limit of 10^{-10} sec. is established for the mean life of such a neutral particle, assuming that it would decay in two high energy photons.

S4. Search for Heavy Particles from Stopped Mesons.* W. Y. CHANG, *Princeton University.*—A cloud chamber of 12 inches diameter, 5 inches depth and having small dead space was constructed for studying meson absorption by nuclei. A vertical meson beam is selected by a three-fold coincident telescope, which is put above the chamber and protected against side-showers by anticoincident counters. The lower circumference of the chamber is surrounded with many anticoincident counters, so that the chamber ex-

pands only when a particle stops in the chamber or in the chamber and counter walls. Before entering the telescope the mesons pass through a lead block of 35 cm to increase the slow meson intensity. The chamber is kept in a constant-temperature room and found to work satisfactorily for days without readjustment. The operation of the chamber, the lights, camera, etc. is controlled automatically by an electronic unit. Thin iron (0.028 inch) and lead (0.018 inch) foils have been separately put inside the chamber. Our preliminary results (more than ten pictures) show no evidence of star production or emission of a single heavily ionizing particle when a meson appears to stop at a foil. The emission of a neutral particle such as a neutral meson seems, therefore, to be necessary after nuclear capture of a negative meson. The effect being studied is smaller than any one of the effects due to side-showers, absorption by the chamber and counter walls, inefficiency of the anticoincident counters, scattering from the top of the chamber, etc. These have made the experiment fairly difficult. Improvements are being made and further results will be reported.

* This work was supported in part by Office of Naval Research.

S5. The Time Distribution of Decay Electrons from Mesons Stopped in Magnesium at 3500 m Altitude.* R. D. SARD AND A. H. BENADE, *Washington University.*—Two sets of G-M tubes, above (*I*) and below (*II*) a 7.6 cm Mg block respond respectively to the incident meson and the decay electron. The circuit[1] records delayed coincidences of the pulses from *I* and *II* in ten contiguous channels ranging from 0.5 to 6.5 μsec. Beneath *II* is a counter tray, *C*, separated from it by a Pb slab thick enough to stop any decay electron from the Mg. The circuit can be switched to respond only if *C* discharges within 0.5 μsec after *I*. In this way the distributions of counter lags greater than 0.5 μsec is determined. Measurements of these lags and of decay electrons were alternated; frequent calibrations were made. There were enough spontaneous lags in the first channel to necessitate an appreciable correction to the decay data for this channel. A differential plot of the 1663 points in the later channels (1.1 to 6.5 μsec) gives a smooth curve, closely fitting that calculated assuming equal numbers of positive and negative stopped mesons, with mean lives of 2.2 and 1.0 μsec respectively.[2] A single exponential with a mean life of 1.7 μsec gives not as good a fit.

* We are indebted to the U. S. Navy for support, and to M. Schein and E. F. Fahy for permission to use the University of Chicago Laboratory at Climax, Colorado.
[1] Based on a design of M. L. Sands: B. Rossi, M. Sands, and R. D. Sard, Phys. Rev. **72**, 120 (1947).
[2] H. K. Ticho and G. E. Valley; results obtained independently and communicated at the Chicago Meeting, American Physical Society, Dec. 30, 1947.

S6. Decay of Mesons in Carbon. C. W. KISSINGER AND D. COOPER, *University of Maryland* (*Introduced by D. Cooper*).—A method is being used for determining the life times of positive and negative mesons in carbon. Geiger-counters in coincidence define a solid angle. Slow positive and negative mesons are separated in a magnetic field and deflected into graphite blocks placed outside the solid angle. The decay electrons are detected as they emerge from the respective graphite blocks. The time between the pulse from the meson and the pulse from the decay electron is measured on a servoscope by photographing the trace. Anticoincidence counters are used to prevent sweeping of the servoscope by mesons that are not deflected into an absorbing block. Preliminary results indicate that both positive and negative mesons decay in carbon with the ejection of an ionizing particle. These results are in agreement with the results of other experiments on the decay of negative mesons in elements of low atomic number.[1,2,3]

[1] M. Conversi, E. Pancini, and O. Piccioni, Phys. Rev. **71**, 209 (1947).
[2] H. K. Ticho and M. Schein, Phys. Rev. **73**, 81 (1948).
[3] G. E. Valley and B. Rossi, Phys. Rev. **73**, 177 (1948).

S7. On the Energy Dependence of the Positive Meson Excess.* M. H. SHAMOS, M. G. LEVY, AND I. S. LOWEN, *New York University.*—The numbers of decay electrons (delayed more than 1 μsec.) from carbon and aluminum have been measured under 10 cm, 30 cm, and 50 cm, of Pb at sea level. The relative sizes of the absorbers were chosen in the ratio of the ranges of the decay electrons in the two materials so as to assure equal probability for detection. Measurements on the mean life are consistent with the value 2.15 μsec. (with a precision of ±10 percent). Under the assumption that both positive and negative mesons decay in carbon, while only the positive mesons decay in aluminum, the relative yields (after subtracting background) permit the comparison of the total number of mesons with the number of positive mesons. The results show no significant dependence upon energy (in the range ~200–800 Mev) in agreement with cloud chamber results,[1] but are in agreement with a 20 percent positive excess only if negative mesons do undergo decay in aluminum, the fraction decaying (beyond 1 μsec.) being ~.30±.16. Extrapolation of this fraction to zero time, assuming the apparent mean life of negative mesons in aluminum is ~0.7 μsec.,[2] would indicate that *all negative mesons decay in aluminum.* Although the precision of this result is rather poor, it is fairly certain that some fraction of the negative mesons decay in aluminum.

* Supported by the Office of Naval Research.
[1] V. J. Hughes, Phys. Rev. **57**, 592 (1940).
[2] G. E. Valley and B. Rossi, Phys. Rev. **73**, 177 (1948).

S8. Slow Mesons in the Atmosphere.* MATTHEW SANDS, *Massachusetts Institute of Technology.*—Further measurements have been made, at altitudes between sea level and 11,000 meters, of the intensity of mesons near the end of their range. The apparatus was similar to that used previously and the results agree with those reported.[1] Measurements were made also with 7.5 cm of lead above the apparatus. The altitude variation of the counting rate was the same as that observed without lead. The same selection technique has been used with a different geometry to determine directly the differential range spectrum and the absolute intensity at sea level of mesons with ranges between zero and 30 cm of lead. The vertical intensity at sea level of mesons which stop and decay in 15 g cm^{-2} of carbon was found to be $(4.4\pm0.3)\times10^{-5}$ sec.$^{-1}$ sterad^{-1}. The intensity of mesons which penetrate 166 g cm^{-2} of lead and stop in 15 g cm^{-2} of carbon was found to be

$(5.1\pm0.3)\times10^{-5}$ sec.$^{-1}$ sterad^{-1}, which value agrees with the result of Koenig.[2]

* The work reported was supported in part by the Office of Naval Research. The aircraft used was provided by the Army Air Forces.

[1] B. Rossi, M. Sands and R. F. Sard, Phys. Rev. **72**, 120 (1947).
[2] H. P. Koenig, Phys. Rev., **69**, 590 (1946).

S9. An Interpretation of Dual-Cosmic Ray Events. R. M. LANGER, *Bureau of Ships*, AND HERMAN YAGODA, *National Institute of Health.*—Three *II*-pronged events recorded in nuclear emulsions exposed at sea level cannot be attributed to nuclear evaporations of component atoms. The three events are related in that the energy and momenta of the particles producing the tracks are explicable on the transformation of heavy primary mesotrons into charged mesotrons of smaller mass. The first event is represented by a 1 Mev proton track and a meson with a recorded track length of 2170 microns having an angle between tracks of 100°. In the second event the track of a 13 Mev alpha particle and a 4.1 Mev secondary mesotron diverge at an angle of 120° and terminate in the emulsion layer. The emergent mesotron has a range of 613 microns and appears to be identical with the *u*-mesotrons described by the British investigators. Momenta considerations indicate a mass of 630 m_e for the incident particle. The third event is comprised of the tracks of two mesotrons of 6 and 1 Mev kinetic energy divirging at an angle of 138°. If their masses be assumed equal (200 m_e), the incident mass corresponds to 400 m_e. The spatial orientation of the events in the original AgBr-gelatin layer suggests that the incident mesotrons were probably uncharged.

S10. Emission of Radiation in the Disintegration of Mesons. DANIEL B. FEER, *Harvard University.*—When a meson of integral spin disintegrates into an electron and neutrino, the acceleration of charge should be accompanied by electromagnetic radiation. The amount of such radiation has been calculated by second-order Dirac perturbation theory for various types of coupling. In common with other second-order radiative effect calculations, the total cross section diverges logarithmically (infra-red catastrophe), so that the lifetime for this process alone cannot be calculated. The ratio of the mean radiation energy emitted to the energy available from the disintegration gives a measure of the probability of the process. For all models considered this ratio is about 0.85 $e^2/ch=0.6$ percent, and varies logarithmically with the meson mass. It is too small to be observed in the experiments designed to detect 50 Mev photons from the decay of mesons of spin one-half.

S11. Trajectories of Charged Meson Test Particles in the Similarity Geometry. BANESH HOFFMANN, *Queens College.*—With the same physical identifications of the components of the basic similarity tensor $S_{\sigma\tau}$ as in the unitary field equations of the gravitational, electromagnetic, and vector meson fields,* the geodesic-like variational principle

$$\delta\int\left\{s_{\sigma\tau}\frac{dx^\sigma}{dt}\frac{dx^\tau}{dt}\right\}^{\frac{1}{2}}dt=0 \qquad (s_{\sigma\tau}\equiv S_{\sigma\tau}/S_{00}),$$

yields the correct equations for the trajectories of charged meson test particles. The ideas behind the similarity theory reveal a close relationship between the hitherto diverse unitary theories of Weyl and Kaluza. The geometers showed that four-dimensional conformal geometry deals with conformal tensors having 6^2 components. Though not incorporating these two extra degrees of freedom, Weyl's geometry is fundamentally conformal. Kaluza's "five-dimensional" theory uses one extra degree of freedom in a projective way such that it may properly be regarded, as can Weyl's theory from a different point of view, as an embryonic form of a general conformal theory.

* B. Hoffmann, Phys. Rev. **72**, 458 (1947); *ibid.* **73**, 30 (1948)

Artificial Radioactive Substances

T1. Double Beta Decay.* E. FIREMAN, *Princeton University.*—There exist a number of stable isobaric nuclei that differ by two in charge and may differ by several Mev in mass. The heavier should decay into the lighter with simultaneous emission of two electrons. The decay probability depends markedly upon whether or not the two electrons are accompanied by two neutrinos. No neutrinos are emitted if they obey the Majorana equation or if the interaction is composed of linear combinations of the usual interactions. Furry's calculations using Majorana wave functions have been extended to linear combinations that arise from symmetry considerations and meson theories. Isobars belonging to a triple set are the most promising for double beta decay since the middle one is near the minimum of the isobaric mass defect curve. Therefore, $_{40}Zr^{96}$ and $_{50}Sn^{124}$ were investigated with a Geiger counter coincidence arrangement. Their activity was compared with elements that are stable against all types of decay. No difference was detected. On the basis of these measurements and the assumption of two-Mev mass difference, the lifetime of $_{50}Sn^{124}$ is greater than $3\cdot10^{15}$ years. This result rules out the polar vector, axial vector, and tensor interactions with Majorana wave functions and the more important linear combinations.

* This work was supported in part by Navy contract.

T2. Measurement of Absorption Coefficients for Gamma-Rays in Various Elements.* ARTHUR L. HUGHES AND CLYDE L. COWAN, *Washington University.*—The availability in the past year of a number of radio-isotopes from the Atomic Energy Commission has permitted measurements to be made of absorption coefficients for a range of gamma-ray energies heretofore impracticable. Insofar as possible, monoenergetic gamma-sources with long half-lives were selected which covered the energy spectrum from 0.4 to 2.8 Mev. A geometry was sought which would yield results whose accuracy was limited only by statistics and by natural background corrections. The source, absorbers of area just sufficient to completely intercept all detected gamma-rays, and G.M. tube were suspended outdoors about 25 feet above the ground. The lowest obtainable background with source present was of the order of four times natural background and was a function of the ac-

tivity of the source. This was due to back scattering by the air. Sufficient data were taken at each point to reduce the statistical error to less than one percent. The following sources were used: Cr-51, Au-198, Cs-135, Sc-46, Zn-65, Co-60, Sb-124, Na-24 and Cs-134. Absorbers used were Pb, Sn, Cu, Al and C. The results, where there is good reason to believe that the gamma-rays were monoenergetic, exhibit remarkable agreement with the values predicted by Heitler.

* This work was supported in part by the Office of Naval Research.

T3. Gamma-Ray Absorption Measurements. CHARLOTTE M. DAVISSON AND ROBLEY D. EVANS, *Massachusetts Institute of Technology.*—The absorption of γ-rays in Al, Cu, Sn, Ta, and Pb has been measured in "good geometry" using the γ-rays from I^{131}, Cu^{64}, Mn^{54}, Co^{60}, Zn^{65}, and Na^{24}. The absorption curves of I^{131} showed the presence of a 0.65 Mev γ-ray 15 percent as abundant as the 0.367 Mev γ-ray. The absorption coefficients of Mn^{54} (0.835 Mev), Zn^{65} (1.14 Mev), Co^{60} (1.16 and 1.31 Mev), and Na^{24} (2.76 Mev separated from 1.38 Mev by coincidence counting) showed agreement within 0.5 percent to 2 percent with the absorption coefficients expected from the theories of Klein-Nishina,[1] Hulme *et al.*,[2] and Bethe and Heitler.[3] Transmissions were measured to about 0.01–0.005 with Zn^{65}, Na^{24}, Cu^{64}, and I^{131}, and to about 0.001 or lower with Mn^{54} and Co^{60}. As one check on the apparatus, absorption measurements were made with Ra γ-rays. These showed that the apparatus has excellent collimation since the results agreed both with those of other workers and with those expected theoretically.

[1] Klein and Nishina, Zs. f. Phys. **52**, 853 (1929).
[2] Hulme, McDougall, Buckingham, and Fowler, Proc. Roy. Soc. **149A**, 131 (1935).
[3] Bethe and Heitler, Proc. Roy. Soc. **146A**, 83 (1934).

T4. A Method for Measuring Short Period Activities.* A. D. SCHELBERG, M. B. SAMPSON, AND A. C. G. MITCHELL, *Indiana University.*—By photographing an oscilloscope it is possible to measure short periods which range from 0.1 second to 5 seconds. The pulses from a Geiger counter are fed into the x-axis amplifier of an oscilloscope using no sweep. A General Radio Oscillograph Recorder is used to photograph the cathode ray tube so that a record is obtained. The activated target is moved from the bombardment position to the counting position in about 0.2 second by means of a pneumatic tube. Exposure of calcium to a 23 Mev alpha-particle beam results in an activity with a half-life of 0.58 ± 0.04 second. This activity may be assigned to Ti^{43} produced by the reaction $Ca^{40}(\alpha,n)Ti^{43}$.

* Supported by Office of Naval Research.

T5. The Formation of Be^{10}. C. EGGLER, D. J. HUGHES, AND C. HUDDLESTON, *Argonne National Laboratory.*—The radioisotope Be^{10} is of great interest because its half-life is extremely long in spite of the expected allowed nature of its disintegration. As part of a program of study of this activity we have investigated methods of making Be^{10} in the pile. The formation of Be^{10} by the (n,γ) and the (n,α) reactions has already been reported.[1] Because of the small yields of these reactions it was decided to investigate the (n,p) as well. Although the latter is slightly exothermic the penetrability of the proton and the self protection of the sample for slow neutrons will make the formation of Be^{10} by the thermal neutrons extremely small. The main source of Be^{10} was expected to be the fast neutrons so some amorphous boron was irradiated near the uranium lumps in the Hanford pile. Beryllium carrier was added to the boron and then separated using the basic acetate process. The final beryllium showed an activity which did not decay and had the correct absorption curve for Be^{10}. The specific activity obtained gives a cross section for fast pile neutrons of 3 millibarns and shows no appreciable contribution from thermal neutrons.

[1] Hughes, Eggler and Huddleston, Phys. Rev. **71**, 269 (1947).

T6. The β-Spectrum of Be^{10}. D. J. HUGHES AND C. EGGLER, *Argonne National Laboratory.*—The disintegration of Be^{10} is expected to be allowed on the basis of spin difference and of comparison with the mirror nucleus C^{10}. However, its half-life of about 3×10^6 years indicates a highly forbidden disintegration. It is therefore of interest to determine if the β-distribution is of an allowed or a highly forbidden shape. Because of the great half-life and low cross section for the formation of Be^{10} (preceding abstract) it seems likely that material will not be available for a spectrometer determination of the spectrum for some time. We are measuring the spectrum, therefore, by comparison with "standard" spectra, which can be measured accurately in the spectrometer. The comparison is made both by means of the shape of β-absorption curves and by observing the β-energy distributions in a helium filled cloud chamber. Assumption of a linear decrease of intensity with absorber thickness allows a simple conversion from absorption curve to spectrum shape, and study of standard spectra (W^{185}, Au^{198}, P^{32}, Cu^{64}) shows good correlation with their known β-distributions. The β-spectrum of Be^{10} given by the absorption method is found to have the allowed shape within experimental error.

T7. A New 20-Second Activity Induced in Boron by High Energy Protons.* R. SHERR, H. R. MUETHER, AND M. G. WHITE, *Princeton University.*—When elemental boron or boron compounds such as boric acid are bombarded in a thin copper cell by 16–18-Mev protons, the resulting C^{11} radioactivity may be partially extracted as CO_2 by blowing a gas through the cell. Strong activities can be blown 40 feet in a fraction of a second into a thin-walled container placed adjacent to a tape-recording Geiger counter. In addition to C^{11} we find a new 20-sec. positron activity which closely follows the C^{11} in chemical tests which are specific for CO_2. The radioactive gas was shaken with BaOH, precipitated as $BaCO_3$, filtered and followed in decay. A second and more involved test using NaOBr removed the possibility that SO_2 might have been in the precipitate. Preliminary absorption measurements give an upper limit of $\sim$2 Mev to the 20-sec. activity. When CaF_2BF_3 enriched in B^{10} is bombarded and the gas caught by NaOH on asbestos, we find considerable enhancement

of the 20-sec. period relative to the C^{11} 20.5-min. period. We, therefore, believe this short activity is C^{10} and that the 8.8-sec. activity earlier ascribed to C^{10} was due to an impurity in the boron target.

* Supported in part by Navy contract.

T8. The Beta-Ray Spectra of C^{14} and S^{35}. JANE L. BERGGREN AND ROBERT K. OSBORNE, *Massachusetts Institute of Technology.*—The beta-ray spectra of C^{14} and S^{35} were investigated with a magnetic lens spectrometer. C^{14} sources were made of elemental carbon containing 27 atom percent C^{14}, and S^{35} sources were made of "no carrier added" sulfur estimated to have a specific activity of 0.7 mc per mg of solid. Counter windows of about 0.4 mg/cm² mica were used, and sources of average thickness 0.1 mg/cm² for C^{14} and 0.05 mg/cm² for S^{35} were mounted on 0.02 mg/cm² of "Formvar." The energy distribution was found to be within 3 percent of the allowed distribution for energies above 40 kev for both spectra. The endpoints obtained were 155 ± 2 kev for C^{14} and 169 ± 3 kev for S^{35}. Comparison with the theory of forbidden spectra shows that both the observed energy distributions are compatible with the theoretical distribution for $\Delta I=1$ (yes) for both Fermi and Gamow-Teller interactions. For the Fermi interaction a second forbidden transition with a spin change $0\rightarrow1$ gives a distribution for C^{14} which would be distinguishable from the observed spectrum. Careful measurements were made of the energy distribution near the end-points. It was found that the rest mass of the neutrino must be less than 1/100 of the electron rest mass.

T9. Some Notes on Radioactive Carbon of High Specific Activity. L. D. NORRIS AND ARTHUR H. SNELL, *Clinton National Laboratories.*—There has been described recently the preparation of several C^{14} samples, as barium carbonate, of appreciably higher specific activity than any material heretofore available.[1] The histories of these samples will be discussed, with emphasis on the radioactivity assays and the effect of sample impurities upon the calculation of carbon isotopic ratios from such assays. The samples were originally described as having specific activities corresponding to isotopic concentrations of 19 percent and 27 percent, respectively. However, more recent counting data indicates that these figures were somewhat low, and that the samples actually have specific activities corresponding to 22 percent and 32 percent, respectively. It has been pointed out that the isotopic concentrations obtained from radioactivity measurements would be minima, and that suspected impurities in the samples would make the ratios of C^{14} to total carbon appreciably higher.[1] That this is the case has been verified by F. A. Jenkins, who has observed band intensities on grating spectrograms prepared from these samples. C^{14} concentrations of 27 percent and 40 percent are obtained. Small corrections occasioned by dilution of the materials in the spectrum tubes would make these concentrations slightly higher.[2] This paper is based on work done for the Manhattan Project.

[1] L. D. Norris and Arthur H. Snell, Phys. Rev. 73, 254 (1948).
[2] F. A. Jenkins, Dep't of Physics, Univ. of Cal., Private communication.

T10. Spectrometer Measurement of Cyclotron-Induced Gamma-Radiation. DAVID E. ALBURGER, *Yale University.**—A thin-lens magnetic spectrometer has been adapted to measure energies of gamma-rays emitted by targets under cyclotron bombardment. The cyclotron beam is deflected out through an extension tube to a target located in front of the spectrometer radiator. Gamma-rays from the target produce photo- and Compton-recoil electrons from the radiator, the energy spectrum of these being determined by varying the lens coil current. Openings in the spectrometer end-plate and a gasket arrangement permit evacuation of the spectrometer by the cyclotron pumps. To reduce the serious defocusing effect of the cyclotron stray magnetic field on the spectrometer 20 iron rings 1" wide and ¼" thick spaced ½" apart along the spectrometer tube on either side of the coil effectively shield this region from the vertical disturbing field. The rings have negligible effect on the axial horizontal field of the lens coil since the spacings result in high reluctance in this direction. A preliminary electron spectrum using a lead radiator has been obtained with the gamma-rays resulting from the deuteron bombardment of PbO. From rough calibration this indicates that a gamma-ray of 0.93 ± 0.09 Mev is present. This is in agreement with the 0.86-Mev first excited state of the O^{17} nucleus as found[1] by Pollard and Davison from the $O^{16}(dp)O^{17}$ reaction.

* Assisted by the Office of Naval Research.
[1] Ernest Pollard and Perry W. Davison, Phys. Rev. 72, 736 (1947).

T11. The Beta-Ray Spectrum of P^{32}. E. J. SCOTT, *University of Michigan.*—The shape of the continuous spectrum of the electrons emitted by P^{32} has been investigated by means of the semi-circular focussing electromagnet type of spectrometer. A Geiger tube with an extremely thin window was used to count the electrons. When a moderately thin source of low specific activity was used, the distribution followed that predicted by the theory of Fermi[1] for electron energies in excess of 200 Kev. Electrons of energies below this value showed an increasingly greater abundance than predicted by this theory. This result is nearly the same as that of Siegbahn,[2] whose corresponding value was about 100 Kev. However, when an extremely thin source of high specific activity (carrier free) was used, the distribution showed an increasing deficiency as the electron energy fell below about 1 Mev. Further experiments relative to internal scattering at the source are being continued to evaluate this discrepancy and to bring the results in accord. This research was supported in part by the Office of Naval Research.

[1] E. Fermi, Zeit. f. Physik. 88, 161 (1934).
[2] Kai Siegbahn, Phys. Rev. 70, 127 (1946).

T12. The Disintegration of Sc^{46}.* CHARLES L. PEACOCK AND ROGER G. WILKINSON, *Indiana University.*—The beta- and gamma-rays of Sc^{46} have been studied using a small 180° spectrometer of good resolution. Weak samples produced by bombarding Sc_2O_3 with the cyclotron deuteron beam, and very strong samples obtained from the Oak Ridge pile were used. Sc^{46} is found to emit a beta-ray hav-

ing a maximum energy of 0.36 Mev, the resulting Ti^{48} returning to the ground state by the cascade emission of two gamma-rays with energies of 0.89 and 1.12 Mev. These results are in agreement with the work of others.[1] In addition, both neutron and deuteron induced activities are found to have a second beta-ray group of very low intensity with an end point at 1.49 Mev. This high energy group represents about 2 percent of the total number of beta-rays and is consistent with the decay scheme previously suggested.[2] Thin source technique and the results of auxiliary experiments make it unlikely that these electrons are due to scattering in the instrument, source thickness or Compton electrons. The gamma-rays are found to be converted with K-conversion coefficients of .0008 and .0004, respectively, for the 0.89 and the 1.12-Mev gamma-rays.

* Supported by the Office of Naval Research.
[1] Miller and Deutsch, Phys. Rev. 72, 527 (A) (1947). Feister and Curtiss, J. Research Nat. Bur. Stand. 38, 411 (1947).
[2] Peacock and Wilkinson, Phys. Rev. 72, 251 (1947).

T13. A Search for Crossover Gamma-Ray Transitions in Co^{60} and Se^{46}.† R. G. Fluharty and Martin Deutsch, *Massachusetts Institute of Technology.*—The Szilard-Chalmers calcium permanganate method of measuring weak neutron intensities was used to search for photoneutrons produced from Be.* The threshold energy of the photoneutrons eliminates any effects due to the lower energy cascade gammas. Calibration by means of Na^{24} and Y^{86} demonstrated that 1 microcurie of these activities is equivalent to 15 c.p.m. of Mn^{56} by beta-ray measurements. Using 60 millicuries of Co^{60} and 15 millicuries of Sc^{46}, no effect was observed. In the case of Co^{60}, 10 c.p.m. above background could be detected, thus the abundance of gamma-rays having an energy above 1.63 Mev is less than 1.1×10^{-5} per disintegrations. By reducing background effects, 4 c.p.m. over background could be detected for Sc^{46}, and thus the high energy gamma-rays have an abundance of less than 1.7×10^{-5} per disintegration.

† This work was supported in part by the Office of Naval Research.
* R. W. Dodson, M. Goldblatt, J. H. Sullivan, L. A. D. C., p. 260.

T14. Auger Electrons Following K-capture in Cu^{64}. C. Sharp Cook and Lawrence M. Langer, *Indiana University.**—In addition to emitting negatrons or positrons, Cu^{64} can also transform to Ni^{64} by the absorption of an electron from the K shell. The K-capture transition goes either to the ground state of Ni^{64} or infrequently to an excited state about 1.3 Mev above the ground level.[1] An intense group of Auger electrons, corresponding to the filling of the vacancy left in the K shell of Ni^{64}, has been measured in a large 180° magnetic spectrometer. The electrons were detected by a thin window counter having a transmission down to 4 kev. An accelerating potential of 4 kev, applied between the detecting slit and the counter helped drive the electrons through the counter window. The source was a chemically separated deposit of less than 0.1 mg/cm² on a backing of 0.02 mg/cm². After empirically correcting for the residual absorption of the counter window, for the self-absorption of the source, and for the efficiency of production of Auger electrons, we obtain for the ratio of K-capture to positron emission a value of 3.5 ± 1.0. This is in good agreement with the value predicted from the Fermi theory.

* This research was supported by the Frederick Gardner Cottrel. Fund of the Research Corporation and the Office of Naval Research.
[1] H. Bradt *et al.*, Hels. Phys. Acta. 19, 219 (1946). M. Deutsch, Phys. Rev. 72, 729 (1947).

Phosphors

U3. The Temperature Dependence of the Long Period. Phosphorescence of Zinc Silicate. Walter C. Michels and Louise Gaus, *Bryn Mawr College.*—The integrated phosphorescent light from zinc silicate with 0.85 percent Mn* has been measured as a function of time at ten fixed temperatures between 210°K and 337°K. It is found that the decay of phosphorescence at all temperatures can be represented as the sum of four exponential decays, each of which has a half-life independent of temperature. The observed half-lives are, in seconds, 133 ± 7 percent, 21 ± 10 percent, 3.5 ± 10 percent, and 0.67 ± 10 percent. The initial intensity corresponding to each decay rate varies with temperature in a manner similar to the intensity variation in a glow curve.[1] The constant decay rates seem to indicate that the long period phosphorescence may be due to direct decay from the trapping states, without thermal excitation to the conduction band. If so, the temperature determines only the relative populations of the various traps, and the glow curves must be interpreted making allowance for finite transition probabilities from the traps to the ground state.

* Supplied by Dr. H. C. Froelich of the General Electric Lamp Development Laboratory, Nela Park, Cleveland, Ohio.
[1] J. T. Randall, and M. H. F. Wilkins, *Proc. Roy. Soc.* **A184**, 347 (1945).

U4. Optical Properties and Constitution of Calcium Silicate-Lead Phosphors. Frank J. Studer and Gorton R. Fonda, *General Electric.*—Calcium silicate phosphors were prepared by firing appropriate mixtures of calcium oxide, silica, and lead oxide. The mixtures were fired below 1200°C, in platinum boats, and an atmosphere of steam was used to facilitate completion of the reaction. The spectrum of the luminescence excited by 2537A was found to vary with the conditions of preparation of the phosphor. Three emission bands are evident at approximately 3000A, 3340A and 3500A, anyone of which may be predominant. The excitation spectrum also varies widely, having several maxima between 2000A and 3000A. When the phosphor is excited by the 2288A line from a low pressure cadmium arc, a fourth broad band appears in the emission, which peaks about 3850A and extends far enough to the longer wave lengths to be easily observed visually. X-ray analysis with a Philips Geiger-counter spectrometer demonstrates that the emission band at 3000A is due to the α-metasilicate, the one at 3500A to the β-metasilicate while the 3340A band is due to the β-ortho-silicate. During the firing process the orthosilicate is formed first by the reaction between the calcium oxide and silica in equi-molar proportions, and it reacts thereafter with additional silica to form the metasilicate.

U5. Magnetic Properties of the ZnF_2:Mn Phosphor.* Peter D. Johnson and Ferd E. Williams, *University*

of North Carolina.—The specific magnetic susceptibility of ZnF_2:Mn and its components have been measured. The unexcited Mn^{++} is apparently in the ^6S state. The susceptibility of fluoride phosphors as a function of activator concentration coupled with energy and entropy calculations indicate that there exists appreciable spin interaction between activator ions and therefore departure from random distribution of Mn^{++} over Zn^{++} sites. Using the interaction energy obtained from susceptibility data and making the theoretically sound assumption that only non-adjacent activator ions are responsible for the emission process, the luminescent efficiency *versus* activator concentration has been successfully computed. The variation in excitation spectrum and efficiency with crystallization temperature has been qualitatively explained by the theory. The change in paramagnetic susceptibility with excitation, predicted by Williams and Eyring,[1] has been measured for ZnF_2:Mn. The phosphor was excited in a vacuum magnetic balance by radiation from a high voltage hydrogen discharge. Corrections for heating and radiation pressure were applied. The change in susceptibility corresponds to a decrease of the order of magnitude of one Bohr magneton per excited activator. The change in multiplicity has also been observed with Zn_2SiO_4:Mn and pure MnF_2.

* This work was supported by the Office of Naval Research.
[1] F. E. Williams and H. Eyring, J. Chem. Phys. 15, 289 (1947).

U6. Theory of Electron Retrapping in Infra-Red Phosphors.* R. C. Herman, C. F. Meyer, and H. S. Hopfield, *The Johns Hopkins University.*—The variations of the brightness and conductivity of infra-red phosphors have been studied theoretically on the basis of a set of non-linear differential equations originally proposed by de Groot[1] and subsequently studied by others.[2] One of the important parameters in these equations is ϵ, the ratio of the cross sections for the capture of a conduction electron into an empty trap and an empty luminescent center. For intensities of the stimulating infra-red light used in most experiments the fundamental equations can be solved approximately. From the solutions of these equations it is possible to determine the value of ϵ from experimental data on the brightness and photocurrent. In this treatment the effect of light absorption in the phosphor is neglected so that the results are strictly applicable to thin samples. In the paper following by W. L. Parker and J. J. Dropkin, an example is given of the application of this theory to experimental data.

* This work was supported by the Bureau of Ordnance, U. S. Navy.
[1] W. de Groot, Physica 6, 275 (1939).
[2] R. C. Herman and C. F. Meyer, J. App. Phys. 17, 743 (1946); 18, 258 (1947); H. A. Klasens and M. E. Wise, Nature 158, 483 (1946).

U7. Stimulated Phosphorescence and Photoconductivity of Infra-Red Phosphors.* W. L. Parker and J. J. Dropkin, *Polytechnic Institute of Brooklyn.*—The photoconductivity and brightness of an infra-red phosphor under stimulation have been measured simultaneously. The phosphor polarizes rapidly with resultant decrease in the current. A technique for depolarizing the sample has been worked out and will be described. This permits the measurement of the decay curves of both brightness and photoconductivity as a function of the time of stimulation. Logarithmic plots of brightness *vs.* time, photocurrent *vs.* time, and photocurrent *vs.* brightness become straight lines at moderately small times. If the brightness and photocurrent are extrapolated to zero time to get the initial values B_0 and i_0, then a plot of i/i_0 *vs.* $(Bi_0)/(B_0 i)$ should be a normalized plot of the number of conduction electrons *vs.* the number of empty luminescent centers. The experimental data show approximate agreement with the theoretical curves of this type described by Herman, Meyer, and Hopfield in the preceding paper. The data indicate that the ratio of the cross sections for retrapping and luminescence is less than one—probably of the order of one-tenth for the samples studies.

* This work was supported by the Bureau of Ships, U. S. Navy.

U8. The Response of Certain Inorganic Phosphors in the Extreme Ultraviolet Region.* E. M. Pell and D. H. Tomboulian, *Cornell University.*—In the investigation of the use of photomultipliers for the detection of ultra-soft x-rays, a preliminary study of certain fluorescent substances was undertaken with the object of finding their responses to radiation in the 100 to 400A region. A grazing incidence vacuum spectrograph was used to disperse the radiation. A highly condensed capillary spark discharge, as well as the L-emission band from an aluminum target, was utilized as a source. A thin layer of the phosphor to be tested was deposited on a strip of celluloid which was placed in contact with the Rowland circle and backed with orthochromatic film. The tests indicate that tetragonal $CaWO_4$:Pb, $BaSO_4$:$PbSO_4$, and tetragonal $CaWO_4$:[W] give excellent conversion in this region. Monoclinic Mg_2WO_5:[W] gives fair conversion, while rhombohedral Zn_2SiO_4:Mn, monoclinic $CdWO_4$:[W], and $Ca_3(PO_4)_2$:Ce respond weakly. No definite evidence of a significant variation of conversion efficiency with incident intensity has been found over an intensity range of the order of 1000:1. We believe the response of phosphors in this region has not been investigated previously. Acknowledgments are due Mr. H. W. Leverenz of RCA Laboratories for the samples used in the investigation.

* Assisted by the Office of Naval Research.

Apparatus of Nuclear Physics

X1. Redesign of the Princeton Cyclotron to Yield 18 Mev Protons.* M. G. White, H. W. Fulbright, P. Gugelot, R. R. Bush, *Princeton University.*—The 35″ Princeton cyclotron magnet can be operated at 19,500 gauss with a maximum $H\rho$ at $n=0.2$ of 6.5×10^6. Full utilization of this $H\rho$ would give 21 Mev protons, but if operated as a conventional cyclotron would require about 500 kev energy gain perrevolution and the necessary radio frequency power at 29.3 megacycles would be very high. A redesign to frequency-modulation operation has thus far yielded an inside average current of 1–1.5 microamperes at 18 Mev, with only 10 kev on the single dee. The central field was 18,300 gauss. A rotating vacuum condenser varies the frequency by 8 percent at repetition rates up

to 3600 c.p.s. The over-all stability and reliability of operation have been gratifying. The beam current varies with modulator repetition frequency in close agreement with the theory of Bohm and Foldy, but the variation of beam current with dee voltage is complicated by interactions between dee voltage and ion-source. Beam homogeneity in energy is surprisingly good, about 100 kv, showing that the center of rotation is more sharply defined than is customary with cyclotrons. Measurements on an internal probe show very little activity at distances greater than 5×10^{-2} cm from the inside edge.

* Supported in part by Navy contract.

X2. Gas Scattering in the Electron Synchrotron. J. MAYO GREENBERG AND T. H. BERLIN, *Johns Hopkins University.*—Elastic single scattering losses from an equilibrium orbit in a circular synchrotron have been obtained as a function of the residual gas pressure and the electron injection energy. The losses have been calculated for a synchrotron of radius 100 cm having a doughnut of radius 4 cm and a 20 c.p.s. magnetic field with peak value 8000 gauss. Injection energies range from 40 to 500 kev and pressures from 10^{-3} to 10^{-6} mm Hg. At 10^{-5} mm the losses range from 1.1 to 4.8 percent; at 10^{-4} mm from 7.1 to 23.4 percent; and at 10^{-3} mm from 14 to 36 percent. The actual losses are greater because of the scattering from the oscillating orbits,[1] the inelastic scattering, and the multiple scattering. For pressures less than 10^{-4} mm, the multiple scattering contributes very considerably to the loss. Calculations are in progress which will yield the scattering losses from the oscillating orbits, the contribution of inelastic scattering, and a more accurate estimation of the contribution of multiple scattering.

[1] D. M. Dennison and T. H. Berlin, Phys. Rev. **70**, 58 (1946).

X3. Two Cavity Operations of Yale Linear Electron Accelerator. R. L. MCCARTHY, J. A. LOCKWOOD, P. J. RICE, H. L. SCHULTZ, *Yale University.**—Description of this accelerator[1] and results of preliminary operation of single cavities with respect to electron energy spectra and beam characteristics have been reported previously.[2] A highly stable frequency source has been employed to drive two triode amplifiers. Each amplifier feeds one resonator of a set of two mutually uncoupled resonators of 3 in. and 7 in. length whose resonant frequencies have been adjusted to be the same. Relative phase between the oscillations in each were controlled by a phase shifting section between one amplifier and its associated resonator. Results of experiments on acceleration of electrons in this system will be reported in detail.

* Assisted by the Office of Naval Research.
[1] H. L. Schultz *et al.*, Phys. Rev. **72**, 346 (1947).
[2] Bull. Am. Phys. Soc. 1947 Annual Meeting.

X4. Electron Ballistics in the Yale Linear Accelerator. C. L. CLARK, *Yale University.**—Results will be presented of detailed calculations on the motion of electrons in the first two cavities of the Yale linear accelerator.[1] In this design cavities driven by separate amplifiers operating from a common master oscillator are kept so loosely coupled that *the relative phase of the fields in successive stages can be held at any desired value.* General features of both axial and radial motions will be discussed, and their bearing on design problems indicated. Numerical results to be reported concern homogeneity,[1] bunching, and focusing. The compatibility of these last will be discussed, and the argument from Earnshaw's theorem[2] will be considered in the light of the arbitrariness of phases in the Yale design. Assumed parameters are approximately as follows: continuous injection at 5 kev; first cavity 3 in. long, second cavity 7 in., each dissipating 400 Kw in the TM_{010} mode at 600 Mc/sec. The chief departure from experimental conditions[3] lies in assuming rectangular pulses, those obtained in practice being more nearly triangular.

* Assisted by the Office of Naval Research.
[1] H. L. Schultz *et al.*, Phys. Rev. **72**, 346 (1947).
[2] Ginzton, Hansen, and Kennedy, Rev. Sci. Inst. **19**, 89 (1948) and references therein cited.
[3] H. L. Schultz *et al.*, Bull. Am. Phys. Soc. **23**, No. 229 (January, 1948).

X5. Compact Electrostatic Generator for Positive Ion Acceleration.* C. P. SWANN AND E. L. HUDSPETH, *Bartol Research Foundation.*—The Bartol generator[1] has been greatly improved in reliability of operation through changes made during the past several months. Textolite control rods, which caused one fire, have been replaced by Pyrex rods. Storage tanks were installed so that a freon-nitrogen mixture may be used as the insulating gas. An all-glass ion source, of the capillary type, operating with 120 volts d.c. and a 15-watt oxide-coated filament, gives an arc of over 500 milliamperes. Tube currents vary from a few tenths to several microamperes of resolved ions. The freon-nitrogen mixture may be pumped from the pressure vessel, the latter hoisted to expose the main elements of the generator, the pressure vessel replaced and operation resumed in less than three hours. Maximum operating voltage at present is 1.75 Mev, which corresponds to 350 kilovolts per foot of accelerating tube. This limit is imposed by the tube itself, and indications are that it may be increased quite appreciably.

* Assisted by the Office of Naval Research.
[1] W. E. Danforth and E. L. Hudspeth, Phys. Rev. **60**, 170 (1941). An account of all phases of work on this generator will be published soon by Danforth, Hudspeth, Mandeville, and Swann.

X6. Methane Proportional Counter for Beta-Counting. C. J. BORKOWSKI AND E. FAIRSTEIN, *Oak Ridge National Laboratory.*—Counters filled with methane and operated in the proportional region with a gas amplification of 10,000 have been developed for precision counting of beta particles, gamma rays, X-rays, and soft conversion electrons. Plateaux of 400 volts are obtained with a slope of 1 percent or less per 100 volts. Using 0.5 mil tungsten center wire and methane at one atmosphere, the operating voltage is 2200 volts. With a specially designed chamber similar to the one described by J. A. Simpson[1] and a continuous flow of methane at atmospheric pressure, the counting of soft radiation is made possible without window or air absorption. H^3 beta-particles have been counted from solid sources in this type of counter. Counting yields as high as 75 percent are obtained for beta-emitters like C^{14}, S^{35},

P^{32}. These counters have been operated continuously for more than a year with no change of characteristics.

High speed counting is possible since the coincidence loss is only 1 percent per 100,000 counts per minute.

Energies of beta particles below 50 kev may be determined with this type counter since the counter is operating in the proportional region. This document is based on work performed for the Atomic Energy Project.

[1] J. A. Simpson, Jr., Rev. Sci. Inst. **18**, 884 (1947).

X7. Deadtime Theory.* S. S. FRIEDLAND, *Memorial Hospital and New York University*, AND A. D. KRUMBEIN, *New York University.*—The deadtime of a self quenching counter is defined as the time it takes the positive ion sheath formed in the vicinity of the central wire, to move from there to a distance such that the field surrounding the wire will have recovered sufficiently to support an observable avalanche. Stever[1] has derived an expression for the deadtime. In his derivation, he assumed the mobility of the positive ion sheath was constant even though it was moving through a region of variable E/p. An examination of Hershey's[2] data, shows that we can approximate the variation of the mobility in deadtime region by the expression $k=Ar$, where k is the mobility, r is the distance of the sheath from the wire center, and A is a constant. Stever's experimental values disagree with theory by a factor of 4. If we insert the above expression into his equations, and again solve for the dead-time, we find that the experimental values now agree with theory within 2 percent.

* This work was supported in part by the Office of Naval Research.
[1] H. G. Stever, Phys. Rev. **61**, 38 (1942).
[2] A. V. Hershey, Phys. Rev. **56**, 908 (1939).

X8. A Proposed Self-Controlled Cloud Chamber. MARTIN J. COHEN, *Princeton University.**—Preliminary results indicate that the functions of a Wilson cloud chamber and a pulse ionization chamber can be performed in the same volume of gas. The mechanism is the following: A heavy ionizing event produces electrons and positive ions in the gas mixture (argon and alcohol). The electrons are collected as such within 10 microseconds by the signal electrode which is connected to a high gain, wide band amplifier (model 100). After amplification the signal short-circuits the electron collection field and expands the cloud chamber to produce "tracks" on the less mobile positive ions. A conventional cloud chamber with a rubber diaphragm is used. The signal electrode is a transparent conducting layer on the front surface of the chamber. It is connected directly to the first grid of the preamplifier. The negative potential is applied to an insulated, perforated brass plate to which the black velvet background is also attached. Measurements show that the condensible vapor in the cloud chamber does not capture electrons to a sufficient extent to preclude operation of the combination of a cloud and ion chamber. Ethyl, N-propyl, iso-amyl alcohols and cyclohexanol have been tried.

* This work is performed under Contract with the Office of Naval Research.

X9. Background Eradication of Nuclear Emulsions by Accelerated Fading of the Latent Image. HERMAN YAGODA AND NATHAN KAPLAN, *National Institute of Health.*—A study of the factors controlling the rate of fading of the latent image produced by densely ionizing radiations in fine-grained emulsions reveal that traces of H_2O_2 in the vapor phase cause very rapid destruction of the latent image. After desiccation of the plate the emulsion is restored to its original sensitivity. This permits the eradication of the accumulated background of alpha-ray tracks arising from continuous registration by internal radioactive impurities prior to exposure to feeble sources of radiation under study. By maintaining the exposure in a dry, H_2O_2 free atmosphere at low temperature quantitative recording is possible for periods longer than 2 months. Under these conditions single α-tracks accumulate at a rate of 8–100/cm²/day depending on emulsion purity and thickness. Low energy alpha-ray stars originating from successive decay of traces of Th and Rd Th in the gelatin generate ~0.3 multiple events/cm²/day. Near sea level, the controlled exposure indicates a daily rate of proton and meson tracks of 0.03–.06/cm^{-2}; and a population of 0.0005/cm² nuclear evaporations induced by cosmic radiations. This method is applicable only to fine-grained nuclear type emulsions as Eastman NTA and Ilford Conc. With coarse-grained, light-sensitive emulsions the H_2O_2 vapor produces pseudophotographic effects. Mechanism of spontaneous fading will be described.

X10. Particle Tracks in Emulsions Showing Grain Gradation. W. VAN DER GRINTEN, *General Electric Company.*—Current photographic processing techniques, carrying the development of nuclear plates practically to completion do not lead to significant differentiation among the amounts of silver precipitated on individual grains. A new technique for producing such differentiation will be described involving the use of a special developer combined with partial development. Thus silver halide grains, struck by a particle of low specific ionization, produce a track composed of small transparent silver specks, whereas similar grains, struck by a particle of high specific ionization produce larger and opaque specks. This "grain gradation" greatly facilitates the differentiation between alpha and proton tracks. So far, low-concentration developing agents active only in the form of ions carrying two or more negative charges have been found to produce grain gradation. The bromide concentration is not critical and may be kept low. This allows one to bring practically all developable grains to the level of visibility. A minimum developer temperature exists below which grain gradation disappears. It is believed that the rate of growth of individual development centers has been homogenized under present conditions and that, consequently, grain gradation is a measure of the number of development centers per grain. Photomicrographs, including betatron stars, will be shown.

X11. Removal of Latent Image in the Powell Photographic Plate Technique. JOSEPH DE FELICE, *Stevens Institute of Technology.* (*Introduced by G. J. Yevick*).—For the absolute count of cosmic ray events at high altitudes it would be convenient to have plates free from tracks prior to the balloon flight. The procedure of Liebermann and Barschall[1] proved satisfactory for the removal of all

latent images from 100 micron Ilford C2 plates. The effect of this process on the grain count for alpha tracks from uranium was determined as follows: Two groups of plates were used; the first group was put through the removal process while the second group was untouched. These two groups were then loaded with uranyl nitrate. The grain density (number of grains per unit length) of the first group turned out to be about one-fifth less than that of the second group. This is compensated in part by the fact that the length of the tracks in the first group was slightly longer (about one-tenth) than the second group. This appears to be due to a swelling of the emulsion. The absolute number of grains per track in the first group was about one-tenth less than the second.

[1] Liebermann and Barschall, Rev. Sci. Inst. **14**, 89, 1943.

X12. Scintillation Counting with Anthracene. P. R. BELL AND R. C. DAVIS, *Oak Ridge National Laboratory.**—Anthracene has proved more satisfactory for use with 1P21 photomultiplier as a scintillation counter than napthalene. Cobalt 60 gamma-rays produce 3.5 times larger pulses in anthracene than in naphthalene permitting the use of a lower background counting rate. A polonium beryllium neutron source gave five times greater counting rate with anthracene than with naphthalene. The maximum pulse size was also five times as great in anthracene. The counts were shown to be due to fast neutrons by an absorption curve in lead and in cadmium. The fast neutron detection efficiency seems to be 10–15 percent.

* This work as done under Contract No. W-35-058, eng. 71.

X13. A Gamma-Ray Isodosimeter. L. D. MARINELLI AND G. J. HINE, *Sloan-Kettering Institute.*—The investigation of the spatial variation of γ-ray dose in the vicinity of extended 3-dimensional sources is tedious and cumbersome. This applies to both experimental methods and numerical calculations. The apparatus to be described records automatically lines of equal radiation doses (isodoses) in a given plane. The isodose curves obtained in different parallel planes complete the radiation field of an extended γ-ray source. The instrument consists of an ionization chamber, a feed-back amplifier and a servomechanism. The latter moves the chamber linearly to or from the slowly rotating γ-ray source according to whether the amplified ionization current is smaller or greater than a pre-set value. The motion of the chamber is recorded on a platform which rotates synchronously with the source. Preliminary results show good agreement with calculations made of linear sources.[1] Further observations with metal foils irradiated in nuclear reactors will be presented.

[1] E. H. Quimby, Radiology **43**, 572, 1944.

Molecular Structure and Nuclear Moments

Y1. Nuclear Quadrupole Moments of N^{14} and I^{127}.* C. H. TOWNES, *Columbia University.*—Nuclear quadrupole moments of Cl and Br have been obtained from microwave measurements of quadrupole couplings and using atomic orbitals as an approximation to molecular wave functions near the nucleus.[1] Atomic beam measurement of the Cl^{35} quadrupole moment shows that the result obtained is essentially correct in the case of Cl^2. A similar calculation from microwave data gives a value for the I^{127} quadrupole moment -0.75×10^{-24} cm^2, somewhat larger than the value $-0.45\pm.15\times10^{-24}$ obtained from atomic emission spectra.[3] The N^{14} quadrupole is more difficult to obtain because the atomic orbital approximation is less accurate for light elements and because of uncertainties in the nitrogen bond structure. However, a comparison of the N^{14} quadrupole coupling in various molecules shows that the normal nitrogen bonds involve considerable s,p hybridization. This conclusion, as well as comparison with the quadrupole coupling in AsF_3, allows a fairly definite determination of the quadrupole moment sign as positive and an approximate evaluation of its magnitude as 0.02×10^{-24} cm^2.

* Work supported by the Signal Corps.
[1] C. H. Townes, Phys. Rev. **71**, 909 (1947).
[2] L. Davis, B. T. Feld, C. W. Zabel, and J. R. Zacharias, Phys. Rev. **73**, 525 (1948).
[3] K. Murakawa, Zeits. f. Physik. **114**, 651 (1939).

Y2. Microwave Rotational Absorption in D_2O.* M. W. P. STRANDBERG, *Massachusetts Institute of Technology.*—A rotational absorption in heavy water, at 20460.40 mc/sec. has been observed and has been identified on the basis of its Stark effect. The observed Stark pattern shows a simple displacement of the absorption according to the formula,

$$\Delta\nu = 1.052E^2 \text{ mc/sec.}$$

where E is the electric field strength in kilovolts per centimeter. The line intensity is the order of magnitude of that of the $6_{-3}-5_{-1}$ transition in H_2O and the 5_1-5_0 transition in HDO. On the basis of the known term values[1] no obvious identification is possible. However, if the relative values of the 3_{-2} and 2_2 terms are interchanged a reasonable fit can be made with the observed Stark effect. If the term value of the 3_{-2} level is taken to be 73.81 cm^{-1} and the 2_2 level taken as 74.50 cm^{-1} the theoretical Stark effect for this transition proves to be

$$\Delta\nu = \mu^2E^2(.2472-.01261M^2) \text{ mc/sec.}$$

This is fitted to the observed pattern with a dipole moment of $2.04\pm.04$ Debye units. Though some dependence on the magnetic quantum number is indicated the fit seems good enough since the dipole moment is reasonable and the predicted intensity[2] checks well with the observed value. On the basis of this identification a relation between the extreme reciprocal moments of inertia is readily calculated as

$$a = .2502+3.1994c \text{ cm}^{-1}.$$

Minimizing the change in the Fuson, Randall, Dennison values $a=15.38$, $c=4.83$, this equation gives $a=15.55$ cm^{-1} and $c=4.79$ cm^{-1}.

* This work has been supported in part by the Signal Corps, the Air Materiel Command, and O.N.R.
[1] N. Fuson, H. M. Randall, and D. M. Dennison, Phys. Rev. **56**, 982 (1939).
[2] G. W. King, R. M. Hainer, and P. C. Cross, Phys. Rev. **71**, 433 (1947).

Y3. Pure Rotational Spectrum of AsF_3. B. P. DAILEY, K. RUSINOW, R. G. SHULMAN, AND C. H. TOWNES,*

Columbia University.—Twelve lines of the rotational transition $J=1\rightarrow J=2$ of AsF_3 were observed by the Stark modulation method near 23,500 mc. Ten of these lines are produced by the $K=0$ and $K=1$ levels of the ground vibrational state. They fit the hyperfine pattern expected from the nuclear quadrupole moment of As. This confirms a spin of $\frac{3}{2}$ for As^{75}. The remaining two lines are probably due to excited vibrational states. Calculated intensities are approximately 10^{-7} nepers/cm. From the frequencies of the observed lines, values of $B_0=.19610$ cm^{-1} and of $I_B=142.7\ 10^{-40}$ g-cm^2 may be calculated. Assuming the F−As−F angle 100±5°, the As−F internuclear distance is 1.712±.006A as compared with 1.73±.02A from electron diffraction measurements.[1] The quadrupole coupling constant, $eQ(\partial^2V/\partial z^2)$, is −235 mc. Since the quadrupole moment as As^{75} is 0.3×10^{-24} cm^2, this large coupling indicates considerable s,p hybridization of the As bond rather than a pure p-orbital.

* Work supported by the Signal Corps.
[1] L. Pauling and L. O. Brockway, J. Am. Chem. Soc. **57**, 2685 (1935).

Y4. Microwave Zeeman Spectra of Methyl-Chloride and Some Nuclear Properties of Chlorine.* C. K. JEN, *Harvard University.*—It has been shown previously[1] that the microwave Zeeman spectrum of $N^{14}H_3$ can be satisfactorily explained on the basis of approximately equal g-factors for nuclear and molecular magnetic moments in the spin-rotation coupling scheme. This explanation was later substantiated by experiments on $N^{15}H_3$ which, having no nuclear electric quadrupole coupling, yielded directly a molecular g-factor for $N^{15}H_3$ in good agreement with the molecular g-factor deduced theoretically for $N^{14}H_3$. Further experiments have since been done on CH_3Cl. The $J=0\rightarrow1$ rotational lines for both CH_3Cl^{35} and CH_3Cl^{37}, already published,[2] have been found here, using a resonant cavity as the absorption cell. In a weak magnetic field, the central line for either molecule remains at the same position but is considerably weakened, while each of the two side lines is split into a symmetrically displaced doublet. Within the experimental limitations of resolution and sensitivity, the Zeeman pattern and the frequency separations are consistent with theoretical calculations, if we assume, for either Cl isotope, a spin $I=\frac{3}{2}$ together with the known value for the nuclear g-factor, and a negligible contribution due to the molecular magnetic moment.

* This research is supported jointly by the Office of Naval Research and the Signal Corps.
[1] C. K. Jen, Bulletin, Am. Phys. Soc., Vol. 23, No. 2, January, 1948 (abstract G2).
[2] W. Gordy, J. W. Simons, and A. G. Smith, Phys. Rev. **72**, 344 (1947).

Y5. Microwave Determination of the Molecular Structures and Nuclear Couplings of Methyl Chloride, Methyl Bromide, and Methyl Iodide.* JAMES W. SIMMONS, WALTER GORDY, AND A. G. SMITH, *Duke University.*—Accurate measurements on the pure rotation spectra of methyl chloride, bromide, and iodide have been made with multiples of the standard 10 mc frequency of WWV. The measurements, with the I_A values** previously determined by infra-red spectroscopy, allow a complete determination of the structures of CH_3Cl and CH_3Br. The I_B values for the ground vibrational state in g-cm$^2\times10^{-40}$ are: 63.1138 for CH_3Cl^{35}, 64.1009 for CH_3Cl^{37}, 87.6835 for CH_3Br^{79}, 88.0180 for CH_3Br^{81}, and 111.505 for CH_3I^{127}. The molecular dimensions obtained are: for methyl chloride, $d_{CH}=1.109$A, $d_{CCl}=1.779$A, $\angle HCH=110°\ 0'$; for methyl bromide, $d_{CH}=1.104$A, $d_{CBr}=1.936_5$A, $\angle HCH=110°\ 15'$; for methyl iodide, $d_{CH}=1.105$A, $d_{CI}=2.132$A, $\angle HCH=110°\ 15'$ (assumed). The nuclear quadrupole couplings, $eQ(\partial^2V/\partial z^2)$, are: for Cl^{35}, −75.13 mc; for Cl^{37}, −59.03 mc; for Br^{79}, 577.0 mc, for Br^{81} 482.0, for I^{127}, −1934 mc. Second-order effects in the hyperfine structure were observed for methyl bromide and methyl iodide.

* The research described in this report was supported by Contract with the Army Air Forces.
** The value of h used is 6.624×10^{-27} erg sec.

Y6. A Note on the Stark Effect in Diatomic Molecules. W. A. NIERENBERG AND M. SLOTNICK, *Columbia University.*—The hyperfine structure arising from the orientation dependent interaction of each nucleus with the other charges of a polar diatomic molecule in a constant electric field are considered. For weak fields, a method is given for determining the level splittings for a general type of nuclear interaction, but where one nucleus interacts more strongly than the other. For both weak and strong fields, explicit formulas are given for the case of a quadrupole interaction of one of the nuclei (nucleus 1) and a cosine or "$I\cdot J$" interaction of both nuclei. The "$I_2\cdot J$" interaction removes the degeneracy with respect to nucleus 2 and causes an additional splitting of the usual quadrupole hyperfine structure levels.[1] This splitting is observed in recent molecular beam experiments of Trischka with CsF and KF. It is found that the perturbation due to $I\cdot J$ interactions may be treated as independent of the mixing of J states arising from a strong electric field.

[1] U. Fano, J. Research Nat. Bur. Stand. March, 1948.

Y7. Saturation Effects in Microwave Spectra.* R. J. WATTS, WILLIAM J. PIETENPOL, JOHN D. ROGERS, AND DUDLEY WILLIAMS, *The Ohio State University.*—Saturation effects in microwave spectra have been observed by numerous investigators. The published data on the changes in absorption coefficients are in essential agreement, but data on line broadening are in disagreement. Townes[1] and Pond and Cannon[2] report pronounced line broadening, while Gordy and Kessler[3] and Smith and Carter[4] have reported their failure to observe appreciable broadening. The results reported here are in essential agreement with those of Pond and Cannon. Changes in observed line heights and widths of the ammonia 6,6 line with changes in incident power level will be discussed. The observed results can be interpreted in terms of a disturbance of the normal Boltzmann distribution of molecules between ground and excited state when radiation density is high.

* Work done under Contract W28-099-ac-179 between Watson Laboratories of the Air Materiel Command and the Ohio State University Research Foundation.
[1] C. H. Townes, Phys. Rev. **70**, 665 (1946).
[2] T. A. Pond and W. F. Cannon, Phys. Rev. **72**, 1121 (1947).
[3] W. Gordy and M. Kessler, Phys. Rev. **71**, 640 (1947).
[4] W. V. Smith and R. L. Carter, Phys. Rev. **72**, 638 (1947).

Y8. New Bands in the Vibration-Rotation Spectrum of Water Vapor. W. S. BENEDICT, *National Bureau of*

Standards.—Reinvestigation of the vibration-rotation spectrum of H_2O from the atmospheric absorption in the solar spectrum λ6600 to λ13495[1] has yielded several new features. Over 1600 lines have been assigned on the basis of relative intensity and constant combination differences in the ground state, to higher rotational transitions in known bands, and to ten new, relatively weak, satellite bands. Some of the new bands are of the parallel type. Perturbations of rotational levels of one vibrational state by its neighbors make it difficult to obtain accurate effective moments of inertia. The identification, position of the zero level, approximate effective reciprocals of inertia, and approximate relative intensity of the new bands are listed:

Upper Level Symmetry								
V_1	V_2	V_3	Species	ν_0 (cm^{-1})	Ae (cm^{-1})	Be (cm^{-1})	Ce (cm^{-1})	Intensity [(111) = 50]
1	3	0	A_1	8273.98	39.9	14.7	8.7	3
0	3	1	B_1	8373.90	38.9	14.7	8.8	15
2	1	0	A_1	8761.5	28.1	14.5	8.9	4
0	1	2	A_1	9000.14	28.9	14.4	8.9	6
0	4	1	B_1	9834.9	45.8	14.9	8.6	1
1	2	1	B_1	10328.9	32.1	14.5	8.6	12
1	0	2	A_1	10867.8	25.3	14.1	8.9	5
1	3	1	B_1	11813.44	37.1	14.6	8.4	1
1	1	2	A_1	12407.65	27.8	14.2	8.7	1
2	2	1	B_1	13652.65	31.4	14.2	8.5	1

[1] H. D. Babcock and C. E. Moore, Carnegie Inst., Washington, Publication 579 (1947).

Y9. An Analysis of the 2.6 Mu Band of H_2S by Punched-Card Methods.* GILBERT W. KING AND R. M. HAINER, *Arthur D. Little, Inc.*—A rather poorly resolved band of H_2S at 2.6 mu was described[1] several years ago, but has hitherto not been analyzed. Using punched-card methods we assumed moments of inertia for the ground state obtained from an analysis[2] of the band at 9911 cm^{-1} and calculated the expected spectrum for thirty-five choices of upper-state moments and ten different slit-shape functions. A fairly satisfactory fit was found for moments 2.71, 2.90, 6.02×10^{-40} g-cm^2 and band center 3789 cm^{-1}. The induced dipole is definitely parallel to the least moment, although excellent fits in the P and R branch could equally well be made for the moment parallel to the intermediate moment. The effective slit width for the observed spectrum was determined, and seems to change from 1 cm^{-1} in the P branch to 5 cm^{-1} in the R branch. The appearance of the calculated and observed spectrum was computed for wider slits (10 cm^{-1}) and found to agree very well with prism data.[3]

* This work was done with support of the Office of Naval Research.
[1] H. H. Nielsen and E. F. Barker, Phys. Rev. **37**, 727 (1931).
[2] P. C. Cross and B. L. Crawford, Jr., J. Chem. Phys. **5**, 621 (1937).
[3] E. A. Wilson, Ph.D. Thesis, Brown University, 1947.

Y10. Infra-Red Absorption Spectra of Ethyl and of *n*-Propyl Alcohol. E. K. PLYLER AND S. L. KRUEGEL, *National Bureau of Standards.*—The infra-red absorption spectra of the vapors of ethyl and of *n*-propyl alcohol have been measured in the region from 2 to 40 microns. To obtain good resolution throughout this region, prisms of LiF, NaCl, KBr, and TlBr−I were used. In ethyl alcohol, 19 bands have been observed, 7 of which are sufficiently strong to be found with cells of short length. A meter path was required to bring out some of the weaker bands. Some of the bands have been related to the C−H, O−H, and C−O vibrations within the molecule. Considering the arrangement of the two C and the O atoms as a simple triatomic molecule, 3 observed bands can be related to the vibrations of this skeletal structure. A band found in the region of 40μ is attributed to the hindered rotation within the molecule. Seventeen bands have been observed in the vapor of *n*-propyl alcohol. The classification of these bands in relation to the structure of the molecule is similar to that for ethyl alcohol, except in the skeletal vibrations where three C and an O are involved. This gives rise to additional bands in the 6.5 to 13μ region.

Y11. Force Constant Calculations for the X_4Y_6 Molecule. HAROLD W. WOOLLEY, *National Bureau of Standards.*—Force constant calculations have been carried out for the tetrahedrally symmetric X_4Y_6 molecule using symmetry coordinates and the matrix methods of Wilson. With 24 internal degrees of freedom, there are 300 quadratic potential energy terms involving 19 force constants. Vibrational frequencies of the A_1, E, and T_1 symmetry classes involve quadratic equations while the T_2 symmetry class has a quartic equation. Only the T_1 vibrations are inactive in both infra-red and Raman, With only 8 frequencies observable in principle and without data for the isotopic molecules, the force constants are not definitely determinable. Examples of the X_4Y_6 molecule are P_4O_6 and As_4O_6. Calculations have been made in regard to a postulated B_4O_6 molecule, using force constants and observed frequencies based on other molecules involving B and O, including solid $(B_2O_3)_x$.

Y12. An Explicit Solution of the Problem of the Asymmetric Rotator According to Quantum Mechanics.* ENOS E. WITMER, *University of Pennsylvania.*—An explicit and exact solution of the problem of the asymmetric rotator according to quantum mechanics has been obtained. Both the energy and the wave functions are in the form of infinite series. This solution is an elaboration or improvement of the one previously published by the writer.[1] The new solution takes account of K-type doubling and gives all the wave functions. This solution is in very close correspondence with the solution of the asymmetric rotator according to the old quantum theory published by the writer.[2] As in that theory the domain of variation of the parameters is divided into two parts and different expansions are used in the two parts. The correspondence principle and numerical checks lead us to believe that the new series for each of the partial domains are convergent over the whole of that partial domain. The formulas may be written so that the coefficients after the first one are functions of the quantum numbers alone. Numerical tables of the coefficients in these series are being made.

* Supported by Bureau of Ships, Department of the Navy.
[1] E. E. Witmer, Proc. Nat. Acad. Sci. **13**, 60 (1927).
[2] E. E. Witmer, Proc. Nat. Acad. Sci. **12**, 602 (1926).

Y13. Fluorescence of Fluorobenzene.* ARNOLD M. BASS AND H. SPONER, *Duke University.*—The fluorescence of fluorobenzene vapor corresponding to the absorption spectrum in the near ultraviolet was examined. The fluorescence was excited by light from various sparks, chiefly a Sn spark which has a strong line at 2643A practically coincident with the 0, 0 absorption band. The

observed fluorescence conforms to the conditions of "high pressure" fluorescence. In order to control the exciting wave-length region, cut-off filters of organic solutions were used. The spectrum was photographed in a medium Bausch and Lomb quartz spectrograph. It extends from about 2640 to 2900A and consists of discrete bands the number of which varies with conditions of excitation. Discrete fluorescence bands of fluorobenzene have been observed before by Monypenny and Russell[1] upon exciting the vapor by the light from a mercury arc. A comparison between their results and ours gives only partial agreement. A preliminary analysis reveals that ground state frequencies of 800,999 and 1027 cm^{-1} occur single, and in multiples and combinations. These frequencies have also been found in the absorption spectrum and in the Raman effect. Although most bands can be explained in analogy to the absorption spectrum, there are several interesting differences between fluorescence and absorption bands which need further clarification.

* This work was supported by the Office of Naval Research.

[1] H. W. Monypenny and A. Russell, J. Chem. Soc. 2436 (1929).

Artificial Radioactive Substances

Z1. Radioactive Ga^{67}, Ge^{69}, As^{73}, and As^{74}. D. A. McCown, L. L. Woodward, M. L. Pool, and H. L. Finston, *The Ohio State University.*—Ge^{70}, in the form of GeO_2 powder, enriched electromagnetically from 21.2 percent to about 90 percent,* has been bombarded with alpha-particles with simultaneous bombardment of GeO_2 containing germanium of normal isotopic constituency. Both samples showed a strong activity of 7.1-hour half-life which has been assigned to Se^{73}. Neither sample showed evidence of the 50-hour As^{73} period. The existence of a 50-hour arsenic period is thus very improbable. Gallium has been bombarded with deuterons to obtain confirmation of the 195-day Ge^{69} period. From intensity considerations this period should have occurred if it exists. No evidence of this period was found. The above alpha-particle bombardment of enriched Ge^{70} also locates the 90-day arsenic period as an As^{73} isotope. The half-life of As^{74}, as a result of alpha-particle bombardment of gallium followed over a period of 10 half-lives, and also from deuteron bombardment of germanium followed over a period of 8 half-lives, is found to be 17.5 ± 0.1 days. The half-life of Ga^{67}, from alpha-particle bombardment of zinc followed over a period of 10 half-lives is found to be 3.26 ± 0.03 days.

* Supplied by the Y-12 plant, Carbide and Carbon Chemicals Corporation, through the Isotopes Division, U. S. Atomic Energy Commission, Oak Ridge, Tennessee.

Z2. Beta- and Gamma-Radiations of Arsenic[16]. C. S. Wu, W. W. Havens, Jr., and L. J. Rainwater, *Columbia University.*—A source of Arsenic AS^{76} obtained from the Oak Ridge pile was investigated, with respect to its beta- and gamma-rays, by the use of a helical focusing magnetic spectrometer and coincidence counting methods. Gamma-ray energies of the AS^{76} were determined from photoelectric lines produced with a thin lead radiator and also from Compton electrons produced in brass. The energies of the stronger lines are 0.557 and 1.22 Mev. The weak one has energy 1.78 Mev. The beta-ray spectrum was measured with an extremely thin source on a backing of 0.08μ Collodin film. Fermi plot of the data gives three groups with end points which agreed well with the energies of the gamma-rays determined. Beta-gamma coincidences were also measured. A scheme of disintegration will be proposed. A search for positrons put the upper limit of the number of positrons less than 0.1 percent of that of electrons. This document is based on work performed for the Atomic Energy Commission.

Z3. Radiations from the Long Period Activity of Zirconium.* M. V. Scherb and C. E. Mandeville, *Bartol Research Foundation.*—The 63-day activity was induced in zirconium hydroxide, irradiated by slow neutrons in the Clinton pile. Chemical purification was carried out for the removal of calcium, iron, and phosphorous as possible impurities. The beta rays of Zr^{95}, separated from its daughter elements of columbium, had a maximum energy of 0.40 Mev, measured by aluminum absorption. The maximum energy of the gamma-rays was 0.91 Mev as measured by coincidence absorption. The beta-gamma coincidence rate was 0.21×10^{-3} coincidence per beta-ray, independent of the beta-ray energy, suggesting a simple spectrum. The gamma-gamma coincidence rate, greater than the beta-gamma coincidence rate, was $(0.29 \pm 0.02) \times 10^{-3}$ coincidence per gamma-ray. A comparison of these coincidence rates with those of Sc^{46} shows that the 0.91 Mev gamma-ray is non-coincident with the beta-rays and may be related to some other decay process. This in turn suggests the possibility of a confusion of isotopic assignments in the zirconium region.

* Assisted by the Office of Naval Research.

Z4. Radioactive Ru and Tc. D. T. Eggen* and M. L. Pool, *The Ohio State University.*—During a detailed study of the reported radioisotopes of Ru and Tc, a new isotope of Ru and one of Tc were found by bombarding Mo with alpha-particles. The Ru activity decays with a half-life of 1.65 ± 0.05 hours and emits 1.1-Mev positrons, 0.7-A x-rays and 0.95-Mev gamma-rays. Fast neutron bombardment of Ru also produces this activity. The Tc activity decays with a period of 20.0 ± 0.5 hours and emits 0.7-A x-rays and 0.78-Mev gamma-rays. The Tc activity also is produced by proton bombardment of Mo and as a daughter product of the 1.65-hour Ru activity. Using electromagnetically separated isotopes,[1] alpha-bombardments were made on Mo^{92}, enriched to 92 percent abundance, and Mo^{94}, enriched to 75 percent abundance. This made possible the assignment of the 1.65-hour and 20-hour activities to Ru^{95} and Tc^{95}, respectively. In addition, it is possible to definitely assign the reported[2] 2.8-day Ru activity to Ru^{97}.

* Research Fellow of the National Institute of Health.

[1] Supplied by the Y-12 plant, Carbide and Carbon Chemicals Corporation through the Isotope Division, United States Atomic Energy Commission, Oak Ridge, Tennessee.

[2] W. H. Sullivan, N. R. Sleight, and E. M. Gladrow, Phys. Rev. 70, 778 (1946).

Z5. Nuclear Isomers Produced by Slow Neutron Capture. M. Goldhaber and C. O. Muehlhause, *Argonne National Laboratory.*—A systematic investigation of nuclear isomers produced by slow neutron capture has been under way for some time. Some of the results are the

following: The 48-minute isomeric transition in Cd is assigned to Cd^{111*} by observing the (n,γ) reaction in enriched Cd^{110}. The 17.5-sec. isomeric transition in Se is assigned to Se^{77*} by observing the (n,γ) reaction in enriched Se^{76}. Thus for both Cd and Se the metastable state is assigned to an odd mass nucleus in agreement with Mattauch's rule. The 72-sec. In^{114} isomer is produced by bombarding enriched In^{113} with thermal neutrons. The partial isotopic cross section is found to be $(2\pm0.3)\times10^{-24}$ cm^2, ~3 percent of the capture cross section of In^{113}. The metastable state of Cs^{134} is assigned to the 3-hour period. Internal conversion electrons as well as characteristic $K\alpha$ radiation of Cs are observed. The energy of the transition is ~160 kv. The internal conversion electrons from the 6.6 min. isomeric transition in Cb^{94} have been observed, as well as characteristic $K\alpha$ radiation of Cb. The energy of the transition is found to be ~50 kv. It leads to a long-lived ground state, the activity of which has so far not been detected ($T\gg100$ years).

Z6. Cloud-Chamber Measurements of Cadmium Capture Gamma-Rays. C. D. MOAK AND J. W. T. DABBS, *Oak Ridge National Laboratory* (*Introduced by E. O. Wollan*).—A study of the capture gamma-rays from cadmium has been made by measuring the energy of the pairs produced in a 0.008 cm. Pb radiator in a cloud chamber operated in a magnetic field of about 1400 gauss. To reduce the errors arising from scattering, the chamber was filled with helium at a pressure of 3 atmospheres. About 30,000 stereoscopic photographs have been taken which have yielded some 400 acceptable pairs. The pair distribution *versus* energy plot, and the corresponding gamma-ray intensity *versus* energy curve will be presented. Measurements so far made on about 100 pairs show a peaking of the gamma-ray intensity at about 5 Mev.

Z7. Separation of the Isomers of Indium 112 and Indium 114 in an Electric Field.* G. J. GOLDSMITH, *Purdue University*.—It has been shown[1] and confirmed that chemical changes induced in a molecule by the isomeric transition of one of its nuclei produce ions which can be collected on an electrode placed in a non-conducting solution of the compound. Indium 114 dissolved in chloroform as the 8-hydroxy quinolate was subjected to a field of the order of 8000 volts per centimeter between nickel electrodes (2×3 cm.) spaced about 1 or 2 mm. apart for various periods up to twenty minutes. The deposit on the anode was found to have the expected half life of 72 seconds superimposed on a weak background of the long lived upper state. Similarly, in the case of the In^{112} isomers, the 9 minute period of the ground state was found confirming the growth curve analysis of Smith, Tendam and Bradt.[2]

* Supported by the Office of Naval Research.
[1] Capron, Stokkink, and van Meerssche, Nature **157**, 806 (1946).
[2] Tendam, and Bradt, Phys. Rev. **72**, 1118 (1947).

Z8. Gamma-Radiation from Tellurium and Samarium. J. M. CORK, R. G. SHREFFLER, AND C. M. FOWLER, *University of Michigan*.—As a result of the many previous investigations on tellurium it had been concluded that, from the 8 known stable isotopes, 8 radioactive emitters, consisting of four sets of isomers, existed. A sample of metallic tellurium given a particularly long exposure in the Oak Ridge pile fails to show certain of the activities that might be expected. Long-lived emitters appear to be present, with half-lives of 8 days, 29.5 days and 25 yrs. The 8-day activity is undoubtedly due to iodine 131. The 144-day activity previously ascribed to tellurium 121 is believed to be an excited state of one of the stable isotopes. This conclusion is based both on its mode of formation and the nature of its radiation. Several conversion electron groups are observed, indicating gamma-energies of 87, 108, and 157 kev. Other higher energy gamma-radiation is revealed by absorption. The K−L−M differences in certain of the conversion groups are characteristic of tellurium and not of antimony as would be expected if K capture or positron emission occurred first. In a samarium sample given a similar long exposure, a short lived (47-hr.) activity is observed which yields a converted gamma-ray of energy 102.1 kev. Terbium is present in most of the rare-earth elements with its strongly converted gamma-radiation of half-life 78 days. An additional samarium activity of longer half-life, emits a gamma-ray of energy 242.4 kev which is converted.

Z9. Internal Conversion Electrons Accompanying Slow Neutron Capture in Gd. O. SALA,* P. AXEL, AND M. GOLDHABER, *University of Illinois*.—Amaldi and Rasetti[1] have observed that approximately one internal conversion electron of an energy of ~70 kev is emitted for each slow neutron captured in Gd. They attempted to find, by a mechanical method, whether the electron is delayed and found an upper limit for the mean lifetime of 10^{-3} sec. We have resumed these attempts with an electronic method in the following way: Neutrons from a Po−α−Be source are slowed down in paraffin. The capture gamma-rays emitted when the slow neutrons are absorbed by Gd are recorded by a gamma-ray Geiger counter. The pulse from this counter sets off a fast sweep (0.2 microsec./inch) on an oscilloscope. The internal conversion electrons are recorded with a thin mica end window Geiger counter. The pulse from this counter produces a vertical deflection. The trace is intensified only when the two events occur within a microsecond. This makes photographic recording possible. In this way we find that the internal conversion electron of Gd is emitted with a mean lifetime $<10^{-7}$ sec. relative to the capture gamma-rays.

* Rockefeller Fellow of the University of São Paulo, São Paulo, Brazil.
[1] E. Amaldi and F. Rasetti, Ricerca Scient. **10**, 115 (1939).

Z10. Radioactive Eu, Gd, and Tb. N. L. KRISBERG AND M. L. POOL, *Ohio State University*, AND CARL T. HIBDON, *University of Colorado*.—An 18.0-hour period and a weaker 5.5-day period have been produced by neutron bombardment of gadolinium resulting in a saturation intensity ratio of 25. A deuteron bombardment of gadolinium gave

a ratio of 3. The 18.0-hour period decays by emission of negatrons of 0.85 Mev and a γ-ray of approximately 0.3 Mev. The 5.5-day period decays by emission of negatrons of 0.5 Mev and γ-rays of 1.28 Mev. Neither period is produced by fast neutron bombardment of Tb but there is some evidence that both are produced by fast neutron bombardment of Dy. Accordingly the 18.0-hour and 5.5-day periods are tentatively assigned Gd^{161} and Tb^{161}, respectively. The 62-day and 22-year periods have been produced by a deuteron bombardment of europium. The latter figure has been estimated from observations extending over five years. The decay is by emission of negatrons of 0.9 Mev and by γ-rays. The 62-day period is probably attributable to Gd^{153} and the 22-year period to Eu^{154}.

Z11. The Beta- and Gamma-Radiation of W^{187} and Au^{198}.* ROGER G. WILKINSON AND CHARLES L. PEACOCK, *Indiana University.*—The radiation of W^{187} produced both by deuteron and neutron bombardment has been re-investigated.[1] The beta-ray spectrum consists of two groups with end points at 0.63 and 1.33 Mev. Four gamma-rays are observed with energies of 0.69, 0.62, 0.48, and 0.21 Mev. There is some evidence of another gamma-ray at 0.14 Mev, but owing to strong counter window cut-off in this region, the presence of this and other low energy gamma-rays reported by Valley[2] cannot be substantiated. A tentative decay scheme for W^{187} will be proposed. Our determination of the radiations from Au^{198} are in good agreement with that of Siegbahn.[3] The beta-ray spectrum appears simple with an end-point at 0.97 Mev, each beta-ray being followed by a 0.41 Mev gamma-ray. The gamma-ray is converted with a K conversion coefficient of 2.5 percent.

* Supported by the Office of Naval Research.
[1] Schwartz and Pool, Phys. Rev. **71**, 122 (1947).
[2] Valley, Phys. Rev. **59**, 686 (1941).
[3] Siegbahn, Proc. Roy. Soc. **189**, 527 (1947).

Z12. A Study of the Radiations of Two Radioactive Isotopes of Iridium.* C. E. MANDEVILLE AND M. V. SCHERB, *Bartol Research Foundation.*—The nineteen-hour activity of Ir^{194} was induced in IrO_2, irradiated by slow neutrons for thirty minutes in the Clinton pile. Coincidence absorption experiments disclosed the presence of a gamma-ray of energy 1.43 Mev. A momentum distribution of secondary electrons ejected from a thick aluminum radiator in a magnetic spectrograph indicated an energy of 1.35 $\pm$0.03 Mev. The beta-gamma coincidence rate corrected for the presence of Ir^{192}, decreased from 0.06×10^{-3} coincidence per beta-ray at zero absorber thickness to zero at 0.150 g/cm^2. An inner beta-ray group, coupled with gamma-rays, then has an end point at 0.48 Mev. The 2.2 Mev beta-rays are non-coincident with gamma-radiation. A gamma-gamma coincidence rate of $(0.54\pm0.05)\times10^{-3}$ coincidence per gamma ray was also present in Ir^{194}. The 68-day activity of Ir^{192} was found to emit beta-rays of energy 0.56 Mev. The beta-gamma coincidence rate was 0.41×10^{-3} coincidence per beta-ray, independent of the beta-ray energy suggesting a simple spectrum and agreeing with an earlier report.[1] A gamma-gamma coincidence rate of $(0.23\pm0.01)\times10^{-3}$ coincidence per gamma-ray was also observed. The beta-gamma coincidence rate suggests that each beta-ray is followed by 0.6 Mev of gamma-ray energy.

* Assisted by the Office of Naval Research.
[1] M. L. Wiedenbeck and K. Y. Chu, Phys. Rev. **72**, 1164 (1947).

SUPPLEMENTARY PROGRAMME

SP1. Relativistic Field Theories.* T. S. CHANG, *Carnegie Institute of Technology* (*Introduced by F. Seitz*).—In a relativistic field theory, it is important to introduce Schroedinger functionals on any space-like surface and study their changes as the surface changes, as recently pointed out by Dirac. We consider here fields $q(x)$ satisfying the usual Lagrangian principle. Let S be any surface, (u_1, u_2, u_3) its curvilinear coordinates, and let $\langle q(u)S|\rangle$ be the Schroedinger functional on it, with the nature of the functions $q(u)$ not specified for the moment. The Schroedinger equation will be

$$\langle q(u)S'|\rangle-\langle q(u)S|\rangle=J\langle q(u)S|\rangle, \qquad (1)$$

where S' is a surface slightly different from S, and J is an operator operating on $q(u)$ and depending on S,S' and the choice of their coordinates. J are found so that (i) (1) is integrable. (ii) If we construct properly the expectation value of q at a point P from $\langle q(u)S|\rangle$, S being a surface passing through P, the expectation value is independent of choice of S and its coordinates u, and satisfies the required field equations. The special cases in which S are planes and J are simply related to the energy momentum tensors or angular momentum tensors are studied.

* To be given after Session E if the Chairman grants time.

SP2. An Explicit Formula for the Energy Levels of the Asymmetric Rotator According to Quantum Mechanics.* ENOS E. WITMER, *University of Pennsylvania.*[1]—Starting with the determinant formula given by Dennison[2] for the energy levels of the asymmetric rotator the writer has obtained an explicit formula for the energy in the form of an infinite series. Actually there are two such series, because the domain of variation of the parameters must be divided into two partial domains with one series for each partial domain. These series formulas are the same as those mentioned in Abstract No. Y12, where they were obtained by another method. Due to the relation between the two formulas only one need be used for calculation. The formula is complicated but highly systematized and can be written so that the coefficients after the first one

are functions of the quantum numbers alone. There are recurrence formulae for the coefficients. The formulas for many coefficients in this series have been obtained already and many more will be obtained. Numerical tables of the coefficients as functions of the quantum numbers are being calculated in order to make the formula as useful as possible.

* To be given after Session Y if the Chairman grants time.
[1] Supported by Bureau of Ships, Department of the Navy.
[2] D. M. Dennison, Rev. Mod. Phys. 3, 280 (1931).

SP3. A Coincidence Investigation of Lanthanum (140).* C. E. MANDEVILLE AND M. V. SCHERB,[1] *Bartol Research Foundation.*—La_2O_3, irradiated by neutrons in the Clinton pile, was separated into calcium, phosphorous, barium, and lanthanum. The beta-gamma coincidence rate was 1.63×10^{-3} coincidence per beta-ray and appeared to be independent of the beta-ray energy. A strong gamma-gamma coincidence rate, $(0.85\pm0.03)\times10^{-3}$ coincidence per gamma-ray was also present. Using a gamma-ray counter of "low Z" materials and the beta-gamma coincidence rate of Sc^{46} as a calibration point, it was concluded that on the average, each beta-ray is followed by 2.3 Mev of gamma-ray energy. On the other hand, assumption of a detection efficiency independent of the quantum energy leads to the conclusion that two gamma-rays follow each beta-ray, in agreement with the earlier Indiana University report.[2]

* To be given after Session Z if the Chairman grants time.
[1] Assisted by the Office of Naval Research.
[2] A. C. G. Mitchell, L. M. Langer, and L. J. Brown, Phys. Rev. 71, 140 (1947).

SP4. A High Pressure Ion Chamber Using Fast Electron Collection.*, ** H. W. FULBRIGHT AND R. J. BRITTEN, *Princeton University.*—A high pressure ion chamber has been built for use in analyzing the distribution in energy of inelastically scattered protons. Fast collection of electrons in argon gas at pressures up to 50 atmospheres is used. The collector is shielded from the region into which the protons are shot by a "Frisch grid" which has the effect of making all electrons freed along the proton tracks equally effective in carrying current to the collector. Pulses from the chamber are fed through a fast linear amplifier into a ten channel pulse height discriminator of the type designed by Matt Sands. With 40 atmospheres pressure the two peaks from normal uranium alpha particle groups can easily be resolved. Protons can enter the chamber through a 1.5 mil steel window. Curves showing the collection time and pulse height for various pressures and voltages will be shown.

* This work was supported in part by Navy contract.
** To be given after Session X if the Chairman grants time.

Author Index to Papers Presented at the Washington Meeting

Aiken, Howard—No. W1
Alburger, David E.—No. T10
Aldrich, L. T. and Alfred O. Nier—No. I11
Allen, James S., H. R. Paneth, and A. H. Morrish—No. I7
Aller, L. H., C. W. Ufford, and J. H. Van Vleck—No. C1
Allison, S. K., H. V. Argo, W. R. Arnold, L. del Rosario, H. A. Wilcox, and C. N. Yang—No. P6
Alvarez, Luis W.—No. F11
Andrews, C. L.—No. L7
Andrews, Donald H.—No. Q1
Anderson, H. L.—No. N5
Antonoff, George—No. K1
Banks, Floyd R., Jr.—No. B9
Band, William and Lothar Meyer—No. Q7
Bass, Arnold M. and H. Sponer—No. Y13
Bell, P. R. and R. C. Davis—No. X12
Belock, H., E. Bromberg, S. Fifer, U. Manfredi, R. McCoy, and H. Zagor—No. L1
Bender, R. S., F. C. Shoemaker, S. G. Kaufmann, and G. M. B. Bouricius—No. A6
Benedikt, Elliot T.—No. E6
Benedict, W. S.—No. Y8
Bennett, Willard H.—No. H9
Berggren, Jane L. and Robert K. Osborne—No. T8
Bergmann, Peter G.—No. C6
Bershader, D. and R. Ladenburg—No. K9
Beyer, R. T. and J. A. Krumhans—No. B3
Birnbaum, George—No. D11
Bitter, Francis—No. N4
Blair, J. M., William Sleator, Jr., George Freier, E. E. Lampi, and J. H. Williams—No. A3
Blatt, John M.—No. A5
Bless, A. A.—No. C9
Bloom, Evelyn G., Fred L. Mohler, J. H. Lengel, and C. E. Wise—No. H12
Bockstahler, Lester I. and Harmon Plumb—No. Q6
Bonner, T. W., J. E. Evans, J. C. Harris, and G. C. Phillips—No. J10
Borkowski, C. J. and E. Fairstein—No. X6
Borowitz, S.—No. F3
Bottom, Virgil E.—No. G2
Boyer, R. L.—No. H8
Bray, Ralph—No. G3
Brickwedde, F. G.—No. H1
Buechner, W. W., R. J. Van de Graaff, E. N. Strait, C. G. Stergiopoulos, and A. Sperduto—No. J5
Bundy, F. P., A. B. Gregg, and H. M. Strong—No. H7
Burgy, M., D. J. Hughes, and J. Wallace—No. B5
Bush, R. R. and H. W. Fulbright—No. A8
Caldwell, Wallace C. and Lloyd P. Smith—No. B8
Chang, T. S.—No. E10, SP1
Chang, W. Y.—No. S4
Christensen, H. and C. J. Calbick—No. G9
Chupp, W. W., and E. M. McMillan—No. F10
Clark, C. L.—No. X4
Cohen, Martin J.—No. X8
Coles, D. K.—No. V4
Cook, C. Sharp and Langer, Lawrence M.—No. T14
Cork, J. M., R. G. Shreffler, and C. M. Fowler—No. Z8
Courant, E. D.—No. J3
Critchfield, Charles L.—No. A4
Curtiss, L. F.—No. R5
Dailey, B. P., K. Rusinow, R. G. Shulman, and C. H. Townes—No. Y3
Darrow, K. K.—No. M1
Davis, Luther, Jr., and Carroll W. Zabel—No. D10
Davis, W. H., A. O. Williams, Jr., and R. T. Beyer—No. C3
Davison, Perry W.—No. P5
Davisson, Charlotte M. and Robley D. Evans—No. T3
Davisson, J. W.—No. G5
De Felice, Joseph—No. X11

Dempster, A. J.—No. I12
Dresden, M.—No. Q9
Eckert, W. J.—No. W3
Eggen, D. T. and M. L. Pool—No. Z4
Eggler, C., D. J. Hughes, and C. Huddleston—No. T5
Eisenbud, L.—No. A9
Everhart, Edgar, and Sanborn C. Brown—No. D2
Falk, C. E., E. Creutz, and F. Seitz—No. J4
Farnsworth, H. E.—No. G8
Feer, Daniel B.—No. S10
Feshback, H., J. Eisenstein, and J. S. Schwinger—No. I3
Feynman, R. P.—No. E4
Fireman, E.—No. T1
Fitzpatrick, J. A., Thomas Kankovsky, and William J. Thaler—No. K2
Fluharty, R. G. and Martin Deutsch—No. T13
Follin, James W., Jr.—No. L9
Foner, S. N., A. Kossiakoff, and F. T. McClure—No. H10
Fox, R. E., A. Langer, and J. A. Hipple—No. H11
Fox, F. E. and V. Griffing—No. K5
Franzen, W., I. C. Corong, and W. E. Stephens—No. P8
Friedland, S. S. and A. D. Krumbein—No. X7
Fulbright, H. W. and R. R. Bush—No. A7
Fulbright, H. W. and R. J. Britten—No. SP4
Fuson, Nelson—No. Q2
Gardner, Eugene, and C. M. G. Lattes—No. S1
Garrett, M. W.—No. L6
Gartlein, C. W.—No. C4
Goldhaber, M. and C. C. Muehlhause—No. Z5
Goldsmith, G. J.—No. Z7
Golian, S. E., C. Y. Johnson, and M. Kuder—No. EA7
Good, W. M., E. O. Wollan, and W. A. Strauser—No. I14
Green, J. B. and Howard N. Maxwell—No. C2
Greenberg, J. Mayo and T. H. Berlin—No. X2
Greenfield, M. A.—No. F1
Gugelot, P. C., and M. G. White—No. F2
Halliday, David, and John Wheatley—No. D6
Halpern, I.—No. P9
Hardy, R. C., and R. L. Cottington—No. H2
Harris, S. P., and A. S. Langsdorf, Jr.—No. F6
Havens, W. W., Jr., L. J. Rainwater, C. S. Wu, and J. R. Dunning—No. F5
Heitler, W.—No. S12
Henry, Hugh F.—No. L10
Hereford, Frank L.—No. I10
Herlin, Melvin A., and Sanborn C. Brown—No. D1
Herman, R. C., C. F. Meyer, and H. S. Hopfield—No. U6
Hewitt, William H., Jr.—No. D9
Heydenburg, N. P., C. M. Hudson, D. R. Inglis, and W. D. Whitehead Jr.—No. J7
Hickam, W. M.—No. H13
Hicks, B. L.—No. K14
Hoffmann, Banesh—No. S11
Hoge, Harold J.—No. H4
Hudspeth, E. L. and C. P. Swann—No. J9
Hughes, Arthur L. and Clyde L. Cowan—No. T2
Hughes, D. J. and C. Eggler—No. T6
Humphreys, R. F., and H. T. Motz—No. P1
Hunter, Joseph L.—No. K4
Iberall, A. S. and W. A. Wildhack—No. K11
Inglis, D. R.—No. J8
James, Hubert M.—No. G4
Jen, C. K.—No. Y4
Jenkins, James F., Jr.—No. EA3
Johnson, E. A.—No. B1
Johnson, Peter D. and Ferd E. Williams—No. U5
Judson, L. V.—No. R1
Katcoff, S., J. A. Miskel, and C. W. Stanley—No. I13
Kê, T'in-Sui—No. G10
Kennard, E. H.—No. K12
King, Gilbert W. and R. M. Hainer—No. Y9
Kissinger, C. W. and D. Cooper—No. S6
Kittel, Charles—No. B4, V2
Knable, N., E. O. Lawrence, C. E. Leith, B. J. Moyer, and R. L. Thornton—No. F9
Koehler, J. S.—No. G6
Krisberg, N. L., M. L. Pool, and Carl T. Hibdon—No. Z10
Kusch, P.—No. M3
Ladenburg, R., C. C. Van Voorhis, and J. Winckler—No. K8
Lamb, W. E.—No. M2
Langer, R. M. and Herman Yagoda—No. S9
Langsdorf, Alexander, Jr.—No. F8
Lattes, C. M. G. and Eugene Gardner—No. S2
Lauer, James L.—No. L11
de Launay, Jules and M. C. Steele—No. Q4
Levine, Harold, and Julian Schwinger—N. E3
Ling, D. S. and D. L. Falkoff—No. I6
Lyons, H.—No. R6
Lyons, Harold, George Birnbaum, and S. J. Kryder—No. D3
McCarthy, R. L., J. A. Lockwood, P. J. Rice, and H. L. Schultz—No. X3
McCormack, R. L., J. Cardell, and W. B. Nottingham—No. U1
McCown, D. A., L. L. Woodward, M. L. Pool, and H. L. Finston—No. Z1
McMillan, E. M.—No. A1
Mack, J. E.—No. C5
Mandeville, C. E. and M. V. Scherb—No. Z12, SP3
Marcus, Paul M.—No. K6
Markstein, George H.—No. K13
Marinelli, L. D. and G. J. Hine—No. X13
Marlow, Douglas, C. R. Nisewanger, and W. M. Cady—No. K7
Masi, J. F.—No. H3
Mason, R. C.—No. G12
Maxwell, E., P. M. Marcus, and J. C. Slater—No. Q3
Meggers, W. F.—No. R2
Meyer, Lothar and William Band—No. Q8
Michels, Walter C. and Louise Gaus—No. U3
Miller, P. H., Jr., and J. J. Markham—No. G1
Millikan, R. A.—No. EA1
Moak, C. D. and J. W. T. Dabbs—No. Z6
Morrison, P.—No. I9
Moshinsky, Marcos, and E. P. Winger—No. E5
Motz, H. T., and R. F. Humphreys—No. P2
Nafe, John—No. M4
Nelson, Edward B., and John E. Nafe—No. D4
Nierenberg, W. A. and M. Slotnick—No. Y6
Norris, L. D. and Arthur H. Snell—No. T9
Onsager, L. and J. E. Robinson—No. Q5
Parker, W. L. and J. J. Dropkin—No. U7
Peacock, Charles and Roger G. Wilkinson—No. T12
Peaslee, D. C.—No. I5
Peck, R. A., Jr.—No. P3
Pell, E. M. and D. H. Tomboulian—No. U8
Pensak, L.—U2
Perlow, G. J., E. Krause, and C. Schroeder—No. EA8
Piccioni, Oreste—No. S3
Pietenpol, William J., John D. Rogers, and Dudley Williams—No. Y7
Plyler, E. K. and S. L. Kruegel—No. Y10
Pollard, E., V. L. Sailor, and L. D. Wyly—No. P4
Pound, R. V.—No. N3
Rado, G. T., M. Maloof, and H. Rosenblatt—No. B2
Rarita, William—No. I1
Reynolds, S. E., and E. J. Workman—No. L3
Rose, M. E., and M. M. Shapiro—No. E7
Sachs, R. G.—No. I4
Saibel, Edward—No. G11
Sala, O., P. Axel, and M. Goldhaber—No. Z9
Sanderson, J. A., J. A. Curcio, and Dorothy Estes—No. H5
Sands, Matthew—No. S8
Sard, R. D. and A. H. Benade—No. S5
Schelberg, A. D., M. B. Sampson, and A. C. G. Mitchell—No. T4
Scherb, M. V. and C. E. Mandeville—No. Z3
Schwarz, Guenter and J. A. Bearden—No. C8
Schwinger, Julian—No. E2
Scott, E. J.—No. T11
Segrè, Emilio—No. A2
Shamos, M. H., M. G. Levy, and I. S. Lower—No. S7
Sherr, R., H. R. Muether, and M. G. White—No. T7
Shoupp, W. E., and B. Jennings—No. P7
Silsbee, F. B.—No. R3
Simmons, James, Walter Gordy and A. G. Smith—No. Y5

Simpson, J. A., Jr.—No. EA5
Singer, S. F.—No. EA4
Slack, C. M., L. F. Ehrke, C. Zavales, D. Dickson, and R. G. Young—
—No. L2
Snell, Arthur H., and L. C. Miller—No. F12
Snyder, R. L.—No. W2
Sommers, H. S., Jr., P. R. Weiss, and W. Halpern—No. D5
Staub, Hans—No. N2
Steinberger, J. and G. C. Wick—No. B6
Stimson, H. F.—No. R4
Strait, E. N., C. G. Stergiopoulos, A. Sperduto, and W. W. Buechner—
No. J6
Strandberg, M. W. P.—No. V5, Y2
Strong, H. M., and F. P. Bundy—No. H6
Studer, Frank J. and Gorton R. Fonda—No. U4
Swann, C. P. and E. L. Hudspeth—No. X5
Swann, W. F. G.—No. EA6
Szilard, L., S. Bernstein, B. Feld, and J. Ashkin—No. F4
Taub, A. H.—No. K15
Teichmann, T.—No. I2
Tisza, L.—No. E9
Tomlinson, E. P.—No. L4
Townes, C. H.—No. V5, Y1
Van der Grinten, W.—No. X10
Vineyard, George H.—No. C7
Wahlin, H. B. and Harry Knop—No. B7
Waldman, Bernard and Walter C. Miller—No. J1
Weidner, R. T., P. R. Weiss, and C. A. Whitmer—No. D8
Weimer, Paul K.—No. G7
Weinberg, Joseph W.—No. E1
Weiss, P. R.—No. V1
Weissler, Alfred—No. K3
Wheatley, John, David Halliday, and J. H. Van Vleck—No. D7
White, M. G., H. W. Fulbright, P. Gugelot, and R. R. Bush—No. X1
Whitmer, Robert M.—No. L5
Wildhack, W. A.—No. K10
Wilkinson, Roger G. and Charles L. Peacock—No. Z11
Wilson, E. Bright—No. V6
Winckler, John—No. EA2
Winsberg, Lester, David Meneghetti, and S. S. Sidhu—No. F7
Witmer, Enos E.—No. Y12, SP2
Woffenstein, Lincoln—No. I8
Woodward, W. M. and I. Halpern—No. J2
Woolley, Harold W.—No. Y11
Workman, E. J., and S. E. Reynolds—No. L8
Wu, C. S., W. W. Havens, Jr., and L. J. Rainwater—No. Z2
Yagoda, Herman and Nathan Kaplan—No. X9
Yevick, G. J.—No. E8
Zacharias, J. R.—No. N1

Minutes of the Meeting at Madison, June 21–23, 1948

THE 286th meeting of the American Physical Society, being the 1948 Summer Meeting in "the East," was held on Monday, Tuesday, and Wednesday, June 21, 22, and 23, in the buildings of the University of Wisconsin at Madison. The Secretary, having been unable to be present, takes leave to quote from the Vice President: "The meeting was a very pleasant and successful one and apparently went off smoothly and was enjoyed by all who were there. . . . The University of Wisconsin did us particularly well. The accommodations in the dormitory were ideally pleasant, and the dormitory was extraordinarily well run, in a beautiful location." To this encomium be it added that the Chairman of the Local Committee was Professor R. G. Sachs. The dinner of the Society was held on the evening of June 21 in the Loraine Hotel.

Invited papers in the general programme numbered eleven. They are listed hereinafter: the last of the list was inserted as a post-deadline paper (under authority of the by-law adopted by the Society in January 1948) in replacement of the two contributed papers numbered **D9** and **D10**. Invited papers sponsored by the Division of Electron Physics numbered six, and these also are listed below.

The Council elected to Fellowship three candidates and to Membership one hundred and twenty-six candidates; their names are appended.

Reports have reached the office of the Society that we have lost through death the following Fellows and Members: Ernest Merritt (retired from Cornell University; first Secretary and ninth President of the Society), John Mills (retired from Bell Telephone Laboratories), Monroe H. Sheppard (Rutgers University), Joyce C. Stearns (Washington University, St. Louis), Richard R. Syrdal (Minneapolis-Honeywell Company), and William Wilson (retired from Bell Telephone Laboratories, lately at North Carolina State College).

Elected to Fellowship: J. G. Aston, W. O. Milligan, F. T. Rodgers, Jr.

Elected to Membership: Pierre R. Aigrain, Niels Y. Andersen, Jr., Joseph O. Artman, David Balber, John L. Balderston, Jr., Norman Bauer, Lt. Col. Wilmer Kersey Benson, Manfred A. Biondi, Kenneth A. Block, Marsden Scott Blois, Jr., Donald E. Bode, Leonard Bogdan, Milton Irving Brand, Samuel Bresticker, Edmond Brown, Charles I. Browne, James W. Brownson, Carlo L. Calosi, Chester F. Carlson, Robert Lee Cason, Jr., William Joseph Conner, Jr., Robert Francis Cotellessa, William B. Cottrell, Leo J. Cronin, Jose Luis Garcia de Quevedo, Channing Dichter, John Richard Drake, Jr., Thomas Herbert Ellison, Hussein M. A. El-Sum, John E. Faulkner, William J. Flett, Edward S. Foster, Jr., Walter H. Gardner, Willard H.

Gardner, Myron Garfunkel, Eric Paul George, Haskell Ginns, John Wallington Glen, Robert L. Gluckstern, Frank J. Gordon, Mary Beth Gorman, Michael Anthony Grace, Ernest P. Gray, Farno L. Green, William D. Gwinn, Ibrahim Hamouda, Benjamin Harmatz, Donald B. Harris, Saul Joseph Harris, Shirley W. Harrison, Walter Hauser, Edward Kenneth Heffner, Richard L. Henkel, Barbara Coe Herbst, Richard Wagner Hoffman, Alexander F. Holser, Donald Edwin Hudson, Harry H. Hummel, Dan W. Johnson, Jr., Orlando T. Johnson, T. B. Jones, James W. Kent, James Gus Kereiakes, Charles W. Kissinger, Leon Knopoff, George E. Koch, Herbert J. C. Kouts, Max Krook, Shea L. Kruegel, Rolf William Landauer, Igor Limansky, Peter Lindenfeld, Paul Lorrain, Robert Clinton Ludwig, James B. Maginnis, Herbert Malamud, Claudine Maroni, Thomas P. Martin, Robert S. Marvin, J. C. D. Milton, John W. Morfitt, Eric Bromfield Morris, Alfred Wachlin Nyquist, Stefan Albert Ochs, Albert W. Overhauser, Joe R. Patton, Beverly L. Paxson, Alphonso C. Pecora, Willis D. Perkins, Rolf E. Peterson, Milton A. Pogorelskin, Robert H. Pry, Guy S. Rambie, Jr., William J. Rand, Charles V. Robinson, John M. Robson, John Thomas Sample, Carl C. Sartain, Nathan Sclar, Nathan Seeman, Gordon Alexander Shifrin, Elwood D. Shipley, David C. Skillman, Albert Eugene Smith, Edward V. Somers, Irwin David Stein, William A. Stewart, Henry Stone, Charles L. Storrs, Jr., Walter Summer, Paul McCullough Sutton, Ross D. F. Thompsen, Ivan Tolstoy, Jay E. Treat, Jr., Robert R. Unterberger, Nathan Wainfan, Thomas S. Walton, John E. Warren, C. F. v. Weizsäcker, Molly Jean Wilson, Rolf G. Winter, L. D. Wyly, Jr., Ralph F. Wyrick, Carl A. Zapffe, Abe M. Zarem, Ernest Jakob Zingg.

KARL K. DARROW, *Secretary*
American Physical Society
Columbia University
New York 27, New York

Invited Papers on the General Programme

Nuclear Reactions and Level Widths. E. P. WIGNER, *Princeton University.*

Remarks on Recent Developments in Quantum Electrodynamics. GREGOR WENTZEL, *University of Chicago.*

Review of Electrostatic Generator Techniques and Recent Results. R. G. HERB, *University of Wisconsin.*

Structure and Behavior of Rubberlike Materials. H. M. JAMES, *Purdue University.*

Structure of Liquids from Other than X-Ray Evidence. G. ANTONOFF, *Fordham University.*

The Utilization of Physicists and Other Scientists During World War II. M. W. WHITE, *Pennsylvania State College.*

Line-Breadths in Radiofrequency and Microwave Absorption Spectra. J. H. VAN VLECK, *Harvard University.*

The Interpretation of the Magnetic Moments of Light Nuclei. R. G. SACHS, *University of Wisconsin.*

Nuclear Spins and Moments Obtained from Microwave Spectra. ARTHUR ROBERTS, *State University of Iowa.*

Absorption of 10–20 Mev Quanta. G. D. ADAMS AND A. T. NORDSIECK, *University of Illinois.*

Cosmic-Ray Investigation at 9500 Feet: Equipment and Results. E. J. LOFGREN, E. P. NEY, AND FRANK OPPENHEIMER, *University of Minnesota.*

Invited Papers Sponsored by the Division of Electron Physics

Imprisonment of Resonance Radiation in Ionized Gases, T. HOLSTEIN, *Westinghouse.*

Cathode-Emission Processes in Townsend Discharges. J. P. MOLNAR AND J. A. HORNBECK, *Bell Telephone Laboratories.*

Electrical Discharges in Gases at Microwave Frequencies. M. A. HERLIN, *Massachusetts Institute of Technology.*

Mass Spectrometry. A. O. C. NIER, *University of Minnesota.*

Sorption of Gases by Metals at Low Pressure: A Study of Getters. L. A. WOOTEN, *Bell Telephone Laboratories.*

The Long-Term Decay of Phosphors under Ultraviolet Excitation. E. F. LOWRY, *Sylvania Electric Products.*

Invited Papers

B1. Nuclear Reactions and Level Widths. E. P. WIGNER, *Princeton University.*

B2. (Title to be announced). GREGOR WENTZEL, *University of Chicago.*

B3. Review of Electrostatic Generator Techniques and Recent Results. R. G. HERB, *University of Wisconsin.*

C1. Structure and Behavior of Rubberlike Materials. H. M. JAMES, *Purdue University.*

C2. Structure of Liquids from Other than X-Ray Evidence. G. ANTONOFF, *Fordham University.*

C3. The Utilization of Physicists and Other Scientists during World War II. M. W. WHITE, *Pennsylvania State College.*

Invited Papers of the Division of Electron Physics

F1. Imprisonment of Resonance Radiation in Ionized Gases. T. HOLSTEIN, *Westinghouse.*

F2. Cathode-Emission Processes in Townsend Discharges. J. P. MOLNAR AND J. A. HORNBECK, *Bell Telephone Laboratories.*

F3. Electrical Discharges in Gases at Microwave Frequencies. M. A. HERLIN, *Massachusetts Institute of Technology.*

G1. Mass Spectrometry. A. O. C. NIER, *University of Minnesota.*

G2. Sorption of Gases by Metals at Low Pressure—a Study of Getters. L. A. WOOTEN, *Bell Telephone Laboratories.*

G3. The Long-Term Decay of Phosphors under Ultraviolet Excitation. E. F. LOWRY, *Sylvania Electric Products.*

Invited Papers

I1. Line-Breadths in Radiofrequency and Microwave Absorption Spectra. J. H. VAN VLECK, *Harvard University.*

I2. The Interpretation of the Magnetic Moments of Light Nuclei. R. G. SACHS, *University of Wisconsin.*

I3. Nuclear Spins and Moments Obtained from Microwave Spectra. ARTHUR ROBERTS, *State University of Iowa.*

I4. Absorption of 10–20 Mev Quanta. G. D. ADAMS AND A. T. NORDSIECK, *University of Illinois.*

Solid and Liquid States

A1. Observations on Superlattices in Order-Disorder Alloys Using Neutron Diffraction. SIDNEY SIEGEL AND C. G. SHULL, *Oak Ridge National Laboratory.*—The presence of superlattices in the order-disorder alloys Cu_3Au and FeCo subsequent to various heat treatments has been investigated using the neutron diffraction technique. The neutrons emerge from the Oak Ridge National Laboratory reactor and are monochromated by a (200) reflection from a NaCl crystal. After passing through the sample, consisting of filings of the alloy, in a cell chosen to give about 70 percent transmission, the diffracted radiation is detected with a BF_3 counter. In the case of Cu_3Au, for which the neutron scattering cross sections are 7 and 10×10^{-24} cm², respectively, no superlattice lines can be found in the neutron diffraction pattern for samples known to be ordered by conventional x-ray evidence. In the case of FeCo superlattice lines indicating complete order are found in samples slowly cooled from 800°C, whereas no order is found in the case of samples quenched from elevated temperatures or severely cold-worked. In the case of FeCo the neutron technique is successful because of the relatively large difference in nuclear scattering cross section, 12×10^{-24} cm² for Fe, 1.5×10^{-24} cm² for Co, while x-ray methods are made difficult because of the nearly identical electronic scattering cross section for x-rays of neighboring elements.

A2. Theory of Electrical Resistivity in Tellurium* V. A. JOHNSON, *Purdue University.*—By using an a.c. method to eliminate the Ettingshaussen effect, Bottom[1] has obtained Hall curves as functions of temperature between 85°K and 600°K for a number of tellurium samples. The samples were made by grinding, melting, and casting either commercial or purified tellurium; the ingots so produced were practically isotropic. Bottom has also measured the resistivities of these samples over the same temperature range. Analysis of these curves shows that the theory of resistivity[2] developed from the study of germanium alloys explains the resistivity behavior of tellurium. The low temperature resistivity may be treated as the sum of resistivities due to scattering by lattice ions and by impurity ions. The hole mobility, associated with lattice scattering only, is given approximately by $2.7\times10^{6}T^{-\frac{1}{2}}$ cm²/volt sec. The ratio of electron to hole mobility is calculated as 1.0. The intrinsic activation energy is found to be about 0.38 ev.

* This work was assisted by a Signal Corps contract.
[1] V. E. Bottom, Bull. Am. Phys. Soc. **23**, No. 3, 21 (1948), G2.
[2] K. Lark-Horovitz and V. A. Johnson, Phys. Rev. **69**, 258 (1946).

A3. Neutron-Bombarded Germanium Semiconductors. R. E. DAVIS,* W. E. JOHNSON, K. LARK-HOROVITZ,* and S. SIEGEL, *Purdue University* and Oak Ridge National Laboratory.*—It has been shown recently[1] that in germanium semiconductors bombarded by deuterons and alpha-particles lattice defects are produced which act as acceptors, thus producing "hole" conduction (*P*-type) (as tested by direction of rectification, Hall effect, and photo-effect). *P*- and *N*-type germanium samples with known electrical characteristics have been irradiated with neutrons in the Oak Ridge reactor; resistivities in *N*-type semiconductors increase under neutron irradiation until the donators are neutralized, and the resistance reaches a maximum; under continued irradiation the conductivity increases again. In *P*-type germanium the conductivity increases steadily with neutron irradiation and values 100 to 200 times the original conductivity have been reached. Whereas the deuteron induced lattice defects are healed by prolonged heat treatment at 400°C, only part of the induced neutron defects are healed in a comparable time interval. Experiments with commercial *N*-type germanium rectifiers indicate changes in the forward and backward direction in agreement witht he conclusion that the *N*-type germanium has been converted to *P*-type. The effect seems more pronounced in Cd-shielded samples.

* The work at Purdue was supported by a Signal Corps Contract.
[1] K. Lark-Horovitz, Bleuler, R. Davis, and D. Tendam, Bull. Am. Phys. Soc. **23**, No. 3, 25 (1948), K3.

A4. On the Measurement of the Hall Effect in Semiconductors.* I. ISENBERG, B. R. RUSSELL, AND R. F. GREENE, *University of Pennsylvania.*—An investigation was made of the short circuiting due to the electrodes in Hall effect experiments on rectangular samples. Formulas derived give the ratio of the measured voltage to Hall voltage as a function of l, the length across which the voltage is applied, w, the width across which the Hall voltage is measured, and the point of measurement. It is found, for example, that for $l/w=2$ the ratio of voltage measured at the center of the sample to Hall voltage is 0.930. If $l/w\geq4$, the error made is less than 0.3 percent. In terms of the ratio of measured voltage to applied voltage the greatest sensitivity is obtained for $l/w<\frac{1}{4}$. This ratio is equal to $0.742\mu B$ and, for this geometry, is independent of l/w. μ is the mobility of the carrier and B the magnetic field strength. It has been shown for homogeneous slabs that, when point electrodes are used, the Hall voltage depends only on the total current, the magnetic field, and the thickness of the sample but is otherwise independent of the shape of the slab. Experiments verifying these results will be described.

* This work was supported in part by Bureau of Ships.

A5. Small Angle Bragg Reflections from Collagen. PAUL KAESBERG, H. N. RITLAND, AND W. W. BEEMAN, *University of Wisconsin.*—The large periodicities in collagen have been investigated using a two crystal spectrometer in the parallel position. The spectrometer is then equivalent to a slit geometry of high resolution. Samples were placed midway between the two crystals and the scattered x-rays scanned by rotation of the second crystal.

The first through seventh orders and the ninth order have been completely resolved with wet collagen and relative intensities determined with an accuracy of about 10 percent. With dry collagen, the reflections are much less intense. The first order reflection from wet collagen has a full width at half-maximum of about 20 seconds with FeKα radiation. The periodicity calculated from the order spacings was 675A. for wet collagen and 643A for dry collagen, in good agreement with results of other investigators using standard diffraction methods.[1]

[1] R. S. Bear, J. Am. Chem. Soc. **66**, 1297 (1944).

A6. Electron Microscopy of Monolayers. H. T. EPSTEIN, *University of Michigan.*—With the aid of the shadow-casting technique of Williams and Wyckoff it has been possible to study the structure of organic acid monolayers with the electron microscope. The layers were deposited on collodion-covered microscope screens by the Langmuir-Blodgett dipping technique. Heights of mono- and multilayers of stearic acid and cerotic acid were measured and were found to agree well with heights given by previous indirect methods. The use of monolayers in finding the heights of minute objects will be discussed. It may also be possible to report on preliminary work with the oleophobic type of monolayer.

A7. Breaking Strength Dispersion in Nylon Yarns. WALLER GEORGE AND RICHARD LATORRE, *Naval Research Laboratory.*—Measurements of breaking strength of continuous multifilament low twist Nylon yarns (8 g.p.d.) are usually observed to lie within a wide range of strength values. Relatively large numbers of strength measurements using constant rate of load application techniques are reported for a sixfold increase in nominal gauge length. The observed frequency distributions and cumulative distributions for various specimen lengths are analyzed for the existence of a probability density function determining the frequency of observation of particular strength values for tests of unit volumes of the material. Distributions from Nylon yarns are given which indicate that the probability density, if it exists, is not Gaussian. However, more detailed analysis of data for short relative to longer gauges shows that the corresponding ratio of statistical sample sizes is independent of strength only for the region of low strengths. For the remaining region this ratio increases rapidly with strength indicating either that the "effective" length of the short sample increases, which is unlikely, or more probably that this "effective" length for longer lengths decreases with increasing strength. This suggests that for low twist and short gauge lengths twist is unimportant, while for longer specimens of same unit twist the total twist limits the length effective in determining the sample size and, correspondingly, increasing the dispersion in the higher strength ranges.

A8. A Twin Transducer for Measuring Mechanical Properties of Rubberlike Solids at Audiofrequencies. ROBERT S. MARVIN,* EDWIN R. FITZGERALD, AND JOHN D. FERRY, *University of Wisconsin.*—Apparatus has been developed for measuring the dynamic viscosity and rigidity of rubberlike solids in small oscillating deformations. A plate rigidly attached between two identical coils in two permanent magnet loudspeakers shears a pair of disk-shaped samples when a driving current is passed through one coil. The output voltage from the other coil is compared in amplitude and phase with the driving current. The amplitude of motion is extremely small. Representative data for the dynamic viscosity and rigidity of polyisobutylene over the range 30 to 700 c.p.s. will be given.

* Carbide and Carbon Chemicals Corporation Fellow in Physical Chemistry.

A9. The Fracture of Liquids. JOHN C. FISHER, *General Electric Research Laboratory.*—A liquid subjected to negative pressure is metastable; vapor bubbles form spontaneously and grow until the pressure of the system rises to the equilibrium vapor pressure. The rate of bubble formation is calculated from the theory of nucleation, and the negative pressure p_t that gives one bubble (i.e., fracture) in t seconds is determined. p_t is very nearly independent of t and is proportional to σ^4 where σ is the surface tension. Subcooled liquids such as glass also are metastable under negative pressure; cracks form spontaneously and grow until the pressure rises to the equilibrium vapor pressure. Nucleation theory leads to an expression for the fracture stress of glass that is proportional to $(E^2\sigma^3)^{\frac{1}{5}}$ where E is the elastic modulus. The transition from high temperature cavity-nucleated fracture to low temperature crack-nucleated fracture is examined. Fracture strengths calculated from nucleation theory agree satisfactorily with the maximum experimental values, and are an order of magnitude smaller than the forces required for simultaneous separation of all atom pairs cut by a plane surface. The frequent occurrence of premature failure is associated with the presence of pre-existing surface cracks in glass, and of positive contact-angle impurity in contact with liquids.

Reactions of Transmutation; Cosmic Rays

D1. Absolute Voltage Determinations of Three Nuclear Reactions. R. G. HERB, S. C. SNOWDEN, AND O. SALA, *University of Wisconsin.*—The large electrostatic analyzer constructed in 1946 at the University of Wisconsin[1] was used to give independent absolute voltage determination of three nuclear reactions. The reactions chosen were, on the old Li 440 Mev scale, the Li(p,n) threshold at 1.86 Mev, the Al(p,γ) resonance at .985 Mev, the F(p,γ) resonance at .862 Mev. Ion beam energies for these reactions were determined from measurements of the analyzer geometry and of the voltages applied to the analyzer. As a check on the dependability of the results the analyzer geometry was changed substantially after one series of runs and all measurements were repeated. Values obtained from the two series of determinations were consistent to better than .05 percent. Final values cannot be given safely until two further measurements are made. A voltage divider which was used in this work is to be checked at the National Bureau of Standards, and the effect of the

earth's magnetic field, which has been only roughly estimated, must be carefully explored. Our values now check closely with those obtained by Hanson[2] and final results will be available in June.

[1] R. E. Warren, J. L. Powell, and R. G. Herb, Rev. Sci. Inst. 18, 559 (1947).
[2] A. O. Hanson and D. L. Benedict, Phys. Rev. 65, 33 (1944).

D2. Thresholds for Some Photo-Nuclear Reactions. J. McElhinney, A. O. Hanson, and R. B. Duffield, *University of Illinois.*—The x-rays from the 22-Mev betatron were used to determine (γ,n) and (γ,p) threshold energies. The majority were detected by the induced radioactivity; the others, by the activity induced in rhodium foils by the ejected neutrons. Energies were determined by fixing the observed thresholds of the reactions, $C^{12}(\gamma,n)C^{11}$, $Cu^{63}(\gamma,n)Cu^{62}$, and $H^2(\gamma,n)H^1$, at 18.7±0.1, 10.9±0.1 and 2.18 Mev, respectively.

Reaction	Half-life	Observed Threshold (Mev)	Detected by
$N^{14}(\gamma,n)N^{13}$	9.9 Min.	10.6±0.2	Activity
$Mg^{26}(\gamma,p)Na^{24}$	14.8 Hr.	13.2±0.5*	Activity
$Mg^{26}(\gamma,p)Na^{25}$	1.0 Min.	15.6±0.5*	Activity
$P^{31}(\gamma,n)P^{30}$	2.5 Min.	12.4±0.2	Activity
$K^{39}(\gamma,n)K^{38}$	7.7 Min.	13.3±0.2	Activity
$Fe^{54}(\gamma,n)Fe^{53}$	8.9 Min.	13.9±0.3	Activity
$Cu^{65}(\gamma,n)Cu^{64}$	12.8 Hr.	10.2±0.4	Activity
$Br^{79}(\gamma,n)Br^{78}$	6.4 Min.	10.8±0.2	Activity
$Br^{81}(\gamma,n)Br^{80}$	18 Min, 4.4 Hr.	10.3±0.2	Activity
$Sb^{121}(\gamma,n)Sb^{120}$	17 Min.	9.3±0.2	Activity
$I^{127}(\gamma,n)I^{126}$	13 days	9.4±0.2	Neutrons
$Ta^{181}(\gamma,n)Ta^{180}$	8.2 Hr.	7.8±0.3	Activity
$Bi^{209}(\gamma,n)Bi^{208}$	—	7.3±0.2	Neutrons

* True thresholds may be 1–2 Mev lower.

D3. Proton-Neutron Thresholds in Cl^{37} and K^{41}. H. T. Richards and R. V. Smith, *University of Wisconsin.*—Protons from the Wisconsin electrostatic generator and analyzed by 90° electrostatic deflection have been used to bombard targets of NaCl and K_2O. A BF_3 counter surrounded by paraffin served as a neutron detector. The $Li^7(p,n)Be^7$ reaction was used to calibrate the energy scale by arbitrarily assuming $E_p=1.880$ Mv for the lithium threshold. The $p-n$ threshold in chlorine was then observed to be at 1.639±.003 Mv. Mass values necessitate assigning the reaction to the Cl^{37} isotope. The Q value is then −1.596 Mv which fixes the mass difference of $A^{37}-Cl^{37}$ as 0.903±.02 mMμ. The large probable error is from the uncertainty of the $n-p$ mass difference. A rough calculation of the reaction cross section for protons 50 kv above threshold gives $\sigma(Cl^{37})=10^{-26}$ cm². In the case of the potassium reaction low neutron intensity near threshold prevented comparable precision in the threshold determination. Radioactivity data and abundance considerations indicate that the reaction should be attributed to the K^{41} isotope. The observed threshold is at 1.25±.06 mv corresponding to a $Q=-1.22$ Mv. The mass difference $Ca^{41}-K^{41}$ is then 0.50±.07 mMμ. The cross section for protons 100 kv above threshold is estimated to be $\sigma(K^{41})=10^{-27}$ cm².

D4. Proton-Neutron Thresholds in V^{51} and Mn^{55}. R. V. Smith and H. T. Richards, *University of Wisconsin.*—Targets of V_2O_5 and metallic manganese have been bombarded by monochromatic protons from the Wisconsin electrostatic generator. Thresholds for neutron emission have been observed and reaction cross sections estimated. If the $Li^7(p,n)Be^7$ threshold is arbitrarily taken to be 1.880 Mv for the proton energy, then the V^{51} threshold is 1.564±.003 Mv proton energy and corresponds to a Q value of −1.534 Mv. Therefore the mass difference $Cr^{51}-V^{51}$ is 0.837±.02 mMμ with the $n-p$ mass difference accounting for the uncertainty. The cross sections of V^{51} is estimated to be 10^{-28} cm² for protons 50 kv above threshold. The manganese threshold occurs at 1.175±.01 Mv proton energy and corresponds to a $Q=-1.16$ Mv. The mass difference $Fe^{55}-Mn^{55}$ is .44±.02 mMμ. The reaction cross section is about 5×10^{-28} cm² for protons 50 kv above threshold. The cross section estimates are based upon a value of 3×10^{-25} cm² for the lithium $p-n$ reaction.

D5. Protons from the $Li^7(d,p)Li^8$ Reaction.* E. N. Strait, C. G. Stergiopoulos, and W. W. Buechner, *Massachusetts Institute of Technology.*—The reaction $Li^7(d,p)Li^8$ is well known, but the resulting proton group has hitherto been unobserved. A search for this group has been made using a 180-degree annular magnet to analyze the reaction products. Thin lithium targets have been bombarded with deuterons from an electrostatic accelerator, the analysis being at 90 degrees to the incident beam. Photographic detection has been employed. Using this technique, it is possible to distinguish between the reaction protons and the deuterons scattered inelastically from the target backing. A sharp peak of protons is observed, the energy of which is 750 kev when the incident deuteron energy is 1.36 Mev. This leads to a Q of −0.18 Mev, in good agreement with that obtained[1] from the excitation function for the production of radioactive Li^8.

* This work was supported in part by the Office of Naval Research
[1] Rumbaugh, Roberts, and Hafstad, Phys. Rev. 54, 657 (1938).

D6. Energy and Angle Variation of $C^{12}(d,p)C^{13}$. D. R. Inglis,* N. P. Heydenburg, and E. M. Hafner,** *Carnegie Institution of Washington.*—The yield of protons from the $C^{12}(d,p)C^{13}$ reaction has been observed from 1.5 to 3.6 Mev, at angles 10°, 90°, and 132.5°. At 10° the resonances observed are in reasonable agreement with those observed for gamma-rays and neutrons by Bailey, Frier, and Williams.[1] The resonances at 2.5, 2.65, and 2.95 Mev do not appear in the 90° yield curve. These are also much less prominent at 132.5°. Angular distribution curves have been taken in the vicinity of several of these resonances. Near 2.95 Mev, these curves show that the resonance is most pronounced near 20°. The short range proton group from $C^{12}(d,p)C^{13*}$ has also been observed at the higher deuteron energies. These have less range than the scattered deuterons, and were observed at 132.5° and 160° using a thin target of india ink on silver foil of 0.5 mm stopping power. The Q for this reaction was calculated to be −0.46 Mev in fair agreement with the value −0.52 ±0.7 Mev given by Bennett, Bonner, Hudspeth, and Watt. A search was made for a proton group giving an exicted state of C^{13} at 0.8 Mev above the ground state which has been found in the reaction $B^{10}(\alpha,p)C^{13}$. Such a group was not observed.

* Johns Hopkins University.
** Brookhaven National Laboratory.
[1] Bailey, Frier, and Williams, Phys. Rev. 73, 274 (1948).

D7. Absolute Thick Target Yields from Several (*D*,*n*) Reactions.* LYLE W. SMITH and P. GERALD KRUGER, *University of Illinois.*—The thick target neutron yields of several elements bombarded with 10-Mev deuterons have been obtained by comparing the activity induced in a large tank of $MnSO_4$ solution with the activity induced by a standard Ra-Be source. The yields in all cases are somewhat larger than would be expected from the extrapolation of the available low energy data. The results for deuterium in conjunction with the data of Curtis, Rosen, and Fowler[1] indicate a significant maximum in the yield between 2 and 10 Mev which is expected on theoretical grounds. The yields range in value from $3.7\pm0.4\times10^{10}$ neutrons/sec/μa for Be to $0.054\pm0.007\times10^{10}$ neutrons/sec/μa for Au. The largest uncertainty in the experiment is caused by the Ra-Be neutron standard.

* This work was supported in part by the Office of Naval Research.
[1] Curtis, Rosen, and Fowler, Phys. Rev. **73**, 648(A) (1948).

D8. Yield of Photo-neutrons from U^{235} Fission Products in Be. S. BERNSTEIN, F. L. TALBOTT, J. K. LESLIE, AND C. P. STANFORD, *Oak Ridge National Laboratory.*—The yield of photo-neutrons from a sample of 25 fission products at the center of a nine-inch diameter Be sphere has been studied. Samples of U^{235} were exposed in the pile for periods of 30 seconds, 15 minutes, six hours, and 74 hours. The photo-neutrons were observed from 0.3 second to about four weeks after the end of the exposure. Curves showing the photo-neutron yield relative to the delayed neutron yield as a function of time are given for these exposure and observation times. A comparison is made between the photo-neutron yield of infinite thicknesses of D_2O and Be for a six-hour exposure. This comparison shows that the yield from Be is less than that for D_2O for times less than about one-half hour after the end of the exposure and that the yield from Be becomes increasingly greater than that for D_2O for times greater than one-half hour. A possible explanation of the relative yields of Be and D_2O with time in terms of the variations of the photo-disintegration cross sections with energy and the average variation of fission product gamma-ray energy with time is proposed.

D9. Equipment for Photographing Cosmic-Ray Cloud-Chamber Tracks at 100,000 Ft. WALTER FRICK, EDWARD J. LOFGREN, FRANK OPPENHEIMER, AND EDWARD P. NEY, *University of Minnesota.*—We have been able to photograph cosmic-ray tracks at an altitude of 100,000 ft. The cloud chambers are carried aloft by a balloon and remain at altitude for several hours. Details of the temperature regulation and the cloud-chamber control equipment will be discussed. The apparatus is housed in a 30″ diameter aluminum sphere and weighs about 60 lb. The constant temperature is maintained by a thermostatically controlled blower which can circulate air from the hot upper part of the sphere which is painted black and the cooler lower section which is polished. The two sections are separated by an insulating barrier. The cloud chamber is in the lower section. The temperature is maintained constant at the lower altitude before the solar engine begins to function by a battery operated heater. This battery is parachute released at an altitude of about 50,000 feet.

D10. Data Obtained from Cosmic-Ray Cloud Chamber Tracks Taken at 100,000 Feet. EDWARD J. LOFGREN, EDWARD P. NEY, AND FRANK OPPENHEIMER, *University of Minnesota.*—Information contained in the pictures of cosmic-ray cloud-chamber tracks taken at an altitude of 100,000 feet will be summarized. Preliminary data on the occurrence of large numbers of heavily ionizing particles which penetrate ½ inch of lead will be presented. The pictures also gives data on the relative amount of soft, penetrating and heavily ionizing components as a function of altitude.

D11. On the Compton Effect for Protons. J. L. POWELL, *University of Wisconsin.*—The scattering of γ-rays by free protons has been studied on the hypothesis that the proton is a Dirac particle whose magnetic moment is described by the well-known Pauli term. The angular distribution[1] of the scattered γ-rays and the total cross section have been calculated for a particle of arbitrary magnetic moment. The total cross section increases linearly with the energy in the extreme relativistic limit. At intermediate energies it is larger than the cross section obtained without the Pauli term (Klein-Nishina formula). Experimental study of this effect would be very difficult on account of the small cross section ($\sim2\times10^{-31}$ cm² at 100 Mv). However, it is conceivable that one could observe the recoil protons from Compton scattering of 100-Mv γ-rays. At this energy, one does not expect the meson production which would confuse the results at higher energy. The calculated angular distribution is fairly uniform, and the recoil particles have energies up to 15 Mv. Comparison of quantitative experimental results with this theory would give information concerning the structure of the proton.

[1] The angular distribution has been given, for the special case of a particle of zero magnetic moment, by Batdorf and Thomas, Phys. Rev. **59**, 621 (1941).

D12. On the Bremsstrahlung Produced by Protons. R. G. SACHS AND J. L. POWELL, *University of Wisconsin.*—If the anomalous magnetic moment of the proton can be described in terms of a Pauli interaction with the electromagnetic field, the cross section for bremsstrahlung will increase more rapidly with energy than that of an ordinary Dirac particle. Therefore it might be expected that the high energy primary protons in the cosmic rays will produce an appreciable number of showers. The extreme relativistic cross sections for scattering by pure and cut-off Coulomb fields have been calculated by one of us (J.P.) using the perturbation method. For a pure Coulomb field the cross section increases more rapidly than that of the electron by a factor E^2 (E=proton energy). For the cut-off field the energy dependence for the ratio is reduced to E, in agreement with the results of the method of Weizsäcker and Williams.[1] The failure of the latter method for

the pure Coulomb field is a consequence of the importance of the contribution of short γ-ray wave-lengths to the cross section. One can conclude that for proton energies above 10^{13} ev it is necessary to consider proton-proton collisions within the nucleus as a major factor in bremsstrahlung production. This effect will reduce the cross section because of the recoil of the proton, while on the other hand the greater strength of nuclear forces may increase it.

[1] Batdorf and Thomas, Phys. Rev. **59**, 621 (1941).

General Nuclear Physics; Apparatus of Nuclear Physics

E1. Binding Energies of α-Particles in Medium-Heavy Nuclides.* TRUMAN P. KOHMAN, *University of Chicago.*—Binding energies of α-particles in medium-heavy nuclides have been estimated by means of the mass equation of Bohr and Wheeler[1] and the packing fraction curve of Mattauch and Flügge.[2] Most nuclides above mass number 140 are energetically capable of α-emission, and are only stabilized by the nuclear potential barrier, the effect of which has also been calculated. The α-disintegration energy generally increases with increasing Z for isobars and with decreasing A for isotopes. Consequently, sufficiently light isotopes of elements in the region from the rare-earths to lead should be α-active. The lighter naturally occurring isotopes of some of the event elements in this region may exhibit barely detectable α-activity. Bombardment with $\gtrsim$100-Mev photons[3] and particles[4,5] should produce sufficiently neutron-deficient nuclides to allow artificial alpha-activity to be observed in competition with β-decay processes in this region.

* Work begun at the Metallurgical Laboratory, Manhattan Engineer District, in 1946.
[1] N. Bohr and J. A. Wheeler, Phys. Rev. **56**, 426 (1939).
[2] J. Mattauch and S. Flügge, *Nuclear Physics Tables* (Julius Springer, Berlin, 1942; Interscience, New York, 1946).
[3] G. C. Baldwin and G. S. Klaiber, Phys. Rev. **70**, 259 (1946).
[4] G. T. Seaborg *et al.*, Phys. Rev. **72**, 739, 740 (1947).
[5] D. H. Templeton, U.S.A.E.C. Document MDDC-1525 (Abstract).

E2. The Ionization Produced by Alpha-Particles in Argon as a Function of Their Energy. WILLIAM P. JESSE AND HAROLD FORSTAT, *Argonne National Laboratory.*—Recently[1] we have shown that the energy of an alpha-particle may be accurately determined by comparison of its total ionization in argon with that of a standard alpha-particle of known energy in cases where the energy difference between the two is small. To compare thus particles of widely differing energies it is necessary to establish first a calibration curve relating the ionization produced by an alpha-particle with its energy. To this end, we have made preliminary measurements of the relative ionization produced by alphas from six natural radioactive substances in the region from 5 to 9 Mev, where the energies are known with high precision. Here the ionization-energy plot is a straight line which, when extrapolated, passes through the origin. In the region of lower energies, where reaction energies are not known with as high precision, it would seem possible to detect any marked change in slope of the above line by measuring the ionization of each of the two particles emerging from an extremely thin sheet, as for instance in the (n,α) reaction for ^{6}Li or ^{10}B. The ratio of the particle energies may be calculated from the consideration of the conservation of momentum. Tentative experiments of this sort are in progress.

[1] W. P. Jesse and H. Forstat, Phys. Rev. **73**, 926 (1948).

E3. Angular Distribution of α's Coincident with U^{235} Fission. L. MARSHALL, *Argonne National Laboratory and University of Chicago.*—From among 7000 U^{235} fissions made by thermal neutrons in uranium impregnated Eastman photographic emulsion *NTB*, 70 α-particles* coincident[1-4] with fission have been found. An analysis has been made of the variation in their average range and numbers with angle between α and short (heavy) fission fragment. The data will be given on slides. No α's less than 4 Mev have been included. The low energy α's emerge more frequently at acute angles to the short fission fragment. The energetic α's emerge at about right angles, as previously found by Wollan *et al.*[4] The longest range α's seem to emerge most probably at about 100° to the short fragment. This agrees qualitatively with the greater electrostatic repulsion of the heavy fragment due to its higher charge. When the two fission tracks are of very different length, the coincident α tends to have an acute angle with the short range fragment and to be of low energy.

* These α-particles were first observed by L. Alvarez. See quotation in 2.
[1] Demers, Phys. Rev. **70**, 974 (1946).
[2] Farwell, Segre, Wiegand, Phys. Rev. **71**, 327 (1947).
[3] San-Tsiang, Zah-wei, Chastel, and Vigneron, Phys. Rev. **71**, 383 (1947).
[4] Wollan, Moak, Sawyer, Phys. Rev. **72**, 447 (1947).

E4. Preliminary Data on the Production of $\pm$ Electron Pairs in the Field of an Electron.* J. A. PHILLIPS AND P. GERALD KRUGER, *University of Illinois.*—A 12″ cloud chamber is irradiated with a collimated beam of gamma-rays from CaF_2 bombarded by 10 Mev molecular hydrogen ions. The cloud chamber is situated outside of the tanks surrounding the cyclotron and is provided with a magnetic field of 1535±1 percent oersteds. Only those pairs and triplets occurring in the gas of the chamber are considered. Operating at a pressure of 1.75 atmospheres, 5372 stereoscopic pictures with air gave 509±electron pairs and 18 triplets. With methane, 13,362 pictures gave 1430 electron pairs and 97 triplets. From these data the ratio of the cross sections for pair to triplet production, assuming a Z^2/Z dependence, has the value for air ($Z^2/Z\simeq 7.2$) of 3.94, and for methane ($Z^2/Z\simeq 4$) of 3.69, which are in agreement within statistical limits. A plot of the logarithm of the number of the slow negative electron of the triplets in equal momentum intervals *versus* momentum of the slow negative electron appears to be a straight line.

* This work in part supported by the Office of Naval Research.

E5. Angular Distribution of the Disintegration Products from the $D-D$ Reaction; 1 to 4 Mev. J. M. BLAIR, W. SLEATOR, JR., GEORGE FREIER, E. E. LAMPI, AND

J. H. WILLIAMS. *University of Minnesota.**—The angular distributions of the He^3, produced when deuterons bombard deuterons in the energy range from 1 to 4 Mev have been measured using the scattering chamber previously described.[1] These particles can be counted separately from the elastically scattered particles by virtue of their differences in range and ionizing ability. We find that the distribution of the He^3 cannot be described by $(1+A\cos^2\theta)$ as reported by Bennett, Mandeville, and Richards for the neutrons from the same reaction.[2] There are more particles in the forward direction than can be accounted for by that expression and, for the higher energies, there are further anomalies at 90° in the center of mass coordinate system. Work is being done on the distributions of the H^1 and H^3 from the same reaction.

* This work was supported in part by the Office of Naval Research.
[1] Sleator, Blair, Lampi, and Williams, Bull. Am. Phys. Soc. 23, No. 2 (1948).
[2] Bennett, Mandeville, and Richards, Phys. Rev. 70, 101A (1946).

E6. Angular Distribution of 1 to 4 Mev Deuterons Scattered by Deuterons. WILLIAM SLEATOR, JR., J. M. BLAIR, GEORGE FREIER, EUGENE LAMPI, AND J. H. WILLIAMS. *University of Minnesota.**—Using the gas filled chamber previously described,[1] cross sections for the elastic scattering of deuterons by deuterons have been measured at energies ½ Mev apart from 1 to 4 Mev, and at angles from 10° to 45°. The reaction products H^1, H^3, and He^3 are also registered in the proportional counter, but these can be distinguished, as described in the previous paper, from the scattered deuterons, and thus the yield of the latter determined. Typical values of the elastic scattering cross sections at two energies, corrected for H^1 and He^3, but not for H^3, which is estimated to contribute one or two percent, are given in barns per unit solid angle in the table.

θ cm	20°	30°	40°	50°	60°	70°	80°	90°
1.50 Mev	4.22	1.30	0.67	.466	.352	.311	.281	.273
3.55 Mev	1.23	0.59	.396	.309	.266	.222	.195	

Results at other energies are similarly regular.

* This work was supported in part by the Office of Naval Research.
[1] Sleator, Blair, Lampi, and Williams, Phys. Rev. 73, 1241A (1948).

E7. A Simple All-Electronic Cloud Chamber Control Circuit. S. BASHKIN AND H. T. RICHARDS, *University of Wisconsin.*—A modified Wynn-Williams thyratron ring circuit functions as a control circuit for a Wilson chamber built for use with the Wisconsin electrostatic generator. The 100 ma delivered by the miniature 2D21 thyratrons obviate relays. Three such thyratrons, with plates capacitively coupled, form a ring circuit with three stable states, in each of which only one thyratron conducts. In the first state, the magnetically operated expansion valve is closed. The plate voltage from one of the non-conducting thyratrons charges a condenser in a variable RC circuit (25–150 sec.) until a neon bulb fires, thereby switching the ring circuit to the next stable state in which the chamber is expanded and the camera solenoid activated. A similar RC circuit (0–1 sec.) transfers the system to its third stable state with the camera closed and the chamber still expanded. A pulse from a third RC circuit (5–20 sec.) closes the cycle, recompressing the chamber. Other variable RC circuits fire neon bulbs to trigger a flash tube and pulse an ion beam on a target coincident with the chamber's sensitive time. This circuit can be easily adpated to counter control or expanded to have more stable states.

E8. Stabilized High Voltage Supply for Electrostatic Analyzer. R. L. HENKEL AND B. PETREE, *University of Wisconsin.*—A system for measuring and controlling the beam energy of the University of Wisconsin electrostatic generator has been described by Hanson.[1] The high voltage supply for the electrostatic analyzer used in his system has been modified to give better energy control and to simplify voltage adjustment. The new supply furnishes continuously adjustable voltages from 4000 to 40,000 volts to the analyzer with stability better than 0.01 percent. High voltage from a rectifier circuit is compared, by means of a voltage divider, to a potentiometer. The difference or error voltage is amplified about 10^7 times by a galvanometer-phototube amplifier, and the amplified error voltage is applied to the grids of variable-impedance tubes in the high voltage transformer primary so as to decrease the error. Oscillation is prevented with differentiated feed-back. Rapid line voltage fluctuations are not completely compensated for by the galvanometer-phototube amplifier because of its relatively slow response, but these fluctuations are avoided by supplying power to the high voltage transformer from a motor-alternator set with electronic field regulation. With this new method, the beam energy automatically follows adjustments of the potentiometer.

[1] A. O. Hanson, Rev. Sci. Inst. 15, 57 (1944).

E9. Design of Electrostatic Generator for the University of São Paulo, Brazil. O. SALA, *University of S. Paulo** AND R. G. HERB, *University of Wisconsin.*—A high pressure electrostatic generator for the University of São Paulo is being designed for a maximum voltage of 3.5–4 Mv following the Wisconsin horizontal arrangement. Important design considerations are low cost, simplicity, minimum time for construction, easy operation and high beam current. The pressure tank is to have an inside diameter of 7 feet, a length of 21 feet and a maximum operating pressure of 150 p.s.i. The tank is arranged to roll back for easy access to equipment inside. Inside structure is supported by four textolite tubes, each 10 feet long, giving an insulating length of 9 feet. Two accelerating tubes are provided, one for the ion beam and one for an electron beam to give voltage control. The second tube will also be used for differential pumping. Two concentric high potential electrodes will be used.

* Now at the University of Wisconsin as a Rockefeller Fellow.

E10. Performance of the Allen Type Multiplier Tube for Lithium Ion Counting. A. H. MORRISH AND J. S. ALLEN, *University of Chicago.*—Information concerning the efficiency of an electron multiplier[1] tube used for detection of single Li ions is necessary for He^6 recoil experiments now in progress. Li ions were produced by thermionic emission from a coating of spodumene on a platinum

filament. After being accelerated, they were bent by the plates of an electrostatic analyzer through a slit into the multiplier tube. This arrangement prevented the tube from "looking" directly at the ion source. The counting rate was compared to the current, which was determined by sweeping the ions through a larger slit, connected to a balanced type d.c. amplifier. The relative transmission of the slits was determined by comparing counting rates of a beam swept through each slit. Ions from 4.9 to 6.5 kv were used, and showed almost constant counting rates. Pulse height distribution curves were taken for 4.9 and 6.0 kv ions, and were of the same general shape, the 6.0 kv ions giving more counts at all points on the curve. The efficiency for ions of low energy is being investigated.

[1] J. S. Allen, Rev. Sci. Inst. **18**, 739 (1947).

E11. Neutral Region in the Space Charge of a Self-Quenching G-M Counter. C. V. ROBINSON, *University of Wisconsin.*—It is not uncommon for a G-M counter to collect more than twice the original charge, Q_0, on the wire. This is inconsistent with (1) immediate collection of the electrons which leave a purely positive space charge; (2) nearness of space charge to the wire; (3) non-negative field throughout the counter. To explain this large charge collection, assumption (1) may be discarded leading to the following mechanism. In a length dx of the counter, ions produced by avalanching, build out radially leaving a weak field near the wire in which delayed quanta produce ion pairs. In about 10^{-9} sec. ionization has ceased, and the length dx of wire is discharged and surrounded by a neutral region (of + ions and electrons) within a purely positive sheath whose charge is a little more than Q_0dx. As the outer + ions move out, the electrons in the neutral region move in, releasing an equal number of electrons and + ions. The process continues until all electrons are collected and all + ions freed. Then the wire recharges. W. W. Beeman suggested the delayed electron collection.

E12. Multivibrator Quenching of Geiger-Mueller Tubes.[1] B. J. THAMER AND A. F. VOIGT, *Iowa State College.*—Lowering or reversing the sign of the potential on the anode of a Geiger-Mueller tube is an effective way of quenching the tube discharge and allowing the tube to regain its sensitivity rapidly, thus reducing the counting loss at high counting rates. An electronic circuit capable of applying a quenching pulse of any desired width and magnitude has been developed. The amplified G-M tube pulse actuates a multivibrator which triggers the quenching tube.[2] A series of dead-time determinations was made on several G-M tubes using paried samples, keeping the width of the quenching pulse at 12 microseconds and varying its magnitude from 0 to a value sufficient to make the center wire 50 volts negative with respect to the cathode. Quenching pulses in the range from 0 to 400 volts gave dead-times of roughly 290 microseconds. Important factors were the previous history of the tube and its operating potential. When the quenching pulse brought the wire potential within ±50 volts of the cathode, the dead-times were approximately 40 microseconds.

[1] This work was done under contract with the Atomic Energy Commission.

[2] For a similar application see J. A. Simpson, Jr., Phys. Rev. **66**, 39 (1944).

X-Rays and Optical Spectroscopy

H1. The MnK Absorption Edges of Manganese and Manganese Compounds. H. P. HANSON AND W. W. BEEMAN, *University of Wisconsin.*—The x-ray K absorption edge of manganese, in the metal and in various compounds, has been measured with a double crystal spectrometer. Striking differences are observed between the edges in homopolar complexes and in ionic crystals. With anions which are not strongly electronegative in their effect, one observes some absorption into levels on the long wave-length side of the main $4p$ absorption. This absorption occurs at the same energy as the $3d$ levels.

H2. Method of Measuring Ratio of Bremsstrahlung Cross Sections. L. H. LANZL, J. S. LAUGHLIN, AND L. S. SKAGGS, *University of Illinois.*—The ratio of cross sections for the production of Bremsstrahlung in elements of nuclear charge Z_1 and Z_2 is measured as follows: two sets of thin, uniform foils, one set of alternate Z_1 and Z_2 foils, the other set all of Z_1 foils, are placed perpendicular to an electron beam and irradiated. The activities of the odd position foils of both sets (Z_1 in both cases) are then measured and plots are made of initial radioactivity *vs.* foil position normalized to the first foil of one of the sets. Such plots are linear[1] if the total foil thickness is small compared to the range of the electrons. The ratio of Bremsstrahlung cross sections for that part of the spectrum above the threshold of Z_1 is then obtained from the ratio of the slopes of the two curves and the number of atoms per unit area in each foil. Using 15.5 Mev electrons from the betatron, the Bremsstrahlung cross section ratio of Ta and Cu, measured under four different conditions, was $6.89 \pm .21$. Elementary theory predicts that the ratio should vary as Z^2 giving for Ta−Cu 6.34. In this measurement Cu corresponded to Z_1 and therefore was the element in which the activity was measured.

[1] L. S. Skaggs, J. S. Laughlin, A. O. Hanson and J. J. Oriin, Phys. Rev. **73**, 420 (1948).

H3. A Photoelectric Technique for Spectral Emissivity Determination Illustrated by Results on Tungsten.* W. B. NOTTINGHAM AND W. E. MUTTER, *Massachusetts Institute of Technology.*—A method of measuring spectral emissivity at a narrow band width over a range of wave-lengths from the near ultraviolet to the near infra-red has been developed. The intensity of various parts of the image of a miniature blackbody source is explored by means of a monochrometer and photomultiplier tube arrangement; the emissivity at a given wave-length and temperature is determined from a measurement of the ratio of the intensity from the surface of the specimen to that from the blackbody cavity. Initial results on tungsten over the range 1300 to 2000°K and 380 to 800 millimicrons are represented by the empirical formula $\epsilon_{\lambda T} = 0.5308 + 5.24 \cdot 10^{-6} T - (9187 + 3.90T)10^{-8}\lambda$ The variation of the spectral emissivity with wave-length and temperature is in general agreement with results of Forsythe and Worthing.** However, the absolute values are all 1½ to 2 percent lower.

* This work has been supported in part by the Signal Corps, the Air Materiel Command and the O.N.R.

** W. E. Forsythe and A. G. Worthing, Astrophys. J. **61**, 152 (1925).

H4. Electromagnetic Shift of S Levels in He II.* J. E. MACK AND N. AUSTERN, *University of Wisconsin.*—Work on the line λ4686A ($n=4\rightarrow n=3$) of ionized helium has been continued. The third most intense component ($3_{\frac{1}{2}}-4_{\frac{1}{2}}$) has been spread, presumably into $3s_{\frac{1}{2}}-4p_{\frac{1}{2}}$ and $3p_{\frac{1}{2}}-4d_{\frac{1}{2}}$. A Fabry-Perot etalon with a 15 mm-spacer was crossed with the previously used diffraction grating in order to obtain this result.

* The work is supported by the Office of Naval Research.

H5. The Continuous Absorption Coefficient of the Helium Atom. SU-SHU HUANG, *Yerkes Observatory.* (*Introduced by S. Chandrasekhar.*)—The continuous absorption coefficient of HeI from its ground state as well as its two metastable states has been carried out. The wave functions used for these three states are those of the Hylleraas type derived from the Ritz principle. The constants of these wave functions were determined, as Hylleraas apparently did not solve for them. For the wave functions of the continuous states, the hydrogenic approximation was used. The cross sections for each of the three states have been determined in terms of the matrix elements of the dipole moment, momentum and acceleration and compared in the manner of Chandrasekhar's discussion of the negative hydrogen ion.*

* Astrophys. J. 102, 223, 395, (1945).

H6. Rydberg Denominators in the Principal Series of the Alkali Metal Atoms. J. G. HIRSCHBERG, JR., *University of Wisconsin.*—The Ritz series fit is discussed for the Rydberg denominators calculated from the accurate term values of Kratz.[1]

[1] H. R. Kratz, Ph.D. Thesis University of Wisconsin, 1942; Phys. Rev. (to be published).

H7. Structure of the ^2D-Terms of Li^7. K. W. MEISSNER, L. G. MUNDIE,[1] AND P. STELSON, *Purdue University.*—Interferometric wave-length measurements of the lithium arc spectrum were carried out by employing an atomic beam light source. The great sharpness of the spectral lines permitted determination of the splitting of several ^2D-terms. The values for the first four members of the diffuse series are: $\Delta\nu=0.0372$, 0.015, 0.010, and 0.005 cm^{-1}. All investigated D-terms exhibit regular term order.

[1] Now at Naval Research Laboratory, Washington, D. C.

H8. Infra-Red Dispersion of N_2O and C_2H_4. C. F. HAMMER, A. G. PIEPER, AND R. ROLLEFSON. *University of Wisconsin.*—The indices of refraction of N_2O and C_2H_4 have been measured for wave-lengths between 1 micron and 16 microns. The method has been described previously.[1] The index of refraction is the sum of a series of terms, each term being a function of the characteristics of a particular absorption band. In the infra-red region the terms due to ultraviolet absorption can be lumped into a single term which is almost constant. Each of the remaining terms is of the form $A_i/[2\pi^2C(\nu_i^2-\nu^2)]$; where A_i is the integrated absorption coefficient,[2] and ν_i is the wave number corresponding to the ith band. These measurements, then, make the determination of A_i possible without actually taking measurements in the band. The accuracy of the A_i's is dependent on the magnitude of the absorption intensity and the wave-length region of the particular band. We believe the accuracy to be better than 4 percent for the strongest bands.

[1] R. Rollefson and R. Havens, Phys. Rev. **57**, 710 (1940).
[2] M. Thorndike, A. J. Wells and E. Bright Wilson, Jr., J. Chem. Phys. **15**, 157 (1947).

H9. Band Spectrum of HgTl. J. GIBSON WINANS AND WILLARD J. PEARCE,* *University of Wisconsin.*—Vibrational analyses have been made for the HgTl band systems with maxima of intensity at 6550, 5200, 4580, and 3810A. The light source was a Tesla discharge with external electrodes through a quartz tube containing Hg and Tl. The 3810 system was obtained also in absorption. The following constants were obtained:

ν_{00}	ω_0'	$\omega_0'x_0'$	ω_0''	$\omega_0''x_0''$	D_0'	D_0''
15339.9	82.2	0.157	102.08	2.08	4100 cm^{-1}	1132 cm^{-1}
15289.4	82.27	0.144	100.8	2.29	4100 cm^{-1}	1081 cm^{-1}
22621.5	81.23	0.077	105.97	0.268	4100 cm^{-1}	2015 cm^{-1}
26253.2	15.53	0.060	26.2	0.69	474 cm^{-1}	250 cm^{-1}

* Now at University of Texas, El Paso.

H10. Spin-Orbit Effect in the Hyperfine Structure of the Ammonia Inversion Spectrum. J. M. JAUCH, *State University of Iowa.*—The recent measurement of the hyperfine structure in the ammonia inversion spectrum by Simmons and Gordy[1] indicated a significant discrepancy with the theoretical formula for the satellite separation. It is pointed out that this effect can be interpreted as due to the interaction of the magnetic dipole moment of the nitrogen nucleus with the rotation of the molecule. The interaction term in the Hamiltonian is of the form $-\mu H'(J, I)$, where μ is the magnetic moment of the N^{14} nucleus, H′ the effective magnetic field at the position of the nucleus, J the angular momentum vector of the molecule, and I the spin vector of the nucleus. Theoretically, the constant H′ (J, K) is expected to depend explicitly on the rotational quantum numbers, J, K. However, a rough estimate indicates that the variation of H′ is less than the uncertainty resulting from the measurements. Best agreement with the experimental values is obtained by assuming $H'=15\pm5$ gauss. This explanation permits also a redetermination of the quadrupole interaction parameter which in frequency units is found to be $(eqQ)=4.107\pm0.015$ mc/sec.

[1] J. W. Simmons and W. Gordy, Phys. Rev. **73**, 713 (1948).

H11. Phenomenological Quantum-Electrodynamics. K. WATSON AND J. M. JAUCH, *State University of Iowa.*—The relativistic quantum formalism of the electromagnetic field in a medium characterized by a dielectric constant ϵ and a magnetic permeability μ has been developed. The total energy and momentum of the field do not form a nulvector in this theory. The quantization is given both in the Hamiltonian form as well as in the symmetrical four-dimensional formalism. When the interaction with charges is introduced the longitudinal components can be eliminated with the help of the subsidiary condition. The

resulting Coulomb energy in the Hamiltonian depends explicitly on the velocity of the medium. If the velocity of the medium with respect to the particle exceeds that of $v=C/n$, a particle at rest can radiate spontaneously. This is traced to the fact that in this case light quantas may occur with negative energy. The total emission probability for such radiation is infinite if n is independent of the frequency. Only if dispersion is introduced does the expression become finite. In the latter case it agrees exactly with the classical expression for Čerenkov radiation given by Tamm and Frank.[1]

[1] Comptes Rendus 14, 109 (1937).

Nuclear Spins and Moments; Artificial Radioactive Substances

J1. Hyperfine Structure of 30 Zn^{67}.* O. H. ARROE, *University of Wisconsin.*—A study of the hyperfine structure of the ZnI lines $4s4p\ ^3P_{012}-4s5s\ ^3S_1$, from a sample enriched in Zn^{67} (borrowed from the United States Atomic Energy Commission) shows hyperfine structure intervals verifying the value 5/2 for the nuclear spin of Zn^{67}, tentatively assigned by Rasmussen.[1]

* The work is supported by the Office of Naval Research.
[1] Rasmussen, Zeits. f. Physik 104, 434 (1937).

J2. A Variation of the Nuclear Resonance Experiment. EDWARD R. MANRING, JOHN R. ZIMMERMAN, AND DUDLEY WILLIAMS, *The Ohio State University.*—Roberts has described a method for measuring nuclear gyromagnetic ratios by means of a super-regenerative oscillator circuit and a communications receiver. We have made extensive experiments using a similar arrangement with a specially designed audio amplifier as a detector. With the usual arrangement in which a solid or liquid sample is mounted inside the oscillator coil, saturation effects introduced considerable difficulty, since the r.f. magnetic fields were larger than necessary for the experiment but, owing to inherent characteristics of super-regenerative circuits, could not be satisfactorily reduced. We have attained satisfactorily low values for the r.f. magnetic field by placing the sample between the plates of a condenser and using the r.f. magnetic field associated with the displacement currents. The parallel plate condenser containing the sample is mounted with the plates parallel to the pole faces of a large electromagnet. As the air gap in the magnetic circuit can be made smaller than when the coil is mounted in the magnetic field, more effective use is made of iron in the magnet circuit and, for a given field current, a more favorable Boltzmann factor can be attained. Although the arrangement we have used has been found to be convenient in special cases, its ultimate limitations are essentially the same as those indicated by Bloch and Purcell.

J3. The Beta-Spectrum of C^{14}.* LAWRENCE M. LANGER, C. SHARP COOK, AND H. CLAY PRICE, JR., *Indiana University.*—The momentum distribution of the negatrons emitted by C^{14} has been investigated in the high resolution, 40 cm radius of curvature, shaped field magnetic spectrometer. The sources were prepared from high specific activity material made available at Oak Ridge through the efforts of Norris and Snell. Spectra were obtained using sources of average thickness 0.13 mg/cm², 0.29 mg/cm², and 0.97 mg/cm². The backing in all cases was 0.02 mg/cm² Zapon. The Zapon counter window transmits electrons down to 2.0 kev. Under these conditions, all three sources yield spectra which are the same for all energies from $W=1.12$ mc² to the end point. Over this region, the Fermi plot is not a straight line, but has, rather, a very slight curvature away from the energy axis. This curvature is not explained by the use of Fermi selection rules for a second forbidden transition of the type $J=1$ with no parity change. S^{35}, measured under essentially identical conditions does yield a straight line Fermi plot over the same region which is curved for C^{14}. The extrapolated Fermi end point for C^{14} is at $W_0=1.306$ mc² corresponding to 156.3 ± 1.0 kev. The end point for S^{35} is found to be 169.1 ± 0.5 kev.

* This work is supported by a grant from the Frederick Gardner Cottrell fund of the Research Corporation and by the Office of Naval Research.

J4. Radioactive Isotopes of Germanium and Arsenic. D. A. MCCOWN, L. L. WOODWARD, M. L. POOL, AND H. L. FINSTON, *The Ohio State University.*—The germanium fraction from zinc bombarded with alpha-particles showed long half-life of positron activity, presumed to be the 195-day germanium period. Gallium bombarded with deuterons gave evidence of no period longer than 11 days in the germanium fraction. From intensity considerations, the 195-day period should have occurred if it were Ge^{69}. Hence this long period has been assigned to Ge^{67}. Gallium bombarded with deuterons showed in the germanium fraction a strong positron activity of 1.66-day half-life. Deuteron bombardment of germanium showed a similar period in the germanium fraction, but this period was an electron emitter, being produced by decay of 12-hour Ge^{77} into As^{77}. Hence the positron emitting period of 1.66 days in germanium is assigned to Ge^{69}. A strong sample of radioactive Ge^{71}, decaying with the 11-day half-life, has produced on a curved crystal camera the characteristic x-ray lines of gallium. Simultaneous deuteron bombardment of two samples of selenium, enriched respectively in isotopes 74 and 76,* confirms in the arsenic fraction the location of the positron emitting period of 1.08 days half-life as that due to As^{72}.

* Supplied by the Y-12 plant, Carbide and Carbon Chemicals Corporation, through the Isotopes Division, U. S. Atomic Energy Commission, Oak Ridge, Tennessee.

J5. Artificial Radioactivity from Enriched Se^{74} and Se^{76}. L. L. WOODWARD, D. A. MCCOWN, M. L. POOL, AND H. L. FINSTON, *The Ohio State University.*—A radioactive Br^{75} isotope of 106-minute half-life has been produced by $Se^{74}(d,n)$ and $Se^{74}(p,\gamma)$ reactions. The Se^{74} used was enriched electromagnetically from 0.9 percent to 14.1 percent.* The period was not observed by similar reactions on Se^{76}, enriched from 9.5 percent to 41.5 percent.* A positron end-point energy of about 1.5 Mev was observed. No evidence of gamma-radiation has been found in the activity. A radioactive Br^{77} isotope of about 58-hour half-

life has been produced by a (d,n) reaction on enriched Se^{76} and by an (α,p) reaction on enriched Se^{74}. A radioactive Kr^{77} isotope of 65-minute half-life has been produced by a $Se+\alpha$ reaction, and located by an α-particle bombardment of enriched Se^{74}. A positron end-point energy of 1.7 Mev has been observed by aluminum absorptions. Gamma-radiation and K-capture have also been observed. The Kr^{79} isotope has been produced by an (α,n) reaction on enriched Se^{76}. The half-life of this isotope is computed as 1.40-days with gamma-radiation present. The 4.4-hour Br^{80} isotope has been produced by a $Se(\alpha,p)$ reaction. Positron emission has been observed with an end-point energy of about 0.8 Mev.

* Supplied by the Y-12 plant, Carbide and Carbon Chemicals Corporation, through the Isotopes Division, U. S. Atomic Energy Commission, Oak Ridge, Tennessee.

J6. Evidence for a Double Isomer in Rh^{103}. H. F. GUNLOCK AND M. L. POOL, *The Ohio State University.*—The x-ray activities in the previously reported 17-day Pd^{103} and 56-minute Rh^{103} have been photographed and found to be the K-series of rhodium. No shift or doubling, due to a possible double electron jump, appears when comparison is made with the spectrum of fluorescent rhodium. Spectrograms of 39.9 and 42.7 Kev electron groups have been obtained from samples of $Rh+d$ and $Ru+d$. These cannot be interpreted as L- and M-conversion electrons, since no group is found where the K-conversion electrons, required by the K-series x-rays, would appear. Considering the two groups as K-electrons, no L- or M-electrons are found near 60 Kev. The gamma-rays responsible for the K-conversion would have energies near 63.1 and 65.9 Kev. These, if present, are of very low intensity. The data appear to indicate two isomers of stable Rh^{103}. The metastable states would have energies of 63.1 and 65.9 Kev and decay to the ground state by emission of gamma-rays which appear to be entirely converted in the K-shell alone.

J7. "Cross-Over" Transitions in Gamma-Ray Spectra. V. MYERS AND A. WATTENBERG, *Argonne National Laboratory.*—The possibility was investigated of there being very weak high energy gamma-rays in certain isotopes than are known at present. In some instances, these gamma-rays may be "cross-over" transitions, i.e., transitions directly from the higher levels to the ground state rather than a cascade process. The technique consisted of placing the radio-isotope inside a beryllium or heavy water target, and a BF_3 pulse ion chamber was used to detect any photoneutrons emitted. 37-minute Cl^{38} and 60-day Sb^{124} produced photoneutrons in D_2O (2.18 Mev threshold) while 34-hour Br^{82} produced photoneutrons in Be (1.63 Mev threshold). It is not known whether the Cl^{38} gamma-ray is a "cross-over" transition, or whether it is the "2.15"-Mev gamma reported by Siegbahn[1] and lying just at the limit for photo-disintegration in heavy water.

[1] K. Siegbahn, Arkiv. F. Math. Astr. och Fys. **32A**, 9 (1945).

J8. The Decay Scheme of 47-hr Sm^{153}. S. B. BURSON AND C. O. MUEHLHAUSE, *Argonne National Laboratory.*—As seen by an ordinary argon filled mica end window counter the 47-hr period in Sm^{153} has been shown to have the following radiations:

.78 Mev β^- ~	100	percent,
EuL x-rays ~	.25	percent,
EuK x-rays ~	.12	percent,
110 Kev γ-rays ~	.03	percent,
610 Kev γ-rays ~	.003	percent.

By coincidence measurements using two mica end window counters we have also shown the existence of direct coincidences of these radiations as follows:

β^-, e^- (e^- ~ L conversion of γ_{110}) ~	90	percent,
β^-, x (K and L-rays) ~	7	percent,
β^-, γ_{110} ~	2	percent,
x, x (K x-rays) ~	.85	percent,
x, γ_{110} (K x-rays) ~	.15	percent.

No delayed coincidences $>1.5\mu s$ were found. We therefore conclude (1) the existence of an almost totally converted level in Eu^{153} of energy <100 kev which is in cascade with γ_{110}, and (2) that the weak γ_{610} must follow a weak β^- branch of ~200 kev from the 47-hr state in Sm.

J9. The Beta-Spectra of W^{185} and Os^{193}. D. SAXON, *Argonne National Laboratory.*—The survey of the heavy elements begun with Au^{198} has been continued in the neighboring region.[1] For W^{185}, the half-life has been determined as $73.2\pm0.5d$, checking the older measurements. The end point from the Kurie extrapolation is 0.430 ± 0.010 Mev. The recent measurement of S. Jnanananda[2] gives 0.675 Mev, a value much outside the experimental errors. Since the end point of Ir^{192} is essentially this value, and in view of the large neutron cross section of Ir^{191} as compared to W^{184}, it is suggested that Jnanananda's sample had $\geq$0.1 percent impurity of Ir^{191}. The half-life of Os^{193} found was 16.1 ± 0.2 days. However the effect of the 100-day Os^{185} K-capture correction could bring this down to the 15-day value found by L. Katzin and M. Pobereskin. The end point found was 142 ± 3 kev. By coincidence methods, Wiedenbeck and Chu obtained 0.64 Mev, a value very close to that for Ir^{192}. From the K, L, and M conversion line the energy of one γ is 127 ± 2 kev, checking that of Cork *et al.* Similarly, the L and M lines of a new low energy γ give 39 ± 1 kev. The above conversion lines all decay with the 16-day period.

[1] D. Saxon, Phys. Rev. **73**, 811 (1948).
[2] S. Jnanananda, Phys. Rev. **72**, 1124 (1947).

J10. Studies on the Radiation of Hf^{181}.* A. F. VOIGT AND B. J. THAMER, *Iowa State College.*—Absorption and coincidence absorption measurements have been made on the radiation from 46-day Hf^{181}, obtained by pile thermal neutron bombardment. The energy of the principal gamma-radiation was found to be 0.52 ± 0.05 Mev while that of the beta-radiation was $0.63\pm.03$ Mev by Feather analysis. Measurement with a magnetic field showed only negative electrons. The coincidence study showed a conversion electron of 0.12 Mev energy in coincidence with the beta-ray. Beta-spectrometer studies have shown a 0.12 Mev electron to be an L conversion electron of a 0.132 Mev gamma-ray which electron is probably the one observed here, the K electron being too soft (0.065 Mev) to be detected. However, DeBenedetti[1] has reported

a 0.11 Mev electron to be emitted in a 22μsec. delayed transition. Since the resolving time of the present circuit[3] is 0.67 μsec. it is impossible that the delayed electron would give the observed coincidence rate. Without knowing whether both of these are L electrons the energies of the coincident and delayed transitions cannot be stated with certainty.

* This work was done under contract with the Atomic Energy Commission.
[1] S. DeBenedetti and F. K. McGowan, Phys. Rev. **70**, 569 (1946).
[2] The coincidence circuit and counter tubes used with it were built by and under the supervision of D. S. Martin.

J11. Activities Produced by Bombardment of TiO_2 with Pile Neutrons.[1] R. E. HEIN AND A. F. VOIGT, *Iowa State College.*—The radioactive isotopes produced by epi-Cd neutron bombardment of titanium dioxide have been investigated using the Argonne heavy water pile. A chemical separation on the irradiated TiO_2 was effected for the purpose of identifying radioactive products from (n,γ), $(n,2n)$, (n,p) and (n,α) processes. The following activities were identified: Ti^{51}, Sc^{46}, Sc^{47}, and Ca^{45}. These identifications were based on observed beta-ray energies and half-life measurements as well as chemical evidence. The cross sections for the formation of these activities from their appropriate titanium isotopes and an upper limit for Sc^{48} were estimated. Since no monitoring sample was present, the estimate for the cross sections was based on measured activities, radiation log and neutron flux. The cross sections for the formation of the listed isotope from the appropriate Ti isotope and based on the total flux of neutrons of all energies are: $Ti^{51}\sigma = 8\times10^{-28}$ cm^2, $Sc^{46}\sigma = 2.5\times10^{-31}$ cm^2, $Sc^{47}\sigma = 6.9\times10^{-30}$ cm^2, $Sc^{48}\sigma = 1.3\times10^{-31}$ cm^2 and $Ca^{45}\sigma = 3\times10^{-32}$ cm^2. The presence of a contaminant, Sb^{123}, with an estimated $\sigma_{act.} = 8\times10^{-24}$ cm^2, hindered the investigation. It is of interest that the 83-hour Sc^{47} was produced by an n,p reaction, while the 44-hour Sc^{48}, which is reported as a product of such a bombardment, was not observed.

[1] This work was done under contract with the Atomic Energy Commission.

Diverse Topics

K1. Secondary Emission from Thoria on Platinum and Tantalum. H. E. MENDENHALL, *Bell Telephone Laboratories.*—Thorium dioxide has been used as a cathode coating material for some magnetrons and power tubes. The secondary emission properties or a film of thoria about 5×10^{-4} cm thick has been studied on platinum and tantalum ribbons. At temperatures up to 400 or 500°C there is evidence from the shape of the δ *vs.* bombarding energy curves of a charging of these surfaces when measurements are made on D.C. At higher temperatures below which primary emission becomes appreciable, the resistance of the coating becomes low enough so that δ's up to 3.4 have been measured without evidence of charging. The thoria coating on tantalum appears to activate when heated to 2000°K probably due to reduction of some thoria to thorium in the coating film.

K2. The Transport Properties of Non-Polar Gases.* JOSEPH O. HIRSCHFELDER, R. BYRON BIRD, AND ELLEN L. SPOTZ, *The University of Wisconsin.*—In the kinetic theory of gases, all of the transport properties are expressed in terms of a set of collision integrals. We have evaluated these on the assumption that the energy of repulsion is inversely proportional to the twelfth power and the energy of attraction to the sixth power of the separation. The transport properties are then reduced to known functions of the reduced mass; the minimum energy of interaction, ϵ; and the collision diameter for low velocity collisions, r_0. The values of ϵ and r_0 for a large number of common gases are determined from recent measurements of viscosity and compared with values previously determined from second virial coefficients. These constants and the tabulated integrals at 84 different temperatures are used to predict the coefficient for thermal diffusion as a function of temperature and the results are very interesting. Our calculations should have a mechanical error of the order of one part in 300, and at the lowest temperatures they must be corrected for quantum effects.

* This work was carried out under contract with the Navy Bureau of Ordnance.

K3. The Equilibrium Assumption in the Theory of Absolute Reaction Rates.* C. F. CURTISS AND J. O. HIRSCHFELDER, *University of Wisconsin.*—The usual theory of absolute reaction rates involves the approximation that the molecules in the transition stage are in statistical equilibrium with the reacting molecules—an approximation difficult to justify. It is shown that this approximation is equivalent to taking the distribution in velocities of the reacting molecules to be Maxwellian. The chemical reaction itself causes the distribution function to deviate somewhat from the equilibrium Maxwellian distribution, since in general only fast molecules react. The perturbed distribution function has been obtained, using a generalization of the Chapman-Enskof methods of kinetic theory. The effect of the perturbation on the rate of a bimolecular reaction has been considered. The influence of the rate of transfer of energy among the various internal degrees of freedom has been obtained by considering two extreme cases. In one case we assumed that the transfer of energy takes place extremely slowly; in the other case that it takes place extremely rapidly. In both cases the rate of reaction obtained differs by less than 8 percent from the value obtained on the basis of the usual approximation.

* This work was carried out under contract with the Navy Bureau of Ordnance.

K4. Unitary Field Theory and Cosmic Magnetism. JEAN MARIANI, *Institute for Advanced Study* (Introduced by L. Brillouin).—We adopt the view that the difficulties in the way of constructing a unified field theory stem from the use of unoperational notions, i.e., notions lacking experimental significance according to L. W. Bridgman. In the present work we consider the notion of an unobservable (an isolated system, a unique electromagnetic field in vacuum, etc.) to be inadmissible. We generalize the law of inertia in a way suggested by Elie Cartan, H. Mandel, and L. P. Eisenhart, using like E. Schrödinger a non-

symmetrical affine connection in Riemannian space-time. We emphasize the fact that the antisymmetrical part of our connection, like Eisenhart's, is a function of the velocity of the test particles in the field, so that the geometry defined by our connection cannot be described independently of the test particles. We base our explanation of electromagnetism upon this fact. Our point of view leads us to a geometry of paths similar to those of O. Veblen, Eisenhart and others. Bodies regarded as electrically neutral in the usual theory are here considered as charged. It follows that a rotating celestial body possesses a magnetic field and it is shown that this leads in the case of static equilibrium to Blackett's formula.

K5. Theory and Applications of the Parallel T Resistance-Capacitance Network. C. E. BERGMAN AND G. H. FETT, *University of Illinois.*—This paper is a general study of the theory and applications of the parallel T resistance-capacitance network, using matrix algebra. The basic theory is presented, and equations are developed for the conditions of null, for the transfer characteristic, and for input (or output) impedance. The effect of loading is considered; simplified equations, resulting from certain special component relationships, are presented. Practical design factors are given. Applications given include reviews and analyses of the uses of the circuit as a compact low-frequency filter to suppress a single frequency, as a filter for a power supply, as a frequency or impedance bridge, and as the feedback loop for a frequency-selective amplifier or frequency-stabilized oscillator. An analysis is given of the problem of imparting band-pass characteristics to the frequency-selective amplifier by means of two parallel T networks.

TO BE READ BY TITLE

T1. Radiations from Columbium (95).* C. E. MANDEVILLE AND M. V. SCHERB, *Bartol Research Foundation of the Franklin Institute.*—The 35-day columbium activity was produced by the fission process in the pile at Oak Ridge. Chemical purification was carried out for the removal of phosphorous, zirconium, copper, and iron as possible impurities. Aluminum absorption indicated the presence of the characteristic soft beta-rays having an energy of about 0.13 Mev. Coincidence absorption of secondary electrons gave a maximum gamma-ray energy of 0.92 Mev. The beta-gamma coincidence rate indicated that the beta-rays are followed by 0.94 Mev of gamma-ray energy. A gamma-gamma coincidence rate of 0.28×10^{-3} coincidence per gamma-ray was also observed. The writers had previously assigned the 0.92 Mev gamma-ray to the zirconium parent element.[1] This apparently resulted from an incomplete chemical separation and from the fact that the 0.92 Mev gamma-ray is very intense. The previously reported[1] coincidence rates of zirconium (95) suggest that only gamma-rays of energy 0.3 or 0.4 Mev follow the zirconium beta-rays.

* Assisted by the Office of Naval Research.

[1] M. V. Scherb and C. E. Mandeville, Bull. Am. Phys. Soc. **23**, No. 3, 56 (1948).

Author Index to Papers Presented at the Madison Meeting

Adams, G. D. and A. T. Nordsieck—No. I4
Antonoff, G.—No. C2
Arroe, O. H.—No. J1
Bashkin, S. and H. T. Richards—No. E7
Bergman, C. E. and G. H. Fett—No. K5
Bernstein, S., F. L. Talbott, J. K. Leslie, and C. P. Stanford—No. D8
Blair, J. M., W. Sleator, Jr., George Freier, E. E. Lampi, and J. H. Williams—No. E5
Burson, S. B. and C. O. Muehlhause—No. J8
Curtiss, C. F. and J. O. Hirschfelder—No. K3
Davis, R. E., W. E. Johnson, K. Lark-Horovitz, and S. Siegel—No. A3
Epstein, H. T.—No. A6
Fisher, John C.—No. A9
Frick, Walter, Edward J. Lofgren, Frank Oppenheimer, and Edward P. Ney—No. D9
George, Waller and Richard LaTorre—No. A7
Gunlock, H. F. and M. L. Pool—No. J6.
Hammer C. F., A. G. Pieper, and R. Rollefson—No. H8
Hanson, H. P. and W. W. Beeman—No. H1
Hein, R. E. and Voigt, A. F.—No. J11
Henkel, R. L. and B. Petree—No. E8
Herb, R. G.—No. B3
Herb, R. G., S. C. Snowden, and O. Sala—No. D1
Herlin, M. A.—No. F3
Hirschberg, J. G., Jr.—No. H6
Hirschfelder, Joseph O., R. Byron Bird, and Ellen L. Spotz—No. K2
Holstein, T.—No. F1
Huang, Su-Shu—No. H5
Inglis, D. R., N. P. Heydenburg, and E. M. Hafner—No. D6
Isenberg, I., B. R. Russell, and R. F. Greene—No. A4
James, H. M.—No. C1
Jauch, J. M.—No. H10
Jesse, William P. and Harold Forstat—No. E2
Johnson, V. A.—No. A2
Kaesberg, Paul, H. N. Ritland, and W. W. Beeman—No. A5
Kohman, Truman P.—No. E1
Langer, Lawrence M., C. Sharp Cook, and H. Clay Price, Jr.—No. J3
Lanzl, L. H., J. S. Laughlin, and L. S. Skaggs—No. H2
Lofgren, Edward J., Edward P. Ney, and Frank Oppenheimer—No. D10
Lowry, E. F.—No. G3
McCown, D. A., L. L. Woodward, M. L. Pool, and H. L. Finston—No. J4
McElhinney, J., A. O. Hanson, and R. B. Duffield—No. D2

Mack, J. E. and N. Austern—No. H4
Mandeville, C. E. and M. V. Scherb—No. T1
Manring, Edward R., John R. Zimmerman, and Dudley Williams—No. J2
Mariani, Jean—No. K4
Marshall, L.—No. E3
Marvin, Robert S., Edwin R. Fitzgerald, and John D. Ferry—No. A8
Meissner, K. W., L. G. Mundie, and P. Stelson—No. H7
Mendenhall, H. E.—No. K1
Molnar, J. P. and J. A. Hornbeck—No. F2
Morrish, A. H. and J. S. Allen—No. E10
Myers, V. and A. Wattenberg—No. J7
Nier, A. O. C.—No. G1
Nottingham, W. B. and W. E. Mutter—No. H3
Phillips, J. A. and P. Gerald Kruger—No. E4
Powell, J. L.—No. D11
Richards, H. T. and R. V. Smith—No. D3
Roberts, Arthur—No. I3
Robinson, C. V.—No. E11
Sachs, R. G.—No. I2
Sachs, R. G. and J. L. Powell—No. D12
Sala, O. and R. G. Herb—No. E9
Saxon, D.—No. J9
Siegel, Sidney and C. G. Shull—No. A1
Sleator, William Jr., J. M. Blair, George Freier, Eugene Lampi, and J. H. Williams—No. E6
Smith, Lyle W. and P. Gerald Kruger—No. D7
Smith, R. V. and H. T. Richards—No. D4
Strait, E. N., C. G. Stergiopoulos, and W. W. Buechner—No. D5
Thamer, B. J. and A. F. Voigt—No. E12
Van Vleck, J. H.—No. I1
Voigt, A. F. and B. J. Thamer—No. J10
Watson, K. and J. M. Jauch—No. H11
Wentzel, Gregor—No. B2
White, M. W.—No. C3
Wigner, E. P.—No. B1
Winans, J. Gibson and Willard J. Pearce—No. H9
Woodward, L. L., D. A. McCown, M. L. Pool, and H. L. Finston—No. J5
Wooten, L. A.—No. G2